



HAL
open science

Synthesis, characterization and bioactivities of dithiocarbazate Schiff base ligands and their metal complexes

May Lee Low

► **To cite this version:**

May Lee Low. Synthesis, characterization and bioactivities of dithiocarbazate Schiff base ligands and their metal complexes. Organic chemistry. Université Pierre et Marie Curie - Paris VI, 2014. English. NNT : 2014PA066148 . tel-01175653

HAL Id: tel-01175653

<https://theses.hal.science/tel-01175653>

Submitted on 11 Jul 2015

HAL is a multi-disciplinary open access archive for the deposit and dissemination of scientific research documents, whether they are published or not. The documents may come from teaching and research institutions in France or abroad, or from public or private research centers.

L'archive ouverte pluridisciplinaire **HAL**, est destinée au dépôt et à la diffusion de documents scientifiques de niveau recherche, publiés ou non, émanant des établissements d'enseignement et de recherche français ou étrangers, des laboratoires publics ou privés.

Université Pierre et Marie Curie

Université de cotutelle

Ecole doctorale ED406

Laboratoire des BioMolécules

**Synthèse, caractérisation et bioactivité de ligands issus de
bases de Schiff dérivées de dithiocarbazate et de leurs
complexes métalliques**

May Lee LOW

Thèse de doctorat de Chimie Moléculaire

Dirigée par Karen Crouse et Clotilde Policar

Présentée et soutenue publiquement le 09 Juillet 2014

Devant un jury composé de :

FARINA Yang, Professeur

YUSOF Nor Azah, Professeur

HASENKNOPF Bernold, Professeur

CROUSE Karen Anne, Professeur

POLICAR Clotilde, Professeur

DELSUC Nicolas, Chargé de recherche

Rapporteur

Rapporteur

Examineur

Directeur de thèse

Directeur de thèse

Invité

All material contained within the thesis, including without limitation text, logos, icons, photographs and all other artwork, is copyright material of Universiti Putra Malaysia unless otherwise stated. Use may be made of any material contained within the thesis for non-commercial purposes from the copyright holder. Commercial use of material may only be made with the express, prior, written permission of Universiti Putra Malaysia.

Copyright © Universiti Putra Malaysia

Abstract of thesis presented to the Senate of Universiti Putra Malaysia and École Doctorale 406 Chimie Moléculaire Université Pierre et Marie Curie in fulfillment of the requirement for the degree of Doctor of Philosophy

**SYNTHESIS, CHARACTERIZATION AND BIOACTIVITIES OF
DITHIOCARBAZATE-SCHIFF BASE LIGANDS AND THEIR METAL
COMPLEXES**

By

LOW MAY LEE

2014

There is an urgent need to discover new drugs with novel mechanisms of action, higher activity and improved selectivity to address the severe challenge of multi-drug resistance in treating bacterial infections and cancer. In view of this, Schiff bases derived from S-substituted dithiocarbamate and their corresponding metal complexes with a plethora of potentially exciting biological activities and coordination chemistry are attractive candidates for consideration. Macroacyclic and open chain metal complexes of tetradentate NNSS and bidentate NS Schiff base ligands derived from the condensation of S-benzylthiocarbamate (SBDTC) and S-methylthiocarbamate (SMDTC) with 2,5-hexanedione, methyl levulinate, levulinic acid, 4-carboxybenzaldehyde and 3-acetylcoumarin have been prepared. The compounds were fully characterized with various physico-chemical and spectroscopic methods. A total of 11 crystals structure were determined throughout this work. In order to provide more insight into the behaviour of the complexes in solution, electron paramagnetic resonance (EPR) and cyclic voltammetry (CV) experiments were performed. Conjugation of the most promising antimicrobial compound (Schiff base of SBDTC with 4-carboxybenzaldehyde) to various vectors (polyarginine, polyethylene glycol (PEG) and phe-arg- β -naphthylamide (PA β N) was

achieved using either standard solid phase or solution synthetic methodologies to prepare improved therapeutic agents. Among the conjugates, the nonaarginine (R9) derivatives showed the most encouraging synergistic effect upon conjugation and complexation to copper ion with enhanced water solubility, bacteria cell membrane permeability and bioactivity. The Cu(II) R9 derivatives possess remarkable antibacterial activity against a wide spectrum of bacteria and in particular, highly efficacious against *S. aureus* with MIC values up to 1-0.5 μM when tested against nine strains of Gram-positive and Gram-negative bacteria. This appears to be the pioneer study to show that the conjugation of polyarginine to dithiocarbamate compounds can greatly influence their therapeutic potential. Cytotoxic assay was also carried out for selected non-conjugated compounds. All the selected Cu(II) complexes assayed against breast cancer cells lines (MCF-7 and MDA-MB-231) exhibited good cytotoxicity with lower IC_{50} values in comparison to their respective ligands. This work highlights the relevance of metal complexation strategy to stabilize the ligands and improve their bioactivity. The structure-activity relationships of the compounds are discussed.

Abstrak tesis yang dikemukakan kepada Senat Universiti Putra Malaysia dan École Doctorale 406 Chimie Moléculaire Université Pierre et Marie Curie sebagai memenuhi keperluan untuk Ijazah Doktor Falsafah

**SINTESIS, PENCIRIAN DAN AKTIVITI BIOLOGI LIGAN
DITIOKARBAZAT-BES SCHIFF DAN KOMPLEKS LOGAM**

Oleh

LOW MAY LEE

2014

Terdapat keperluan segera untuk menemui ubat-ubatan baru dengan mekanisme baru, aktiviti yang lebih tinggi dan tindakan yang lebih khusus bagi menangani cabaran yang serius iaitu rintangan terhadap pelbagai ubat-ubatan dalam rawatan jangkitan bakteria dan kanser. Memandangkan situasi ini, bes Schiff dan kompleks logam yang berasal daripada S-gantian ditiokarbazat yang mempunyai pelbagai potensi aktiviti biologi dan kimia koordinasi menarik merupakan calon-calon yang baik untuk pertimbangan. Kompleks logam bersistem makro-bukan-kitaran dan rangkaian-terbuka masing-masing dengan ligan tetradentat NNSS dan bidentat NS bes Schiff yang berasal daripada kondensasi antara S-benzilditiokarbazat (SBDTC) dan S-metilditiokarbazat (SMDTC) dengan 2,5-heksanadion, metil levulinat, asid levulinik, 4-carboxibenzaldehid dan 3-asetilcoumarin telah disediakan. Semua sebatian tersebut telah dicirikan sepenuhnya dengan pelbagai kaedah fiziko-kimia dan spektroskopi. Sebanyak 11 struktur kristal telah ditentukan sepanjang kajian ini. Untuk memberi gambaran yang lebih jelas terhadap sifat-sifat kompleks dalam larutan, eksperimen elektron resonans paramagnet (EPR) dan voltametri berkitar (CV) telah dijalankan. Konjugasi sebatian yang paling berpotensi antimikrob (bes Schiff SBDTC dengan 4-carboxibenzaldehid) dengan pelbagai vektor (poliarginine, polietilena glikol (PEG) dan phe-arg- β -naptilamida (PA β N)) telah berjaya dicapai

sama ada melalui metodologi sintetik standard peptida fasa pepejal atau larutan bagi penyediaan agen terapeutik yang lebih baik. Antara sebatian yang dikongjugasi, nonaarginine (R9) derivatif menunjukkan kesan sinergi yang paling menggalakkan melalui kongjugasi dan juga pengkompleksan dengan ion kuprum yang turut membawa kepada peringkatan kelarutan dalam air, ketelapan terhadap membran sel bakteria dan bioaktiviti sebatian. Cu(II) R9 derivatif memiliki aktiviti antibakteria yang terbaik terhadap spektrum bakteria yang luas dan khususnya, sangat berkesan terhadap *S. aureus* dengan nilai-nilai MIC sehingga 1-0.5 μM apabila diuji terhadap sembilan jenis bakteria Gram-positif dan Gram-negatif. Ini merupakan kajian perintis yang menunjukkan bahawa kongjugasi antara polyarginine dengan sebatian ditiokarbamat boleh mempengaruhi potensi terapeutik mereka. Kajian sitotoksik juga dijalankan untuk segelintir sebatian yang tidak dikongjugasi. Semua Cu(II) kompleks yang diuji terhadap sel-sel kanser payudara (MCF-7 dan MDA-MB-231) menunjukkan sifat sitotoksik yang baik dengan nilai-nilai IC_{50} yang lebih rendah berbanding dengan ligan masing-masing. Ini menunjukkan kesesuaian strategi pengkompleksan dengan ion logam untuk menstabilkan ligan dan meningkatkan bioaktiviti mereka. Perhubungan di antara struktur dan aktiviti sebatian juga dibincang.

Résumé de thèse présenté au Sénat de Université Putra Malaysia et de l'École
Doctorale Chimie Moléculaire 406 Université Pierre et Marie Curie à
l'accomplissement de l'obligation pour le grade de docteur en philosophie

SYNTHÈSE, LA CARACTÉRISATION ET DE BIOACTIVITÉS
DITHIOCARBAZATE - BASE DE SCHIFF LIGANDS ET LEUR MÉTAL
COMPLEXES

Par

LOW MAY LEE

2014

Il y a de nos jours un besoin urgent de découvrir de nouveaux médicaments avec de nouveaux mécanismes d'action, une activité plus élevée et une meilleure sélectivité pour relever le défi de la multirésistance dans le traitement des infections bactériennes et le cancer. Dans cette perspective, des bases de Schiff dérivées de dithiocarbazates S-substitué et leurs complexes métalliques correspondants sont des candidats intéressants puisqu'ils peuvent être facilement synthétisés et permettent une grande diversité de coordination. Dans cette étude, des complexes macrocycliques tetradentes SSNN et bidente NS dont les ligands sont issus de la condensation de la S-benzylthiocarbazate (SBDTC) ou de la S-methylthiocarbazate (SMDTC) avec la 2,5-hexanedione, le lévulinate de méthyle, l'acide lévulinique, le 4-carboxybenzaldéhyde ou le 3-acétylcoumarine ont été préparés. Les ligands et complexes synthétisés ont été entièrement caractérisés par différentes méthodes spectroscopiques et physico-chimiques. 11 structures cristallines ont été obtenues au cours de ce travail et afin d'étudier en détail la géométrie, la stabilité et les propriétés de ces complexes en solution, des expériences de résonance paramagnétique électronique (RPE), de titration calorimétrique isotherme et de voltamétrie cyclique (CV) ont été réalisées. L'activité

antibactérienne de ces complexes a ensuite été étudiée et a permis de sélectionner un complexe « leader » (plus efficace, stable et fonctionnalisable). Ce complexe a alors été modifié afin d'augmenter sa stabilité en milieux biologiques, sa solubilité dans l'eau ainsi que son activité. Il a été conjugué avec différentes entités : des peptides pénétrants, un polyéthylène glycol (PEG) et un peptide inhibiteur des pompes d'efflux bactériennes (Phe-Arg- β -naphthylamide (PA β N)). Parmi les conjugués obtenus, ceux comportant un peptide avec 9 arginines (R9) ont montré un effet synergique lors de la formation des complexes puisque l'activité anti-bactérienne des complexes s'est avérée meilleure que celle des ligands et du cuivre seuls. Ces complexes ont montré une remarquable activité antibactérienne sur neuf souches de bactéries Gram-positives et Gram-négatives et en particulier, ils se sont avérés très efficaces contre *S.aureus* avec des valeurs de concentration minimale inhibitrice (CMI) de 1 à 0,5 μ M. L'activité anti-cancéreuse des complexes non-conjugués a également été étudiée. Tous les complexes de cuivre sélectionnés et testés sur des cellules de cancer du sein MCF7 et MDA-MB- 231 ont montré une cytotoxicité élevée avec des valeurs de CI50 plus faibles pour les complexes par rapport à leurs ligands respectifs. Ceci met à nouveau en évidence la pertinence d'utiliser les complexes métalliques, pour à la fois stabiliser les ligands et générer des composés plus actifs. Les relations structure-activité des composés sont discutées.

ACKNOWLEDGEMENTS

I am most grateful to my main supervisors Professor Karen A. Crouse, Professor Clotilde Policar and Dr. Nicolas Delsuc for their valuable guidance, advice and support from the very beginning of my PhD journey until the successful completion of this thesis. They are my role models whom I will always hold at the highest esteem. To Professor Karen Crouse, thank you for the inspiration. You instilled in me the love for inorganic chemistry during my undergraduate studies and eventually introduced me to the beauty of synthetic chemistry of dithiocarbazate for my PhD. To Professor Clotilde Policar, thank you for accepting me to your group and giving me the most incredible opportunity to realize this research project. I greatly appreciate that. To Dr. Nicolas Delsuc, I could not have imagined having a better mentor than you. Your enthusiasm, optimism and critical opinions keep me going. Thank you so much.

I would also like to extend my appreciation to my co-supervisors and collaborators for making this research possible Dr. Pierre Dorlet for his kind assistance and suggestions with EPR and CV experiments, Dr. Laure Maigre and Professor Jean-Marie Pagés for antibacterial evaluation, Dr. Régis Guillot and Dr. Mohamed Ibrahim M. Tahir for single crystal XRD structure determination, Professor Rozita Rosli and Dr. Abhimanyu Veerakumarasivam for the access to cytotoxic assay as well as Dr. François Lambert, Dr. Hélène Bertrand and Dr. Thahira Begum for meaningful discussion.

Many thanks to the wonderful present and past members of Laboratoire des BioMolécules (LBM) / Ecole Normale Supérieure (ENS) Héloïse, Sarah, Vincent, Cécile, Margharita, Cillian, Anne-Sophie, Sylvain, Jean-Marie, Julian, Benjamin, Marilyne, Laure, Anais, Nicolas, Mayeul, Geraldine, Rodrique, Laurent, Alex, Roba, Pierluca, Enrique, Jing, Paul, Akansha, Victor and many more people that I had the privilege to know. I could not thank them enough for the kindness that I received throughout my stay in Paris and all the pleasant memories that we shared in and outside the lab. It means a lot to me. My gratitude also to my lab mates in Universiti Putra Malaysia (UPM) Georgiana, Shahedh, Ming Yueh, Shatila and Tan. You are my rock, thanks very much for the friendship.

The financial support for the project from UPM, the Ministry of Higher Education (Malaysia) and French ANR Blanc 2010, METABACT grant is gratefully acknowledged. In addition, I am very thankful for the award of an Erasmus Mundus Maheva Scholarship and a UPM Graduate Research Fellowship (GRF).

And finally, I wish to thank my dearest mom, dad and younger sister for their endless love and encouragement. Thank you for believing in me and teaching me to reach for the stars, to work hard and to always strive to be the very best that I can be. To them I dedicate this work.

Dans la vie, rien n'est à craindre, tout est à comprendre.

Nothing in life is to be feared, it is only to be understood.

- Marie Curie

APPROVAL

I certify that an Examination Committee has met on (**date of viva voce**) to conduct the final examination of **Low May Lee** on her Doctor of Philosophy thesis entitled “**Synthesis, Characterization and Bioactivities of Dithiocarbazate-Schiff Base Ligands and Their Metal Complexes**” in accordance with Universities and University Colleges Act 1971 and the Constitution of the Universiti Putra Malaysia [P.U.(A) 106] 15 March 1998. The Committee recommends that the student be awarded the degree of Doctor of Philosophy.

Members of the Thesis Examination Committee were as follows

Name of Chairperson, PhD

Title (e.g., Professor/Associate Professor/Ir; omit if irrelevant)

Name of Faculty

Universiti Putra Malaysia

(Chairman)

Name of Examiner 1, PhD

Title (e.g., Professor/Associate Professor/Ir; omit if irrelevant)

Name of Faculty

Universiti Putra Malaysia

(Internal Examiner)

Name of Examiner 2, PhD

Title (e.g., Professor/Associate Professor/Ir; omit if irrelevant)

Name of Faculty

Universiti Putra Malaysia

(Internal Examiner)

Name of External Examiner, PhD

Title (e.g., Professor/Associate Professor/Ir; omit if irrelevant)

Name of Department and/or Faculty

Name of Organisation (University/Institute)

Country

(External Examiner)

NORITAH OMAR, PhD

Assoc. Prof. and Deputy Dean

(Thesis and Publication)

School of Graduate Studies

Universiti Putra Malaysia

Date

APPROVAL

This thesis was submitted to the Senate of Universiti Putra Malaysia and has been accepted as fulfillment of the requirement for the degree of Doctor of Philosophy. The members of the Supervisory Committee are as follows

Karen Anne Crouse, PhD

Professor
Faculty of Science
Universiti Putra Malaysia
(Chairman)

Clotilde Policar, PhD

Professor
Laboratoire des BioMolécules (UMR 7203)
Université Pierre et Marie Curie
(Member)

Nicolas Delsuc, PhD

Chargé de Recherche CNRS
Laboratoire des BioMolécules (UMR 7203)
Université Pierre et Marie Curie
(Member)

Mohamed Ibrahim Mohamed Tahir, D.Phil

Senior Lecturer
Faculty of Science
Universiti Putra Malaysia
(Member)

Thahira B.S.A Ravoof, PhD

Senior Lecturer
Faculty of Science
Universiti Putra Malaysia
(Member)

Rozita Rosli, PhD

Professor
Faculty of Medical and Health Science
Universiti Putra Malaysia
(Member)

BUJANG BIN KIM HUAT, PhD

Professor and Dean
School of Graduate Studies
Universiti Putra Malaysia

Date

DECLARATION

I hereby confirm that

- this thesis is my original work;
- quotations, illustrations and citations have been duly acknowledged;
- ownership of intellectual property from the thesis is as stipulated in the Memorandum of Agreement (MoA), or as according to the Universiti Putra Malaysia (Research) Rules 2012, in the event where the MoA is absent;
- permission from supervisor and the office of Deputy Vice-Chancellor (Research and Innovation) are required prior to publishing it (in the form of written, printed or in electronic form) including books, journals, modules, proceedings, popular writings, seminar papers, manuscripts, posters, reports, lecture notes, learning modules or any other materials as stated in the Universiti Putra Malaysia (Research) Rules 2012;
- there is no plagiarism or data falsification/fabrication in the thesis, and scholarly integrity is upheld as according to the Universiti Putra Malaysia (Graduate Studies) Rules 2003 (Revision 2012-2013) and the Universiti Putra Malaysia (Research) Rules 2012. The thesis has undergone plagiarism detection software.

Signature _____ Date _____

Name and Matric No: Low May Lee (GS26866)

DECLARATION

This is to confirm that

- the research conducted and the writing of this thesis was under our supervision;
- supervision responsibilities as stated in the Universiti Putra Malaysia (Graduate Studies) Rules 2003 (Revision 2012-2013) are adhered to.

Signature _____
Karen Anne Crouse, PhD
Professor

Signature _____
Clotilde Policar, PhD
Professor

Signature _____
Mohamed Ibrahim Mohamed Tahir,
D.Phil
Senior Lecturer

Signature _____
Nicolas Delsuc, PhD
Chargé de Recherche CNRS

Signature _____
Dr. Thahira B.S.A Ravoof, PhD
Senior Lecturer

Signature _____
Rozita Rosli, PhD
Professor

LIST OF TABLES

Table		Page
3.1	Selected bond lengths for SBPY, SMHD, CuSMHD and CuSBHD.	59
3.2	Selected bond angles for CuSMHD, CuSBHD, CuATSM (Blower et al., 2003) and CuAATSM.	59
3.3	Selected bond lengths for SMML, SBML, SBEL and SBLA.	65
3.4	Selected bond angles for SMML, SBML, SBEL and SBLA.	65
3.5	Intermolecular hydrogen bonds for SMML, SBML, SBEL and SBLA.	66
3.6	Selected dihedral angles between the two planes for SMML, SBML, SBEL and SBLA.	66
3.7	Selected bond lengths for Cu(SMML) ₂ and Cu(SMLA) ₂ .	69
3.8	Selected bond angles for Cu(SMML) ₂ and Cu(SMLA) ₂ .	69
3.9	Main bond lengths (Å) and angles (°) in the coordination sphere around the rhenium atom.	74
3.10	Bond lengths (Å) and angles (°) in the dithiocarbazate fragments.	74
3.11	EPR parameters measured from the spectra of the copper(II) complexes.	85
3.12	Electrochemical data for CuSMHD and CuSBHD versus Ag/AgCl.	90
3.13	Electrochemical data for the Cu(II) complexes vs Ag/AgCl at 0.1V.	92
3.14	Electrochemical data for the Cu(SMML) ₂ vs Ag/AgCl at various scan rate (V/s).	94
4.1	Selected ligands and their Cu(II) complexes that were synthesized and studied.	105
4.2	LC-ES-MS data for all Cu(II) dithiocarbazate Schiff base ligand-conjugates and R1-SB4CB for comparison.	136

4.3	Thermodynamic parameters of conjugated ligand complexation with copper determined by ITC at 25 °C.	138
4.4	EPR parameters measured from the spectra of the copper(II) complexes.	141
4.5	Electrochemical data vs Ag/AgCl.	143
5.1	Bacteria strains.	157
5.2	Antimicrobial activity of the tetradentate series.	162 - 163
5.3	Antimicrobial activity of non-conjugated bidentate series.	168 - 169
5.4	Antimicrobial activity of bioconjugate series.	176 - 177
5.5	Final antimicrobial evaluation against 9 strains of bacteria.	181 - 182
5.6	Cytotoxic assay results.	187

LIST OF FIGURES

Figure		Page
1.1	(a) Decade-wise approval of new antibiotics and (b) prevalence of MRSA.	2
2.1	Various S-substituents at position R ₁ in dithiocarbazates.	5
2.2	Examples of different series of carbonyl compounds that have been used for the preparation of dithiocarbazate ligands.	6
2.3	Examples of different dithiocarbazate derivatives (a) with sugars, amino acid and calixarene (b) with modifications at N ₁ atom.	7
2.4	Different conformations of dithiocarbazate.	8
2.5	(a) Thione-thiol tautomerism (b) C=S and S=C conformers.	9
2.6	Compounds with antimigratory activity.	11
2.7	(a) Schiff bases of SBDTC with 2-acetylpyridine, 2-benzoylpyridine and 6-methyl-2-formylpyridine, respectively in thione form (b) saccharinate anion.	14
2.8	Mixed ligand Pt(II) and Pd(II) complexes with Schiff base (derived from SBDTC and 2-hydroxyacetophenone) and phosphine ligands.	19
2.9	Ternary structures of VO complexes and the phenanthroline bases used.	20
3.1	RP-HPLC chromatogram of SBHD at 220 nm (top) and 280 nm (bottom).	53
3.2	RP-HPLC chromatogram of CuSBHD.	53
3.3	RP-HPLC chromatogram of SMML.	53
3.4	RP-HPLC chromatogram of Cu(SMML) ₂ .	54
3.5	RP-HPLC chromatogram of SM4CB.	54
3.6	FT-IR spectra recorded for ligand SBHD and complex CuSBHD.	57
3.7	FT-IR spectra recorded for ligand SMML and complex Cu(SMML) ₂ .	57

3.8	ORTEP drawing of (a) SMHD (b) SBPY (c) CuSMHD and d) CuSBHD. Ellipsoids are drawn at the 50% probability level.	58
3.9	ORTEP diagrams and intermolecular hydrogen bonds (shown as <i>dotted line</i>) of (a) SMML (b) SBLA (c) SBML (d) SBEL. Ellipsoids are drawn at the 50% probability level.	62 - 63
3.10	ORTEP diagrams of (a) Cu(SMML) ₂ and (b) Cu(SMLA) ₂ with intermolecular hydrogen bonds (shown as <i>dotted lines</i>) in (c). Ellipsoids are drawn at the 50% probability level.	68
3.11	ORTEP diagram and intermolecular interactions (shown as <i>dotted red line</i>) for Re ₂ (SBCM) ₂ . Ellipsoids are drawn at the 50% probability level.	72 - 73
3.12	¹ H NMR and ¹³ C NMR spectra of SMML.	77
3.13	¹ H NMR and ¹³ C NMR spectra of SB4CB.	78
3.14	(a) UV-vis spectra recorded at 25 μM in DMSO using a cell length of 1 cm. The insert shows the d-d band of the two complexes at concentration of 1 mM. (b) UV-Vis spectra recorded for SMML and Cu(SMML) ₂ at 25 μM. Insert shows d-d band of the complex at 1 mM.	81
3.15	UV-Vis spectra obtained by addition of Cu(OAc) ₂ .H ₂ O at 25°C to a solution of SM4CB (ca. 2.5 x 10 ⁻⁵ M) at a) in DMSO solution as well as in 0.1M acetate buffer, pH6.	82
3.16	The EPR spectrum of CuSMHD, CuSBHD, Cu(SMML) ₂ and Cu(SM4CB) ₂ at 1 mM in frozen DMF. Microwave frequency 9.50 GHz, microwave power 0.25 mW, modulation amplitude 0.2 mT, modulation frequency 100 kHz, time constant 164 ms, T=50 K.	84
3.17	<i>Transoid</i> and <i>cisoid</i> ligands conformation.	85
3.18	The EPR spectrum of Cu(R1-SB4CB) ₂ at 1 mM in various solvents. #: major species, *: minor species.	87
3.19	The EPR spectrum of Cu(R9-SB4CB) ₂ at 1 mM in various solvents. #: major species, *: minor species.	88
3.20	The different possible species of the Cu(II) complexes that could exist in solution.	88

3.21	Cyclic voltammograms of the Cu complexes at 1.7 mM in anhydrous deoxygenated DMF containing 0.1 M tetrabutylammonium hexafluorophosphate as the supporting electrolyte. Working electrode glassy carbon; counter electrode Pt wire; reference electrode Ag/AgCl, scan rate 100 mV/s. All sweeps were initiated in the direction of the arrow.	90
3.22	Cyclic voltammograms of the Cu(SMML) ₂ at 1.7 mM in anhydrous deoxygenated DMF containing 0.1 M tetrabutylammonium perchlorate as the supporting electrolyte. Working electrode glassy carbon; counter electrode Pt wire; reference electrode Ag/AgCl. (a) and (b) Scan rate= 0.1 V/s. (c) Various scan rates= 0.02, 0.05, 0.1, 0.2, 0.5 V/s. All sweeps were initiated in the direction of the arrow.	93
3.23	Plot of the anodic (I _{pa}) and cathodic (I _{pc}) current with the square root of scan rate for Cu(SMML) ₂ .	94
4.1	Schematic diagram of a functionalized bis(thiosemicarbazone) conjugated to a biologically active molecule (BAM).	99
4.2	Applications of cell-penetrating peptides as molecular delivery vehicles.	101
4.3	CPP loading and targeting strategies.	102
4.4	Chromatograms of PEG-SB4CB synthesized via Fmoc strategy. (a) Crude (b) Purified. Detection at $\lambda = 220$ nm (top) and 280 nm (bottom). The peak at 17.5 min corresponds to the expected product.	121
4.5	RP-HPLC chromatograms obtained on a C8 column. Samples were eluted using a gradient of acetonitrile from 5 to 95% in water over 30 min with 1 mL min ⁻¹ flow rate at room temperature (both solvents contain 0.1% TFA). Detection: $\lambda = 220$ nm (top) and 280 nm (bottom).	124
4.6	Chromatograms of PA β N-SB4CB synthesized in solution. (a) Crude (b) Purified. The peak at 21.5 min corresponds to the expected product.	126
4.7	¹ H and ¹³ C spectra of the Schiff base-conjugate (R1-SB4CB).	129
4.8	MALDI spectra of R9-SB4CB. The hydrolyzed fragment (cleavage of C=N bond) is noticeable during MALDI characterization.	130

- 4.9 UV-Vis titration of various ligands (concentration set at ca. 2.5×10^{-5} M) with $\text{Cu}(\text{OAc})_2 \cdot \text{H}_2\text{O}$ (concentration set at ca. 5×10^{-4} M) at 25°C . a) Titration of R1-SB4CB in methanol and its corresponding titration curve monitored at 340 nm. b) Titration of SM4CB in acetate buffer pH 6 and its corresponding titration curve monitored at 340 nm. c) Titration of R9-SM4CB in acetate buffer pH 6 and its corresponding titration curve monitored at 340 nm. 132 - 133
- 4.10 UV-Vis spectra obtained by addition of $\text{Cu}(\text{OAc})_2 \cdot \text{H}_2\text{O}$ at 25°C to a solution of R9-SB4CB (ca. 2.5×10^{-5} M) at a) pH 4 (0.1 M acetate buffer), b) pH 7.4 (0.01 M PBS buffer) and at c) pH 9 (0.1 M borate buffer). 134 - 135
- 4.11 LC chromatogram of $\text{Cu}(\text{R1-SB4CB})_2$ (top) and R1-SB4CB (bottom) showing the two isomeric peaks with similar molecular mass. A linear gradient elution developed from holding time of 5 min at 100% (0.1% formic acid in water) and then from 0-60% (0.1% formic acid in acetonitrile) in 30 min. Experiments were carried out at a flow rate of $10 \mu\text{L min}^{-1}$ at room temperature with peaks detection at 220 nm and 280 nm. 137
- 4.12 ITC titration of $\text{Cu}(\text{R9-SB4CB})_2$, $\text{Cu}(\text{OAc})_2$ (concentration at ca. 5×10^{-5} M) was added every 300 s to the ligand R9-SB4CB solution (concentration at ca. 1×10^{-5} M) in 0.1M acetate buffer at pH 6. The top curve represents the corrected heat flow with time. The bottom curve represents the heat of reaction (measured by peak integration) as a function of Cu/ligand ratio. The solid line is the best theoretical fit to the experimental data. The three first points were removed for the fitting. 139
- 4.13 The EPR spectra of both parent and conjugated compounds (1 mM) in frozen DMF were indicative of the same species being formed with approximate calculated g_{\perp} and g_{\parallel} values of ~ 2.05 and ~ 2.15 , respectively. Microwave frequency 9.50 GHz, microwave power 0.25 mW, modulation amplitude 0.2 mT, modulation frequency 100 kHz, time constant 164 ms, $T = 50$ K. 140
- 4.14 EPR spectra of 1mM $\text{Cu}(\text{R9-SB4CB})_2$ and $\text{Cu}(\text{OAc})_2$ in frozen acetate buffer pH 6 (0.1 M) are different from one another. Microwave frequency 9.50 GHz, microwave power 0.2 mW, modulation amplitude 0.2 mT, modulation frequency 100 kHz, time constant 164 ms, $T = 50$ K. 141
- 4.15 Cyclic voltammograms of $\text{Cu}(\text{R1-SB4CB})_2$ and $\text{Cu}(\text{SB4CB})_2$, 1.7 mM in anhydrous deoxygenated DMF with 0.1 M tetrabutylammonium perchlorate as the supporting electrolyte. Working electrode glassy carbon; counter electrode Pt wire; reference electrode Ag/AgCl, scan rate 100 mV/s. All sweeps were initiated in the direction of the arrow. 142

5.1	Structural features of the cell wall that distinguishes the Gram-positive from the Gram-negative bacteria.	146
5.2	Mechanism of antimicrobial agents.	148
5.3	The membrane target of antimicrobial peptides of multicellular organisms and the basis of specificity.	150
5.4	(a) Diagrammatic comparison of the five families of efflux pumps (b) Targeting the efflux pump. Illustrations of various targets in the efflux pump complex of RND family.	152
5.5	Example of a metallodrug consists of hydroxamic acid and an ancillary ligand.	155
5.6	Influence of DMSO on the growth of bacteria strains over time. (a) AG100 and (b) EA289.	161
5.7	Effect of complexation on the non-conjugated bidentate series of molecules against the different strains of <i>E. coli</i> (AG100 T and AG100A acrAB-) and <i>E. aerogenes</i> (EA289 acrAB- and EA298 tolC-). The ratio MIC (free ligand) / MIC(complexed ligand) has been calculated with the MIC (in presence of PMBN) reported according to the stoichiometry of the complex.	171
5.8	Effect of complexation on the conjugated bidentate series of molecules against the different strains of <i>E. coli</i> (AG100 T and AG100A acrAB-) and <i>E. aerogenes</i> (EA289 acrAB- and EA298 tolC-).	180
5.9	Effect of complexation on Cu(SB4CB) ₂ , Cu(SM4CB) ₂ Cu(R9-SB4CB) ₂ , Cu(RW9-SB4CB) ₂ , Cu(R9-SM4CB) ₂ , Cu(RW9-SM4CB) ₂ against the different strains without the presence of PMBN.	185
5.10	Effect of complexation on Cu(SB4CB) ₂ , Cu(SM4CB) ₂ Cu(R9-SB4CB) ₂ , Cu(RW9-SB4CB) ₂ , Cu(R9-SM4CB) ₂ , Cu(RW9-SM4CB) ₂ against the different strains in the presence of PMBN.	186

LIST OF SCHEMES

Scheme		Page
3.1	Synthesis of the non-conjugated parent compounds.	49
4.1	Strategies to prepare metal complex conjugated with peptides.	104
4.2	Synthetic pathway for the synthesis of the functionalized copper complexes.	105
4.3	Synthesis of the PEGylated copper complex by Fmoc strategy.	120
4.4	Synthesis of ligand-peptide conjugates by Boc-strategy.	123
4.5	Solution synthesis of PA β N-SB4CB.	125

LIST OF APPENDICES

Figure		Page
A1	^1H NMR spectrum of SBHD	227
A2	^{13}C NMR spectrum of SBHD	227
A3	^1H NMR spectrum of SMHD	228
A4	^{13}C NMR spectrum of SMHD	228
A5	^1H NMR spectrum of SBPY	229
A6	^{13}C NMR spectrum of SBPY	229
A7	^1H NMR spectrum of SMLA	230
A8	^{13}C NMR spectrum of SMLA	230
A9	^1H NMR spectrum of SBML	231
A10	^{13}C NMR spectrum of SBML	231
A11	^1H NMR spectrum of SBLA	232
A12	^{13}C NMR spectrum of SBLA	232
A13	^1H NMR spectrum of SBEL	233
A14	^{13}C NMR spectrum of SBEL	233
A15	^1H NMR spectrum of SM4CB	234
A16	^{13}C NMR spectrum of SM4CB	234
A17	^1H NMR spectrum of SBCM	235
A18	^1H NMR spectrum of $\text{Zn}(\text{SBCM})_2$	235
A19	^1H NMR spectrum of $\text{Re}_2(\text{SBCM})_2$	236
A20	^1H NMR spectrum of PEG-SB4CB	237
A21	^{13}C NMR spectrum of PEG-SB4CB	237
A22	^1H NMR spectrum of PEGAC	238

A23	¹³ C NMR spectrum of PEGAC	238
A24	¹ H NMR spectrum of R1AC	239
A25	¹³ C NMR spectrum of R1AC	239
A26	¹ H NMR spectrum of R4-SB4CB	240
A27	¹ H NMR spectrum of R4-AC	240
A28	¹ H NMR spectrum of R9-SB4CB	241
A29	¹ H NMR spectrum of R9-SM4CB	241
A30	¹ H NMR spectrum of R9AC	242
A31	¹ H NMR spectrum of RW9-SB4CB	242
A32	¹ H NMR spectrum of RW9-SM4CB	243
A33	¹ H NMR spectrum of RW9AC	243
A34	¹ H NMR spectrum of PAβN-SB4CB	244
B1	ESI-MS spectrum of CuSBHD	245
B2	ESI-MS spectrum of CuSMHD	245
B3	ESI-MS spectrum of SBPY	246
B4	HR-MS spectrum of SMML	247
B5	HR-MS spectrum of SMLA	247
B6	HR-MS spectrum of SM4CB	248
B7	HR-MS spectrum of SBML	248
B8	HR-MS spectrum of SBEL	249
B9	HR-MS spectrum of SBLA	249
B10	HR-MS spectrum of SB4CB	250
B11	ESI-MS spectrum of Cu(SMML) ₂	250
B12	ESI-MS spectrum of Cu(SMLA) ₂	251
B13	ESI-MS spectrum of Cu(SM4CB) ₂	251

B14	ESI-MS spectrum of Cu(SBML) ₂	252
B15	ESI-MS spectrum of Cu(SBLA) ₂	252
B16	ESI-MS spectrum of Cu(SB4CB) ₂	253
B17	HR-MS spectrum of SBCM	253
B18	ESI-MS spectrum of Cu(SBCM) ₂	254
B19	ESI-MS spectrum of Zn(SBCM) ₂	254
B20	ESI-MS spectrum of Re ₂ (SBCM) ₂	255
B21	HR-MS spectrum of PEG-SB4CB	255
B22	HR-MS spectrum of PEGAC	256
B23	HR-MS spectrum of R1AC	256
B24	MALDI-TOF-MS full spectrum of R4-SB4CB	257
B25	MALDI-TOF-MS enlarged spectrum of R4-SB4CB	258
B26	MALDI-TOF-MS full spectrum of PAβN-SB4CB	259
B27	MALDI-TOF-MS enlarged spectrum of PAβN-SB4CB	260
B28	MALDI-TOF-MS full spectrum of R9-SB4CB	261
B29	MALDI-TOF-MS enlarged spectrum of R9-SB4CB	262
B30	MALDI-TOF-MS full spectrum of RW9-SB4CB	263
B31	MALDI-TOF-MS enlarged spectrum of RW9-SB4CB	264
B32	MALDI-TOF-MS full spectrum of R9-SM4CB	265
B33	MALDI-TOF-MS enlarged spectrum of R9-SM4CB	266
B34	MALDI-TOF-MS full spectrum of RW9-SM4CB	267
B35	MALDI-TOF-MS enlarged spectrum of RW9-SM4CB	268
B36	MALDI-TOF-MS full spectrum of R4AC	269
B37	MALDI-TOF-MS enlarged spectrum of R4AC	270
B38	MALDI-TOF-MS full spectrum of R9AC	271

B39	MALDI-TOF-MS enlarged spectrum of R9AC	272
B40	MALDI-TOF-MS full spectrum of RW9AC	273
B41	MALDI-TOF-MS enlarged spectrum of RW9AC	274
B42	LC-MS (EMS) spectrum of R1-SB4CB at 17.6 min	275
B43	LC-MS (EPI) spectrum of R1-SB4CB at 17.6 min	275
B44	LC-MS (EMS) spectrum of R1-SB4CB at 15.3 min	276
B45	LC-MS (EPI) spectrum of R1-SB4CB at 15.3 min	276
B46	TIC (EMS) chromatogram of R1-SB4CB	277
B47	TIC (EPI) chromatogram of R1-SB4CB	277
B48	ESI-MS spectrum of Cu(R1-SB4CB) ₂	278
B49	LC-MS [EMS and ER (inset)] spectra of Cu(R1-SB4CB) ₂ at 17.6 min	279
B50	LC-MS (EPI) spectrum of Cu(R1-SB4CB) ₂ at 17.6 min	279
B51	LC-MS [EMS and ER (inset)] spectra of Cu(R1-SB4CB) ₂ at 15.3 min	280
B52	LC-MS (EPI) spectrum of Cu(R1-SB4CB) ₂ at 15.3 min	280
B53	TIC (EMS) chromatogram of Cu(R1-SB4CB) ₂	281
B54	TIC (EPI) chromatogram of Cu(R1-SB4CB) ₂	281
B55	ESI-MS spectrum of Cu(PEG-SB4CB) ₂	282
B56	LC-MS [EMS and ER (inset)] spectra of Cu(PEG-SB4CB) ₂ at 16.1 min	283
B57	LC-MS (EPI) spectrum of Cu(PEG-SB4CB) ₂ at 16.1 min	283
B58	LC-MS [EMS and ER (inset)] spectra of Cu(PEG-SB4CB) ₂ at 15.2 min	284
B59	LC-MS (EPI) spectrum of Cu(PEG-SB4CB) ₂ at 15.2 min	284
B60	TIC chromatogram of Cu(PEG-SB4CB) ₂	285
B61	ESI-MS spectrum of Cu(PAβN-SB4CB) ₂	286

B62	TIC (EMS) chromatogram of Cu(PAβN-SB4CB) ₂	287
B63	TIC (EPI) chromatogram of Cu(PAβN-SB4CB) ₂	287
B64	LC-MS [EMS and ER (inset)] spectra of Cu(PAβN-SB4CB) ₂	288
B65	LC-MS (EPI) spectrum of Cu(PAβN-SB4CB) ₂	288
B66	LC-MS [EMS and ER (inset)] spectra of Cu(R4-SB4CB) ₂ at 14.0 min	289
B67	LC-MS (EPI) spectrum of Cu(R4-SB4CB) ₂ at 14.0 min	289
B68	LC-MS [EMS and ER (inset)] spectra of Cu(R4-SB4CB) ₂ at 17.3 min	290
B69	LC-MS (EPI) spectrum of Cu(R4-SB4CB) ₂ at 17.3 min	290
B70	TIC (EMS) chromatogram of Cu(R4-SB4CB) ₂	291
B71	TIC (EPI) chromatogram of Cu(R4-SB4CB) ₂	291
C1	UV-Vis spectrum of SMLA at 25 μM	292
C2	UV-Vis spectrum of Cu(SMLA) ₂ at 25 μM and 1 Mm	292
C3	UV-Vis spectrum of SBML at 25 μM	292
C4	UV-Vis spectrum of Cu(SBML) ₂ at 25 μM and 1 mM	293
C5	UV-Vis spectrum of SBLA at 25 μM	293
C6	UV-Vis spectrum of Cu(SBLA) ₂ at 25 μM and 1 mM	293
C7	UV-Vis spectrum of SBEL at 25 μM	294
C8	UV-Vis spectrum of SM4CB at 25 μM	294
C9	UV-Vis spectrum of Cu(SM4CB) ₂ at 25 μM	294
C10	UV-Vis spectrum of SB4CB at 25 μM	295
C11	UV-Vis spectrum of Cu(SB4CB) ₂ at 25 μM	295
C12	UV-Vis titration of Cu-R4SB4CB	295
C13	Plot of absorbance against equivalent of Cu for UV-Vis titration of Cu-R4SB4CB	296

C14	UV-Vis titration of Cu-PA β NSB4CB	296
C15	Plot of absorbance against equivalent of Cu for UV-Vis titration of Cu-PA β NSB4CB	296
C16	UV-Vis titration of Cu-PEGSB4CB	297
C17	Plot of absorbance against equivalent of Cu for UV-Vis titration of Cu-PEGSB4CB	297
C18	UV-Vis titration of Cu-RW9SM4CB	297
C19	Plot of absorbance against equivalent of Cu for UV-Vis titration of Cu-RW9SM4CB	298
C20	UV-Vis titration of Cu- RW9SB4CB	298
C21	Plot of absorbance against equivalent of Cu for UV-Vis titration of Cu-RW9SB4CB	298
C22	UV-Vis titration of Cu-R9SB4CB	299
C23	Plot of absorbance against equivalent of Cu for UV-Vis titration of Cu-R9SB4CB	299
C24	UV-vis spectra of SBCM, Cu(SBCM) ₂ , Zn(SBCM) ₂ and Re ₂ (SBCM) ₂ recorded at 25 μ M in DMSO using a cell length of 1 cm. The insert shows the d-d band of the complex Cu(SBCM) ₂ at concentration of 1 mM	300
D1	FT-IR spectrum of SMHD	300
D2	FT-IR spectrum of CuSMHD	300
D3	FT-IR spectrum of SBPY	300
D4	FT-IR spectrum of SMLA	301
D5	FT-IR spectrum of Cu(SMLA) ₂	301
D6	FT-IR spectrum of SBML	301
D7	FT-IR spectrum of Cu(SBML) ₂	302
D8	FT-IR spectrum of SBLA	302
D9	FT-IR spectrum of Cu(SBLA) ₂	302
D10	FT-IR spectrum of SBEL	303

D11	FT-IR spectrum of SM4CB	303
D12	FT-IR spectrum of Cu(SMH4CB) ₂	303
D13	FT-IR spectrum of SB4CB	304
D14	FT-IR spectrum of CuS(SB4CB) ₂	304
D15	FT-IR spectrum of Re ₂ (SBCM) ₂ and SBCM	304
D16	FT-IR spectrum of Cu(SBCM) ₂	305
D17	FT-IR spectrum of Zn(SBCM) ₂	305
F1	RP-HPLC chromatogram of SMHD	311
F2	RP-HPLC chromatogram of CuSMHD	311
F3	RP-HPLC chromatogram of SBPY	311
F4	RP-HPLC chromatogram of SMDTC	312
F5	RP-HPLC chromatogram of SBDTC	312
F6	RP-HPLC chromatogram of SMLA	312
F7	RP-HPLC chromatogram of Cu(SMLA) ₂	313
F8	RP-HPLC chromatogram of SBML	313
F9	RP-HPLC chromatogram of Cu(SBML) ₂	313
F10	RP-HPLC chromatogram of SBLA	314
F11	RP-HPLC chromatogram of Cu(SBLA) ₂	314
F12	RP-HPLC chromatogram of SBEL	314
F13	RP-HPLC chromatogram of CuSM4CB	315
F14	RP-HPLC chromatogram of SB4CB	315
F15	RP-HPLC chromatogram of CuSB4CB	315
F16	RP-HPLC chromatogram of SBCM	316
F17	RP-HPLC chromatogram of Zn(SBCM) ₂	316
F18	RP-HPLC chromatogram of Re ₂ (SBCM) ₂	316

F19	RP-HPLC chromatogram of Cu(SBCM) ₂	317
F20	RP-HPLC chromatogram of R1-SB4CB (crude)	317
F21	RP-HPLC chromatogram of R1-SB4CB (purified)	317
F22	RP-HPLC chromatogram of R4-SB4CB (crude)	318
F23	RP-HPLC chromatogram of R4-SB4CB (purified)	318
F24	RP-HPLC chromatogram of R9-SB4CB (crude)	318
F25	RP-HPLC chromatogram of R9-SB4CB (purified)	319
F26	RP-HPLC chromatogram of RW9-SB4CB (crude)	319
F27	RP-HPLC chromatogram of RW9-SB4CB (purified)	319
F28	RP-HPLC chromatogram of RW9-SM4CB (crude)	320
F29	RP-HPLC chromatogram of RW9-SM4CB (purified)	320
F30	RP-HPLC chromatogram of R1-Ac (crude)	320
F31	RP-HPLC chromatogram of R1-Ac (purified)	321
F32	RP-HPLC chromatogram of R4-Ac (crude)	321
F33	RP-HPLC chromatogram of R4-Ac (purified)	321
F34	RP-HPLC chromatogram of R9-Ac (crude)	322
F35	RP-HPLC chromatogram of R9-Ac (purified)	322
F36	RP-HPLC chromatogram of RW9-Ac (crude)	322
F37	RP-HPLC chromatogram of RW9-Ac (purified)	323
F38	RP-HPLC chromatogram obtained from the SPPS Fmoc synthesis of the aliphatic ligand, SMLA-R9 conjugate. None of the major peaks correspond to the desired product as observed by MALDI-TOF-MS. The coupling and deprotection were difficult and the Schiff base was hydrolysed resulting in the product R9-ketone (<i>m/z</i> : 1521, R _T = 6.5 min) and R9-Fmoc (<i>m/z</i> : 1645, R _T = 10.5 min)	323
G1	Cyclic voltammogram of ferrocene	324
G2	Cyclic voltammograms of the Cu(SMLA) ₂	325

G3	Cyclic voltammograms of the Cu(SM4CB) ₂	326
G4	Cyclic voltammograms of the Cu(SBML) ₂	327
G5	Cyclic voltammograms of the Cu(SBLA) ₂	328
G6	Cyclic voltammograms of the Cu(SB4CB) ₂	329
G7	Cyclic voltammograms of the Cu(SBCM) ₂	330
G8	Plot of the anodic (I _{pa}) and cathodic (I _{pc}) current with the square root of scan rate for Cu(SBCM) ₂ and (above) cyclic voltammograms of Cu(SBCM) ₂ at 0.1 V/s in the range of -1.5 V to 1.5 V	331
H1	ITC titration of Cu(R1-SB4CB) ₂	332
H2	ITC titration of Cu(RW9-SB4CB) ₂	332
H3	ITC titration of Cu(R9-SM4CB) ₂	333
H4	ITC titration of Cu(RW9-SM4CB) ₂	333
H5	ITC titration of Cu(SB4CB) ₂	334
I1	The EPR spectrum of Cu(SMLA) ₂ at 1 mM	335
I2	The EPR spectrum of Cu(SBML) ₂ at 1 mM	335
I3	The EPR spectrum of Cu(SBLA) ₂ at 1 mM	335
I4	The EPR spectrum of Cu(SB4CB) ₂ at 1 mM	336
I5	The EPR spectrum of Cu(R9-SM4CB) ₂ at 1 mM	336
I6	The EPR spectrum of Cu(R1-SB4CB) ₂ at 1 mM	336
I7	The EPR spectrum of Cu(PEG-SB4CB) ₂ at 1 mM	337
I8	The EPR spectrum of Cu(PAβN-SB4CB) ₂ at 1 mM	337
I9	The EPR spectrum of Cu(R4-SB4CB) ₂ at 1 mM	337
I10	The EPR spectrum of Cu(R9-SM4CB) ₂ at 1 mM	338
I11	The EPR spectrum of Cu(RW9-SB4CB) ₂ at 1 mM	338
I12	The EPR spectrum of Cu(RW9-SM4CB) ₂ at 1 mM	338
I13	The EPR spectrum of Cu(SBCM) ₂ at 1 mM	339

Table		Page
E1	Crystallographic data and structure refinement details for compounds SBPY, SMHD, CuSMHD and CuSBHD	306-307
E2	Crystallographic data and structure refinement details for compounds for compounds SMML, SBML and SBEL	308
E3	Crystallographic data and structure refinement details for compounds for compounds SBLA, Cu(SMML) ₂ and Cu(SMLA) ₂	309
E4	Crystallographic data and structure refinement details for compounds for compounds Re ₂ (SBCM) ₂	310
J1	CHNS data	340-341

LIST OF ABBREVIATIONS

<i>A. baumannii</i>	<i>Acinetobacter baumannii</i>
<i>A. fumigates</i>	<i>Aspergillus fumigatus</i>
<i>A. niger</i>	<i>Aspergillus niger</i>
<i>A. ochraceous</i>	<i>Aspergillus ochraceus</i>
ABC	ATP binding cassette
Abs.	Absorbance
ACN	Acetonitrile
ΔH	Enthalpy of the reactions
AMPs	Antimicrobial peptides
ABC	ATP binding cassette
Arg	Arginine
a.u.	Arbitrary unit
<i>B. cereus</i>	<i>Bacillus cereus</i>
<i>B. subtilis</i>	<i>Bacillus subtilis</i>
BAM	Biologically active molecule
BBN	Bombesin
BHT	Buthylatedhydroxytoluene
Boc	Tert-butyloxycarbonyl
<i>C. lusitaniae</i>	<i>Candida lusitaniae</i>
<i>C. albicans</i>	<i>Candida albicans</i>
<i>C. lypolytica</i>	<i>Candida lypolytica</i>
Caov-3	Human ovarian cancer
Cb4PDTC	4-carboxybenzaldehyde

CD3OD	Deuterated methanol
CEM-SS	T-lymphoblastic leukemia
CHCA	alpha-cyano-4-hydroxycinnamic acid
CHNS	Carbon, hydrogen, nitrogen, sulphur
CH ₃ CN	Acetonitrile
CH ₃ OH	Methanol
CI	Chemical ionization
CPPs	Cell penetrating peptides
Cu(OAc) ₂ ·H ₂ O	Copper(II) acetate monohydrate
CV	Cyclic voltammetry
DCM	Dichloromethane
DFO	Desferrioxamine B
DFT	Density functional theory
DIEA	N,N-Diisopropylethylamine
DiSC3(5)	3,3'-Dipropylthiadicarbocyanine iodide
DMEM	Dulbecco's modified Eagle's medium
DMF	Dimethylformamide
DMSO	Dimethyl sulfoxide
DMSO-d ₆	Deuterated dimethyl sulfoxide
DNA	Deoxyribonucleic acid
dpq	Dipyrido[3,2-d:2',3'-f]quinoxaline
dppz	Dipyrido[3,2-a:2',3'-c] phenazine
DTC	Dithiocarbazate
<i>E. aerogenes</i>	<i>Enterobacter aerogenes</i>
<i>E. coli</i>	<i>Escherichia coli</i>

<i>E. histolytica</i>	<i>Entamoeba histolytica</i>
E _p	Peak potentials
E _{1/2}	Half-wave potentials
EPIs	Efflux pump inhibitors
EPR	Electron paramagnetic resonance
ER	Estrogen receptor
ESI-MS	Electrospray ionization-mass spectroscopy
EtOH	Ethanol
F	Phenylalanine
<i>F. oxysporum</i>	<i>Fusarium oxysporum</i>
FAB	Fast atom bombardment
FBS	Fetal bovine serum
FDA	Food and Drug Administration
Fmoc	Fluorenylmethyloxycarbonyl
Fmoc-AEEA-OH	[2-[2-(Fmoc-amino)ethoxy]ethoxy]acetic acid
FT-IR	Fourier transform infrared spectroscopy
FTSC	2-formylpyridine thiosemicarbazone
GRP	gastrin-releasing peptide
HATU	1-[Bis(dimethylamino)methylene]-1H-1,2,3-triazolo[4,5-b]pyridinium 3-oxid hexafluorophosphate
HBTU	N,N,N',N'-Tetramethyl-O-(1H-benzotriazol-1-yl)uraniumhexafluorophosphate, O-(Benzotriazol-1-yl)-N,N,N',N'-tetramethyluronium hexafluorophosphate
HELA	Cervical cancer cells
HEPES	2-[4-(2-hydroxyethyl)piperazin-1-yl]ethanesulfonic acid
HF	Hydrofluoric acid

HIV-TAT	Human immunodeficiency virus - trans-activator of transcription
HL-60	Human promyelocytic leukemia cells
HOAt	1-hydroxy-7-azabenzotriazole
HOBt	Hydroxybenzotriazole
HR-MS	High resolution mass spectroscopy
HT-29	Colon cancer cells
HTS	High throughput screening
IC ₅₀	Inhibition concentration at 50%
INT	Iodonitrotetrazolium
I _{pa}	Anodic current
I _{pc}	Cathodic current
ITC	Isothermal titration calorimetry
K562	Human acute myelocytic leukemia cell line
KAN ^R	Resistance to kanamycin
K _{ass}	Association constant
<i>K. pneumonia</i>	<i>Klebsiella pneumonia</i>
LC-MS	Liquid chromatography–mass spectrometry
LMCT	Ligand-to-metal charge-transfer
LPS	Lipopolysaccharide
<i>M. tuberculosis</i>	<i>Mycobacterium tuberculosis</i>
MATE	Multidrug and toxic compound extrusion
MALDI-TOF-MS	Matrix-assisted laser desorption/ionization-time-of-flight-mass spectroscopy
MBHA	4-Methylbenzhydrylamine
MCF-7	Human breast carcinoma cells expressing nuclear estrogen receptors

MDA-MB-231	Human breast carcinoma cells not expressing nuclear estrogen receptors
MDCK	Madin-Darby canine kidney
MDR	Multi-drug resistance
MeOH	Methanol
Me ₂ S	Dimethylsulfide
MFS	Major facilitator superfamily
MHB	Mueller-Hinton broth
MIC	Minimum inhibitory concentration
<i>m/z</i>	Mass-to-charge ratio
MOPS	3-(N-morpholino)propanesulfonic acid
MPA	3-mercaptopropionic acid
MRSA	Methicillin-resistant <i>Staphylococcus aureus</i>
MTT	3-(4,5-dimethylthiazol-2-yl)-2,5-diphenyltetrazolium bromide
<i>n</i>	Stoichiometry
NHE	Normal hydrogen electrode
NMP	N-Methyl-2-pyrrolidone
NMR	Nuclear magnetic resonance
NS	Nitrogen-sulphur
OPNG	ortho-nitrophenyl-β-D-galactopyranoside
ORTEP	Oak Ridge thermal ellipsoid plot
¹ O ₂	Singlet oxygen
<i>P. aeruginosa</i>	<i>Pseudomonas aeruginosa</i>
PAβN	Phenylalanine-arginine-β-naphthylamide
PBS	Phosphate buffered saline

Pc4PDTC	S4PDTC with pyridine-2-carboxaldehyde
PEG	Polyethylene glycol
phen	1,10-phenanthroline
PMB	Polymyxin B
PMBN	Polymyxin B nonapeptide
PNAs	Polynucleic acids
Pro	Proline
pyta	4-(2-pyridyl)-1,2,3-triazole
QSAR	Quantitative structure-activity relationship
R	Arginine
RND	Resistance-nodulation-division
RP-HPLC	Reversed phase-high performance liquid chromatography
RPM	Revolutions per minute
r.t.	Room temperature
R _T	Retention time
<i>S. aureus</i>	<i>Staphylococcus aureus</i>
<i>S. ceciricaee</i>	<i>Saccaromyces ceciricaee</i>
sac	Saccharinate anion
S2PDTC	S-2-picolylidithiocarbazate
S4PDTC	S-4-picolylidithiocarbazate
SB2ATP	SBDTC-2-acetylthiophene
SB3ATP	SBDTC-3-acetylthiophene
SB4CB	4-(Benzylsulfanylthiocarbonyl-hydrazonomethyl)-benzoic acid
SBCM	N'-[1-(2-Oxo-2H-chromen-3-yl)-ethylidene]-hydrazinecarbodithioic acid benzyl ester

SBDTC	S-benzylthiocarbamate
SBEL	4-(Benzylsulfanylthiocarbonyl-hydrazono)-pentanoic acid ethyl ester
SBHD	N'-[4-(Benzylsulfanylthiocarbonyl-hydrazono)-1-methyl-pentylidene]-hydrazinecarbodithioic acid benzyl ester
SBLA	4-(Benzylsulfanylthiocarbonyl-hydrazono)-pentanoic acid
SBML	4-(Benzylsulfanylthiocarbonyl-hydrazono)-pentanoic acid methyl ester
SBPY	(2,5-Dimethyl-pyrrol-1-yl)-dithiocarbamic acid benzyl ester
SCE	Saturated calomel electrode
SCXRD	Single crystal X-ray diffraction
<i>S. enterica</i>	<i>Salmonella enterica</i>
SM4CB	4-(Methylsulfanylthiocarbonyl-hydrazonomethyl)-benzoic acid
SMDB	S-methyl- β -N-(2-acetylfuran) dithiocarbamate
SMDTC	S-methylthiocarbamate
SMHD	N'-[1-Methyl-4-(methylsulfanylthiocarbonyl-hydrazono)-pentylidene]-hydrazinecarbodithioic acid methyl ester
SMISA	S-methylthiocarbamate with isatin
SMLA	4-(Methylsulfanylthiocarbonyl-hydrazono)-pentanoic acid
SMML	4-(Methylsulfanylthiocarbonyl-hydrazono)-pentanoic acid methyl ester
SMR	Small multidrug resistance
SOD	Superoxide dismutase
SPPS	Solid-phase peptide synthesis
STSC	Salicylaldehyde thiosemicarbazone
TFA	Trifluoroacetic acid
TIS	Triisopropylsilane

TRIS	2-Amino-2-hydroxymethyl-propane-1,3-diol
Trp	Tryptophan
%T	Percentage of transmission
UV-Vis	Ultraviolet-visible
W	Tryptophan
WT	Wild type
XO	Xanthine oxidase
ϵ	Extinction coefficient
α^2	molecular orbital coefficient α^2
$A_{\parallel}, g_{\parallel}, g_{\perp}$	EPR parameters

TABLE OF CONTENTS

	Page
ABSTRACT	iii - iv
ABSTRAK	v - vi
RÉSUMÉ	vii - viii
ACKNOWLEDGEMENTS	ix - x
APPROVAL	xi-xii
DECLARATION	xiii - xiv
LIST OF TABLES	xv - xvi
LIST OF FIGURES	xvii - xxi
LIST OF SCHEMES	xxii
LIST OF APPENDICES	xxiii - xxxii
LIST OF ABBREVIATIONS	xxxiii - xl

CHAPTER

1	INTRODUCTION	1-3
2	LITERATURE REVIEW	
	2.1 S-substituted dithiocarbazate	4
	2.2 Schiff bases and metal complexes	5 - 9
	2.3 Biological activity	
	2.3.1 Anticancer activity	9 - 15
	2.3.2 Antibacterial and antifungal activity	15 - 17
	2.3.3 Iron chelators	17 - 18
	2.3.4 Antituberculosis activity	18
	2.3.5 Antiamoebic activity	18 - 19
	2.3.6 Other biological properties	20 - 22
	2.4 Objectives	23
3	NON-CONJUGATED PARENTS COMPOUNDS	
	3.1 Introduction	
	3.1.1 Types of ligands systems	
	3.1.1.1 Tetradentate NNSS	24 - 26
	3.1.1.2 Potentially bidentate NS or tridentate ONS ligands with an acid or ester functionality	26 - 27
	3.1.1.3 Potentially bidentate NS or tridentate ONS ligands with natural potent aldehyde or ketones moieties	28
	3.1.2 Choice of metals	
	3.1.2.1 Copper	29 - 30
	3.1.2.2 Zinc	30

3.1.2.3 Rhenium	31 - 32
3.2 Methodology	
3.2.1 Materials	32
3.2.2 Instrumentation	32 - 35
3.2.3 Synthesis	
3.2.3.1 Macroacyclic Cu(II) system with tetradentate NNSS ligands	35 - 38
3.2.3.2 Open chain Cu(II) system with bidentate NS ligands with acid or ester functionality	38 - 45
3.2.3.3 Open chain metal system with bidentate NS ligands with natural ketone moiety	45 - 47
3.3 Results and Discussion	
3.3.1 Synthesis	48 - 55
3.3.2 Characterization of metal complexes in solid state	
3.3.2.1 FT-IR	55 - 57
3.3.2.2 Single crystal XRD description	58 - 74
3.3.3 Characterization of metal complexes in solution	
3.3.3.1 NMR	75 - 78
3.3.3.2 UV-VIS	79 - 82
3.3.3.3 EPR	82 - 88
3.3.3.4 Electrochemistry	88 - 94
3.4 Conclusion	94 - 95

4 FUNCTIONALIZED COMPOUNDS

4.1 Introduction	
4.1.1 Key drawbacks of metallodrugs	96 - 98
4.1.2 Conjugated metal complexes	
4.1.2.1 Schiff base conjugates	98 - 99
4.1.2.2 PEGylation	100
4.1.2.3 Cell penetrating peptide as cell delivery vectors	100 - 103
4.1.2.4 Design of metal complex-conjugates	103 - 108
4.2 Methodology	
4.2.1 Materials	108
4.2.2 Instrumentation	109 - 110
4.2.3 Synthesis	110 - 119
4.3 Results and Discussion	
4.3.1 Synthesis	119 - 127
4.3.2 Characterization of ligand conjugates	
4.3.2.1 NMR	127 - 129
4.3.2.2 MALDI-TOF-MS/ESI-MS	130

4.3.3	Characterization of metal-complexes conjugates	
4.3.3.1	UV-VIS	131 - 135
4.3.3.2	LC-MS	135 - 137
4.3.3.3	ITC	137 - 139
4.3.3.4	EPR	139 - 141
4.3.3.5	Electrochemistry	142 - 143
4.4	Conclusion	143 - 144
5	BIOLOGICAL ACTIVITIES	
5.1	Introduction	
5.1.1	Mechanism of actions of antimicrobial agents and multi-drug resistance	145 - 149
5.1.2	Antimicrobial peptides	149 - 150
5.1.3	Efflux pumps and inhibitors	151 - 152
5.1.4	Contribution of metal complexes to the improvement of antimicrobial agents	153 - 155
5.2	Methodology	
5.2.1	Antimicrobial testing (MIC determination)	
5.2.1.1	Bacterial strains, culture media and chemicals	156 - 157
5.2.1.2	Determination of bacterial susceptibility	157 - 158
5.2.2	In vitro cytotoxicity testing	158 - 159
5.3	Results and Discussion	
5.3.1	Antimicrobial evaluation	
5.3.1.1	Macroacyclic Cu(II) system with tetradentate NNSS ligands	159 - 167
5.3.1.2	Open chain Cu(II) system with bidentate NS ligands with acid or ester functionality	167 - 176
5.3.1.3	Functionalized compounds	176 - 186
5.3.2	Cytotoxicity	187 - 189
5.4	Conclusion	189 - 190
6	SUMMARY AND RECOMMENDATION	191 - 193
	REFERENCES	194 - 222
	APPENDICES	223 - 341
	LIST OF PUBLICATIONS AND CONFERENCES ATTENDED	342 - 343
	BIODATA OF STUDENT	344

CHAPTER 1

INTRODUCTION

The use of novel, exotic original compounds from nature's chest to treat diseases has been a quest of mankind since ancient time (Li and Vederas, 2009). Although natural products have historically been a rich source of lead therapeutic molecules, Harvey (2008, p. 894) pointed out that "the difficulties in access and supply, complexities of natural product chemistry and inherent slowness of working with them" have contributed to the de-emphasis of natural products programs in industry over the years. It is foreseeable that developments in the field of synthesis will only continue as synthetic compounds hold the upper hand in meeting the demand of the highly competitive pharmaceutical industry to adapt to the current state-of-the-art advancement in science and technology (Ferguson, 1975; Li and Vederas, 2009; Strohl, 2000).

In term of metal-containing drugs, the platinum drug cisplatin introduced clinically in 1971 and approved by Food and Drug Administration (FDA) in late 1978, has been the most effective metal-based anticancer drug in the market (Hoeschele, 2009; Swarts et al., 2008). The resounding therapeutic success of cisplatin and its analogues has triggered tremendous effort in search of alternative metal-based chemotherapeutic agents in the past few decades (Ronconi and Fregona, 2009; Jakupec et al. 2008). The rationale for these studies is that metal centers other than platinum might open up new avenues in the development of clinically useful drug (Ronconi et al., 2006). Furthermore, there is an urgency to discover and characterize new drugs with enhanced activity, selectivity, bioavailability and fewer side-effects

than conventional drugs to treat current diseases. Figure 1.1 highlights the steady decrease in not only the commercialization but also the discovery for new antibiotics after the 1980s while the serious threat of antimicrobial resistance continues to prevail as reflected in the increasing occurrence of Methicillin-resistant *Staphylococcus aureus* (MRSA) over the same period (Bandow and Metzler-Nolte, 2009; Patra et al., 2012b). In addition, parallel concern over acquired drug resistance and serious side-effects of current anti-cancer drugs in the midst of the rise of cancer, in particular breast cancer as one of the leading causes of death worldwide, also drives the need to develop better alternatives (Ahmad et al., 2013; Yang et al., 2013; Ronconi and Fregona, 2009).

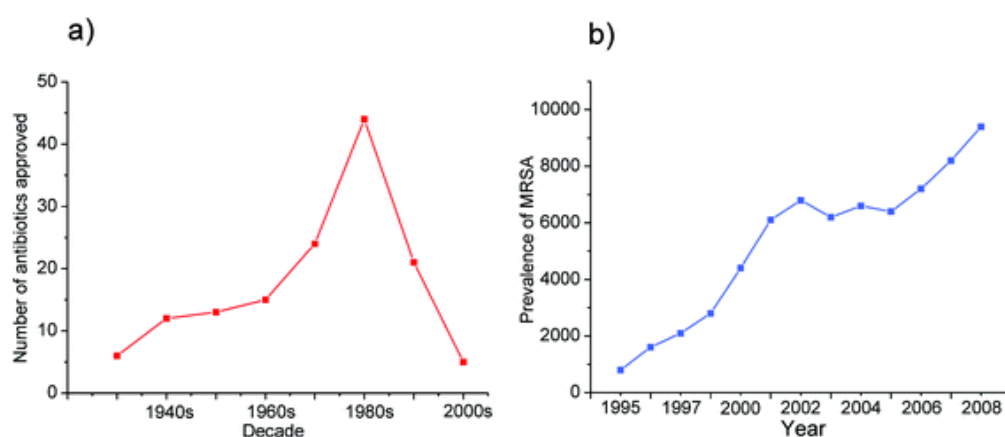


Figure 1.1. (a) Decade-wise approval of new antibiotics and (b) prevalence of MRSA (Source: Patra et al., 2012b)

Many publications have highlighted the rich diversity and potential of metal complexes for the design of novel therapeutic agents (Fricker, 2007; Haas and Franz, 2009; Ronconi and Sadler, 2007; Hambley, 2007; Thompson and Orvig, 2006; Meggers, 2009). The intrinsic nature of metal centers, characteristic coordination modes, accessible redox states and tuneable thermodynamic and kinetic properties allow metal complexes to offer potential advantages over organic agents

alone (Rijt and Sadler, 2009). In addition, Sadler (2009, p. 10647) stated that “the ligands not only control the reactivity of the metal but also play critical roles in determining the nature of interactions involved in the recognition of biological target sites such as deoxyribonucleic acid (DNA), enzymes and protein receptors” (p. 10647). The great expansion of research in the coordination chemistry of nitrogen- and sulphur-containing ligands such as Schiff bases derived from thiosemicarbazones and dithiocarbazates has taken place during recent years (Pelosi, 2010; Beraldo and Gambino, 2004; Ali and Livingstone, 1974). Schiff base metal complexes have played a prominent role in the development of coordination chemistry. This area of research has a wide spectrum, ranging from synthesis to application in many diverse fields. Schiff bases are condensation products of primary amines and aldehydes or ketones (e.g. $RCH=NR'$, where R and R' may represent alkyl and/or aryl substituents) that have often been used as chelating ligands for preparation of complex compounds which are useful as catalysts, in various biological systems, polymers and dyes besides some uses as antifertility and enzymatic agents (Kumar et al., 2009; Soliman and Linert, 2007). Since this class of ligands possess both hard nitrogen and soft sulphur donor atoms, they are capable to act as good chelating agents for various metal ions (Mohamed et al., 2009). The flexibility and bioactivity of nitrogen and sulphur containing Schiff bases have also been associated with the presence of both imino ($-N=CH-$) and thioamino ($-(C=S)-NH-$) moieties in their structures (Tarafder et al., 2008). Coordination of such compounds with metal ions often enhances their activities (Lobana et al., 2009). The low cost as well as the relatively easy preparation of Schiff base derivatives also provide a major attraction in creating novel leads that can be synthesized in a practical and step-economical fashion.

CHAPTER 2

LITERATURE REVIEW

2.1 S-substituted dithiocarbazate

Schiff base ligands formed from dithiocarbazates are a class of particularly important Schiff bases which have been of immense interest owing to their potentially beneficial pharmacological properties and their wide variety of bonding modes and stereochemistry. Dithiocarbazates easily form “an interesting series of ligands whose properties can be modified by introducing different organic substituents” to form stable complexes with a wide variety of metal ions (Tarafder et al., 2002b, p. 2691). In 1974, Ali and Livingstone first reviewed the chemistry of nitrogen-sulphur (NS) chelating ligands. Since then, much has been published about metal complexes with dithiocarbazate. Most of the work has focused upon S-methyl and S-benzyl dithiocarbazate Schiff bases and complexes, while other S-substituted derivatives have been studied recently (Figure 2.1). They include S-allyl (Islam et al., 2014), isomeric S-2-/3-/4-picolyl (Khoo et al., 2014; Crouse et al., 2004; Khoo, 2008), isomeric S-2-/3-/4-methylbenzyl (Ravoof et al., 2011; Ravoof et al., 2010; Ravoof, 2008), S-naphthylmethyl (How, 2008), S-quinolin-2-yl-methyl (How, 2008), S-4-nitrobenzyl (Pavan et al., 2010; Maia et al., 2010) and S-4-chlorobenzyl (Li et al., 2009).

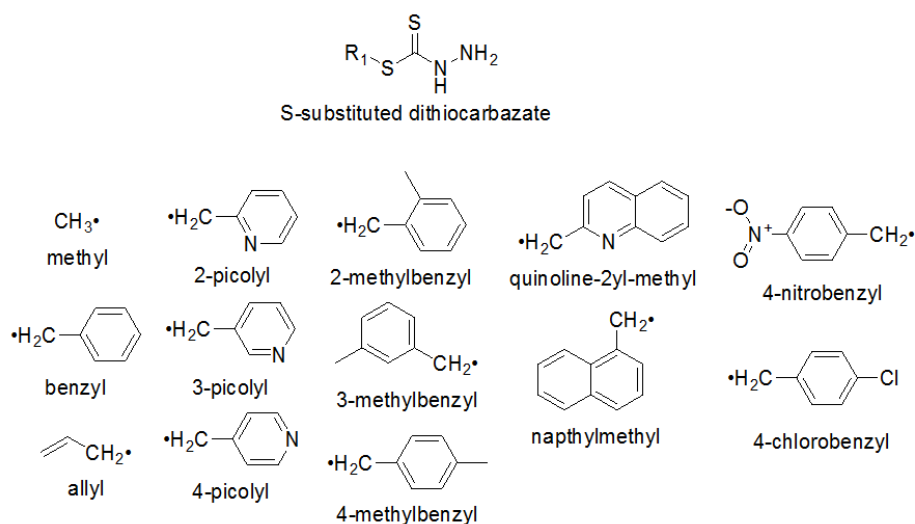
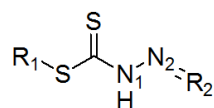


Figure 2.1. Various S-substituents at position R₁ in dithiocarbazates.

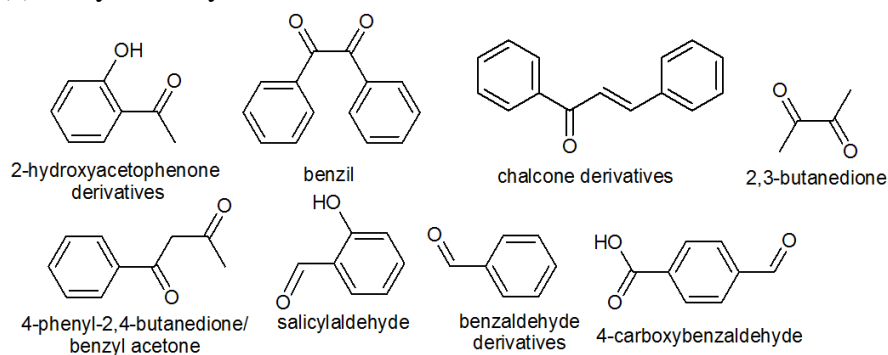
2.2 Schiff bases and metal complexes

Many Schiff base ligands have been obtained by the condensation of an aldehyde or a ketone with dithiocarbazate. Figure 2.2 illustrates the different carbonyl compounds that have been used as precursors for the ligands preparation with condensation at position R₂. The resulting Schiff bases and their respective metal complexes of these selected examples of alkyl, aryl and heteroatomic carbonyl compounds are biologically active and will be discussed in the following section. Other Schiff bases with substituents involving amino acid, sugars and calixarene are shown in Figure 2.3a. Apart from the varied S-substituents, modifications at N₁ atom of the dithiocarbazate derivatives have also been reported (Figure 2.3b). The ligands can be further classified as mono(dithiocarbazate) and bis(dithiocarbazate) which could result in open chain and macrocyclic metal complexes upon complexation. There are also reports of mixed ligand complexes of dithiocarbazate derived ligands with saccharinate ion (Ravoof et al., 2007), phenanthroline bases (Sasmal et al., 2008) and triphenylphosphine (Maia et al., 2010) as co-ligands.



Schiff base

(a) Alkyl and aryl series



(b) Heteroatomic series

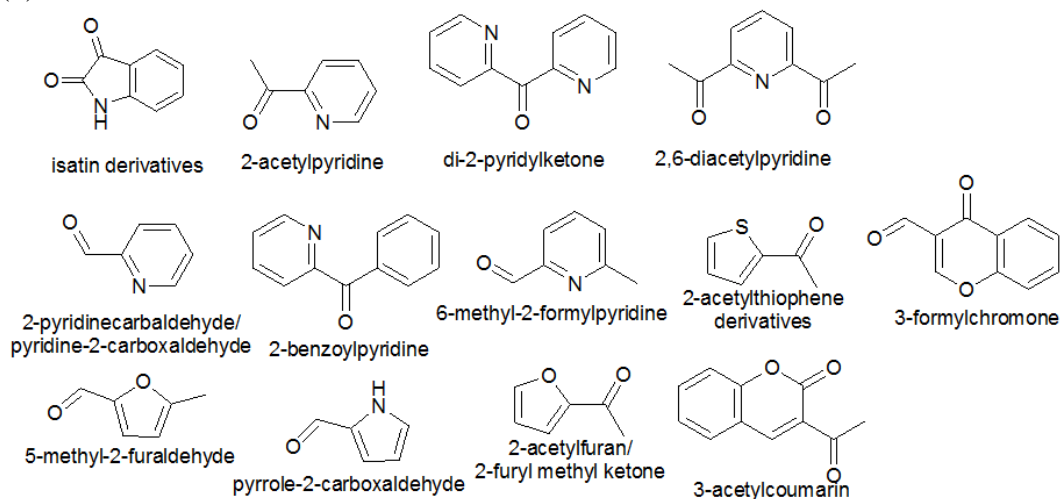
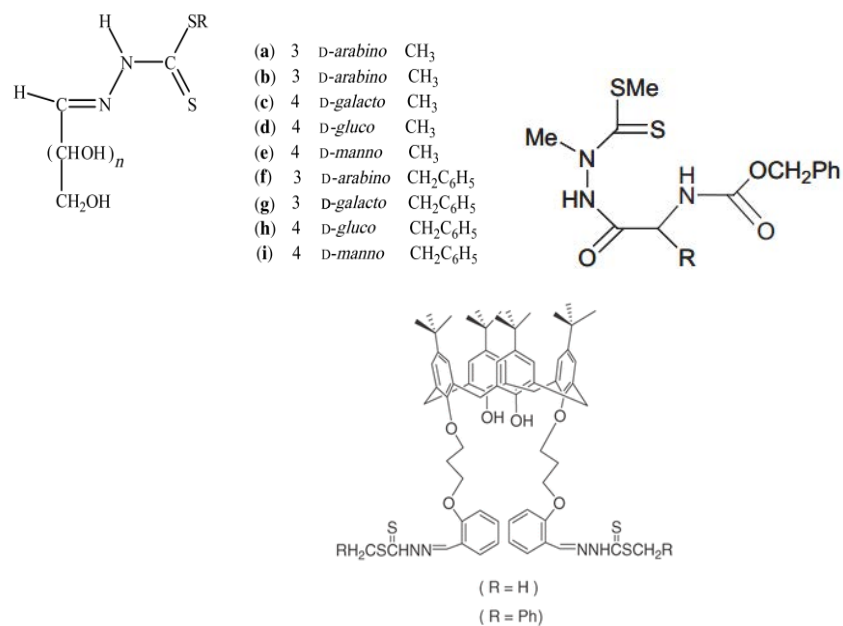


Figure 2.2. Examples of different carbonyl compounds that have been used for the preparation of dithiocarbazate ligands (a) alkyl and aryl series (b) heteroatomic series.

(a) Schiff bases with sugars, amino acid and calixarene.



(Sources: Iskander et al., 2003; Cattabriga et al., 1998; Sun et al., 2009)

(b) Other derivatives with modifications at N₁ atom

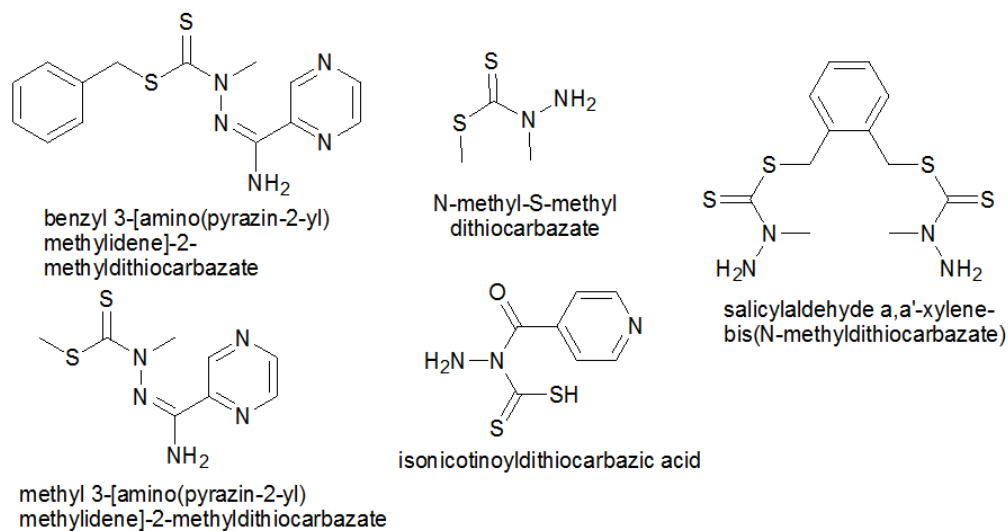


Figure 2.3. Examples of different dithiocarbazate derivatives (a) with sugars, amino acid and calixarene (b) with modifications at N₁ atom

Structural determination show that these dithiocarbazate related compounds could exist differently either as *E* or *Z* diastereoisomers relative to the azomethine C=N bond or as *cis-cis*, *cis-trans*, *trans-cis* and *trans-trans* conformations around the C-N and C-S bonds (Figure 2.4) (Lanfredi et al., 1977). They also form thiol-thione tautomers and, if a hydroxy functional group is present, S=C or C=S conformation could result based on the direction of the thiocarbonyl group either towards or away from the intramolecular hydrogen bonding (Figure 2.5) (Krasowska et al., 2010). In general, dithiocarbazate related compounds normally crystallize in *trans-cis* configuration around the C=S bond in both the S-substituted dithiocarbazate and its Schiff base ligands. They also commonly form intermolecular bonds via NH...S hydrogen bonding and CH...S interactions. The Schiff base coordinates divalent metal ion in its iminothiolate form. Therefore, deprotonation of thioamide N-atom is typical in dithiocarbazate Schiff base coordination chemistry. The conversion of C=S double bond to a single C-S bond is also anticipated due to “tautomerism of the dithiocarbazate ligand to its iminothiolate form” (Ravoof et al., 2007, p 1163). A number of bonding modes and geometries (e.g. tetrahedral, square planar, square pyramidal and octahedral) have been observed for the dithiocarbazate derivatives with transition, non-transition and heavy metals as well as actinides (Tarafder et al., 2002b; Maia et al., 2010; Ravoof et al., 2004; Takjoo et al., 2011).

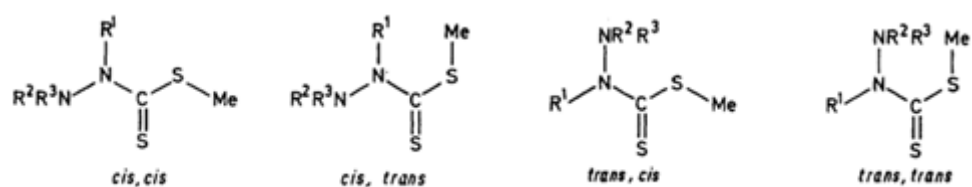


Figure 2.4. Different conformations of dithiocarbazate (Source: Lanfredi et al., 1977)

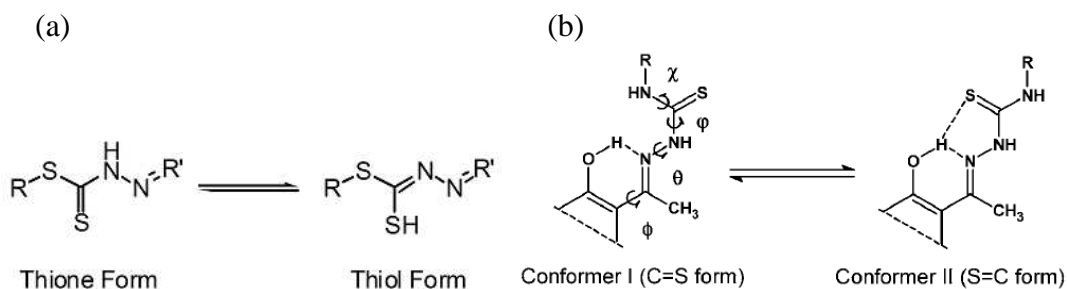


Figure 2.5. (a) Thione-thiol tautomerism (b) C=S and S=C conformers (Source: Krasowska et al., 2010)

2.3 Biological activity

Dithiocarbamate derivatives are of great interest particularly in the development of novel therapeutic compounds because of their vast spectrum of biological activity. Many researchers have synthesized these compounds as target structures and have evaluated their biological activities. A compilation of literature reports focusing on the significant bioactivities of a variety of dithiocarbamate carried out during the past several decades will be presented herein.

2.3.1 Anticancer activity

The Schiff base derived from S-methyldithiocarbamate (SMDTC) with isatin (SMISA) and its Co(II), Ni(II), Cu(II), Zn(II) and Cd(II) metal complexes were evaluated in vitro against MDA-MB-231 (human breast carcinoma cells not expressing nuclear estrogen receptors, ER-) and MCF-7 (human breast carcinoma cells expressing nuclear estrogen receptors, ER+) cancer cell lines. SMISA was found to be inactive, however Ni(SMISA)₂ and Cu(SMISA)₂ exhibited marked activity against the MCF-7 with IC₅₀ (μg/mL) values of 3.5 and 0.45, respectively, whereas Zn(SMISA)₂ and Cd(SMISA)₂ were moderately active. Cd(SMISA)₂ was also active against the MDA-MB-231 with IC₅₀ value of 1.7 μg/mL. The active compounds demonstrated better IC₅₀ values than the standard drug tamoxifen (IC₅₀

against MCF-7= 5.0 $\mu\text{g/mL}$; IC_{50} against MDA-MB-231= 8.0 $\mu\text{g/mL}$) (Manan et al., 2011b). Another closely related study involving S-benzylthiocarbamate (SBDTC) Schiff bases derived from 5-fluoroisatin, 5-chloroisatin, 5-bromoisatin showed that the cytotoxic activity of the halo substituted isatins against the MCF-7 breast cancer cell lines tested was in the order of Br (2.6 $\mu\text{g/mL}$) > F (3.2 $\mu\text{g/mL}$) > Cl (14.0 $\mu\text{g/mL}$) (Manan et al., 2011a). The ONS Schiff base of SBDTC with salicylaldehyde and its Zn(II) and Sb(III) complexes were also strongly active against human cell T-lymphoblastic leukemia CEM-SS (IC_{50} = 2.3 to 4.3 $\mu\text{g/mL}$) while the Cu(II), U(VI) and Th(IV) complexes were moderately active. The Ni(II), Zr(IV) and Cr(III) complexes were found to be inactive. Complexation seems to reduce the cytotoxicity of this ligand (Tarafder et al., 2000a).

A bridged dimeric Cu(II) complex of the Schiff base product of condensation of SBDTC and 2-acetylpyridine, $\text{Cu}_2\text{Cl}_2(\text{L})_2$ (Figure 2.6) was identified as the best inhibitor of cell motility with nanomolar potency from the screening performed by Beshir et al (2008). The compound appeared to be selective for certain cell lines as it was most active towards Madin-Darby canine kidney (MDCK) cells followed by human breast carcinoma T47D cells, less in human breast carcinoma BT20 cells and show a weaker activity in human colorectal carcinoma HCT116 cells. From the structure-activity relationship investigation, Beshir et al. (2008) concluded that a two-ligand structure with bulky nonpolar S-substituents in a *transoid* conformation is important for the antimigratory activity of these metal-ligand complexes.

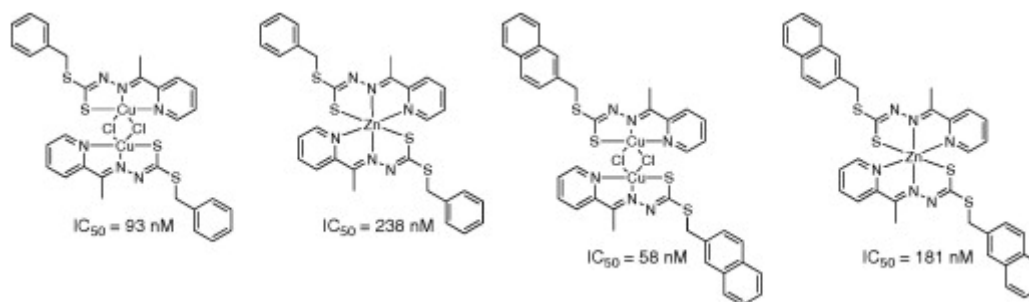


Figure 2.6. Compounds with antimigratory activity (Source: Beshir et al., 2008)

The Schiff base of SMDTC with 2-acetylpyridine and its Mn and Co complexes have been synthesized. The free ligand ($IC_{50} = 21.7 \mu M$) and its metal complexes ($IC_{50} = 4.5 \mu M$ for Mn and $25.4 \mu M$ for Co) exhibited significant and different antitumor activity against human acute myelocytic leukemia cell line (K562) (Chen et al., 2011).

The tridentate NNS Schiff base derived from SMDTC with pyridine-2-carboxaldehyde and the Mn complex of analogous Schiff base prepared by condensing SBDTC with pyridine-2-carboxaldehyde showed significant antitumor activity against leukemia cell line K562 with IC_{50} values in the μM range, $37 \mu M$ and $31 \mu M$, respectively (Zhang et al., 2011a). The Schiff base SBDTC-pyridine-2-carboxaldehyde was also cytotoxic with an IC_{50} value of $5.90 \mu g/mL$ against CEM-SS cells while the Cu(II), Cd(II), Zn(II), Sb(II) and Co(II) complexes were strongly cytotoxic with IC_{50} values of $2.20 \mu g/mL$, $2.30 \mu g/mL$, $5 \mu g/mL$, $1.6 \mu g/mL$ and $0.35 \mu g/mL$, respectively (Tarafer et al., 2000c; Tarafer et al., 2000c). In addition, the Cu(II) and Cd(II) complexes were effective against human colon adenocarcinoma cells (HT-29) with their corresponding IC_{50} values of $2.60 \mu g/mL$ and $3.10 \mu g/mL$ (Tarafer et al., 2001b). Another Schiff base synthesized by

reacting S-4-picolylthiocarbamate (S4PDTC) with pyridine-2-carboxaldehyde (Pc4PDTC) showed moderate cytotoxicity against human myeloid leukemia cells (HL-60) with IC_{50} value of 9 $\mu\text{g}/\text{mL}$ while the Schiff base synthesized by reacting S4PDTC with 4-carboxybenzaldehyde (Cb4PDTC) was inactive. Complexing Pc4PDTC with Cd(II) and Cu(II) enhanced its cytotoxicity from moderately to highly active (IC_{50} value of 1.20-1.70 $\mu\text{g}/\text{mL}$). Pc4PDTC containing two pyridine rings and its Cd(II) and Cu(II) complexes were also highly active against colon cancer cells HT-29 with IC_{50} value ≤ 1.0 $\mu\text{g}/\text{mL}$ (Khoo et al., 2014). S-2-picolylthiocarbamate (S2PDTC) proved moderately active against HT-29 and weakly active toward CEM-SS with IC_{50} values of 9.5 and 24.0 $\mu\text{g}/\text{mL}$, respectively, while among its Schiff bases reported herein, only the NNS Schiff base with pyridine-2-carboxaldehyde showed strong activity toward CEM-SS and HT-29 with IC_{50} values of 2.3 $\mu\text{g}/\text{mL}$. All of the Ni(II) complexes were inactive against CEM-SS cancer cells (Crouse et al., 2004).

SBDTC-2-acetylthiophene (SB2ATP), $IC_{50} = 13$ $\mu\text{g}/\text{mL}$ and Cd(SB3ATP)₂, $IC_{50} = 9$ $\mu\text{g}/\text{mL}$ showed significant bioactivity towards human promyelocytic leukemia cells (HL-60). SB2ATP, SBDTC-3-acetylthiophene (SB3ATP), Co(SB2ATP)₂, Cu(SB2ATP)₂, Cu(SB3ATP)₂, Zn(SB2ATP)₂ and Cd(SB2ATP)₂ were also selective with significant chemotherapeutic activity against MCF-7 with $IC_{50} = 1.4$ – 4.2 $\mu\text{g}/\text{mL}$. The Schiff bases however displayed higher cytotoxic activity compared to their metal complexes except for Cu(SB3ATP)₂ (Chan et al., 2008). The Zn complex of the Schiff base, SBDTC-5-methyl-2-furaldehyde was also found to be highly active against CEM-SS leukemia cell line with IC_{50} value of 2.0 $\mu\text{g}/\text{mL}$, while the Cd complex was slightly less active than that of Zn with IC_{50} value of 4.95

$\mu\text{g/mL}$ (Tarafder et al., 2002a). The Cd(II) complexes of SMDTC with 2-furylmethylketone and 5-methyl-2-furaldehyde and Co(II) complex of SMDTC-2-furylmethylketone were found to be very active against CEM-SS and cervical cancer cells (HELA) with IC_{50} values between 1.8 and 3.6 $\mu\text{g/mL}$ (Chew et al., 2004). The Pb(II) complex of SBDTC with 5-methyl-2-furaldehyde was highly cytotoxic against leukemic cells CEM-SS with IC_{50} of 3.25 $\mu\text{g/mL}$ (Tarafder et al., 2002b). The Cu (II), Ni (II) and Zn (II) complexes of SMDTC with 2-furylmethylketone showed very good activity against CEM-SS cells with IC_{50} values of 1.6, 2.1 and 3.0 $\mu\text{g/mL}$, respectively. The Cu(II) and Zn(II) complexes were also highly active against HELA cells with IC_{50} values of 1.5 and 2.1 $\mu\text{g/mL}$ (Tarafder et al., 2002c).

The comparison of cytotoxic activity of SMDTC-2-benzolpyridine, SBDTC-2-benzolpyridine and their metal complexes indicated that the presence of bulky nonpolar S-substituents on dithiocarbamate moiety and complexation with metals can enhance the cytotoxic activities. In particular, the Zn(II) complex of the S-benzyl derivative effectively inhibited K562 leukemia cell line at a concentration more than 61-fold lower than the Schiff base ligand and the IC_{50} values of both Zn(II) complexes were also higher against the normal hepatocyte QSG7701 cell line, demonstrating that the compounds were able to distinguish the tumor cells from normal cells (Li et al., 2012). The pentadentate Schiff base of 2,6-diacetylpyridine with SBDTC exhibited marked cytotoxicity against CEM-SS giving IC_{50} value of 4.3 $\mu\text{g/mL}$, but its Ni(II) complex was inactive (Ali et al., 2001a). The Schiff bases of both SMDTC- and SBDTC-6-methyl-2-formylpyridine exhibited strong cytotoxicity against human ovarian cancer (Caov-3) cell lines with the S-methyl derivative ($\text{IC}_{50} = 1.0 \mu\text{g/mL}$) being twice as active as the S-benzyl derivative. The

Pt complex of the S-methyl derivative was moderately active but the Pd(II) complex was only weakly active against this cancer. None of the complexes of S-benzyl derivatives are active against the ovarian cancer cell line (Caov-3) (Ali et al., 2006). The mixed-ligand complexes of general formula, [Cu(NNS)(sac)] involving six NNS Schiff bases ligands (SBDTC or SMDTC with 2-acetylpyridine, 2-benzoylpyridine and 6-methyl-2-formylpyridine, respectively) and sac (the saccharinate anion) (Figure 2.7) were found to be highly active against the leukemic cell line HL-60 with IC₅₀ values of 0.25-0.80 µg/mL but only the Cu complex with SBDTC-2-acetylpyridine exhibit strong cytotoxicity against Caov-3, IC₅₀ = 0.40 µg/mL (Ravoof et al., 2007; Ravoof et al., 2004).

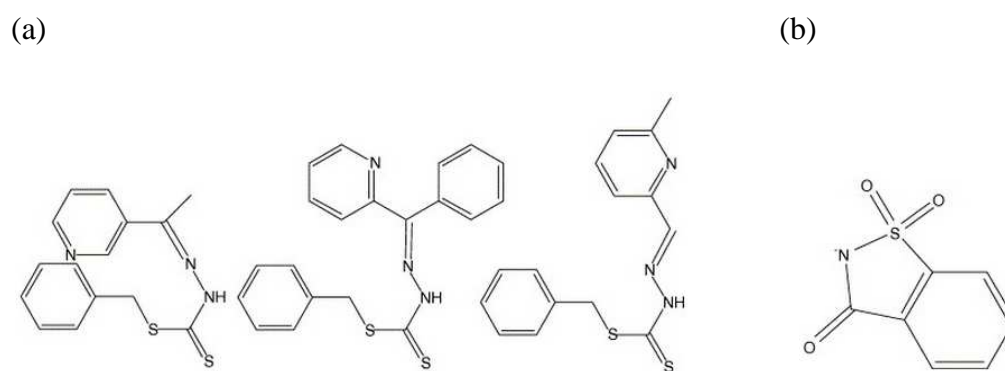


Figure 2.7. (a) Schiff bases of SBDTC with 2-acetylpyridine, 2-benzoylpyridine and 6-methyl-2-formylpyridine, respectively in thione form (b) saccharinate anion (Source: Ravoof et al., 2007)

A tridentate nitrogen-sulfur Schiff base synthesized by condensation of 6-methyl-2-formylpyridine with S-3-methylbenzylthiocarbamate was strongly active against MCF-7 and MDA-MB-231 cell lines with IC₅₀= 0.3 and 2.2 µg/mL, respectively. Its metal complexes also showed high selectivity with Cu(II), Ni(II) and Zn(II) complexes strongly active against only MCF-7, whereas the Cd(II) complex was strongly active only against MDA-MB-231, although the complexes were less active in comparison to the ligand itself (Ravoof et al., 2010).

The OS donor ligand derived from the reaction of SBDTC with benzoyl chloride and its Cu(II), Ni(II) and Pb(II) complexes displayed marked cytotoxicity against HL-60 leukemia cells with $IC_{50} \leq 5.0 \mu\text{g/mL}$ while Cd(II) and Co(II) complexes were only moderately cytotoxic. In this case, the ligand was more potent compared to its metal complexes (How et al., 2008). SBDTC and its Sn(II) complex were very effective against renal carcinoma Tk10 kidney cancer cells and leukemia TK6 cell line. The IC_{50} values were in the range 1.0-4.0 $\mu\text{g/mL}$ with SBDTC being the most active compound. The SNNS quadridentate Schiff base of SBDTC with benzil and its Sn(II) complex were also effective against skin cancer cells (UACC melanoma) with IC_{50} of 5.2 and 2.7 $\mu\text{g/mL}$, respectively (Tarafder et al., 2000b). The NS Schiff base prepared by condensing SBDTC with 2,3-butanedione (1:1 mole ratio) was strongly active against leukemic cells CEM-SS with IC_{50} value of 2.05 $\mu\text{g/mL}$ (Tarafder et al., 2001a).

2.3.2 Antibacterial and antifungal activity

The Schiff base formed from pyridine-2-carboxaldehyde SMDTC and its Zn complex showed marked and broad antimicrobial and antifungal activities compared to the S-benzyl derivatives with MIC values as low as 12.5 $\mu\text{g/mL}$ (Zhang et al., 2011a). The antibacterial activity of the Schiff bases of SBDTC with ferrocene-based chalcones containing a F or Cl substituent in the *para* position or a pyridine ring were the most active in the series and their activity against Gram-negative bacterial (*Escherichia coli* (*E. coli*) and *Pseudomonas aeruginosa* (*P. aeruginosa*)) strains was found to be higher than that for the drugs ketoconazole, kanamycin and penicillin (Liu et al., 2012). In another closely related investigation, the Zn(II) and Cu(II) complexes of SBDTC with ferrocene-based chalcone Schiff base ligand

containing a *para*-Cl substituent and the Zn(II) complex of SBDTC with ferrocene-based chalcone having a methyl group in the aromatic ring were the most active in the series with MIC values in the range of 1.319×10^{-8} M to 3.750×10^{-7} M against bacteria and fungi tested (*Staphylococcus aureus* (*S. aureus*), *Bacillus cereus* (*B. cereus*), *E. coli*, *P. aeruginosa*, *Aspergillus niger* (*A. niger*), *Aspergillus fumigatus* (*A. fumigates*)) (Liu et al., 2013). SMDTC-2-benzolpyridine and its Cu(II) complex showed excellent activity against Gram positive bacteria (*Bacillus subtilis* (*B. subtilis*), *S. aureus*) and yeast (*Candida lusitaniae* (*C. lusitaniae*)) with MIC values of 1-5 µg/mL. It was found that the SMDTC derived ligand was more potent than the SBDTC derivative towards the tested microorganisms and complexation with metals also had a synergetic effect resulting in enhanced antimicrobial activity (Li et al., 2012). Both the Cu(II) complex of the Schiff base S4PDTC with pyridine-2-carboxaldehyde and the Cd(II) complex of S4PDTC 4-carboxybenzaldehyde (Cb4PDTC) showed good antifungal activity against *Candida albicans* (*C. albicans*) with MIC values lower than Nystatin (Khoo et al., 2014). The Schiff base derived from SBDTC with pyrrole-2-carboxaldehyde was a stronger antifungal agent than Nystatin against *Saccharomyces ceciricaee* (*S. ceciricaee*) and *Candida lypolytica* (*C. lypolytica*) (Tarafter et al., 2002a). The NSS Schiff bases of S2PDTC with 2-acetylfuran showed better activity than Nystatin toward against the fungus, *C. lypolytica* while its metal complexes were not active (Crouse et al., 2004). Co(II) complex of SMDTC with 2-furyl-methylketone and Cd (II) complex of SMDTC with 5-methyl-2-furaldehyde gave the most effective activity against fungi tested (*C. lypolytica* and *Aspergillus ochraceus* (*A. ochraceous*)) (Chew et al., 2004) while the Cu(II) complex of SMDTC with 2-furylmethylketone showed clear activity against *C. lypolytica* with better activity than Nystatin (Tarafter et al., 2002c). Bi(III) and

As(III) metal complexes of SBDTC-3-acetylcoumarin (L) with the formula [ClBi(L)₂] and [PhAs(L)₂] showed low MIC values (10 µg/mL for bacterial strain *B. subtilis* and 16 µg/mL for fungal strain *Fusarium oxysporum* (*F. oxysporum*)). The metal complexes were more active against fungal strains compared to bacterial strains and had better activity than the free ligands (Dawara et al., 2012). In the series with salicylaldehyde Schiff base of isonicotinoyldithiocarbazic acid, the best activity was shown by the Ni(II) complex (MIC = 75 µg/mL) against the gram-negative pathogenic strain of *E. coli* (Kalia et al., 2012). The Cd complex of the SNNS Schiff base SBDTC-benzil was active against bacteria *P. aeruginosa* and *B. cereus* with the MIC values better or comparable to kanamycin (Tarafder et al., 2000b). The Cu(II) complex of SBDTC-salicylaldehyde proved to be the best in the series against *B. cereus* (MIC=79.6 µg/mL) (Tarafder et al., 2000a).

2.3.3 Iron chelators

All dithiocarbazate ligands derived from either SBDTC or SMDTC with 2-acetylpyridine, di-2-pyridylketone and 2-pyridinecarbaldehyde were more effective than standard desferrioxamine B (DFO) at releasing intracellular Fe and SMDTC-2-pyridinecarbaldehyde was the most active of all compounds tested. Furthermore, the three SMDTC derivatives were more effective at mobilising intracellular ⁵⁹Fe than their corresponding SBDTC analogues. 2-pyridinecarbaldehyde derivatives with both SMDTC and SBDTC exhibit no apparent cytotoxicity (>10 µM). This property, in combination with their high activity in sequestering intracellular Fe present ideal properties for a chelator in the treatment of Fe overload. The other four dithiocarbazates (with 2-acetylpyridine and di-2-pyridyl ketone) showed moderate to potent anti-proliferative activity which may be problematic for treatment of Fe

overload. On the other hand, the anti-proliferative activity of these compounds can be advantageous in the treatment of cancer (Basha et al., 2012).

2.3.4 Antituberculosis activity

Ni, Co and Zn complexes of a non-Schiff base isonicotinoyldithiocarbamic acid ligand synthesized from isoniazid with carbon disulphide showed MIC values of 2, 2 and 50 µg/mL against *Mycobacterium tuberculosis* (*M. tuberculosis*) H₃₇Rv, and 10, 100 and 50 µg/mL against a multi-drug-resistant strain of *M. tuberculosis*. They had little cytotoxic effect on the transformed human rhabdomyosarcoma cell line RD cells making them potentially useful to treat multi-drug resistant tuberculosis infections (Kanwar et al., 2008). Others dithiocarbamate derivatives such as 2-/3-/4-pyridinecarbonimidoyldithiocarbamic acid esters, methyl 3-[amino(pyrazin-2-yl)methylidene]-2-methyldithiocarbamate and benzyl 3-[amino(pyrazin-2-yl)methylidene]-2-methyldithio carbamate have been studied and were among the promising classes of compounds showing action against tuberculosis (Olczak et al., 2010). In another study by Pavan et al. (2010), dithiocarbamate compounds derived from benzoylacetone showed poor activity. The low activity was associated with the difference in the molecular structures from the potent analogues which contained pyridine rings further affirming that the aromatic heteroatom N moiety played an important role in the anti-tuberculosis activity of the compounds (Pavan et al., 2010).

2.3.5 Antiamoebic activity

Mixed ligand Pt(II) and Pd(II) complexes prepared with ONS Schiff bases derived from SBDTC and 2-hydroxyacetophenone (Figure 2.8) or SBDTC and 4-phenyl-

2,4-butanedione, and neutral phosphine ligands exhibited biological activity on extra- and intra-cellular forms of *Trypanosoma cruzi* in a time- and concentration-dependent manner with IC_{50} values ranging from 7.8 to 18.7 μ M. Nonetheless, the most active compound with $IC_{50} = 0.6 \mu$ M was the ligand SBDTC-4-phenyl-2,4-butanedione which also presented a trypanocidal activity on trypomastigote form better than the drug benznidazole (Maia et al., 2010).

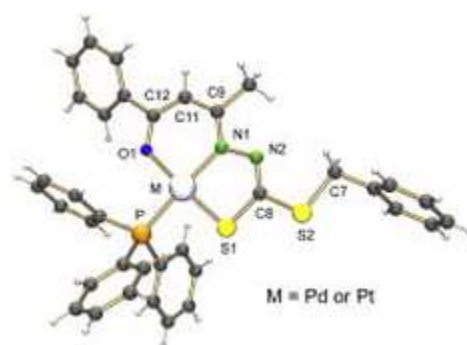


Figure 2.8. Mixed ligand Pt(II) and Pd(II) complexes with Schiff base (derived from SBDTC and 2-hydroxyacetophenone) and phosphine ligands (Source: Maia et al., 2010)

Pd(II) complexes of Schiff bases SMDTC-2-acetylpyridine and SBDTC-2-acetylpyridine also showed potent activity against HK-9 strain of *Entamoeba histolytica* (*E. histolytica*) trophozoites with $IC_{50} = 0.19$ and 0.16μ g/mL, respectively (Neelam et al., 2000). Dioxovanadium(V) complexes of Schiff bases formed between bromo substituted salicylaldehyde and dithiocarbazates ($IC_{50} = 1.35 \mu$ M) (Maurya et al., 2003), the dinuclear potassium dioxovanadium(V) complex of SBDTC-5,5-methylbis(salicylaldehyde) ($IC_{50} = 0.092 \mu$ M) (Maurya et al., 2012) and Pd(II) complex of SBDTC-5-nitrothiophene-2-carboxaldehyde ($IC_{50} = 0.28 \mu$ g/mL) (Bharti et al., 2002) were the most active among their respective series and each showed substantially better amoebocidal action than metronidazole, a commonly used drug against the protozoan parasite *E. histolytica*.

2.3.6 Other biological properties

Methyl 3-phenyldithiocarbazate was found to decrease the rate of brassinin (a crucial plant defense produced by crucifers) detoxification making it among potential detoxification inhibitors (Pedras and Jha, 2006). Oxovanadium(IV) complexes with mixed-ligands SMDTC-salicylaldehyde and *N,N*-donor phenanthroline bases like 1,10-phenanthroline (phen), dipyrdo[3,2-*d*:2',3'-*f*]quinoxaline (dpq) and dipyrdo[3,2-*a*:2',3'-*c*]phenazine (dppz) (Figure 2.9) showed good binding to calf thymus DNA with binding constant values in the range of 7.4×10^4 – $2.3 \times 10^5 \text{ M}^{-1}$. The complexes also showed poor chemical nuclease activity in the dark in the presence of 3-mercaptopropionic acid (MPA) or hydrogen peroxide while both dpq and dppz complexes showed efficient DNA cleavage activity under UV-A radiation (365 nm) via a type-II mechanistic pathway involving formation of singlet oxygen ($^1\text{O}_2$) as the reactive species (Sasmal et al., 2008).

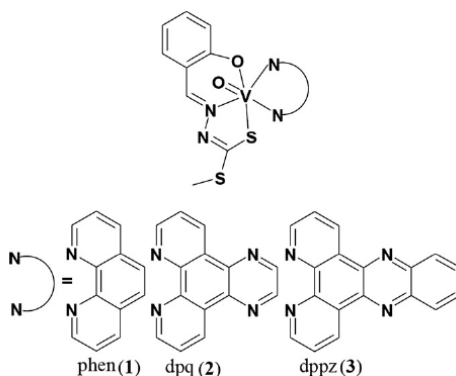


Figure 2.9. Ternary structures of VO complexes and the phenanthroline bases used. (Source: Sasmal et al., 2008)

A series of dithiocarbamate Schiff bases of SBDTC with various hydroxyl-substituted benzaldehydes were tested for their xanthine oxidase (XO) inhibitory activity. The Schiff base with the hydroxy substituent in the *para*-position on the benzaldehyde unit was the most potent. It displayed significantly increased potency over the benchmark allopurinol under the assay conditions employed ($95 \pm 4\%$

inhibition at 50 μM and $\text{IC}_{50} = 0.7 \pm 0.1 \mu\text{M}$) (Leigh et al., 2011). SBDTC (Tarafder et al., 2001b) and the Ni and Cu complexes of SBDTC-2,3-butanedione (Tarafder et al., 2001a) were found to be stronger antioxidants than Vitamin E. Antioxidant properties of SBDTC and two other Schiff bases synthesized by reacting S4PDTC with pyridine-2-carboxaldehyde (Pc4PDTC) and 4-carboxybenzaldehyde (Cb4PDTC) were also found to be comparable to the commercially available synthetic antioxidant butylatedhydroxytoluene (BHT) (Tarafder et al., 2001b; Khoo et al., 2014). Alkyl pyridine-carbonyldithiocarbazates were shown to be uncouplers of oxidative phosphorylation in mitochondria. Greater activity was observed with increasing alkyl chain length, the optimum being C9, indicating the influence of hydrophobicity towards the activity (Terada et al., 1978; Kubota et al., 1978). Technetium-nitrido complexes of the Schiff base S-methyl 3-(2-hydroxyphenyl methylene) dithiocarbazate had been investigated as potential Tc-99m nitrido tumor imaging disposition in mice (Borel et al., 1992). N-methyl-SMDTC had also been effectively used for high-yield preparation of nitrido Tc-99m and Re-188 radiopharmaceuticals (Uccelli et al., 2011; Boschi et al., 2010). The anti-fertility data indicated a highly significant decline in the motility of sperm as well as in sperm count in the treated animals in the case of dimethyltin(IV) complex derived from SBDTC-4-nitrobenzanilide (Singh et al., 2009). The results suggested that the ligand of SBDTC-3-acetylcoumarin was most effective in reducing fertility and complexation with bismuth and arsenic enhanced its activity (Dawara et al., 2012). The pesticide activity and DNA cleavage activity of Ge(IV) complex with SBDTC-3-fomylchromone Schiff base were found to be better in comparison to the ligand itself (Dawara et al., 2011).

At this stage, it is impossible to draw any meaningful correlations from this limited and diverse group. A library of compounds must be systematically designed and their activities determined in order to achieve that. The above reports on dithiocarbazate, its Schiff bases and metal complexes highlight that even subtle change in the structures lead to dramatic alterations of the biological properties of this class of compounds. The pharmacological activities of these metal complexes depend on the type of metal ion, its ligands and the structure of the compounds. These factors play important roles in the recognition of target sites. In conjunction with the continuous effort to develop new derivatives that possess potent biological activities, the major aim of the present work is to expand the synthesis involving multidentate dithiocarbazate derivatives to include bioconjugation and to explore the biological potential of the compounds synthesized to determine their cytotoxicity and their potencies against selected bacterial strains expressing a multi-drug resistance phenotype. Although many new dithiocarbazate derivatives have been added to the family in recent years, there is still no clear structure-activity relationship to explain their activity. The actual mechanism of action is still unknown. Electron paramagnetic resonance (EPR) and electrochemistry have been carried out in this work to connect the biological activities to their structures and redox properties in order to identify features that promote better activity. It is expected that this structure-activity analysis will serve to orient further synthetic efforts towards determining the optimum features essential to promote higher bioactivities and ultimately to guide future work designed to reveal their mode of action.

2.4 Objectives

1. To synthesize bioactive Schiff bases (i.e. potentially bi-, tri- or tetradentate ligands) and their open chain or macroacyclic metal complex systems derived from S-substituted dithiocarbazates.
2. To incorporate grafting work with vectors (i.e. polyarginine, polyethylene glycol (PEG) and phe-arg- β -naphthylamide (PA β N)) in order to prepare improved therapeutic agents.
3. To characterize the synthesized compounds using various physico-chemical and spectroscopic techniques.
4. To study the biological activity of the compounds prepared and to attempt to elucidate their structure-activity relationships.

CHAPTER 3

NON-CONJUGATED PARENTS COMPOUNDS

In this work, three series of parent compounds: (i) tetradentate NNSS ligands (ii) potentially bidentate NS or tridentate ONS ligands with acid or ester functionalities and (iii) potentially bidentate NS or tridentate ONS ligands with natural ketone moiety were prepared by condensation of S-substituted dithiocarbazates with 2,5-hexanedione, methyl levulinate, levulinic acid, 4-carboxybenzaldehyde and 3-acetylcoumarin. All were complexed with copper to synthesize their respective metal complexes.

3.1 Introduction

3.1.1 Ligand systems

3.1.1.1 Tetradentate NNSS

Macrocyclic and macroacyclic Schiff bases have been widely studied (Vigato and Tamburini, 2004). They show various coordination abilities and potential applications in biology which range from therapeutic drug candidates to diagnostic agents (Holland et al., 2008) and they provide synthetic models for the metal containing sites in metalloproteins and metalloenzymes (Gennari et al., 2012). It is therefore worthwhile to explore these interesting properties by investigating the synthesis and characterization of new Cu(II) bis(dithiocarbazate) in this work. The compounds are analogues of the Cu(II) bis(thiosemicarbazone) that have garnered much attention resulting in biological breakthroughs (Paterson and Donnelly, 2011) particularly as radiopharmaceuticals (Donnelly, 2011).

It is anticipated that the replacement of nitrogen atom with sulphur may provide interesting results warranting further exploration into dithiocarbazate compounds. Moreover, to form the Schiff bases, the 2,5-hexanedione has been chosen to expand the ligand flexibility by introducing backbones containing more than two carbons. This enhanced flexibility may facilitate increased tetrahedral distortion leading to incorporation of metal cations that prefer non-square planar geometries such as Cu(I) ion. Previous studies have shown that physico-chemical properties such as redox potential as well as biological activity have been related to the geometry at the metal site (Durot et al., 2005; Drew et al., 1995; Rorabacher, 2004; Basha et al., 2012; Jansson et al., 2010). These were fine examples demonstrating the marked influence of ligand environment towards the redox potential of their respective Cu(II)/Cu(I), Fe(III)/Fe(II) and Mn(III/II) metal systems. While choice of the metal ions and substituent functional groups of the ligands have been carefully chosen to affect the geometry of metal complexes (Ostermeier et al., 2010; Jones and McCleverty, 1970; Cowley et al., 2004; Stefani et al., 2012), the studies by Diaz et al. (1998;1999) that highlighted the differences in coordination geometry identified using EPR by comparing the open chain and cyclic metal complex system which subsequently affect their biological activity was found to be particularly attractive since this analytical tool enabled a structural view of the complexes in solution. The group noted that the Cu(II) complexes of the open chain mono(thiosemicarbazone) with a higher degree of tetrahedral distortion should be further explored as potentially better SOD-like mimics than the macrocyclic bis(thiosemicarbazone) complexes. Although the reports were primarily focused on superoxide dismutase (SOD) mimics, it would also be meaningful to carry out such comparison in this

work as the open chain system will be envisaged to offer interesting diversity and aid towards the understanding of the structure-bioactivity relationship.

3.1.1.2 Potentially bidentate NS or tridentate ONS ligands with an acid or ester functionality

The open chain series in this work consisting ligands of methyl levulinate and levulinic acid with SBDTC and SMDTC as well as their corresponding Cu(II) complexes will be a worthy comparison to their macroacyclic Cu(II) tetradentate system with 2,5-hexanedione bis(dithiocarbamate). Furthermore, the Schiff base derivatives containing the acid or ester functional group have proved to be attractive from both biological and physico-chemical aspects. For instance, recent attention was dedicated to metal complexes of α -ketoglutaric acid (Baldini et al., 2004) and pyruvic acid thiosemicarbazone (Diaz et al., 1994; Wiecek et al., 2009). These aliphatic ligands with a variety of potential donor atoms and many possible conformations provided a versatile chelating behavior. In addition, the metal complexes were found to be potent against the selected human leukemia and cancer cell lines tested and thus may be regarded as potentially significant antitumor agent (Baldini et al., 2004; Diaz et al., 1994; Wiecek et al., 2009). Similarly, the analogous Schiff base keto-ester methylpyruvate with SMDTC has been screened by the National Cancer Institute, Bethesda, Maryland and has been found to exhibit promising activity against leukemia cells as mentioned by Ali et al. (2001b). The authors also stated that the “ligand coordinated to the metal(II) ion as a uninegatively charged tridentate chelating agent via the carbonylic oxygen atom, the azomethine nitrogen atom and the thiolato sulfur atom” but resulted in varied conformation geometry with different metal (Ali et al., 2001b p. 1037). The Cu(II)

complexes have the general formula, CuLX (L= Schiff base; X=Cl⁻, Br⁻) with a distorted square-planar structure whereas the Zn(II), Cd (II) and Ni(II) complexes of empirical formula, ML₂ supported a six-coordinate distorted octahedral structure for these complexes as confirmed by the X-ray crystallographic structural analysis (Ali et al., 2001b; Ali et al., 1999; Ali et al., 2004). To date, metal complexes of methyl levulinate or levulinic acid dithiocarbazate have not been reported although semicarbazone derivatives of levulinic acid have been identified as potent anticonvulsant agents showing broad spectrum of activity with low neurotoxicity (Navneet and Pradeep, 2005).

Since the carbonylic oxygen atom and the azomethine nitrogen atom are further apart with three carbons in between them, these ligands could adapt NS bidentate chelation ability different from the ONS chelating ligands with α -ketoglutaric acid, pyruvic acid or methyl pyruvate. In addition, 4-carboxybenzaldehyde was utilized to form the Schiff bases in order to provide insight on the influence of an aromatic acid. As most sulphur-nitrogen chelating ligands and their complexes are highly hydrophobic and their low solubility in water imposes experimental limitations in biological studies, the introduction of a hydrophilic group such as -COOH in systems should permit increased solubility in water (Pogni et al., 2000). Besides that, the presence of a carboxylic functional group would allow for further ligand optimization via bioconjugation to improve the properties of the compounds and their applications.

3.1.1.3 Potentially bidentate NS or tridentate ONS ligands with natural potent aldehyde or ketones moieties.

In order to expand the synthesis and exploration of dithiocarbazate derivatives, attention was also directed herein to aromatic dithiocarbazate derived from natural aldehydes or ketones that had well established medicinal properties. The rationale behind this attempt was based on the prospect of the synergistic effects developed from integration of the promising bioactivity of individual components (i.e. metal center and ligand comprising the carbonyl group and substituted dithiocarbazate moiety). A number of publications had highlighted the potential of utilizing such natural aromatic compounds like chromone (Barve et al., 2006; Khan et al., 2009), chalcone (Zhang et al., 2011b) and curcumin (Padhye et al., 2009). This prompted the preparation of new metal complexes with Schiff base formed from the condensation of SBDTC and 3-acetylcoumarin in this work. Coumarin derivatives are attractive because of their wide variety of biological activities including antioxidant, antibacterial, antifungal and cytotoxic (Datta et al., 2011; Bagihalli et al., 2008; Phaniband et al., 2011; Kulkarni et al., 2009; Creaven et al., 2009). Moreover, the reported coumarin Schiff bases and their metal complexes were shown to exhibit outstanding luminescence properties which may provide advantage for application of these compounds as probes (Datta et al., 2011). Further findings reveal that the coumarin derivatives interact strongly with DNA and can cause DNA cleavage (Phaniband et al., 2011; Kulkarni et al., 2009).

3.1.2 Choice of metals

3.1.2.1 Copper

Copper complexes represent a class of compounds that have been subjected to intensive research because of their potential therapeutic applications (Duncan and White, 2012) in particular as effective antitumor (Chakraborty et al., 2010; Afrasiabi et al., 2003) and antibacterial agents (Li et al., 2000; Joseph et al., 2012). A number of related thiosemicarbazone copper complexes have been found to be active in cell destruction, as well as in the inhibition of DNA synthesis (Ferrari et al., 2002a; Ferrari et al., 2002b; Bisceglie et al., 2012; Ferrari et al., 2004) Cancer cells have also been shown to take up greater amounts of copper than normal cells (Jansson et al., 2010). The altered metabolism of cancer cells and the differential response between normal and cancer cells to copper are the basis for the development of copper complexes endowed with anticancer characteristics (Gandin et al., 2013). Recently, copper(II) complexes of thiosemicarbazone NNSS ligands have been explored extensively as radiopharmaceuticals for the specific targeting of hypoxic tissue (Donnelly, 2011). They are also known to be stable ($K_{\text{ass}} = 10^{18}$), neutral and can easily cross cellular membranes (Paterson and Donnelly, 2011; Donnelly, 2011; Ngarivhume et al., 2005). Copper complexes with such multidentate Schiff base ligands are attractive for study because of their rich spectroscopic and magnetic properties that often change during the course of enzyme catalysis (Ferrari et al., 2002b). Copper also exhibits different oxidation states affirming its important role as a model to provide better understanding of biological metalloenzymes and metalloprotein systems (Balamurugan et al., 2006; Knoblauch et al., 1999; Ďuračková et al., 1999). For instance, the CuN_2S_2 chromophore is present in blue copper proteins such as plastocyanine (Donnelly, 2011; Sarkar et al., 2009). With

these examples in mind and following the interest concerning the electrochemical investigation into the Cu(I)-Cu(II) redox couple, it is only logical for copper ion to serve as an excellent choice in the continuing search for new and effective metallodrugs.

3.1.2.2 Zinc

In addition to Cu(II) complexes, another two metal complexes, zinc(II) and rhenium(I) will be presented as well. Both are important as their complexes are diamagnetic and this facilitates complementary methods of detection to EPR spectroscopy for the Cu(II) complex through the use of nuclear magnetic resonance (NMR) spectroscopy for Zn(II) and Re(I) species (Kirin et al., 2005). In addition, one of the most promising previous findings by Awidat (2005) was that bis (S-methyl- β -N-(2-acetylfuran)dithiocarbazate) (SMDB) complexed with zinc was found to show remarkable selectivity towards brain cancer cells with a toxicity towards normal cells that was relatively much lower than tamoxifen, the current drug of choice in the treatment of brain cancer. The IC₅₀ values for SMDB-Zn on glioma cell lines A172, U87MG, T98G and normal brain cell line HCN-2 were at 3.7 μ g/mL, 1.76 μ g/mL, 2.7 μ g/mL and 7 μ g/mL, respectively (Awidat, 2005). Zn(II) complexes of the analogous bis(thiosemicarbazone) were also found to be weakly fluorescent owing to intraligand excitation and this fluorescence has been used to track the uptake and intracellular distribution of the Zn(II) complexes in diverse cancer cell lines (Lim et al., 2010). The understanding of intracellular distribution of these complexes is important to design compounds that are selective towards specific tissues and organelles (Holland et al., 2007).

3.1.2.3 Rhenium

Although different dithiocarbazate metal complexes have been investigated, few works deal with Re complexes (Mevellec et al., 2002; Boschi et al., 2010) and none has yet to report on a Re(I) tricarbonyl core. Much significant progress in targeted rhenium (Re-188 and Re-186) radiopharmaceuticals recently has focused on the use of the Re carbonyl core (Donnelly, 2011). The use of radionuclides has increased the demand for new complexes containing carrier-free radionuclides having reasonable half lives and proper energy of radiation (Fuks et al., 2010). The carbonyl approach exploits the stability of the metal tricarbonyl core whilst allowing a variety of bi- and tridentate ligands to react with it to further functionalize these with biomolecules or targeting vectors (Donnelly, 2011; Amoroso et al., 2007; Santos et al., 2004; Clède et al., 2013). Because of the small size and charge of the *fac*- $\text{Re}(\text{CO})_3^+$ group, it does not significantly influence biological properties of even the smallest biomolecules used in the synthesis of radiopharmaceuticals making it an attractive candidate not just for medicinal therapeutic application but also as diagnostic agents (Fuks et al., 2010; François et al., 2014; Clède et al., 2012) For instance, an innovative approach to prepare a rhenium tricarbonyl complex with a 4-(2-pyridyl)-1,2,3-triazole (pyta) ancillary ligand endowed with luminescent and infrared properties allowed a relevant bio-imaging correlative study using both infrared (IR) and luminescence modalities (Clède et al., 2012). Vibrational spectroscopies are attractive for bio-imaging as in the case of vibrational excitations in the IR region where no photo-bleaching is induced in contrast to what is observed with organic fluorophores in the visible or UV-range. Furthermore, IR-probes also show advantages in their stability in biological environments and intense absorption

in the 1800-2200 cm^{-1} range which is the transparent IR window of biological media (Clède et al., 2013; Clède et al., 2012; Policar et al., 2011).

3.2 Methodology

3.2.1 Materials

All chemicals and solvents were of analytical grade and were used as received without further purification. Common solvents for solution synthesis were obtained from either Carlo Ebra or VMR. Anhydrous DMF was from Sigma Aldrich or Acros Organics and DMSO of HPLC grade was from Alfa Aesar. Chemicals: Benzyl chloride (Aldrich), iodomethane (Merck), potassium hydroxide (Merck), hydrazinium hydroxide (Merck), carbon disulfide (Merck), 2,5-hexanedione (Merck), methyl levulinate (Alfa Aesar), levulinic acid (Janssen), 4-carboxylbenzaldehyde (Acros Organics), 3-acetylcoumarin (Aldrich), copper (II) acetate monohydrate (HmbG chemicals), zinc (II) acetate (Touzart), rhenium (I) pentacarbonyl chloride (Strem chemicals), tetrabutylammonium perchlorate (Fluka), tetrabutylammonium hexafluorophosphate (Fluka). SBDTC and SMDTC were prepared as previously reported (Chan et al., 2008; Chew et al., 2004).

3.2.2 Instrumentation

The IR spectra were recorded in the range of 550–4000 cm^{-1} on a Perkin-Elmer 100 series FT-IR spectrophotometer in ATR mode. Microanalyses were carried out using either a Leco CHNS-932 analyzer, a LECO TruSpec CHN/CHNS instrument or performed at the CNRS (Gif-sur-Yvette and Vernaison, France). The UV–Vis spectra were recorded on a Cary 300 bio spectrophotometer (200-800 nm) or Perkin Elmer Lambda 45 with a 1 cm optical path quartz cuvette. ^1H NMR and ^{13}C NMR

spectra were recorded with Bruker DRX300 spectrometers. The chemical shifts (δ /ppm) were calibrated relative to residual solvent signals. Electrospray-ionization (ESI) mass spectra were recorded with a Finnigan Mat 95S in the BE configuration at low resolution. High resolution (HR) mass spectra were obtained on a JEOL MS 700 spectrometer (CI or FAB) or on a Bruker hybride APEX spectrometer. EPR spectra were recorded on an X-band Bruker Elexsys 500 spectrometer equipped with a continuous flow helium cryostat (Oxford Instruments) and a temperature control system. The field modulation frequency was 100 kHz. The spectra were all recorded under non-saturating conditions. Cyclic voltametry (CV) measurements were recorded under argon using a 620C electrochemical analyzer (CH Instruments, Inc). The working electrode was a glassy carbon disk, a Pt wire was used as counter-electrode and the reference electrode was an Ag/AgCl electrode (0.223 V versus NHE). Immediately before the measurement of each voltammogram, the working electrode was carefully polished with alumina suspensions (1, 0.3 and 0.05 μm , successively), sonicated in an ethanol bath and then washed carefully with ethanol. The solutions were made up of 100 μL of the complexes in anhydrous deoxygenated DMF (0.01 M) with 0.5 mL of tetrabutylammonium perchlorate or tetrabutylammonium hexafluorophosphate (0.1 M) as the supporting electrolyte. Peak potentials, E_p , and half-wave potentials, $E_{1/2}$, were referenced to the ferrocene/ferrocinium couple, 0.54 V in DMF versus SCE. The ferrocene/ferrocinium half-wave potential under the conditions used was 0.07 V. RP-HPLC analysis was carried out using Waters HPLC system connected to Breeze software that consisted of combination of a dual wavelength UV-Vis absorbance detector (Waters 2487) and a binary pump (Waters 1525) equipped with an analytical cell for reaction monitoring or purity checking. The analytical

measurements were performed using either a ACE C8 or C18 column (250x4.5mm) packed with spherical 5 μm particles of 300 \AA pore size. Experiments were carried out at a flow rate of 1 mL min^{-1} at room temperature. Injection volume was 50 μL . Sample concentration was approximately 1 mg/mL . Two methods were employed for single crystal X-ray diffraction (SCXRD) determination:

For CuSMHD, CuSBHD and SMHD: A crystal mounted on a glass fiber using perfluoropolyether oil and cooled rapidly to 150 K in a stream of cold N_2 was analyzed using an Oxford Cryosystems Cobra unit. Diffraction data were measured using an Agilent Xcaliber Eos Gemini diffractometer (graphite-monochromated $\text{Mo K}\alpha$ radiation, $\lambda = 0.71073 \text{ \AA}$). Intensity data were processed with the CrysAlis Pro software suite (Pro, 2011). The structures were solved using the direct-methods program SIR92 (Altomare et al., 1994) which located all non-hydrogen atoms. Subsequent full-matrix least-squares refinement was carried out using CRYSTALS Program Suite (Betteridge et al., 2003). Coordinates and anisotropic thermal parameters of all non-hydrogen atoms were refined. All H atoms were located in a difference map. Those attached to carbon atoms were repositioned geometrically. The H atoms were initially refined with soft restraints on the bond lengths and angles to regularize their geometry, after which the positions were refined with riding constraints.

For SBPY, SMML, SBML, SBEL, SBML, Cu(SMLA)_2 , Cu(SMML)_2 and $\text{Re}_2(\text{SBCM})_2$: X-ray diffraction data was collected by using a Kappa X8 APPEX II Bruker diffractometer with graphite-monochromated $\text{Mo K}\alpha$ radiation ($\lambda = 0.71073 \text{ \AA}$). The crystal was mounted on a CryoLoop (Hampton Research) with Paratone-N (Hampton Research) as cryoprotectant and then flash frozen in a nitrogen-gas stream at 100 K. The temperature of the crystal was maintained at the selected value (100K)

within an accuracy of ± 1 K by means of a 700 series Cryostream cooling device. The data were corrected for Lorentz polarization, and absorption effects. The structure was solved by direct methods using SHELXS-97 (Sheldrick, 1997a) and refined against F^2 by full-matrix least-squares techniques using SHELXL-97 (Sheldrick, 1997b) with anisotropic displacement parameters for all non-hydrogen atoms. Hydrogen atoms were located on a difference Fourier map and introduced into the calculations as a riding model with isotropic thermal parameters. All calculations were performed by using the crystal structure crystallographic software package WINGX (Farrugia, 1999).

3.2.3 Synthesis

3.2.3.1 Macroacyclic Cu(II) system with tetradentate NNSS ligands

SBHD The title compound was synthesized with some modification of the method described by Ali et al. (1987). 2,5-hexanedione (0.587 mL, 0.005 mol, 1 equiv) was added to a hot solution of SBDTC (1.983 g, 0.01 mol, 2 equiv) in absolute ethanol (150 mL) and the mixture was further heated for 5 min. A white precipitate was formed and was immediately filtered off, washed with cold ethanol and dried in vacuo over silica gel to yield the expected Schiff base (0.997 g, Yield 42%). Elemental analysis for $C_{22}H_{26}N_4S_4$: Calcd. C 55.66, H 5.52, N 11.80; Found C 54.79, H 5.59, N 11.75. 1H NMR (300 MHz, DMSO- d_6) δ 12.18 (s, 2H), 7.39 -7.20 (m, 10H), 4.40 (s, 4H), 1.96 (s, 6H). ^{13}C NMR (75 MHz, DMSO- d_6) δ 197.16, 158.26, 137.15, 129.15, 128.41, 127.05, 37.56, 34.05, 17.74. IR: ν (cm^{-1}) = 3147 (m, b), 1640 (w), 1054 (s), 981 (m), 828 (m). UV-Vis in DMSO: λ_{max} nm ($\log \epsilon$) = 276 (4.32), 308 (4.41), \approx 360 (3.32, sh). RP-HPLC: R_T (min) = 15.3, 18.3, 22.4.

SMHD SMDTC (1.222 g, 0.01 mol, 2 equiv) was dissolved in hot ethanol (150 mL) and 2,5-hexanedione (0.587 mL, 0.005 mol, 1 equiv) was added to this solution. The mixture was heated while being stirred to reduce the volume to 1/3 of the original volume. The mixture was kept at 4°C overnight and white precipitate was formed. The product was filtered off, washed with cold ethanol and dried in vacuo over silica gel to afford 1.129 g of SMHD (Yield 70%). The compound was further recrystallized from methanol and crystals suitable for X-ray diffraction analysis were obtained from the same solvent through slow evaporation at room temperature. Elemental analysis for C₁₀H₁₈N₄S₄: Calcd. C 37.24, H 5.63, N 17.37; Found C 37.86, H 4.87, N 17.84. ¹H NMR (300 MHz, DMSO-d₆) δ 12.13 (s, 2H), 2.57 (s, 4H), 2.43 (s, 6H), 2.00 (s, 6H). ¹³C NMR (75 MHz, DMSO-d₆) δ 198.95, 157.63, 33.97, 17.77, 16.94. IR: ν (cm⁻¹) = 3111 (m, b), 1628 (m), 1046 (s), 988 (m), 827 (m). UV-Vis in DMSO: λ_{max} nm (log ϵ) = 276 (4.25), 305 (4.37), \approx 360 (2.75, sh). RP-HPLC: R_T (min) = 6.4, 11.1, 18.7.

CuSBHD The copper complex was prepared by adding copper (II) acetate monohydrate, Cu(OAc)₂·H₂O (0.020 g, 0.0001 mol, 1 equiv) in acetonitrile (20 mL) to a solution of SBHD (0.047 g, 0.0001 mol, 1 equiv) in acetonitrile (150 mL) at room temperature. The solution was stirred for an hour and then concentrated to reduce volume before being placed at 4°C overnight. The product was filtered off to yield 0.039 g (Yield 73%). The compound was recrystallized from acetonitrile and black crystals of diffraction quality were obtained from the same solvent after several days through slow evaporation at 4°C. Elemental analysis for C₂₂H₂₅CuN₄S₄: Calcd. C 49.27, H 4.51, N 11.85; Found C 49.40, H 4.63, N 10.46. ESI-MS: m/z = [M+H]⁺ Calcd. 536.04, Found 536.02; [M+Na]⁺ Calcd. 558.02, Found 558.01;

$[M+K]^+$ Calcd. 573.99, Found 573.98; $[2M+3H]^+$ Calcd. 1073.08, Found 1073.04. IR: ν (cm^{-1}) = 1629 (m), 1606 (w), 992 (s), 955 (s), 857 (m). UV-Vis in DMSO: λ_{max} nm ($\log \epsilon$) = 275 (4.37), ≈ 294 (4.26, sh), ≈ 340 (4.01, sh), ≈ 400 (3.55, sh), ≈ 600 (2.45, sh). RP-HPLC: R_T (min) = 28.5.

CuSMHD The copper complex was prepared by adding $\text{Cu}(\text{OAc})_2 \cdot \text{H}_2\text{O}$ (0.200 g, 0.001 mol, 1 equiv) in methanol (20 mL) to a hot solution of the above SMHD (0.322 g, 0.001 mol, 1 equiv) in methanol (100 mL). The reaction was heated until the volume reduced to 1/3 of the original volume and then placed at 4°C overnight. The product which formed was filtered off to afford 0.296 g of CuSMHD (Yield 77%). The compound was further recrystallized from acetonitrile and black crystals of diffraction quality were obtained from the same solvent after several weeks through slow evaporation at room temperature. Elemental analysis for: $\text{C}_{10}\text{H}_{17}\text{CuN}_4\text{S}_4$: Calcd. C 31.27, H 4.20, N 14.59; Found C 31.35, H 4.24, N 14.64. ESI-MS: $m/z = [M + H]^+$ Calcd. 383.97, Found 383.96; $[M+\text{Na}]^+$ Calcd. 405.96, Found 405.94; $[M+K]^+$ Calcd. 421.93, Found 421.92. IR: ν (cm^{-1}) = 1628 (m), 1611(w), 1000 (s), 964 (s), 821 (m). UV-Vis in DMSO: λ_{max} nm ($\log \epsilon$) = 273 (4.34), ≈ 294 (4.24, sh), ≈ 340 (3.99, sh), ≈ 400 (3.49, sh) ≈ 600 (2.43, sh). RP-HPLC: R_T (min) = 23.3.

SBPY SBPY was a side product from the initial attempt to synthesize SBHD. Prolonged heating and purification via column chromatography caused the desired compound to undergo cyclization forming a pyrrole. Single crystals of diffraction quality were obtained from DMSO and analyzed by single crystal X-ray diffraction. ESI-MS: $m/z = [M + H]^+$ Calcd. 277.08, Found 277.08; $[M + \text{Na}]^+$ Calcd. 299.07,

Found 299.06. ^1H NMR (300 MHz, DMSO- d_6): δ (ppm) = 12.29 (s, 1H), 7.45 – 7.20 (m, 5H), 5.69 (s, 2H), 4.45 (s, 2H), 2.00 (s, 6H). ^{13}C NMR (75 MHz, DMSO- d_6): δ (ppm) = 204.09, 136.30, 129.02, 128.55, 127.43, 126.50, 104.34, 38.17, 10.99. IR: ν (cm^{-1}) = 3264 (m), 2917 (w), 1055 (s), 972 (w), 828 (w). UV-Vis in DMSO: λ_{max} nm ($\log \epsilon$) = 282 (4.02). RP-HPLC: R_T (min) = 22.3.

3.2.3.2 Open chain Cu(II) system with bidentate NS ligands with acid or ester functionality

Preparation of ligands

The general procedure used to prepare the ligands can be summarized as follows: to a solution (the solvent differs depending on the compound; each is reported below) of S-substituted dithiocarbazate, an equimolar amount of levulinic acid/ methyl levulinate/4-carboxybenzaldehyde (dissolved in the same solvent) was added dropwise. The mixture was heated to reduce the volume by about 1/3 of the original volume and then placed in the refrigerator overnight. The products formed were filtered, washed with diethyl ether and dried in vacuo over silica gel. Each compound was recrystallized from the solvent used for its synthesis and crystals suitable for X-ray diffraction analysis were obtained from the same solvent through slow evaporation at room temperature. The structures of four ligands were successfully solved by SCXRD analysis. The purity and stability of the products dissolved in the minimum quantity of CH_3OH or DMSO-water mixture were checked by RP-HPLC.

SMML 1.222 g (0.01 mol, 1 equiv) of SMDTC was solubilized in 100 mL of hot ethanol. An equimolar amount (1.22 mL, 0.01 mol, 1 equiv) of methyl levulinate was added dropwise to the solution of the dithiocarbazate, heated and stirred for one

to two hours until the volume was reduced to yield 1.062 g of product (Yield 45 %). HR-MS: $m/z = [M+Na]^+$ Calcd. 257.03889, Found 257.03934. 1H NMR (300 MHz, CD_3OD) δ 3.66 (s, 3H), 2.65 (s, 4H), 2.51 (s, 3H), 1.99 (s, 3H). ^{13}C NMR (75 MHz, CD_3OD) δ 202.68, 175.37, 156.36, 52.27, 34.23, 30.81, 30.61, 17.79, 17.31. IR: ν (cm^{-1}) = 3224 (m) 1717 (s) 1640 (m) 1025 (s) 990 (s) 834 (m). UV-Vis in DMSO: λ_{max} nm ($\log \epsilon$) = 274 (3.97), 304 (4.29). RP-HPLC: R_T (min) = 6.4 (SMDTC) and 15.3 (SMML).

SMLA 0.611 g (0.005 mol, 1 equiv) of SMDTC was solubilized in 50 mL of hot acetonitrile. An equimolar amount (0.50 mL, 0.005 mol, 1 equiv) of levulinic acid was added dropwise to the solution of the dithiocarbazate, heated and stirred for one to two hours until the volume was reduced to yield 0.357 g of product (Yield 33 %). HR-MS: $m/z = [M+Na]^+$ Calcd. 243.02324, Found 243.02334. 1H NMR (300 MHz, CD_3OD) δ 2.63 (s, 4H), 2.52 (s, 3H), 1.99 (s, 3H). ^{13}C NMR (75 MHz, CD_3OD) δ 202.70, 176.84, 156.56, 34.39, 30.69, 17.81, 17.38. IR: ν (cm^{-1}) = 3163 (w, b) 1715 (m) 1638 (m) 1067 (s) 923 (w) 819 (m). UV-Vis in DMSO: λ_{max} nm ($\log \epsilon$) = 273 (4.05), 304 (4.32). RP-HPLC: R_T (min) = 6.3 (SMDTC) and 11.7 (SMLA).

SBML 1.000 g (0.005 mol, 1 equiv) amount of SBDTC was solubilized in 50 mL of hot ethanol. An equimolar amount (0.61 mL, 0.005 mol, 1 equiv) of methyl levulinate was added dropwise to the solution of the dithiocarbazate, heated and stirred for one to two hours until the volume was reduced to yield 0.911 g of product (Yield 59 %). HR-MS: $m/z = [M+Na]^+$ Calcd. 333.07019, Found 333.07034. 1H NMR (300 MHz, CD_3OD) δ 7.40 – 7.20 (m, 5H), 4.44 (s, 2H), 3.47 (s, 3H), 2.61 (s, 4H), 1.98 (s, 3H). ^{13}C NMR (75 MHz, CD_3OD) δ 200.87, 175.39, 156.61, 138.50,

130.53, 129.65, 128.40, 52.12, 40.01, 34.15, 30.47, 17.38. IR: ν (cm^{-1}) = 3201 (w) 1717 (s) 1642 (w) 1029 (s) 984 (m) 782 (m). UV-Vis in DMSO: λ_{max} nm ($\log \epsilon$) = 275 (4.15), 306 (4.33). RP-HPLC: R_T (min) = 15.3 (SBDTC) and 20.0 (SBML).

SBLA SBDTC (2.000 g, 0.01 mol, 1 equiv) was dissolved in 100 mL of hot acetonitrile. An equimolar amount (1 mL, 0.01 mol, 1 equiv) of levulinic acid was added dropwise to the solution of the dithiocarbazate, heated and stirred for one to two hours until the volume was reduced to yield 1.595 g of product (Yield 54 %). HR-MS: $m/z = [M+Na]^+$ Calcd. 319.05454, Found 319.05468. ^1H NMR (300 MHz, CD_3OD) δ 7.40 – 7.17 (m, 5H), 2.60 (s, 4H), 4.47 (s, 2H), 1.98 (s, 3H). ^{13}C NMR (300 MHz, CD_3OD) δ 200.88, 176.77, 156.91, 138.70, 130.47, 129.59, 128.30, 39.81, 34.38, 30.64, 17.44. IR: ν (cm^{-1}) = 3116 (w, b) 1698 (s) 1652 (w) 1047 (s) 925 (s) 778 (m). UV-Vis in DMSO: λ_{max} nm ($\log \epsilon$) = 275 (4.10), 306 (4.28). RP-HPLC: R_T (min) = 15.3 (SBDTC) and 17.5 (SBML).

SBEL 1.000 g (0.005 mol, 1 equiv) of SBDTC was solubilized in 50 mL of hot ethanol. An equimolar amount (0.61 mL, 0.005 mol, 1 equiv) of levulinic acid was added dropwise to the solution of the dithiocarbazate, heated and stirred for one to two hours until the volume was reduced to yield 0.327 g of product. (Yield 44%). HR-MS: $m/z = [M+Na]^+$ Calcd. 347.08584, Found 347.08601. ^1H NMR (300 MHz, CD_3OD) δ 7.39 – 7.20 (m, 5H), 4.44 (s, 2H), 3.93 (q, $J = 6$, 2H), 2.59 (s, 3H), 1.98 (s, 4H), 1.02 (t, $J = 6$, 3H). ^{13}C NMR (75 MHz, CD_3OD) δ 200.83, 174.98, 156.62, 138.43, 130.57, 129.69, 128.43, 61.68, 40.09, 34.09, 30.64, 17.43, 14.50. IR: ν (cm^{-1}) = 3217 (w) 1717 (s) 1642 (w) 1029 (s) 983 (m) 782 (m). UV-Vis in DMSO: λ_{max}

nm ($\log \epsilon$) = 275 (4.11), 306 (4.30). RP-HPLC: R_T (min) = 15.3 (SBDTC) and 21.1 (SBEL).

SM4CB 0.611 g (0.005 mol, 1 equiv) amount of SMDTC was solubilized in 40 mL of hot acetonitrile. An equimolar amount (0.751 g, 0.005 mol, 1 equiv) of 4-carboxybenzaldehyde was dissolved in 200 mL of hot acetonitrile, added dropwise to the solution of the dithiocarbazate, heated and stirred for 2 hours until the volume was reduced to yield 0.817 g of product. (Yield 73%). HR-MS: $m/z = [M+H]^+$ Calcd. 255.02565, Found 255.02574. ^1H NMR (300 MHz, DMSO- d_6) δ 13.44 (s, 1H), 13.16 (s, 1H), 8.29 (s, 1H), 7.92 (dd, $J = 55.5, 9, 4\text{H}$), 2.54 (s, 3H). ^{13}C NMR (75 MHz, DMSO- d_6) δ 199.01, 166.83, 145.14, 137.40, 132.25, 129.90, 127.43, 16.82. IR: ν (cm^{-1}) = 3108 (w, b) 1688 (s) 1612 (w) 1046 (s) 927 (s) 795 (m). UV-Vis in DMSO: λ_{max} nm ($\log \epsilon$) = 348 (4.54), ≈ 360 (4.48,sh). RP-HPLC: R_T (min) = 13.3.

SB4CB 0.496 g (0.0025 mol, 1 equiv) amount of SBDTC was dissolved in 20 mL of hot acetonitrile. An equimolar amount (0.375 g) of 4-carboxybenzaldehyde was dissolved in 150 mL of hot acetonitrile, added dropwise to the solution of the dithiocarbazate, heated and stirred for 2 hours until the volume was reduced to yield 0.462 g of product. (Yield 56 %). HR-MS: $m/z = [M+H]^+$ Calcd. 331.05695, Found 331.05700. ^1H NMR (300 MHz, DMSO- d_6) δ 13.48 (s, 1H), 13.15 (s, 1H), 8.29 (s, 1H), 7.89 (dd, $J = 57, 9, 4\text{H}$), 7.46-7.24 (m, 5H), 4.49 (s, 2H). ^{13}C NMR (75 MHz, DMSO- d_6) δ 197.13, 166.81, 145.47, 137.26, 136.63, 132.30, 129.90, 129.31, 128.54, 127.50, 127.31, 37.69. IR: ν (cm^{-1}) = 3089 (w, b) 1688 (s) 1611 (w) 1036 (s) 929 (m) 797 (s). UV-Vis in DMSO: λ_{max} nm ($\log \epsilon$) = 349 (4.51), ≈ 364 (4.44,sh). RP-HPLC: R_T (min) = 16.8.

Preparation of Cu(II) complexes

To a solution of the ligand (the solvent differs depending on the compound and is reported below), a solution containing an half-molar amount of $\text{Cu}(\text{OAc})_2 \cdot \text{H}_2\text{O}$ dissolved in methanol was added dropwise. The resulting mixture was stirred overnight at room temperature, concentrated and then let to stand at room temperature. Only for obtaining complexes with the ligands SM4CB and SB4CB, was the solution heated to reduce the volume by about 1/3 of the original volume and then let to cool to room temperature or placed in the refrigerator overnight. The black or brown products formed were filtered, washed with pentane and dried in vacuo over silica gel. The structures of two Cu(II) complexes were successfully solved by single crystal X-ray analysis. The purity and stability of the products dissolved in the minimum quantity of $\text{CH}_3\text{OH}/\text{DMSO}$ -water mixture were analyzed by RP-HPLC.

Cu(SMML)₂ 0.234g (0.001 mol, 1 equiv) of SMML was solubilized in 50 mL of methanol. 0.100 g (0.0005 mol, 0.5 equiv) of $\text{Cu}(\text{OAc})_2 \cdot \text{H}_2\text{O}$ was then dissolved in 10 mL of methanol, added to the ligand solution, and stirred overnight. Black solid was precipitated. The solid was collected by filtration, washed with pentane and dried to give $\text{Cu}(\text{SMML})_2$ (0.419 g, 79 %). Black crystals of diffraction quality were obtained from ethanol solution after several days through slow evaporation at room temperature. Elemental analysis for $\text{C}_{16}\text{H}_{26}\text{CuN}_4\text{S}_4\text{O}_4$: Calcd. C 36.24, H 4.94, N 10.64; Found C 36.41, H 5.03, N 10.64. ESI-MS: $m/z = [\text{M}+\text{H}]^+$ Calcd. 530.03, Found 530.02; $[\text{M}+\text{Na}]^+$ Calcd. 552.01, Found 552.00. IR: ν (cm^{-1}) = 1726 (s), 1610 (m), 1009 (s) 983 (s) 860 (m). UV-Vis in DMSO: λ_{max} nm ($\log \epsilon$) = 273 (4.45), 428 (3.32), ≈ 607 (3.08,sh). RP-HPLC: R_T (min) = 14.1 and 21.4.

Cu(SMLA)₂ 0.131 g (0.0006 mol, 1 equiv) of SMLA was solubilized in 25 mL of methanol. 0.060 g (0.0003 mol, 0.5 equiv) of Cu(OAc)₂·H₂O was then dissolved in 10 mL of methanol, added to the ligand solution, and stirred overnight. The solution was concentrated to reduce volume, triturated with acetonitrile and allow to stand. Black solid was precipitated. The solid was collected by filtration, washed with pentane and dried to give Cu(SMLA)₂ (0.065 g, 43 %). Black crystals of diffraction quality were obtained from methanol after several weeks through slow evaporation at 4°C. Elemental analysis for C₁₄H₂₆CuN₄S₄O₆: Calcd. C 31.24, H 4.87, N 10.41; Found C 31.58, H 4.31, N 10.48. ESI-MS: $m/z = [M+H]^+$ Calcd. 502.00, Found 501.99; $[M+Na]^+$ Calcd. 523.98, Found 523.97. IR: ν (cm⁻¹) = 3660- 2160 (b) 1701 (s) 1608 (m) 948 (s) 914 (m) 853 (m). UV-Vis in DMSO: λ_{\max} nm (log ϵ) = 270 (4.46), 307 (4.14,sh), 428 (3.10), \approx 488(3.00,sh) \approx 608 (2.85,sh). RP-HPLC: R_T (min) = 16.6.

Cu(SBML)₂ 0.186 g (0.0006 mol, 1 equiv) of SBML was solubilized in 30 mL of toluene. 0.060 g (0.0003 mol, 0.5 equiv) of Cu(OAc)₂·H₂O was then dissolved in 10 mL of methanol, added to the ligand solution, and stirred overnight. The solution was concentrated to reduce volume, triturated with pentane and allow to stand. Black solid was precipitated. The solid was collected by filtration, washed with pentane and dried to give Cu(SBML)₂ (0.131 g, 64%). Elemental analysis for C₂₈H₃₄CuN₄S₄O₄: Calcd. C 49.28, H 5.02, N 8.21; Found C 50.07, H 5.09, N 8.31. ESI-MS: $m/z = [M+Na]^+$ Calcd. 704.08, Found 704.06. IR: ν (cm⁻¹) = 1726 (s) 1614 (m) 1009 (s) 981 (s) 764 (m). UV-Vis in DMSO: λ_{\max} nm (log ϵ) = 273 (4.51), 433 (3.28), \approx 496 (3.18,sh), \approx 608 (3.05,sh). RP-HPLC: R_T (min) = 19.0 and 25.0.

Cu(SBLA)₂ 0.178 g (0.0006 mol, 1 equiv) of SBLA was solubilized in 30 mL of toluene. 0.060 g (0.0003 mol, 0.5 equiv) of Cu(OAc)₂·H₂O was then dissolved in 10 mL of ethanol, added to the ligand solution, and stirred overnight. The solution was concentrated to reduce volume, triturated with pentane and allow to stand. Black solid was precipitated. The solid was collected by filtration, washed with pentane and dried to give Cu(SBLA)₂ (0.125 g, 64%). Elemental analysis for C₂₈H₃₀CuN₄S₄O₄: Calcd. C 47.72, H 4.62, N 8.56; Found C 47.15, H 4.64, N 8.51. ESI-MS: $m/z = [M+Na]^+$ Calcd. 676.04, Found 676.03. IR: ν (cm⁻¹) = 3330-2300 (b) 1698 (s) 1613 (w) 1600 (w) 948 (s) 919 (s) 763 (w). UV-Vis in DMSO: λ_{\max} nm (log ϵ) = 272 (4.48), 431 (3.30), \approx 471(3.24, sh), \approx 608 (3.05, sh). RP-HPLC: R_T (min) = 16.8 and 21.2.

Cu(SM4CB)₂ 0.203 g (0.0008 mol, 1 equiv) of SM4CB was solubilized in 150 mL of hot acetonitrile. 0.080 g (0.0004 mol, 0.5 equiv) of Cu(OAc)₂·H₂O was then dissolved in 20 mL of acetonitrile, added to the ligand solution, and heated at 82°C (reflux temperature) with stirring for one-two hour until the volume was reduced. The solution was allowed to stand at 4°C overnight. Brown solid was precipitated. The solid was collected by filtration, washed with pentane and dried to give Cu(SM4CB)₂ (0.167 g, 73 %). Elemental analysis for C₂₀H₁₈CuN₄S₄O₄: Calc C 42.13, H 3.18, N 9.83; Found C 41.84, H 3.39, N 9.65. ESI-MS: $m/z = [M+3Na-2H]^+$ Calcd. 635.91, Found 635.90; $[M+2Na-H]^+$ Calcd. 613.93, Found 613.92; $[M+Na]^+$ Calcd. 591.95, Found 591.94. IR: ν (cm⁻¹) = 3280-2320 (b) 1687 (s) 1607 (m) 964 (m) 939 (m) 819 (m). UV-Vis in DMSO: λ_{\max} nm (log ϵ) = 322 (4.45). RP-HPLC: R_T (min) = 13.3.

Cu(SB4CB)₂ 0.1322 g (0.0004 mol, 1 equiv) of SB4CB was solubilized in 75 mL of acetonitrile. 0.040 g (0.0002 mol, 0.5 equiv) of Cu(OAc)₂·H₂O was then dissolved in 10 mL of acetonitrile, added to the ligand solution, and heated at 82°C (reflux temperature) with stirring for one-two hour until the volume was reduced. The solution was allowed to stand at 4°C overnight. Brown solid was precipitated. The solid was collected by filtration, washed with pentane and dried to give Cu(SB4CB)₂ (0.106 g, 73 %). Elemental analysis for C₃₂H₂₆CuN₄S₄O₄: Calcd. C 53.21, H 3.63, N 7.76; Found C 53.39, H 3.81, N 7.65. ESI-MS: $m/z = [M+3Na-2H]^+$ Calcd. 787.98, Found 787.96, $[M+2Na-1H]^+$ Calcd. 765.99, Found 765.98, $[M+Na]^+$ Calcd. 744.01, Found 744.00. IR: ν (cm⁻¹) = 3280-2350 (b) 1687 (s) 1605 (m) 958 (m) 915 (m) 816 (m). UV-Vis in DMSO: λ_{max} nm (log ϵ) = 322 (4.48). RP-HPLC: R_T (min) = 16.8.

3.2.3.3 Open chain Cu(II) system with bidentate NS ligands with natural ketone moiety

SBCM This compound was prepared by a slight modification of a previously reported procedure (Dawara et al., 2012). SBDTC (0.397 g, 0.002 mol) was dissolved in hot absolute ethanol (40 mL). An equimolar amount of 3-acetylcoumarin also dissolved in hot absolute ethanol (0.378 g, 60 mL) was added dropwise to the solution of the dithiocarbazate. The mixture was heated over 2-3 hours until finally the volume was 1/3 of the original volume to produce orange precipitate. The solution was allowed to stand for a few hours at 4°C. The product was filtered off, washed with pentane and dried in vacuo over silica gel to afford 0.619 g of SBCM (Yield 84 %). HR-MS: $m/z = [M+Na]^+$ Calcd. 391.05454, Found 391.05492. ¹H NMR (300 MHz, DMSO-d₆) δ 12.56 (s, 1H), 12.50 (s, 0H), 8.19 (s, 1H), 8.10 (s, 0H), 7.85 (dd, $J = 7.8, 1.4$, 1H), 7.77 – 7.60 (m, 2H), 7.50 – 7.21 (m,

12H), 4.48 (s, 2H), 4.42 (s, 1H), 2.34 (s, 3H), 2.20 (s, 1H). IR: ν (cm^{-1}) = 3025 (w) 2872 (w) 1700 (s) 1559 (m) 1042 (m) 999 (s) 841 (m). UV-Vis in DMSO: λ_{max} nm ($\log \epsilon$) = 286 (4.22), \approx 342 (4.12, sh). RP-HPLC: R_{T} (min) = 23.7.

Cu(SBCM)₂ The ligand (0.0368g, 0.0001 mol, 1 equiv) was dissolved in hot solution of ethanol:acetonitrile (2:1 ratio, 100 mL). Cu(OAc)₂·H₂O (0.010 g, 0.00005 mol, 0.5 equiv) dissolved in 10 ml of ethanol was added and the reaction mixture was stirred at room temperature overnight. The solution was concentrated to reduce volume and allow to stand. Dark brown solid was precipitated. The solid was collected by filtration, washed with pentane and dried under vacuum to afford the expected complexes Cu(SBCM)₂. (0.031 g, 78 %) Elemental analysis for C₃₈H₃₀CuN₄S₄O₄: Calcd. C 57.16 H 3.79 N 7.02; Found C 56.53, H 3.80, N 7.02. ESI-MS: m/z = [M+K]⁺ Calcd. 836.02, Found 836.01; [M+Na]⁺ Calcd. 820.04, Found 820.03; [M+H]⁺ Calcd. 798.06, Found 798.05. IR: ν (cm^{-1}) = 1726 (s) 1565 (m) 986 (s) 965 (s) 853 (w) 839 (w). UV-Vis in DMSO: λ_{max} nm ($\log \epsilon$) = 285 (4.48), \approx 341 (4.42, sh), 606 (2.95). RP-HPLC: R_{T} (min) = 23.5 and 28.0.

Zn(SBCM)₂ The ligand (0.0368g, 0.0001 mol, 1 equiv) was dissolved in hot solution of ethanol:acetonitrile (2:1 ratio, 100 mL). Zn(OAc)₂ (0.009 g, 0.00005 mol, 0.5 equiv) dissolved in 10 ml of ethanol was added and the reaction mixture was stirred at room temperature overnight. The solution was concentrated to reduce volume allow to stand. White solid was precipitated. The solid was collected by filtration, washed with pentane and under vacuum to afford the expected complexes Zn(SBCM)₂. (0.033 g, 83%) Elemental analysis for C₃₈H₃₀ZnN₄S₄O₄: Calcd. C 57.03, H 3.78, N 7.00; Found C 56.49, H 3.84, N 7.10. ESI-MS: m/z = [M+H]⁺

Calcd. 799.1, Found 799.5. ^1H NMR (300 MHz, DMSO- d_6) δ 8.22 (s, 2H), 7.76 (t, J = 7.1, 4H), 7.52 (dd, J = 16.7, 8.4, 4H), 7.36 – 7.20 (m, 10H), 3.87 (s, 4H), 2.53 (s, 6H). IR: ν (cm^{-1}) = 1706 (s) 1567 (m) 984 (s) 952 (m) 843 (w). UV-Vis in DMSO: λ_{max} nm ($\log \epsilon$) = 292 (4.50), \approx 344 (4.41, sh). RP-HPLC: R_T (min) = 23.4.

Re(SBCM) $_2$

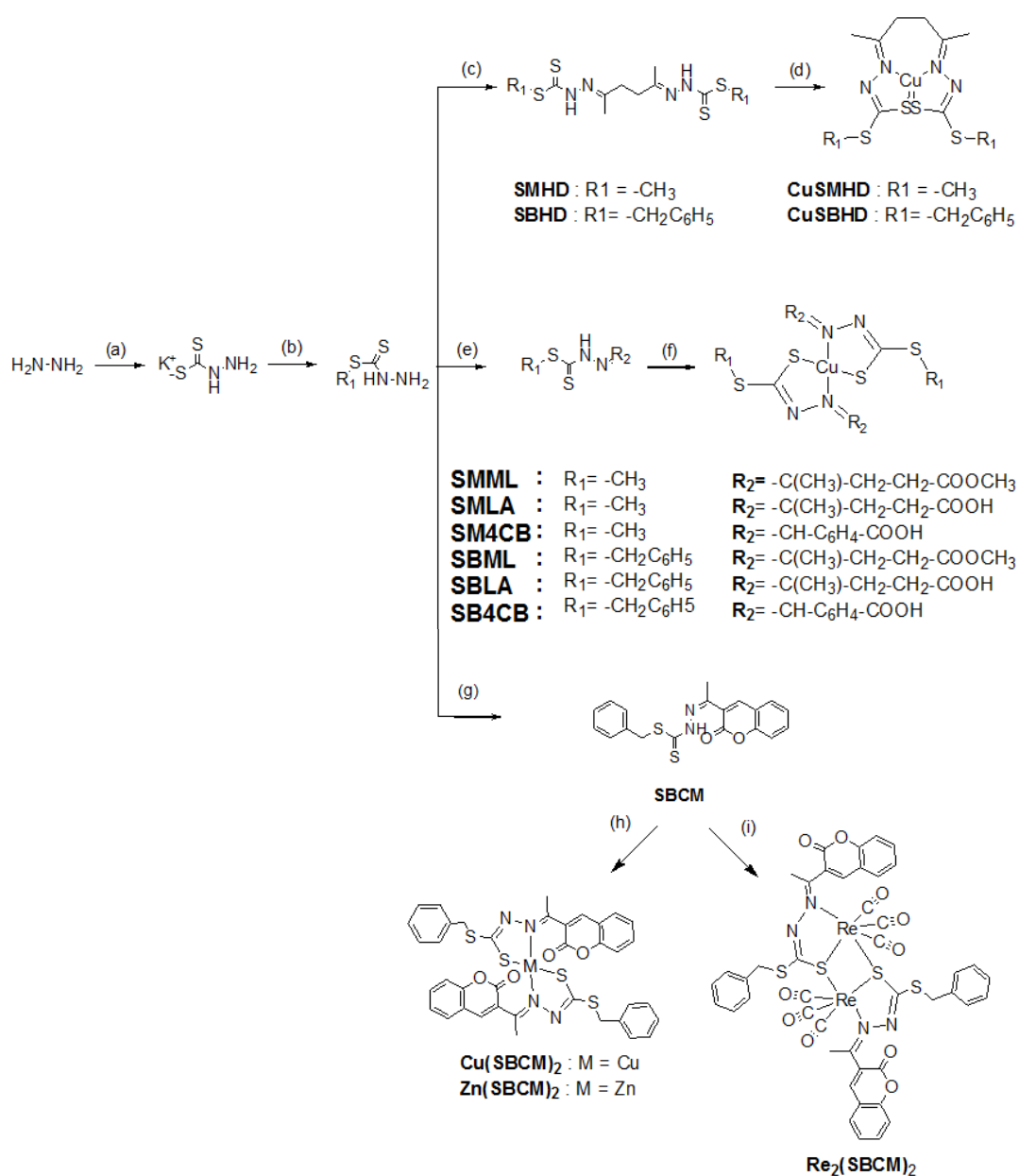
The ligand (0.074 g, 0.0002 mol, 1 equiv) was dissolved in toluene (30 mL) at 110 °C. $\text{Re}(\text{CO})_5\text{Cl}$ (0.072 g, 0.0002 mol, 1 equiv) was added and the reaction mixture was refluxed overnight. A yellow precipitate appeared. The reaction was cooled down to room temperature, filtered and the solid was washed with toluene. The solid dried under vacuum to afford the expected complexes (0.0441 g, 33 %). Yellow-orange crystals of diffraction quality were obtained from toluene after several weeks through slow evaporation at room temperature. Elemental analysis for $\text{C}_{44}\text{H}_{30}\text{ReN}_4\text{S}_4\text{O}_{10}$: Calcd. C 41.44, H 2.37, N 4.39; Found C 40.04, H 2.41, N 4.43. ESI-MS: m/z = $[\text{M}+\text{H}]^+$ Calcd. 1275.00, Found 1275.00, $[\text{M}+\text{Na}]^+$ Calcd. 1296.98, Found 1296.98. ^1H NMR (300 MHz, DMSO- d_6) δ ^1H NMR (300 MHz, DMSO) δ 8.30 (s, 2H), 7.73 – 7.65 (m, 4H), 7.50 – 7.40 (m, 8H), 7.38 – 7.24 (m, 7H), 4.45 (s, 4H), 2.52 (s, 4H). IR: ν (cm^{-1}) = 2017 (s) 1914 (s) 1892 (s) 1724 (s) 1566 (m) 1022 (m) 1004(m) 846 (w) UV-Vis in DMSO: λ_{max} nm ($\log \epsilon$) = 2.86 (4.53), \approx 325 (4.44,sh). RP-HPLC: R_T (min) = 25.7.

3.3 Results and discussion

3.3.1. Synthesis

The synthesis of S-substituted dithiocarbazates were performed as already described (Chan et al., 2008; Chew et al., 2004). Carbon disulfide and hydrazine were reacted in basic ethanolic conditions. After workup the expected dithiocarbazate was directly engaged into the nucleophilic substitution with methyl iodide or benzyl chloride to afford SMDTC and SBDTC, respectively. The tetradentate NNSS Schiff base ligands were then prepared with variations from the method described by Ali et al. (1987) involving the condensation reaction between the respective S-substituted dithiocarbazates and 2,5-hexanedione in 2:1 ratio (Scheme 3.1: a-d). The initial attempt to synthesize the ligand SBHD with prolonged heating or purification using column chromatography showed that this compound underwent cyclization to its pyrrole derivative as confirmed by NMR, ESI, elemental analysis and single crystal X-ray diffraction. The bis(dithiocarbazate) was postulated to form first, subsequently hydrolyzed into mono(dithiocarbazate) and SBDTC (Patel et al., 2009; Chaviara et al., 2005). It is likely that the mono(dithiocarbazate) then underwent cyclization to a pyrrole via the Paal-Knorr reaction. However, such a side reaction was not previously described during the formation of bis(thiosemicarbazone) with 2,5-hexanedione (Gingras et al., 1962) although there have been reports of the formation of pyrazole upon reaction with 1,3-diketones (Ali et al., 2013b; Iskander et al., 1982; Casas et al., 2008; Centore et al., 2013) and others cyclic byproducts from related reactions (Christlieb and Dilworth, 2006; Ali et al., 2013a). To our knowledge, this is the first description of a pyrrole derived from a dithiocarbazate. Encouraged by the remarkable pharmacological properties of functionalized pyrrole (Liu et al., 2008; Fürstner, 2003), the compound was tested for its antimicrobial activity and the

results are discussed in Chapter 5. The Schiff base SBHD was finally obtained by either stirring the dione and SBDTC at room temperature for 30 min or by heating for only 5 min.



Scheme 3.1. Synthesis of the non-conjugated parent compounds. (a) CS₂, KOH, EtOH, 0°C, 1 hr (b) CH₃I or PhCH₂Cl, EtOH, 0°C, 5 hr (c) For SMHD (2,5-hexanedione, EtOH, 79°C, 1 hr), for SBHD (2,5 hexanedione, EtOH, 79°C, 5 min) (d) For CuSMHD (Cu(OAc)₂·H₂O, MeOH, 65°C, 1hr), for CuSBHD (Cu(OAc)₂, acetonitrile, r.t., 1hr). (e) For SMML and SBML (methyl levulinate, EtOH, 79°C, 1 hr), for SMLA and SBLA (levulinic acid, acetonitrile, 82°C, 1h), for SM4CB and SB4CB (4-carboxy benzaldehyde, acetonitrile, 82°C, 2h) (f) For Cu(SMML)₂ and Cu(SMLA)₂ (Cu(OAc)₂·H₂O, MeOH, r.t, overnight), for Cu(SBML)₂ and Cu(SBLA)₂ (Cu(OAc)₂·H₂O, toluene, r.t, overnight), for

Cu(SM4CB)₂ and Cu(SB4CB)₂ (Cu(OAc)₂·H₂O, acetonitrile, 82°C, 2h). (g) 3-acetylcoumarin, EtOH, 79°C, 2 hr. (h) Cu(OAc)₂·H₂O or Zn(OAc)₂, EtOH:ACN (2:1 ratio), r.t, overnight (i) Re(CO)₅Cl, toluene, 110 °C, overnight.

White precipitates were formed. The SMHD ligand was synthesized by heating to reduce the volume without the occurrence of such side reaction. The expected compound SMHD that precipitated was filtered off and recrystallized to afford pure SMHD with good yields. The tetra-coordinated Cu(II) complexes with NNSS coordination of these ligands were obtained from the reaction of copper(II) acetate with equimolar amounts of the respective ligand in acetonitrile for SBHD and in methanol for SMHD. The complexes were isolated by filtration with yields of 77% and 73% for CuSMHD and CuSBHD, respectively. Black crystals were grown from acetonitrile.

Six bidentate Schiff base ligands with acid or ester functionality were prepared via the condensation reaction between the respective S-substituted dithiocarbazates and carbonyl compounds in equimolar amount (Scheme 3.1: a,b,e-f). The reactions with methyl levulinate were carried out in ethanolic solution at 79°C whereas the reactions involving both levulinic acid and 4-carboxybenzaldehyde containing the acid-COOH functionality were done in hot acetonitrile solution. The attempt to synthesize the ligand SBLA in ethanol did not yield the expected compound. Instead, an esterification reaction occurred with the concomitant formation of a ligand bearing an ethyl ester (SBEL). The reaction of copper(II) acetate salts with the Schiff base ligands in 1:2 ratio yielded crystalline complexes of the formula, CuL₂ in which the ligands were bidentate. Depending on the ligands, different reaction conditions have been set up in order to optimize the yield and purity of the

complexes. Early trials at high temperature and in polar alcoholic solution often resulted in oily products and further efforts to crystallize the complexes were futile. The structures of four Schiff bases (SMML, SBML, SBEL, SBLA) and two Cu (II) complexes, Cu(SMML)₂ and Cu(SMLA)₂ were confirmed by single-crystal X-ray analyses.

The synthesis of the bidentate NS Schiff base with natural ketone moiety, SBCM and its proposed structures of metal complexes are schematically represented in Scheme 3.1 (a,b,g-i). The complexes Cu(SBCM)₂ and Zn(SBCM)₂ were prepared by reacting SBCM with metal(II) acetate in ethanol:acetonitrile (2:1 ratio) solution mixture at room temperature whereas the adduct, Re₂(SBCM)₂, was obtained by refluxing the free ligand with ReCl(CO)₅ in toluene. The single crystal of the Re(I) complex was also grown from toluene.

The purity and stability of the ligands and their corresponding complexes at physiological pH are important prerequisites for the evaluation of their biological activity. Therefore RP-HPLC experiments have been performed to gain insights into their stability in aqueous solutions. The tetradentate ligands and their respective Cu(II) complexes were eluted on a C18-column with an increasing amount of acetonitrile (CH₃CN) in H₂O (from 5% to 100% of CH₃CN over 30 minutes), containing 0.1 % trifluoroacetic acid (TFA) to maintain the pH. The compounds were detected using a UV detector at 220 nm and 280 nm. The chromatograms of the pure ligands of the tetradentate series showed 3 peaks that could correspond respectively to the hydrolyzed hydrazone, the expected ligand and the pyrrole byproduct (Figure 3.1) whereas the complexes showed only a single peak

corresponding to the copper complexes (Figure 3.2). The bidentate series with acid or ester functionality were also eluted on a RP-HPLC C8-column with a solvent system similar to those used for the tetradentate ligands. For the aliphatic Schiff bases (SMML, SMLA, SBML, SBLA, SBEL), the chromatograms of the ligands showed two peaks corresponding to the starting S-substituted dithiocarbamate and the expected ligand whereas the complexes showed mainly a single peak corresponding to the copper complexes. Another peak (the intensity differed from one compound to the other) was also visible for the copper(II) complexes that may be due to either isomerization or to dissociation to 1:1 Cu:L complexes. The chromatograms of SMML and Cu(SMML)₂ are shown in Figure 3.3 and 3.4 respectively as examples, the rest of the chromatograms can be found in the Appendices. The aromatic acid Schiff bases (SM4CB and SB4CB) on the other hand showed only one peak corresponding to the ligands which indicated their enhanced stability as compared to their aliphatic counterparts (Figure 3.5). Similarly, the chromatograms of SBCM and its complexes showed mainly a single peak highlighting the stability of the aromatic coumarin derivatives. In conclusion, the observations indicated that the -C=N- hydrazone bond in the aliphatic free ligands could undergo hydrolysis but when complexed, the stability of the ligands was significantly increased in acidic conditions and it appears clearly that aromatic Schiff bases were more stable. The difference in the ligands and metal complexes stability is noteworthy as metal-complexation could then be used as a mean to protect the ligand from degradation that could occur in the biological before it could reach its target.

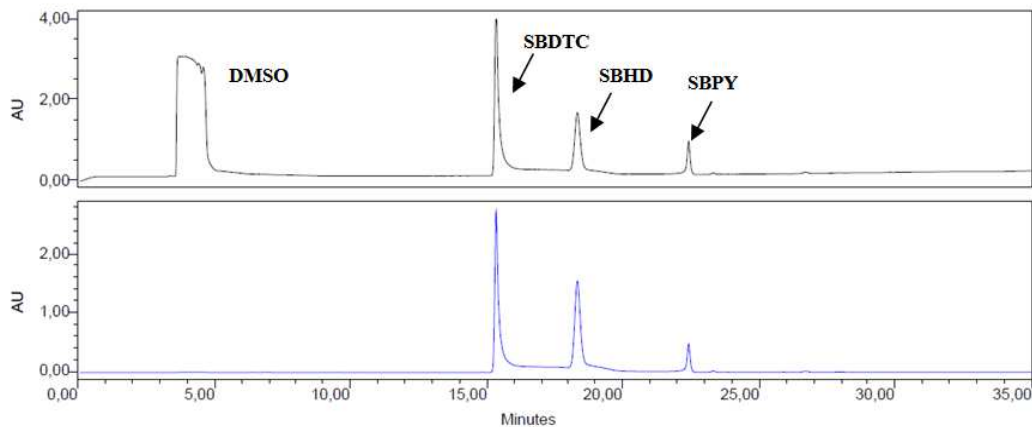


Figure 3.1. RP-HPLC chromatogram of SBHD at 220 nm (top) and 280 nm (bottom).

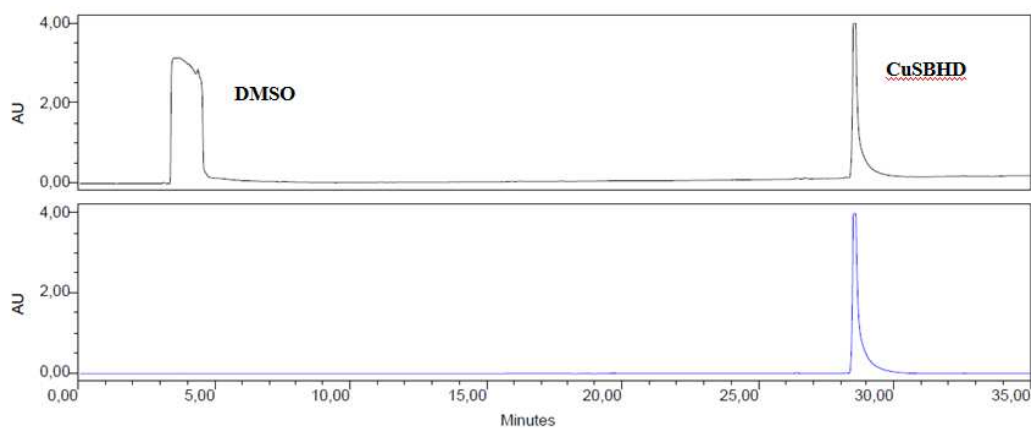


Figure 3.2. RP-HPLC chromatogram of CuSBHD.

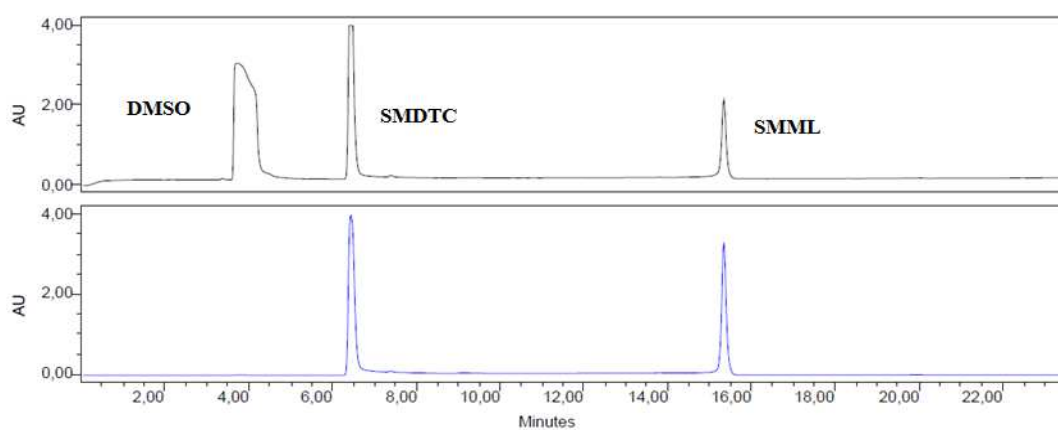


Figure 3.3. RP-HPLC chromatogram of SMML.

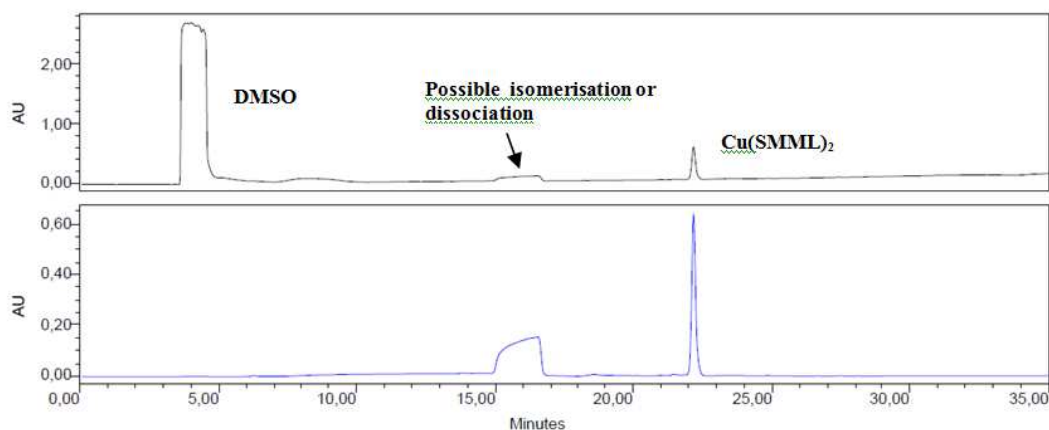


Figure 3.4. RP-HPLC chromatogram of Cu(SMML)₂.

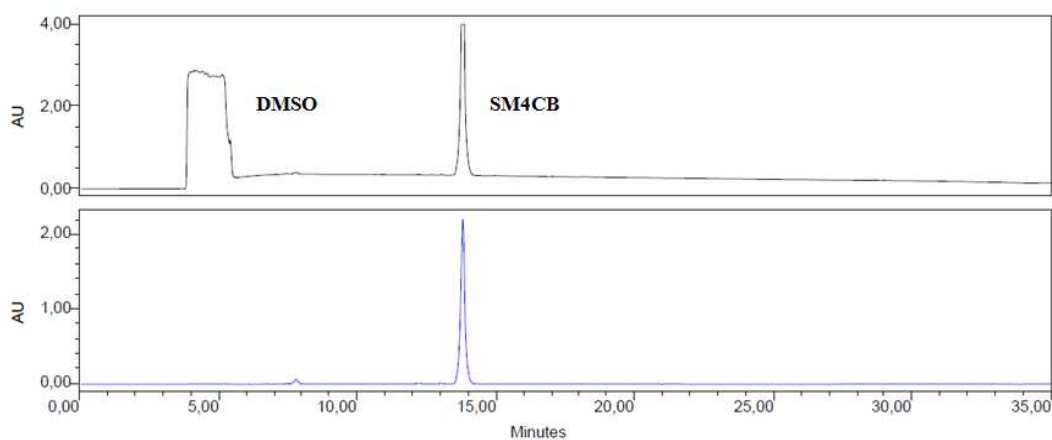


Figure 3.5. RP-HPLC chromatogram of SM4CB.

The proposed structures and stoichiometry was initially established by elemental analysis and mass spectrometry. The analytical data for the metal complexes agreed well with the formulations proposed. All the mass spectra show signals corresponding to the molecular weight of either the protonated complexes or the complexes with sodium or potassium. These results confirm 1:1 metal to ligand stoichiometry for CuSMHD, CuSBHD and a dimeric $\text{Re}_2(\text{SBCM})_2$ whereas $\text{Cu}(\text{SMML})_2$, $\text{Cu}(\text{SMLA})_2$, $\text{Cu}(\text{SBML})_2$, $\text{Cu}(\text{SBLA})_2$, $\text{Cu}(\text{SM4CB})_2$, $\text{Cu}(\text{SB4CB})_2$, $\text{Cu}(\text{SBCM})_2$ and $\text{Zn}(\text{SBCM})_2$ demonstrated 1:2 metal to ligand stoichiometry. Upon complexation of metal ion with S-substituted dithiocarbazate derived Schiff base ligand, a deprotonation of the nitrogen of the dithiocarbazate is expected, leading to an iminothiolate. Coordination via NS atoms would be anticipated. However, the O

atom present in the ligands containing acid, ester or coumarin moiety could also potentially participate in metal coordination. In order to confirm the formation of the metal complexes and to characterize them, several other techniques were employed.

3.3.2 Characterization of metal complexes in solid state

3.3.2.1 FT-IR

Two examples of the FT-IR spectra used to monitor complexation, one from tetradentate series and the other from bidentate series are shown in Figure 3.6 and 3.7, respectively. The IR spectra for the rest of the compounds can be found in the Appendices. The IR spectra of the tetradentate ligands and bidentate SMML and SBML ligands exhibit characteristic bands ν_{NH} at *ca.* 3130 and 3200 cm^{-1} , respectively. Strong broad structured bands spanning from around 3300–2300 cm^{-1} appeared in the spectra of the ligands SMLA, SBLA, SM4CB and SB4CB which contained the acid functionality and their respective Cu(II) complexes due to ν_{OH} , ν_{NH} and ν_{CH} overlapping stretching vibrations. The IR spectrum of coumarin-derived SBCM however showed only a weak band at 3056 cm^{-1} assignable to $\nu(\text{NH})$ stretching. Another band attributed to $\nu(\text{SH})$ was noticeable at 2872 cm^{-1} . These observations demonstrated that while most of the ligands existed in thione form, SBCM existed in both thione and thiolate forms in the solid state. In addition, all the ligands possess bands $\nu(\text{C}=\text{N})$ at 1652-1559 cm^{-1} , $\nu(\text{C}=\text{S})$ at 1067-1025 cm^{-1} , $\nu(\text{CSS})$ at 990-923 cm^{-1} and $\nu(\text{NN})$ at 841-778 cm^{-1} . Upon formation of the complexes, the band corresponding to the $\nu(\text{NH})$ stretching of the ligands disappeared. The $\nu(\text{C}=\text{N})$ attributed to azomethine bond was observed to experience a downward shift of 5-40 cm^{-1} in most of the spectra with the exception of metal complexes of SBCM that shifted to higher wavenumbers ($\sim 1566 \text{ cm}^{-1}$). A

second band due to $\nu(\text{N}=\text{C})$ in complexes containing anionic dithiocarbazate moieties was also resolved (Rapeal et al., 2007) for CuSMHD, CuSBHD and Cu(SBLA)₂. The hydrazinic $\nu(\text{N}-\text{N})$ band also shifted to either higher and lower wavenumbers upon complexation. All these observations indicates the deprotonation of the Schiff base ligands and coordination via the azomethine nitrogen atom during complexation with metal ion which resulted in the adoption of a more stable structure where the conjugated system was elongated in the complexes as compared to the free ligands. The disappearance of $\nu(\text{C}=\text{S})$ and the splitting of the asymmetric $\nu(\text{CSS})$ band into two peaks in the spectra of the all metal complexes were strong evidence of coordination via the thiolate sulfur atoms (Crouse et al., 2004; Akbar Ali and Tarafdar, 1977). In the bidentate series, the strong band at 1717-1687 cm^{-1} of the ligands can be assigned to the carbonyl $\nu(\text{C}=\text{O})$. The band remained unchanged upon complexation in the spectra of Cu(SM4CB)₂, Cu(SB4CB)₂ and Cu(SBLA)₂ but slightly shifted for Cu(SMML)₂, Cu(SBML)₂, Cu(SMLA)₂, Cu(SBCM)₂, Zn(SBCM)₂ and Re₂(SBCM)₂. Despite the shift in wavenumbers, the X-ray structures solved for Cu(SMML)₂, Cu(SMLA)₂ and Re₂(SBCM)₂ revealed that the metal ions were coordinated by the bidentate ligands via only the azomethine nitrogen and thiolate sulfur atoms. No coordination via the carbonylic oxygen was observed. Such a shift can be interpreted as being caused by the vibrational coupling of the C=O in the solid state H-bonded structure (Ferrari et al., 2000). Single crystal X-ray analyses of the ligands and complexes indicated the formation of intermolecular hydrogen bonds involving the carbonylic oxygen and the presence of other short contacts. Previous publications had also reported comparable shifting that did not correspond to coordinated O atoms (Creaven et al., 2009). *Fac*-geometry

around the rhenium atom is also confirmed by the three characteristic Re-(CO) vibrations at 2017, 1914 and 1892 cm^{-1} .

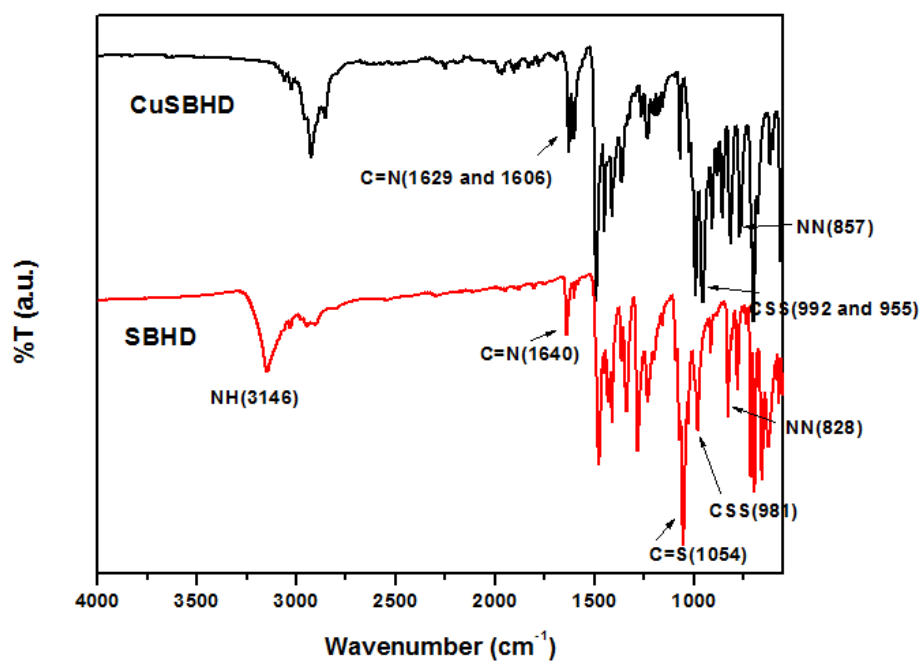


Figure 3.6. FT-IR spectra recorded for ligand SBHD and complex CuSBHD.

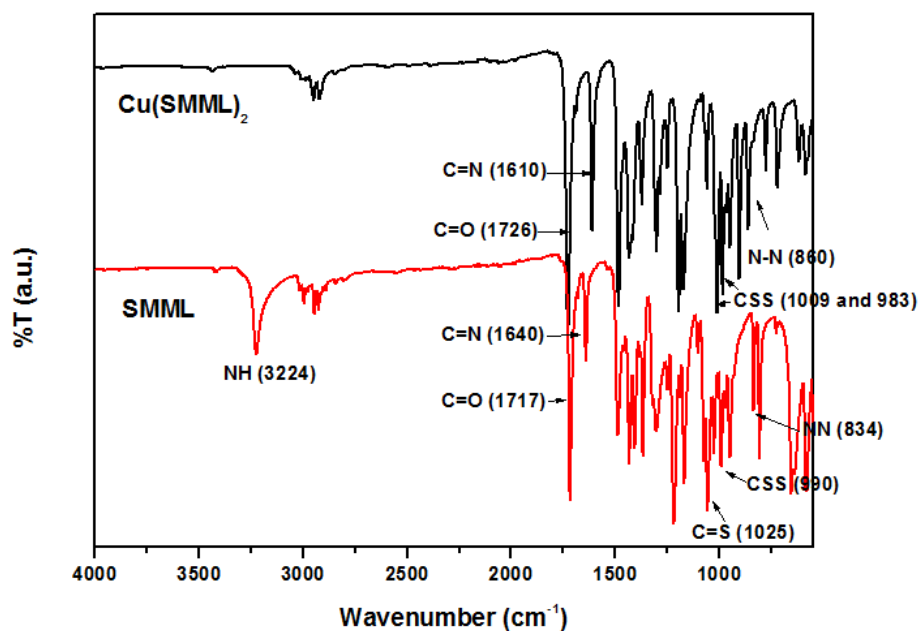


Figure 3.7. FT-IR spectra recorded for ligand SMML and complex Cu(SMML)₂.

3.3.2.2 Single crystal XRD description

The ORTEP diagrams of the compounds in the tetradentate series SBPY, SMHD, CuSMHD and CuSBHD with atomic numbering schemes are shown in Figure 3.8.

Selected bond lengths and bond angles are depicted in Table 3.1 and 3.2.

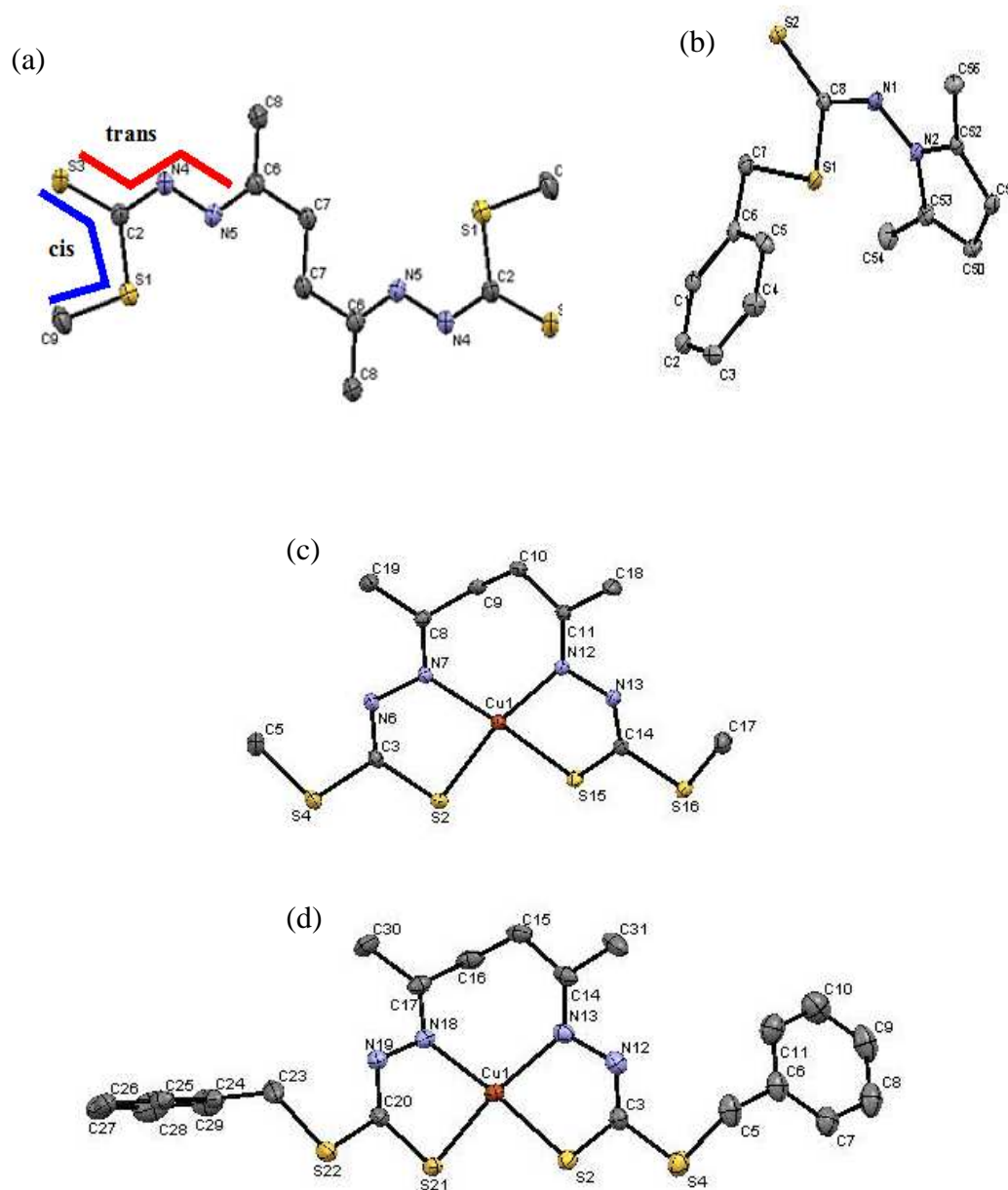


Figure 3.8. ORTEP drawing of (a) SMHD (b) SBPY (c) CuSMHD and (d) CuSBHD. Ellipsoids are drawn at the 50% probability level.

Table 3.1. Selected bond lengths for SBPY, SMHD, CuSMHD and CuSBHD.

Compound	Bond lengths (Å)				
	C=S	C-S	C-N	N-N	C=N
SMHD	1.657(4)	1.763(3)	1.337(4)	1.392(3)	1.281(4)
CuSMHD	1.738(2), 1.737(1)	1.753(1), 1.758(2)	1.290(2), 1.289(2)	1.407(1), 1.418(2)	1.288(2), 1.292(2)
CuSBHD	1.734(2), 1.740(2)	1.758(2), 1.756(2)	1.287(2), 1.287(2)	1.418(2), 1.401(2)	1.291(2), 1.284(2)
SBPY	1.647(2)	1.748(2)	1.354(2)	1.380(2)	1.386(2), 1.389(2)
	N-Cu	N-Cu	S-Cu	S-Cu	N-Cu
CuSMHD	2.071(1)	1.993(1)	2.246(4)	2.266(4)	2.071(1)
CuSBHD	1.978(1)	2.056(1)	2.252(4)	2.248(4)	1.978(1)

Table 3.2. Selected bond angles for CuSMHD, CuSBHD, CuATSM (Blower et al., 2003) and CuAATSM (Cowley et al., 2004).

Bond angles (°)	CuSMHD	CuSBHD	CuATSM	CuAATSM
S-Cu-N	85.75(3)	84.36(4)	85.13	86.79(5)
N-Cu-N	104.21(5)	99.61(5)	80.60	96.10(7)
N-Cu-S	84.89(3)	85.26(4)	85.11	85.60(5)
S-Cu-S	92.80(2)	91.67(2)	109.23	91.74(2)

The crystal structure of SMHD reveals an (E, E') conformation with respect to the hydrazone bond and a center of symmetry at the middle of the C7-C7' single bond. The molecule crystallized in *trans-cis* configuration around the S(NH)C=S moiety (highlighted in Figure 3.8 (a)) very similar to most Schiff bases derived from dithiocarbazate (Low et al., 2013; Ravooft et al., 2007). The S-methyl group was *cis* across the C2-S1 bond while the ketone moiety was *trans* along the C2-N4 bond with respect to the terminal thione S atom. The bond lengths N5-C6 (1.281 Å) and S3-C2 (1.657 Å) are consistent with a double-bond of a hydrazone and a thiocarbonyl, respectively. The values are comparable to related NNSS tetradentate ligands (Jasinski et al., 2003; Xu et al., 2002; Paterson et al., 2010). The bond lengths N4-C2 (1.337 Å) and S1-C9 (1.763 Å) are shorter than typical covalent

single-bond distance (N-C 1.47 Å and C-S 1.81 Å), indicating higher order bond character. This can result from delocalization of electron density within the dithiocarbazate S1-C2(=S3) and N4-C2(=S3) π -systems. The ligand appears essentially planar in the solid state and no hydrogen bonding was observed. The pyrrole byproduct SBPY crystallized in a monoclinic system with a space group of $P2_1/c$. The central C7S1C8S2N1 residue is planar while both the benzyl and pyrrole rings are inclined to this plane forming interplanar angles of 71.87° and 88.30°, respectively. A comparison of the selected bond lengths and bond angles with SMHD show that the molecule also crystallized in *trans-cis* configuration around the S(NH)C=S moiety similar to the Schiff bases with intermediate bond length indicative of extensive conjugation and π -delocalization over the molecules and other intermolecular interactions.

It is expected that the Cu(II) ion would be four-coordinated by the ligands in their iminothiolate form. N-deprotonation is typical in dithiocarbazate Schiff base coordination chemistry (Manan et al., 2011b; Jasinski et al., 2003; Paterson et al., 2010). Tautomerism of the dithiocarbazate ligand to its iminothiolate form is also anticipated to convert the C=S bond to a single C-S bond but in most cases the bond length lies between the C-S single bond (1.82 Å) and C=S double bond (1.56 Å) indicative of a partial double bond character (Ravoof et al., 2007). This is the case for both complexes where the C-S distance is 1.738 Å and 1.734 Å for CuSMHD and CuSBHD, respectively. The increase in the C-S bond distance as compared to the uncoordinated neutral ligand showed that the ligand is dianionic upon coordination. In addition, the C2-N4 bond length is about 1.337 Å in the free ligand whereas this bond shortened in both metal complexes (1.290 Å and 1.287 Å for

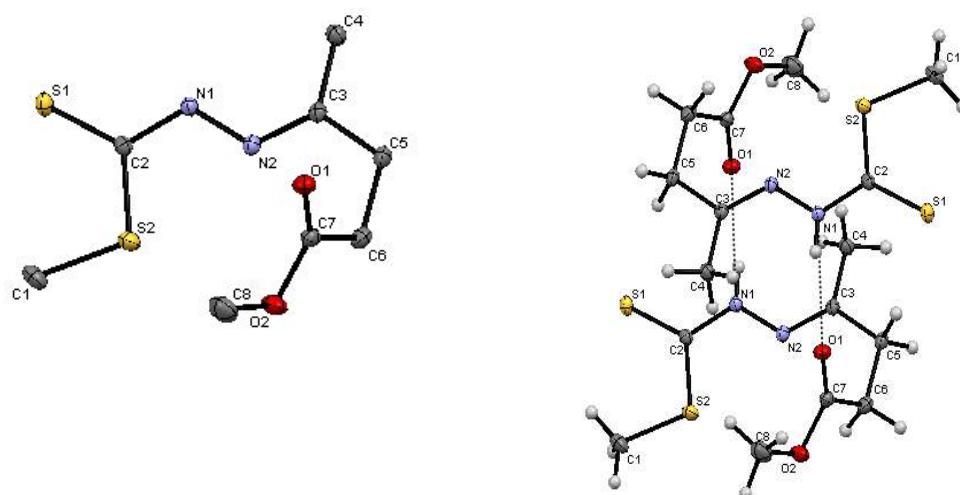
CuSMHD and CuSBHD, respectively) suggesting an enhancement of their double bond character. In order to accommodate the metal, the ethylene from the hexanedione adopts a *gauche* conformation forming a seven-membered chelate ring surrounding the Cu ion. It has been reported that seven membered chelate rings with two hydrazone bonds have a tendency to favour tetrahedral coordination of metal ions (Nandi et al., 1984). The deviation from planarity can be assessed by measuring the sum of the four angles, N-Cu-S, S-Cu-S, S-Cu-N and N-Cu-N, for which 360° would be obtained for an ideal planar arrangement and 437.6° for an ideal tetrahedral arrangement (Knoblauch et al., 1999). The sum of these angles around the central copper metal in this complex are consistent with a slightly distorted square planar geometry with CuSMHD showing a more significant distortion than CuSBHD (367.65° and 360.9° respectively). The interplanar angles between two N-Cu-S planes of 35.65° and 31.22° for CuSMHD and CuSBHD, respectively, confirms that CuSBHD is the more planar molecule. The Cu-N (1.98-2.07 Å) and Cu-S (2.24-2.27 Å) bond distances of both CuSMHD and CuSBHD are almost similar to the typical Cu(II) N₂S₂ complexes of related ligands (Blower et al., 2003; Cowley et al., 2004). When compared with other Cu(II) complexes of the same family with zero (CuATSM), one (CuAATSM) or two carbons (CuSMHD and CuSBHD) linking the two hydrazones, it appears clearly that the distortion from planar geometry increases with the number of carbons (360.07° , 360.23° , 360.9° and 367.65° for CuATSM, CuAATSM, CuSBHD and CuSMHD respectively).

Since the substituents are remote from the metal center, the solid state structures of the two complexes are almost identical. In the crystallographic lattice, the two benzyl groups adopt different orientations (*syn/anti*) with respect to their adjacent

coordinated S-donor atoms similar to the Cu(II) complex reported by Ali *et al.* (2013b). Together these data show that the tetradentate Cu(II) complexes are indeed formed and adopt a slightly distorted square planar geometry.

The crystal structures of the Schiff base ligands (SMML, SBML, SBEL, SBLA) and two Cu(II) complexes (CuSMML and CuSMLA) with their atom numbering schemes and intermolecular hydrogen bonds are shown in Figures 3.9 and Figure 3.10. Selected bond lengths and bond angles are given in Tables 3.3 to 3.8.

(a)



(b)

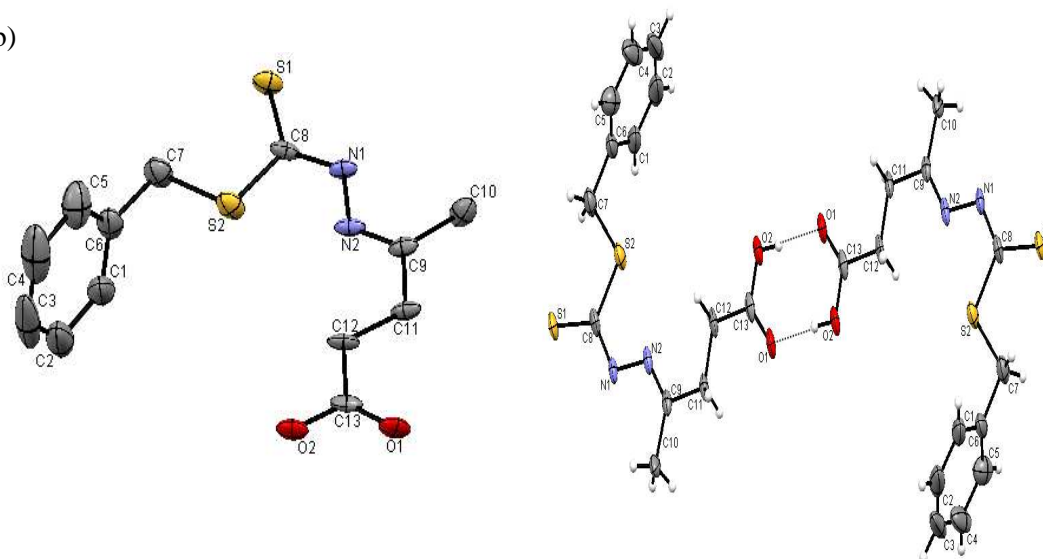


Figure 3.9. ORTEP diagrams and intermolecular hydrogen bonds (shown as *dotted line*) of (a) SMML and (b) SBLA. Ellipsoids are drawn at the 50% probability level.

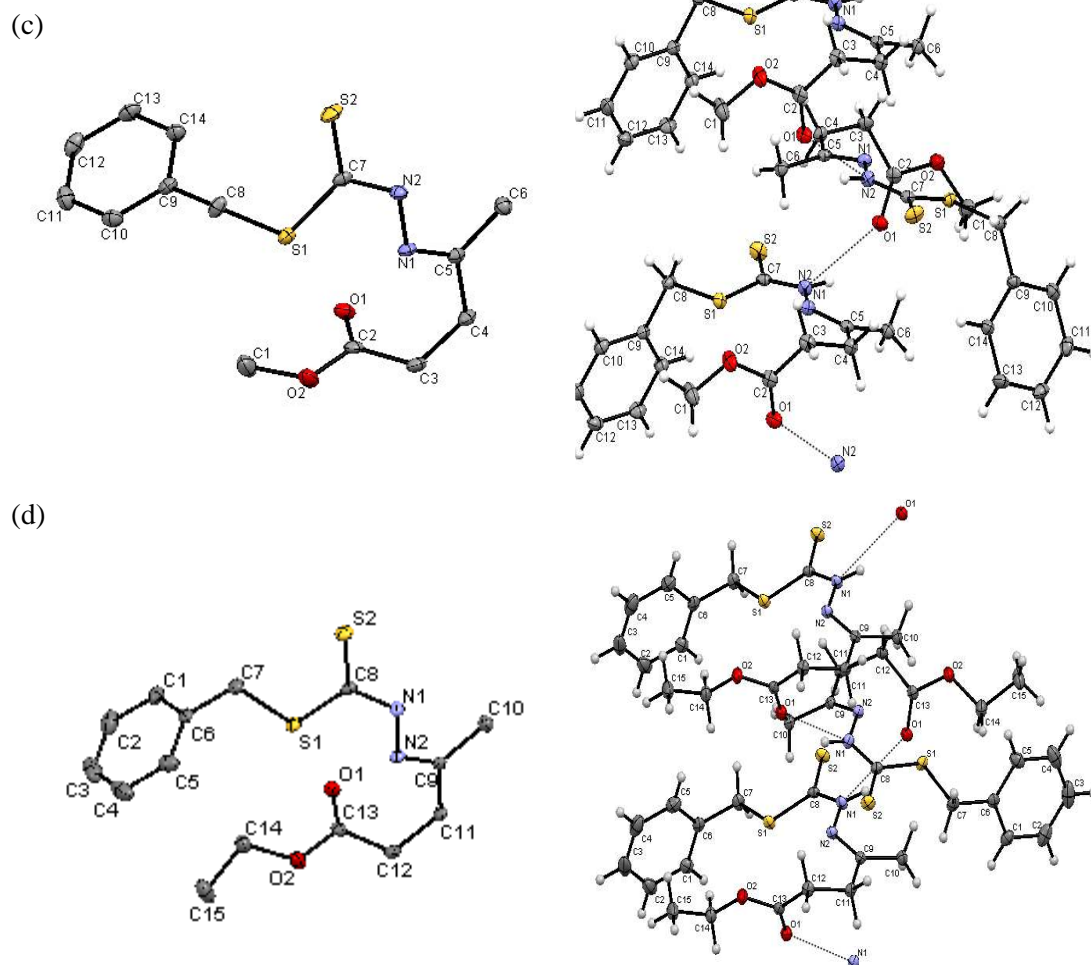


Figure 3.9 (continued). ORTEP diagrams and intermolecular hydrogen bonds (shown as *dotted line*) of (c) SBML (d) SBEL. Ellipsoids are drawn at the 50% probability level.

SBML and SBEL crystallized in space group of $P 2_1/n$ whereas SMML and SBLA crystallized in space groups $P 2_1/c$ and $P-1$, respectively. The Schiff bases are in the thione form with C=S bond distances ranging from 1.662 to 1.681 Å. As observed for the tetradentate ligands, the bond lengths were intermediate between a C–S single bond and a C=S double bond possibly due to the extensive conjugation over the C=N–N–C chain and other intermolecular interactions. The N–N bond distance varied from 1.378 to 1.394 Å in the Schiff bases, showing that the bond was shorter

than a single bond, indicating significant π -charge delocalization along the dithiocarbazate moiety. The attachment of the methyl levulinate/levulinic acid groups to the imino nitrogen atoms was probably responsible for the shortening of the N-N distance. *Trans-cis* conformation was observed in all the Schiff bases around the -SC(=S)NH- moiety. The methyl levulinate/levulinic acid moiety was *trans* with respect to the terminal thione S atom about the C-N bond while the S-methyl/S-benzyl group was *cis* with respect to the terminal thione S atom about the C-S bond. The bond angles in the Schiff bases were close to 120° consistent with sp^2 hybridization. The C–O (carbonylic) and C–O (hydroxylic) distances of 1.21 and 1.33 Å demonstrate typical localized bonds like those reported for carboxylic groups in thiosemicarbazone α -ketoglutaric acid (Ferrari et al., 2002a).

SMML and SBLA featured centrosymmetric H-bonded dimeric motifs held by strong intermolecular hydrogen bonds (N–H \cdots O, 2.932 Å) and (O–H \cdots O, 2.662 Å), respectively. The (N–H \cdots O) motif was also observed in SBML and SBEL but they were different from the dimeric SMML. Two (N–H \cdots O) bonds linked the dimeric SMML together while the individual (N–H \cdots O, 2.902 Å for SBEL and 2.933 Å for SBML) bond from one ligand were linked to two separate ligands forming a continuous chain in both SBML and SBEL.

The Schiff bases are also not planar. Both the benzyl rings and the methyl levulinate/levulinic acid moieties are in a twisted conformation at particular angles. A remarkable difference in the Schiff bases is the orientation of the =C(CH₃)CH₂CH₂COOR chains (where R = H, CH₃, CH₂CH₃) highlighted by the varied inclination angles between the allylic (=C(CH₃)CH₂CH₂) and the terminal

carbocyclic acid/ester (-COOR) planes. The deviation from planarity between the two plans can be arranged as $SBLA < SBML < SBEL < SMML$ while the order of planarity of the dithiocarbazate plane with respect to the allylic plane in the Schiff bases can be placed as follows $SBLA > SMML > SBML > SBEL$. The benzyl ring in all S-benzyl derivatives was almost perpendicular to the dithiocarbazate plane. The perpendicularity of the benzyl ring towards the dithiocarbazate plane can be ordered $SBLA > SBEL > SBML$.

Table 3.3. Selected bond lengths for SMML, SBML, SBEL and SBLA.

Compound	Bond lengths (Å)			
	C=S	C-S	C-N	N-N
SMML	1.6635	1.7560	1.3427	1.3797
SBLA	1.6806	1.7758	1.3624	1.3940
SBEL	1.6663	1.7567	1.3390	1.3989
SBML	1.6617	1.7636	1.3418	1.3941
Compound	C=N	C=O	C-O	
SMML	1.2846	1.2112	1.3352	
SBLA	1.2944	1.2418	1.3303	
SBEL	1.2853	1.2110	1.341	
SBML	1.2854	1.2102	1.3346	

Table 3.4. Selected bond angles for SMML, SBML, SBEL and SBLA.

Compound	Bond angles (°)			
	S-C=S	S=C-N	N-N=C	S-C-N
SMML	125.24	121.55	119.04	113.19
SBLA	124.30	122.81	120.49	112.89
SBEL	125.68	121.47	116.00	112.83
SBML	126.64	120.57	116.37	112.79

Table 3.5. Intermolecular hydrogen bonds for SMML, SBML, SBEL and SBLA.

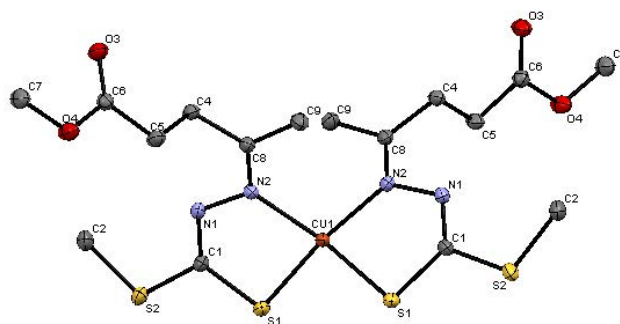
Compound	D-H-A (Å)
SMML	N1-H1···O1 (2.932)
SBLA	O1-H1···O2 (2.662)
SBEL	N1-H1···O1 (2.902)
SBML	N2-H1···O1 (2.933)

Table 3.6. Selected dihedral angles between the two planes for SMML, SBML, SBEL and SBLA.

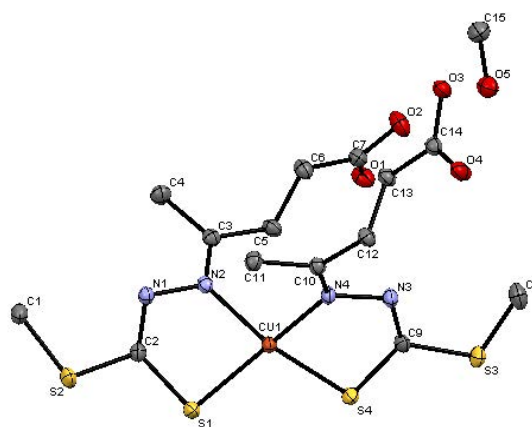
Compound	Dihedral angles (°)	Compound	Dihedral angles (°)
SMML		SBEL	
S2C2S1N1N2 (dithiocarbazate) and C3C4C5C6 (ML)	5.74	S1C8 S2N1N2 (dithiocarbazate) and C9C10C11C12 (EL)	30.62
S2C8S1N1N2 (dithiocarbazate) and O1C7O2C8(ML)	77.67	S1C8 S2N1N2 (dithiocarbazate) and O1C13O2C14C15 (EL)	68.59
C3C4C5C6 (ML) and O1C7O2C8(ML)	79.19	S1S2C8N1N2 (dithiocarbazate) and C1C2C3C4C5C6C7 (benzyl)	77.52
		C9C10C11C12 (EL) and O1C13O2C14C15 (EL)	74.96
SBLA		SBML	
S2C8S1N1N2 (dithiocarbazate) and C9C10C11C12 (LA)	3.49	S1C7S2N2N1 (dithiocarbazate) and C3C4C5C6 (ML)	18.64
S2C8S1N1N2 (dithiocarbazate) and C13O2O1(LA)	2.68	S1C7S2N2N1 (dithiocarbazate) and O1C2O2C1(ML)	77.62
S2C8S1N1N2 (dithiocarbazate) and C1C2C3C4C5C6C7 (benzyl)	78.54	S1C7S2N2N1 (dithiocarbazate) and C8C9C10C11C12C13C14 (benzyl)	72.71
C9C10C11C12 (LA) and C13O2O1(LA)	2.48	C3C4C5C6 (ML) and O1C2O2C1(ML)	74.43

Cu(SMML)₂ crystallized in the *C* 2/*c* space group as a centrosymmetric complex in which the two ligands were symmetrically related to each other and have the same bond angles and distances. The central copper atom was bis-chelated by the uninegatively charged bidentate ligand through the azomethine nitrogen atoms (N2) and thiolate sulfur atoms (S1). Both nitrogen and sulfur atoms in the two ligands are coordinated at the same position relative to each other. The sum of the four angles, N-Cu-S, S-Cu-S, S-Cu-N, and N-Cu-N, in the complex was 374.33° confirming significant deviation from the square-planar geometry about the copper ions. Neither the carbonylic nor hydroxylic oxygen of the methyl levulinate moiety participated in complexation. The conjugation system of the moieties was influenced by coordination with the metal as shown by slight lengthening of the N–N bond distance (1.407 Å). The bond lengths in the dithiocarbazate moiety that are expected to be most affected by coordination are azomethine C–N and C–S. The C1–S1 and C1–N1 bond lengths in the complex were 1.737 and 1.296 Å respectively. The C1–S1 distance was longer than that observed in the Schiff base, SMML, indicating single bond character as expected when complexation involves the ligand in its thiol form. The C1–N1 bond distances in the complex were also typical for double bonds in Schiff bases compounds clearly indicating that complexation involves deprotonation at N1.

(a)



(b)



(c)

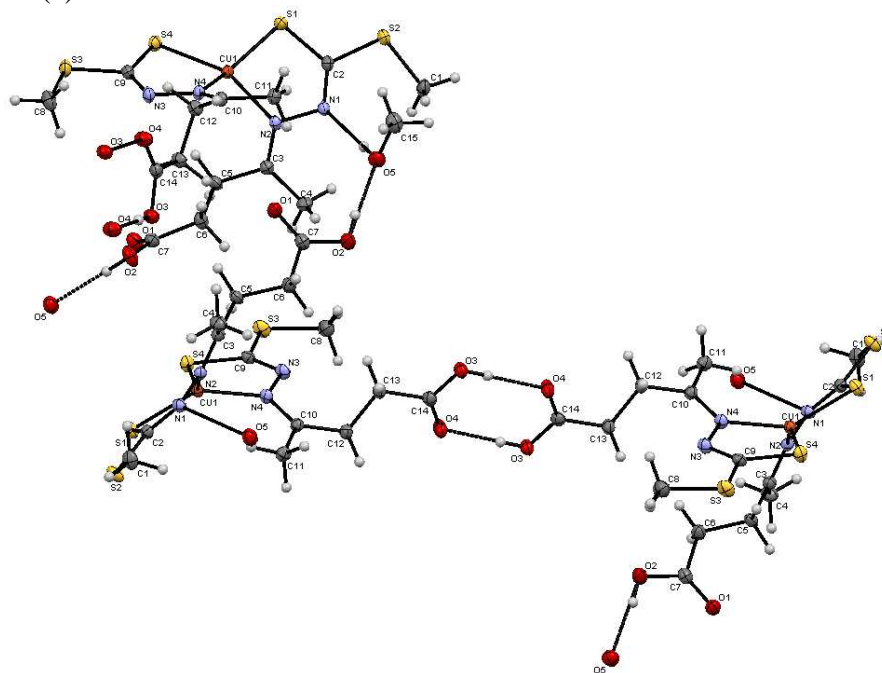


Figure 3.10. ORTEP diagrams of (a) Cu(SMML)₂ and (b) Cu(SMLA)₂ with intermolecular hydrogen bonds (shown as *dotted lines*) in (c). Ellipsoids are drawn at the 50% probability level.

Table 3.7. Selected bond lengths for Cu(SMML)₂ and Cu(SMLA)₂

Compound	Bond lengths (Å)				
	C=S	C-S	C-N	N-N	C=N
Cu(SMML) ₂	1.7366	1.7466	1.2958	1.4066	1.2962
Cu(SMLA) ₂	1.7423(1)	1.7372(1)	1.2987	1.4096(1)	1.2875(1)
	1.7420(1)	1.7469(1)	1.2861(1)	1.4099(1)	1.2873(1)
	N-Cu	N-Cu	S-Cu	S-Cu	
Cu(SMML) ₂	2.0109	2.0109	2.2195	2.2195	
Cu(SMLA) ₂	1.9898(1)	1.9912(1)	2.2356(1)	2.2287(1)	

Table 3.8. Selected bond angles for Cu(SMML)₂ and Cu(SMLA)₂

Bond angles (°)	Cu(SMML) ₂	Cu(SMLA) ₂
	S-Cu-N	86.15
N-Cu-N	106.43	102.28
N-Cu-S	86.15	85.89
S-Cu-S	95.60	107.38

Cu(SMLA)₂ crystallized in $P 2_1/n$ space group within an asymmetric unit in which two nonequivalent ligand molecules were present with one methanol molecule. Similar to Cu(SMML)₂, deprotonation of the ligand lead to tautomerization to the iminothiolate. While coordinating in the iminothiolate form, the negative charge generated on the sulfur atom was delocalized in the C=N-N=C chain as indicated by the intermediate C(2)-N(1) = (1.2987 and 1.2861(1) Å), N(1)-N(2) = (1.4096(1) and 1.4099(1) Å) and N(2)-C(3) = (1.2875(1) and 1.2873(1) Å) bond lengths. The lengthening of the C-S bond in the complex can be attributed to enethiolization. The 380.12° sum of angles around the Cu²⁺ ion in Cu(SMLA)₂ indicated that the complex was appreciably distorted from regular square-planar geometry. The Cu-S (2.2356(1) and 2.2287(1) Å) and Cu-N (1.9898(1) and 1.9912(1) Å) bond lengths are similar to those of the bis-chelated four coordinate copper(II) complex of the related isatin Schiff base of SMDTC (Manan et al., 2011b; Ali et al., 2008). The

difference between the bond lengths in the same complex can be ascribed to the constraints imposed by chelation. The packing for Cu(SMLA)₂ was also determined. In addition to the interactions between the (O3-H···O4) bond involving two neighbouring independent molecules similar to its free ligand SBLA, an extended network of hydrogen bonds involving the crystallized methanol molecule and the other ligand in Cu(SMLA)₂ that was closed to the solvent molecule was also observed. The linkage involved the hydroxylic oxygen atom (O2) of one complex molecule, the alcoholic oxygen atom (O3) of methanol and the uncoordinated azomethine nitrogen atom (N1) from another complex molecule. The continuous hydrogen bond networks developed were (O2–H2···O5, 2.655 Å) and (O5–H5···N1, 2.854 Å). As a consequence of these H-bond systems, the two ligands were not planar in the portion involved in metal coordination and the terminal chains with the carboxylic group which bridged the adjacent molecule were fairly distorted as can be seen from the dihedral angles involving the levulinic acid moiety (84.78° for C3–C4–C5 and C6–C7–O1–O2, 89.31° for C10–C11–C12 and C13–C14–O4–O3). The presence of methanol in the lattice highlights the spatial effect in which the terminal chains with the carboxylic group were forced to align in parallel whereas in Cu(SMML)₂ the ester terminal chains were almost 180° from one another minimizing steric constraints. This explains the observation that Cu(SMLA)₂ was more distorted from square planar than Cu(SMML)₂.

The ORTEP diagram of Re₂(SBCM)₂ complex with atomic numbering scheme is shown in Figure 3.11. Selected bond lengths and bond angles are given in Tables 3.9 and 3.10. The complex crystallized in *P* 2₁/*c* space group with unit cell parameters a=14.7072(4), b=12.6588(3), c=12.1386(3) and α=90°, β=99.374(1)°, γ=90°. A

number of thiosemicarbazone complexes of Re(I) carbonyl compounds have been studied by X-ray diffraction (Carballo et al., 2002; Santos et al., 2004). However, to date, this is the first Re(I) tricarbonyl complex with a dithiocarbazate Schiff base ligand to have been characterized structurally by X-ray diffractometry. Crystallographic analysis of the complex $\text{Re}_2(\text{SBCM})_2$ in this work showed that the rhenium atom was octahedrally coordinated to (i) three carbonyl carbon atoms in *fac* arrangement, (ii) the N and S atoms of the deprotonated bidentate dithiocarbazate Schiff base ligand with 3-acetylcoumarin in which the metal forms a five-membered chelate ring and (iii) the sulfur atom of a neighbouring molecule that had replaced the chloride atom resulting in a centrosymmetric dimer. The Re-S-Re bridge (Re-S = 2.4669 (1) and 2.5565 (1) Å) was more asymmetric than Re complex (a) (data adopted from Carballa et al., 2002). Like Re complex (a), the planar Re_2S_2 diamond for $\text{Re}_2(\text{SBCM})_2$ in which the Re-Re distance was too long for any significant bonding interaction, had bond angles close to 90°. The three Re-C distances were close to one another with an average bond distance of 1.916 Å in the range shown by numerous other Re(I) complexes containing the $\text{Re}(\text{CO})_3^+$ core (Czerwieniec et al., 2005; Fuks et al., 2010). The Re-N (2.2002(1) Å), Re-S (2.4669(1) Å) and Re-S' (2.5565(1) Å) distances do not differ significantly from those determined for Re complex (a). Therefore, it can be concluded that in the dimeric $\text{Re}_2(\text{SBCM})_2$ complex the geometry around each Re center was slightly distorted octahedral. The C12-S1 was shorter (1.7755 Å) in this complex in comparison to (a), but it was longer than in most free dithiocarbazate Schiff bases (*ca* 1.6 Å) suggesting a predominantly thiol character upon complexation. This conclusion was reinforced by the observed shortening of N2-C12 (*ca*. 1.34 Å from the previous series in this work and 1.2638 Å in $\text{Re}_2(\text{SBCM})_2$). The configuration

around this latter bond was *Z* (because of the N1-S1 chelation to the rhenium) and the configuration with respect to C10-N1 was *E* ($C8C10N1N2 = 179.94$). The dihedral angle between the dithiocarbazate plane and the plane of the coumarin ring was 83.07° whereas the dithiocarbazate plane and the plane of benzyl ring were at 75.22° to one another. The experimentally found N1-Re-S1 bond angle was only 79.13° . Such deviation from the ideal value of 90° can be explained by the relatively strong tensions in the six-membered ring formed by the bidentate ligand and the Re(I) cation. It can be also seen that both C-Re-S axial angles are about 174° . The two CO molecules present in the equatorial plane form with Re(I) the angles 96.43° and 93.16° , respectively. There were also intermolecular interactions from the apical carbonyl oxygen from one molecule to the equatorial carbonyl oxygen and the uncoordinated nitrogen of the neighbouring molecule forming (O5-O3, 2.932 \AA and O5-N2, 2.906 \AA) bonds. It is plausible that the short distances were due to hydrogen bonding.

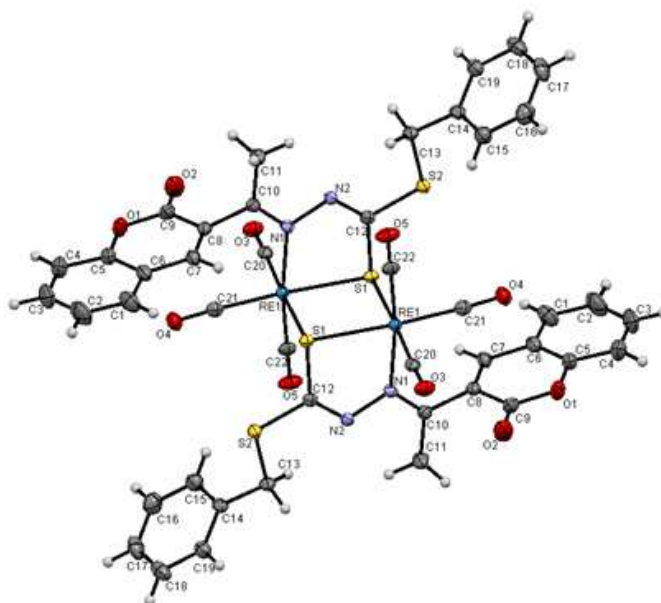


Figure 3.11. ORTEP diagram and intermolecular interactions (shown as *dotted red line*) for $\text{Re}_2(\text{SBCM})_2$. Ellipsoids are drawn at the 50% probability level.

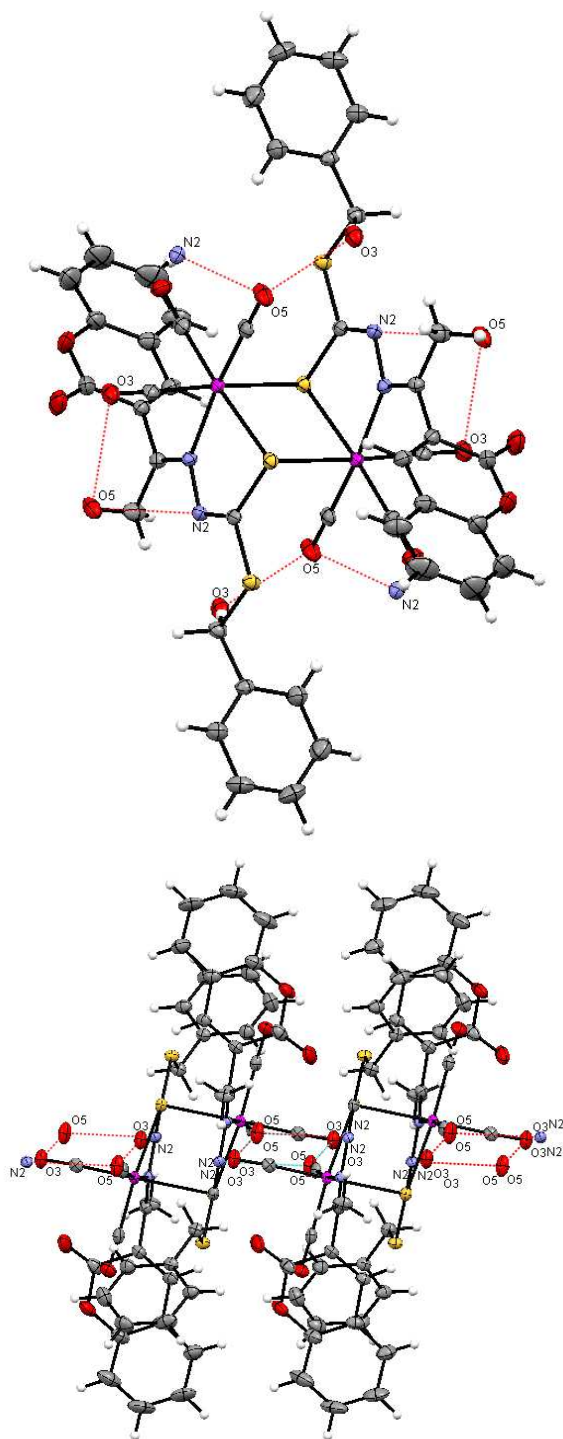


Figure 3.11 (continued). ORTEP diagram and intermolecular interactions (shown as *dotted red line*) for $\text{Re}_2(\text{SBCM})_2$. Ellipsoids are drawn at the 50% probability level.

Table 3.9. Main bond lengths (Å) and angles (°) in the coordination sphere around the rhenium atom.

Bond lengths	Re ₂ (SBCM) ₂	(a)	Bond angles	Re ₂ (SBCM) ₂	(a)
Re1-C20	1.9161	1.868(17)	C20-Re-C22	90.26	90.3(6)
Re1-C22	1.9185	1.924(13)	C20-Re-C21	88.8	88.7(6)
Re1-C21	1.9123	1.901(14)	C22-Re-C21	86.74	91.1(5)
Re-N	2.2002	2.210(9)	C20-Re-N	89.06	91.3(5)
Re-S	2.4669	2.465(3)	C22-Re-N	172.13	171.7(4)
Re-S	2.5565	2.537(4)	C21-Re-N	101.08	97.1(4)
Re-Re'	3.7830	3.794(11)	C20-Re-S	96.43	90.8(5)
C20-O3	1.1421	1.162(16)	C22-Re-S	93.16	94.1(4)
C22-O5	1.1416	1.135(14)	C21-Re-S	174.77	174.8(4)
C21-O4	1.1539	1.159(15)	N-Re-S	79.13	77.8(3)
Reference for compound (a): Data adopted from (Carbolla et al., 2002)			C20-Re-S'	175.62	172.0(4)
			C22-Re-S'	93.99	91.5(4)
			C21-Re-S'	92.5	99.0(5)
			N-Re-S'	86.58	85.8(3)
			S-Re-S'	82.29	81.34(12)
			Re-X-Re'	97.71	98.66(12)
			C12-S-Re	95.48	95.4(4)
			C10-N-Re	128.54	130.0(8)
			N2-N1-Re	118.98	116.4(7)

Table 3.10. Bond lengths (Å) and angles (°) in the dithiocarbazate fragments.

Bond lengths	Re ₂ (SBCM) ₂	Bond angles	Re ₂ (SBCM) ₂
S1-C12	1.7755	C12-N2-N1	116.70
S2-C12	1.7509	C10-N1-N2	111.83
N2-C12	1.2638	N2-C12-S2	119.94
N2-N1	1.4203	N2-C12-S1	127.24
N1-C10	1.2887	S1-C12-S2	112.78
C8-C10	1.4879	N1-C10-C8	120.79

3.3.3 Characterization of metal complexes in solution

3.3.3.1 NMR

The NMR spectra of ligands SMML (Figure 3.12), SMLA, SBML, SBLA and SBEL were recorded in CD₃OD whereas SM4CB, SB4CB (Figure 3.13), SBCM, SMHD, SBHD, Zn(SBCM)₂ and Re₂(SBCM)₂ were carried out in DMSO-d₆ due to their low solubility in CD₃OD at room temperature. The NH signal was not observed in any of the ¹H NMR spectra in CD₃OD due to fast exchange with solvent. However, the spectra illustrated the expected hydrogens for each compound. The S-methyl derivatives (SMML and SMLA) showed characteristic signals at *ca.* 2.52 ppm attributed to S-CH₃ while the S-benzyl derivatives (SBML, SBLA and SBEL) displayed distinct multiplets of their five aromatic protons and singlets of their S-CH₂ protons at *ca.* 7.40-7.17 ppm and 4.45 ppm, respectively. The proton signals for the two CH₂ groups of both levulinic acid and methyl levulinate were found to be identical at *ca.* 2.62 ppm whereas the -CH₃ group was at *ca.* 1.98 ppm. Other distinctive signals arising from the protons of the ester Schiff bases were observed at 3.66 ppm (-OCH₃ of SMML), 3.47 ppm (-OCH₃ of SBML) and 3.93 ppm in addition to 1.02 ppm (-OCH₂CH₃ of SBEL). The spectra of aromatic acid ligands SM4CB and SB4CB in DMSO-d₆ demonstrated signals at 8.29 ppm and 8.01-7.80 ppm attributed to -CH=N and aromatic hydrogens of 4-carboxybenzaldehyde moiety, respectively. Both ligands also showed characteristic signals of their S-substituted dithiocarbazate similar to those discussed above. The -NH (dithiocarbazate) signal of both SM4CB and SB4CB occurred at *ca.* 13 ppm whereas for SMHD and SBHD occurred at *ca.* 12.15 indicating the presence of thioimine NH. This signal and the absence of the C-SH signal at *ca.* 4 ppm indicated that in solution the thione tautomer remains as the predominant species (Roy et al., 2007).

The NH signals above 12 ppm indicate that the *Z*-configurational isomer is predominant (Rebolledo et al., 2005). The presence of -SC(=S)NH- at *ca.* 200 ppm in the ¹³C NMR spectra of all the Schiff bases indicated that the thione form predominates in solution. This signal was shifted downfield due to the deshielding effect of the neighbouring amine nitrogen and electronegative sulphur. The C=N signal appeared at *ca.* 156 ppm of the result of hydrazone bond formation when carbonyl compounds react with the *S*-substituted dithiocarbazate. The -S-CH₂ peak occurred upfield at *ca.* 40 ppm while the S-CH₃ peak was found at *ca.* 17 ppm. The aromatic carbons were observed at *ca.* 138 - 127 ppm as expected. The ¹H NMR spectrum of SBCM in DMSO-d₆ however showed double set of signals due to existence of SBCM in two isomeric forms. Such observation has been reported by Hunoor et al. (2010) with 3-acetylcoumarin-isonicotinoylhydrazone. The relative percentage of the two isomers was found to be 60% and 40%. The singlets at 12.56, 4.48 and 2.34 are assigned to -NH, -CH₂-S-, -CH₃ (3-acetylcoumarin), respectively. Overlapping signals from the coumarin and benzyl rings were observed in the aromatic region at 7.85-7.21 ppm. Upon complexation of SBCM with Zn(II) and Re(I), the hydrazone proton signal disappeared, which clearly indicates deprotonation of NH by enolisation. The downfield shift of methyl protons for both complexes further supports the coordination through azomethine nitrogen. The others protons in the ¹H NMR spectra of the complexes have not shown considerable change. Due the low solubility of the coumarin derivatives, it was impossible to record good ¹³C-NMR spectra.

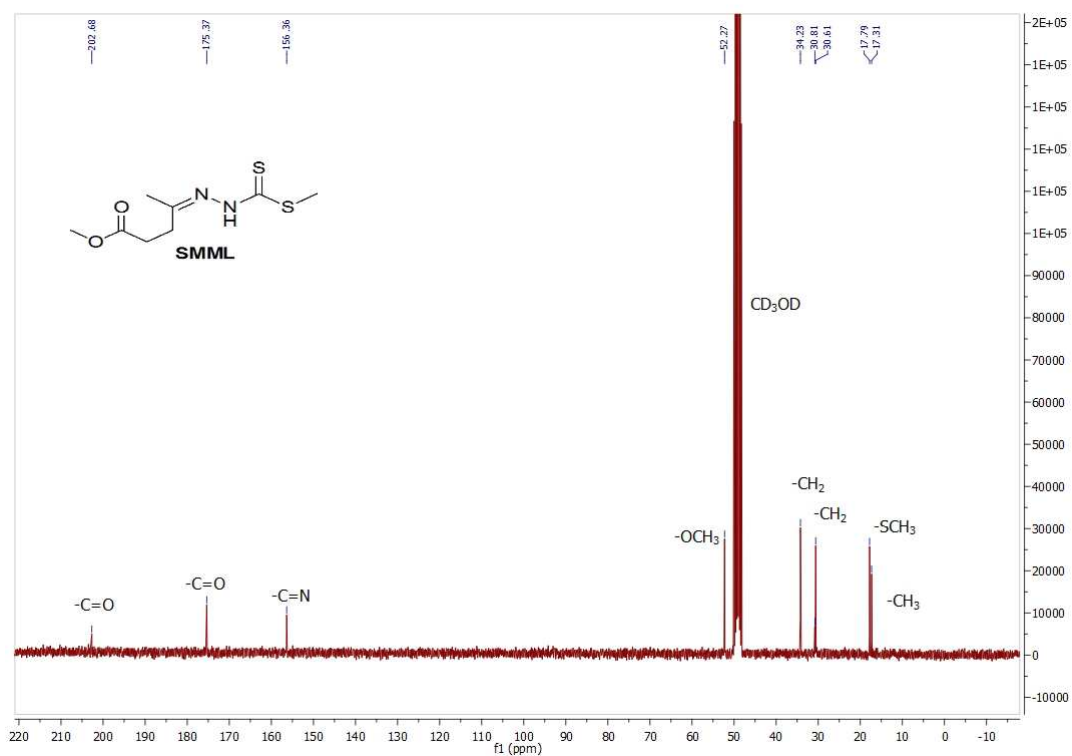
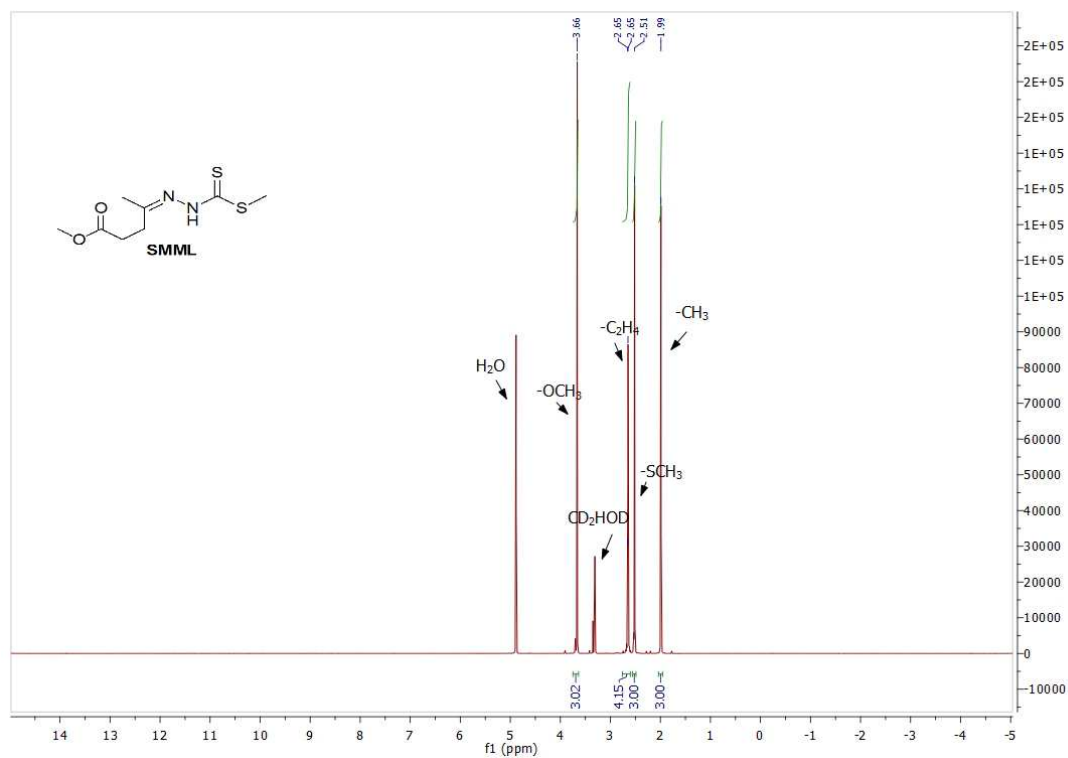


Figure 3.12. ^1H NMR and ^{13}C NMR spectra of SMML

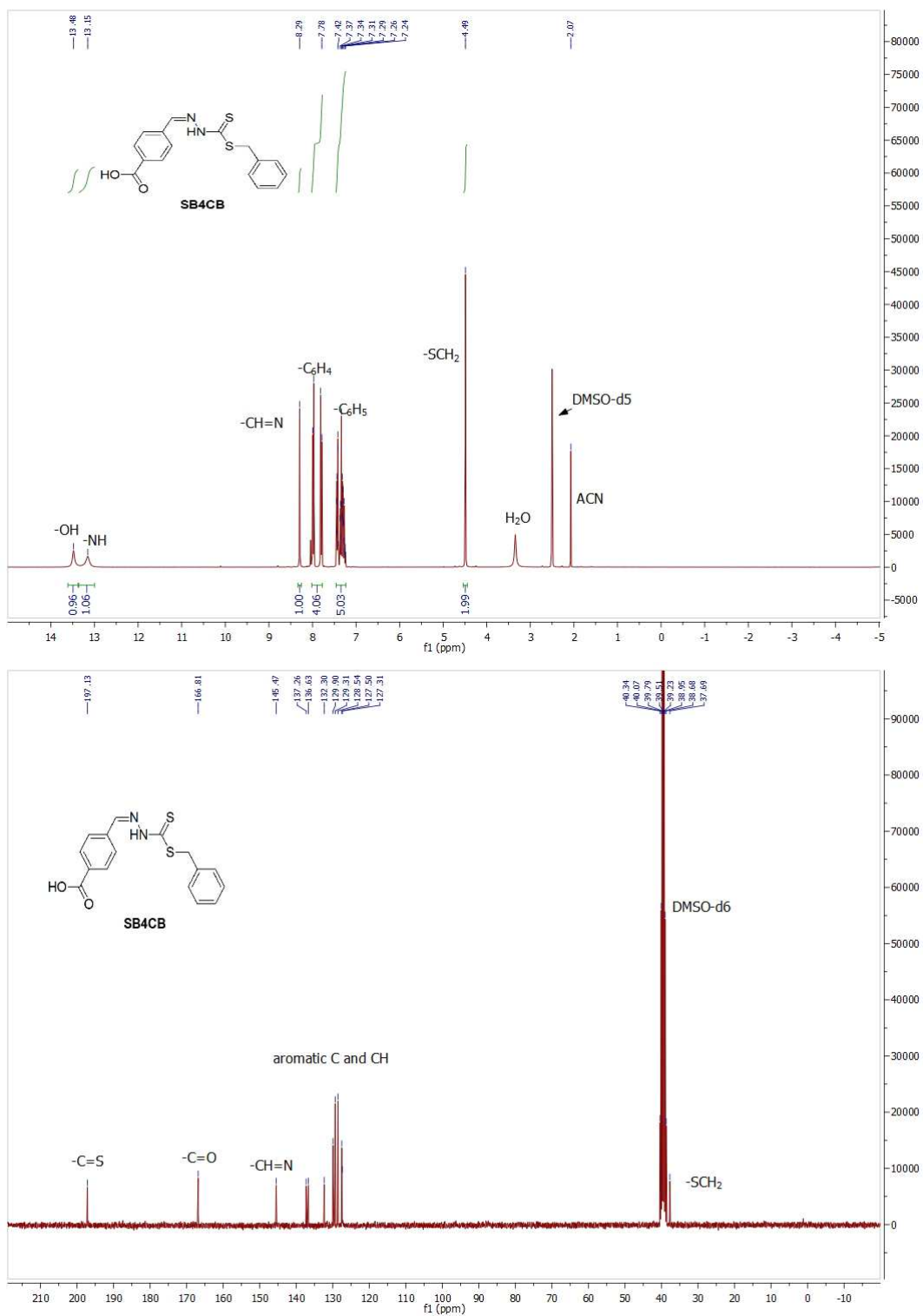


Figure 3.13. ¹H NMR and ¹³C NMR spectra of SB4CB

3.3.3.2 UV-VIS

Electronic spectra of all the metal complexes in DMSO were scanned in the region 200–800 nm at concentrations between 25 μ M and 1 mM. The electronic spectra of the Schiff bases showed two bands, from *ca.* 273 nm to 364 nm arising from $\pi \rightarrow \pi^*$ and $n \rightarrow \pi^*$ transitions. For all the metal complexes, the first band corresponding to the $\pi \rightarrow \pi^*$ (256–300 nm) transition is always observed, whereas the second intraligand band at higher wavelength (300–400 nm) ascribed to $n \rightarrow \pi^*$ band showed either a blue shift with a reduction of intensity or disappeared. This is due to donation of the lone pair of electrons to the metal and hence the coordination of the azomethine group (Latheef and Kurup, 2008). Most Cu(II) complexes with the exception of Cu(SM4CB)₂ and Cu(SB4CB)₂ showed the presence of ligand-to-metal charge transfer (LMCT) band (400–450 nm) arising from S \rightarrow M(II) interaction. Some spectra of the d⁹ Cu(II) complexes also revealed the presence of a broad d-d band at *ca.* 604 nm attributed to ${}^2B_{1g} \rightarrow {}^2A_{1g}$ for a distorted square planar environment around the copper(II) ion due to Jahn-Teller distortion (West et al., 1993; Nair and Joseyphus, 2008). There was a slight hypsochromic shift at 325 nm in the spectrum of the Re₂(SBCM)₂ complex whereas in the Zn(SBCM)₂ complex a slight bathochromic shift was seen at 292 nm. Two examples of the UV-Vis spectra each for tetradentate series and bidentate series are shown in Figure 3.14.

Cu(SM4CB)₂ and Cu(SB4CB)₂, however, showed neither the sulfur-to-copper LMCT band at 400 nm nor the d-d band. The absence of these bands even at high concentration (1 mM) suggests that the ligand does not have a suitable low-lying antibonding π^* orbital (Ali et al., 2001b). These two complexes showed a broad band spanning 300–400 nm with λ max at *ca.* 322 nm. The spectra of the complexes

were different from those of the free ligands that showed intra-ligand transitions at *ca.* 349 nm and 362 nm. The changes observed for the complexes were in agreement with the results of titration experiment carried out in both DMSO and 0.1M acetate buffer solution in order to ascertain the formation of the Cu(II) complexes with the proposed 1:2 metal to ligand stoichiometry. In these titration experiments, the changes in the UV-Vis spectra were obvious with an absorption band at 300-325 nm arising when the complex formed while the intensity of ligand band at $\lambda_{\text{max}} \approx 345$ nm decreased upon addition of Cu(OAc)₂. Complexation proceeded with a sharp endpoint at 0.5 equivalents with clear isosbestic points indicative of a single complexation event (Figure 3.15).

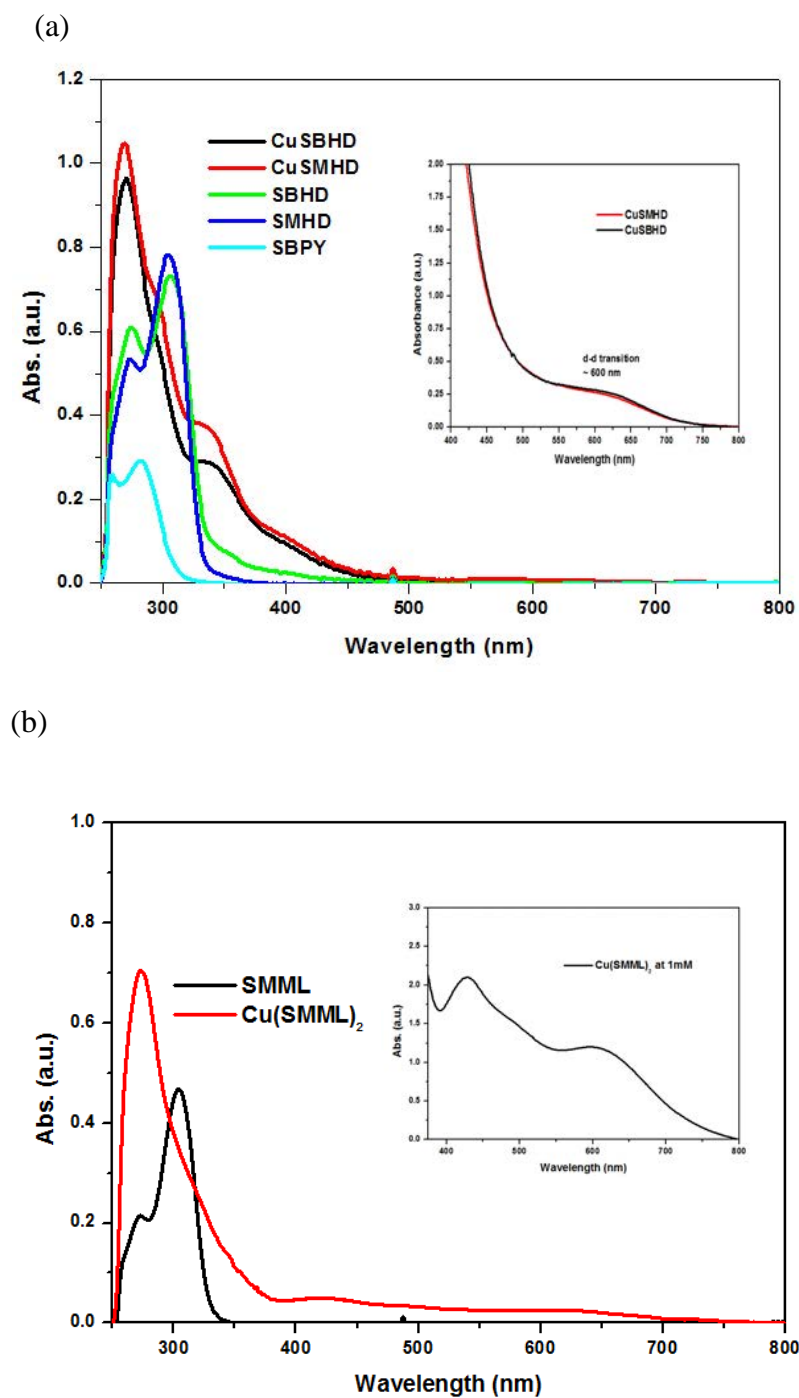


Figure 3.14. (a) UV-Vis spectra recorded for tetradentate series at 25 μM in DMSO using a cell length of 1 cm. The insert shows the d-d band of the two complexes at concentration of 1 mM. (b) UV-Vis spectra recorded for SMML and $\text{Cu}(\text{SMML})_2$ at 25 μM . Insert shows d-d band of the complex at 1 mM.

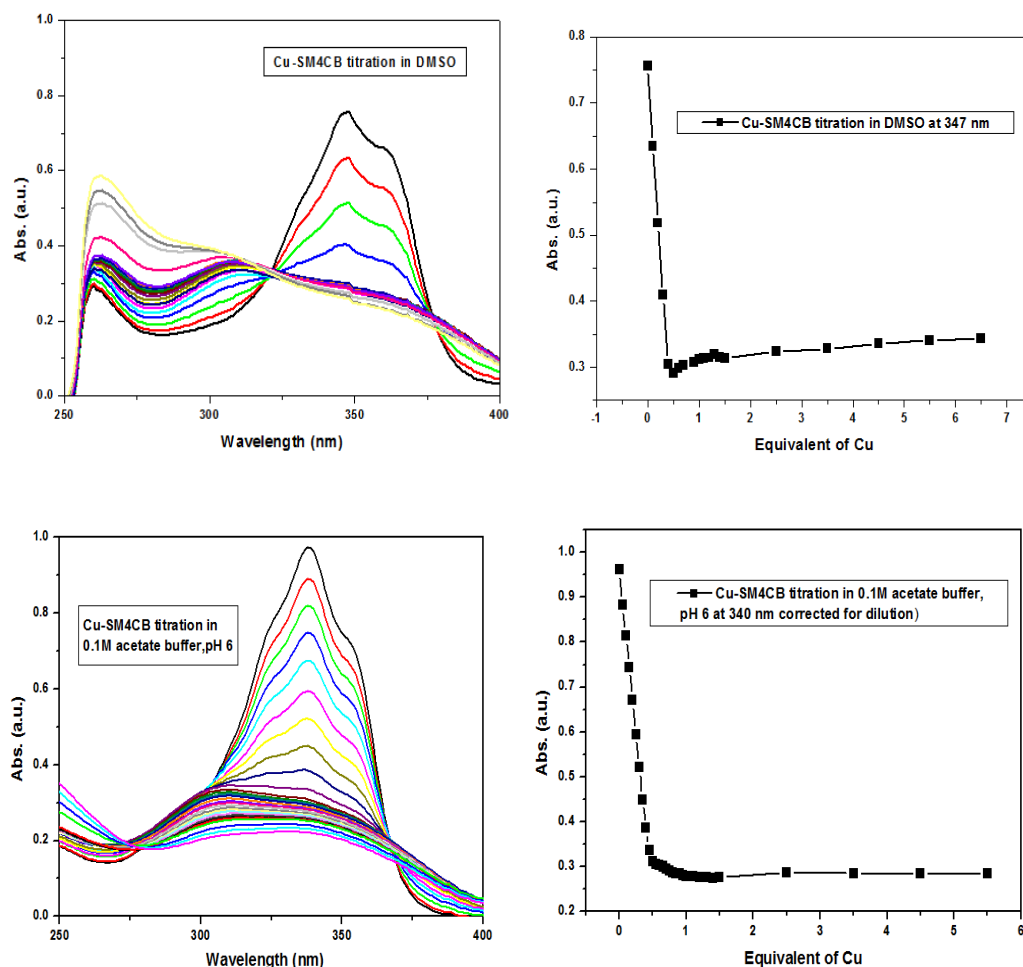


Figure 3.15. UV-Vis spectra obtained by addition of $\text{Cu}(\text{OAc})_2 \cdot \text{H}_2\text{O}$ at 25°C to a solution of SM4CB (*ca.* 2.5×10^{-5} M) in DMSO solution as well as in 0.1 M acetate buffer, pH6.

3.3.3.3 EPR

Examples of EPR spectra are shown in Figure 3.16. EPR parameters for all complexes are summarized in Table 3.11. Spectra of the frozen solutions for all tetradentate and bidentate Schiff base Cu(II) parent complexes in DMF showed the presence of one major species. They are typical of mononuclear d^9 Cu(II) complexes with axial symmetry and distorted square planar geometry with the unpaired electrons lying mainly in the $d_x^2-d_y^2$. The spectra also exhibited partially resolved superhyperfine features. The g_{\parallel} values for all the complexes are similar to those previously reported for $\text{Cu}(\text{II})\text{N}_2\text{S}_2$ complexes (Jasinski et al., 2003; Diaz et al.,

1998; Hueting et al., 2010). It has been reported that g_{\parallel} higher than 2.3 are indicative of a predominantly ionic character for metal-ligand bonds, whereas g_{\parallel} smaller than 2.3 reveal metal-ligand bonds with predominantly covalent character, which was the case here. In addition, the relatively small g_{\parallel} value (g_{\parallel} near 2.20) suggested a strong nitrogen character in the singly occupied molecular orbital (Kivelson and Neiman, 2004; Chikate et al., 2005). EPR spectroscopy is sensitive to angular distortions at the Cu(II) centre, particularly those involving distortions from planar to tetrahedral geometry. As a general rule, distortion from planar towards tetrahedral geometry results in a decrease in A_{\parallel} and an increase in g_{\parallel} (Ali et al., 2005). The empirical factor f ($= g_{\parallel}/A_{\parallel}$) (Joseph et al., 2012; Krishna et al., 2008) is a measure of deviation from idealized geometry. Its value ranges between 105 and 135 cm for square planar complexes, depending on the nature of coordinated atoms, while for a structure distorted toward the tetrahedron the values can be much larger and values from 160 to 242 cm suggest a moderate to considerable distortion in the geometry. For macroacyclic Cu(II) complexes, CuSBHD reflects only a slightly higher degree of tetrahedral distortion compared with CuSMHD in solution but both complexes appear close to square planar geometry. They are however less planar than other reported C-C backbone analogues most likely due to the extension of carbon backbone (Jasinski et al., 2003; Diaz et al., 1998; Hueting et al., 2010). In the bidentate series, the complexes with aliphatic acid or ester substituents (Cu(SMML)₂, Cu(SMLA)₂, Cu(SBML)₂ and Cu(SBLA)₂) were more distorted (with f values at *ca.* 147 cm) than those with aromatic acid or coumarin substituents (Cu(SM4CB)₂ and Cu(SB4CB)₂ at *ca.* 125 cm; Cu(SBCM)₂ at $f = 135$ cm), which are within the perfect range for square planar complexes. Finally, molecular orbital

coefficient α^2 (in-plane σ -bonding) was calculated using the equations below (Rapheal et al., 2007; Chandra and Sangeetika, 2004) :

$$\alpha^2 = (A_{\parallel}/0.036) + (g_{\parallel} - 2.0036) + 3/7(g_{\perp} - 2.0036) + 0.04$$

The α^2 value of 0.5 indicates complete covalent bonding, while 1.0 suggests complete ionic bonding. The observed values between 0.61 and 0.70 for all series indicated that these copper complexes have some covalent character as suggested above.

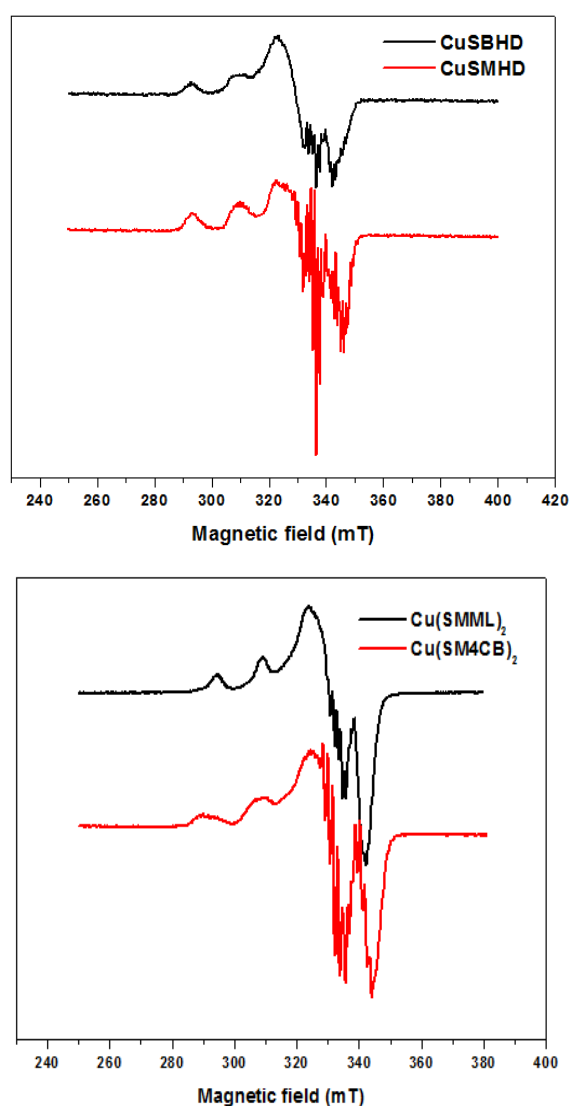


Figure 3.16. The EPR spectrum of CuSMHD, CuSBHD, Cu(SMML)₂ and Cu(SM4CB)₂ at 1 mM in frozen DMF. Microwave frequency 9.50 GHz, microwave power 0.25 mW, modulation amplitude 0.2 mT, modulation frequency 100 kHz, time constant 164 ms, T=50 K.

Table 3.11. EPR parameters measured from the spectra of the copper(II) complexes.

Compound	g_{\parallel}	g_{\perp}	A_{\parallel} ^[a]	f ^[b]	α^2
CuSMHD	2.15	2.06	460 (153)	141	0.64
CuSBHD	2.16	2.06	451 (150)	143	0.64
Cu(SMML) ₂	2.15	2.05	438 (146)	147	0.61
Cu(SMLA) ₂	2.15	2.06	438 (146)	147	0.62
Cu(SBML) ₂	2.15	2.05	438 (146)	147	0.61
Cu(SBLA) ₂	2.15	2.05	443 (148)	145	0.61
Cu(SM4CB) ₂	2.15	2.05	504 (168)	128	0.67
Cu(SB4CB) ₂	2.15	2.05	531 (177)	121	0.70
Cu(SBCM) ₂	2.15	2.05	478 (159)	135	0.65

[a] Unit in MHz, in bracket = $A_{\parallel} \times 10^{-4} \text{ cm}^{-1}$ [b] Unit in cm.

The spectra in DMF (see Appendices) for all Cu(II) parent complexes also show the presence of an additional minor component. Because of their lability, the bidentate Schiff base Cu(II) complexes may exhibit different solution and solid state structures (Jansson et al., 2010). In particular, *transoid* or *cisoid* ligands conformation (Figure 3.17) with respect to the central metal-coordinated rings may exist for such complexes in an open chained system (Beshir et al., 2008; Blumberg and Peisach, 2003; Da Silva et al., 1999).

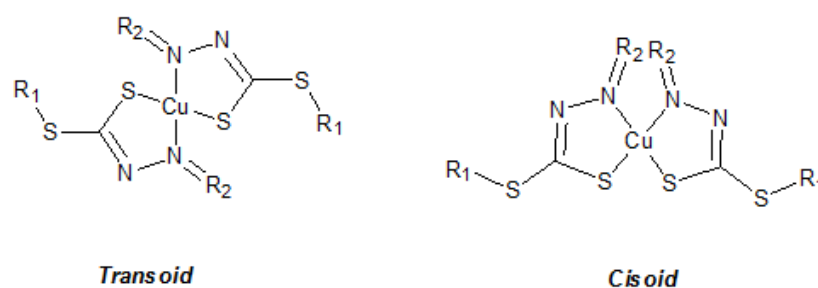


Figure 3.17. *Transoid* and *cisoid* ligands conformation.

The aliphatic acid or ester substituted parent compounds Cu(SMML)₂, Cu(SBML)₂, Cu(SMLA)₂ and Cu(SBLA)₂ demonstrated that the g_{\parallel} region for the minor species shifted further to the left of the magnetic field whereas for aromatic Cu(SM4CB)₂

and $\text{Cu}(\text{SB4CB})_2$, the presence of the minor species was further to the right of the magnetic field relative to the dominant species. Although there is no evidence to make a definitive assignment, single crystals of both $\text{Cu}(\text{SMML})_2$ and $\text{Cu}(\text{SMLA})_2$ were determined by X-ray diffraction to adopt *cisoid* orientation. It can be argued that the predominant orientation in the solid may be indicative of an energetically preferred state in solution. Thus, the observation may serve as an indirect indication that the *cisoid* orientation is more favourable in aliphatic Cu(II) complexes and can be tentatively assigned as the major species. The difference observed in the aromatic series $\text{Cu}(\text{SM4CB})_2$ and $\text{Cu}(\text{SB4CB})_2$ could point toward that both compounds have stronger preference for a *transoid* conformation since the *cisoid* structure will result in more steric hindrance especially with the presence of the aromatic ring. This ordering of the structures is also consistent with the interpretation of EPR results that the mainly *transoid* $\text{Cu}(\text{SM4CB})_2$ and $\text{Cu}(\text{SB4CB})_2$ were more planar as compared to their aliphatic counterparts as indicated by the f values. This proposal is also in agreement with the LC-MS results for the Cu(II)-bioconjugate in this work that showed two peaks with the same mass.

Other possibilities that can also be taken into account are previous findings that reported partial dissociation of CuL_2 upon dissolution to afford the corresponding 1:1 Cu/ligand complexes (Jansson et al., 2010; Diaz et al., 1998; Pogni et al., 2000). The observed EPR spectra of the complexes could be a composite of the 1:2 and 1:1 Cu/ligand complexes. In the case for 1:1 complex, DMF solvent molecules (also O-donors) are expected to participate in coordination to form $\text{CuL}(\text{DMF})_2$ complex. Assuming that the minor species is a 1:1 and the dominant species is 1:2, the $g//$ region for 1:1 should shift further to the left of the magnetic field (Faller et al.,

2012). This was observed only for compound $\text{Cu}(\text{SMML})_2$, $\text{Cu}(\text{SBML})_2$, $\text{Cu}(\text{SMLA})_2$ and $\text{Cu}(\text{SBLA})_2$. In addition, solvent molecules are known to be able to alter the geometry of the $\text{Cu}(\text{II})$ complexes although their coordination is weak (Umamaheswari et al., 2014). Thus, water or an DMF molecule could potentially coordinate in the apical position of the $\text{Cu}(\text{II})$ complexes giving rise to a penta-coordinated compound with rhombic symmetry. The spectra of conjugated complexes $\text{Cu}(\text{R1-SB4CB})_2$ and $\text{Cu}(\text{R9-SB4CB})_2$ in aqueous solution revealed the minor species observed in pure DMF as the dominant species (Figure 3.18 and 3.19). However, this analogy is not definitive as the observation could only be the result of solvent effect. Other hypotheses could involve the presence of $\text{Cu}(\text{II})$ -DMF complex although this can in fact be ruled out in this instance since the free Cu^{2+} species in DMF did not match the parent compounds. Figure 3.20 illustrates possible representation of the $\text{Cu}(\text{II})$ complexes that could exist in solution.

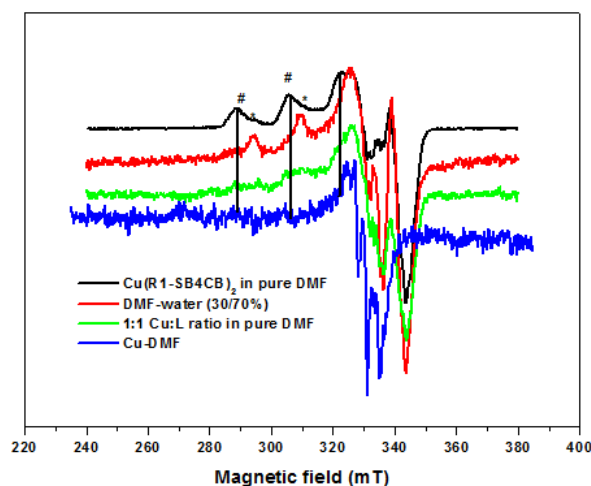


Figure 3.18. The EPR spectrum of $\text{Cu}(\text{R1-SB4CB})_2$ at 1 mM in various solvents. #: major species, *: minor species.

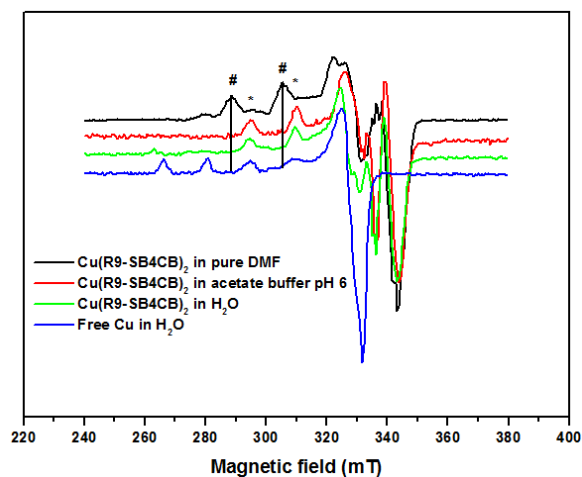


Figure 3.19. The EPR spectrum of $\text{Cu}(\text{R9-SB4CB})_2$ at 1 mM in various solvents. #: major species, *: minor species.

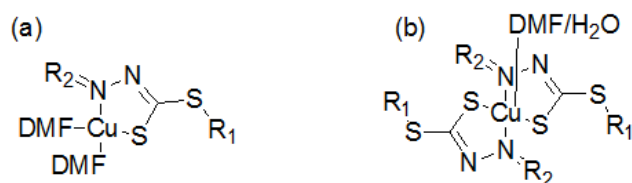


Figure 3.20. The different possible species of the $\text{Cu}(\text{II})$ complexes that could exist in solution.

3.3.3.4 Electrochemistry

As redox properties have been linked to bioactivity (i.e. SOD and anticancer properties) of metal complexes (Ďuračková et al., 1999; Jansson et al., 2010) and in order to gain a better understanding of the influence of different functional group have on the electronic properties of coordinated metal centers, the electrochemical properties of the various $\text{Cu}(\text{II})$ complexes were described herein. Figure 3.21 and Table 3.12 show the profile of the $\text{Cu}(\text{II})$ complexes obtained with SMHD and SBHD at a scan rate of 100 mVs^{-1} . Both complexes undergo an electrochemically irreversible one-electron reduction at $E_{\text{pc}} = -0.328$ and $-0.285 \text{ V}/(\text{Ag}/\text{AgCl})$ and standard $\text{Fc}/\text{Fc}^+ = 0.56 \text{ V}$), respectively, coupled with an oxidation at $E_{\text{pa}} = 0.069$ and $0.129 \text{ V}/(\text{Ag}/\text{AgCl})$. These waves can be assigned to the irreversible

oxidation/reduction wave for Cu(II)/Cu(I) (Paterson et al., 2010). The redox properties of the ligands were also investigated but they were found to be innocent. The irreversible nature of the copper-centered redox waves in the present study differed from the analogues CuATSM and CuAATSM (Blower et al., 2003; Cowley et al., 2004) previously reported to demonstrate quasi-reversible reduction. The loss of reversibility observed in this work is most likely related to the differences in geometry rearrangement of Cu(II)/Cu(I) ions in this ligand system that possesses two carbons between the two hydrazones functions. The Cu(II)/Cu(I) redox potentials of CuSMHD and CuSBHD are also more positive than the previous examples. The ease of deformation away from planarity seems to favour reduction. The differences in redox potential between CuSMHD and CuSBHD can also be due to changes in inductive effects of the substituents. Altering the terminal S-substituent (from methyl to benzyl) induces a weak effect on the Cu redox potentials which could be rationalized by a stronger electron-donating effect of the methyl group (Basha et al., 2012). The oxidation process at higher positive potential has previously been assigned to the copper(III/II) redox couple. It is interesting to note occurrence of an additional peak, which can be attributed to the reduction of a species produced by the second oxidation. However, the nature of this oxidized complex has not been determined.

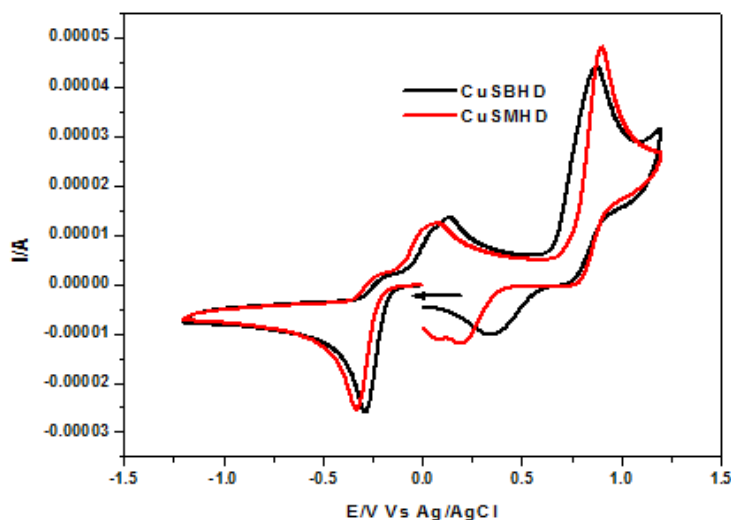


Figure 3.21. Cyclic voltammograms of the Cu complexes at 1.7 mM in anhydrous deoxygenated DMF containing 0.1 M tetrabutylammonium hexafluorophosphate as the supporting electrolyte. Working electrode: glassy carbon; counter electrode: Pt wire; reference electrode: Ag/AgCl, scan rate: 100 mV/s. All sweeps were initiated in the direction of the arrow.

Table 3.12. Electrochemical data for CuSMHD and CuSBHD versus Ag/AgCl.

	Cu(II)/Cu(I)		Cu(III)/Cu(II)	
	E_{pc}/V	E_{pa}/V	E_{pc}/V	E_{pa}/V
CuSMHD	-0.328	0.069	0.195	0.899
CuSBHD	-0.285	0.129	0.357	0.870

All bidentate parent compounds displayed qualitatively similar redox behaviour in the series, yet the characteristic one-electron Cu(II)/Cu(I) quasi reversible reduction waves were shifted depending on the ligand (Table 3.13). The measured reduction potentials clearly correlate with the electron-donating ability of the functional group and also the S-substituted dithiocarbazate. Similar to the previous tetradentate series, the S-methyl derivatives showed lower Cu(II)/Cu(I) reduction potential at $E_{pc} = -0.092$ to -0.114 V as compared to the S-benzyl derivatives at $E_{pc} = -0.021$ to -0.079

V. Among the functional groups the reduction potential towards the more negative can be arranged in the following order $\text{Cu}(\text{SMML})_2 < \text{Cu}(\text{SMLA})_2 < \text{Cu}(\text{SM4CB})_2$. Cyclic voltammograms were also recorded at different scan rates between 0.4 V and -0.4 V vs. Ag/AgCl from 0.02 V/s to 0.5V/s for all the compounds which showed similar trend. Taking $\text{Cu}(\text{SMML})_2$ as an example (Figure 3.22), the peak currents were still found to be proportional to scan rates with the peak currents ratio of the anodic signal and the cathodic signal (i_{pa}/i_{pc}) remained close to 1 (Table 3.14) independent of the sweep rate used indicating the reversibility and stability of the electrochemically generated product (Evans et al., 1983). Furthermore, when plotting the peak current as a function of the square root of the scan rate for reversible electron transfer, a linear correlation was found although not particularly perfect suggesting that the redox process is confined to the surface (Figure 3.23). However, another indicator of reversible electron transfer called the current function, whose values were given by $(i_p / v^{1/2})$ were not entirely constant anymore for all scan rates and the most obvious indication that the process was not completely reversible was the separation of anodic and cathodic peak potential. Inspection of the voltammetric data shows that at increasing scan rates, the reduction (E_{pc}) and oxidation (E_{pa}) peaks are shifted to more negative and positive values respectively. The separation between them, ΔE_p , exceeds the Nernstian requirement of 59 mV expected for a reversible one-electron process. For $\text{Cu}(\text{SMML})_2$, this value increases from $\Delta E_p = 78$ mV at 0.05 V/s to $\Delta E_p = 135$ mV at 5 V/s indicating a kinetic inhibition of the electron transfer process (dos Santos-Claro, 2005). This behavior cannot be attributed to some uncompensated solution resistance, as the internal standard Fc/Fc^+ couple, that shows rapid heterogeneous electron transfer in most of the solvents, gave a ΔE_p value of 51 mV (measured at $v = 0.1$ V/s). Thus,

any possible uncompensated resistance is sufficiently small so that the resulting voltage drops are negligible compared to the ΔE_p values attributable to kinetic effects (Parajón-Costa et al., 2004). Therefore the reaction of higher scan rates can be considered to be quasi-reversible and this quasi-reversibility associated with the reduction process probably arises as a consequence of a geometry change towards a distorted tetrahedral environment around the Cu(I) species

Table 3.13. Electrochemical data for the Cu(II) complexes vs Ag/AgCl at 0.1V

	Cu(II)/Cu(I)				i_{pa}/i_{pc}	Cu(II)
	E_{pa} [V]	E_{pc} [V]	$\Delta E_p = E_{pa} - E_{pc}$ [mV]	$\Delta E_{1/2} = 0.5 (E_{pa} + E_{pc})$ [V]		/Cu(III)
	E_{pa} [V]	E_{pc} [V]				E_{pa} [V]
Cu(SMML) ₂	0.002	-0.092	94	-0.045	1.00	1.000
Cu(SMLA) ₂	-0.014	-0.095	81	-0.055	0.60	0.998
Cu(SM4CB) ₂	-0.011	-0.114	103	-0.063	1.11	1.006
Cu(SBML) ₂	0.021	-0.066	87	-0.023	1.01	1.001
Cu(SBLA) ₂	0.008	-0.078	86	-0.035	0.84	0.985
Cu(SB4CB) ₂	0.015	-0.079	94	-0.032	0.88	1.029
Cu(SBCM) ₂	0.077	-0.021	98	0.028	1.19	0.973

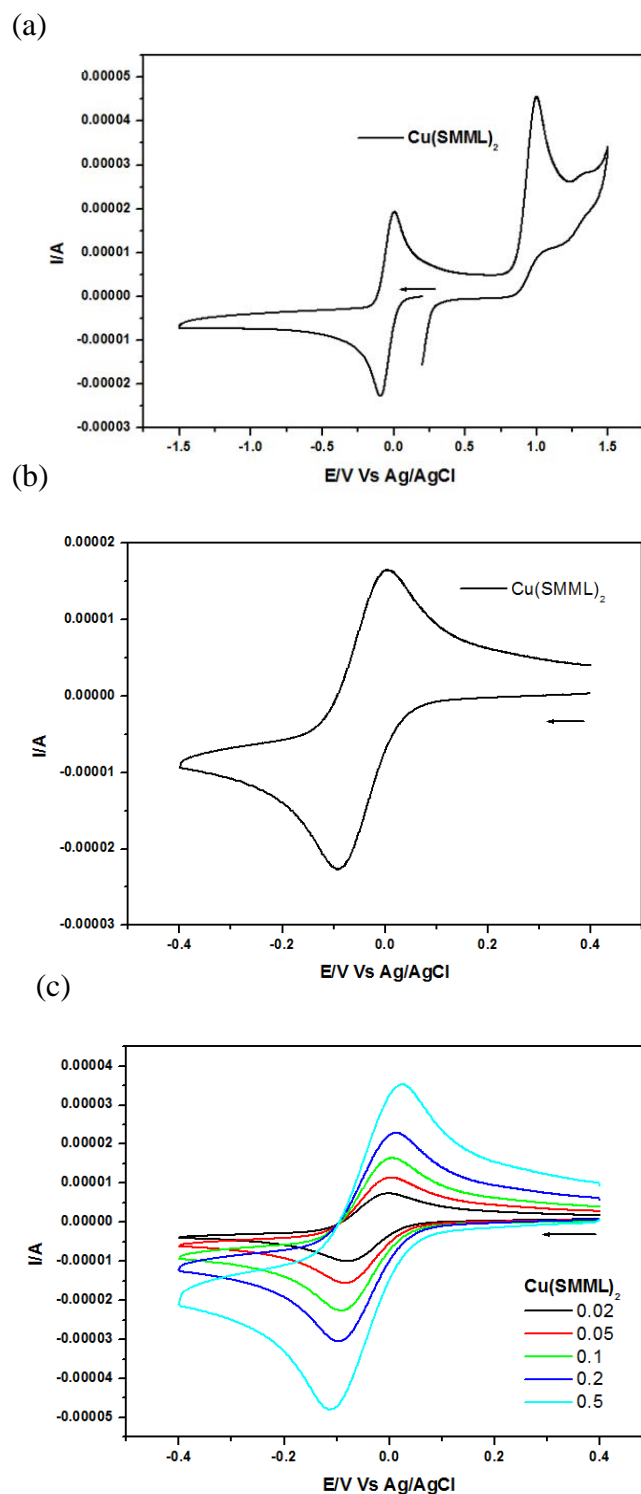


Figure 3.22. Cyclic voltammograms of the $\text{Cu}(\text{SMML})_2$ at 1.7 mM in anhydrous deoxygenated DMF containing 0.1 M tetrabutylammonium perchlorate as the supporting electrolyte. Working electrode: glassy carbon; counter electrode: Pt wire; reference electrode: Ag/AgCl. (a) and (b) Scan rate= 0.1 V/s. (c) Various scan rates= 0.02, 0.05, 0.1, 0.2, 0.5 V/s. All sweeps were initiated in the direction of the arrow.

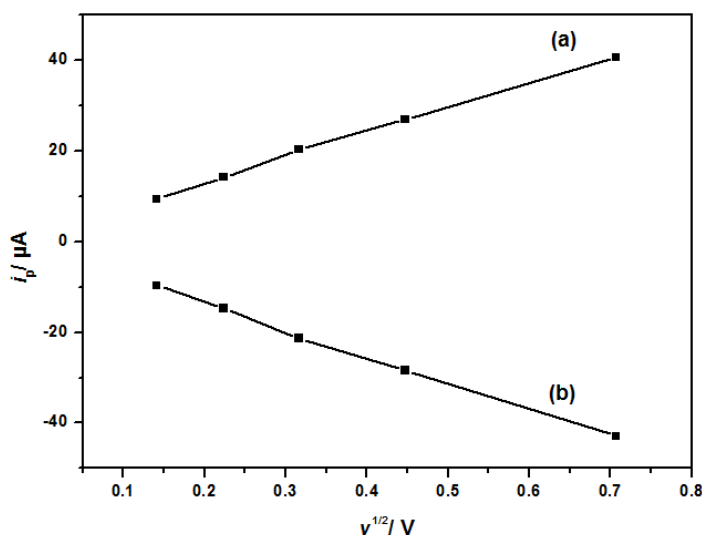


Figure 3.23. Plot of the anodic (I_{pa}) and cathodic (I_{pc}) current with the square root of scan rate for $Cu(SMML)_2$.

Table 3.14. Electrochemical data for the $Cu(SMML)$ vs $Ag/AgCl$ at various scan rate (V/s).

$Cu(SMML)_2$	Cu(II)/Cu(I)					i_a/i_c	$i_p / v^{1/2}$
	$E_{pa}[V]$	$E_{pc}[V]$	$\Delta E_p = E_{pa} - E_{pc}[mV]$	$\Delta E_{1/2} = 0.5 (E_{pa} + E_{pc}) [V]$			
0.02	-0.001	-0.079	78	-0.040	0.97	-68.32	
0.05	0.002	-0.085	87	-0.042	0.96	-65.87	
0.10	0.002	-0.092	94	-0.045	1.00	-67.45	
0.20	0.012	-0.097	109	-0.043	0.95	-63.50	
0.50	0.021	-0.114	135	-0.047	0.95	-60.61	

3.4 Conclusion

Two series of metal complexes (either macrocyclic or open chain) with dithiocarbamate Schiff base chelating ligands have been successfully synthesized and characterized. Although the Schiff bases derived from the keto-ester (methyl levulinate), keto-acid (levulinic acid and 4-carboxybenzaldehyde) and natural ketone derivative, 3-acetylcoumarin, contained O atoms that could potentially participate in coordination, the ligands behaved as bidentate NS ligands coordinating to the central metal through the azomethine nitrogen atom and the thiolate sulphur atom in all

complexes. Eleven structures of the compounds have been determined by single crystal X-ray crystallographic analysis. The ^1H , ^{13}C NMR and FTIR spectra of the Schiff bases indicated that the ligands retained the thione form in both solid state and solution. Only the ligand SBCM existed in both thione and thiolate form in solid state. RP-HPLC analysis of the free ligands showed that the aromatic ligands were more stable than the aliphatic ligands. Their stability was further improved upon complexation. Electronic and EPR spectra showed that most of the paramagnetic Cu(II) complexes had distorted square planar geometries with the exception of $\text{Cu}(\text{SB4CB})_2$, $\text{Cu}(\text{SM4CB})_2$ and $\text{Cu}(\text{SBCM})_2$ as demonstrated from their empirical factor f ($= g_{\parallel}/A_{\parallel}$). Cu(II) complexes with aliphatic acid and ester bidentate ligands (145-147 cm) confirm slightly higher degree of tetrahedral distortion than those with tetradentate ligands (141 and 143 cm) in solution. However, $\text{Cu}(\text{SM4CB})_2$, $\text{Cu}(\text{SB4CB})_2$ and $\text{Cu}(\text{SBCM})_2$ that possess aromatic acid or coumarin substituents ($\text{Cu}(\text{SM4CB})_2$ and $\text{Cu}(\text{SB4CB})_2$ at *ca.* 125 cm; $\text{Cu}(\text{SBCM})_2$ at $f = 135$ cm) are in the square planar range. The Re(I) and Zn(II) complexes were diamagnetic. There were also differences between the macroacyclic and open chain Cu(II) complexes with regard to their electrochemistry. The latter series showed Cu(II)/Cu(I) quasi reversibility at more positive potential whereas the former series was not reversible suggesting that the open chain Cu(II) complexes can accommodate Cu(I) more easily as a result of their flexibility. To sum up, this chapter demonstrated that by using a convergent synthesis strategy, a library of complexes with tune stabilities, geometries and electrochemical properties can be generated. In addition, the introduction of carboxylic acid functions opens the possibility to conjugate these complexes with vectors. The biological activities of all these compounds were evaluated and are discussed in Chapter 5.

CHAPTER 4

FUNCTIONALIZED COMPOUNDS

4.1 Introduction

4.1.1 Key drawbacks of metallodrugs

In the past years, much effort has been devoted to synthesis and testing of metal complexes in search of new metal metallodrugs for biological application. However, only a fraction of the thousands of tested metal compounds has entered clinical trials or has been approved worldwide with many challenging issues in terms of favorable selectivity, solubility, and stability as well as knowledge about their mode of action remaining unsolved (Fricker, 2007; Timerbaev et al., 2006).

The poor water solubility of many metal complexes is one of the key drawbacks “in the course of their analysis or application” (Miklán et al., 2007, p. 108). Studies in aqueous and buffer solutions are of utmost importance for an understanding of the mechanism of action of bioactive molecules and the design of stronger chelators (Milunovic et al., 2012). Such is the case for thiosemicarbazone derived Schiff base metal complexes (Enyedy et al., 2010; Raja et al., 2011). There is relatively few information that is available in the literature for these families of compounds as such investigations are often hampered by the low aqueous solubility of the compounds. There are also cases in which a high amount of DMSO is used to pre-dissolve the metal complexes in order to overcome their poor solubility in aqueous media during biological studies. However, the use of DMSO affects the reliability of the results obtained. DMSO has been shown to considerably retard the growth of fungi and cancerous cells and lead to bacteria and cell death at above certain concentrations

(Dolan et al., 2013; Ng et al., 2013). Therefore, compounds that are highly water-soluble are preferred for biological applications as they enable preclinical development of a drug candidate without the use of solubilizers (Bacher et al., 2013).

Apart from that, cell uptake and metal complex accumulation are also challenges for medicinal and bioinorganic chemistry. The efficient and rapid passage of metal complexes into cells remains a major hurdle in the design of potential therapeutic agents. A significant number of drug candidates and probe molecules fail because of insufficient cell uptake, requiring high quantities of drug administration, which often leads to undesirable side effects (Rijt et al., 2011) Only molecules in a narrow range of molecular weight and polarity are able to directly cross the plasma membrane by passive diffusion (Brunner and Barton, 2006). It is therefore critical to optimize the properties of their cellular uptake in the effort to develop potent and selective metal complexes as chemotherapeutic or diagnostic agents.

The capability to design and synthesize new molecules with tuned functions offers a powerful and efficacious way to overcome these shortcomings. Recently, new strategies have been developed in an attempt to maximize the impact of drugs on cancer cells and minimize the problem of adverse side effects through effective delivery of complexes with tumour-targeting properties and biologically-active ligands (Hambley, 2007; Storr et al., 2006; Thompson and Orvig, 2006; Thompson and Orvig, 2003). The use of multifunctional ligands that adequately bind metal ions and also include specific targeting features is an attractive choice which is gaining popularity today with applications at the forefront of all areas of medicinal inorganic

chemistry research. The field has benefited greatly from advances in targeted ligand design, which lead to the development of improved therapeutic agents (Ronconi and Sadler, 2007).

4.1.2 Conjugated metal complexes

By combining ligands or metal complexes with vectors, a large number of new bioconjugates with interesting biological properties can be prepared. An excellent review by Nils Metzler-Nolte (2010, p. 195) gives an overview of the use of peptides “as targeting vectors for the directed delivery of metal-based drugs or probes for biomedical investigations”. The numerous peptides that have been utilized “include neuropeptides (enkephalin, neuropeptide Y, neurotensin), uptake peptides (TAT and poly-Arg) and intracellular localization sequences”. These bioconjugates display biomedical applications in radiopharmaceutical, as anticancer and antibacterial drugs or targeted CO-releasing molecules as well as in biosensor applications.

4.1.2.1 Schiff base conjugate

As this work involves dithiocarbazate derivatives, the development of Schiff base metal complex bioconjugates from the family of nitrogen-sulphur donor ligands will be specifically highlighted (Donnelly, 2011; Paterson and Donnelly, 2011). To date, the concept of bifunctional ligands has been most successfully applied to radioimaging with Cu(II) bis(thiosemicarbazone) (Figure 4.1). Many new tetradentate bifunctional bis(thiosemicarbazone) chelators have been designed and conjugated to various vectors such as the tumor targeting bombesin derivative BBN(7-14)-NH₂ that has high affinity for gastrin-releasing peptide (GRP) receptors

(Paterson et al., 2010; Hueting et al., 2010), somatostatin derived octreotide that detects somatostatin-receptor-positive tumors (Cowley et al., 2007), pyrene fluorophore tags for cellular imaging (Lim et al., 2010) and water-soluble glucose derivatives (Holland et al., 2007) to name a few.

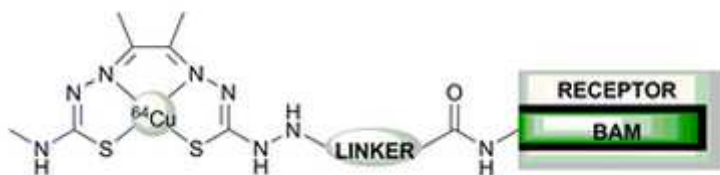


Figure 4.1. Schematic diagram of a functionalized bis(thiosemicarbazone) conjugated to a biologically active molecule (BAM) (Source: Hueting et al., 2010).

Conjugates of tridentate salicylaldehyde thiosemicarbazone (STSC) and 2-formylpyridine thiosemicarbazone (FTSC) coupled to a single amino acid of L- or D-proline (Pro) with good chelating properties and improved aqueous solubility have recently been reported (Milunovic et al., 2012; Bacher et al., 2013). As a result, various techniques have been used to conduct detailed studies on the stoichiometry and thermodynamic stability of metal ions with the Pro-TSC conjugates in a water/DMSO mixture. Most importantly, conjugation resulted in enhancement of their antiproliferative activity. While several studies exploring the multifunctional ligand-peptide conjugates concept using thiosemicarbazone derivatives have been highlighted, there are no reports of its application to dithiocarbamate analogues prior to this work. In the following parts, focus will be directed to polyethylene glycol (PEG) and cell penetrating peptides (CPPs) which are vectors used for conjugation in this work.

4.1.2.2 PEGylation

PEGylation describes the covalent modification of proteins, peptides, antibody fragments or non-peptide small drug molecules by attachment to one or more polyethylene glycol (PEG) chains. PEG is a non-toxic, non-immunogenic, non-antigenic polymer that is highly water soluble and has been approved by FDA. PEGylation is used as a well-recognized approach for drug delivery (Harris and Chess, 2003; Riley and Riggs-Sauthier, 2008; Veronese and Pasut, 2005). The introduction of PEG into pharmaceuticals improves their pharmacokinetics with “a prolonged residence in body, a decreased degradation by metabolic enzymes and a reduction or elimination of protein immunogenicity” (Veronese and Pasut, 2005, p 1451). There is an emerging interest in the use of metal-PEG complexes in biological studies (Stephan et al., 2005; Heldt et al., 2004) including work on the modification of cisplatin with PEG (Dhar et al., 2011; Ohya et al., 2001) as well as PEGylated iridium cyclometalated complexes that showed improved aqueous solubility and cell permeability (Li et al., 2010).

4.1.2.3 Cell penetrating peptide as cell delivery vectors

Crossing the plasma membrane is a challenge for some molecules with many potential drugs not displaying the required balance between lipophilicity and positive charge allowing for membrane permeability while supporting aqueous solubility. These limitations greatly prevent them from reaching their desired target in cellulo and results in the reduction of their therapeutics efficacy (Stewart et al., 2008). Others like polynucleic acids (PNAs) would not be able to penetrate into cells due to the presence of their high negative charge (Walrant et al., 2011). Over the past two decades, CPPs, also called “Trojan horse peptides”, have attracted

tremendous attention and found numerous applications in biology and medicine (Vives, 2005; Fonseca et al., 2009). CPPs are short peptides (5-30 amino acids)

capable of translocation through the cellular plasma membrane on their own or together with cargoes. They often contain basic amino acid side chains and are in many cases amphipathic. The first CPPs were derived from naturally occurring proteins such as TAT from HIV-TAT and penetratin from the *Antennapedia homeodomain* (Regberg et al., 2012, p. 991).

Subsequently, many new CPPs either protein-derived or synthetic derivatives have been produced and optimized as cell delivery agents (Regberg et al., 2012; Dietz and Bähr, 2004; Lundberg and Langel, 2003). Their unique ability to cross the plasma membrane and internalize in cells make them very powerful tools to revolutionize the transportation of a great variety of different substances ranging from small therapeutic drugs to large proteins and DNA (Figure 4.2).

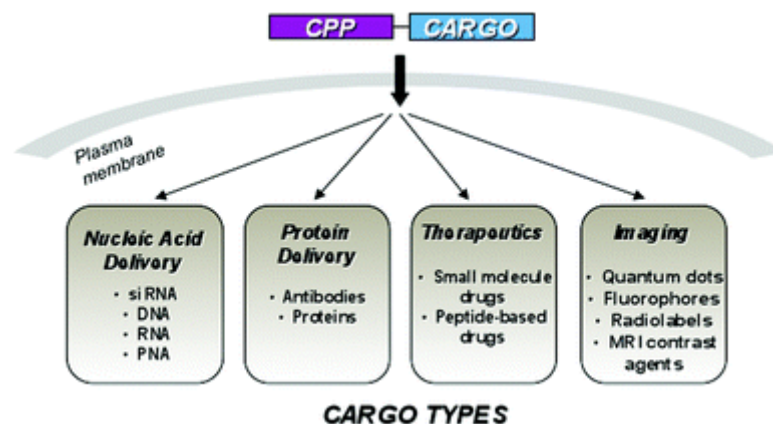


Figure 4.2. Applications of cell-penetrating peptides as molecular delivery vehicles (Source: Stewart et al., 2008).

The use of CPPs as molecular vehicles also offers a number of benefits over other delivery vectors which include lower toxicity and controlled administration. CPPs are obviously an excellent vector to transport various materials across the cell membrane and will continue to attract much interest for further exploration in the synthetic front (Figure 4.3) and prospective applications (Regberg et al., 2012).

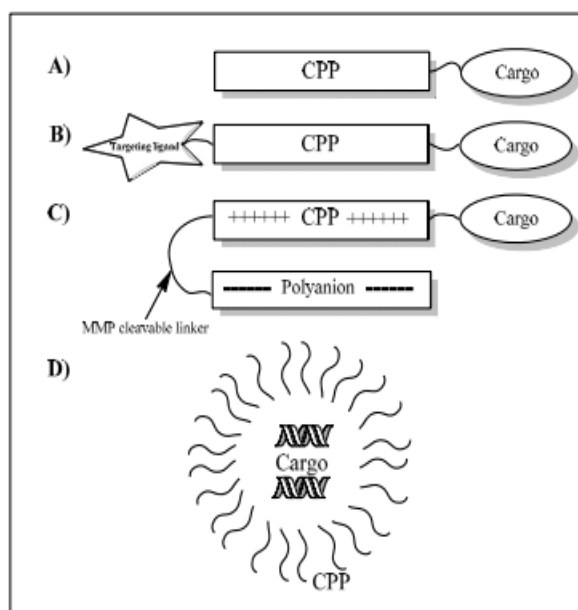


Figure 4.3. CPP loading and targeting strategies. (Source: Regberg et al., 2012)

(A) Covalent conjugation of CPP to cargo

(B) CPP coupled to targeting ligand and cargo

(C) Activatable CPP, after cleavage of the linker the peptide dissociates from the polyanion and becomes an active CPP

(D) Non-covalent complex of CPPs and cargo (oligonucleotides or other macromolecules) formed by electrostatic and hydrophobic interactions.

Among the CPPs, arginine-rich derivatives of human immunodeficiency virus-trans-activator of transcription (HIV-TAT) are the most studied. The importance of guanidinium-side chain of arginine (Arg) has been demonstrated. When the positively charged Arg groups were replaced with neutral alanine amino acids, it led to drastic reduction of cell uptake. Furthermore, polyarginine are known to penetrate cells more successfully than other polycationic peptides of equal length containing lysine, ornithine and histidine (Mitchell et al., 2000). High cell uptake for polyarginine were observed for chain lengths of 8 to 15 arginine residues with the optimum range being 7 to 9 (Wender et al., 2000) whereas chain lengths longer than 15 arginine residues were less efficient to cross the cell membrane (Miklan et al., 2007; Rijt et al., 2011; Brunner and Barton, 2006). Although polyarginine had efficiently delivered diverse conjugated proteins and peptides, only limited reports are available on its capacity to enhance delivery of metallodrugs. For instance, a great increase in nuclear accumulation has been observed by Barton and coworkers

(Brunner and Barton, 2006; Puckett and Barton, 2009) for rhodium and ruthenium-octaarginine conjugates that target DNA mismatches. Dolan et al. (2013) described the very water soluble iridium polyarginine conjugate that displayed a doubling of increase cytotoxicity with a decrease in IC_{50} values as compared to the parent complex. The conjugate significantly accumulated in the nucleus whereas the parent did not. A few prominent papers have established the influence of the peptide chain length on bioactivity. For instance, Rijt et al. (2011) showed that the

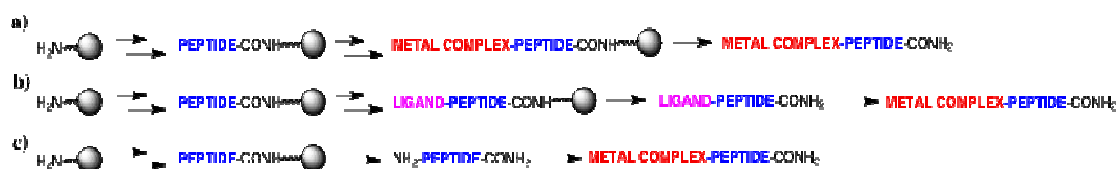
there is a correlation between longer arginine chain length and cell uptake, nuclear uptake, DNA binding, and cytotoxicity of the osmium conjugates in the following order: eight arginine residues \gg five arginine residues $>$ one arginine \sim unfunctionalized.

As will be discussed in Chapter 5, antimicrobial evaluation of non-conjugated copper(II) complexes exhibit promising biological activities but suffer from low water solubility and poor membrane permeability across bacteria. The molecular design strategy employed to circumvent these main drawbacks as well as the synthetic efforts made to prepare complexes with enhanced bioactivity will be presented herein.

4.1.2.4 Design of the metal complex-peptide conjugates

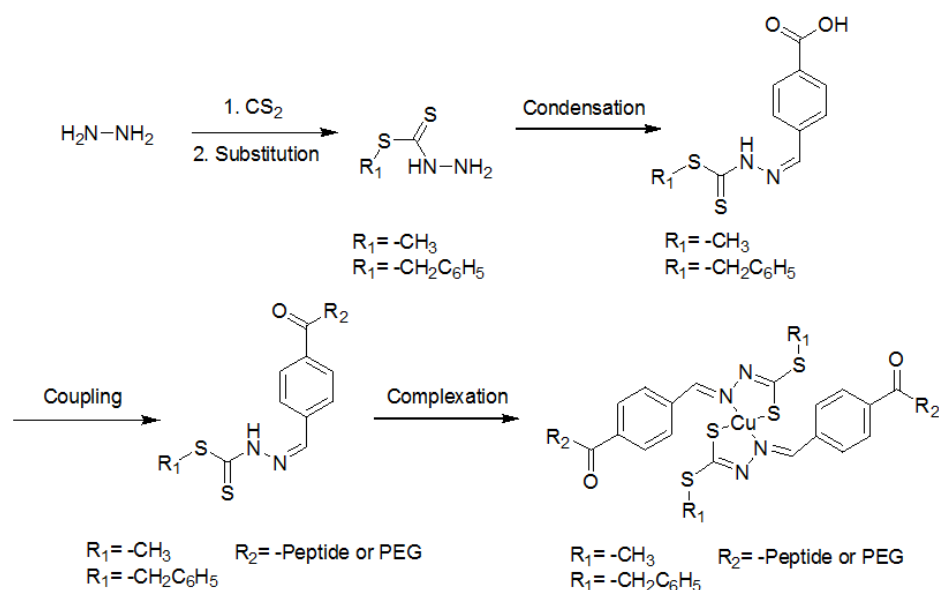
There are several strategies available to prepare metal complex-peptide conjugates (Metzler-Nolte, 2010; Splith et al., 2010; Dirscherl and Koenig, 2008; Heinze et al., 2008; Kirin et al., 2005; Liolios et al., 2012; Dirscherl et al., 2007) (Scheme 4.1). The most common is to couple the metal complex during solid-phase peptide synthesis (SPPS) while the peptide is still retained on the resin (Scheme 4.1a). This method carries the benefit of advantages from SPPS of convenient, flexible incorporation of metal complexes at any position of the amino acid sequence, high

yield and high purity of the conjugates providing the compound is stable enough to survive all SPPS manipulations. Alternatively, the peptide-ligand can be synthesized first via SPPS followed by in situ solution complexation with metal ions (Scheme 4.1b). The other is to attach the metal complexes in solution after the peptide synthesis has been completed on the resin, cleaved and purified (Scheme 4.1c). The post-labeling second and third options are definitely preferable for metal-complexes (option b) or ligands (option c) that are sensitive towards SPPS conditions. These two strategies prevent demetallation and decomposition of the metal complexes.



Scheme 4.1. Strategies to prepare metal complex conjugated with peptides.

To generate the copper complexes in this work, the strategy based on Scheme 4.1b with bidentate ligands was employed as shown below (Scheme 4.2). To allow the conjugation of the complexes with various vectors (PEG, peptides), the presence of a reactive function in the ligand structure is required. Among the orthogonal reactive functions, carboxylic acid has been chosen since it is an easy-to-handle group that can react with the terminal amine function of the peptides and the PEG derivative. Table 4.1 summarized the conjugates that were synthesized and characterized in this work.



Scheme 4.2. Synthetic pathway for the synthesis of the functionalized copper complexes.

Table 4.1. Selected ligands and their Cu(II) complexes conjugates that were synthesized and studied.

	R ₁	R ₂	Compounds abbreviation	Cu(II) complexes abbreviation
Parent compound	-CH ₂ C ₆ H ₅	-OH	SB4CB	Cu(SB4CB) ₂
Conjugates	-CH ₂ C ₆ H ₅	-NH-(EtO) ₂ -CH ₂ CONH ₂	PEG-SB4CB	Cu(PEG-SB4CB) ₂
	-CH ₂ C ₆ H ₅	-NH-R-CONH ₂	R1-SB4CB	Cu(R1-SB4CB) ₂
	-CH ₂ C ₆ H ₅	-NH-R4-CONH ₂	R4-SB4CB	Cu(R4-SB4CB) ₂
	-CH ₂ C ₆ H ₅	-NH-R9-CONH ₂	R9-SB4CB	Cu(R9-SB4CB) ₂
	-CH ₂ C ₆ H ₅	-NH-RW9-CONH ₂	RW9-SB4CB	Cu(RW9-SB4CB) ₂
	-CH ₂ C ₆ H ₅	-NH-FR-CONH-Naphth.	PAβN-SB4CB	Cu(PAβN-SB4CB) ₂
Parent compound	-CH ₃	-OH	SM4CB	Cu(SM4CB) ₂
Conjugates	-CH ₃	-NH-R9-CONH ₂	R9-SM4CB	Cu(R9-SM4CB) ₂
	-CH ₃	-NH-RW9-CONH ₂	RW9-SM4CB	Cu(RW9-SM4CB) ₂

Note: R is the one letter nomenclature for arginine and RW9 corresponds to the sequence RRWRRWRR in which W is tryptophan. F is phenylalanine. Naphth. is naphthylamide.

In this strategy, symmetrical ligands are involved leading to complexes bearing two functionalizing groups. Since most of the conjugation work in the literature focuses on tetradentate bis(thiosemicarbazones) containing only a single targeting agent (for

radiopharmaceutical purposes), having two functional groups may or may not produce the desired results. In fact, in some instances, it could be counterproductive as this can further compromise the pharmacokinetics. On the other hand, this bivalent approach could also impart higher affinity and selectivity. Ma et al. (2011) described the preparation of ligands with two carboxylate functional groups that bear two tumor-targeting peptides. The presence of dimeric CPPs in ligands (Hoyer et al., 2012) and Pt complexes (Abramkin et al., 2012) have been reported to dramatically improve their capacity to enter various cells increasing their cytotoxicity potential.

A complex having a PEG was first designed to increase the water solubility. PEG is a neutral water solubilizing agent that does not show any antimicrobial activity. Therefore it was to be anticipated that this conjugation would highlight only the bioactivity of the complex itself, while enhancing its water solubility. In addition, PEG functionalized with carboxylic acid and amine is commercially available. To eventually modulate the bacteria uptake of the complexes, the ligands were also conjugated to a CPP R9. As mentioned before, cell uptake is optimum for peptides having from 8 to 15 arginine residues. Since the complexes preparation involved two equivalents of ligand in which two peptides were to be introduced leading to a total of 18 arginine residues, thus in addition to R9, different peptide chain with lengths of one (R1) or four arginines (R4) were introduced to determine their potential influence on the antimicrobial activity of the conjugates. In addition to that, some CPPs and antimicrobial peptides (AMPs) are known to share several common characteristics such as high density in basic residues and an amphipathic secondary structure (a hydrophobic side and a cationic side) in membrane environments (Strøm et al., 2003). Recent reports have shown that conjugation of metal binding ligands

with AMPs significantly enhances the permeability and activity of the compounds against bacteria that have developed cross-resistance against conventional antibiotics (Chantson et al., 2005; Chantson et al., 2006; Pagès et al., 2013). Since these bioactive peptide sequences consist mainly of arginine and tryptophan, it would also be desirable to utilize RW9 (a CPP derived from penetratin) as a vector for bioconjugation in search of new improved antibacterial agent (Walrant et al., 2011). And not least, a peptide known as an inhibitor of bacteria efflux pumps was grafted also. The challenge of multi-drug resistance has become a pressing issue in treating bacterial infections and one resistance pathway of multi-drug resistant bacteria involves the “over-expression of efflux pumps which expel structurally unrelated antibiotics thus decreasing their intracellular concentration” (Nikaido and Pagès, 2012, p. 340; Pagès and Amaral, 2009). Recent attention has been directed to the discovery of small molecules that inhibit the efflux pumps of the “resistance-nodulation-division (RND) family in gram-negative bacteria” (Okandeji et al., 2011, p. 7679). These compounds “act by competitively binding the substrate interacting sites of RND-family efflux” (Santos et al., 2012, p. 292) and for that reason, the efflux pumps inhibitors (EPIs) are often used as adjuvants to restore susceptibility of MDR bacterial pathogens to drugs. “The prototypical inhibitor of RND-family efflux pumps in gram-negative bacteria is” a C-capped dipeptide, MC-207,110 (Phe-Arg- β -naphthylamide, PA β N) (Okandeji et al., 2011, p. 7679). In this work, the adjuvant PA β N was directly linked to the antibacterial agent, namely the Cu(II) complex in order to eventually reveal any synergistic effect. At this moment, there is no knowledge of the mechanism of antimicrobial activity of dithiocarbamate derived Schiff base compounds and therefore efflux pumps give us a potential starting target. It was hoped that during the pursuit of this target, light would be shed on the

problem and show the path to improving the activity and pharmacological properties of our lead compounds.

4.2 Methodology

4.2.1 Materials

All chemicals and solvents used were similar to those mentioned in Chapter 3 unless stated otherwise herein. Peptide synthesis: 4-Methylbenzhydrylamine (MBHA) resin (0.54 mmol/g, Iris Biotech GmbH), fluorenylmethyloxycarbonyl(Fmoc)-link amide resin MBHA resin (0.52 mmol/g, Iris Biotech GmbH), tert-butoxycarbonyl (Boc)-L-Arg (Tos)-OH (Iris Biotech GmbH), Boc-L-Trp (CHO)-OH (Neosystem Laboratoire), Fmoc-AEEA-OH (Iris Biotech GmbH), PA β N (Bachem), hydroxybenzotriazole, HOBt (Molekula), N,N,N',N'-Tetramethyl-O-(1H-benzotriazol-1-yl)uraniumhexafluorophosphate, O-(Benzotriazol-1-yl)-N,N,N',N'-tetramethyluronium hexafluorophosphate, HBTU (Novabiochem), 1-[bis(dimethylamino)methylene]-1H-1,2,3-triazolo[4,5-b]pyridinium3-oxid hexafluorophosphate, HATU (Iris Biotech GmbH), 1-hydroxy-7-azabenzotriazole, HOAt (GL BioChem (Shanghai) Ltd/ Applied Biosystems), N,N-diisopropylethylamine, DIEA (Alfa Aesar), piperidine (Carlo Erba RS), TFA (Carlo Erba RS), hydrofluoric acid, HF (Merck), triisopropylsilane, TIS (Merck), N-methyl-2-pyrrolidone, NMP (Merck), acetic acid (AnalaR Normapur, VMR chemicals). Buffers: Acetate buffer pH 4 and 6, 0.1 M (Na acetate-Janssen Chimica, acetic acid-AnalaR Normapur, VMR chemicals), PBS pH 7.4, 0.01M (Sigma Aldrich tablet) and borate buffer pH 9 (Na tetraborate-Acros Organics).

4.2.2 Instrumentation

All instrumentations were similar to those mentioned in Chapter 3 unless stated otherwise herein. Peptides and conjugates were characterized by MALDI-TOF-MS in the positive ion reflector mode on an ABI Voyager DE-Pro MALDI-TOF mass spectrometer (Applied Biosystems) using as matrix a saturated solution of CHCA in CH₃CN/H₂O/TFA (50:50:0.1 v:v:v). LC-MS was carried out using an Applied Biosystems QTRAP LC-MS/MS System with a linear gradient elution developed from holding time of 5 min at 100% A and then from 0-60% B in 30 min. Eluent A was 0.1% formic acid in water, while eluent B was 0.1% formic acid in acetonitrile. Experiments were carried out at a flow rate of 10 $\mu\text{L min}^{-1}$ at room temperature with a microLC C18 column 1 mm in diameter with UV detector. Peaks were detected at 220 nm and 280 nm. ITC titrations were performed and analysed using the Nano ITC standard volume calorimetry (TA Instruments) apparatus. Aliquots (10 μL) of the Cu(II)(OAc)₂ solution were added to the solution of the ligand in 0.1M acetate buffer at pH 6. An equilibration time of 300 s was allowed between each addition. Measurements were conducted at 25 °C in a 983 μL cell volume with a 250 μL syringe with stirring rate 300 RPM. The concentrations of the metal salts and of the ligands were adjusted to yield total conversion and a good signal/noise ratio for each experiment. All enthalpy of reactions (ΔH) values were corrected against the heat of dilution. ITC results were analyzed using the Nano Analyze software supplied (version 2.1.6), utilizing a one binding site model. The crude products (conjugated ligands) were analyzed and purified by RP-HPLC using three Waters HPLC systems connected to Breeze software:

System A was similar to Chapter 3.

System B consisted of combination of a dual wavelength UV-Vis absorbance detector (Waters 2487) and a binary pump (Waters 1525) equipped with and a semi-preparative cell for purification purposes. Purification of crude products was achieved with C8 semi preparative column (250×10mm, 5 μm particles of 300 Å pore size). Experiments were carried out at a flow rate of 4 mL min⁻¹ at room temperature. Injection volume was 1.5 mL. Sample concentration was approximately 10 mg/mL.

System C consisted of a dual wavelength UV-Vis absorbance detector (Waters 2487) and a Waters 600 preparative pump. Purification of crude products was achieved with a Waters X-bridge C18 preparative column (19×50mm, 5 μm particles of 300 Å pore size). Experiments were carried out at a flow rate of 10 mL min⁻¹ at room temperature. Injection volume was 1.5 mL. Sample concentration was approximately 10 mg/mL.

All the peaks were detected at 220 nm and 280 nm. All the HPLC experiments were performed using water containing 0.1% of TFA as eluent A and acetonitrile containing 0.1% of TFA as eluent B. Several elution gradients were developed for the different compounds as detailed in the synthetic section.

4.2.3 Synthesis

General procedure A

The PEG derivative was synthesized on solid support by Fmoc strategy using Fmoc protected MBHA Rink amide resin (loading 0.52 mmol/g). The resin was swollen in DCM one hour prior to use. Fmoc removal was performed by using 20% (v:v) piperidine in NMP once for 1 min and then once for 15 min. The resin was washed five times with NMP. Then, a solution of Fmoc-AEEA-OH (3 equiv) was

preactivated with HBTU/HOBt (3 equiv/3 equiv) and DIEA (6 equiv) in NMP (1 mL for 0.1 g of resin) and added to the resin in a reaction vessel (polypropylene syringe). After completion (monitored by Kaiser test for primary amines, in case of positive Kaiser test, the same amino acid was condensed again until a negative test is obtained) the Fmoc group of the PEG derivative was removed as previously described. A solution of Schiff base (SB4CB) (3 equiv) was preactivated with HATU/HOAt (3 equiv/3 equiv) and DIEA (6 equiv) in NMP (1 mL for 0.1 g of resin) and added to the resin. The mixture was allowed to react on the automatic shaker for 2 hours. Cleavage from the resin was performed by shaking for 3 h with a solution of 5 mL of TIS (2.5%), deionised water (2.5%), and TFA (95%). The mixture was then filtered and the volume of the solution was reduced by evaporation. Cold diethyl ether was then added to precipitate the compound, which was then centrifuged for 5 min at 8000 RPM (three times). The compound was solubilized in deionised water and lyophilized. The crude product was then purified with preparative RP-HPLC. For N-terminus acetylated PEG, instead of the coupling with the ligand, the acetylation was performed with 10% acetic anhydride in DCM for 1 hour at room temperature. The compound was cleaved as described but no precipitation occurred upon addition of diethyl ether. The crude was purified by silica-gel column chromatography.

PEG-SB4CB

To PEG-NH₂ on Fmoc-MBHA Rink amide resin (0.25 g, 0.13 mmol) was added a solution of SB4CB (0.129 g, 0.39 mmol, 3 equiv), HATU (0.148 g, 0.39 mmol, 3 equiv), HOAt (0.053 g, 0.39 mmol, 3 equiv) and DIPEA (0.136 mL, 0.78 mmol, 6 equiv) in DMF (2.5 mL). The crude peptide material was purified with System C:

gradient elution of 5 to 100% of B in A for 10 min. The peak eluted at 7.2 min. The fraction was freeze-dried to give PEG-SB4CB as a cream powder. Analytical RP-HPLC (System A: gradient elution of 5 to 100% of B in A for 30 min): $R_T = 17.5$ min. HR-MS: $m/z = [M+Na]^+$ Calcd. 497.12877, Found 497.12892. 1H NMR (300 MHz, CD_3OD) δ 8.57 (s, 1H), 8.08 (s, 1H), 7.82 (dd, $J = 19.5, 9, 4H$), 7.45 – 7.21 (m, 5H), 4.52 (s, 2H), 3.96 (s, 2H), 3.69 (s, 6H), 3.59 (d, $J = 6, 2H$). ^{13}C NMR (75 MHz, CD_3OD) δ (ppm) 200.29, 175.93, 169.77, 145.41, 138.40, 138.36, 137.28, 130.54, 129.71, 129.02, 128.71, 128.49, 72.11, 71.38, 71.22, 70.71, 41.05, 39.91.

AcPEG-NH₂ (PEGAC)

PEG-NH₂ on Fmoc-MBHA Rink amide resin (0.784 g, 0.42 mmol) was acetylated with 10% acetic anhydride in DCM for 1 hour at room temperature. The crude was purified by silica-gel column chromatography eluted with a gradient of MeOH in DCM from 4/96 to 10/90 (v:v) MeOH/DCM to yield the expected compound. The expected compound fraction was evaporated to give AcPEG-NH₂ as a colourless oily solid (88 mg, 98%). HR-MS: $m/z = [M+Na]^+$ Calcd. 227.10023, Found 227.10031. 1H NMR (300 MHz, CD_3OD) δ 3.99 (s, 2H), 3.72-3.64 (m, 4H), 3.56 (t, $J = 6, 2H$), 3.40 – 3.34 (m, 2H), 1.95 (s, 3H). ^{13}C NMR (75 MHz, CD_3OD) δ 175.95, 173.71, 72.06, 71.38, 71.22, 70.89, 40.54, 22.65.

General procedure B

Side-chain protected polyarginine (R1, R4, R9 and RW9) were assembled on MBHA resin (loading 0.54 mmol/g) either manually or using the peptide synthesizer (Applied Biosystem 433A) with HBTU/HOBt as coupling agents. All amino acids were coupled as Boc derivatives. The side chain Arg residue was protected by a

tosyl group and the tryptophan side chain was protected by a formyl group. For RW9, deformylation was performed with 20% piperidine in NMP for approximately 2 hours (sequential time length addition 1 min, 3 min, 5 min, 7 min, 15 min, 30 min and finally 60 min) prior to Boc removal and coupling to the Schiff base. Boc removal was performed by using TFA for 1 min (twice) and washed with 10% DIEA in DCM. Coupling was the same as for Fmoc synthesis. Cleavage from the resin and tosyl protecting group removal was performed using HF in the presence of dimethyl sulfide for 2 hours at 0°C. After HF removal, cold diethyl ether was added to precipitate the peptide. The precipitate was collected, redissolved using 10% acetic acid in water and lyophilized. For N-terminus acetylated peptides, the acetylation was performed with 10% acetic anhydride in DCM for 1 hour at room temperature.

R1-SB4CB

To R1-NH₂ on MBHA resin (0.25 g, 0.135 mmol) was added a solution of SB4CB (0.135 g, 0.405 mmol, 3 equiv), HATU (0.154 g, 0.405 mmol, 3 equiv), HOAt (0.055 g, 0.405 mmol, 3 equiv) and DIPEA (0.140 mL, 0.810 mmol, 6 equiv) in DMF (2.5 mL). The crude peptide material was purified with System C: gradient elution of 5 to 100% B in A for 10 min. The peak eluted at 6.06 min. The fraction was freeze-dried to give R1-SB4CB as a cream powder. Analytical RP-HPLC (System A: gradient elution of 5 to 100% of B in A for 30 min): R_T = 16.1 min. LC-MS: $m/z = [M+H]^+$ Calcd. 486.17, Found 486.10. ¹H NMR (300 MHz, CD₃OD) δ 8.10 (s, 1H), 7.86 (dd, $J = 27, 9, 4$ H), 7.44 – 7.22 (m, 5H), 4.61 (dd, $J = 9, 3, 1$ H), 4.53 (s, 2H), 3.24 (td, $J = 7.5, 3, 2$ H), 2.06 – 1.94 (m, 1H), 1.90 – 1.63 (m, 3H). ¹³C NMR (75 MHz, CD₃OD) δ = 200.36, 176.66, 169.66, 158.79, 145.29, 138.74,

138.35, 136.70, 130.53, 129.71, 129.26, 128.70, 128.50, 54.55, 42.12, 39.93, 30.44, 26.65

R4-SB4CB

To R4-NH₂ on MBHA resin (0.25 g, 0.135 mmol) was added a solution of SB4CB (0.135 g, 0.405 mmol, 3 equiv), HATU (0.154 g, 0.405 mmol, 3 equiv), HOAt (0.055 g, 0.405 mmol, 3 equiv) and DIPEA (0.140 mL, 0.810 mmol, 6 equiv) in DMF (2.5 mL). The crude peptide material was purified with System C: gradient elution of 30 to 50% B in A for 10 mins. The peak eluted at 3.34 min. The fraction was freeze-dried to give R4-SB4CB as a cream powder. Analytical RP-HPLC (System A: gradient elution of 5 to 100% of B in A for 30 min): R_T = 14.0 min. MALDI-TOF-MS: $m/z = [M+H]^+$ Calcd. 954.48, Found 954.49. ¹H NMR (300 MHz, CD₃OD) δ 8.10 (s, 1H), 7.87 (dd, $J = 27, 6$, 4H), 7.44 – 7.23 (m, 5H), 4.55 – 4.47 (m, 3H), 4.43 – 4.31 (m, 3H), 3.28 – 3.13 (m, 8H), 2.00 – 1.61 (m, 16H).

R9-SB4CB

To R9-NH₂ on MBHA resin (0.25 g, 0.135 mmol) was added a solution of SB4CB (0.135 g, 0.405 mmol, 3 equiv), HATU (0.154 g, 0.405 mmol, 3 equiv), HOAt (0.055 g, 0.405 mmol, 3 equiv) and DIPEA (0.140 mL, 0.810 mmol, 6 equiv) in DMF (2.5 mL). The crude peptide material was purified with System C: gradient elution of 5 to 100% B in A for 10 min. The peak eluted at 4.86 min. The fraction was freeze-dried to give R9-SB4CB as a cream powder. Analytical RP-HPLC (System A: gradient elution of 5 to 100% of B in A for 30 min): R_T = 13.3 min. MALDI-TOF-MS: $m/z = [M]^+$ Calcd. 1733.98, Found 1733.93. ¹H NMR (300 MHz,

CD₃OD) δ 8.11 (s, 1H), 7.89 (dd, $J = 39, 9, 4$ H), 7.44 – 7.23 (m, 5H), 4.53 (s, 2H), 4.40 – 4.17 (m, 9H), 3.30 – 3.09 (m, 18H), 2.02 – 1.52 (m, 36H).

RW9-SB4CB

To RW9-NH₂ on MBHA resin (0.25 g, 0.135 mmol) was added a solution of SB4CB (0.135 g, 0.405 mmol, 3 equiv), HATU (0.154 g, 0.405 mmol, 3 equiv), HOAt (0.055 g, 0.405 mmol, 3 equiv) and DIPEA (0.140 mL, 0.810 mmol, 6 equiv) in DMF (2.5 mL). The crude peptide material was purified with System C: gradient elution of 5 to 100% B in A for 10 min. The peak eluted at 5.69 min. The fraction was freeze-dried to give RW9-SB4CB as a cream powder. Analytical RP-HPLC (System A: gradient elution of 5 to 100% of B in A for 30 min): $R_T = 16.5$ min. MALDI-TOF-MS: $m/z = [M]^+$ Calcd. 1823.91, Found 1823.27. ¹H NMR (300 MHz, CD₃OD) δ 8.06 (s, 1H), 7.79 (dd, $J = 45, 9, 4$ H), 7.55 (d, $J = 6, 1$ H), 7.46 – 7.22 (m, 10H), 7.17 – 6.84 (m, 9H), 4.61 (dd, $J = 9, 6, 1$ H), 4.54 (s, 2H), 4.48 (td, $J = 4.5, 3, 2$ H), 4.33 – 4.21 (m, 3H), 4.14 – 4.00 (m, 3H), 3.35 (s, 5H), 3.27 – 2.95 (m, 15H), 1.97 – 1.37 (m, 24H).

R9-SM4CB

To R9-NH₂ on MBHA resin (0.25 g, 0.135 mmol) was added a solution of SM4CB (0.089 g, 0.405 mmol, 3 equiv), HATU (0.154 g, 0.405 mmol, 3 equiv), HOAt (0.055 g, 0.405 mmol, 3 equiv) and DIPEA (0.140 mL, 0.810 mmol, 6 equiv) in DMF (2.5 mL). After cleavage, the crude peptide material was purified with System C: gradient elution of 5 to 100% B in A for 10 min. The peak eluted at 4.32 min. The fraction was freeze-dried to give R9-SM4CB as a cream powder. Analytical RP-HPLC (System A: gradient elution of 5 to 100% of B in A for 30 min): $R_T = 11.8$

min. MALDI-TOF-MS: $m/z = [M+H]^+$ Calcd. 1658.95, Found 1658.78. ^1H NMR (300 MHz, CD_3OD) δ 8.11 (s, 1H), 7.91 (dd, $J = 39, 9, 4\text{H}$), 4.42 – 4.20 (m, 9H), 3.30 – 3.11 (m, 18H), 2.60 (s, 3H), 2.04 – 1.55 (m, 36H).

RW9-SM4CB

To RW9-NH₂ on MBHA resin (0.25 g, 0.135 mmol) was added a solution of SM4CB (0.089 g, 0.405 mmol, 3 equiv), HATU (0.154 g, 0.405 mmol, 3 equiv), HOAt (0.055 g, 0.405 mmol, 3 equiv) and DIPEA (0.140 mL, 0.810 mmol, 6 equiv) in DMF (2.5 mL). The crude peptide material was purified with System C: gradient elution of 20 to 50% B in A for 10 min. The peak eluted at 6.11 min. The fraction was freeze-dried to give RW9-SM4CB as a cream powder. Analytical RP-HPLC (System A: gradient elution of 5 to 100% of B in A for 30 min): $R_T = 14.0$ min. MALDI-TOF-MS: $m/z = [M+H]^+$ Calcd. 1748.89, Found 1748.45. ^1H NMR (300 MHz, CD_3OD) δ 8.07 (s, 1H), 7.95 (d, $J = 9, 2\text{H}$), 7.77 (d, $J = 6, 2\text{H}$), 7.55 (d, $J = 6, 1\text{H}$), 7.46 – 7.28 (m, 5H), 7.19 – 6.84 (m, 9H), 4.57 (dd, $J = 15, 9, 1\text{H}$), 4.49 – 4.36 (m, 2H), 4.33 – 4.17 (m, 3H), 4.14 – 3.96 (m, 3H), 3.28 – 2.96 (m, 15H), 2.61 (s, 3H), 1.94 – 1.27 (m, 24H).

AcR1-NH₂ (R1AC)

To R1-NH₂ on MBHA resin (0.25 g, 0.135 mmol), the acetylation was performed with 10% acetic anhydride in DCM for 1 hour at room temperature. The crude peptide material was purified with System C: gradient elution of 0 to 30% B in A for 10 mins. The peak eluted at 3.26 min. The fraction was freeze-dried to give R4AC as a cream powder. Analytical RP-HPLC (System A: gradient elution of 0 to 30% of B in A for 30 min): $R_T = 4.0$ min. HR-MS: $m/z = [M+H]^+$ Calcd. 216.14550,

Found 216.14556. ^1H NMR (300 MHz, CD_3OD) δ 4.35 (dd, $J = 9, 6, 1\text{H}$), 3.28 – 3.17 (m, 2H), 2.01 (s, 3H), 1.96 – 1.83 (m, 1H), 1.75 – 1.59 (m, 3H). ^{13}C NMR (75 MHz, CD_3OD) δ 176.79, 173.61, 54.00, 42.09, 30.38, 26.46, 22.66.

AcR4-NH₂ (R4AC)

To R4-NH₂ on MBHA resin (0.25 g, 0.135 mmol), the acetylation was performed with 10% acetic anhydride in DCM for 1 hour at room temperature. The crude peptide material was purified with System C: gradient elution of 0 to 30% B in A for 10 min. The peak eluted at 4.36 min. The fraction was freeze-dried to give R4AC as a cream powder. Analytical RP-HPLC (System A: gradient elution of 0 to 30% of B in A for 30 min): $R_T = 6.8$ min. MALDI-TOF-MS: $[\text{M}+\text{K}]^+$ Calcd. 836.02, Found 722.33; $[\text{M}+\text{Na}]^+$ Calcd. 820.04, Found 706.37; $[\text{M}+\text{H}]^+$ Calcd. 684.45, Found 684.38. ^1H NMR (300 MHz, CD_3OD) δ 4.38 – 4.24 (m, 4H), 3.21 (t, $J = 6.6, 8\text{H}$), 2.02 (s, 3H), 1.98 – 1.56 (m, 16H).

AcR9-NH₂ (R9AC)

To R9-NH₂ on MBHA resin (0.25 g, 0.135 mmol), the acetylation was performed with 10% acetic anhydride in DCM for 1 hour at room temperature. The crude peptide material was purified with System B: gradient elution of 0 to 30% B in A for 30 min. The peak eluted at 9 min. The fraction was freeze-dried to give R9AC as a cream powder. Analytical RP-HPLC (System A: gradient elution of 5 to 100% of B in A for 30 min): $R_T = 6.0$ min. MALDI-TOF-MS: $[\text{M}+\text{K}]^+$ Calcd. 836.02, Found 1486.90; $[\text{M}+\text{Na}]^+$ Calcd. 1502.87, Found 1486.90; $[\text{M}+\text{H}]^+$ Calcd. 1464.95, Found 1464.93. ^1H NMR (300 MHz, CD_3OD) δ 4.35 – 4.12 (m, 9H), 3.28 – 3.16 (m, 18H), 2.04 (s, 3H), 1.96 – 1.63 (m, 36H).

AcRW9-NH₂ (RW9AC)

To RW9-NH₂ on MBHA resin (0.25 g, 0.135 mmol), the acetylation was performed with 10% acetic anhydride in DCM for 1 hour at room temperature. The crude peptide material was purified with System B: gradient elution of 5 to 100% B in A for 30 mins. The peak eluted at 12 min. The fraction was freeze-dried to give RW9AC as a cream powder. Analytical RP-HPLC (System A: gradient elution of 5 to 100% of B in A for 30 min): R_T = 10.6 min. MALDI-TOF-MS: [M+K]⁺ Calcd. 836.02, Found 1593.72; [M+Na]⁺ Calcd. 820.04, Found 1577.75; [M+H]⁺ Calcd. 1554.89, Found 1554.78. ¹H NMR (300 MHz, CD₃OD) δ 7.56 (d, *J* = 9, 1H), 7.48 – 7.30 (m, 5H), 7.14 – 6.89 (m, 9H), 4.60 (dd, *J* = 9, 6, 1H), 4.44 (dd, *J* = 15, 9, 2H), 4.34 – 4.21 (m, 2H), 4.15 – 3.98 (m, 4H), 3.36 (d, *J* = 5.7, 1H), 3.29 – 2.94 (m, 16H), 2.05 (s, 3H), 1.89 – 1.29 (m, 24H).

Procedure C (Solution synthesis)

PAβN-SB4CB

The ligand SB4CB (10 mg, 0.061 mmol, 1 equiv), PAβN.2HCl (23.5 mg, 0.091 mmol, 1.5 equiv), HATU (17.3 mg, 0.091 mmol, 1.5 equiv) and HOAt (6.2mg, 0.091 mmol, 1.5 equiv) were placed in a round-bottom flask under argon. Dried DMF (1 mL) was added followed by DIEA (0.026 mL, 0.303 mmol, 5 equiv). The reaction mixture was stirred overnight at room temperature. Analytical HPLC showed conversion of starting material into a less polar product >50%. After dilution with water, the crude peptide material was purified with System C: gradient elution of 5 to 100% B in A for 10 min. The peak eluted at 8.57 min. The fraction was freeze-dried to give PAβN-SB4CB as a yellowish solid. Analytical HPLC: R_T = 21.5 min. MALDI-TOF-MS: *m/z* = [M+H]⁺ Calcd. 759.29, Found 759.24. ¹H NMR

(300 MHz, CD₃OD) δ 8.19 (d, $J = 3$, 1H), 8.06 (s, 1H), 7.86 – 7.73 (m, 7H), 7.58 – 7.05 (m, 14H), 4.83 (dd, $J = 9, 6$, 1H), 4.58 (dd, $J = 15, 6$, 1H), 4.53 (s, 2H), 3.29 – 3.07 (m, 4H), 2.04 – 1.61 (m, 4H).

Preparation of copper (II) complexes, CuL₂

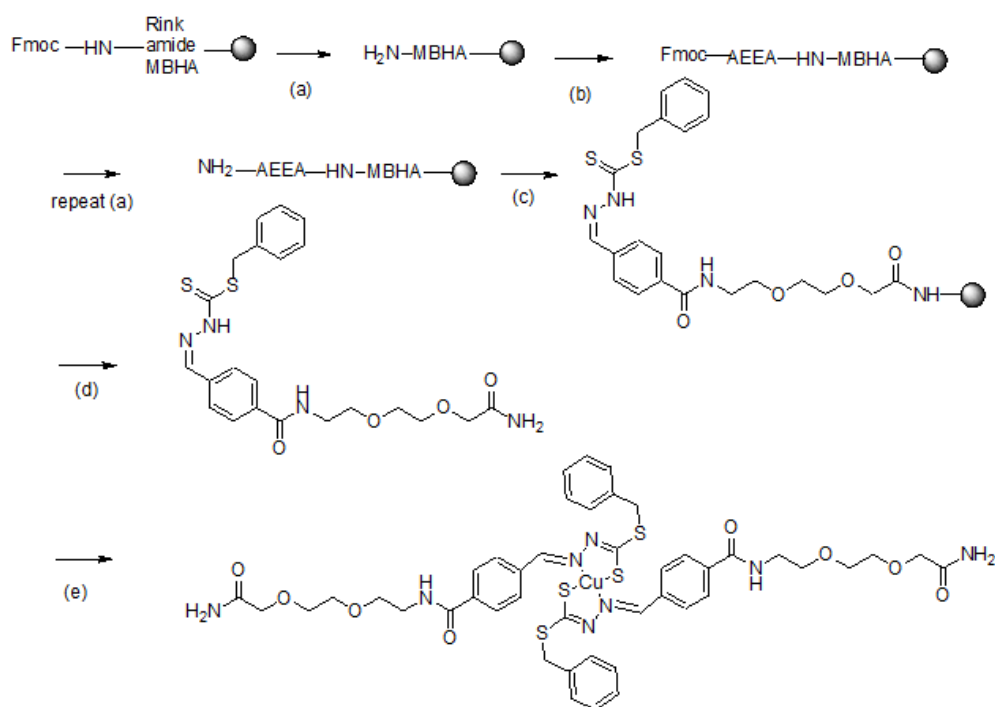
To the bioconjugate L (mmol, 2 equiv) in methanol was added a solution of Cu(OAc)₂·H₂O (mmol, 1 equiv), the solution mixture was stirred overnight and then evaporated to dryness to give brown oily solid.

4.3 Results and discussion

4.3.1 Synthesis

The synthesis of the bidentate dithiocarbazate Schiff base ligand bioconjugates with PEG and peptides are reported here for the first time as well as the synthesis of their Cu(II) complexes. The preparation of eight new ligand-vector conjugates and their Cu complexes containing Schiff base ligands derived from the condensation of SMDTC/SBDTC with 4-carboxybenzaldehyde and various vectors comprising CPPs, PEG and EPI are detailed in this work. In addition, five acetylated vectors were also prepared for meaningful comparison during the antimicrobial evaluation. The compounds were synthesized using either solid phase peptide synthesis techniques or solution phase coupling conditions. The presence of metal ion and/or Schiff base in the system can interfere with standard conjugation synthetic procedures. Therefore, the procedure needs to be optimized accordingly for each compound to prevent hydrolysis, decomposition and demetallation.

In the case of Schiff base ligand-PEG conjugate, the conjugation was performed via Fmoc strategy using a rink amide resin (Scheme 4.3). The synthesis for PEG conjugates was relatively straightforward. The PEG amino acid was coupled using standard HBTU and HOBt coupling reagents in basic conditions. After Fmoc deprotection, the coupling of the Schiff base was performed using HATU and HOAt. Cleavage from the resin of the ligand-PEG conjugate was achieved in the cocktail mixture of 95% TFA, 2.5% TIS and 2.5% water. Only one major peak assignable to the product was observed in the crude chromatogram (Figure 4.4). The ligand was purified by reverse-phased HPLC and the complex was formed in MeOH. The acetylated PEG carboxamide was synthesized similarly to be used as a control compound for the biological tests.



Scheme 4.3. Synthesis of the PEGylated copper complex by Fmoc strategy. (a) 20% piperidine in NMP, 1 × 5 min, 1 × 30 min. (b) HBTU, HOBt, DIEA, Fmoc-AEEA-OH, anhydrous DMF, 30 min-1 hr. (c) HATU, HOAt, DIEA, Schiff base ligand, anhydrous DMF, 2 hr (d) 95% TFA, 2.5% TIS and 2.5% H₂O, 3 hr (e) Cu(OAc)₂ in MeOH, r.t. overnight.

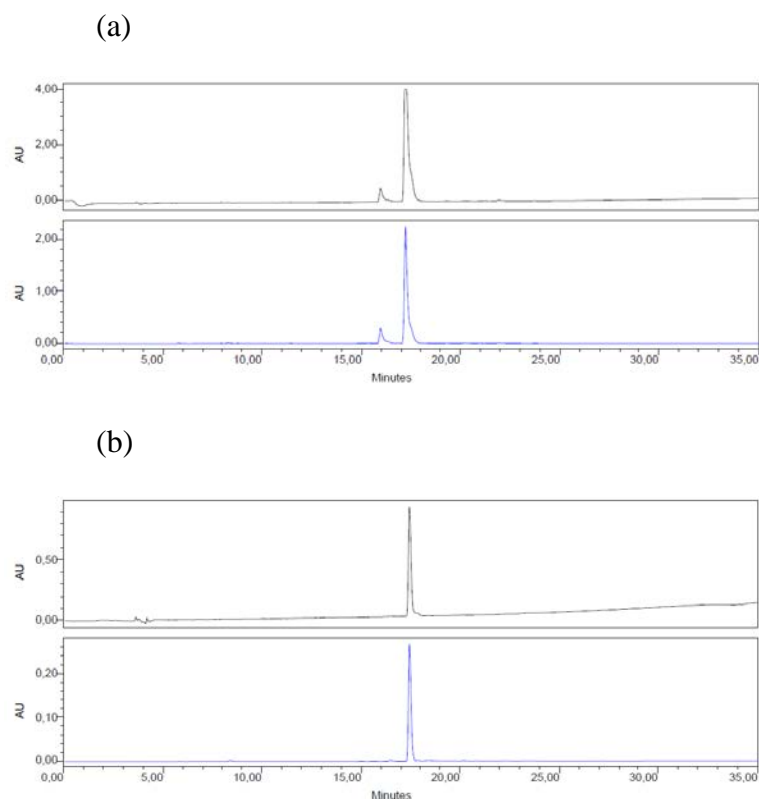
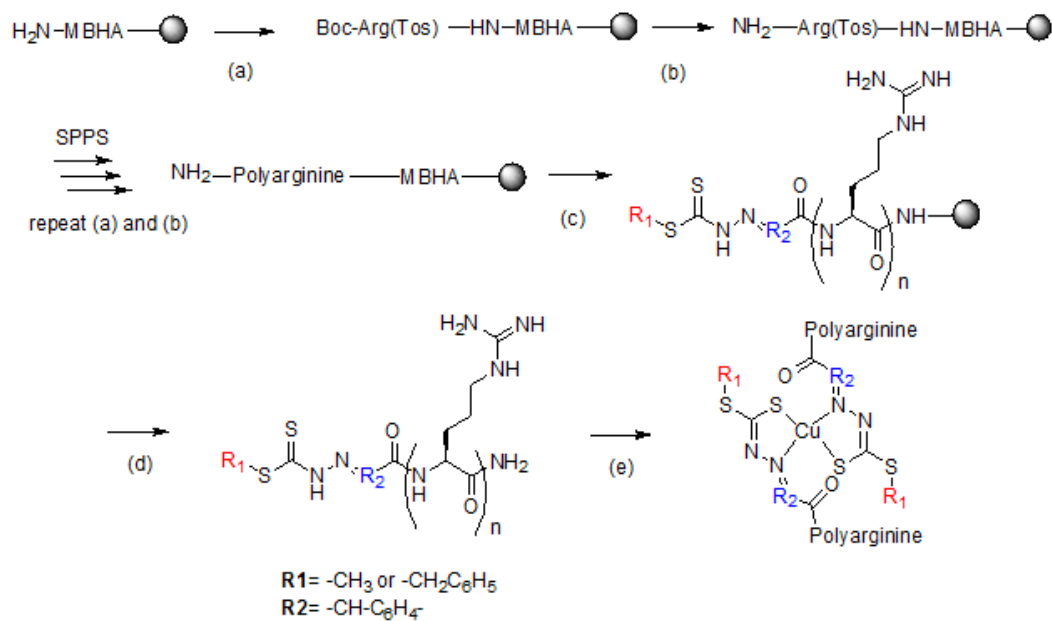


Figure 4.4. Chromatograms of PEG-SB4CB synthesized via Fmoc strategy. (a) Crude (b) Purified. Detection at $\lambda = 220$ nm (top) and 280 nm (bottom). The peak at 17.5 min corresponds to the expected product.

While the Fmoc strategy was relatively straightforward for PEG conjugates, the synthesis was problematic for polyarginine conjugates. Problems arose because the CPPs themselves were difficult to assemble using Fmoc strategy which required multiple repeat couplings and long reaction times. Although the synthesis was monitored by the Kaiser test which indicated that the coupling and deprotection at each step was successful, the final result after cleavage of the conjugates from the resin was not satisfactory with the presence of a mixture of polyarginine (R9, R8, R7) or Fmoc-protected polyarginine in the chromatograms of crude products. In addition to that, the HPLC profile was not always reproducible and at times, hydrolysis of the Schiff base hydrazone moiety was observed with the hydrolyzed byproduct peak being almost equal to the peak of the desired product. As a result,

preparation of the polyarginine peptides was then performed using Boc-strategy on MBHA resin to obtain C-carboxamide peptides. The CPPs couplings were performed using tosyl and formyl as side-chain protecting groups for arginine and tryptophan respectively and HBTU/HOBt as coupling reagents (Scheme 4.4). The Boc groups were removed using pure TFA for 1 min the first time and repeat for 5 mins. The ligands were introduced at the N-terminal amino group of the protected resin bound polyarginine with HATU/HOAt as coupling agents for efficient coupling without the need for repeat coupling. The compounds were removed from the resin simultaneously with the cleavage of the tosyl side-chain protecting groups in HF in the presence of anisole and dimethylsulfide (Me_2S) as radical scavengers. However, in some cases the presence of anisole led to an unexpected byproduct, which has a very similar retention time to that of the expected compound, consequently, only Me_2S was employed (Figure 4.5). If the conjugates were found to contain formyl-protected tryptophan, the formyl deprotection was subsequently carried out with 20% piperidine in NMP prior to coupling with Schiff base ligands. Otherwise, when deformylation was carried out after the coupling of the Schiff base, total hydrolysis of the Schiff base moiety resulted. The product was purified by RP-HPLC and compounds were obtained as yellow powders readily soluble in either water or organic solvents such as DMSO, DMF and methanol. N-acetylated versions were synthesized for all conjugated peptides by following the same procedures. The final acetylation was performed using acetic anhydride in DCM 10/90 v:v.



Scheme 4.4. Synthesis of ligand-peptide conjugates by Boc-strategy. (a) HBTU, HOBT, DIEA and Boc-Arg(Tos)-OH in NMP for 30 min. (b) Neat TFA, 2 × 1 min then 20% DIEA in DCM. (c) HATU, HOAt, DIEA and Schiff base ligands in anhydrous DMF for 2 hr. (d) HF and Me₂S for 2 hr at 0°C. (e) Cu(OAc)₂ in MeOH, r.t. overnight.

(a)

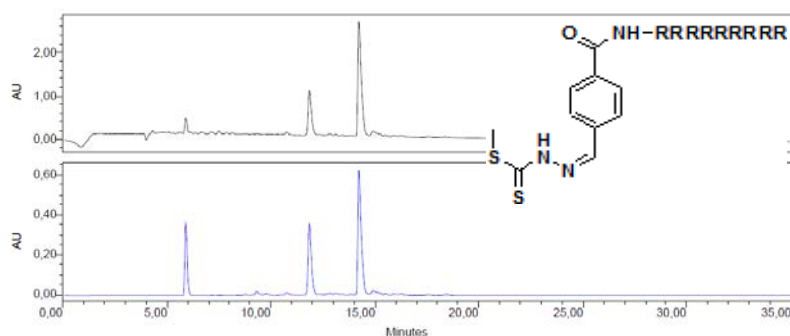
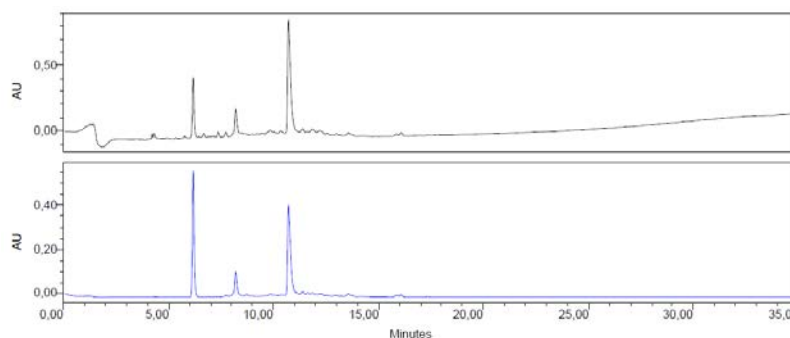


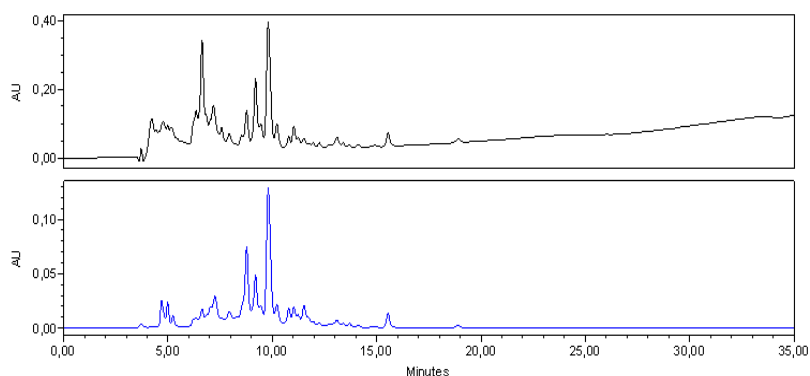
Figure 4.5. RP-HPLC chromatograms obtained on a C8 column. Samples were eluted using a gradient of acetonitrile from 5 to 95% in water over 30 min with 1 mL min^{-1} flow rate at room temperature (both solvents contain 0.1% TFA). Detection: $\lambda = 220\text{ nm}$ (top) and 280 nm (bottom)

(b)



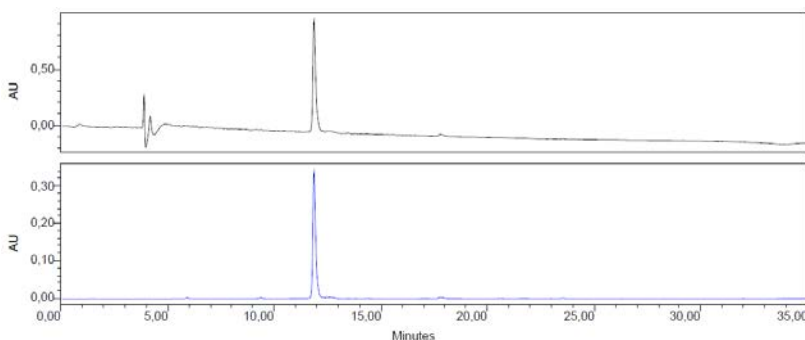
(a) HPLC profile of the crude R9-SM4CB conjugate from Boc-strategy with the addition of anisole during HF-cleavage. The peak at $\sim 6\text{ min}$ is the hydrolyzed compound, the peak at 11.8 min is the desired product while the peak at $\sim 14.5\text{ min}$ is the byproduct caused by anisole.

(c)



(b) RP-HPLC profile of the crude R9-SM4CB conjugate from Boc-strategy without the addition of anisole during HF-cleavage. The byproduct observed in (a) caused by anisole was no longer visible.

(d)

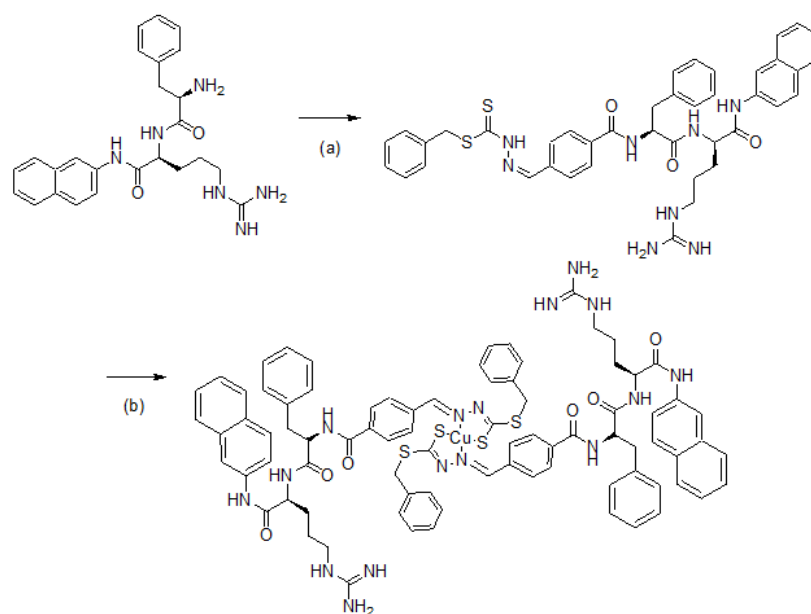


(c) RP-HPLC elution profile of the crude R9-SM4CB conjugate from Fmoc-strategy. The profile was less well resolved as compared to Boc-strategy and not always reproducible.

(d) RP-HPLC elution profile of the purified R9-SM4CB.

It should also be noted that among the early attempts to functionalize the parent compounds, aliphatic side chain ligands from levulinic acid were utilized. However, the standard SPPS were unsuccessful as they resulted in total hydrolysis of the Schiff base moiety. Although alternative approaches were adopted to synthesize the conjugate in solution via ring-opening of succinic anhydride and formation of acyl chloride, the ligands were found to be unstable under these reaction conditions. This showed that aliphatic side chain ligands are not suitable for use in bioconjugation. The rigid carboxylate benzyl ring in 4-carboxylbenzaldehyde derivatives (SM4CB and SB4CB) provided suitable stability and functionality for coupling by SPPS. The ability to survive the synthesis and purification conditions is important and the stable 4-carboxybenzaldehyde derived Schiff base ligands were deemed most suitable for bioconjugation in this work.

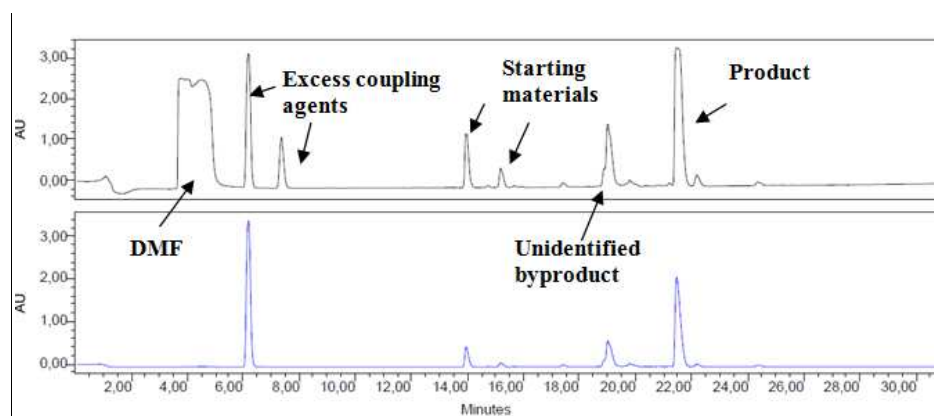
The conjugation of SB4CB with the efflux pump inhibitor PA β N was effected through solution synthesis (Scheme 4.5).



Scheme 4.5. Solution synthesis of PA β N-SB4CB (a) HATU, HOAt, DIEA and Schiff base ligand mixture in anhydrous DMF overnight at r.t. (b) in MeOH overnight.

The carboxyl group of SB4CB was coupled to the free N-terminal amino group of phenylalanine with the coupling agents HATU/HOAt in anhydrous DMF. The reaction progress was monitored by RP-HPLC. Although an excess of PA β N was used, the reaction did not proceed to completion even after 24 hours with the peaks corresponding to the starting materials still visible in the chromatograms (Figure 4.6). The product PA β N-SB4CB along with the unreacted starting material were separated using preparative HPLC.

(a)



(b)

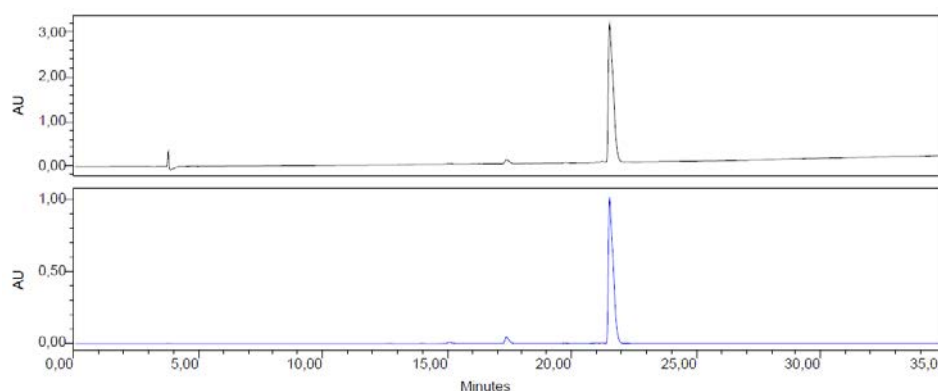


Figure 4.6. Chromatograms of PA β N-SB4CB synthesized in solution. (a) Crude (b) Purified. The peak at 21.5 min corresponds to the expected product.

The purity of each ligand and acetylated peptide was confirmed by the presence of a single peak in the reverse-phased HPLC chromatogram. The purity for all the compounds was ensured to be >95%. The copper complexes were finally obtained

by mixing a 0.5 equivalent of $\text{Cu}(\text{OAc})_2$ to the ligand in MeOH. All ligand conjugates and their respective complexes were comprehensively characterized spectroscopically.

4.3.2 Characterization of ligands conjugates

4.3.2.1 NMR

All ligands were analyzed by NMR spectroscopy in order to confirm the integrity of the Schiff base hydrazone moiety. For illustration, the example of R1-SB4CB will be discussed here while the rest of the spectra are available in the Appendices. ^1H and ^{13}C spectra of R1-SB4CB in CD_3OD are shown in Figure 4.7. The presence of the Schiff base is immediately apparent from the NMR spectra of the bioconjugates. R1-SB4CB possesses peaks that corresponds to the SB4CB moiety: characteristic resonance signals at δ 8.10 ppm and 7.90-7.80 ppm attributed to $-\text{CH}=\text{N}$ and the aromatic ring of 4-carboxybenzaldehyde moiety, the 5 aromatic protons of SBDTC in the region of 7.43-7.23 ppm and the presence of a singlet of the S- CH_2 protons observed at 4.53 ppm. These chemical shifts of SB4CB moiety are consistent in almost all the NMR spectra of the bioconjugates with exception of RW9-SB4CB and PA β N-SB4CB in which the SB4CB aromatic region multiplets overlapped with the peptides tryptophan, phenylalanine and naphthylamide protons. For SM4CB derived conjugates, the aromatic ring in the region of 7.43-7.23 ppm and S- CH_2 protons at 4.53 ppm were absent while the distinctive methyl signal for SMDTC was clearly visible at 2.61 ppm. Signals arising from the protons of arginine were observed at *ca.* 4.85-4.59 ppm, 3.26-3.21 ppm and 2.06-1.62 ppm corresponding to α -CH, δ - CH_2 and β , γ - CH_2 respectively. The α - CH_2 peaks shifted highfield with increasing number of arginine with the signals observed at *ca.* 4.40-4.17 ppm for

R9-SB4CB. In RW9 derivatives, the tryptophan β -CH₂ signal partially overlapping with the arginine δ -CH₂ protons as well as the CD₃OD solvent peak while the α -CH of tryptophan can be easily located between *ca.* 4.60-4.45 ppm. Such overlappings were also observed for PA β N-SB4CB in which the protons of α -CH and β -CH₂ each overlapped with the CD₃OD solvent peaks at 4.78 ppm and 3.31 ppm. For PEG-SB4CB, the 10 protons of PEG can be found in the region *ca.* 4.00-3.50 ppm. In principle, dithiocarbazate derivatives can exhibit thione-thiol tautomerism due to the presence of thioamide function -NH-C(S)SR. In the ¹³C NMR spectra of R1-SB4CB, the presence of -NH-C(=S)S at δ 200.36 ppm indicates that the Schiff bases predominate as the thione form in solution (if thiol form is present, a signal at *ca.* 158 ppm will be observed) (How, 2008). This signal was shifted downfield due to the deshielding effect of the neighbouring amine nitrogen and electronegative sulphur. The CH=N signal of the Schiff base occurred at 145.29 ppm indicative of the hydrazone bond which was formed when 4-carboxybenzaldehyde reacted with the SBDTC. The -S-CH₂ peak occurred relatively upfield at 39.93 ppm. The aromatic carbons were observed around 138-128 ppm as expected for carbons in aromatic rings. In addition, the spectrum also showed the expected signals with carbon atoms of arginine giving four signals at δ 26.65, 30.44, 42.12 and 54.55 ppm while the two amide and one amine carbon atoms gave signals at δ 176.66, 169.66 and 158.79 ppm. Overall, the NMR spectra of all the bioconjugates were comparable and in agreement with the expected structure, which confirm their formation.

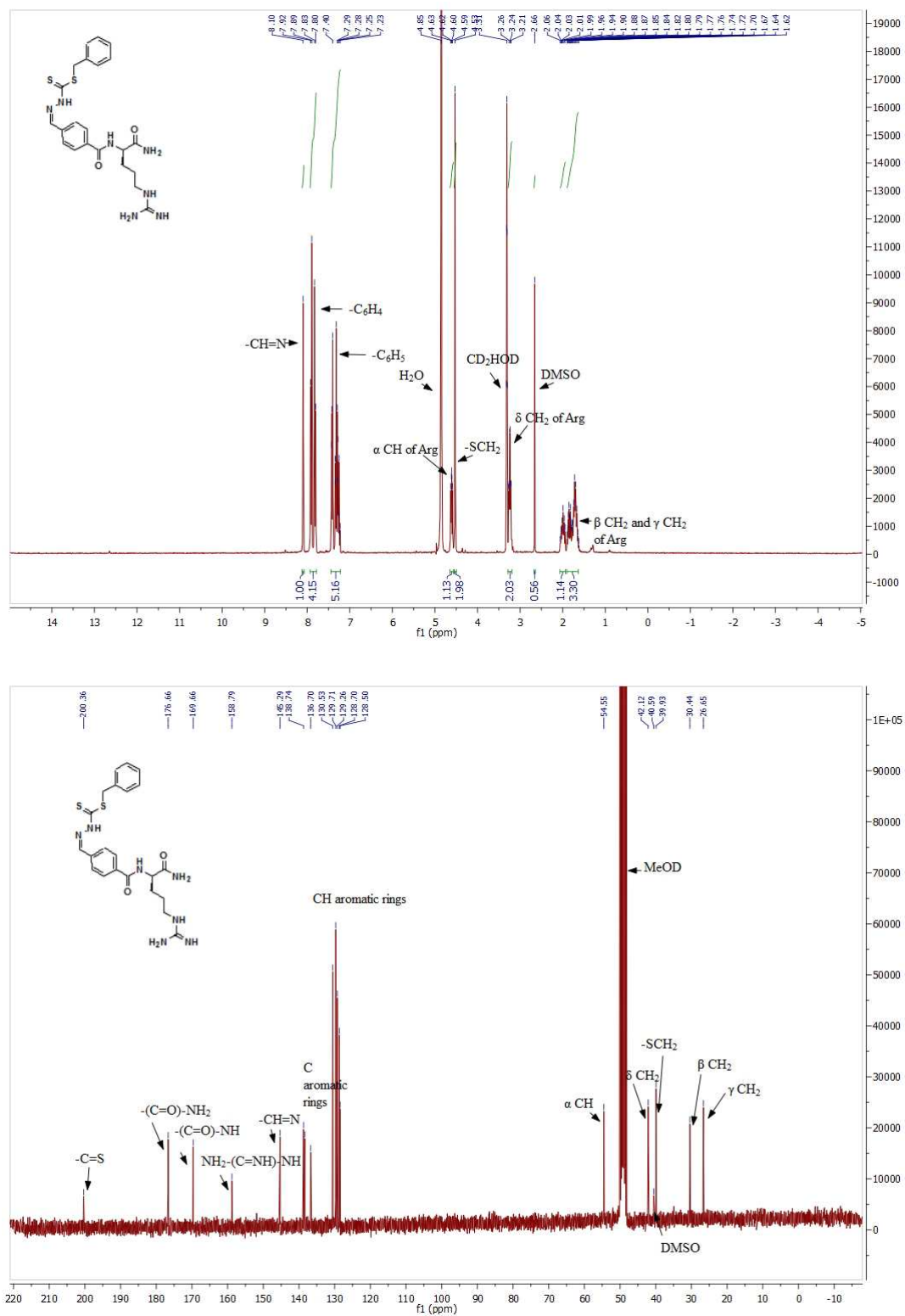


Figure 4.7. ^1H and ^{13}C spectra of the Schiff base-conjugate (R1-SB4CB).

4.3.2.2 MALDI-TOF-MS/ESI-MS

In addition to NMR, the ligand-conjugates were also analyzed with mass spectrometry either MALDI-TOF-MS or ESI-MS for molecules of molecular weight less than 500. The mass spectral data of the compounds are shown in the Appendices. As an example, the mass spectrum of one of the ligand-conjugates, R9-SB4CB, is shown in Figure 4.8. The MALDI mass spectra of the new ligand conjugates mainly gave peaks that correspond to their protonated form. The MALDI mass spectra of all ligands also showed the fragment corresponding to the hydrolyzed Schiff base moiety (cleavage of C=N bond). Since the MALDI analysis involves laser irradiation and the use of an acidic matrix, it was anticipated that this observed hydrolysis could occur during the mass experiment. In some cases, this peak was the main peak with a larger relative abundance than that of the targeted ligand-conjugate itself.

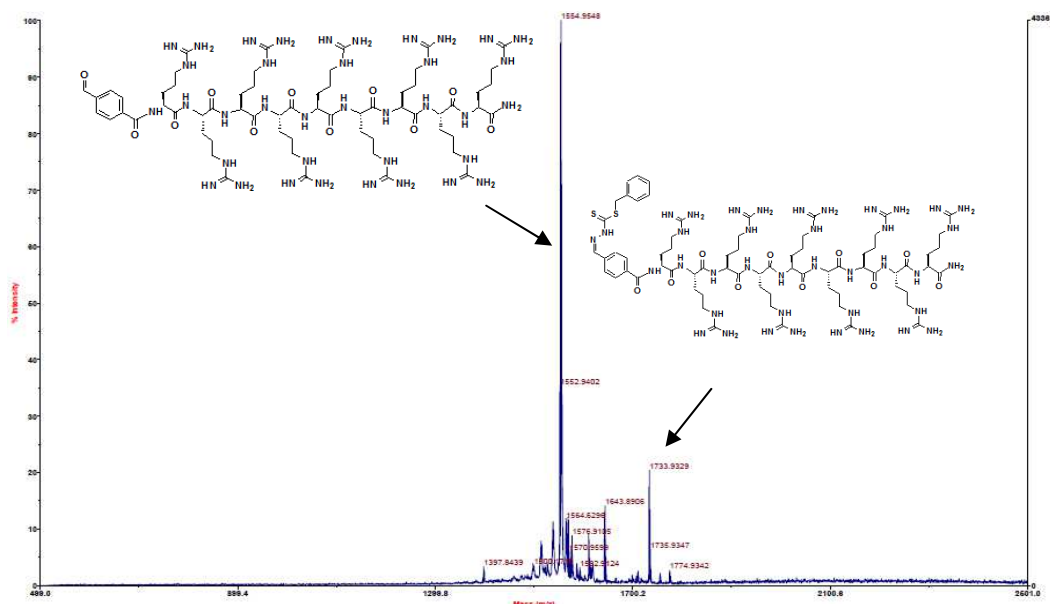


Figure 4.8. MALDI spectra of R9-SB4CB. The hydrolyzed fragment (cleavage of C=N bond) is noticeable during MALDI characterization.

4.3.3 Characterization of metal-complexes conjugates

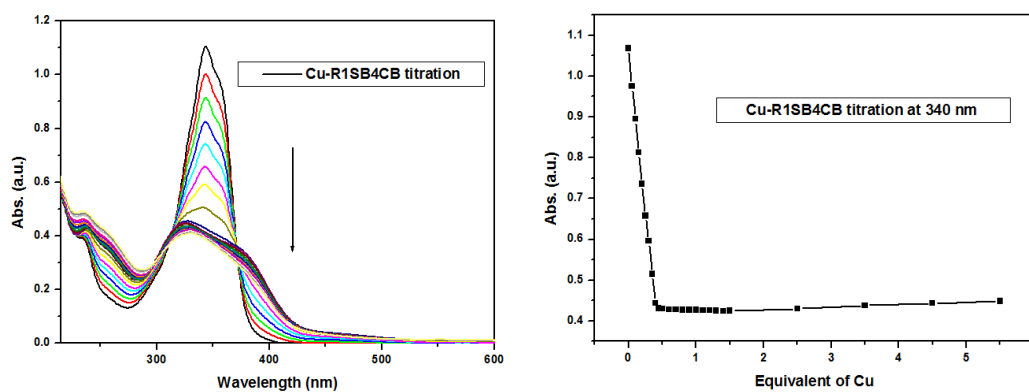
The targeted Cu(II) complexes of the above described bidentate Schiff base ligands involve two identical ligands and a copper(II) ion. Consequently, all the bioconjugate complexes were prepared in situ by mixing methanolic solutions of the ligands and Cu(II)(OAc)₂ in a 2:1 ratio. The hydrophilic polyarginine may contain many bound water molecules and trifluoroacetate counterions. Therefore, it is difficult to ascertain the actual peptide concentration based on the weight of the lyophilized conjugate. The concentration was thus determined with reference to the extinction coefficient of the Schiff base chromophore that absorbs at 340 nm. Upon complexation, the colour of the reaction mixture changes to brown, which serves evidence for complexation in the duration when left to stir overnight. As both the ligands and metal complexes showed the same retention time in RP-HPLC, the reaction could not be monitored or purified using HPLC. The expected complexation was monitored by UV-Vis spectroscopy and the identification of the complexes was further confirmed by EPR, LC-MS and ITC as discussed below.

4.3.3.1 UV-Vis

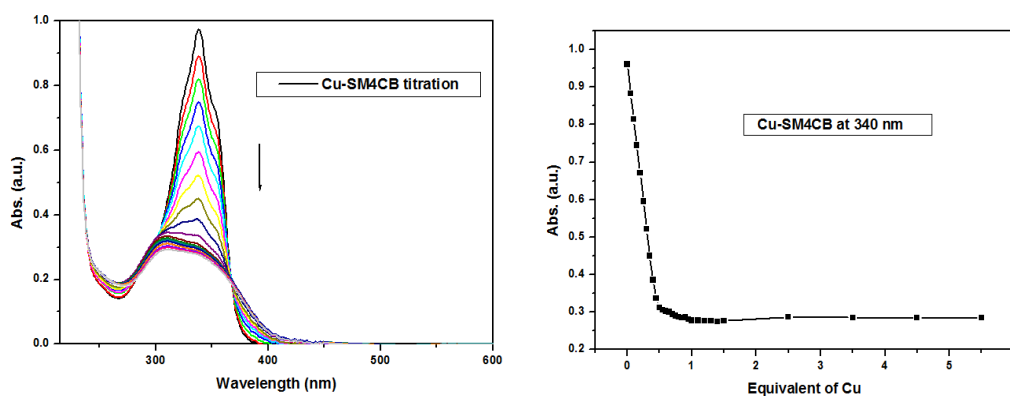
UV-Vis titrations were performed to ascertain the formation of the expected ML₂ complex. The titration was carried out in MeOH, which mirrored the actual synthetic procedure and also in acetate buffer pH 6 for aqueous solution studies. Upon addition of Cu(OAc)₂, the changes in UV-Vis spectra are noticeable with a broad absorption band arising from the formed complex which range from 300-400 nm with $\lambda_{\text{max}} \sim 325$ nm ($\log \epsilon = 3.96$) while the intensity of the band corresponding to ligands at $\lambda_{\text{max}} \sim 340$ nm ($\log \epsilon = 4.64$) decreases. For all the ligands, the titration, performed at a concentration in the range of 10^{-5} M, proceeds with a sharp end-point

at 0.5 equivalent with clear isosbestic points indicative of a single complexation event. This low-energy region of the UV-Vis spectrum is the same for the conjugated ligands and the parent compounds, which strongly suggests an identical Cu coordination into the Schiff base ruling out possible coordination to peptide chains of the bioconjugate. The 1:2 stoichiometry of the complex was verified by the plot of absorbance (abs.) against equivalent of Cu. Examples of UV-Vis titration curves obtained are shown in Figure 4.9.

(a)



(b)



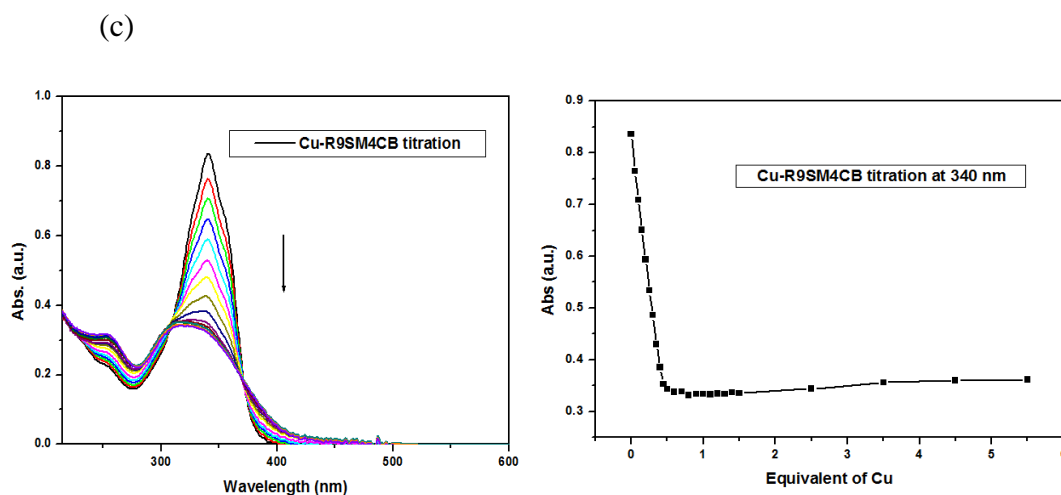


Figure 4.9. UV-Vis titration of various ligands (concentration set at ca. 2.5×10^{-5} M) with $\text{Cu}(\text{OAc})_2 \cdot \text{H}_2\text{O}$ (concentration set at ca. 5×10^{-4} M) at 25°C . a) Titration of R1-SB4CB in methanol and its corresponding titration curve monitored at 340 nm. b) Titration of SM4CB in acetate buffer pH 6 and its corresponding titration curve monitored at 340 nm for comparison with conjugated compounds. c) Titration of R9-SM4CB in acetate buffer pH 6 and its corresponding titration curve monitored at 340 nm.

Understanding the behavior of these compounds in aqueous and buffer systems under physiological conditions (pH range 6.0-7.4) is important for the study of biological activity. Many Schiff bases derived from S-substituted dithiocarbamate prepared to date and their metal complexes suffer from poor aqueous solubility that hinders investigation of their properties. The tremendous increase in solubility of their bioconjugate derivatives allows for some investigations to be carried out as well as their complexation in aqueous solution. The complexation of Cu(II) was confirmed to be pH dependent. After screening a range of aqueous buffer solutions, acetate buffer (pH 6) was utilized as it does not interfere with the UV absorption and the complexation proceeded well. Attempts were unsuccessful with water (no complexation) and buffers such as HEPES (no complexation), TRIS (no complexation), MOPS (changes in the UV-Vis signature too small for analysis), PBS (precipitation of the ligands) and borate buffer (reduction of the Cu(II) ion /

formation of hydroxide at high pH). When the reaction solutions were monitored by UV-Vis, the distinct λ_{max} shift and end-point at 0.5 equivalents were observed at pH 6 (0.1 M acetate buffer) and pH 7.4 (0.01M PBS) but were not observed at pH 4 (0.1 M acetate buffer) and 9 (0.1 M borate buffer) (Figure 4.10). As mentioned earlier, Schiff bases derived from DTC readily undergo thiol-thione tautomerism at equilibrium mixture in solution (Ali et al., 2003). In the presence of metal ions, the equilibrium state is more favourable towards the thiol form that spontaneously deprotonate to give a thiolate anion for metal coordination (Hossain et al., 1996; Tarafder et al., 2002a). At low pH, the deprotonation required for coordination is presumably suppressed. Furthermore, the thione sulphur has strong electron withdrawing effect that causes the amide proton to be slightly acidic which is stabilized in strong acidic condition. No complexation at high pH could be due to hydrolysis of Schiff bases, reduction of the Cu(II) ion or formation of hydroxide that resulted in precipitation.

(a)

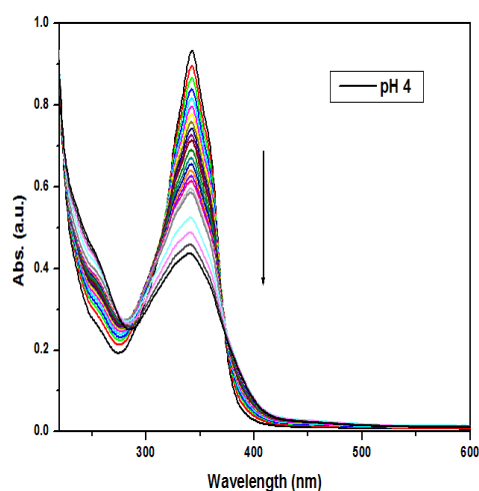
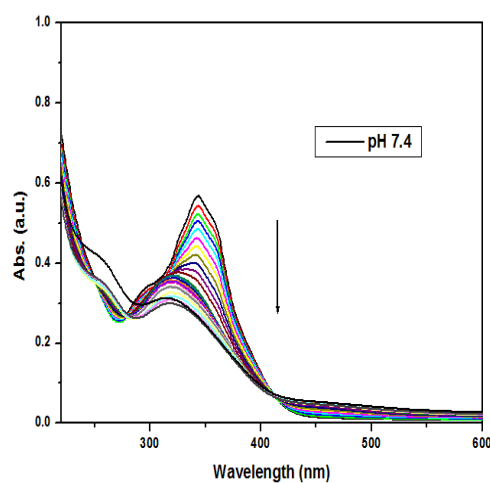


Figure 4.10. UV-Vis spectra obtained by addition of Cu(OAc)₂.H₂O at 25°C to a solution of R9-SB4CB (*ca.* 2.5×10^{-5} M) at a) pH 4 (0.1 M acetate buffer), b) pH 7.4 (0.01 M PBS buffer) and at c) pH 9 (0.1 M borate buffer).

(b)



(c)

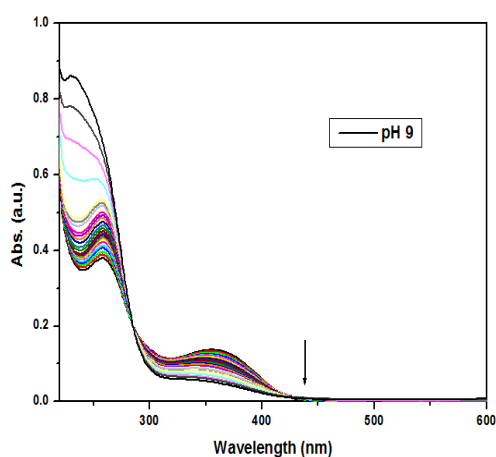


Figure 4.10 (continued). UV-Vis spectra obtained by addition of $\text{Cu}(\text{OAc})_2 \cdot \text{H}_2\text{O}$ at 25°C to a solution of R9-SB4CB (*ca.* 2.5×10^{-5} M) at a) pH 4 (0.1 M acetate buffer), b) pH 7.4 (0.01 M PBS buffer) and at c) pH 9 (0.1 M borate buffer).

4.3.3.2 LC-MS

The identities of all metal complexes were verified by LC-MS experiments involving an electron spray ionisation. Table 4.2 summarizes the data for all Cu(II) dithiocarbamate Schiff base ligand-conjugates in solution in MeOH. Both copper complexes $\text{Cu}(\text{R1-SB4CB})_2$ and $\text{Cu}(\text{PEG-SB4CB})_2$ gave the expected signals in the electrospray mass spectra (positive ion detection mode) which correspond to the

protonated cations with the expected isotope pattern. The identities of Cu(PAβN-SB4CB)₂ and Cu(R4-SB4CB)₂ were confirmed by their respective double charged (2+) ions.. As shown in Figure 4.11, the chromatogram of R1-SB4CB showed two well-separated peaks with identical MS spectra and the same behavior was observed for its metal complex Cu(R1-SB4CB)₂. This may highlight the presence of diastereoisomers (*E/Z* hydrazone bound or *cisoid/transoid* complexes). The same was observed for Cu(R4-SB4CB)₂ and Cu(PEG-SB4CB)₂ but for Cu(PAβNSB)₂ the second peak was not very obvious. It is also interesting to note that the isotopic pattern of Cu(R1-SB4CB)₂ and Cu(PEG-SB4CB)₂ seems to be the result of an overlapping of two isotopic patterns. The copper (II) complexes also showed several similar fragment ions of [CuL]⁺ and the ligand [L+H]⁺ most likely due to decomposition in the gas phase. The hydrolyzed ligand signal appeared when MALDI was used however was not apparent in the ES-MS spectra due to the fact that electron-spray ionization is generally considered a “softer” technique.

Table 4.2. LC-ES-MS data for all Cu(II) dithiocarbazate Schiff base ligand-conjugates and R1-SB4CB for comparison.

Compound	Rt [min]	Exact Mass _{calcd} [MH ⁺]	Exact Mass _{expt}
Cu(R1-SB4CB) ₂	15.1 & 17.6	1032.27	[M+H] ⁺ = 1031.9 & 1030.1
R1-SB4CB	15.3 & 17.5	486.18	[M+H] ⁺ = 486.1
Cu(PEG-SB4CB) ₂	15.2 & 16.1	1010.21	[M+H] ⁺ = 1010.6 & 1011.5
Cu(PAβNSB) ₂	15.2	1578.50	[M+2H] ²⁺ = 789.1
Cu(R4-SB4CB) ₂	14.0 & 17.3	1968.87	[M+2H] ²⁺ = 986.1 and 986.1
Cu(R9-SB4CB) ₂	Results pending		
Cu(R9-SM4CB) ₂	Results pending		
Cu(RW9-SB4CB) ₂	Results pending		
Cu(RW9-SM4CB) ₂	Results pending		

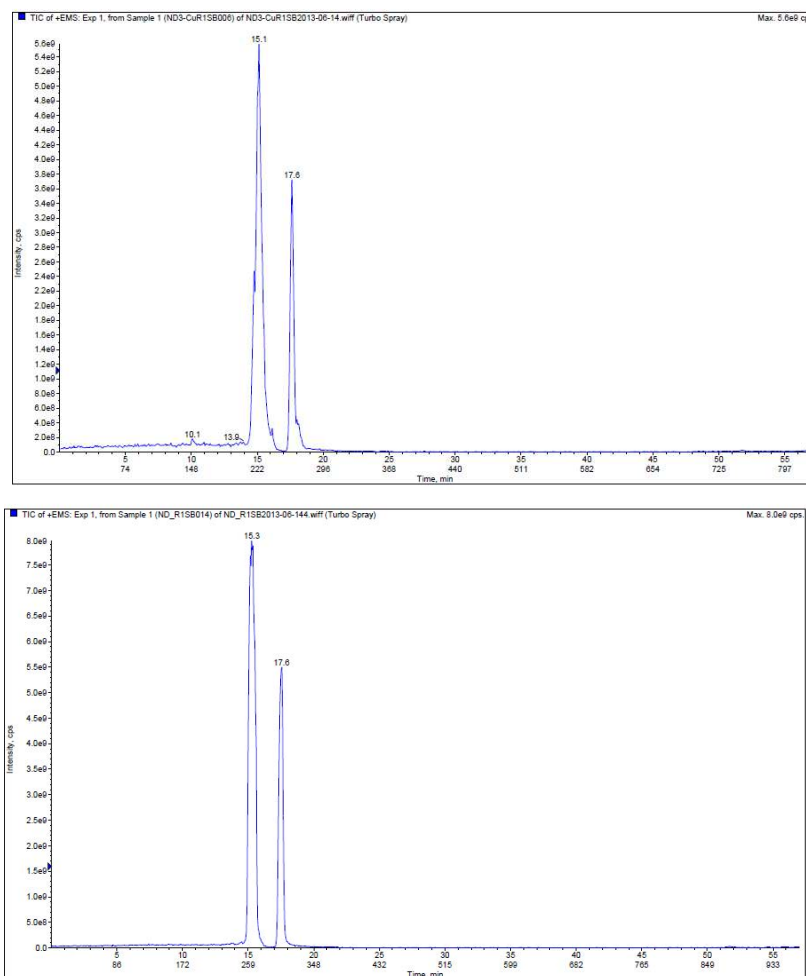


Figure 4.11. LC chromatogram of Cu(R1-SB4CB)₂ (top) and R1-SB4CB (bottom) showing the two isomeric peaks with similar molecular mass. A linear gradient elution developed from holding time of 5 min at 100% (0.1% formic acid in water) and then from 0-60% (0.1% formic acid in acetonitrile) in 30 min. Experiments were carried out at a flow rate of 10 $\mu\text{L min}^{-1}$ at room temperature with peaks detection at 220 nm and 280 nm.

4.3.3.3 ITC

Isothermal Titration Calorimetry (ITC), commonly used in the characterization of interactions between biomolecules, provides a complete thermodynamic characterization of an interaction (Grossoehme et al., 2010; Cisnetti et al., 2012; Ostermeier et al., 2010). In this work, ITC experiments were undertaken to determine the thermodynamic parameters for the interaction of selected peptide conjugate ligands with Cu(II) ions during complexation in aqueous solution. The

metal ion was titrated into the ligand and all experiments were run in duplicate or triplicate and corrected for buffer interactions. ITC directly measures the heat released after each injection of copper. The curves obtained were fitted using the integrated software, which calculates the enthalpy of the reactions (ΔH), the stoichiometry (n) and the association constant (K_{ass}). For the compounds in this work, the reactions were endothermic with ΔH values ranging from 12.2 to 159.8 kJ mol⁻¹ (Table 4.3). For all combinations tested, the association constant ($\log K_{\text{ass}}$) was of the order *ca.* 6, in the same range as the parent compound, and the stoichiometry close to the theoretical value of 0.5. These data strongly support the formation of the expected ML₂ complexes in agreement with the UV-Vis titrations: $\text{Cu}^{2+} + 2(\text{L}) \rightarrow [\text{CuL}_2]^{2+}$. Also, the conjugation doesn't seem to affect the complex formation to a large extent. An example of the ITC experiment for Cu(R9-SB4CB)₂, the most stable complex, is shown below (Figure 4.12).

Table 4.3. Thermodynamic parameters of conjugated ligand complexation with copper determined by ITC at 25 °C.

	$\log(K_{\text{ass}})$	ΔH (kJ mol ⁻¹)	n	ΔS (J mol ⁻¹ K ⁻¹)
Cu(R1-SB4CB) ₂	6.00	74.4	0.42	364.5
Cu(R9-SM4CB) ₂	6.56	12.2	0.53	166.4
Cu(R9-SB4CB) ₂	5.94	24.9	0.49	196.5
Cu(RW9-SB4CB) ₂	6.72	60.8	0.55	332.4
Cu(RW9-SM4CB) ₂	6.75	36.1	0.43	249.0
Cu(SB4CB) ₂ ^[a]	5.30	264.6	0.43	984.2

^[a] Parent compounds are given for the purpose of comparison.

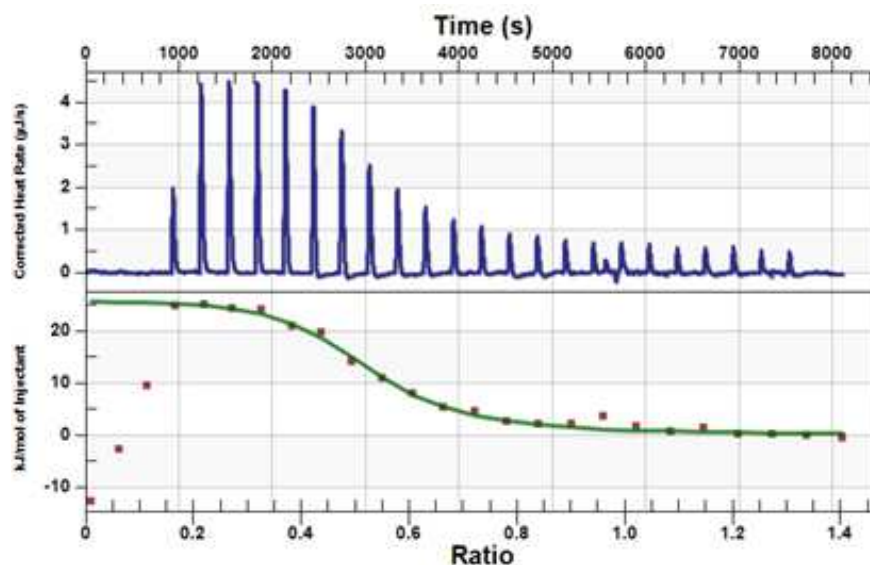


Figure 4.12. ITC titration of $\text{Cu}(\text{R9-SB4CB})_2$, $\text{Cu}(\text{OAc})_2$ (concentration at ca. 5×10^{-5} M) was added every 300 s to the ligand R9-SB4CB solution (concentration at ca. 1×10^{-5} M) in 0.1M acetate buffer at pH 6. The top curve represents the corrected heat flow with time. The bottom curve represents the heat of reaction (measured by peak integration) as a function of Cu/ligand ratio. The solid line is the best theoretical fit to the experimental data. The three first points were removed for the fitting.

Note: ITC experiments had been carried out for R4, PABNSB, PEG-SB4CB and SM4CB but to no avail. R4 suffered from peptide aggregation while PABNSB, PEG-SB4CB and SM4CB were not sufficiently water soluble for meaningful investigations.

4.3.3.4 EPR

Metal binding to the Schiff base ligand-vector conjugates were investigated using EPR spectroscopy for this paramagnetic d^9 Cu(II) system (Table 4.4). The EPR spectra of frozen solutions of the parent compounds $\text{Cu}(\text{SB4CB})_2$ and $\text{Cu}(\text{R9-SB4CB})_2$ in DMF (1 mM) show a well-resolved axial Cu(II) signal with significant separation of g_{\perp} and g_{\parallel} (Figure 4.13). Both spectra, with $g_{\parallel} > g_{\perp}$ are typical of axially symmetric mononuclear d^9 Cu^{II} complexes in a ground state doublet with the unpaired electron residing in a $d_{x^2-y^2}$ orbital. The g and A parameters, and especially g_{\parallel} and A_{\parallel} , indicate that the metal coordination environment involves two nitrogen atoms in a square-planar geometry for all complexes. The EPR spectra of the

bioconjugated complexes are expected to be very similar to those of their parent compounds, as observed here. The close similarity of the spectra is a strong indication that the Cu(II) ion is indeed coordinated to the ligand moiety of SB4CB or SM4CB in the bioconjugated system rather than unspecifically bound to the peptide sequence. Furthermore, the similarity of the EPR parameters of the complexes indicate that conjugation of the C-functionalized Schiff base ligands with polyarginine and other vectors such as PEG and PA β N has very little effect on its Cu(II) chelating behaviour. Due to the importance of water as a medium in biological investigation, the EPR spectrum of Cu(R9-SB4CB)₂ was also recorded in acetate buffer at pH 6 (Figure 4.14). Although the compound showed larger distortion from planarity with the increase of *f* value as compared to the spectra measured in DMF, the *f* value is still within the square planar range. In addition, the spectrum was different from that of aquated Cu(II) ions in aqueous solution indicating that the ligands remained coordinated to Cu(II) ions in that environment.

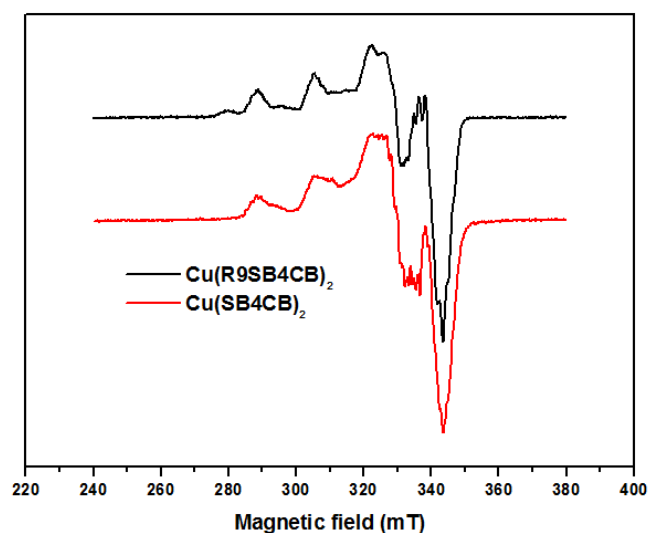


Figure 4.13. The EPR spectra of both parent and conjugated compounds (1 mM) in frozen DMF were indicative of the same species being formed with approximate calculated g_{\perp} and g_{\parallel} values of ~ 2.05 and ~ 2.15 , respectively. Microwave frequency 9.50 GHz, microwave power 0.25 mW, modulation amplitude 0.2 mT, modulation frequency 100 kHz, time constant 164 ms, $T = 50$ K.

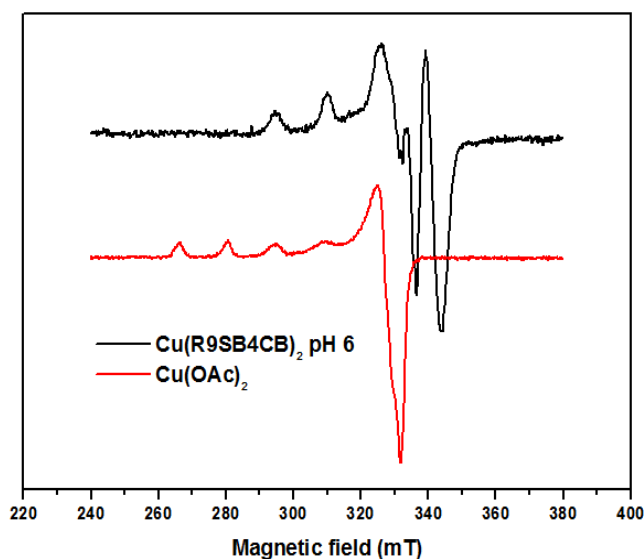


Figure 4.14: EPR spectra of 1mM $\text{Cu}(\text{R9-SB4CB})_2$ and $\text{Cu}(\text{OAc})_2$ in frozen acetate buffer pH 6 (0.1 M) are different from one another. Microwave frequency 9.50 GHz, microwave power 0.2 mW, modulation amplitude 0.2 mT, modulation frequency 100 kHz, time constant 164 ms, $T = 50$ K.

Table 4.4. EPR parameters measured from the spectra of the copper(II) complexes.

Compound	$g_{//}$	g_{\perp}	$A_{//}^{[a]}$	$f^{[b]}$	α^2
$\text{Cu}(\text{R1-SB4CB})_2$	2.16	2.06	523 (174)	124	0.71
$\text{Cu}(\text{PEG-SB4CB})_2$	2.15	2.06	541 (180)	119	0.71
$\text{Cu}(\text{PA}\beta\text{NSB})_2$	2.16	2.06	515 (172)	126	0.70
$\text{Cu}(\text{R4-SB4CB})_2$	2.16	2.06	509 (170)	127	0.69
$\text{Cu}(\text{R9-SB4CB})_2$	2.16	2.06	513 (171)	126	0.70
$\text{Cu}(\text{R9-SM4CB})_2$	2.16	2.06	524 (175)	123	0.71
$\text{Cu}(\text{RW9-SB4CB})_2$	2.16	2.06	514 (171)	126	0.70
$\text{Cu}(\text{RW9-SM4CB})_2$	2.16	2.06	519 (173)	125	0.70
$\text{Cu}(\text{SB4CB})_2^{[c]}$	2.15	2.05	531 (177)	121	0.70
$\text{Cu}(\text{SM4CB})_2^{[c]}$	2.15	2.05	504 (168)	128	0.67
$\text{Cu}(\text{R9-SB4CB})_2\text{-pH 6}$	2.13	2.05	463 (154)	138	0.61

[a] Unit in MHz, in bracket = $A_{//} \times 10^{-4} \text{ cm}^{-1}$ [b] Unit in cm. [c] Parent compounds for comparison purpose.

4.3.3.5 Electrochemistry

The electrochemistry properties of $\text{Cu}(\text{R1-SB4CB})_2$, $\text{Cu}(\text{PEG-SB4CB})_2$ and $\text{Cu}(\text{PA}\beta\text{N-SB4CB})_2$ were also tested in DMF (Table 4.5). The voltametric waves were not reversible unlike those of the parent compounds (Figure 4.15). This observation may be due to slow electron transfer or the bulkiness/hindered structure of the functionalized compounds.

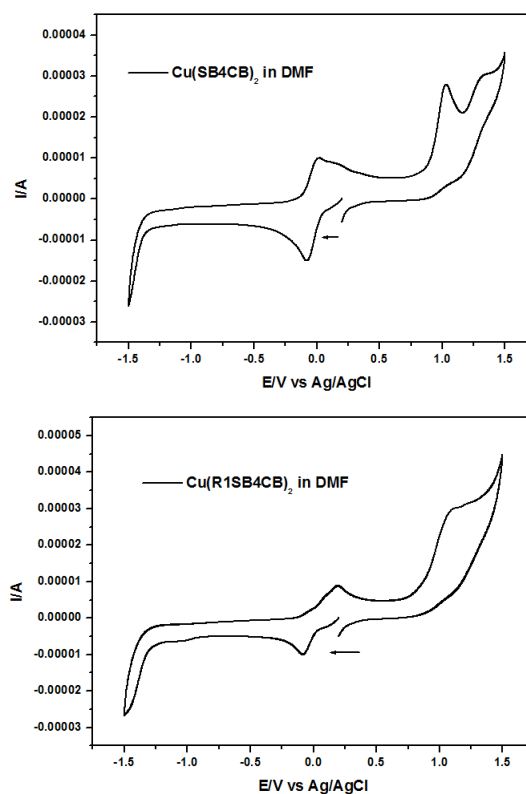


Figure 4.15. Cyclic voltammograms of $\text{Cu}(\text{R1-SB4CB})_2$ and $\text{Cu}(\text{SB4CB})_2$, 1.7 mM in anhydrous deoxygenated DMF with 0.1 M tetrabutylammonium perchlorate as the supporting electrolyte. Working electrode: glassy carbon; counter electrode: Pt wire; reference electrode: Ag/AgCl, scan rate: 100 mV/s. All sweeps were initiated in the direction of the arrow.

Table 4.5. Electrochemical data vs Ag/AgCl.

	Cu(II)/Cu(I)					Cu(II)/ Cu(III)
	E_{pa} [V]	E_{pc} [V]	$\Delta E_p = E_{pa} - E_{pc}$ [mV]	$\Delta E_{1/2} = 0.5 (E_{pa} + E_{pc})$ [V]	i_{pa}/i_{pc}	E_{pa} [V]
Cu(SB4CB) ₂	0.015	-0.079	94	-0.032	0.88	1.029
Cu(R1-SB4CB) ₂	0.200	-0.083	-	-	-	1.103
Cu(PEG-SB4CB) ₂	0.171	-0.098	-	-	-	1.103
Cu(PA β N-SB4CB) ₂	0.193	-0.082	-	-	-	1.090

4.4 Conclusion

This work shows the successful synthesis of copper complexes with bidentate dithiocarbazate Schiff base-conjugates which further demonstrates the ligands versatility for bioconjugation via SPPS for the first time. A series of ligand-bioconjugates were readily synthesized by either SPPS or solution phase synthesis. The synthetic pathways investigated are robust and can be applied to other bioconjugating groups. The conjugated ligands were characterized with HPLC, NMR and MS. Cu(II) ion complexation was achieved in situ and studied by a combination of LC-MS, UV-Vis, EPR, ITC and CV. The results indicate specific structural features of the metal bioconjugate complexes prepared in situ that exactly match those of the parent metal complexes. The formation of the desired complexes has been proven unambiguously and these complexes show dissociation constants in the low micromolar range. The effect of the vector conjugate is evident in the increase of the water solubility of the ligands and their metal complexes thus allowing investigation in aqueous solution to be carried out. The successful conjugation and facile complexation with copper suggest that the Schiff bases SB4CB and SM4CB may be suitable for further optimization with other targeting

groups. Such optimization is anticipated to result in enhanced biological properties as well as offering the possibility of being utilized for radioimaging. In addition, only two different substituents on the S-dithiocarbamate moiety (a methyl and a benzyl) were investigated in this work but many others can be introduced in the same way, which would potentially give access to a larger library of complexes. All the compounds presented here were further evaluated for their potential antimicrobial activity which will be discussed in the next chapter.

CHAPTER 5

BIOLOGICAL ACTIVITIES

5.1 Introduction

5.1.1 Mechanism of action of antimicrobial agents and multi-drug resistance

Bacteria could be broadly classified into Gram-positive and Gram-negative groups based on the outcome of Gram staining. The major difference between both groups is the structural organization outside the plasma membrane as shown in Figure 5.1 (Lolis and Bucala, 2003). According to Salton and Kim (1996), “most Gram-positive bacteria have a thick (20 to 80 nm) and continuous cell wall which is composed largely of peptidoglycan”. The peptidoglycan is linked covalently to “other cell wall polymers such as the teichoic acids, polysaccharides, and peptidoglycolipids”. On the contrary, Gram-negative bacteria have a thin (5 nm to 10 nm) peptidoglycan layer and another outer membrane structure outside the layer. In addition, lipoprotein molecules can be found in between the membrane structure and peptidoglycan layer while the lipopolysaccharides (LPS) are on the exterior surface of the outer membrane structure.

During an infection, “bacterial cells grow and divide, replicating repeatedly to reach large numbers”. In order to do so, bacteria “must synthesize or take up many types of biomolecules” causing cell deaths and disruption of cell function of the host organisms (Neu and Gootz, 1996). Bacteria could also promote infection and disease by producing toxins that can exert their effects directly on a target cell or by disabling the immune system (Deisingh and Thompson, 2002).

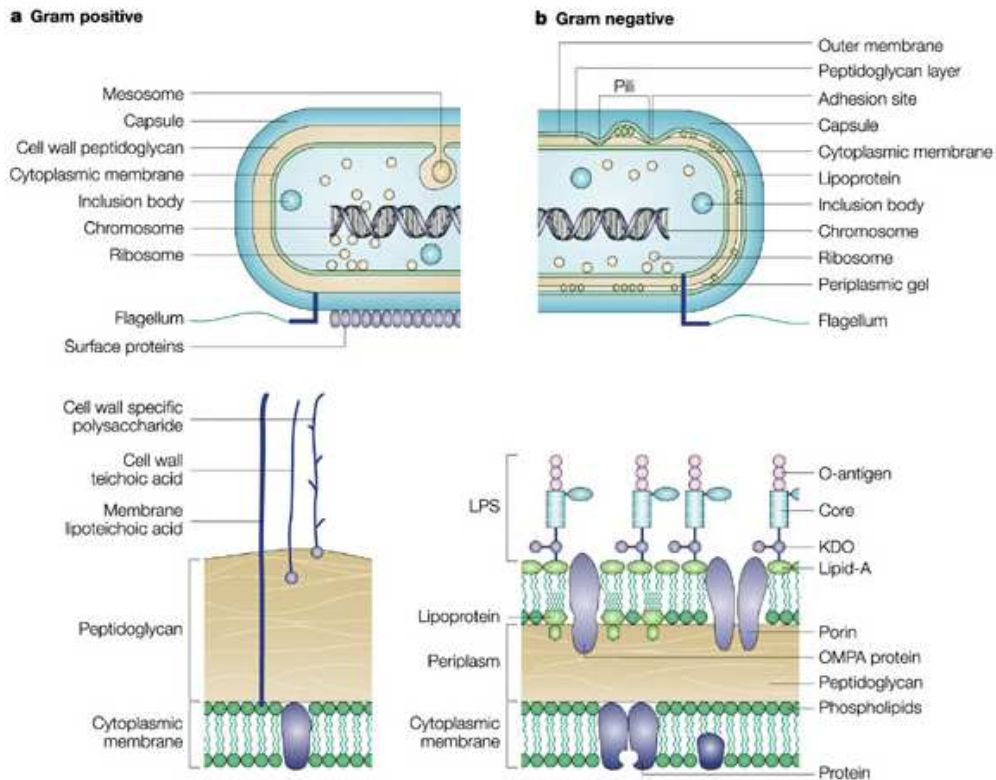


Figure 5.1. Structural features of the cell wall that distinguishes the Gram-positive from the Gram-negative bacteria (Source: Lolis and Bucala, 2003)

Antibacterial agents act against bacteria by interfering with vital processes for growth and division (Figure 5.2) that are specific to bacteria. They can be separated into groups depending on their target as listed by Neu and Gootz (1996) and O'Connell et al. (2013):

(1) Cell walls.

These peptidoglycan cell walls in bacteria and their synthetic pathways are an interesting target for specific treatment. For instance, penicillins and cephalosporins (β -lactam antibiotics) inhibit peptidoglycan polymerization while vancomycin (a glycopeptide) not only inhibits this polymerization but also prevents the polymer cross-linking.

(2) Cytoplasmic membranes.

Polymyxin binds to the bacterial LPS and then disrupts the plasma membrane causing leakage.

(3) Bacterial nucleic acid synthesis.

Quinolones prevent DNA replication by binding to topoisomerase IV or DNA gyrase. Nitroimidazoles such as metronidazole is reduced by an electron transport protein in anaerobic bacteria. The reduced drug damage DNA. Rifampin blocks mRNA synthesis by binding to DNA directed RNA polymerase

(4) Protein synthesis or ribosome function.

Aminoglycosides and tetracycline interfere with ribosome function by binding to the 30S ribosomal subunit and thus preventing translation initiation and tRNA binding. Another class of protein synthesis inhibitors includes chloramphenicol, erythromycin and clindamycin that disrupt translocation and peptidyl transferase activity by binding to the 50S ribosomal subunit.

(5) Metabolic pathway or folate synthesis.

Both sulfonamides and trimethoprim interfere with folate metabolism in the bacterial cell by competitively blocking the biosynthesis of tetrahydrofolate needed for DNA replication.

Antibacterial agents that kill bacteria as demonstrated by antibiotics that inhibit cell-wall construction are categorized as bactericidal while agents that only prevent or slow down the growth of the bacteria as exemplified by tetracyclines which stop protein synthesis are termed as bacteriostatic (O'Connell et al., 2013). In addition, “antimicrobial agents such as penicillin are active against only a narrow spectrum of

bacteria whereas others such as ampicillin inhibit a broad range of Gram-negative and Gram-positive bacteria” (Coates et al., 2002, p. 898). The combination of several antimicrobial agents has been known to display higher activity in comparison to using the individual component alone. For instance, sulfamethoxazole and trimethoprim (also known as co-trimoxazole) are synergistic in inhibiting folic acid metabolism by acting at different sites (Masters et al., 2003). Sulfamethoxazole and trimethoprim have specific affinity for pteridine synthetase and dihydrofolate reductase, respectively. Nonetheless, the combinations of antimicrobial agents should be practiced with caution to ensure that the result is not detrimental in which one agent reduces the efficacy of the other.

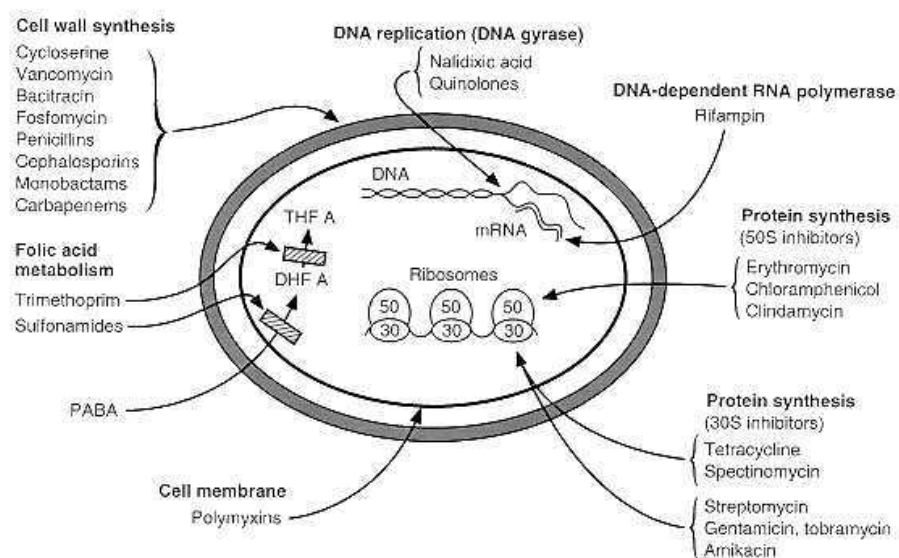


Figure 5.2. Mechanism of antimicrobial agents. (Source: Neu and Gootz ,1996)

Over the years, evolution of bacteria has resulted in varied mechanisms to protect themselves from the toxicity of antibacterials which lead to the challenge of multi-drug resistance (MDR) (Walsh, 2000; Taubes, 2008; Boucher et al., 2009; Stratton, 2003; Cloete, 2003). This has become a severe issue in treating bacterial infections as the worldwide dissemination of resistant bacteria has dramatically compromised

the efficiency of the antibiotic families and consequently increases the frequency of therapeutic failure (Pagès and Amaral, 2009). Tenover (2006, p. S3) has also stated that:

Bacteria may be intrinsically resistant to ≥ 1 class of antimicrobial agents, or may acquire resistance by de novo mutation or via the acquisition of resistance genes from other organisms. Acquired resistance genes may enable a bacterium to produce enzymes that destroy the antibacterial drug, to express efflux systems that prevent the drug from reaching its intracellular target, to modify the drug's target site, or to produce an alternative metabolic pathway that bypasses the action of the drug.

Therefore, continuous effort to discover new antibacterials with novel mechanism of action and to further understand the resistance mechanisms is required in order to fight the issue of MDR. Two classes of antimicrobial agents, the antimicrobial peptides and the efflux pump inhibitors are the focus of the following discussion.

5.1.2 Antimicrobials peptides

Since the synthetic work detailed herein involves CPPs that are known to share similar features with antimicrobial peptides (AMPs), it is worthwhile to highlight this class of compounds to aid interpretation and discussion of the results. The investigation of AMPs as antibacterial agents is currently of great interest as such compounds may offer several advantages over traditional antibacterial agents. The advantages highlighted by O'Connell et al. (2013, p. 10720) include AMPs reduced tendency to create resistance and their appealing “immunomodulatory, anti-inflammatory and anti-endotoxin activities”. These peptides also share the same fundamental structural features: they are relatively small in size ranging from 12 to 50 amino acid residues, they contain a net excess of positively charged residues and around 50% of hydrophobic residues resulting in amphipathic structure which is a crucial prerequisite to interact with the bacteria membrane (Strøm et al., 2003;

O'Connell et al., 2013). The phospholipid membrane of bacterial cells is the main target for AMPs. As shown in Figure 5.3 (Zasloff, 2002), bacterial membranes differ from the membranes of plants and mammals in which the outer leaflet of the bilayer that is exposed to the extracellular environment is composed mainly of negatively charged lipids in bacteria whereas the leaflet in multicellular animal is made of neutral lipids. Many hypotheses have therefore been presented for the mechanism of action of AMPs (Brogden, 2005; Hancock and Lehrer, 1998) including

fatal depolarization of the normally energized bacterial membrane, the creation of physical holes that cause cellular contents to leak out, the activation of deadly processes such as induction of hydrolases that degrade the cell wall, the scrambling of the usual distribution of lipids between the leaflets of the bilayer, resulting in disturbance of membrane functions, and the damaging of critical intracellular targets after internalization of the peptide (Zasloff, 2002, p. 390).

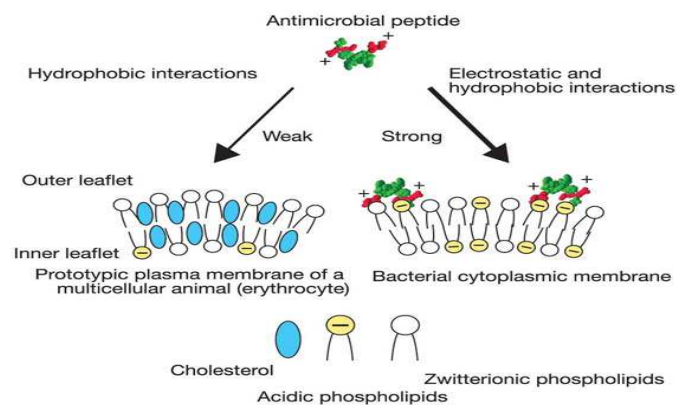


Figure 5.3. The membrane target of antimicrobial peptides of multicellular organisms and the basis of specificity (Source: Zasloff, 2002)

5.1.3 Efflux pumps and inhibitors

As previously mentioned in Chapter 4 (p.107), one primary resistance pathway of multi-drug resistant bacteria involves the over-expression of efflux pumps. The pumps have different affinity towards the diverse antibacterial drugs but most of the drugs are recognized by either one or more than one efflux pumps. From the illustration of Piddock (2006) in Figure 5.4a,

there are five main families of efflux pumps in bacteria: the ATP binding cassette (ABC) family, the major facilitator superfamily (MFS), multi-drug and toxic compound extrusion (MATE) family, the resistance nodulation division (RND) family, and the small multi-drug resistance (SMR) family. While members of the ABC, MFS, MATE and SMR families of efflux pumps are commonly observed in Gram-positive bacteria, efflux pumps in the RND, MFS and ABC families are often found in Gram-negative bacteria (Okandeji et al. 2011, p. 7679).

There is certainly a good deal of attention to combat efflux pumps due to their crucial role in many MRD phenotypes of pathogenic bacteria. According to Okandeji et al. (2011), two strategies can be applied: either circumventing their activity by preparing “derivatives of antibacterial drugs that are poor substrates of efflux pumps” or directly inhibit the efflux pumps through identification of an original anti resistance weapon called the efflux pump inhibitors (EPIs). EPIs cannot be considered as antibiotics but as adjuvants that will help other antibiotics to be efficient. A number of chemicals, such as phenylalanine arginine- β -naphthylamide (PABN), 1-(1-naphthylmethyl)-piperazine, quinoline derivatives as well as natural products like alkaloid reserpine have been found to inhibit bacterial efflux pumps (Kuete et al., 2011; Stavri et al., 2007). The use of these EPIs facilitates significant reduction of resistance to antibiotics in which the isolates were previously resistant (Kuete et al., 2011). In the search of new and potent antimicrobial agents in this study, the role of efflux pump had been investigated using pump-deleted strains and

PAβN-conjugates. The efflux pumps AcrAB and TolC of RND-family were chosen for investigation because they are often linked with the resistance of Gram-negative bacteria that are problematic to treat until now (Pagès and Amaral, 2009; Nikaido and Pagès, 2012; Vecchione et al., 2009; Okandeji et al., 2011; Piddock, 2006; Kuete et al., 2011; Stavri et al., 2007).

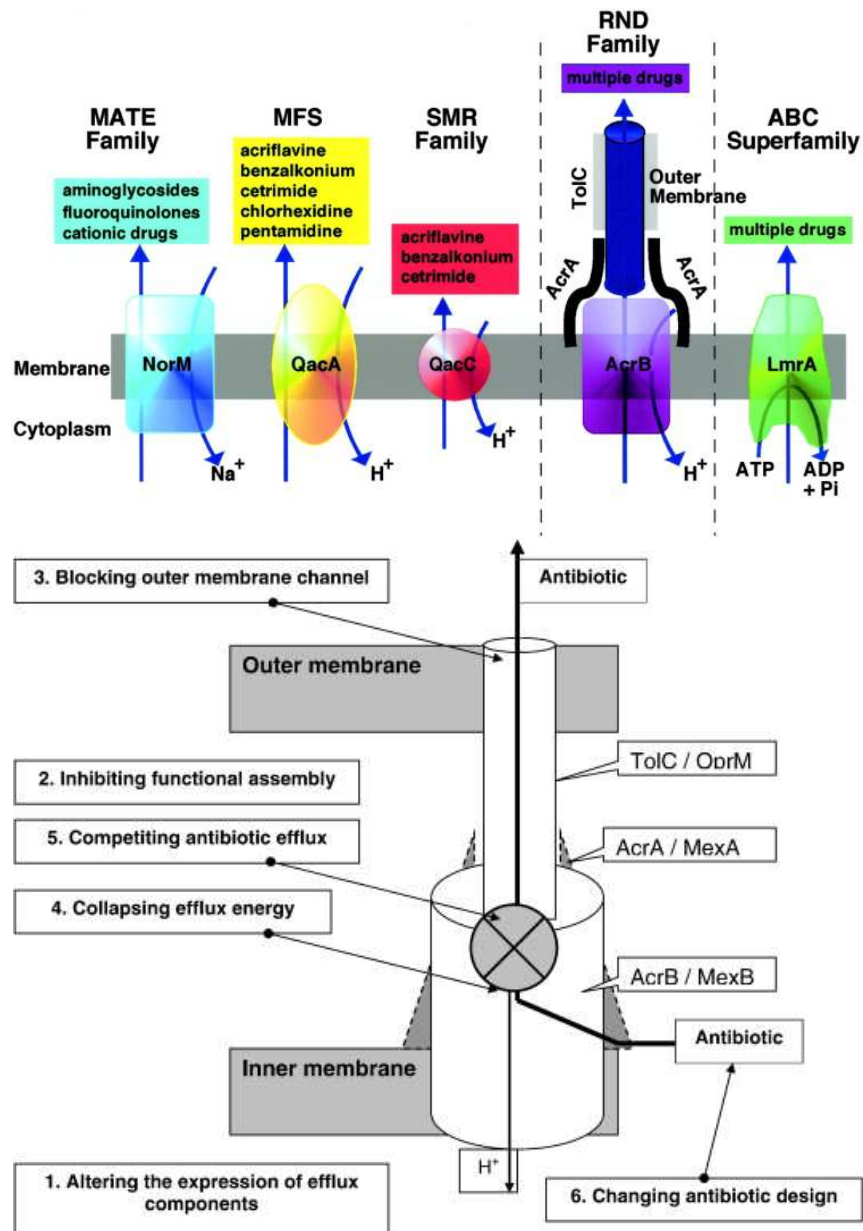


Figure 5.4. (a) Diagrammatic comparison of the five families of efflux pumps (Source: Piddock, 2006) (b) Targeting the efflux pump. Illustrations of various targets in the efflux pump complex of RND family (Source: Pagès and Amaral, 2009)

5.1.4 Contribution of metal complexes to the improvement of antimicrobial agents

The rich coordination geometry of metals offers an exciting platform for the discovery of new and potent metallodrugs with novel mechanisms of action (Sadler: N. J. Farrer and P. J. Sadler, 2011). These attributes may allow antibacterial metal complexes to be less likely to induce resistance in bacteria or at least to delay development of resistance. The geometrical arrangement of ligands in metal complexes, which vary according to the number and types of ligands bound to the metal centre, and to the coordination preference of the metal, affect their bioactivity (Ng et al., 2013). In the past few decades, we have witnessed the development and evolution of potential antibacterial agents derived from metal-based compounds although the mechanisms of their action are still not well understood. Patra et al. (2012b) reviewed work that explored organometallic derivatization of existing drugs as an attractive approach to overcome the resistance issue. For instance, organo ruthenium derivatives of quinolones (topoisomerase II enzyme inhibitor which unwinds DNA and interferes with DNA replication) showed good activity and were proven to have direct interaction with double-stranded DNA (Turel et al., 2010, Chen et al., 2004). It is interesting to note that organometallic derivatives of platensimycin (bacterial fatty acid biosynthesis inhibitor) appeared to completely change the mechanism of action. The compound no longer inhibited FabF enzyme but exhibited multi-causal death effect (Patra et al., 2009; Patra et al., 2012a). The review also discussed metal-specific mode of action of potential metallodrugs derived from arsenic, silver and gold ions. In some cases, it has been shown that the activity of a metal-derivatized drug could be the sum of the activity of the original drug and the inherent toxicity of the metal ion (Patra et al., 2012b). In reviews by

Beraldo and Gambino (2004), and Pelosi (2010) the significant bioactivities of Schiff base ligands derived from semicarbazones and thiosemicarbazones and their metal complexes were demonstrated. Enhancement of activity upon complexation was shown to be related to changes in either lipophilicity or redox effects with possible mechanisms of action involving production of free radicals, metal complex DNA interaction or inhibition of metalloenzymes. In very recent years, modification of metallocenes with peptides has been shown to not only enhance activity but also to alter the specificity of the compounds towards either Gram-positive or Gram-negative bacteria. (Metzler-Nolte, 2010; Chantson et al., 2005; Chantson et al., 2006). This strategy was also utilized by Jean-Marie Pages, Isabelle Artaud and coworkers (Pagès et al., 2013) in preparing a multicomponent metal chelating group-short antimicrobial peptide-fluorescent tag conjugate. The compound proved to be active against multi-drug resistant clinical isolates while the imaging investigation allowed determination of the localization and accumulation of the active compound inside bacteria (Pagès et al., 2013). Previously, the team had developed highly efficient inhibitors of bacterial metalloenzymes involved in the N-formyl-methionine excision pathway of nascent polypeptides (Petit et al., 2009; Huguet et al., 2012; Mamelli et al., 2009). They adopted the strategy of delivering the drug inhibitor via a metal-chaperone (Alimi et al., 2012). Metallodrugs consist of two parts: the drug, usually a hydroxamic acid, and an ancillary ligand as shown in Figure 5.5 below. The mechanism of action involves dissociation of the metallodrugs inside the bacteria promoting the delivery of the drug to its target (Artaud et al., 2014).

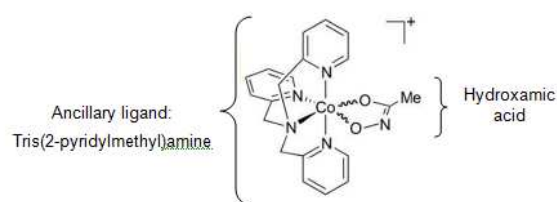


Figure 5.5. Example of a metallodrug that consists of hydroxamic acid and an ancillary ligand (Alimi et al., 2012).

All the examples above clearly demonstrate that there is a need to expand investigations in the field of metals in medicine and they attest to the significant role of metals in combating multi-drug resistance in bacteria to address the toxic effects of antimicrobial agents. Strategies used to search for effective drugs for a given target are of two types. The first involves a detailed knowledge of the target that allows the tailoring of suitable inhibitors whereas the second, a screening procedure, is applied when a compound is expected to show bioactivity but the target(s) against which it is effective is not known (Ferrari et al., 2002a). In this work, latter procedure was adopted. While much developmental effort has focused on the anticancer activity of dithiocarbazate Schiff bases and their metal complexes, study of the antimicrobial activity of these types of compounds has not been thoroughly explored. Therefore, a number of Cu(II) analogs were synthesized without specific molecular targets in view. The compounds were screened against a range of microbes with the intention of subsequently trying to correlate the biological activities with both solid and solution structures and their physico-chemical properties in order to orient further synthetic efforts towards obtaining the optimum geometry around the Cu ion essential to promote higher bioactivities and ultimately to reveal their mode of action.

5.2 Methodology

5.2.1 Antimicrobial testing (MIC determination)

5.2.1.1 Bacterial strains, culture media and chemicals

The bacteria chosen for this study are listed in the Table 5.1 below. The microorganisms studied included reference (from the American Type Culture Collection) and clinical (Laboratory collection) strains of gram negative bacteria *E. coli*, *E. aerogenes*, *A. baumannii*, *K. pneumoniae*, *P. aeruginosa* and *Salmonella enterica* (*S. enterica*) serotype Typhimurium as well as gram positive *S. aureus*. EA289 is an *E. aerogenes* KAN^S (sensitive to kanamycin, MDR isolate that exhibits active efflux of norfloxacin and efflux pump overproduction), EA298 constructed from EA289 is deleted of TolC (Pradel and Pagès, 2002). AG100 is an *E. coli* Wild Type (WT) and AG100A is its KAN^R (resistant to kanamycin) derivative, deleted of AcrAB and hypersensitive to chloramphenicol, tetracycline, ampicillin and nalidixic acid (Viveiros et al., 2005). Strains were grown at 37°C on Mueller-Hinton medium 24 h prior to any assay. Mueller-Hinton broth (MHB) was used for the susceptibility test. Chemicals polymyxin B nonapeptide (PMBN) were obtained from Sigma-Aldrich and the culture medium was purchased from Becton Dickinson.

Table 5.1. Bacteria strains.

Bacteria strains	Features	References
<i>Escherichia coli</i>		
AG100	Wild-type <i>E. coli</i> K-12	(Viveiros et al., 2005)
AG100A	AG100 Δ <i>acrAB</i> ::KAN ^R	(Viveiros et al., 2005)
<i>Enterobacter aerogenes</i>		
EA289	KAN sensitive derivative of EA27	(Pradel and Pagès, 2002)
EA298	EA 289 <i>tolC</i> ::KAN ^R	(Pradel and Pagès, 2002)
<i>Acinetobacter baumannii</i>		
ATCC19606	Reference strain	-
<i>Klebsiella pneumoniae</i>		
ATCC12296	Reference strain	-
<i>Pseudomonas aeruginosa</i>		
PA 01	Reference strain	-
<i>Salmonella enterica serotype Typhimurium</i>		
SL696	Wild-type, metA22, trpB2, strAi20	(Plesiat and Nikaido, 1992)
<i>Staphylococcus aureus</i>		
SA1199	Wild-type clinical, methicilin-susceptible	(Kaatz et al., 1987)

KAN^R, resistance to kanamycin

5.2.1.2 Determination of bacterial susceptibility

The respective minimum inhibition concentration (MIC) of the sample against targeted bacteria were determined using the broth dilution method previously described (Mallea et al., 1998). Susceptibilities were determined in 96-wells microplates with an inoculum of 2×10^5 cfu in 200 μ L of MHB containing two-fold serial dilutions of samples. MICs were determined in the presence of 5 % or 0.5% of DMSO. In the first case, a 20 \times concentration range of each compound was prepared in DMSO 100%. In the second case, a 200 \times concentration range of each compound was prepared in DMSO 100% and then diluted with H₂O to obtain a 20 \times concentration range in DMSO 10%. Then 10 μ l of these ranges were added to 190 μ l of inoculum. The MICs of samples were determined after 18 h incubation at 37°C, following addition (50 μ l) of 0.2 mg/mL iodinitrotetrazolium (INT) and incubation at 37°C for 30 minutes. MIC is defined as the lowest sample

concentration that prevented the color change of the medium and exhibited complete inhibition of microbial growth. The range of samples concentration used for MIC determination is universally accepted to be in doubling dilution steps up and down from 1 mg/L as required (Andrews, 2001). Therefore, the sample dilution range was from 0-128 μ M. Samples were tested alone or in the presence of PMBN at 51.2 mg/L final concentration (1/5 of its direct MIC). All assays were performed in duplicate or triplicate. Ciprofloxacin was used as standard antibiogram reference.

5.2.2 In vitro cytotoxicity testing

The cell lines used for testing, MCF-7 (human breast cancer cells possessing nuclear estrogen receptor) and MDA-MB-231 (human breast cancer cells without nuclear estrogen receptor) were obtained from the National Cancer Institute, U.S.A. Both cell lines were cultured in RPMI-1640 / DMEM (High glucose) (Sigma) medium supplemented with 10% fetal calf serum. The cells were plated into 96-well plate at cell density 6000 cells/well and incubated for 24 hours. After 24 hours, the media (5% serum) were discarded and cells rinsed with PBS solution. 200 μ L of a series of concentrations (50.0, 25.0, 10.0, 5.0, 1.0 and 0.5 μ M) for each sample prepared was added to each well. The 96-well plate was incubated for another 72 hr, after which the well plate was removed from incubator. Cytotoxicity was determined using the microtitration of 3-(4,5-dimethylthiazol-2-yl)-2,5-diphenyltetrazolium bromide (MTT) assay (Sigma, USA) as reported by Mosmann (1983). 20 μ L of MTT solution (5 mg/mL) was added to each well. The plate was wrapped with aluminium foil and incubated for 4 hours. After 4 hours, 200 μ L of sample containing MTT solution was discarded from the well. 200 μ L of DMSO was added to each well to dissolve the formazan crystals formed. The effect of the compound on cell line

viability was measured on an automated spectrophotometric plate reader (model MRX II microplate Elisa reader) at a test wavelength of 570 nm. Cytotoxicity was expressed as IC_{50} , i.e. the concentration that reduced the absorbance of treated cells by 50% with reference to the control (untreated cells). The IC_{50} values were determined from the plotted absorbance data for the dose-response curves. Controls that contained only cells were included for each sample. Tamoxifen was used as the cytotoxic standard.

5.3 Results and discussion

The free Schiff bases and their Cu(II) complexes as well as their bioconjugates described in the previous chapters were tested in collaboration with Dr. Laure Maigre and Professor Jean-Marie Pagès of Facultés de Médecine (UMR-MD1), Université de la Méditerranée, Marseille, France for the compounds ability to inhibit the growth of nine strains of both gram-negative and gram-positive bacteria. The effects of membrane permeabilizing agent (PMBN) and efflux pumps were investigated in an attempt to link the activity of these compounds with the bacteria penetration and the detoxification mechanisms of bacteria. Such investigations constitute the pioneering effort with these dithiocarbazate derivatives.

5.3.1 Antimicrobial evaluation

5.3.1.1 Macroacyclic Cu(II) system with tetradentate NNSS ligands

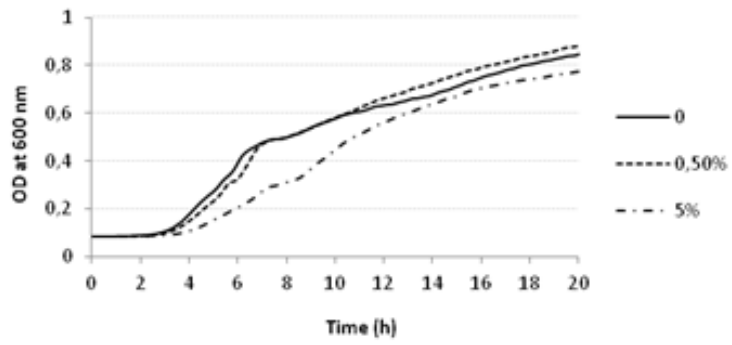
The initial synthesis and MIC evaluation involved tetradentate bis(dithiocarbazate) ligands and their respective Cu(II) complexes as shown in Table 5.2. As noted in previous chapters, a major drawback of these dithiocarbazate-Schiff bases is their poor solubility in aqueous solution. To ensure complete dissolution of the tested

compounds, up to 5% (v:v) of DMSO was used. Indeed, it is not ideal since DMSO could be toxic to bacteria at such a high concentration and/or could modify the membrane permeability (Yu and Quinn, 1994), thus affecting the apparent MIC values.

DMSO effect

It has been shown that solutions from 1% to 10% DMSO considerably affect the growth of fungi and cancerous cells, and with a 15% solution, growth of certain bacteria is effectively eliminated (Notman et al., 2006; Yu and Quinn, 1998; Ng et al., 2013). This is also the case for bacteria strains *A. Baumannii* and *P. Aeruginosa* at 5% of DMSO thus preventing the determination of the MIC under this condition. DMSO has also been reported to enhance permeability of the lipid membrane and also to cause the cell membrane to become less rigid facilitating membrane diffusion of exogenous species (Randhawa, 2006; Ghajar and Harmon, 1968; Anselet al., 1969; Dolan et al., 2013). As shown below (Figure 5.6), in comparison to 5% DMSO, 0.5% DMSO would not significantly affect the growth of the bacteria as compared to 5% DMSO. Therefore, it is important to keep in mind that DMSO is not necessarily innocent.

(a)



(b)

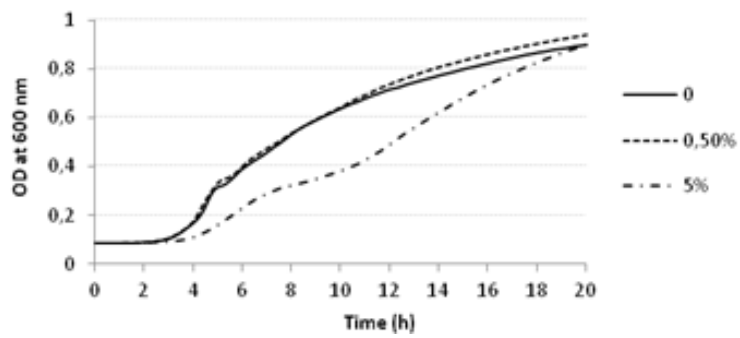
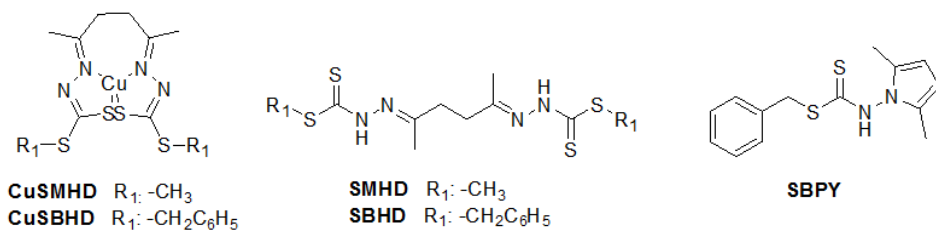


Figure 5.6. Influence of DMSO on the growth of bacteria strains over time. (a) AG100 and (b) EA289

Table 5.2. Antimicrobial activity of the tetradentate series.



Compound	Minimum inhibitory concentration (MIC) (μM)															
	Gram-															
	<i>E. coli</i>				<i>E. aerogenes</i>				<i>A. baumannii</i>	<i>K. pneumoniae</i>	<i>P. aeruginosa</i>	<i>S. enterica</i>		Gram+		
	AG100WT		AG100A <i>acrAB</i> -		EA289 <i>acrAB</i> +		EA298 <i>tolC</i> -		ATCC 19606	ATCC 11296		PA01	SL696		SA1199	
% DMSO	0.5	5	0.5	5	0.5	5	0.5	5	0.5	0.5	5	0.5	0.5	5	0.5	5
SMHD	>128	>128	>128	>128	>128	128-64	>128-128	>128	64	128	64	128-64	>128	>128	32	64-32
+PMBN	32	32	16	16	>128-128	64	128	32	16	64	32-16	16-8	64	32	32-16	64-32
CuSMHD	>128	>128	>128	>128	>128	>128	>128	>128	>128	>128	>128	>128	>128	>128	>128	>128
+PMBN	>128	>128	>128	1-2	>128	>128	>128-128	0.5-1	>128	>128	>128	>128	>128	>128	>128	>128
SBHD	>128	128	>128	128	>128	128-64	>128-128	64	>128	>128	128	>128	>128	>128	>128	64-32
+PMBN	>128	64	128-32	32-16	>128-128	64	>128-64	16-4	128-64	128-64	32-16	64-32	>128	64	16	128
CuSBHD	>128	>128	>128	>128	>128	>128	>128	>128	>128	>128	>128	>128	>128	>128	>128	>128
+PMBN	>128	>128	>128	>128	>128	>128	>128	>128	>128	>128	>128	>128	>128	>128	>128	>128

SBPY	>64	>64	>64	>64	>64	>64	>64	>64	>128	>128	>128	>128	>128	>128	128	128-64
+PMBN	64	64	32	16	>64	64	32	4	>128-128	>128	64	>128-128	64	64-32	128-64	128
Cu(Ac) ₂	>128	>128	>128	>128	>128	>128	>128	>128	>128	>128	>128	>128	>128	>128	>128	>128
+PMBN	>128	>128	>128	>128	>128	>128	>128	>128	>128	>128	>128	>128	>128	>128	>128	>128
Ciprofloxacin	0.03	0.06	0.008	0.015	64	64	32	32	2	0.25	-	0.5-0.25	0.03	-	1	-
+PMBN	0.015	0.03	0.008	0.008	64	128	32	16	2	0.125	-	-	0.03	-	1-0.5	-

Colour code: MIC values or average MIC values $\geq 64 \mu\text{M}$ = red, $\leq 10 \mu\text{M}$ = green, in between $64 \mu\text{M}$ and $10 \mu\text{M}$ = colourless. MIC values higher than $64 \mu\text{M}$ indicate inactivity.

Differences could be observed among the MIC values obtained with different concentrations of DMSO (0.5% or 5%) for certain molecules, particularly for CuSMHD against the mutated strains *E. coli* *acrAB*- and *E. aerogenes* *TolC*-. For this molecule, the MICs obtained with concentrations of DMSO, 2.5%, 1.5% and 1% were all > 128 μ M while with 5% DMSO, the MIC value was in the range 1-2 and 0.5-1 μ M, respectively. Because of the effect of DMSO on bacterial growth, it was not possible to confirm that the value truly reflects specific antimicrobial activity of the compound itself but it more likely corresponds to a synergetic effect of DMSO and the compound. The MIC values at 0.5% DMSO are more significant and will be discussed. However, in 0.5% DMSO, partial precipitation of the compounds could not be excluded which would lead to the determination of overestimated MIC values i.e. underestimation of the biological effect at the apparent concentration.

Influence of membrane permeabilizing agent on bioactivity

Since it has been reported that the low permeability of the outer membrane (Stratton, 2003; Cloete, 2003; Tenover, 2006; Strøm et al., 2003; Zasloff, 2002; Pagès and Amaral, 2009; Nikaido and Pagès, 2012) is a prime factor limiting intracellular activity of potential antimicrobial compounds, it is expected that the presence of a membrane permeabilizing agent would act synergistically with the compounds under study to promote their antimicrobial efficiency by facilitating increased uptake of the compounds. Among the permeabilizing agents, Polymyxin B nonapeptide (PMBN) has been used. PMBN is a cationic cyclic peptide derived from the antibacterial peptide polymyxin B (PMB). PMBN is an extremely poor antimicrobial agent but it is still capable of binding to lipid A of Gram-negative bacteria lipopolysaccharide

(LPS) like its parent compound, rendering the bacteria susceptible to various hydrophobic antibiotics. This capacity of PMBN to bind to bacteria with relatively high affinity and to permeabilize their outer membrane is often referred to as “sensitizing activity” and points to a novel therapeutic direction (Tsubery et al., 2000 and Tsubery et al., 2001). The compounds were therefore tested in the presence and absence of sub-inhibitory concentrations of PMBN (used at 1/5 its direct MIC value). Without PMBN all compounds were inactive against the strains tested (MIC > 64 μ M) except for the ligands SMHD and SBHD against *S. aureus*. However, a significant increase of up to 3-fold improvement of MIC values on both Gram-negative and Gram-positive bacteria was observed for the organic compounds SMHD, SBHD and SBDP in presence of PMBN. These results strongly suggest that the compounds, although toxic, do not penetrate the bacteria membrane efficiently. This lack of penetration hinders their intrinsic toxicity and leads to an apparent high MIC.

Efflux of the compounds

The role of efflux pumps was investigated using pump-deleted strains of Gram-negative *E. coli* and *E. aerogenes*. SMHD also seems more active (16 μ M) towards the isogenic derived strain, in which the efflux pump *AcrAB* genes are deleted as compared to wild-type *E. coli* (64 μ M). No significant activity was observed for SMHD in the absence likewise in presence of efflux pump for *E. aerogenes*. SBPY show differences in the MDR clinical isolate EA289 overexpressing the *AcrAB* efflux pump and on its efflux negative TolC- derivative EA298 with improvement in MIC from >64 μ M to 32 μ M. These results confirmed that SBPY is recognized by the efflux pumps and expelled from the bacteria thus limiting their bioactivity.

Effect of the dithiocarbazate substituent

Nevertheless, the ligand SMHD showed a broad range of moderate activity in the presence of PMBN with the most promising MIC values at or around 16 μM against *E. coli* *acrAB*-, *A. Baumannii*, *P. aeruginosa* and *S. aureus* thus making it a potential candidate for improvement. It is known that the biological activity of dithiocarbazate compounds can be greatly modified in the presence of different substituents. For instance, inhibition of *E. coli* and *S. aureus* by the Schiff base prepared from 2-benzoylpyridine with SMDTC is highly effective whereas that of the SBDTC compound shows no activity (Hossain et al., 1996).

Differences in activity against gram-positive and gram-negative bacteria

Apart from that, both SMHD and SBHD were moderately active against gram positive *S. aureus*. Typically, antibacterial molecules are more active toward Gram-positive than Gram-negative bacteria (Lessa et al., 2012; Bolla et al., 2011), as the additional outer membrane of the latter organisms impairs or slow down the drug uptake, which could be the case here.

Effect of complexation

Contrary to what has been usually reported in the literature that metal complexation enhances the bioactivity of ligands (Nandi et al., 1984; Joseph et al., 2012), in this case, the formation of the copper complexes induces a loss of antibacterial potency of the compounds. Similar losses in activity were previously reported with Pd(II) and Pt(II) complexes with acetone Schiff bases (Ali et al., 2002). The observation for this tetradentate series of compounds can be explained by the lower solubility of the metal complexes or by the lower stability of the hydrazone moiety in the case of

the free ligands. As mentioned before (Chapter 3, p. 51), depending on the pH, the ligands can be hydrolyzed in aqueous solution leading to several reactive products that can be toxic towards bacteria. At this stage it is not possible to deduce a clear structure-activity relationship from the limited number of compounds tested. Nonetheless, the Cu series complexed with tetradentate ligands was found to show a wide range of activity from non-active to active.

5.3.1.2 Open chain Cu(II) system with bidentate NS ligands with acid or ester functionality

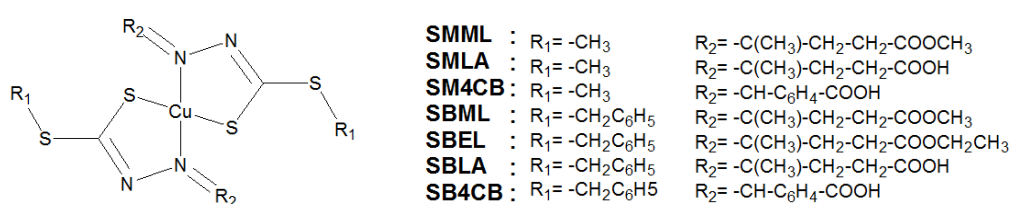
Efforts have been devoted to significantly improve the aqueous solubility of the above-mentioned compounds and to address the lack uptake of compounds due to low permeability of the outer membrane as well as the efficiency of efflux pumps. The synthesis was extended to another series based on Cu(II) complexes of bidentate ligands which are more soluble.

Influence of membrane permeabilizing agent on bioactivity

The bidentate ligands involved aliphatic ester, aliphatic acid or aromatic acid functionalities and were derived from both SMDTC and SBDTC. They were initially screened against a panel of four strains of bacteria with and without the presence of PMBN and the more promising compounds were further tested, in total nine strains of bacteria. These bidentate compounds were much more water soluble than their tetradentate counterparts and MIC studies could be performed with only 0.5% of DMSO. It has been previously shown that this amount does not inhibit the growth of bacteria. The general observations of the results summarized in Table 5.3 indicated that the bidentate series was more active than the tetradentate series in

0.5% DMSO. Upon introduction of PMBN, the impressive improvement in biological activity showed that these compounds also did not cross the cell membrane of Gram-negative bacteria efficiently. In the following discussion only results obtained in presence of PMBN will be discussed.

Table 5.3. Antimicrobial activity of non-conjugated bidentate series.



Compound	Minimum Inhibitory concentration (MIC) (µM)			
	<i>E. coli</i>		<i>E. aerogenes</i>	
	AG100 WT	AG100A AcrAB-	EA289 AcrAB+	EA298 ToIC-
SMML	>128	>128	>128	>128
+ PMBN 1/5	64	32	>128	128 - 64
Cu(SMML) ₂	>128	128	>128	>128
+ PMBN 1/5	64	16	>128-128	64 - 16
SMLA	>128	>128	>128	>128
+ PMBN 1/5	64	32	>128	128 - 64
Cu(SMLA) ₂	>64	>64	>64	>64
+ PMBN 1/5	64	32	>64	32
SBML	>128	128	>128	>128- 128
+ PMBN 1/5	16	16	>128-128	64 - 16
Cu(SBML) ₂	>128	32-16	>128	>128
+ PMBN 1/5	16	4	>128	4
SBLA	>128	128	>128	128
+ PMBN 1/5	32	8	128	64 - 16
Cu(SBLA) ₂	>128	>128	>128	>128
+ PMBN 1/5	32-16	8-4	>128	8
SBEL	>128	>128	>128	>128
+ PMBN 1/5	32	16	>128-128	128 - 16
SM4CB	>64	>64	>64	>64
+ PMBN 1/5	>64	>64 - 32	>64	>64
Cu(SM4CB) ₂	>64	>64	>64	>64

+ PMBN 1/5	64	32	>64	64
SB4CB	>64	>64 - 64	>64	>64
+ PMBN 1/5	32	16	>64	16
Cu(SB4CB) ₂	>64	>64	>64	>64
+ PMBN 1/5	8	8	>64	8 - 4

Colour code: MIC values or average MIC values $\geq 64 \mu\text{M}$ = red, $\leq 10 \mu\text{M}$ = green, in between $64 \mu\text{M}$ and $10 \mu\text{M}$ = colourless. MIC values higher than $64 \mu\text{M}$ indicate inactivity.

Efflux of the compounds

The influence of the efflux pump was verified by the improvement in MIC values against strains of *E. coli* and *E. aerogenes* lacking the selected efflux pump. Most compounds showed at least 2-fold increase in antimicrobial activity towards *E. coli* AcrAB- and *E. aerogene* TolC-. In contrast, only SBML, Cu(SB4CB)₂ and SM4CB showed no difference in activity against pump-deleted strains with the first two compounds having similar MIC values against *E. coli* strains and the latter against *E. aerogenes* strains indicating that the compounds were not driven out by the pump. Therefore, the reduction in antimicrobial activity of most compounds tested, like many of the current antibiotics, can be also primarily attributed to the presence of efflux pumps

Planarity of the ligands

Another factor that could affect the bioactivity of the Schiff bases is their planarity. Investigations by Olczak et al. (2007) has suggested that planarity of the pyridin-2-yl or pyrazin-2-ylformamide thiosemicarbazone fragment could be a prerequisite for tuberculostatic activity. The antimicrobial activity of the ligands SMML, SBML, SBEL and SBLA in which their crystal structures have been solved, can be arranged as SMML < SBEL < SBML < SBLA against all the 4 strains tested. The more active SBLA also appeared to be most planar when considering the inclination angles

between (i) the allylic ($=C(CH_3)CH_2CH_2$) and the terminal carbocyclic acid/ester ($-COOR$) planes (ii) the dithiocarbazate and the allylic planes, but appears to acquire greater perpendicularity of the benzyl ring towards the dithiocarbazate plane.

Stability of the ligand

The results demonstrated that the free ligand SB4CB with the aromatic acid substituent exhibited the lowest MIC values indicating a higher potency among the compounds in this series. This efficacy might be due to the presence of the aromatic ring that increases the stability of the compounds. It has been noted in the Chapter 3 (p. 52) that the aliphatic Schiff bases (SMML, SMLA, SBML, SBLA and SBEL) were hydrolyzed when chromatographed by RP-HPLC with solvent system containing 0.1% TFA. On the other hand, the aromatic Schiff bases (SM4CB and SB4CB) were found to be stable when monitored by HPLC and UV-Vis spectroscopy under similar conditions. No hydrolysis was observed even after 24 hours (18 hours is the duration required for MIC assay).

Effect of complexation

Many of the well known antibiotics like tetracyclines, quinolones and bleomycin are chelating agents and their actions are improved by the presence of metal ions, in particular copper ion (Ming, 2003; Efthimiadou et al., 2008). Thus, the synthesis and study of metal complexes with drugs used in clinical practice as well as promising ligands which may exhibit synergistic activity has attracted much attention as an approach to new drug development (Turel et al., 2010). Upon complexation with copper, most of the non-conjugated bidentate series compounds tested in this work showed equal or lower MIC values. The free copper (II) acetate was also screened

against all strains and was found inactive (MIC >128 μ M). The lack of growth inhibition activity for copper (II) acetate confirmed that the observed growth inhibition within experimental threshold was not due to the intrinsic biological activity of copper (II) free metal (Ng et al., 2013). To compare the complexation effect independently from the efficiency of the ligands, the ratio of MIC of the free ligand to that of the Cu(II) complex (which had been multiplied by 2 due to the coordination of two ligands in a complex) was calculated for the series of molecules and for each strain. A ratio above one is taken to mean that the enhanced biological activity is the result of a synergistic effect afforded by the complexation (the activity is due not only to the ligand itself) whereas a ratio less than one implies that the complexation is deleterious. As shown in Figure 5.7, the beneficial effect of the complexation for the ligands highly depends on the bacteria strain.

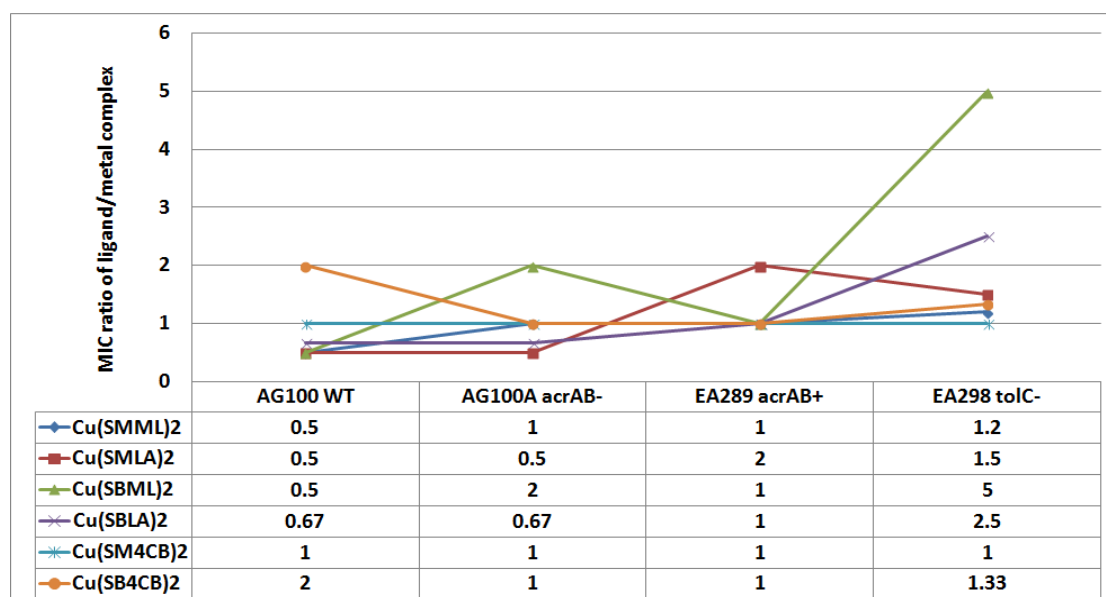


Figure 5.7. Effect of complexation on the non-conjugated bidentate series of molecules against the different strains of *E. coli* (AG100 T and AG100A acrAB-) and *E. aerogenes* (EA289 acrAB- and EA298 tolC-). The ratio MIC (free ligand) / MIC(complexed ligand) has been calculated with the MIC (in presence of PMBN) reported according to the stoichiometry of the complex.

The complexation did not play a crucial role on the three first tested strains *E. coli* WT, *E. coli* *acrAB*⁻ and *E. aerogenes* *acrAB*⁺ since majority of the MIC ratio values were 1. Only Cu(SB4CB)₂, Cu(SBML)₂ and Cu(SMLA)₂ showed positive complexation effect towards *E. coli* WT, *E. coli* *AcrAB*⁻ and *E. aerogenes* *AcrAB*⁺, respectively. Interestingly, the complexation improved the activity for most of compounds with the exception of Cu(SM4CB)₂ against the efflux pump TolC deleted *E. aerogenes* strain whereas such an effect is not observed on the strain possessing the TolC pump. This also demonstrated that complexation effectively decreases the efflux of the active molecules in the TolC pump deleted strain. The observed efficiency of the metal complexes could be linked to the significant changes in the physico-chemical properties of the compounds upon chelation. For instance, the molecular weight is doubled, the spatial geometry varied and new redox properties appear since the compounds now involved a metal. Besides that, the polarity of the metal complex is reduced to a greater extent in comparison to its free ion because of the overlap of the ligand orbital and partial sharing of the positive charge of the metal ion with the donor groups. Furthermore, it increases the delocalization of π -electrons over the whole chelate ring and enhances the lipophilicity of complexes in aqueous solutions, which may modify the interactions with cellular membranes (Raman, et al., 2003; Tiwari et al., 2012; Lobana et al., 2009). The changes in the metal complexes may also be compatibility with the hydrophobic pocket in the target site of the bacteria which further strengthen the binding of the complexes to the microbe contributing to their enhanced activity (Ming, 2003; Efthimiadou et al., 2008).

Effect of the dithiocarbazate substituent

There is also a general trend that the S-benzyl derived ligands and their metal complexes showed better activity than the S-methyl derivatives in this series. There have been mixed past reports on the bioactivity between SBDTC derivatives as compared to the SMDTC (Hossain, et al., 1996; Pavan et al., 2010). The stronger activity of S-benzyl derivatives could possibly be attributed to a higher cellular uptake due to an increased lipophilicity. In order to further access the structure-activity relationship, the biological activities of the compounds were correlated with the electrochemical properties as well as their structures in both solid state (SCXRD) and solution (EPR).

Redox potential of metal complexes

The redox potentials for the two series were recorded by cyclic voltammetry in anhydrous DMF. The obvious differences between the two series were that Cu(II) complexes of the bidentate series revealed a quasi-reversible reduction wave for Cu(II)/Cu(I) couples with E_{pc} ranging from -0.066 V to -0.114 V/(Ag/AgCl with $Fc/Fc^+ = 0.563$ V) (Chapter 3, page 88-94). On the other hand, both CuSMHD and CuSBHD in the tetradentate ligands series underwent an electrochemically irreversible one-electron reduction at $E_{pc} = -0.328$ and -0.285 V which were more negative than their bidentate counterparts. The more positive redox potential could be an explanation for the greater activity of the bidentate series. A higher redox potential means that Cu(II) reduction is easier, and consequently a higher content of Cu(I) could be continuously generated due to the reversibility. Cu(I) is prone to participate in Fenton-type reactions that produce reactive oxygen species (ROS), which can damage biomolecules within cells (Jansson et al., 2010). Radical

generation has also been proposed as a mechanism of cytotoxicity of Cu(II) and Fe(III) thiosemicarbazone (Jansson et al., 2010). This certainly suggests that the role of the reduction of the Cu(II) complexes in the antimicrobial action of the compounds cannot be excluded. In both series, the redox potentials were higher in the case of the benzyl-substituted compound than in the case of the methyl, which could be explained by a weaker electron-donating effect of the benzyl group. Again, the complexes having the higher redox potential were found to be more active. This supports the suggestion that the easier reduction to Cu(I) may be responsible for the increased activity.

Geometry of metal complexes

As previously mentioned in Chapter 3 (page 25, 88), there are correlation among redox potential, geometry and biological activity. Because of the difference in geometric preferences for Cu(II) (Jahn-Teller distortion favors square planar geometry) and Cu(I) (as a d^{10} ion, there is no electronic preference for a particular geometry) (Rorabacher, 2004), it would be anticipated that compounds with more positive Cu(II)/Cu(I) reduction potential (which goes with Cu(I) being more stable) are the least planar. The enhanced flexibility of the bidentate series as compared to the tetradentate series may facilitate increased square planar distortion leading to incorporation of Cu(I) ion that prefer non-square planar geometries. The information with regard to the deviation from planarity in the solid state can be accessed from the crystal structures. The crystal structures were obtained for Cu(SMML)₂, Cu(SMLA)₂, CuSMHD and CuSBHD. The bond angles about the central copper metal were consistent with a distorted square planar geometry with the sum of the angles around Cu exceeds 360°. The bidentate series, Cu(SMML)₂ and Cu(SMLA)₂

(374.33° and 380.12°, respectively) displayed a more significant distortion than CuSMHD and CuSBHD (367.65° and 360.9° respectively). The angles between two N-Cu-S planes confirmed the deviation from planarity of the complexes in the order Cu(SMLA)₂ > Cu(SMML)₂ > CuSMHD > CuSBHD. The bidentate series with more positive Cu(II)/Cu(I) redox potentials also demonstrated higher antimicrobial activity than their more planar tetradentate counterparts although the difference in bioactivity between the compounds in the same series was less pronounced. The EPR spectra recorded in DMF for both series indicated distorted square planar geometry for most Cu(II) complexes. Referring to the empirical factor $f (= g_{\parallel}/A_{\parallel})$ (Joseph et al., 2012; Krishna et al., 2008) of the compounds shown in Chapter 3 (p. 83), Cu(II) complexes with aliphatic acid and ester bidentate ligands (145-147 cm) confirm slightly higher degree of tetrahedral distortion than those with tetradentate ligands (141 and 143 cm) in solution. However, there are exceptions with Cu(SM4CB)₂ and Cu(SB4CB)₂ formed by the more active aromatic acid bidentate ligands. Both complexes revealed lower f values (128 and 121 cm, respectively) which are in the square planar range.

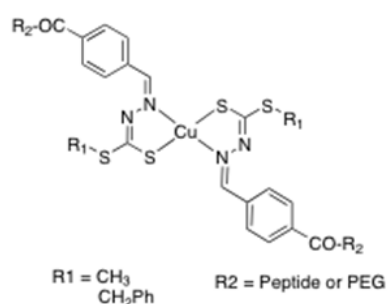
At this stage, the growth inhibitory mechanism of action and molecular target for the compounds carried out in this work is unclear. Nonetheless, others mechanisms of action are possible. For example, square planar Cu(II) complexes have often been associated with their ability to interact with DNA, the central target for most therapeutic agents (Manikandamathavan, et al., 2013). One of the proposed mechanism for these complexes involved the reduction of the DNA-intercalated Cu(II) complexes by glutathione or ascorbate, and followed by reoxidation of Cu(I) with dioxygen or in the presence of hydrogen peroxide. This leads to the generation

of active radicals which cause oxidative stress with irreversible damage to DNA resulting in induction of apoptosis (Gilbert et al., 1999; da Silveira et al, 2008; Borrás et al., 2007). Different binding interactions that affect metabolic pathways or even equally critical cellular processes have also been observed for Cu(II) thiosemicarbazone analogues. Their anti-tumour activity has been attributed to either inhibition of the enzyme ribonucleotide reductase, topoisomerase IIa or more recently a multi-drug resistance protein (MDR1) (Bisceglie, et al., 2012; Ferrari, et al., 2004; Finch, et al., 2000; Kovala-Demertzi et al., 1999). Although these proposed mechanisms are ambiguous, results point towards structure and redox potential dependent antimicrobial efficacy of the dithiocarbamate compounds.

5.3.1.3 Functionalized compounds

Having identified the most promising ligand (SB4CB) and Cu(II) complex, Cu(SB4CB)₂, the ligand was further functionalized with various vectors and the MIC values are shown in Table 5.4.

Table 5.4. Antimicrobial activity of bioconjugate series.



Compound	Minimum Inhibitory concentration (MIC) (μ M)			
	<i>E. coli</i>		<i>E. coli</i>	
	AG100 WT	AG100A <i>acrAB</i> -	EA289 <i>acrAB</i> +	EA298 <i>tolC</i> -
PEGAC	>128	>128	>128	>128
+ PMBN 1/5	>128	>128	>128	>128

PEG-SB4CB	>128	64	>128	>128
+PMBN 1/5	16	8	>128	16
Cu(PEG-SB4CB) ₂	>128	>128	>128	>128
+ PMBN 1/5	16	4	>128	8-4
PAβN-SB4CB	>128	>128	>128	>128
+ PMBN 1/5	>128	>128	>128	>128
Cu(PAβN-SB4CB) ₂	>128	>128	>128	>128
+ PMBN 1/5	>128	>128	>128	>128
R1AC	>128	>128	>128	>128
+ PMBN 1/5	>128	>128	>128	>128
R1-SB4CB	>128	32	>128-128	128-64
+PMBN 1/5	16	8	128	16
Cu(R1-SB4CB) ₂	>128	64	>128	128-64
+ PMBN 1/5	16-8	4	>128	8-4
R4AC	>128	>128	>128	>128
+ PMBN 1/5	>128	>128	>128	>128
R4-SB4CB	32	16-8	64	16
+PMBN 1/5	16	4	64	8-4
Cu(R4-SB4CB) ₂	16-8	8-4	>64-32	8
+ PMBN 1/5	8	2	>64-64	4-2
R9-Ac	8	8	8	8
+ PMBN 1/5	4	4	8	8
R9-SB4CB	8	8	8	4
+PMBN 1/5	4	4	4	4
Cu(R9-SB4CB) ₂	4	4	4	4
+ PMBN 1/5	2	2	4	2
RW9-Ac	2	2	8 - 4	2
+ PMBN 1/5	2	2	4	2
RW9-SB4CB	16 - 4	16	16 - 8	8
+ PMBN 1/5	8	8	8	8
Cu(RW9-SB4CB) ₂	8 - 4	8 - 4	16 - 8	8 - 4
+ PMBN 1/5	8	4	8	8

Colour code: MIC values or average MIC values $\geq 64 \mu\text{M}$ = red, $\leq 10 \mu\text{M}$ = green, in between $64 \mu\text{M}$ and $10 \mu\text{M}$ = colourless. MIC values higher than $64 \mu\text{M}$ indicate inactivity.

Influence of membrane permeabilizing agent on bioactivity

The antimicrobial activity and water solubility of this series were observed to be improved with conjugation in comparison to the parent compounds with the exception of PAβN conjugates. The PEG and R1 conjugates demonstrated significant improved activity only upon introduction of PMBN. This indicates that the addition of a neutral PEG and a positive charge from R1 were not sufficient for

uptake across the cell membrane of the bacteria. In contrast, it is positive to highlight that R4, R9 and RW9 conjugates were already active without the presence of PMBN. The increase in the cationic nature of the polyarginine derivatives allows better interaction and subsequently permeability across the negatively charged bacteria membrane as anticipated. Therefore, the MIC values obtained for these compounds either showed no difference or improved only 2-fold with the presence of PMBN. The slightly better activity in some cases of the polyarginine derivatives with PMBN point out that conjugation has yet to bring about optimum uptakes and the improved MIC values may be a result of synergistic effect between PMBN and conjugated ligands. Nonetheless, polyarginine conjugates appeared to be most efficient in crossing the cell membrane compared to the unconjugated compounds and other vectors.

Efflux of the compounds

The PEG, R1 and R4 conjugates also showed at least 2-fold increase in MIC values against pump deleted strains *E. coli* AcrAB- and *E. aerogene* TolC-. However, for R9 and RW9 derivatives, the MIC values remained the same with or without the presence of efflux pump. This is another encouraging observation that conjugation to CPP R9 and RW9 is beneficial as they are not affected by the efflux pumps. The PA β N conjugate was inactive against all strains tested. This conjugate was initially designed to assess the effect of efflux pump as well as to reveal any synergistic effect of the conjugate with possible new mechanism of action. However, the lack of activity reported with regards to this conjugate certainly demised the potential for positive synergistic effect.

Influence of arginine chain lengths on bioactivity

In addition to the noticeable trend with PMBN and efflux pumps, there is also correlation of higher bacterial growth inhibition potency with arginine chain lengths. The improvement of the MIC values averaged against all four strains upon conjugation of SB4CB to polyarginine is in the following order: R9-SB4CB > RW9-SB4CB > R4-SB4CB > R1-SB4CB > SB4CB. In order to identify the contribution of each moiety in the conjugates, acetylated free peptides and PEG were tested as well. The acetylated vectors PEGAC, R1AC and R4AC were totally inactive with MIC >128 μ M. The improved activity observed for the conjugates of these three vectors could have benefited from the better water solubility, permeability and cell uptakes of the conjugates. In contrast, RW9AC proved to be highly active against all the strains while R9AC also showed activity against them. As previously mentioned (Chapter 5, p. 149), CPPs and antimicrobial peptides are known to show similar characteristics, in particular amphiphilicity, which is a crucial factor determining the antibacterial activity of peptides. This seems to be the case for the CPP RW9. Noting the antimicrobial activity of the acetylated R9AC and RW9AC, these two vectors could have contributed their activity to the improved MIC values as demonstrated by the conjugates.

Effect of complexation

According to the Figure 5.8, most of the bioconjugated Cu(II) complexes showed equal or lower MIC values compared to the ligands indicating that complexation with Cu(II) did not contribute significantly to the observed activity of the ligands. The conjugates also showed resemblance to the parent compound in which complexation improved the efficiency against *E. aerogenes* TolC- strain as

demonstrated by the compounds $\text{Cu}(\text{PEG-SB4CB})_2$ and $\text{Cu}(\text{R1-SB4CB})_2$. On the other hand, both compounds showed deleterious ligands effect against *E. coli* WT.

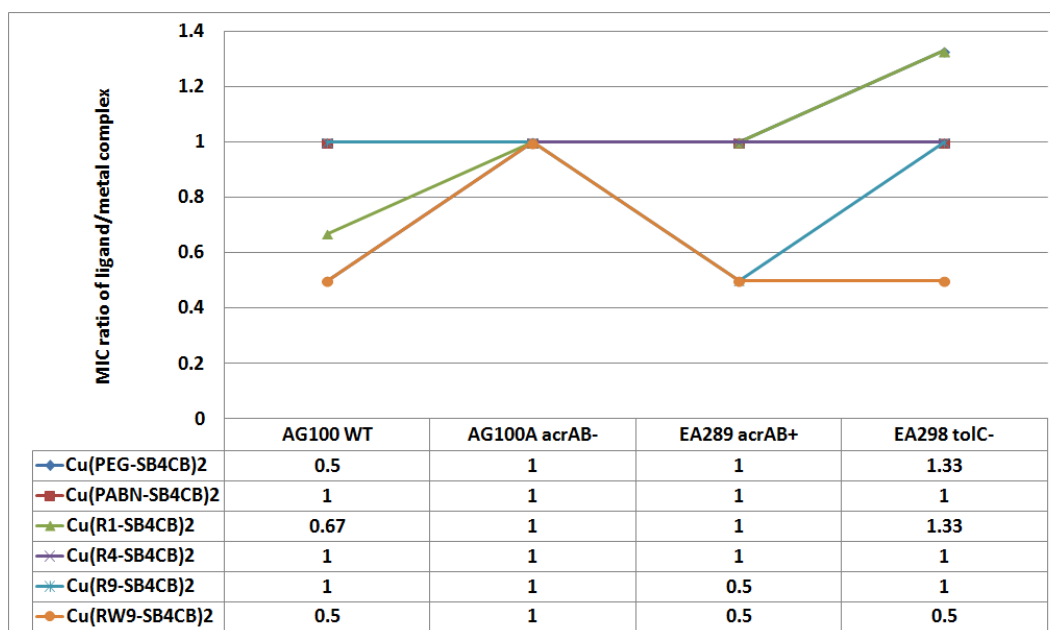


Figure 5.8. Effect of complexation on the conjugated bidentate series of molecules against the different strains of *E. coli* (AG100 T and AG100A *acrAB*-) and *E. aerogenes* (EA289 *acrAB*- and EA298 *tolC*-)

Final antimicrobial evaluation against 9 strains of bacteria

Despite the MIC ratio values, R9 and RW9 conjugates proved to be most potent derivatives that could escape from the efflux pump and penetrate cell membrane with good aqueous solubility. It therefore worthwhile to further explore their antimicrobial activity by extending the MIC determination to another five strains of bacteria for the conjugates, the acetylated vectors as well as the parent compounds for comparison (Table 5.5). The parent compounds SB4CB and $\text{Cu}(\text{SB4CB})_2$ were most active against gram positive bacteria *S. aureus* even without the presence of PMBN and both compounds also showed a wide spectrum of activity against the other gram negative strains in the presence of PMBN.

Table 5.5. Final antimicrobial evaluation against 9 strains of bacteria

Compound	Minimum inhibitory concentration (MIC) (µM)								
	Gram-								Gram+
	<i>E. coli</i>		<i>E. aerogenes</i>		<i>A. baumannii</i>	<i>K. pneumoniae</i>	<i>P. aeruginosa</i>	<i>S. enterica</i>	<i>S. aureus</i>
	AG100WT	AG100A <i>acrAB</i> -	EA289 <i>acrAB</i> +	EA298 <i>tolC</i> -	ATCC 19606	ATCC 11296	PA01	SL696	SA1199
SB4CB	>64	>64 - 64	>64	>64	128	>128	>128	>128	16
+ PMBN 1/5	32	16	>64	16	32	32	32	32	8
Cu(SB4CB)2	>64	>64	>64	>64	>128	>128	>128	>128	8 - 4
+ PMBN 1/5	8	8	>64	8 - 4	32	>128	64	64	8
SM4CB	>64	>64	>64	>64	>128	>128	>128	>128	64 - 32
+ PMBN 1/5	>64	>64 - 32	>64	>64	64	128	32	>128	64
Cu(SM4CB)2	>64	>64	>64	>64	>128	>128	>128	>128	16
+ PMBN 1/5	64	32	>64	64	>128	>128	128	>128	32
R9-Ac	8	8	8	8	>128	16	>128	64 - 16	>128
+ PMBN 1/5	4	4	8	8	>128	16	>128	8 - 4	64 - 32
R9-SB4CB	8	8	8	4	32	32	128 - 64	16	4
+ PMBN 1/5	4	4	4	4	32	16	128	8	4
Cu(R9-SB4CB)2	4	4	4	4	64	32	32	8	2
+ PMBN 1/5	2	2	4	2	64	16	32	4	1
R9-SM4CB	8	8	16 - 8	16 - 8	64	32 - 16	128	16	8
+ PMBN 1/5	4	4	8	8	32	16 - 8	>128	4	2
Cu(R9-SM4CB)2	8 - 4	4	8	4	64	16	64	8	8 - 4
+ PMBN 1/5	4	2	4	4	64	8	128	4 - 2	1 - 0.5

RW9-Ac	2	2	8 - 4	2	64 - 32	16 - 8	64 - 32	4 - 2	4
+ PMBN 1/5	2	2	4	2	128 - 64	8	4 - 2	1	2
RW9-SB4CB	16 - 4	16	16 - 8	8	32	32	16	8	4
+ PMBN 1/5	8	8	8	8	32	>16	8	4	2
Cu(RW9-SB4CB)2	8 - 4	8 - 4	16 - 8	8 - 4	64 - 32	32	16	8	4 - 2
+ PMBN 1/5	8	4	8	8	32	>16	8	4	1
RW9-SM4CB	8 - 2	8 - 4	8 - 4	4	8	16 - 8	16	4 - 2	2 - 1
+ PMBN 1/5	8	4	8	8	16	16	16 - 8	2 - 1	1
Cu(RW9-SM4CB)2	2	8 - 4	8	4	16 - 8	16 - 8	16	2 - 1	1
+ PMBN 1/5	4	2	4	4	16	16	8	1	1 - 0.5
Ciprofloxacin	0.03	0.008	64	32	2	0.25	0.5- 0.25	0.03	1
+ PMBN 1/5	0.015	0.008	64	32	2	0.125	-	0.03	1 - 0.5

Colour code: MIC values or average MIC values $\geq 64 \mu\text{M}$ = red, $\leq 10 \mu\text{M}$ = green, in between $64 \mu\text{M}$ and $10 \mu\text{M}$ = colourless. MIC values higher than $64 \mu\text{M}$ indicate inactivity.

It is likely that the complexes were more active against the Gram-positive bacteria due to the ease of penetration through the cell wall as compared to the Gram-negative bacteria. It should be noted that SM4CB, the less active S-methyl analogue of SB4CB ligand was also functionalized with R9 and RW9 in order to better understand the conjugation effect. This led to further positive results including the synthesis of a new compound, R9-SM4CB that was active against most of the bacteria. It is particularly interesting to note the construct of active R9-SM4CB against *S. aureus* with MIC values of 8 μ M (without the presence of PMBN) from R9AC (MIC >128 μ M) and SM4CB (MIC= 64 μ M), both of which were inactive under identical conditions. Comparing the efficacy of the compounds against the different strains of bacteria, the MIC values of the ligands conjugates were considerably better as compared to the parent compounds. Upon conjugation, the functionalized compounds exhibited improved antimicrobial activity with MIC values in the micromolar concentration range, as low as 1-0.5 μ M. However, in comparison with the R9 and RW9 acetylated free peptides, the improvement in MIC values of the conjugates were less striking although there were some exceptions that will be discussed herein. RW9AC proved to be active against *E. coli*, *E. aerogenes*, *K. pneumoniae*, *S. enterica* and *S. aureus* but less active against *A. baumannii* and *P. aeruginosa*. While R9AC also showed activity against some of the bacteria strains, it was completely inactive against *A. baumannii*, *P. aeruginosa* and *S. aureus*. Conjugation to R9 did not essentially change the antibacterial activity of R9 against gram-negative bacteria *E. coli*, *E. aerogenes* ArcAB+, *K. pneumoniae*, *P. aeruginosa* and *S. enterica*. The no improvement observation could mean that the activity is only due to the peptide and not to the parent compound. The RW9 conjugates showed either similar or increased MIC values as compared to acetylated

RW9 when evaluated against *E. coli*, *E. aerogenes*, *K. pneumoniae* and *S. enterica*. The conjugation of Schiff base with RW9 apparently compromises the antimicrobial activity of RW9 although the compounds were still active with respect to the bacteria mentioned previously. Notwithstanding this, R9 conjugates displayed 2 to 4- fold of enhancement in activity against *A. baumannii* from inactive R9AC (MIC > 128 μ M) to moderately active (MIC 32 and 64 μ M for R9-SB4CB and R9-SM4CBCB, respectively). Likewise, RW9-SM4CB (MIC 8 μ M) also showed improvement from RW9AC with the same strain. The highlight of the MIC results was definitely the high activity against the Gram-positive *S. aureus* in which R9-SB4CB, R9-SM4CB and RW9-SM4CB all showed better MIC values than their parent ligands as well as their respective acetylated free peptides. In addition, the MIC values of the conjugates were even more effective than ciprofloxacin against the *E. aerogenes* strains and also showed comparable MIC values with the standard drug towards *S. aureus*.

Since the parent compounds already showed activity without the introduction of PMBN against *S. aureus* and also PMNB does not significantly improve the MIC values of R9 and RW9 conjugates, the complexation effect will be discussed using MIC values ratio with and without PMBN as shown in Figure 5.9 and 5.10. Among the conjugates, only $\text{Cu}(\text{R9-SM4CB})_2$, $\text{Cu}(\text{RW9-SB4CB})_2$ and $\text{Cu}(\text{RW9-SM4CB})_2$ showed positive synergistic complexation effect against *P. aeruginosa*, *E. coli* AcrAB- and *E. coli* WT respectively, without the presence of PMBN. In the presence of PMBN, the efficacy of complexation effect towards *S. aureus* was evident from the MIC ratio values of 2 and 1.33 for $\text{Cu}(\text{R9-SB4CB})_2$ and $\text{Cu}(\text{R9-SM4CB})_2$, respectively. It was also apparent that complexation exacerbates the

ligand effect of RW9 derivatives with the most ratios less than 1 as observed in both graphs. However, the complexation effect was more favourable towards R9 derivatives as shown by Cu(R9-SB4CB)₂ with ratio of 2 against *P. aeruginosa* and *S. aureus* and Cu(R9-SM4CB)₂ with ratio of 1.33 against *S. aureus* in the presence of PMBN.

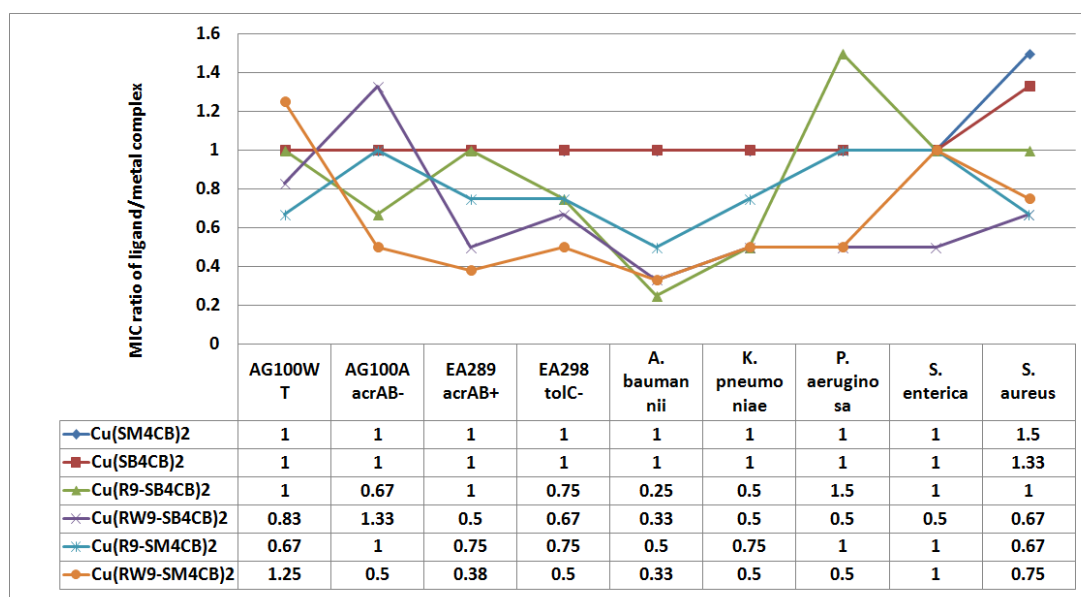


Figure 5.9. Effect of complexation on Cu(SB4CB)₂, Cu(SM4CB)₂, Cu(R9-SB4CB)₂, Cu(RW9-SB4CB)₂, Cu(R9-SM4CB)₂, Cu(RW9-SM4CB)₂ against the different strains without the presence of PMBN.

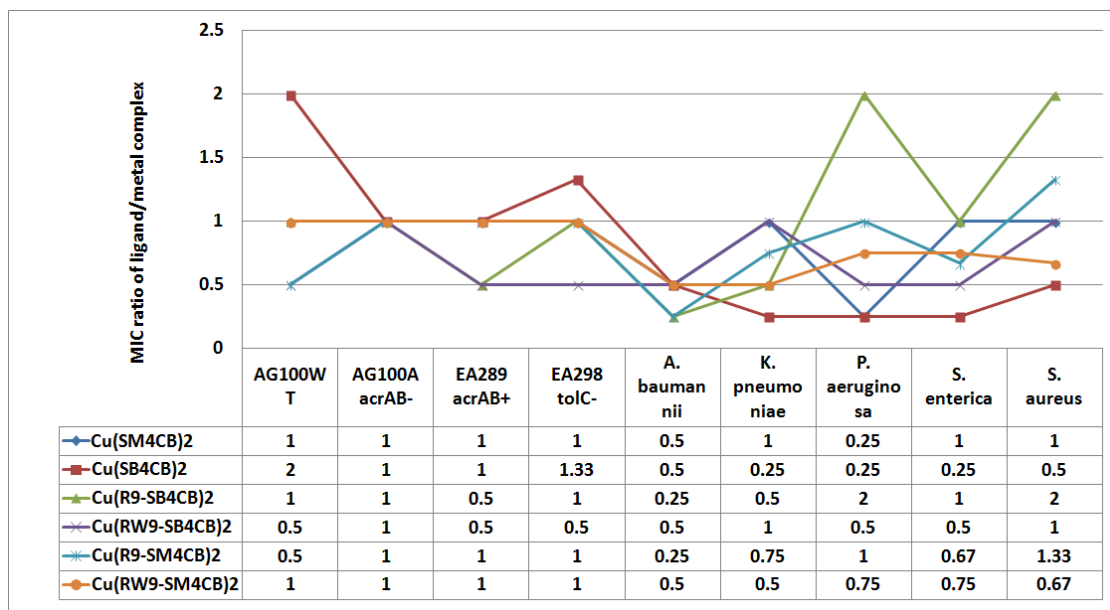


Figure 5.10. Effect of complexation on Cu(SB4CB)₂, Cu(SM4CB)₂, Cu(R9-SB4CB)₂, Cu(RW9-SB4CB)₂, Cu(R9-SM4CB)₂, Cu(RW9-SM4CB)₂ against the different strains in the presence of PMBN.

The EPR spectra for all of the Cu(II) bioconjugates were recorded and the redox potentials for Cu(R1-SB4CB)₂, Cu(PEG-SB4CB)₂ and Cu(PAβNSB)₂ were also evaluated (Chapter 4, p. 142). A general observation demonstrated that the EPR properties of the bioconjugates were similar to their parent compounds adopting a square planar geometry in solution. From the electrochemistry investigation, the Cu(II) bioconjugates showed a non-reversible negative shift of the redox couple Cu(II)/Cu(I) potential in the range -0.083 to -0.098 V as compared to Cu(SB4CB)₂ at -0.072 V. The loss of reversibility observed herein does not compromise the bioactivity of the compounds Cu(R1-SB4CB)₂ and Cu(PEG-SB4CB)₂, instead the bioconjugates derivatives showed enhanced antimicrobial efficacy. This could suggest a difference type of mechanism for the bioconjugates.

5.3.2 Cytotoxicity

In view of the well known cytotoxic activity of sulfur–nitrogen Schiff base chelating agents and their metal complexes and also to judge their utility for further development as anticancer agents, selected compounds were tested for their cytotoxicity against two breast cancer cell lines MDA-MB-231 (human breast carcinoma cells not expressing nuclear estrogen receptors, ER-) and MCF-7 (human breast carcinoma cells expressing nuclear estrogen receptors, ER+). Measurement of the cytotoxicity was carried out using MTT assay (Mosmann, 1983) based on the metabolic reduction of tetrazolium salt to form water insoluble formazan crystals with tamoxifen as standard. DMSO was used as negative control in the assay and the final content of DMSO for each compound tested was 0.5% or less. The concentration required to reduce growth of cancer cells by 50% (IC₅₀) are shown in Table 5.6 for both tetradentate series and bidentate NS series derived from 3-acetylcoumarin.

Table 5.6. Cytotoxic assay results.

	IC ₅₀ (μM)	
	MCF7	MDA-MB231
Tetradentate series		
SMHD	138.90	9.61
SBHD	9.69	1.05
CuSMHD	2.60	2.34
CuSBHD	1.49	0.71
Bidentate series		
SBCM	inactive	inactive
Re ₂ (SBCM) ₂	19.41	8.61
Zn(SBCM) ₂	inactive	inactive
Cu(SBCM) ₂	5.97	8.31
Tamoxifen	11.20	13.40

For the tetradentate series, it is interesting to note that the structure-activity relationship observed in the antibacterial tests differed from their cytotoxicity. Both ligands displayed at least 9-fold better toxicity towards the MDA-MB231 cell line that does not express estrogen nuclear receptors, indicating that ligand toxicity is not only mediated by these receptors. The more lipophilic SBHD exhibits a stronger toxicity in comparison to SMHD (Pavan et al., 2010). Complexation of Schiff base ligands with metal ions has been found to produce synergistic effects on the antiproliferative activities of the parent ligands since the complexes showed a marked cytotoxicity with IC_{50} values $< 5.0 \mu\text{M}$ towards both cell lines. Again the bioactivity of the complexes does not involve estrogen receptors because they are more active on MDA-MB231 cells. On both cell lines, the benzyl substituted complex CuSBHD showed slightly better IC_{50} values. The stronger activity of CuSBHD could possibly be attributed to a higher cellular uptake due to an increased lipophilicity. Likewise, the 3-acetylcoumarin derived bidentate series also highlighted that complexation played a significant role in improving the bioactivity of the compound. The ligand SBCM was found to be inactive towards both MCF-7 and MDA-MB231 cell lines. However, complexation of the Schiff base ligand with Cu(II) and Re(I) with the exception of Zn(II) showed marked cytotoxicity with IC_{50} values $< 10 \mu\text{M}$. $\text{Re}_2(\text{SBCM})_2$ displayed better selectivity towards MDA-MB231 whereas $\text{Cu}(\text{SBCM})_2$ was more potent against MCF7. All the Cu(II) complexes were most potent in both series and have lower IC_{50} values in comparison to standard tamoxifen making them potential anticancer agents for consideration. The difference in selectivity observed between the Cu(II) complexes of bidentate (MCF7) and tetradentate (MDA-MB231) series may result from their differences in ligand substituents, physico-chemical and redox potential. The bioactive $\text{Re}_2(\text{SBCM})_2$ with

the presence of tricarbonyl core may also offer novel exploratory derivatives for future investigations in the treatment of cancer as novel pharmaceutical as well as potential probe for sub-cell imaging. While the mechanism of action against breast cancer cell lines for dithiocarbazate compounds has yet to be definitively determined but an *in vitro* study by Cheah (2007) and Awidat (2005) on some dithiocarbazate compounds suggested that they induce apoptosis by DNA fragmentation and suppression of the expression of certain oncogenes. Previously mentioned mechanisms in the antimicrobial section i.e. inhibition of the enzyme ribonucleotide reductase, topoisomerase IIa or multi-drug resistance protein as well as production of ROS have also been linked to their anti-cancer activity.

5.4 Conclusion

It was demonstrated that the bidentate Schiff base (SB4CB) and its Cu(II) complex $\text{Cu}(\text{SB4CB})_2$ with aromatic acid functionality possess the most remarkable antibacterial effect against a wide spectrum of bacteria. The pioneering conjugation strategy investigated in this work demonstrated the utility of the combination of functionalized dithiocarbazate derivatives with vectors (CPPs) to generate bioconjugates with enhanced antimicrobial activity, membrane permeability and water solubility. The results highlighted various trends and factors that govern antimicrobial activities of the tested compounds. It was clearly evident that antimicrobial activities of the compounds are strongly dependent on their substituents. Introduction of the carboxylic acid moiety and SBDTC increases the antimicrobial activity within the bidentate series. The complexation with copper has a synergetic effect on the antimicrobial activity of these compounds. The increased activity of the complexes could be associated with their increased lipophilicity,

better fitness and size of the molecules towards binding sites as well as various geometrical arrangements including square planar and distorted forms inducing a tuning in redox potential. The observed cyclic voltammetric behaviour of bidentate copper(II) complexes showed a Cu(II)/Cu(I) redox quasi-reversibility and a positive shift as compared to the tetradentate series which may also contribute to their toxicity. In addition, the biological activity depends on factors such as the bacteria strain and the vectors used for bioconjugation. A deep understanding of the structure and activity of metal complexes against microorganisms is invaluable toward future development of antibiotic agents. The antimicrobial activity of the compounds can be summarized as follows:

Tetradentate series (S-benzyl derivatives<S-methyl derivatives, Cu (II) complexes<Ligands) <Bidentate series (Aliphatic<Aromatic, S-methyl derivatives<S-benzyl derivatives, Ligands<Cu (II) complexes) <Peptide conjugate series (PAβN<PEG<R1<R4<RW9/R9)< their Cu (II) complexes (MIC \approx 1-0.5 μ M)

All the selected Cu(II) complexes assayed against breast cancer cells lines (MCF-7 and MDA-MB-231) exhibited good cytotoxicity with lower IC₅₀ values (0.71-8.31 μ M) in comparison to their respective ligands and standard drug tamoxifen. This highlights the relevance of metal complexation strategy to stabilize the ligands and improve their bioactivity.

CHAPTER 6

CONCLUSION AND RECOMMENDATIONS

In conclusion, a total of 43 compounds were synthesized and characterized in this work. These compounds comprised of 10 Schiff base ligands derived from either SMDTC or SBDTC, 8 ligand-peptides/PEG conjugates, 5 acetylated peptides/PEG and 19 metal complexes. Single crystal structures were solved for 11 compounds. Only SMHD and SBHD were NNSS tetradentate ligands while the others behaved as bidentate NS ligands coordinating to the central metal through the azomethine nitrogen atom and the thiolate sulphur atom in their respective complexes. The antimicrobial activity of the compounds showed improvement going from macroacyclic tetradentate series to open chain bidentate series and finally the bioconjugates series. This work also allows new insight into the relationship between the structural/electrochemical properties and biological activity of the compounds. The bidentate series demonstrated higher antimicrobial activity than their more planar tetradentate counterparts as in the solid state, the crystal structures of $\text{Cu}(\text{SMML})_2$ and $\text{Cu}(\text{SMLA})_2$ from the bidentate series displayed a more significant distortion from square planar than CuSMHD and CuSBHD of the macroacyclic tetradentate series. EPR data also support the slightly greater distortion of the bidentate series in comparison to the tetradentate series in solution with the exception of $\text{Cu}(\text{SB4CB})_2$ and $\text{Cu}(\text{SM4CB})_2$ that fall in the square planar range. Both series also differed in their electrochemical properties in which bidentate series showed $\text{Cu}(\text{II})/\text{Cu}(\text{I})$ quasi reversibility at more positive potential whereas tetradentate series was not reversible. The $\text{Cu}(\text{II})$ R9 derivatives of SB4CB and SM4CB possess the most remarkable antibacterial effect against a wide spectrum of

bacteria. In addition, these R9-conjugates managed to address drawbacks that are often associated with most metal complexes involving the issues of poor water solubility and lack of uptake of the compounds due to low permeability of the outer membrane as well as the efficiency of bacteria efflux pump. The successful conjugation and facile complexation with copper for Schiff bases SB4CB and SM4CB offer exciting potential for them to be further optimized with different vectors in the future. The selected Cu(II) compound assayed against breast cancer cells also exhibited good cytotoxicity. The fact that the Cu (II) complexes are more efficient than the ligands is appealing. Taking into account, the serious side effects and upcoming resistance of clinical reference drugs, these new compounds are useful lead candidates for the development of novel therapeutic agents to treat bacterial infections and cancer.

Hitherto, the mechanism of action of the compounds has yet to be verified. Therefore, efforts to determine the concentration and location of the compounds inside cells will be the next crucial step for intracellular understanding. This is important in order to increase the compounds chances of succeeding in in vivo assay, clinical trials and ultimately to be used as therapeutic drugs. Attaching the lead compound to a probe or fluorescence moiety would allow cell imaging experiments to be carried out. Parallel studies involving the recognition of biomolecules as specific targets such DNA binding and cleavage, protein or enzyme inhibitors as well as depolarization 3,3'-Dipropylthiadicarbocyanine iodide (DiSC3(5)) or *ortho*-nitrophenyl- β -D-galactopyranoside (OPNG) membrane permeabilization assay (for bacteria) are also essential in order shed light on the mode of action of these compounds under biological conditions. It is also expected

that the application of computational analysis like docking will facilitate a deeper understanding of the molecular interaction. In addition, Density Functional Theory (DFT) and Quantitative Structure-Activity Relationship (QSAR) studies will enable elucidation of key structural and chemical parameters required to develop potent compounds. The data compilation will be beneficial in the long run as the information may allow utilization of virtual high throughput screening (HTS) approach to prescreen lead dithiocarbamate compounds in silico for diseases prior to synthesis or bioactivity assay validation. This approach would be an excellent strategy in both time- and cost-effective manner as compared to the carpet bombing strategy.

REFERENCES

- Abramkin, S., Valiahd, S. M., Jakupec, M. A., Galanski, M., Metzler-Nolte, N., & Keppler, B. K. (2012). Solid-phase synthesis of oxaliplatin-TAT peptide bioconjugates. *Dalton Transactions*, 41(10), 3001-3005.
- Afrasiabi, Z., Sinn, E., Padhye, S., Dutta, S., Padhye, S., Newton, C., ... & Powell, A. K. (2003). Transition metal complexes of phenanthrenequinone thiosemicarbazone as potential anticancer agents: synthesis, structure, spectroscopy, electrochemistry and in vitro anticancer activity against human breast cancer cell-line, T47D. *Journal of Inorganic Biochemistry*, 95(4), 306-314.
- Ahmad, J. Ma, A. Jemal, (2013) in *Breast Cancer Metastasis and Drug Resistance*, Springer New York, pp. 1.
- Ali, M. A., & Livingstone, S. E. (1974). Metal complexes of sulphur-nitrogen chelating agents. *Coordination Chemistry Reviews*, 13(2), 101-132.
- Ali, M. A., & Tarafdar, M. T. H. (1977). Metal complexes of sulphur and nitrogen-containing ligands: Complexes of S-benzylthiocarbamate and a Schiff base formed by its condensation with pyridine-2-carboxaldehyde. *Journal of Inorganic and Nuclear Chemistry*, 39(10), 1785-1791.
- Ali, M. A., Hossain, S. M., Majumder, S. M. M. H., Uddin, M. N., & Tarafder, M. T. H. (1987). Synthesis and characterization of some new nickel (II), zinc (II) and cadmium (II) complexes of quadridentate SNNS ligands. *Polyhedron*, 6(8), 1653-1656.
- Ali, M. A., Nazimuddin, M., Shaha, R., Butcher, R. J., & Bryan, J. (1999). Synthesis and characterization of bis-chelated nickel (II) complexes of the methylpyruvate Schiff bases of S-alkylthiocarbamates and the X-ray crystal structure of the [Ni (ONSM₂)₂] complex. *Polyhedron*, 17(22), 3955-3961.
- Ali, M. A., Mirza, A. H., Butcher, R. J., Tarafder, M. T. H., & Ali, M. A. (2001a). Synthetic, spectroscopic, biological and X-ray crystallographic structural studies on a novel pyridine-nitrogen-bridged dimeric nickel (II) complex of a pentadentate N₃S₂ ligand. *Inorganica Chimica Acta*, 320(1), 1-6.
- Ali, M. A., Mirza, A. H., & Butcher, R. J. (2001b). Synthesis and characterization of copper (II) complexes of the methylpyruvate Schiff base of S-methylthiocarbamate (Hmpsme) and the X-crystal structures of Hmpsme and [Cu (mpsme) Cl]. *Polyhedron*, 20(9), 1037-1043.
- Ali, M. A., Mirza, A. H., Butcher, R. J., Tarafder, M. T. H., Keat, T. B., & Ali, A. M. (2002). Biological activity of palladium (II) and platinum (II) complexes of the acetone Schiff bases of S-methyl- and S-benzylthiocarbamate and the X-ray crystal structure of the [Pd(asme)₂](asme= anionic form of the acetone Schiff base of S-methylthiocarbamate) complex. *Journal of Inorganic Biochemistry*, 92(3), 141-148.

Akbar Ali, M., Mirza, A. H., Nazimuddin, M., Ahmed, R., Gahan, L. R., & Bernhardt, P. V. (2003). Synthesis and characterization of mono-and bis-ligand zinc (II) and cadmium (II) complexes of the di-2-pyridylketone Schiff base of S-benzyl dithiocarbazate (Hdpksbz) and the X-ray crystal structures of the $[Zn (dpksbz)_2]$ and $[Cd (dpksbz) NCS]_2$ complexes. *Polyhedron*, 22(11), 1471-1479.

Ali, M. A., Mirza, A. H., & Fong, G. A. (2004). Synthesis, characterization and x-ray crystal structures of the bis-ligand zinc (II) and cadmium (II) complexes of the methylpyruvate schiff base of S-methyldithiocarbazate. *Transition Metal Chemistry*, 29(6), 613-619.

Ali, M. A., Mirza, A. H., Fereday, R. J., Butcher, R. J., Fuller, J. M., Drew, S. C., ... & Murray, K. S. (2005). Synthetic, EPR spectroscopic, magnetic and X-ray crystallographic structural studies on copper (II) complexes of the tridentate N_2S donor ligand formed from 6-methyl-2-formylpyridine and S-methyldithiocarbazate (Hmpsme). *Inorganica Chimica Acta*, 358(13), 3937-3948.

Ali, M. A., Mirza, A. H., Butcher, R. J., & Crouse, K. A. (2006). The preparation, characterization and biological activity of palladium (II) and platinum (II) complexes of tridentate NNS ligands derived from S-methyl- and S-benzyl dithiocarbazates and the X-ray crystal structure of the $[Pd (mpasme) Cl]$ complex. *Transition Metal Chemistry*, 31(1), 79-87.

Ali, M. A., HJ Abu Bakar, H. J., Mirza, A. H., Smith, S. J., Gahan, L. R., and Bernhardt, P. V. (2008) Preparation, spectroscopic characterization and X-ray crystal and molecular structures of nickel(II), copper(II) and zinc(II) complexes of the Schiff base formed from isatin and S-methyldithiocarbazate (Hisa-sme). *Polyhedron* 27, 71-79

Ali, M. A., Mirza, A. H., Mei, C. C., Bernhardt, P. V., & Karim, M. R. (2013a). Template synthesis and X-ray structural characterization of nickel (II) and zinc (II) complexes of tetradentate SNNS ligands formed by condensation of phthalaldehyde with S-methyldithiocarbazate and 4N -methyl-3-thiosemicarbazide. *Polyhedron*, 49 (1), 277-283.

Ali, M. A., Bernhardt, P. V., Brax, M. A., England, J., Farlow, A. J., Hanson, G. R., ... & Wieghardt, K. (2013b). The trivalent copper complex of a conjugated bis-dithiocarbazate Schiff base: Stabilization of Cu in three different oxidation states. *Inorganic Chemistry*, 52(3), 1650-1657.

Alimi, M., Allam, A., Selkti, M., Tomas, A., Roussel, P., Galardon, E., & Artaud, I. (2012). Characterization of cobalt (III) hydroxamic acid complexes based on a tris (2-pyridylmethyl) amine scaffold: Reactivity toward cysteine methyl ester. *Inorganic Chemistry*, 51(17), 9350-9356.

Altomare, A. G. C. A. M. C. G. M., Cascarano, G., Giacovazzo, C., Guagliardi, A., Burla, M. C., Polidori, G. T., & Camalli, M. (1994). SIRPOW. 92-a program for automatic solution of crystal structures by direct methods optimized for powder data. *Journal of Applied Crystallography*, 27(3), 435-436.

Amoroso, A. J., Coogan, M. P., Dunne, J. E., Fernández-Moreira, V., Hess, J. B., Hayes, A. J., ... & Williams, C. (2007). Rhenium fac tricarboxyl bishydrazone complexes: biologically useful fluorochromes for cell imaging applications. *Chemical Communications*, (29), 3066-3068.

Andrews, J. M. (2001). Determination of minimum inhibitory concentrations. *Journal of Antimicrobial Chemotherapy*, 48(suppl 1), 5-16.

Ansel, H. C., Norred, W. P., & Roth, I. L. (1969). Antimicrobial activity of dimethyl sulfoxide against *Escherichia coli*, *Pseudomonas aeruginosa*, and *Bacillus megaterium*. *Journal of Pharmaceutical Sciences*, 58(7), 836-839.

Artaud, I., Allam, A., Alimi, M., Maigre, L., Galardon, E., de Sousa, R. A., & Pages, J. (2014, March). Metallodrugs, as new strategy to improve cell uptake in bacteria of molecules known to be active in vitro. In *Journal of Biological Inorganic Chemistry* (Vol. 19, pp. S185-S185). 233 Spring St, New York, NY 10013 USA: SPRINGER.

Awidat, K. (2005). *Biological Activities and Molecular Analysis of Novel Dithiocarbamate Complex Compoundson Glioma Cell Lines* (Doctoral dissertation, Universiti Putra Malaysia).

Bacher, F., Enyedy, E. A., Nagy, N. V., Rockenbauer, A., Bognár, G. M., Trondl, R., ... & Arion, V. B. (2013). Copper (II) complexes with highly water-soluble l-and d-proline-thiosemicarbazone conjugates as potential inhibitors of topoisomerase IIa. *Inorganic Chemistry*, 52(15), 8895-8908.

Bagihalli, G. B., Avaji, P. G., Patil, S. A., & Badami, P. S. (2008). Synthesis, spectral characterization, in vitro antibacterial, antifungal and cytotoxic activities of Co (II), Ni (II) and Cu (II) complexes with 1, 2, 4-triazole Schiff bases. *European Journal of Medicinal Chemistry*, 43(12), 2639-2649.

Balamurugan, R., Palaniandavar, M., & Halcrow, M. A. (2006). Copper (II) complexes of sterically hindered Schiff base ligands: synthesis, structure, spectra and electrochemistry. *Polyhedron*, 25(5), 1077-1088.

Baldini, M., Belicchi-Ferrari, M., Bisceglie, F., Dall'Aglio, P. P., Pelosi, G., Pinelli, S., ... & Tarasconi, P. (2004). Copper (II) complexes with substituted thiosemicarbazones of α -ketoglutaric acid: synthesis, X-ray structures, DNA binding studies, and nuclease and biological activity. *Inorganic Chemistry*, 43(22), 7170-7179.

Bandow, J. E., & Metzler-Nolte, N. (2009). New ways of killing the beast: Prospects for inorganic-organic hybrid nanomaterials as antibacterial agents. *ChemBioChem*, 10(18), 2847-2850.

Barve, V., Ahmed, F., Adsule, S., Banerjee, S., Kulkarni, S., Katiyar, P., ... & Sarkar, F. H. (2006). Synthesis, molecular characterization, and biological activity of novel synthetic derivatives of chromen-4-one in human cancer cells. *Journal of Medicinal Chemistry*, 49(13), 3800-3808.

- Basha, M. T., Chartres, J. D., Pantarat, N., Ali, M. A., Mirza, A. H., Kalinowski, D. S., ... & Bernhardt, P. V. (2012). Heterocyclic dithiocarbazate iron chelators: Fe coordination chemistry and biological activity. *Dalton Transactions*, 41(21), 6536-6548.
- Beraldo, H., & Gambino, D. (2004). The wide pharmacological versatility of semicarbazones, thiosemicarbazones and their metal complexes. *Mini Reviews in Medicinal Chemistry*, 4(1), 31-39.
- Beshir, A. B., Guchhait, S. K., Gascon, J. A., & Fenteany, G. (2008). Synthesis and structure–activity relationships of metal–ligand complexes that potentially inhibit cell migration. *Bioorganic & Medicinal Chemistry Letters*, 18(2), 498-504.
- Betteridge, P. W., Carruthers, J. R., Cooper, R. I., Prout, K., & Watkin, D. J. (2003). CRYSTALS version 12: software for guided crystal structure analysis. *Journal of Applied Crystallography*, 36(6), 1487-1487.
- Bharti, N., Naqvi, F., & Azam, A. (2002). Synthesis, characterization, and screening for antiamebic activity of palladium (II), platinum (II), and ruthenium (II) complexes with ns-donor ligands. *Helvetica Chimica Acta*, 85(9), 2713-2720.
- Bisceglie, F., Pinelli, S., Alinovi, R., Tarasconi, P., Buschini, A., Mussi, F., ... & Pelosi, G. (2012). Copper (II) thiosemicarbazone molecular modifications modulate apoptotic and oxidative effects on U937 cell line. *Journal of Inorganic Biochemistry*, 116, 195-203.
- Blower, P. J., Castle, T. C., Cowley, A. R., Dilworth, J. R., Donnelly, P. S., Labisbal, E., ... & Went, M. J. (2003). Structural trends in copper (II) bis (thiosemicarbazone) radiopharmaceuticals. *Dalton Transactions*, (23), 4416-4425.
- Blumberg, W. E., & Peisach, J. (2003). Bis (thiosemicarbazone) and other nitrogen and sulfur ligated complexes of copper (II). *The Journal of Chemical Physics*, 49(4), 1793-1802.
- Bolla, J. M., Alibert-Franco, S., Handzlik, J., Chevalier, J., Mahamoud, A., Boyer, G., ... & Pagès, J. M. (2011). Strategies for bypassing the membrane barrier in multi-drug resistant Gram-negative bacteria. *FEBS letters*, 585(11), 1682-1690.
- Borel, M., Rappi, M., Pasqualini, R., Madelmont, J. C., Godeneche, D., & Veyre, A. (1992). Synthesis of potential ^{99m}Tc nitrido tumor imaging disposition in mice. *International Journal of Radiation Applications and Instrumentation. Part A. Applied Radiation and Isotopes*, 43(3), 425-436.
- Borrás, J., Alzuet, G., González-Alvarez, M., García-Giménez, J. L., Macías, B., & Liu-González, M. (2007). Efficient DNA cleavage induced by copper (II) complexes of hydrolysis derivatives of 2, 4, 6-tri (2-pyridyl)-1, 3, 5-triazine in the presence of reducing agents. *European journal of inorganic chemistry*, 2007(6), 822-834.

- Boschi, A., Massi, A., Uccelli, L., Pasquali, M., & Duatti, A. (2010). PEGylated N-methyl-S-methyl dithiocarbazate as a new reagent for the high-yield preparation of nitrido Tc-99m and Re-188 radiopharmaceuticals. *Nuclear Medicine and Biology*, 37(8), 927-934.
- Boucher, H. W., Talbot, G. H., Bradley, J. S., Edwards, J. E., Gilbert, D., Rice, L. B., ... & Bartlett, J. (2009). Bad bugs, no drugs: no ESKAPE! An update from the Infectious Diseases Society of America. *Clinical Infectious Diseases*, 48(1), 1-12.
- Brogden, K. A. (2005). Antimicrobial peptides: pore formers or metabolic inhibitors in bacteria? *Nature Reviews Microbiology*, 3(3), 238-250.
- Brunner, J., & Barton, J. K. (2006). Targeting DNA mismatches with rhodium intercalators functionalized with a cell-penetrating peptide. *Biochemistry*, 45(40), 12295-12302.
- Cattabriga, M., Marchi, A., Marvelli, L., Rossi, R., Vertuani, G., Pecoraro, R., ... & Ferretti, V. (1998). Synthesis and structural characterization of technetium and rhenium complexes containing derivatized amino acids. *J. Chem. Soc., Dalton Transactions*, (9), 1453-1460.
- Carballo, R., Casas, J. S., García-Martínez, E., Pereiras-Gabián, G., Sánchez, A., Sordo, J., ... & Abram, U. (2002). Reaction of bromopentacarbonylrhenium (I) with ferrocenylcarbaldehyde thiosemicarbazones: the first X-ray diffraction studies of metal carbonyl complexes containing bidentate thiosemicarbazone ligands. *Journal of Organometallic Chemistry*, 656(1), 1-10.
- Casas, J. S., Castellano, E. E., Ellena, J., García-Tasende, M. S., Pérez-Parallé, M. L., Sánchez, A., ... & Touceda, Á. (2008). New Pd (II) and Pt (II) complexes with N, S-chelated pyrazolonate ligands: Molecular and supramolecular structure and preliminary study of their *in vitro* antitumoral activity. *Journal of Inorganic Biochemistry*, 102(1), 33-45.
- Centore, R., Takjoo, R., Capobianco, A., & Peluso, A. (2013). Ring to open-chain transformation induced by selective metal coordination in a new dithiocarbazate ligand. *Inorganica Chimica Acta*, 404, 29-33.
- Chakraborty, A., Kumar, P., Ghosh, K., & Roy, P. (2010). Evaluation of a Schiff base copper complex compound as potent anticancer molecule with multiple targets of action. *European Journal of Pharmacology*, 647(1), 1-12.
- Chan, M. H. E., Crouse, K. A., Tahir, M. I. M., Rosli, R., Umar-Tsafe, N., & Cowley, A. R. (2008). Synthesis and characterization of cobalt (II), nickel (II), copper (II), zinc (II) and cadmium (II) complexes of benzyl N-[1-(thiophen-2-yl) ethylidene] hydrazine carbodithioate and benzyl N-[1-(thiophen-3-yl) ethylidene] hydrazine carbodithioate and the X-ray crystal structure of bis {benzyl N-[1-(thiophen-2-yl) ethylidene] hydrazine carbodithioate} nickel (II). *Polyhedron*, 27(4), 1141-1149.

- Chandra, S., & Sangeetika, X. (2004). EPR, magnetic and spectral studies of copper (II) and nickel (II) complexes of schiff base macrocyclic ligand derived from thiosemicarbazide and glyoxal. *Spectrochimica Acta Part A: Molecular and Biomolecular Spectroscopy*, 60(1), 147-153.
- Chantson, J. T., Falzacappa, M. V. V., Crovella, S., & Metzler-Nolte, N. (2005). Antibacterial activities of ferrocenoyl-and cobaltocenium-peptide bioconjugates. *Journal of Organometallic Chemistry*, 690(21), 4564-4572.
- Chantson, J. T., Vittoria Verga Falzacappa, M., Crovella, S., & Metzler-Nolte, N. (2006). Solid-phase synthesis, characterization, and antibacterial activities of metallocene-peptide bioconjugates. *ChemMedChem*, 1(11), 1268-1274.
- Chaviara, A. T., Cox, P. J., Repana, K. H., Pantazaki, A. A., Papazisis, K. T., Kortsaris, A. H., ... & Bolos, C. A. (2005). The unexpected formation of biologically active Cu (II) Schiff mono-base complexes with 2-thiophene-carboxaldehyde and dipropylenetriamine: crystal and molecular structure of $Cu(dpta)SCl_2$. *Journal of Inorganic Biochemistry*, 99(2), 467-476.
- Cheah, P. S., Ling, K. H., Crouse, K. A., & Rosli, R. (2007). Characterization of the S-benzylthiocarbamate effects on cell proliferation and oncogene expression in human breast cancer cells. *J Med Biol Sci*, 1, 1-7.
- Chen, C. L., Zhu, X. F., Li, M. X., Guo, H. M., & Niu, J. Y. (2011). Antitumor activity of manganese (II) and cobalt (III) complexes of 2-acetylpyridine schiff bases derived from S-methyldithiocarbamate: Synthesis, characterization, and crystal structure of the manganese (II) complex of 2-acetylpyridine S-methyldithiocarbamate. *Russian Journal of Coordination Chemistry*, 37(6), 435-438.
- Chen, X. B., Ye, Q., Wu, Q., Song, Y. M., Xiong, R. G., & You, X. Z. (2004). The first organometallic carbonyl tungsten complex of antibacterial drug norfloxacin. *Inorganic Chemistry Communications*, 7(12), 1302-1305.
- Chew, K. B., Tarafder, M. T. H., Crouse, K. A., Ali, A. M., Yamin, B. M., & Fun, H. K. (2004). Synthesis, characterization and bio-activity of metal complexes of bidentate N-S isomeric Schiff bases derived from S-methyldithiocarbamate (SMDTC) and the X-ray structure of the bis [S-methyl- β -N-(2-furyl-methylketone) dithiocarbamate] cadmium (II) complex. *Polyhedron*, 23(8), 1385-1392.
- Chikate, R. C., Belapure, A. R., Padhye, S. B., & West, D. X. (2005). Transition metal quinone-thiosemicarbazone complexes 1: Evaluation of EPR covalency parameters and redox properties of pseudo-square-planar copper (II)-naphthoquinone thiosemicarbazones. *Polyhedron*, 24(8), 889-899.
- Christlieb, M., & Dilworth, J. R. (2006). Ligands for molecular imaging: the synthesis of bis (thiosemicarbazone) ligands. *Chemistry - A European Journal*, 12(24), 6194-6206.

Cisnetti, F., Maréchal, J. D., Nicaise, M., Guillot, R., Desmadril, M., Lambert, F., & Policar, C. (2012). Metal Complexation of a D-Ribose-Based Ligand Decoded by Experimental and Theoretical Studies. *European Journal of Inorganic Chemistry*, 2012(20), 3308-3319.

Clède, S., Lambert, F., Sandt, C., Gueroui, Z., Refregiers, M., Plamont, M.-A., Dumas, P., Vessieres, A., and Policar, C. (2012). A rhenium tris-carbonyl derivative as a single core multimodal probe for imaging (SCoMPI) combining infrared and luminescent properties. *Chemical Communications* 48, 7729-7731.

Clède, S., Lambert, F., Sandt, C., Kascakova, S., Unger, M., Harté, E., ... & Policar, C. (2013). Detection of an estrogen derivative in two breast cancer cell lines using a single core multimodal probe for imaging (SCoMPI) imaged by a panel of luminescent and vibrational techniques. *Analyst*, 138(19), 5627-5638.

Cloete, T. E. (2003). Resistance mechanisms of bacteria to antimicrobial compounds. *International Biodeterioration & Biodegradation*, 51(4), 277-282.

Coates, A., Hu, Y., Bax, R., & Page, C. (2002). The future challenges facing the development of new antimicrobial drugs. *Nature Reviews Drug Discovery*, 1 (11), 895-910.

Cowley, A. R., Dilworth, J. R., Donnelly, P. S., Gee, A. D., & Heslop, J. M. (2004). Acetylacetonate bis (thiosemicarbazone) complexes of copper and nickel: towards new copper radiopharmaceuticals. *Dalton Transactions*, (16), 2404-2412.

Cowley, A. R., Dilworth, J. R., Donnelly, P. S., Heslop, J. M., & Ratcliffe, S. J. (2007). Bifunctional chelators for copper radiopharmaceuticals: the synthesis of [Cu (ATSM)-amino acid] and [Cu (ATSM)-octreotide] conjugates. *Dalton Transactions*, (2), 209-217.

Crouse, K. A., Chew, K. B., Tarafder, M. T. H., Kasbollah, A., Ali, A. M., Yamin, B. M., & Fun, H. K. (2004). Synthesis, characterization and bio-activity of S-2-picolylidithiocarbazate (S2PDTC), some of its Schiff bases and their Ni (II) complexes and X-ray structure of S-2-picolyl-β-N-(2-acetylpyrrole) dithiocarbazate. *Polyhedron*, 23(1), 161-168.

Creaven, B. S., Devereux, M., Karcz, D., Kellett, A., McCann, M., Noble, A., & Walsh, M. (2009). Copper (II) complexes of coumarin-derived Schiff bases and their anti-*Candida* activity. *Journal of Inorganic Biochemistry*, 103(9), 1196-1203.

Czerwieniec, R., Kapturkiewicz, A., & Nowacki, J. (2005). Re (I)(tricarbonyl)⁺ complexes with anionic N∩S⁻ thioxalato ligand. *Inorganic Chemistry Communications*, 8(1), 34-37.

Da Silva, A. S., De Silva, M. A. A., Carvalho, C. E. M., Antunes, O. A. C., Herrera, J. O. M., Brinn, I. M., & Mangrich, A. S. (1999). Coordination complexes of bifunctional compounds: I. Synthesis and properties of bis [5-(2-oxophenyl)-3-phenyl-1, 2, 4-oxadiazolyl] copper (II). A fluorescent coordination compound of Cu (II). *Inorganica Chimica Acta*, 292(1), 1-6.

Da Silveira, V. C., Luz, J. S., Oliveira, C. C., Graziani, I., Ciriolo, M. R., & Ferreira, A. M. D. C. (2008). Double-strand DNA cleavage induced by oxindole-Schiff base copper (II) complexes with potential antitumor activity. *Journal of inorganic biochemistry*, 102(5), 1090-1103.

Datta, P., Mukhopadhyay, A. P., Manna, P., Tiekink, E. R., Sil, P. C., & Sinha, C. (2011). Structure, photophysics, electrochemistry, DFT calculation, and *in-vitro* antioxidant activity of coumarin Schiff base complexes of Group 6 metal carbonyls. *Journal of Inorganic Biochemistry*, 105(4), 577-588.

Dawara, L., Fahmi, N., & Singh, R. V. (2011). Synthesis, characterization, antimicrobial, pesticidal and DNA cleavage activity of germanium (IV) derivatives of 3-(2-methyl-2, 3-dihydro-benzthiazo-2-yl)-chromen-2-one and N'-[1-2-oxo-2H-chrome-3yl-ethylidene]-hydrazinecarbodithionic acid benzyl ester ligands. *Main Group Metal Chemistry*, 34(5-6), 139-146.

Dawara, L., Joshi, S. C., & Singh, R. V. (2012). Synthesis, characterization, and antimicrobial and antispermatic activity of bismuth (iii) and arsenic (iii) derivatives of biologically potent nitrogen and sulfur donor ligands. *International Journal of Inorganic Chemistry*, 2012, 1-9.

Deisingh, A. K., & Thompson, M. (2002). Detection of infectious and toxigenic bacteria. *Analyst*, 127(5), 567-581.

Dhar, S., Kolishetti, N., Lippard, S. J., & Farokhzad, O. C. (2011). Targeted delivery of a cisplatin prodrug for safer and more effective prostate cancer therapy *in vivo*. *Proceedings of the National Academy of Sciences*, 108(5), 1850-1855.

Diaz, A., Cao, R., & Garcia, A. (1994). Characterization and biological properties of a copper (II) complex with pyruvic acid thiosemicarbazone. *Monatshefte für Chemie/Chemical Monthly*, 125(8-9), 823-825.

Diaz, A., Pogni, R., Cao, R., & Basosi, R. (1998). EPR characterization of a series of mono- and bis-thiosemicarbazone copper (II) complexes. *Inorganica Chimica Acta*, 275, 552-556.

Diaz, A., Cao, R., Frago, A., & Sánchez, I. (1999). Interpretation of the sod-like activity of a series of copper (II) complexes with thiosemicarbazones. *Inorganic Chemistry Communications*, 2(8), 361-363.

Dietz, G. P., & Bøhr, M. (2004). Delivery of bioactive molecules into the cell: the Trojan horse approach. *Molecular and Cellular Neuroscience*, 27(2), 85-131.

Dirscherl, G., Knape, R., Hanson, P., & König, B. (2007). Solid-phase synthesis of metal-complex containing peptides. *Tetrahedron*, 63(23), 4918-4928.

Dirscherl, G., & Koenig, B. (2008). The use of solid-phase synthesis techniques for the preparation of peptide-metal complex conjugates. *European Journal of Organic Chemistry*, 2008(4), 597-634.

Dolan, C., Moriarty, R. D., Lestini, E., Devocelle, M., Forster, R. J., & Keyes, T. E. (2013). Cell uptake and cytotoxicity of a novel cyclometalated iridium (III) complex and its octaarginine peptide conjugate. *Journal of Inorganic Biochemistry*, 119, 65-74.

Donnelly, P. S. (2011). The role of coordination chemistry in the development of copper and rhenium radiopharmaceuticals. *Dalton Transactions*, 40(5), 999-1010.

dos Santos Claro, P. C., González-Baró, A. C., Parajón-Costa, B. S., & Baran, E. J. (2005). Spectroscopic and electrochemical behavior of the methyl and ethyl derivatives of bis (acetylacetonato) oxovanadium (IV). *Zeitschrift für anorganische und allgemeine Chemie*, 631(10), 1903-1908.

Drew, M. G., Harding, C. J., McKee, V., Morgan, G. G., & Nelson, J. (1995). Geometric control of manganese redox state. *J. Chem. Soc., Chem. Commun.*, (10), 1035-1038.

Duncan, C., & White, A. R. (2012). Copper complexes as therapeutic agents. *Metallomics*, 4(2), 127-138.

Đuračková, Z., Mendiola, M. A., Sevilla, M. T., & Valent, A. (1999). Thiohydrazone copper (II) complexes. The relationship between redox properties and superoxide dismutase mimetic activity. *Bioelectrochemistry and Bioenergetics*, 48(1), 109-116.

Durot, S., Policar, C., Cisnetti, F., Lambert, F., Renault, J. P., Pelosi, G., ... & Mahy, J. P. (2005). Series of Mn complexes based on n-centered ligands and superoxide-reactivity in an anhydrous medium and SOD-like activity in an aqueous medium correlated to MnII/MnIII redox potentials. *European Journal of Inorganic Chemistry*, 2005(17), 3513-3523.

Efthimiadou, E. K., Katsarou, M. E., Karaliota, A., & Psomas, G. (2008). Copper (II) complexes with sparfloxacin and nitrogen-donor heterocyclic ligands: structure-activity relationship. *Journal of Inorganic Biochemistry*, 102(4), 910-920.

Enyedy, É. A., Nagy, N. V., Zsigó, É., Kowol, C. R., Arion, V. B., Keppler, B. K., & Kiss, T. (2010). Comparative solution equilibrium study of the interactions of copper (II), iron (II) and zinc (II) with triapine (3-aminopyridine-2-carbaldehyde thiosemicarbazone) and related ligands. *European Journal of Inorganic Chemistry*, 2010(11), 1717-1728.

Evans, D. H., O'Connell, K. M., Petersen, R. A., & Kelly, M. J. (1983). Cyclic voltammetry. *Journal of chemical education*, 60(4), 290.

Faller, P., Hureau, C., Dorlet, P., Hellwig, P., Coppel, Y., Collin, F., & Alies, B. (2012). Methods and techniques to study the bioinorganic chemistry of metal-peptide complexes linked to neurodegenerative diseases. *Coordination Chemistry Reviews*, 256(19), 2381-2396.

Farrugia, L. J. (1999). WinGX suite for small-molecule single-crystal crystallography. *Journal of Applied Crystallography*, 32(4), 837-838.

Ferrari, M. B., Gasparri Fava, G., Pelosi, G., & Tarasconi, P. (2000). Versatile chelating behavior of aliphatic thiosemicarbazones in zinc and cobalt complexes. *Polyhedron*, 19(16), 1895-1901.

Ferrari, M. B., Bisceglie, F., Pelosi, G., Sassi, M., Tarasconi, P., Cornia, M., ... & Pinelli, S. (2002a). Synthesis, characterization and X-ray structures of new antiproliferative and proapoptotic natural aldehyde thiosemicarbazones and their nickel (II) and copper (II) complexes. *Journal of Inorganic Biochemistry*, 90(3), 113-126.

Ferrari, M. B., Bisceglie, F., Fava, G. G., Pelosi, G., Tarasconi, P., Albertini, R., & Pinelli, S. (2002b). Synthesis, characterization and biological activity of two new polymeric copper (II) complexes with α -ketoglutaric acid thiosemicarbazone. *Journal of Inorganic Biochemistry*, 89(1-2), 36-44.

Ferrari, M. B., Bisceglie, F., Pelosi, G., Tarasconi, P., Albertini, R., Dall'Aglio, P. P., ... & Sava, G. (2004). Synthesis, characterization and biological activity of copper complexes with pyridoxal thiosemicarbazone derivatives. X-ray crystal structure of three dimeric complexes. *Journal of Inorganic Biochemistry*, 98(2), 301-312.

Ferguson, L. N. (1975) Cancer. How can chemists help? *Journal of Chemical Education*, 52(11), 688.

Finch, R. A., Liu, M. C., Grill, S. P., Rose, W. C., Loomis, R., Vasquez, K. M., ... & Sartorelli, A. C. (2000). Triapine (3-aminopyridine-2-carboxaldehyde-thiosemicarbazone): A Potent Inhibitor of Ribonucleotide Reductase Activity with Broad Spectrum Antitumor Activity. *Biochemical Pharmacology*, 59(8), 983-991.

Francois, A., Auzanneau, C., Le Morvan, V., Galaup, C., Godfrey, H. S., Marty, L., Boulay, A., Artigau, M., Mestre-Voegtle, B., Leygue, N., Picard, C., Coulais, Y., Robert, J., and Benoist, E. (2014). A functionalized heterobimetallic $^{99m}\text{Tc}/\text{Re}$ complex as a potential dual-modality imaging probe: synthesis, photophysical properties, cytotoxicity and cellular imaging investigations. *Dalton Transactions* 43, 439-450.

Fonseca, S. B., Pereira, M. P., & Kelley, S. O. (2009). Recent advances in the use of cell-penetrating peptides for medical and biological applications. *Advanced Drug Delivery Reviews*, 61(11), 953-964.

Fricker, S. P. (2007). Metal based drugs: from serendipity to design. *Dalton Transactions*, (43), 4903-4917.

Fuks, L., Gniazdowska, E., & Koźmiński, P. (2010). Tricarbonylrhenium (I) complexes with anionic ligands containing S and O Donor atoms—potential radiopharmaceutical precursors. *Polyhedron*, 29(1), 634-638.

- Fürstner, A. (2003). Chemistry and biology of roseophilin and the prodigiosin alkaloids: a survey of the last 2500 years. *Angewandte Chemie International Edition*, 42(31), 3582-3603.
- Gandin, V., Porchia, M., Tisato, F., Zanella, A., Severin, E., Dolmella, A., & Marzano, C. (2013). Novel mixed-ligand copper (I) complexes: role of dihydrazone ligands on cytotoxicity and genotoxicity. *Journal of Medicinal Chemistry*, 56(18), 7416-7430.
- Gennari, M., Pécaut, J., Collomb, M. N., & Duboc, C. (2012). A copper thiolate centre for electron transfer: mononuclear vs. dinuclear complexes. *Dalton Transactions*, 41(11), 3130-3133.
- Ghajar, B. M., & Harmon, S. A. (1968). The effect of dimethyl sulfoxide (DMSO) on permeability of *Staphylococcus aureus*. *Biochemical and Biophysical Research Communications*, 32(6), 940-944.
- Gilbert, B., Walton, P., & Whitwood, A. (1999). DNA damage via intercalation of copper complexes and activation by ascorbate and peroxides: direct EPR evidence for hydroxyl radical formation and reaction. *Journal of the Chemical Society, Perkin Transactions 2*, (9), 1891-1895.
- Gingras, B. A., Suprunchuk, T., & Bayley, C. H. (1962). The preparation of some thiosemicarbazones and their copper complexes: Part III. *Canadian Journal of Chemistry*, 40(6), 1053-1059.
- Grossoehme, N. E., Spuches, A. M., & Wilcox, D. E. (2010). Application of isothermal titration calorimetry in bioinorganic chemistry. *Journal of Biological Inorganic Chemistry*, 15(8), 1183-1191.
- Haas, K. L., & Franz, K. J. (2009). Application of metal coordination chemistry to explore and manipulate cell biology. *Chemical Reviews*, 109(10), 4921-4960.
- Hambley, T. W. (2007). Developing new metal-based therapeutics: challenges and opportunities. *Dalton Transactions*, (43), 4929-4937.
- Hancock, R. E., & Lehrer, R. (1998). Cationic peptides: a new source of antibiotics. *Trends In Biotechnology*, 16(2), 82-88.
- Harris, J. M., & Chess, R. B. (2003). Effect of pegylation on pharmaceuticals. *Nature Reviews Drug Discovery*, 2(3), 214-221.
- Harvey, A. L. (2008). Natural products in drug discovery. *Drug Discovery Today*, 13(19), 894-901.
- Heinze, K., Beckmann, M., & Hempel, K. (2008). Solid-phase synthesis of transition-metal complexes. *Chemistry - A European Journal*, 14(31), 9468-9480.

- Heldt, J. M., Fischer-Durand, N., Salmain, M., Vessieres, A., & Jaouen, G. (2004). Preparation and characterization of poly (amidoamine) dendrimers functionalized with a rhenium carbonyl complex and PEG as new IR probes for carbonyl metallo immunoassay. *Journal of Organometallic Chemistry*, 689(25), 4775-4782.
- Hoeschele, J. D. (2009) In remembrance of Barnett Rosenberg. *Dalton Transactions*, 48, 10648-10650.
- Holland, J. P., Aigbirhio, F. I., Betts, H. M., Bonnitcha, P. D., Burke, P., Christlieb, M., ... & Warren, J. E. (2007). Functionalized bis (thiosemicarbazonato) complexes of zinc and copper: Synthetic platforms toward site-specific radiopharmaceuticals. *Inorganic Chemistry*, 46(2), 465-485.
- Holland, J. P., Barnard, P. J., Bayly, S. R., Betts, H. M., Churchill, G. C., Dilworth, J. R., ... & Hueting, R. (2008). Synthesis, radiolabelling and confocal fluorescence microscopy of styrene-derivatised bis(thiosemicarbazonato) zinc and-copper Complexes. *European Journal of Inorganic Chemistry*, 2008(12), 1985-1993.
- Hossain, M. E., Alam, M. N., Begum, J., Akbar Ali, M., Nazimuddin, M., Smith, F. E., & Hynes, R. C. (1996). The preparation, characterization, crystal structure and biological activities of some copper (II) complexes of the 2-benzoylpyridine Schiff bases of S-methyl-and S-benzyl-dithiocarbazate. *Inorganica Chimica Acta*, 249(2), 207-213.
- How, F. N. F., Crouse, K. A., Tahir, M. I. M., Tarafder, M. T. H., & Cowley, A. R. (2008). Synthesis, characterization and biological studies of S-benzyl- β -N-(benzoyl) dithiocarbazate and its metal complexes. *Polyhedron*, 27(15), 3325-3329.
- How, F. N. F. (2008). *Synthesis, Characterization and Elucidation of the Structure–Activity Relationship of Heteroatom Donor Ligands and Their Complexes Derived From Substituted Dithiocarbazate Derivatives* (Doctoral dissertation, Universiti Putra Malaysia).
- Hoyer, J., Schatzschneider, U., Schulz-Siegmund, M., & Neundorff, I. (2012). Dimerization of a cell-penetrating peptide leads to enhanced cellular uptake and drug delivery. *Beilstein Journal of Organic Chemistry*, 8(1), 1788-1797.
- Hueting, R., Christlieb, M., Dilworth, J. R., Garayoa, E. G., Gouverneur, V., Jones, M. W., ... & Tourwé, D. A. (2010). Bis (thiosemicarbazones) as bifunctional chelators for the room temperature 64-copper labeling of peptides. *Dalton Transactions*, 39(15), 3620-3632.
- Huguet, F., Melet, A., Alves de Sousa, R., Lieutaud, A., Chevalier, J., Maigre, L., ... & Artaud, I. (2012). Hydroxamic acids as potent inhibitors of Fe(II) and Mn(II) *E. coli* methionine aminopeptidase: Biological activities and x-ray structures of oxazole hydroxamate–cmetap-Mn complexes. *ChemMedChem*, 7(6), 1020-1030.

Hunoor, R. S., Patil, B. R., Badiger, D. S., Vadavi, R. S., Gudasi, K. B., Chandrashekhar, V. M., & Muchchandi, I. S. (2010). Spectroscopic, magnetic and thermal studies of Co (II), Ni (II), Cu (II) and Zn (II) complexes of 3-acetylcoumarin–isonicotinoylhydrazone and their antimicrobial and anti-tubercular activity evaluation. *Spectrochimica Acta Part A: Molecular And Biomolecular Spectroscopy*, 77(4), 838-844.

Iskander, M. F., El-Sayed, L., El-Toukhy, A., & Tawflk, M. (1982). Coordination compounds of hydrazine derivatives with transition metals. Part 24. Coordination chemistry of hydrazine-S-methyl carbodithioate schiff bases derived from β -dicarbonyl compounds. *Transition Metal Chemistry*, 7(3), 135-140.

Iskander, M. F., Shaban, M. A., & El-Badry, S. M. (2003). Sugar hydrazone–metal complexes: transition-and non-transition metal complexes of monosaccharide S-alkylhydrazonocarbodithioates and dehydro-l-ascorbic acid bis (S-alkylhydrazonocarbodithioates). *Carbohydrate Research*, 338(22), 2341-2347.

Islam, M. A. A. A., Sheikh, M. C., Alam, M. S., Zangrando, E., Alam, M. A., Tarafder, M. T. H., & Miyatake, R. (2014) Synthesis, characterization and bio-activity of a bidentate NS Schiff base of S-allyldithiocarbazate and its divalent metal complexes: X-ray crystal structures of the free ligand and its nickel (II) complex. *Transition Metal Chemistry*, 1-9.

Jakupec, M. A., Galanski, M., Arion, V. B., Hartinger, C. G., & Keppler, B. K. (2008). Antitumour metal compounds: more than theme and variations. *Dalton Transactions*, (2), 183-194.

Jansson, P. J., Sharpe, P. C., Bernhardt, P. V., & Richardson, D. R. (2010). Novel thiosemicarbazones of the ApT and DpT series and their copper complexes: identification of pronounced redox activity and characterization of their antitumor activity. *Journal of Medicinal Chemistry*, 53(15), 5759-5769.

Jasinski, J. P., Bianchani, J. R., Cueva, J., El-Saied, F. A., El-Asmy, A. A., & West, D. X. (2003). Spectral and structural studies of the copper (II) complexes of 3, 4-hexanedione bis (3-azacyclothiosemicarbazones). *Zeitschrift Für Anorganische Und Allgemeine Chemie*, 629(2), 202-206.

Jones, C. J., & McCleverty, J. A. (1970). Complexes of transition metals with Schiff bases and the factors influencing their redox properties. Part I. Nickel and copper complexes of some diketone bithiosemicarbazones. *Journal of the Chemical Society A: Inorganic, Physical, Theoretical*, 2829-2836.

Joseph, J., Nagashri, K., & Janaki, G. B. (2012). Novel metal based anti-tuberculosis agent: Synthesis, characterization, catalytic and pharmacological activities of copper complexes. *European Journal of Medicinal Chemistry*, 49, 151-163.

Kaatz, G. W., Barriere, S. L., Schaberg, D. R., & Fekety, R. (1987). The emergence of resistance to ciprofloxacin during treatment of experimental *Staphylococcus aureus* endocarditis. *Journal of Antimicrobial Chemotherapy*, 20(5), 753-758.

- Kalia, S., Lumba, K., and Sharma, A. (2012) Screening of some newly synthesized transition metal complexes of salicylaldehyde schiff base of isonicotinoyldithiocarbamic acid against some pathogenic microbial strains. *International Journal of advances in Pharmacy, Biology and Chemistry*, 1(4), 461-464.
- Kanwar, S. S., Lumba, K., Gupta, S. K., Katoch, V. M., Singh, P., Mishra, A. K., & Kalia, S. B. (2008). Synthesis and mycobactericidal properties of metal complexes of isonicotinoyldithiocarbamic acid. *Biotechnology Letters*, 30(4), 677-680.
- Khan, K. M., Ambreen, N., Hussain, S., Perveen, S., & Iqbal Choudhary, M. (2009). Schiff bases of 3-formylchromone as thymidine phosphorylase inhibitors. *Bioorganic & Medicinal Chemistry*, 17(8), 2983-2988.
- Khoo, T. J. (2008). *Structure Elucidation And Biological Activity Of Dithiocarbamate Derivatives, Their Schiff Base Ligands And Metal Complexes* (Doctoral dissertation, Universiti Putra Malaysia).
- Khoo, T. J., Break, M. K. B., Crouse, K. A., Tahir, M. I. M., Ali, A. M., Cowley, A. R., ... & Tarafder, M. T. H. (2014). Synthesis, characterization and biological activity of two Schiff base ligands and their nickel (II), copper (II), zinc (II) and cadmium (II) complexes derived from S-4-picolyldithiocarbamate and X-ray crystal structure of cadmium (II) complex derived from pyridine-2-carboxaldehyde. *Inorganica Chimica Acta*. 413, 68-76.
- Kivelson, D., & Neiman, R. (2004). ESR studies on the bonding in copper complexes. *The Journal of Chemical Physics*, 35(1), 149-155.
- Kirin, S. I., Dübon, P., Weyhermüller, T., Bill, E., & Metzler-Nolte, N. (2005). Amino acid and peptide bioconjugates of copper (II) and zinc (II) complexes with a modified N, N-bis (2-picoly) amine ligand. *Inorganic Chemistry*, 44(15), 5405-5415.
- Knoblauch, S., Benedix, R., Ecke, M., Gelbrich, T., Sieler, J., Somoza, F., & Hennig, H. (1999). Synthesis, crystal structure, spectroscopy, and theoretical investigations of tetrahedrally distorted copper (ii) chelates with [CuN₂S₂] coordination sphere. *European Journal of Inorganic Chemistry*, 1999(8), 1393-1403.
- Kovala-Demertzi, D., Miller, J. R., Kourkoumelis, N., Hadjikakou, S. K., & Demertzis, M. A. (1999). Palladium (II) and platinum (II) complexes of pyridine-2-carbaldehyde thiosemicarbazone with potential biological activity. Synthesis, structure and spectral properties. Extended network via hydrogen bond linkages of [Pd (PyTsc) Cl]. *Polyhedron*, 18(7), 1005-1013.
- Krasowska, M., Kochel, A., & Filarowski, A. (2010). The conformational analysis of 2-hydroxyaryl Schiff thiosemicarbazones. *CrystEngComm*, 12(6), 1955-1962.

- Krishna, P. M., Reddy, K. H., Pandey, J. P., & Siddavattam, D. (2008). Synthesis, characterization, DNA binding and nuclease activity of binuclear copper (II) complexes of cuminaldehyde thiosemicarbazones. *Transition Metal Chemistry*, 33(5), 661-668.
- Kubota, S., Uda, M., Mori, Y., Kametani, F., and Terada, H. (1978) Syntheses and uncoupling activities of alkyl dithiocarbazates and alkyl pyridinecarbonyldithiocarbazates. *Journal of Medicinal Chemistry* 21, 591-594.
- Kuete, V., Alibert-Franco, S., Eyong, K. O., Ngameni, B., Folefoc, G. N., Nguemeving, J. R., ... & Pagès, J. M. (2011). Antibacterial activity of some natural products against bacteria expressing a multi-drug-resistant phenotype. *International Journal of Antimicrobial Agents*, 37(2), 156-161.
- Kulkarni, A., Patil, S. A., & Badami, P. S. (2009). Synthesis, characterization, DNA cleavage and *in vitro* antimicrobial studies of La (III), Th (IV) and VO (IV) complexes with Schiff bases of coumarin derivatives. *European Journal of Medicinal Chemistry*, 44(7), 2904-2912.
- Kumar, S., Dhar, D. N., & Saxena, P. N. (2009). Applications of metal complexes of Schiff bases - a review. *J Sci Ind Res*, 68(3), 181-187.
- Lanfredi, A. M. M., Tiripicchio, A., Camellini, M. T., Monaci, A., & Tarli, F. (1977). X-Ray and infrared structural studies on the methyl ester of dithiocarbazic acid and its N-substituted derivatives. *Journal of The Chemistry Society., Dalton Transactions*, (5), 417-422.
- Latheef, L., & Prathapachandra Kurup, M. R. (2008) Spectral and structural studies of nickel (II) complexes of salicylaldehyde 3-azacyclothiosemicarbazones. *Polyhedron* 27, 35-43.
- Leigh, M., Raines, D. J., Castillo, C. E., & Duhme-Klair, A. K. (2011). Inhibition of xanthine oxidase by thiosemicarbazones, hydrazones and dithiocarbazates derived from hydroxy-substituted benzaldehydes. *ChemMedChem*, 6(6), 1107-1118.
- Lessa, J. A., Reis, D. C., Da Silva, J. G., Paradizzi, L. T., da Silva, N. F., de Fátima A Carvalho, M., ... & Beraldo, H. (2012). Coordination of thiosemicarbazones and bis (thiosemicarbazones) to bismuth (III) as a strategy for the design of metal-based antibacterial agents. *Chemistry & Biodiversity*, 9(9), 1955-1966.
- Li, J. W. H., & Vederas, J. C. (2009). Drug discovery and natural products: end of an era or an endless frontier? *Science*, 325(5937), 161-165.
- Li, H.-Q., Luo, Y., Li, D.-D., and Zhu, H.-L. (2009) (E)-4-Chlorobenzyl 3-(3-nitrobenzylidene) dithiocarbazate. *Acta Crystallographica, Section E* 65, o3101.
- Li, M. X., Zhang, L. Z., Chen, C. L., Niu, J. Y., & Ji, B. S. (2012). Synthesis, crystal structures, and biological evaluation of Cu (II) and Zn (II) complexes of 2-benzoylpyridine Schiff bases derived from S-methyl-and S-phenyldithiocarbazates. *Journal of Inorganic Biochemistry*, 106(1), 117-125.

- Li, Q. X., Tang, H. A., Li, Y. Z., Wang, M., Wang, L. F., & Xia, C. G. (2000). Synthesis, characterization, and antibacterial activity of novel Mn (II), Co (II), Ni (II), Cu (II), and Zn (II) complexes with vitamin K₃-thiosemicarbazone. *Journal of Inorganic Biochemistry*, 78(2), 167-174.
- Li, S. P. Y., Liu, H. W., Zhang, K. Y., & Lo, K. K. W. (2010). Modification of luminescent iridium (III) polypyridine complexes with discrete poly (ethylene glycol)(PEG) pendants: synthesis, emissive behavior, intracellular uptake, and PEGylation properties. *Chemistry - A European Journal*, 16(28), 8329-8339.
- Lim, S., Price, K. A., Chong, S. F., Paterson, B. M., Caragounis, A., Barnham, K. J., ... & Donnelly, P. S. (2010). Copper and zinc bis (thiosemicarbazonato) complexes with a fluorescent tag: synthesis, radiolabelling with copper-64, cell uptake and fluorescence studies. *JBIC Journal of Biological Inorganic Chemistry*, 15(2), 225-235.
- Liolios, C. C., Zikos, C., Fragogeorgi, E., Benaki, D., Pelecanou, M., Pirmettis, I., ... & Varvarigou, A. D. (2012). A bombesin copper complex based on a bifunctional cyclam derivative. *European Journal of Inorganic Chemistry*, 2012(17), 2877-2888.
- Liu, K., Lu, H., Hou, L., Qi, Z., Teixeira, C., Barbault, F., ... & Xie, L. (2008). Design, synthesis, and biological evaluation of N-carboxyphenylpyrrole derivatives as potent HIV fusion inhibitors targeting gp41. *Journal of Medicinal Chemistry*, 51(24), 7843-7854.
- Liu, Y. T., Lian, G. D., Yin, D. W., & Su, B. J. (2012). Synthesis and antimicrobial activity of some novel ferrocene-based Schiff bases containing a ferrocene unit. *Research on Chemical Intermediates*, 38(3-5), 1043-1053.
- Liu, Y. T., Lian, G. D., Yin, D. W., & Su, B. J. (2013). Synthesis, characterization and biological activity of ferrocene-based Schiff base ligands and their metal (II) complexes. *Spectrochimica Acta Part A: Molecular and Biomolecular Spectroscopy*, 100, 131-137.
- Lobana, T. S., Sharma, R., Bawa, G., & Khanna, S. (2009). Bonding and structure trends of thiosemicarbazone derivatives of metals - an overview. *Coordination Chemistry Reviews*, 253(7), 977-1055.
- Lolis, E., & Bucala, R. (2003). Therapeutic approaches to innate immunity: severe sepsis and septic shock. *Nature Reviews Drug Discovery*, 2(8), 635-645.
- Low, M. L., Ravoof, T. B. S., Tahir, M. I. M., Crouse, K. A., & Tiekink, E. R. (2013). (Pyridin-4-yl) methyl N'-(3-phenylallylidene) hydrazinecarbodithioate. *Acta Crystallographica Section E: Structure Reports Online*, 69(2), o167-o168.
- Lundberg, P., & Langel, Ü. (2003). A brief introduction to cell-penetrating peptides. *Journal of Molecular Recognition*, 16(5), 227-233.

Ma, M. T., Cooper, M. S., Paul, R. L., Shaw, K. P., Karas, J. A., Scanlon, D., ... & Donnelly, P. S. (2011). Macrobicyclic cage amine ligands for copper radiopharmaceuticals: A single bivalent cage amine containing two Lys3-bombesin targeting peptides. *Inorganic Chemistry*, 50(14), 6701-6710.

Maia, P. I. D. S., Fernandes, A. G. D. A., Silva, J. J. N., Andricopulo, A. D., Lemos, S. S., Lang, E. S., ... & DeFlon, V. M. (2010). Dithiocarbazate complexes with the $[M(PPh_3)]^{2+}$ (M= Pd or Pt) moiety: Synthesis, characterization and anti-Tripanosoma cruzi activity. *Journal of Inorganic Biochemistry*, 104(12), 1276-1282.

Mallea, M., Chevalier, J., Bornet, C., Eyraud, A., Davin-Regli, A., Bollet, C., & Pages, J. M. (1998). Porin alteration and active efflux: two in vivo drug resistance strategies used by Enterobacter aerogenes. *Microbiology*, 144(11), 3003-3009.

Mamelli, L., Petit, S., Chevalier, J., Giglione, C., Lieutaud, A., Meinel, T., ... & Pagès, J. M. (2009). New antibiotic molecules: bypassing the membrane barrier of gram negative bacteria increases the activity of peptide deformylase inhibitors. *PLoS One*, 4(7), e6443.

Manan, M. A. F. A., Crouse, K. A., Tahir, M. I. M., Rosli, R., How, F. N. F., Watkin, D. J., & Slawin, A. M. (2011a). Synthesis, characterization and cytotoxic activity of s-benzylidithiocarbazate schiff bases derived from 5-fluoroisatin, 5-chloroisatin, 5-bromoisatin and their crystal structures. *Journal of Chemical Crystallography*, 41(11), 1630-1641.

Manan, M. A. F. A., Tahir, M. I. M., Crouse, K. A., Rosli, R., How, F. N. F., & Watkin, D. J. (2011b). The crystal structure and cytotoxicity of centrosymmetric copper (II) complex derived from S-methyldithiocarbazate with isatin. *Journal of Chemical Crystallography*, 41(12), 1866-1871.

Manikandamathavan, V. M., & Unni Nair, B. (2013). DNA binding and cytotoxicity of copper (II) imidazole terpyridine complexes: Role of oxyanion, hydrogen bonding and π - π interaction. *European Journal of Medicinal Chemistry*, 68, 244-252.

Masters, P. A., O'Bryan, T. A., Zurlo, J., Miller, D. Q., & Joshi, N. (2003). Trimethoprim-sulfamethoxazole revisited. *Archives of Internal Medicine*, 163(4), 402-410.

Maurya, M. R., Khurana, S., Azam, A., Zhang, W., & Rehder, D. (2003). Synthesis, characterisation and antiamoebic studies of dioxovanadium (V) complexes containing ONS donor ligands derived from S-benzylidithiocarbazate. *European Journal of Inorganic Chemistry*, 2003(10), 1966-1973.

Maurya, M. R., Haldar, C., Khan, A. A., Azam, A., Salahuddin, A., Kumar, A., & Costa Pessoa, J. (2012). Synthesis, characterization, catalytic and antiamoebic activity of vanadium complexes of binucleating bis (dibasic tridentate ONS donor) ligand systems. *European Journal of Inorganic Chemistry*, 2012(15), 2560-2577.

- Meggers, E. (2009). Targeting proteins with metal complexes. *Chemical Communications*, (9), 1001-1010.
- Metzler-Nolte, N. (2010). Biomedical applications of organometal–peptide conjugates. In *Medicinal Organometallic Chemistry* (pp. 195-217). Springer Berlin Heidelberg.
- Mevellec, F., Roucoux, A., Noiret, N., & Patin, H. (2002). Novel six-coordinate oxorhenium (V) '3+ 2' mixed-ligand complexes carrying the SNO/SN donor atom set. *Inorganica Chimica Acta*, 332(1), 30-36.
- Miklán, Z., Szabó, R., Zsoldos-Mády, V., Reményi, J., Bánóczy, Z. and Hudecz, F. (2007). New ferrocene containing peptide conjugates: Synthesis and effect on human leukemia (HL-60) cells. *Peptide Science*, 88(2), 108-114.
- Milunovic, M. N., Enyedy, E. A., Nagy, N. V., Kiss, T., Trondl, R., Jakupec, M. A., ... & Arion, V. B. (2012). L- and D-proline thiosemicarbazone conjugates: coordination behavior in solution and the effect of copper (II) coordination on their antiproliferative activity. *Inorganic Chemistry*, 51(17), 9309-9321.
- Ming, L. J. (2003). Structure and function of "metalloantibiotics". *Medicinal Research Reviews*, 23(6), 697-762.
- Mitchell, D. J., Steinman, L., Kim, D. T., Fathman, C. G., & Rothbard, J. B. (2000). Polyarginine enters cells more efficiently than other polycationic homopolymers. *The Journal of Peptide Research*, 56(5), 318-325.
- Mohamed, G. G., Omar, M. M., & Ibrahim, A. A. (2009). Biological activity studies on metal complexes of novel tridentate Schiff base ligand. Spectroscopic and thermal characterization. *European Journal of Medicinal Chemistry*, 44(12), 4801-4812.
- Mosmann, T. (1983). Rapid colorimetric assay for cellular growth and survival: application to proliferation and cytotoxicity assays. *Journal of Immunological Methods*, 65(1), 55-63.
- Nair, M. S., & Joseyphus, R. S. (2008). Synthesis and characterization of Co (II), Ni (II), Cu (II) and Zn (II) complexes of tridentate Schiff base derived from vanillin and DL- α -aminobutyric acid. *Spectrochimica Acta Part A: Molecular and Biomolecular Spectroscopy*, 70(4), 749-753.
- Nandi, A. K., Chaudhuri, S., Mazumdar, S. K., & Ghosh, S. (1984). Crystal and molecular structure of hexan-2,5-dione bis (4-phenylthiosemicarbazonato) nickel (II), (C₂₀H₂₂N₆S₂Ni): a model study of the enhancement of the antibacterial activity of a tetradentate N, S donor ligand on metal complexation. *Inorganica Chimica Acta*, 92(3), 235-240.
- Navneet, A., & Pradeep, M. (2005). Synthesis and evaluation of 4-substituted semicarbazones of levulinic acid for anticonvulsant activity. *Journal of Zhejiang University Science B*, 6(7), 617-621.

Neelam, B., Mannar R, M., Fehmida, N., Alok, B., Sudha, B., & Amir, A. (2000). Palladium (II) complexes of NS donor ligands derived from S-methyl-dithiocarbamate, S-benzyl-dithiocarbamate and thiosemicarbazide as antiamoebic agents. *European Journal of Medicinal Chemistry*, 35(5), 481-486.

Neu HC & Gootz TD. Antimicrobial Chemotherapy. In: Baron S, editor. Medical Microbiology. 4th edition. Galveston (TX): University of Texas Medical Branch at Galveston; 1996. Chapter 11. Available from: <http://www.ncbi.nlm.nih.gov/books/NBK7986/>

Ng, N. S., Leverett, P., Hibbs, D. E., Yang, Q., Bulanadi, J. C., Wu, M. J., & Aldrich-Wright, J. R. (2013). The antimicrobial properties of some copper (II) and platinum (II) 1, 10-phenanthroline complexes. *Dalton Transactions*, 42(9), 3196-3209.

Ngarivhume, T., Díaz, A., Cao, R., Ortiz, M., & Sánchez, I. (2005). Association capacity of ribose bis (thiosemicarbazone) copper (II) with nitric oxide. *Synthesis And Reactivity In Inorganic, Metal-Organic, And Nano-Metal Chemistry*, 35(10), 795-800.

Nikaido, H. & Pagès, J. M. (2012). Broad-specificity efflux pumps and their role in multi-drug resistance of Gram-negative bacteria. *FEMS Microbiology Reviews*, 36(2), 340-363.

Notman, R., Noro, M., O'Malley, B., & Anwar, J. (2006). Molecular basis for dimethylsulfoxide (DMSO) action on lipid membranes. *Journal of the American Chemical Society*, 128(43), 13982-13983.

O'Connell, K. M., Hodgkinson, J. T., Sore, H. F., Welch, M., Salmond, G. P., & Spring, D. R. (2013). Combating multi-drug-resistant bacteria: Current strategies for the discovery of novel antibacterials. *Angewandte Chemie International Edition*, 52(41), 10706-10733.

Ohya, Y., Nagatomi, K., & Ouchi, T. (2001). Synthesis and cytotoxic activity of macromolecular prodrug of cisplatin using poly (ethylene glycol) with galactose residues or antennary galactose units. *Macromolecular Bioscience*, 1(8), 355-363.

Olczak, A., Główska, M. L., Gołka, J., Szczesio, M., Bojarska, J., Kozłowska, K., ... & Orlewska, C. (2007). Is planarity of pyridin-2-yl-and pyrazin-2-yl-formamide thiosemicarbazones related to their tuberculostatic activity? X-ray structures of two pyrazine-2-carboxamide-N'-carbonothioyl-hydrazone. *Journal of Molecular Structure*, 830(1), 171-175.

Olczak, A., Szczesio, M., Golka, J., Orlewska, C., Gobis, K., Foks, H., & Glowka, M. L. (2010). Planarity of heteroaryldithiocarbamic acid derivatives showing tuberculostatic activity. II. Crystal structures of 3-[amino (pyrazin-2-yl) methylidene]-2-methylcarbamic acid esters. *Acta Crystallographica Section C: Crystal Structure Communications*, 67(1), o37-o42.

Okandeji, B. O., Greenwald, D. M., Wroten, J., & Sello, J. K. (2011). Synthesis and evaluation of inhibitors of bacterial drug efflux pumps of the major facilitator superfamily. *Bioorganic & Medicinal Chemistry*, *19*(24), 7679-7689.

Ostermeier, M., Berlin, M. A., Meudtner, R. M., Demeshko, S., Meyer, F., Limberg, C., & Hecht, S. (2010). Complexes of click-derived bistriazolylpyridines: remarkable electronic influence of remote substituents on thermodynamic stability as well as electronic and magnetic properties. *Chemistry - A European Journal*, *16*(33), 10202-10213.

Padhye, S., Yang, H., Jamadar, A., Cui, Q. C., Chavan, D., Dominiak, K., ... & Sarkar, F. H. (2009). New difluoro Knoevenagel condensates of curcumin, their Schiff bases and copper complexes as proteasome inhibitors and apoptosis inducers in cancer cells. *Pharmaceutical Research*, *26*(8), 1874-1880.

Pagès, J. M., & Amaral, L. (2009). Mechanisms of drug efflux and strategies to combat them: challenging the efflux pump of Gram-negative bacteria. *BBA-Proteins and Proteomics*, *1794*(5), 826-833.

Pagès, J. M., Kascàková, S., Maigre, L., Allam, A., Alimi, M., Chevalier, J., ... & Artaud, I. (2013). New peptide-based antimicrobials for tackling drug resistance in bacteria: Single-cell fluorescence imaging. *ACS Medicinal Chemistry Letters*, *4*(6), 556-559.

Parajón-Costa, B. S., Wagner, C. C., & Baran, E. J. (2004, July). Vibrational spectra and electrochemical behavior of bispicolinate copper (II). In *Anales de la Asociación Química Argentina* (Vol. 92, No. 1-3, pp. 109-117). Asociación Química Argentina.

Patel, R. N., Shukla, K. K., Singh, A., Choudhary, M., Patel, D. K., Niclós-Gutiérrez, J., & Choquesillo-Lazarte, D. (2009). Spectroscopic, structural and magnetic studies of nickel (II) complexes with tetra- and pentadentate ligands. *Transition Metal Chemistry*, *34*(2), 239-245.

Paterson, B. M., & Donnelly, P. S. (2011). Copper complexes of bis (thiosemicarbazones): from chemotherapeutics to diagnostic and therapeutic radiopharmaceuticals. *Chemical Society Reviews*, *40*(5), 3005-3018.

Paterson, B. M., Karas, J. A., Scanlon, D. B., White, J. M., & Donnelly, P. S. (2010). Versatile new bis (thiosemicarbazone) bifunctional chelators: synthesis, conjugation to bombesin (7–14)-NH₂, and copper-64 radiolabeling. *Inorganic Chemistry*, *49*(4), 1884-1893.

Patra, M., Gasser, G., Pinto, A., Merz, K., Ott, I., Bandow, J. E., & Metzler-Nolte, N. (2009). Synthesis and biological evaluation of chromium bioorganometallics based on the antibiotic platensimycin lead structure. *ChemMedChem*, *4*(11), 1930-1938.

Patra, M., Gasser, G., Wenzel, M., Merz, K., Bandow, J. E., & Metzler-Nolte, N. (2012a). Sandwich and half-sandwich derivatives of platensimycin: Synthesis and biological evaluation. *Organometallics*, *31*(16), 5760-5771.

- Patra, M., Gasser, G., & Metzler-Nolte, N. (2012b). Small organometallic compounds as antibacterial agents. *Dalton Transactions*, 41(21), 6350-6358.
- Pavan, F. R., Maia, P. I. D. S., Leite, S. R., Deflon, V. M., Batista, A. A., Sato, D. N., ... & Leite, C. Q. (2010). Thiosemicarbazones, semicarbazones, dithiocarbazates and hydrazide/hydrazones: Anti-*Mycobacterium tuberculosis* activity and cytotoxicity. *European Journal of Medicinal Chemistry*, 45(5), 1898-1905.
- Pedras, M. S. C., & Jha, M. (2006). Toward the control of *Leptosphaeria maculans* : Design, syntheses, biological activity, and metabolism of potential detoxification inhibitors of the crucifer phytoalexin brassinin. *Bioorganic & Medicinal Chemistry*, 14(14), 4958-4979.
- Pelosi, G. (2010). Thiosemicarbazone metal complexes: From structure to activity. *Open Crystallography Journal*. 3(1), 16-28.
- Petit, S., Duroc, Y., Larue, V., Giglione, C., Léon, C., Soulama, C., ... & Artaud, I. (2009). Structure–activity relationship analysis of the peptide deformylase inhibitor 5-bromo-1h-indole-3-acetohydroxamic acid. *ChemMedChem*, 4(2), 261-275.
- Phaniband, M. A., Dhumwad, S. D., & Pattan, S. R. (2011). Synthesis, characterization, antimicrobial, and DNA cleavage studies of metal complexes of coumarin Schiff bases. *Medicinal Chemistry Research*, 20(4), 493-502.
- Piddock, L. J. (2006). Clinically relevant chromosomally encoded multi-drug resistance efflux pumps in bacteria. *Clinical Microbiology Reviews*, 19(2), 382-402.
- Plesiat, P., & Nikaido, H. (1992). Outer membranes of Gram-negative bacteria are permeable to steroid probes. *Molecular Microbiology*, 6(10), 1323-1333.
- Polcar, C., Waern, J. B., Plamont, M.-A., Clède, S., Mayet, C., Prazeres, R., Ortega, J.-M., Vessières, A., and Dazzi. (2011). A Subcellular IR imaging of a metal–carbonyl moiety using photothermally induced resonance. *Angewandte Chemie International Edition* 50, 860-864.
- Pogni, R., Baratto, M. C., Diaz, A., & Basosi, R. (2000). EPR characterization of mono (thiosemicarbazones) copper (II) complexes. Note II. *Journal of Inorganic Biochemistry*, 79(1), 333-337.
- Pradel, E., & Pagès, J. M. (2002). The AcrAB-TolC efflux pump contributes to multi-drug resistance in the nosocomial pathogen *Enterobacter aerogenes*. *Antimicrobial Agents and Chemotherapy*, 46(8), 2640-2643.
- Pro, C. (2011). Agilent Technologies. *Yarnton, Oxfordshire, England*.
- Puckett, C. A., & Barton, J. K. (2009). Fluorescein redirects a ruthenium–octaarginine conjugate to the nucleus. *Journal of the American Chemical Society*, 131(25), 8738-8739.

Raja, D.S, Bhuvanesh, N. S., & Natarajan, K. (2011). Biological evaluation of a novel water soluble sulphur bridged binuclear copper (II) thiosemicarbazone complex. *European Journal of Medicinal Chemistry*, 46(9), 4584-4594.

Raman, N., Muthuraj, V., Ravichandran, S., & Kulandaisamy, A. (2003). Synthesis, characterisation and electrochemical behaviour of Cu (II), Co (II), Ni (II) and Zn (II) complexes derived from acetylacetone and *p*-anisidine and their antimicrobial activity. *Journal of Chemical Sciences*, 115(3), 161-167.

Randhawa, M. A. (2006). The effect of dimethyl sulfoxide (DMSO) on the growth of dermatophytes. *Japanese Journal of Medical Mycology*, 47(4).

Rapheal, P. F., Manoj, E., & Prathapachandra Kurup, M. R. (2007). Copper (II) complexes of N(4)-substituted thiosemicarbazones derived from pyridine-2-carbaldehyde: Crystal structure of a binuclear complex. *Polyhedron*, 26(4), 818-828.

Ravoof, T. B., Crouse, K. A., Tahir, M. I. M., Cowley, A. R., & Ali, M. A. (2004). Synthesis, characterization and bioactivity of mixed-ligand Cu (II) complexes containing S-methyldithiocarbazate derivatives and saccharinate ligands and the X-ray crystal structure of the copper-saccharinate complex containing S-methyl- β -N-(6-methylpyrid-2-yl) methylenedithiocarbazate. *Polyhedron*, 23(16), 2491-2498.

Ravoof, T. B., Crouse, K. A., Tahir, M. I. M., Cowley, A. R., & Ali, M. A. (2007). Synthesis, characterization and bioactivity of mixed-ligand Cu (II) complexes containing Schiff bases derived from S-benzylthiocarbazate and saccharinate ligand and the X-ray crystal structure of the copper-saccharinate complex containing S-benzyl- β -N-(acetylpyrid-2-yl)methylenedithiocarbazate. *Polyhedron*, 26(6), 1159-1165.

Ravoof, T. B. (2008). *Synthesis, characterisation and biological activities of nitrogen-sulphur ligands and their transition metal complexes* (Doctoral dissertation, Universiti Putra Malaysia).

Ravoof, T. B., Crouse, K. A., Tahir, M. I. M., How, F. N., Rosli, R., & Watkins, D. J. (2010). Synthesis, characterization and biological activities of 3-methylbenzyl 2-(6-methyl pyridin-2-ylmethylene) hydrazine carbodithioate and its transition metal complexes. *Transition Metal Chemistry*, 35(7), 871-876.

Ravoof, T. B., Crouse, K. A., Tahir, M. I. M., Rosli, R., Watkin, D. J., & How, F. N. (2011). Synthesis, Characterisation and Biological Activities of 2-Methylbenzyl 2-(dipyridin-2-yl methylene) hydrazinecarbodithioate. *Journal of Chemical Crystallography*, 41(4), 491-495.

Rebolledo, A. P., Vieites, M., Gambino, D., Piro, O. E., Castellano, E. E., Zani, C. L., ... & Beraldo, H. (2005). Palladium (II) complexes of 2-benzoylpyridine-derived thiosemicarbazones: spectral characterization, structural studies and cytotoxic activity. *Journal of Inorganic Biochemistry*, 99(3), 698-706.

- Regberg, J., Srimanee, A., & Langel, Ü. (2012). Applications of cell-penetrating peptides for tumor targeting and future cancer therapies. *Pharmaceuticals*, 5(9), 991-1007.
- Rijt, S. H. V., Kostrhunova, H., Brabec, V., & Sadler, P. J. (2011). Functionalization of osmium arene anticancer complexes with (poly) arginine: effect on cellular uptake, internalization, and cytotoxicity. *Bioconjugate Chemistry*, 22(2), 218-226.
- Rijt, S. H., & Sadler, P. J. (2009). Current applications and future potential for bioinorganic chemistry in the development of anticancer drugs. *Drug Discovery Today*, 14(23), 1089-1097.
- Riley, T., & Riggs-Sauthier, J. (2008). The benefits and challenges of PEGylating small molecules. 32(7), 88-94.
- Ronconi, L., Marzano, C., Zanello, P., Corsini, M., Miolo, G., Maccà, C., ... & Fregona, D. (2006). Gold (III) dithiocarbamate derivatives for the treatment of cancer: solution chemistry, DNA binding, and hemolytic properties. *Journal of Medicinal Chemistry*, 49(5), 1648-1657.
- Ronconi, L., & Sadler, P. J. (2007). Using coordination chemistry to design new medicines. *Coordination Chemistry Reviews*, 251(13), 1633-1648.
- Ronconi, L., & Fregona, D. (2009). The Midas touch in cancer chemotherapy: from platinum-to gold-dithiocarbamate complexes. *Dalton Transactions*, (48), 10670-10680.
- Rorabacher, D. B. (2004). Electron transfer by copper centers. *Chemical Reviews*, 104(2), 651-698.
- Roy, S., Mandal, T. N., Barik, A. K., Pal, S., Gupta, S., Hazra, A., ... & Kar, S. K. (2007). Metal complexes of pyrimidine derived ligands—Syntheses, characterization and X-ray crystal structures of Ni (II), Co (III) and Fe (III) complexes of Schiff base ligands derived from S-methyl/S-benzyl dithiocarbamate and 2-S-methylmercapto-6-methylpyrimidine-4-carbaldehyde. *Polyhedron*, 26(12), 2603-2611.
- Sadler, P. J. (2009) *Dalton Transactions themed issue on Metal Anticancer Compounds*. Dalton Transactions , 48, 10647
- Sadler: N. J. Farrer & P. J. Sadler, *Medicinal Inorganic Chemistry: State of Art, New Trends and Vision of the Future in Bioinorganic Medicinal Chemistry*, ed. E. Alessio, Wiley, Weinheim, 2011, Chapter 1
- Salton MRJ & Kim KS. Structure. In: Baron S, editor. Medical Microbiology. 4th edition. Galveston (TX): University of Texas Medical Branch at Galveston; 1996. Chapter 2. Available from: <http://www.ncbi.nlm.nih.gov/books/NBK8477/>

- Santos, I. G., Abram, U., Alberto, R., Lopez, E. V., & Sanchez, A. (2004). Tricarbonylrhenium (I) complexes with thiosemicarbazone derivatives of 2-acetylpyridine and 2-pyridine formamide showing two unusual coordination modes of tridentate thiosemicarbazone ligands. *Inorganic Chemistry*, 43(6), 1834-1836.
- Santos, S., Torcato, I., & Castanho, M. A. (2012). Biomedical applications of dipeptides and tripeptides. *Peptide Science*, 98(4), 288-293.
- Sasmal, P. K., Patra, A. K., & Chakravarty, A. R. (2008). Synthesis, structure, DNA binding and DNA cleavage activity of oxovanadium (IV) N-salicylidene-S-methyldithiocarbazate complexes of phenanthroline bases. *Journal of Inorganic Biochemistry*, 102(7), 1463-1472.
- Sarkar, S., Patra, A., Drew, M. G. B., Zangrando, E., & Chattopadhyay, P. (2009). Copper (II) complexes of tetradentate N2S2 donor sets: synthesis, crystal structure characterization and reactivity. *Polyhedron*, 28(1), 1-6.
- Sheldrick, G. M. SHELXS-97, Program for Crystal Structure Solution, University of Göttingen, Göttingen, Germany, 1997a.
- Sheldrick, G. M. SHELXL-97, Program for the refinement of crystal structures from diffraction data, University of Göttingen, Göttingen, Germany, 1997b.
- Singh, R. V., Chaudhary, P., Chauhan, S., & Swami, M. (2009). Microwave-assisted synthesis, characterization and biological activities of organotin (IV) complexes with some thio Schiff bases. *Spectrochimica Acta Part A: Molecular and Biomolecular Spectroscopy*, 72(2), 260-268.
- Soliman, A. A., & Linert, W. (2007). Structural features of ONS-donor salicylidene Schiff base complexes. *Monatshefte Für Chemie-Chemical Monthly*, 138(3), 175-189.
- Splith, K., Neundorf, I., Hu, W., N'Dongo, H. W. P., Vasylyeva, V., Merz, K., & Schatzschneider, U. (2010). Influence of the metal complex-to-peptide linker on the synthesis and properties of bioactive CpMn (CO) 3 peptide conjugates. *Dalton Transactions*, 39(10), 2536-2545.
- Stavri, M., Piddock, L. J., & Gibbons, S. (2007). Bacterial efflux pump inhibitors from natural sources. *Journal of Antimicrobial Chemotherapy*, 59(6), 1247-1260.
- Stefani, C., Jansson, P. J., Gutierrez, E., Bernhardt, P. V., Richardson, D. R., & Kalinowski, D. S. (2012). Alkyl substituted 2'-benzoylpyridine thiosemicarbazone chelators with potent and selective anti-neoplastic activity: Novel ligands that limit methemoglobin formation. *Journal of Medicinal Chemistry*, 56(1), 357-370.
- Stephan, H., Geipel, G., Appelhans, D., Bernhard, G., Tabuani, D., Komber, H., & Voit, B. (2005). Pegylation of 1, 4, 8, 11-tetraazacyclotetradecane (cyclam) and its Cu (II) complexation. *Tetrahedron Letters*, 46(18), 3209-3212.

- Stewart, K. M., Horton, K. L., & Kelley, S. O. (2008). Cell-penetrating peptides as delivery vehicles for biology and medicine. *Org. Biomol. Chem.*, 6(13), 2242-2255.
- Storr, T., Thompson, K. H., & Orvig, C. (2006). Design of targeting ligands in medicinal inorganic chemistry. *Chemical Society Reviews*, 35(6), 534-544.
- Stratton, C. W. (2003). Dead bugs don't mutate: susceptibility issues in the emergence of bacterial resistance. *Emerging Infectious Diseases*, 9(1), 10.
- Strohl, W. R. (2000). The role of natural products in a modern drug discovery program. *Drug Discovery Today*, 5(2), 39-41.
- Strøm, M. B., Haug, B. E., Skar, M. L., Stensen, W., Stiberg, T., & Svendsen, J. S. (2003). The pharmacophore of short cationic antibacterial peptides. *Journal of Medicinal Chemistry*, 46(9), 1567-1570.
- Swarts, J. C., Cook, M. J., & Baker, E. N. (2008). Metal-containing proteins, macrocycles, and coordination complexes in therapeutic applications and disease. *Metal-Based Drugs*, 2008.
- Sun, J., Liu, D. M., & Yan, C. G. (2009). Transition metal complexes of bidentate p-tert-butylcalix [4] arene S-alkyldithiocarbazate Schiff bases. *Journal of Coordination Chemistry*, 62(14), 2337-2346.
- Takjoo, R., Centore, R., Hakimi, M., Ali Beyramabadi, S., & Morsali, A. (2011). S-allyl-3-(2-pyridyl-methylene) dithiocarbazate ligand and its manganese (II), cobalt (III) and nickel (II) complexes. *Inorganica Chimica Acta*, 371(1), 36-41.
- Tarafder, M. T. H., Ali, M. A., Wee, D. J., Azahari, K., Silong, S., & Crouse, K. A. (2000a). Complexes of a tridentate ONS Schiff base. Synthesis and biological properties. *Transition Metal Chemistry*, 25(4), 456-460.
- Tarafder, M. T. H., Ali, A. M., Elias, M. S., Crouse, K. A., & Silong, S. (2000b). Coordination chemistry and biological activity of bidentate and quadridentate nitrogen-sulfur donor ligands and their complexes. *Transition Metal Chemistry*, 25(6), 706-710.
- Tarafder, M. T. H., Ali, M. A., Saravanan, N., Weng, W. Y., Kumar, S., Umar-Tsafe, N., & Crouse, K. A. (2000c). Coordination chemistry and biological activity of two tridentate ONS and NNS Schiff bases derived from S-benzylidithiocarbazate. *Transition Metal Chemistry*, 25(3), 295-298.
- Tarafder, M. T. H., Saravanan, N., & Crouse, K. A. (2001a). Coordination chemistry and biological activity of nickel (II) and copper (II) ion complexes with nitrogen-sulphur donor ligands derived from S-benzylidithiocarbazate (SBDTC). *Transition Metal Chemistry*, 26(6), 613-618.

Tarafder, M. T. H., Kasbollah, A., Crouse, K. A., Ali, A. M., Yamin, B. M., & Fun, H. K. (2001b). Synthesis and characterization of Zn (II) and Cd (II) complexes of S-benzyl- β -N-(2-pyridyl) methylenedithiocarbazate (HNNS): bioactivity of the HNNS Schiff base and its Zn (II), Cu (II) and Cd (II) complexes and the X-ray structure of the [Zn (NNS)₂] complex. *Polyhedron*, 20(18), 2363-2370.

Tarafder, M. T. H., Jin, K. T., Crouse, K. A., Ali, A. M., Yamin, B. M., & Fund, H. K. (2002a). Coordination chemistry and bioactivity of Ni²⁺, Cu²⁺, Cd²⁺ and Zn²⁺ complexes containing bidentate Schiff bases derived from S-benzylidithiocarbazate and the X-ray crystal structure of bis [S-benzyl- β -N-(5-methyl-2-furylmethylene) dithiocarbazato] cadmium (II). *Polyhedron*, 21(25-26), 2547-2554.

Tarafder, M. T. H., Khoo, T. J., Crouse, K. A., Ali, A. M., Yamin, B. M., & Fun, H. K. (2002b). Coordination chemistry and bioactivity of some metal complexes containing two isomeric bidentate NS Schiff bases derived from S-benzylidithiocarbazate and the X-ray crystal structures of S-benzyl- β -N-(5-methyl-2-furylmethylene) dithiocarbazate and bis [S-benzyl- β -N-(2-furylmethylketone) dithiocarbazato] cadmium (II). *Polyhedron*, 21(27), 2691-2698.

Tarafder, M. T. H., Chew, K. B., Crouse, K. A., Ali, A. M., Yamin, B. M., & Fun, H. K. (2002c). Synthesis and characterization of Cu (II), Ni (II) and Zn (II) metal complexes of bidentate NS isomeric Schiff bases derived from S-methyldithiocarbazate (SMDTC): bioactivity of the bidentate NS isomeric Schiff bases, some of their Cu (II), Ni (II) and Zn (II) complexes and the X-ray structure of the bis [S-methyl- β -N-(2-furyl-methyl) methylenedithiocarbazato] zinc (II) complex. *Polyhedron*, 21(27), 2683-2690.

Tarafder, M. T. H., Islam, M. A. A. A. A., Crouse, K. A., Chantrapromma, S., & Fun, H. K. (2008). (E)-4-(Benzyloxy) benzaldehyde thiosemicarbazone. *Acta Crystallographica Section E: Structure Reports Online*, 64(6), o988-o989.

Taubes, G. (2008). The bacteria fight back. *Science (New York, NY)*, 321(5887), 356-361.

Tenover, F. C. (2006). Mechanisms of antimicrobial resistance in bacteria. *The American Journal of Medicine*, 119(6), S3-S10.

Terada, H., Uda, M., Kametani, F., & Kubota, S. (1978). Structural requirements of alkyl acyldithiocarbazates for the uncoupling of oxidative phosphorylation in mitochondria. *Biochimica et Biophysica Acta (BBA)-Bioenergetics*, 504(2), 237-247.

Thompson, K. H., & Orvig, C. (2003). Boon and bane of metal ions in medicine. *Science*, 300(5621), 936-939.

Thompson, K. H., & Orvig, C. (2006). Metal complexes in medicinal chemistry: new vistas and challenges in drug design. *Dalton Transactions*, (6), 761-764.

- Timerbaev, A. R., Hartinger, C. G., Aleksenko, S. S., & Keppler, B. K. (2006). Interactions of antitumor metallodrugs with serum proteins: advances in characterization using modern analytical methodology. *Chemical Reviews*, *106*(6), 2224-2248.
- Tiwari, K. N., Monserrat, J. P., Hequet, A., Ganem-Elbaz, C., Cresteil, T., Jaouen, G., ... & Jolival, C. (2012). In vitro inhibitory properties of ferrocene-substituted chalcones and aurones on bacterial and human cell cultures. *Dalton Transactions*, *41*(21), 6451-6457.
- Tsubery, H., Ofek, I., Cohen, S., & Fridkin, M. (2000). Structure-function studies of polymyxin b nonapeptide: implications to sensitization of gram-negative bacteria. *Journal of Medicinal Chemistry*, *43*(16), 3085-3092.
- Tsubery, H., Ofek, I., Cohen, S., & Fridkin, M. (2001). N-terminal modifications of polymyxin B nonapeptide and their effect on antibacterial activity. *Peptides*, *22*(10), 1675-1681.
- Turel, I., Kljun, J., Perdih, F., Morozova, E., Bakulev, V., Kasyanenko, N., ... & Osheroff, N. (2010). First ruthenium organometallic complex of antibacterial agent ofloxacin. Crystal structure and interactions with DNA. *Inorganic Chemistry*, *49*(23), 10750-10752.
- Uccelli, L., Pasquali, M., Boschi, A., Giganti, M., & Duatti, A. (2011). Automated preparation of Re-188 lipiodol for the treatment of hepatocellular carcinoma. *Nuclear Medicine and Biology*, *38*(2), 207-213.
- Umamaheswari, V., Cias, P., Pöppl, A., Kaupp, M., & Gescheidt, G. (2014). Ligand spheres in asymmetric hetero Diels–Alder reactions catalyzed by Cu (II) box complexes: experiment and modeling. *Dalton Transactions*, *43*(2), 698-705
- Vecchione, J. J., Alexander, B., & Sello, J. K. (2009). Two distinct major facilitator superfamily drug efflux pumps mediate chloramphenicol resistance in *Streptomyces coelicolor*. *Antimicrobial Agents and Chemotherapy*, *53*(11), 4673-4677.
- Veronese, F. M., & Pasut, G. (2005). PEGylation, successful approach to drug delivery. *Drug Discovery Today*, *10*(21), 1451-1458.
- Vigato, P. A., & Tamburini, S. (2004). The challenge of cyclic and acyclic schiff bases and related derivatives. *Coordination Chemistry Reviews*, *248*(17), 1717-2128.
- Viveiros, M., Jesus, A., Brito, M., Leandro, C., Martins, M., Ordway, D., ... & Amaral, L. (2005). Inducement and reversal of tetracycline resistance in *Escherichia coli* K-12 and expression of proton gradient-dependent multi-drug efflux pump genes. *Antimicrobial Agents and Chemotherapy*, *49*(8), 3578-3582.
- Vives, E. (2005). Present and future of cell-penetrating peptide mediated delivery systems: "is the Trojan horse too wild to go only to Troy?". *Journal of Controlled Release*, *109*(1), 77-85.

Walrant, A., Correia, I., Jiao, C. Y., Lequin, O., Bent, E. H., Goasdoué, N., ... & Alves, I. D. (2011). Different membrane behaviour and cellular uptake of three basic arginine-rich peptides. *Biochimica et Biophysica Acta (BBA) - Biomembranes*, 1808(1), 382-393.

Walsh, C. (2000). Molecular mechanisms that confer antibacterial drug resistance. *Nature*, 406(6797), 775-781.

Wender, P. A., Mitchell, D. J., Pattabiraman, K., Pelkey, E. T., Steinman, L., & Rothbard, J. B. (2000). The design, synthesis, and evaluation of molecules that enable or enhance cellular uptake: peptoid molecular transporters. *Proceedings of the National Academy of Sciences*, 97(24), 13003-13008.

West, D. X., Liberta, A. E., Padhye, S. B., Chikate, R. C., Sonawane, P. B., Kumbhar, A. S., & Yerande, R. G. (1993). Thiosemicarbazone complexes of copper (II): structural and biological studies. *Coordination Chemistry Reviews*, 123(1), 49-71.

Wiecek, J., Dokorou, V., Ciunik, Z., & Kovala-Demertzi, D. (2009). Organotin complexes of pyruvic acid thiosemicarbazone: synthesis, crystal structures and antiproliferative activity of neutral and cationic diorganotin complexes. *Polyhedron*, 28(15), 3298-3304.

Xu, L., Zhou, J. H., Chen, X. T., & You, X. Z. (2002). Dibenzyl 2, 2'-(ethane-1, 2-diylidene) dihydrazinecarbodithioate bis (dimethylformamide) solvate. *Acta Crystallographica Section C: Crystal Structure Communications*, 58(8), o513-o514.

Yang, G., Nowsheen, S., Aziz, K., & Georgakilas, A. G. (2013). Toxicity and adverse effects of Tamoxifen and other anti-estrogen drugs. *Pharmacology & Therapeutics*, 139(3), 392-404.

Yu, Z., & Quinn, P. (1994). Dimethyl sulphoxide: a review of its applications in cell biology. *Bioscience Reports*, 14, 259-281.

Yu, Z. W., & Quinn, P. J. (1998). The modulation of membrane structure and stability by dimethyl sulphoxide (Review). *Molecular Membrane Biology*, 15(2), 59-68.

Zaslhoff, M. (2002). Antimicrobial peptides of multicellular organisms. *Nature*, 415(6870), 389-395.

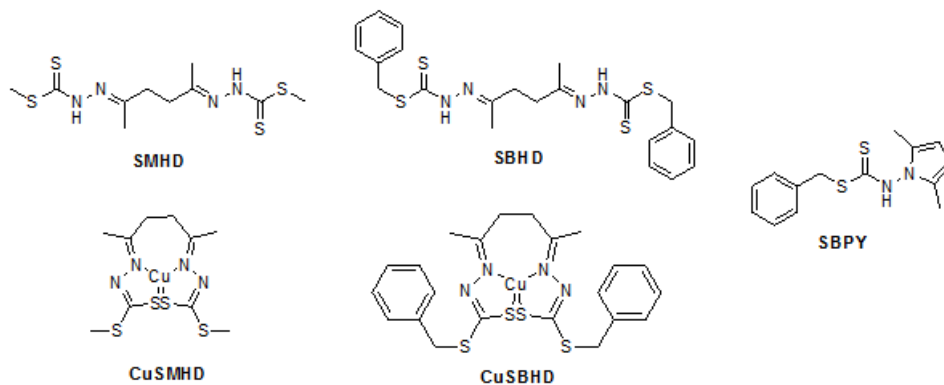
Zhang, L. Z., Ding, T., Chen, C. L., Li, M. X., Zhang, D., & Niu, J. Y. (2011a). Biological activities of pyridine-2-carbaldehyde Schiff bases derived from S-methyl- and S-benzylthiocarbazate and their zinc (II) and manganese (II) complexes. Crystal Structure of the Manganese (II) complex of pyridine-2-carbaldehyde S-benzylthiocarbazate. *Russian Journal of Coordination Chemistry*, 37(5), 356-361.

Zhang, H. J., Qian, Y., Zhu, D. D., Yang, X. G., & Zhu, H. L. (2011b). Synthesis, molecular modeling and biological evaluation of chalcone thiosemicarbazide derivatives as novel anticancer agents. *European Journal of Medicinal Chemistry*, 46(9), 4702-4708.

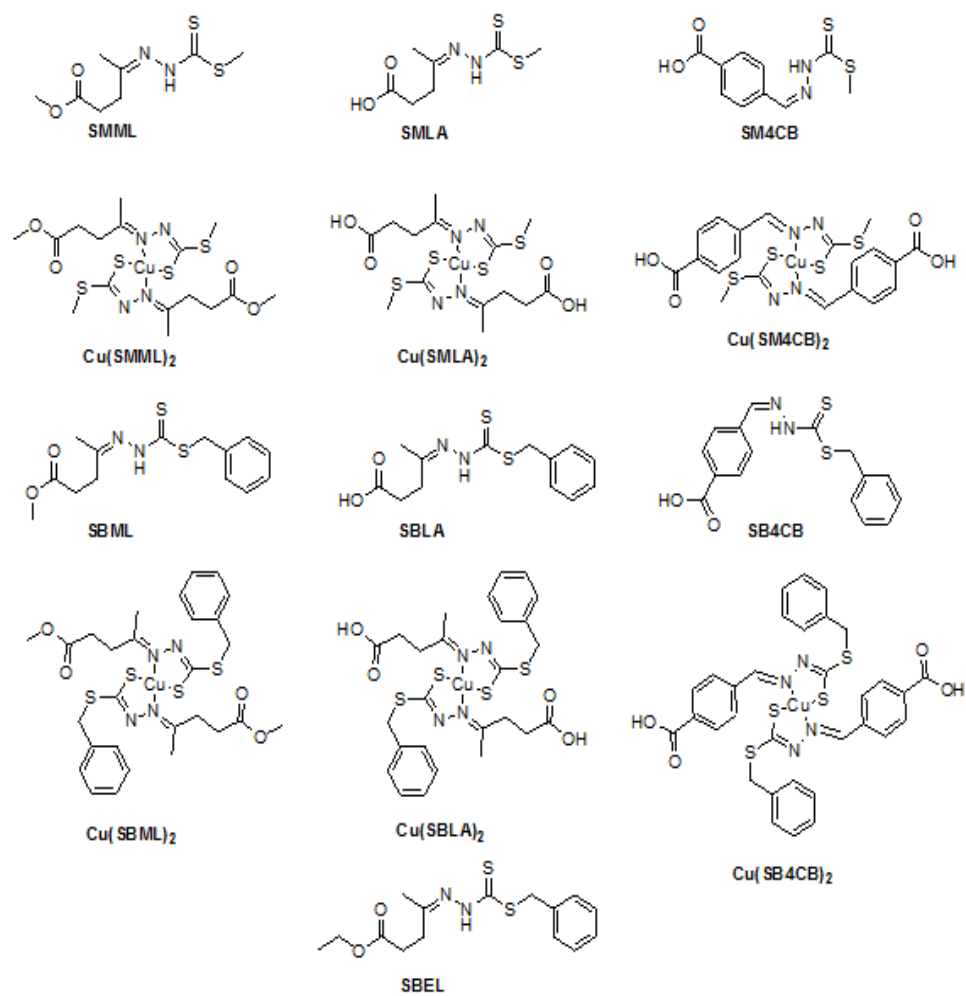
APPENDICES

Molecular structures of all compounds synthesized and characterized in this work.

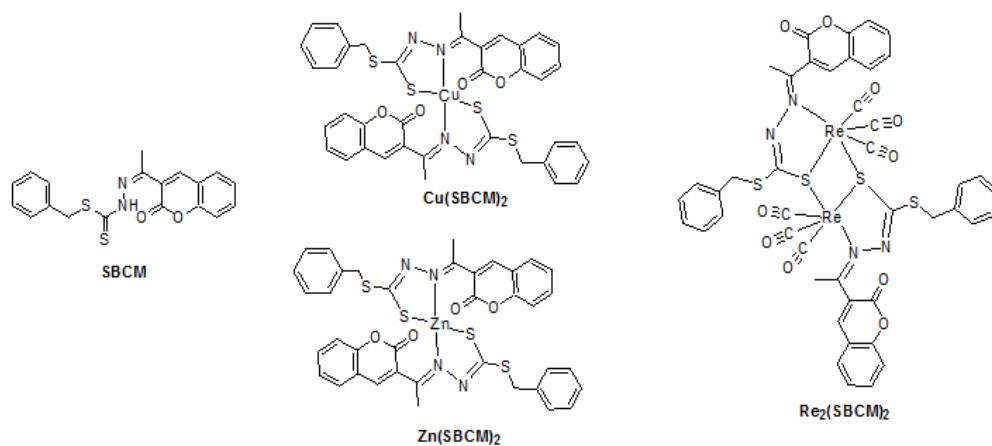
(a) Macroacyclic Cu(II) system with tetradentate NNSS ligands.



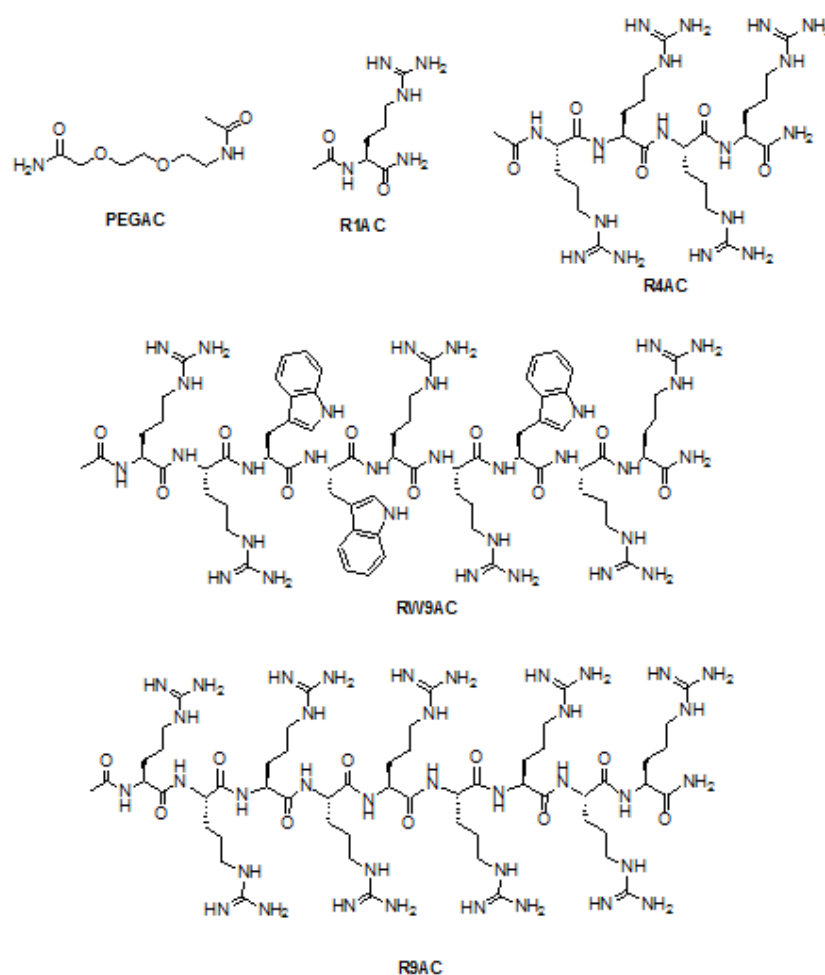
(b) Open chain Cu(II) system with bidentate NS ligands with acid or ester functionality.



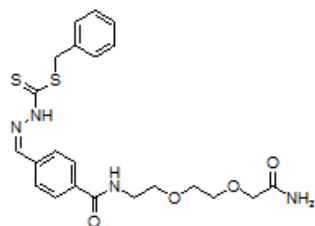
(c) Open chain metal system with bidentate NS ligands with natural ketone moiety.



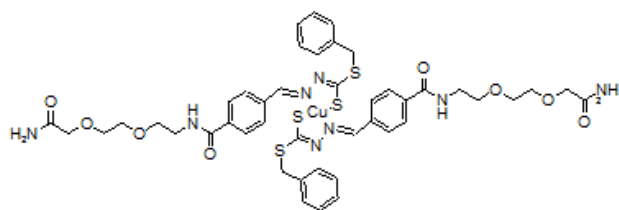
(d) Acetylated vectors.



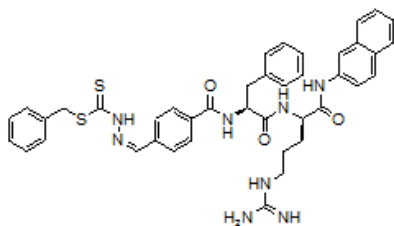
(e) Functionalized compounds.



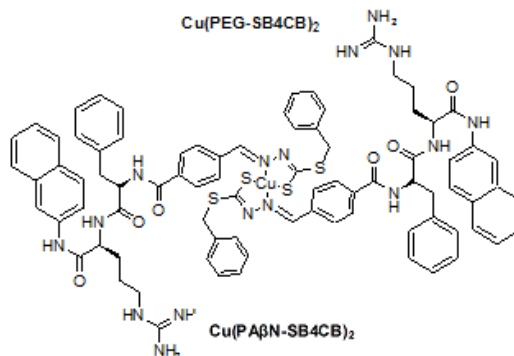
PEG-SB4CB



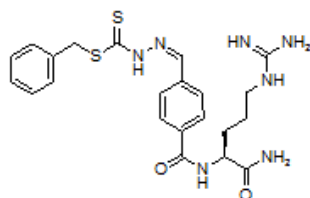
$\text{Cu}(\text{PEG-SB4CB})_2$



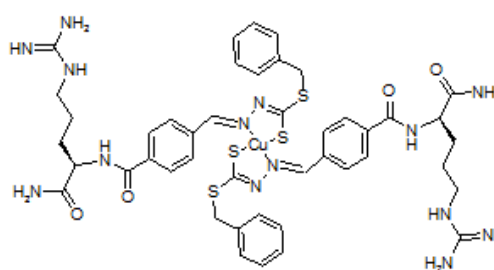
PAβN-SB4CB



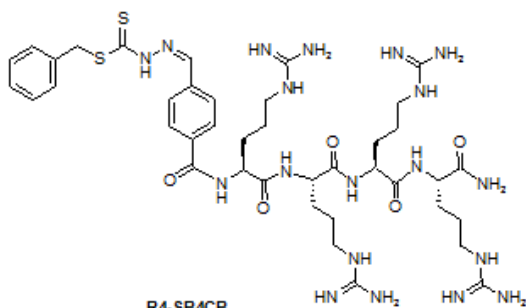
$\text{Cu}(\text{PA}\beta\text{N-SB4CB})_2$



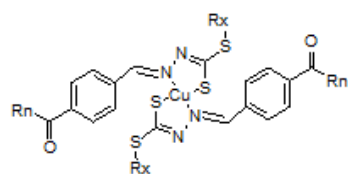
R1-SB4CB



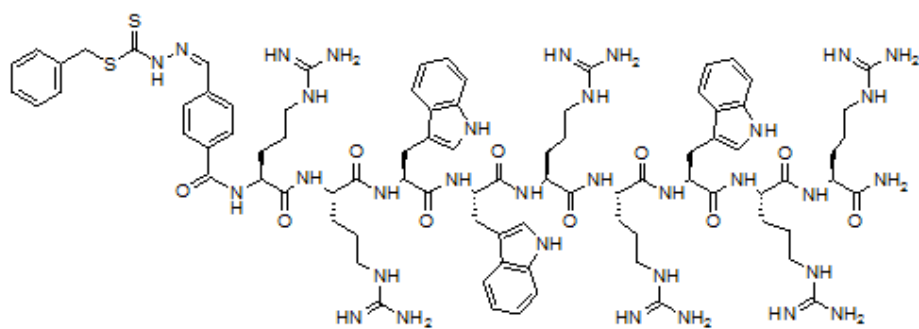
$\text{Cu}(\text{R1-SB4CB})_2$



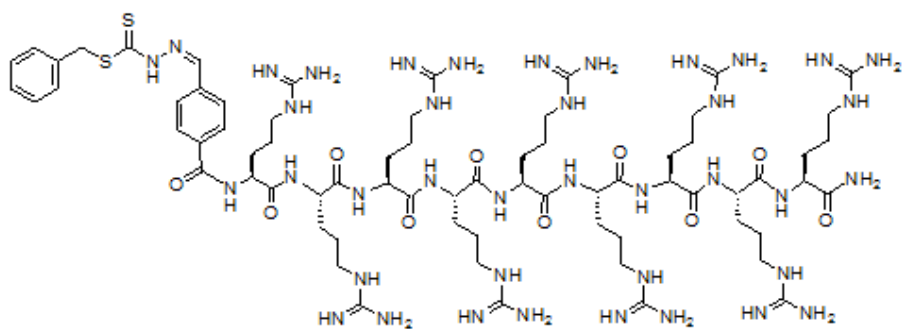
R4-SB4CB



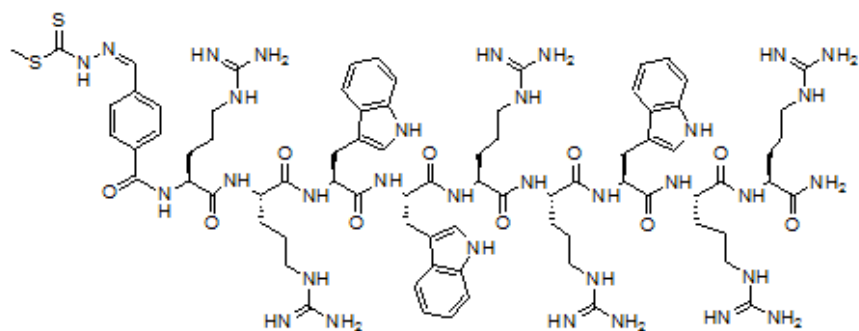
$\text{Cu}(\text{R4-SB4CB})_2$: Rx=CH₂Ph, Rn=R4
 $\text{Cu}(\text{RW9-SB4CB})_2$: Rx=CH₂Ph, Rn=RW9
 $\text{Cu}(\text{R9-SB4CB})_2$: Rx=CH₂Ph, Rn=R9
 $\text{Cu}(\text{RW9-SM4CB})_2$: Rx=CH₃, Rn=RW9
 $\text{Cu}(\text{R9-SM4CB})_2$: Rx=CH₃, Rn=R9



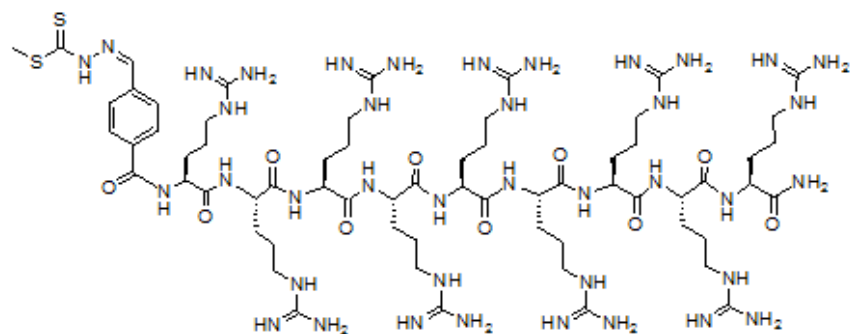
RW9-SB4CB



R9-SB4CB



RW9-SM4CB



R9-SM4CB

A. NMR spectra

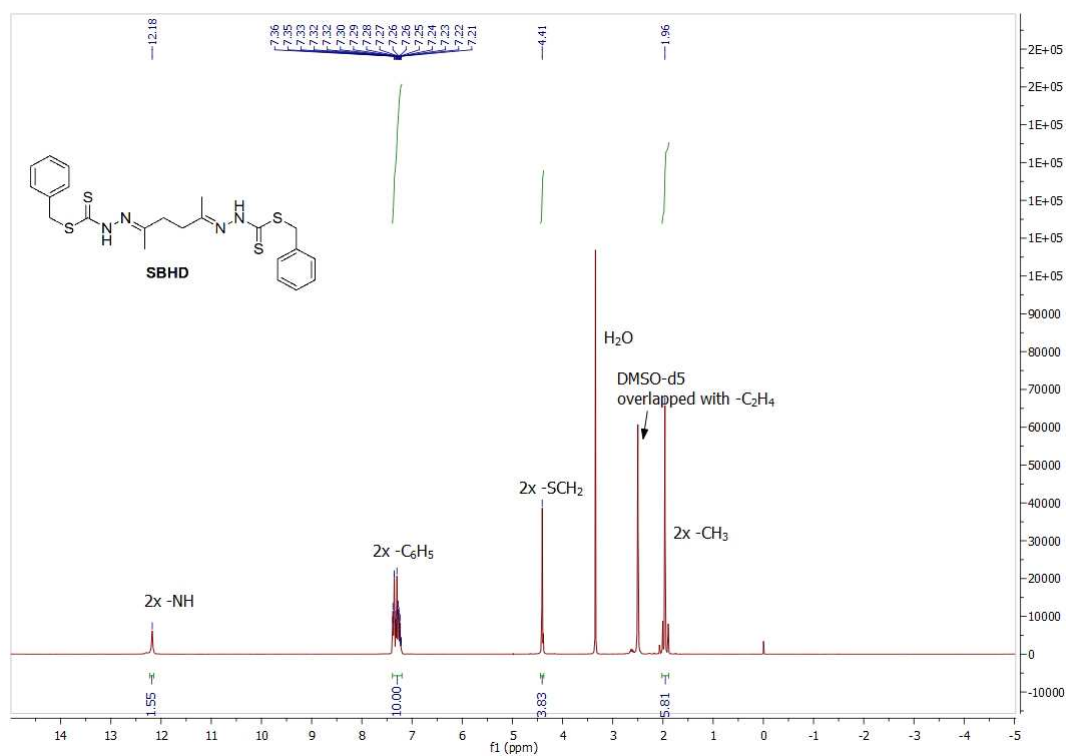


Figure A1. ^1H NMR spectrum of SBHD

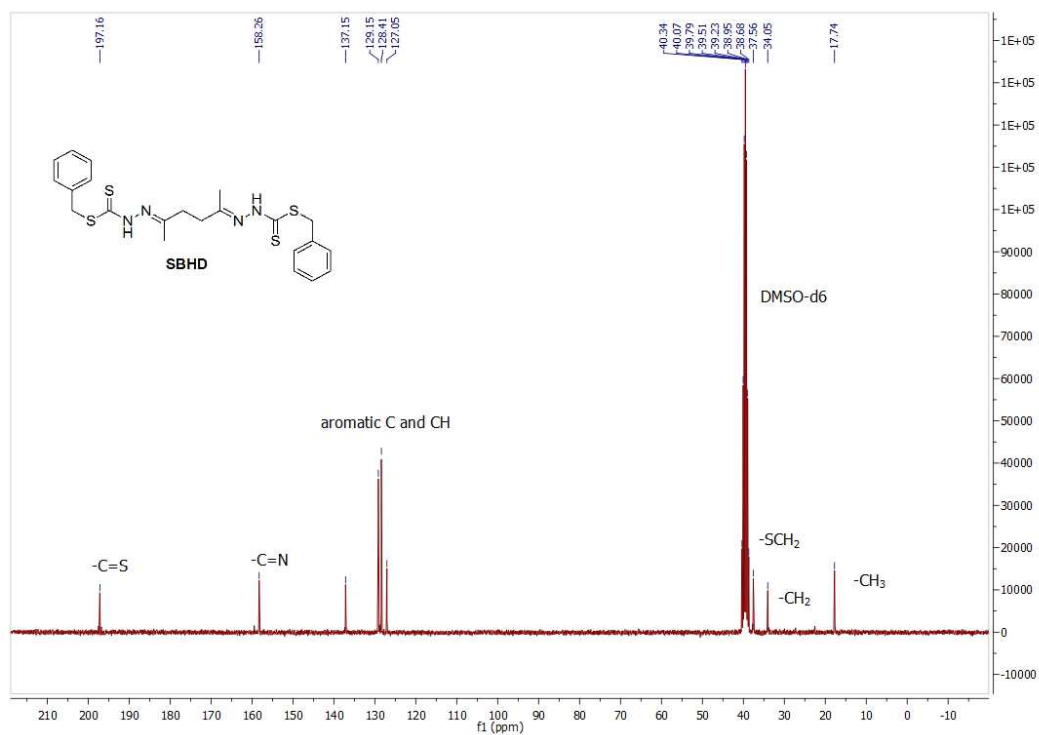


Figure A2. ^{13}C NMR spectrum of SBHD

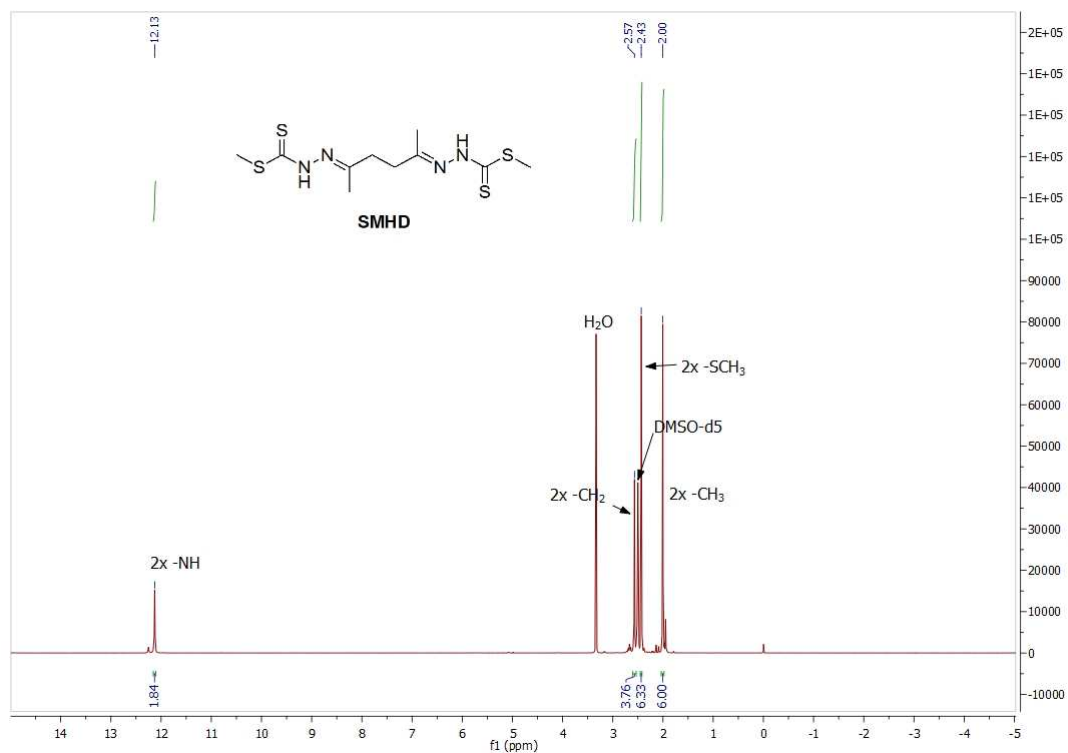


Figure A3. ^1H NMR spectrum of SMHD

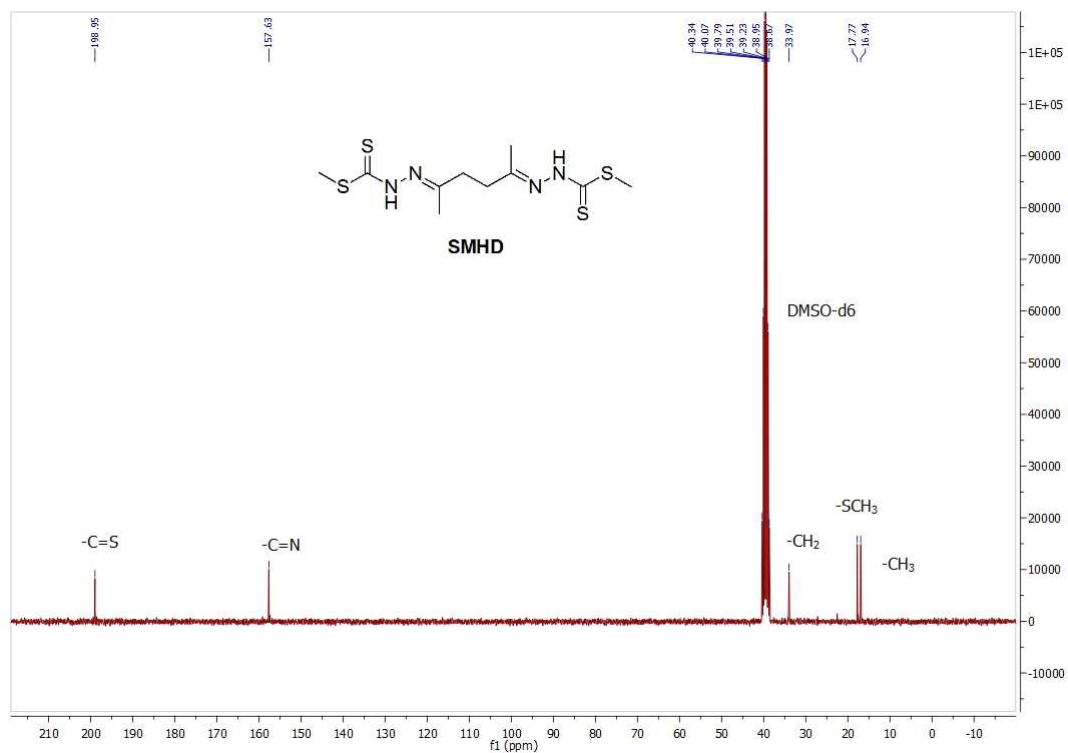


Figure A4. ^{13}C NMR spectrum of SMHD

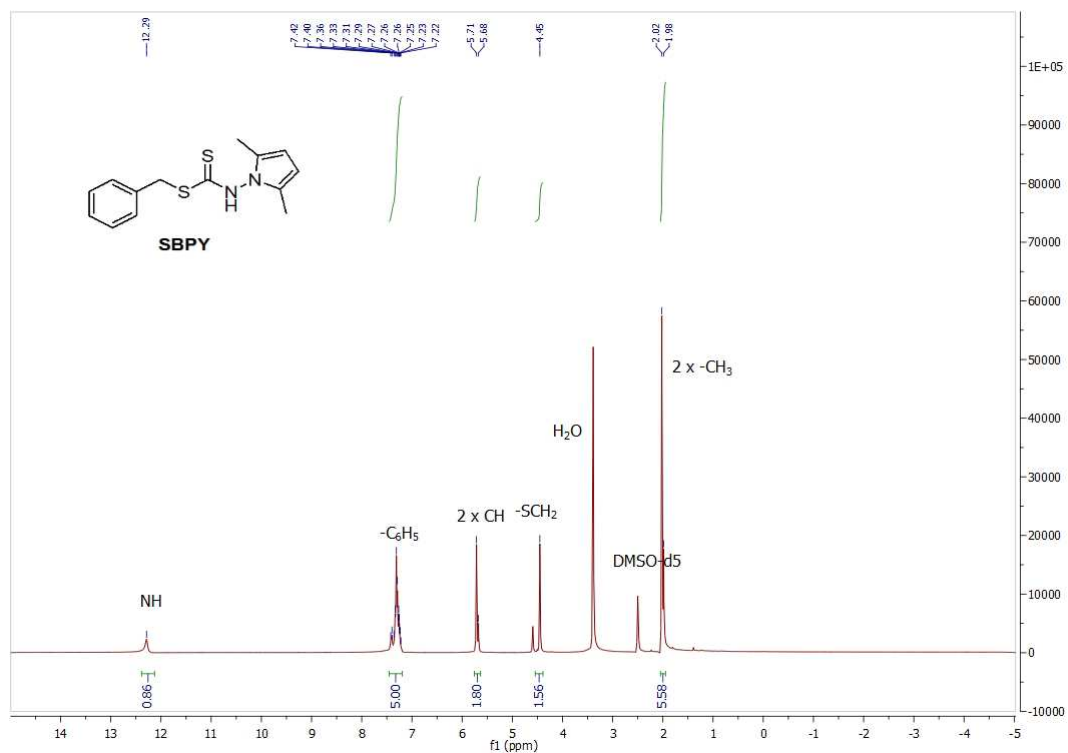


Figure A5. ¹H NMR spectrum of SBPY

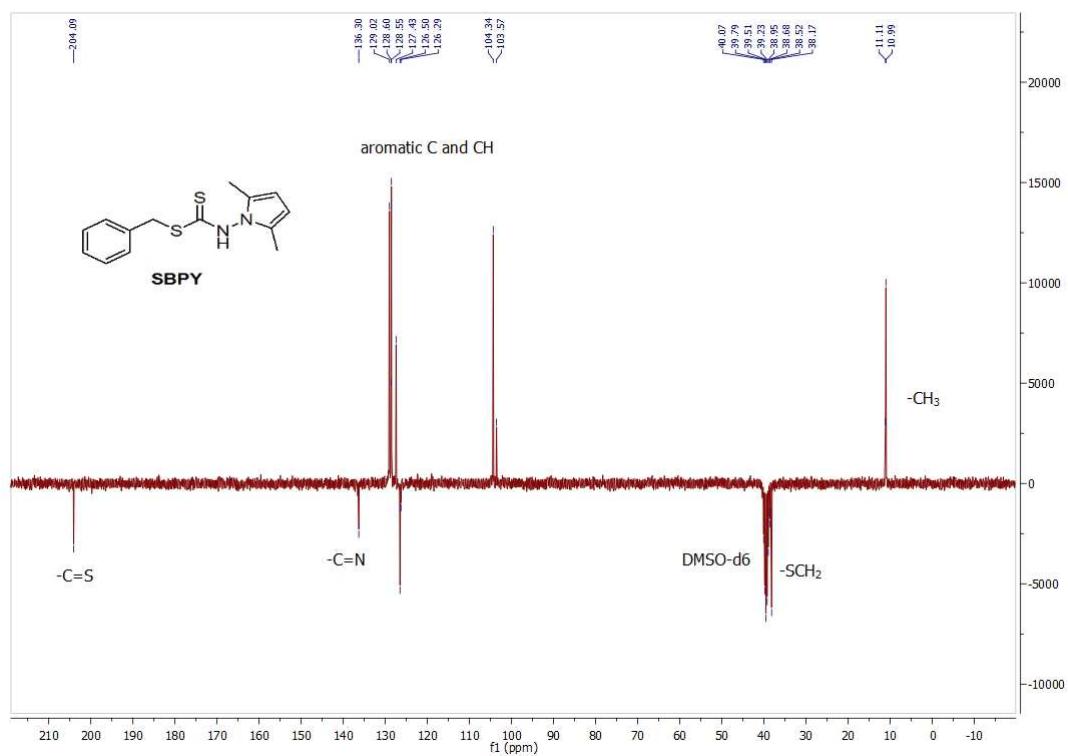
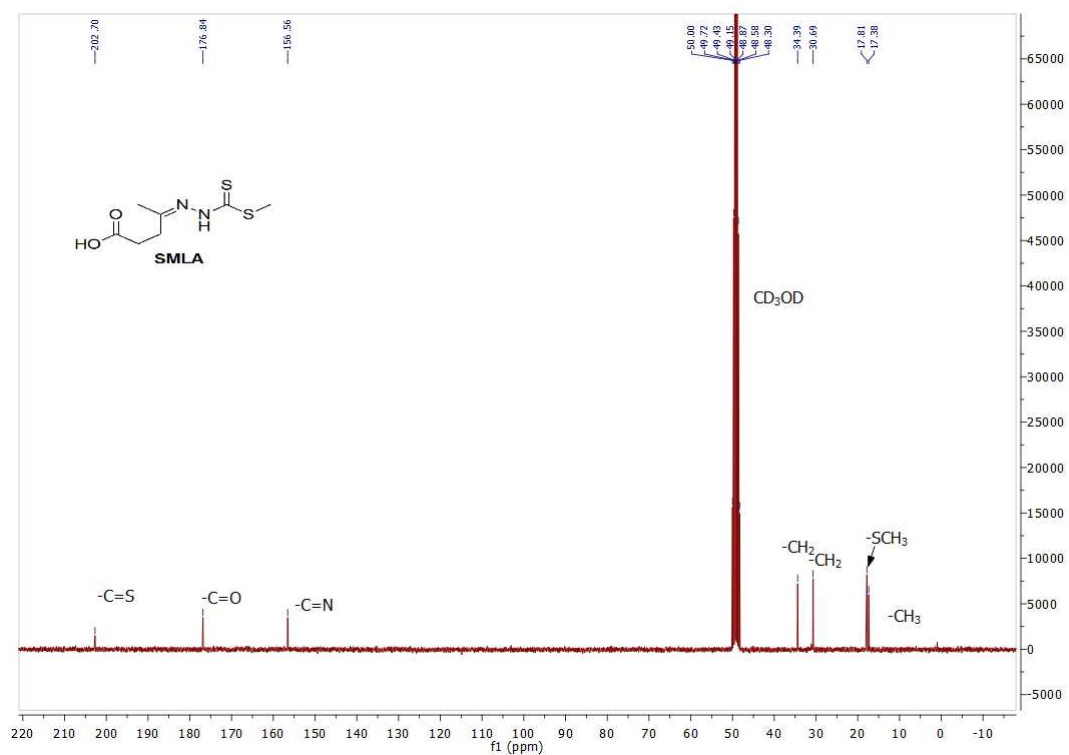
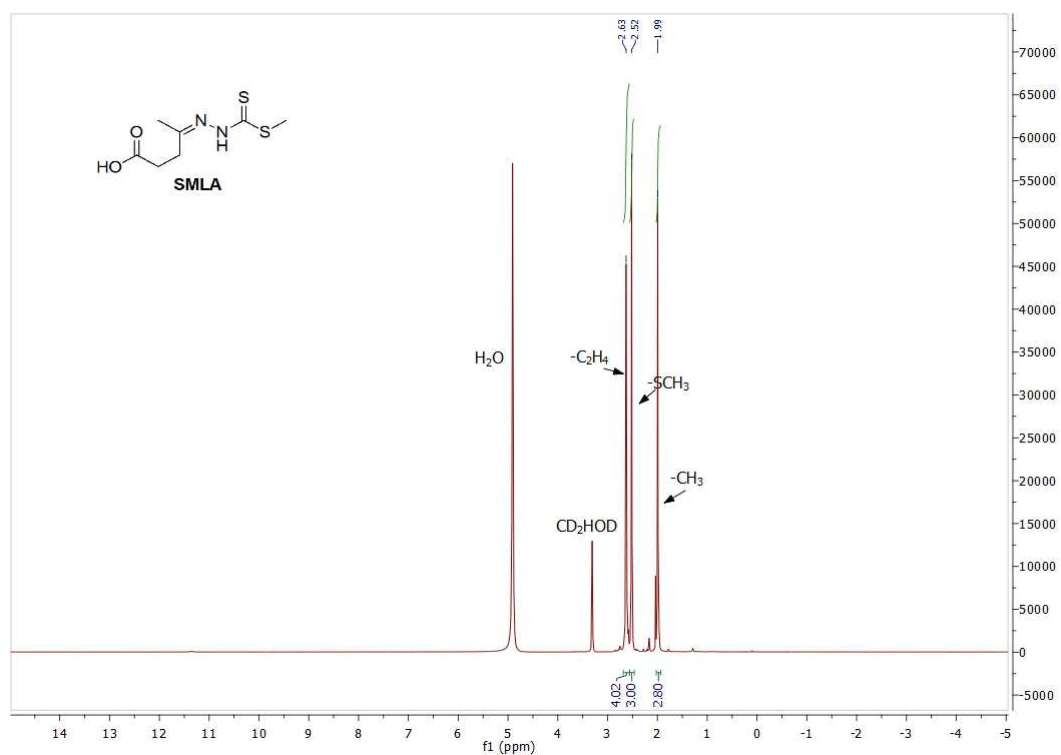
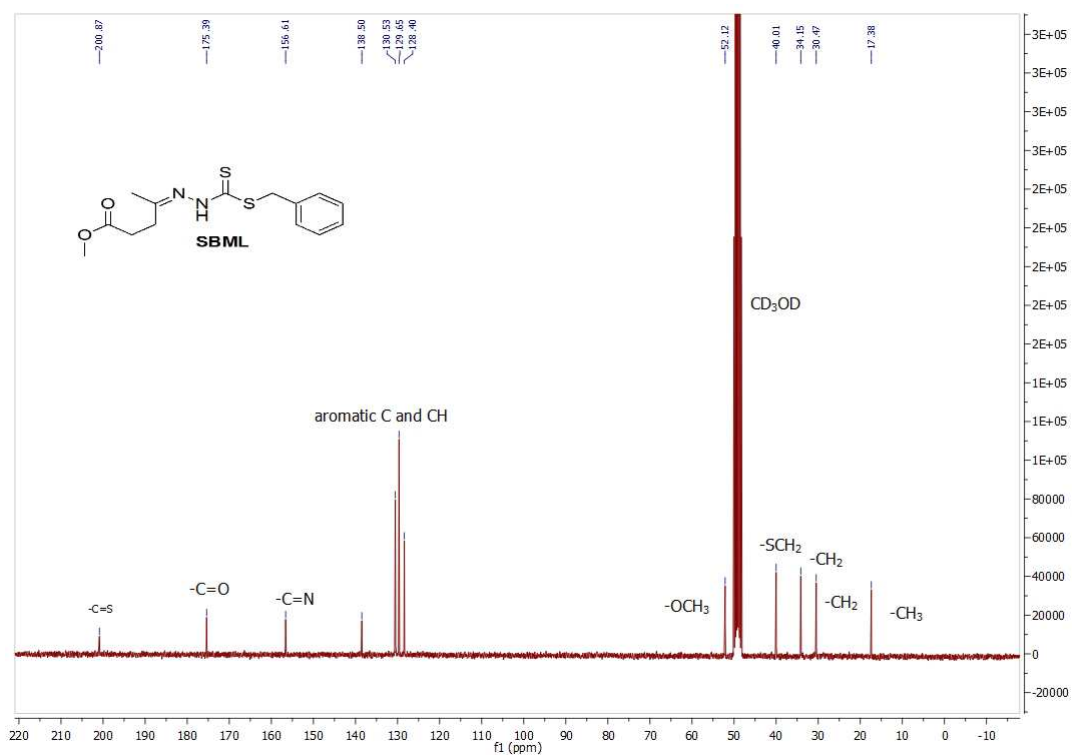
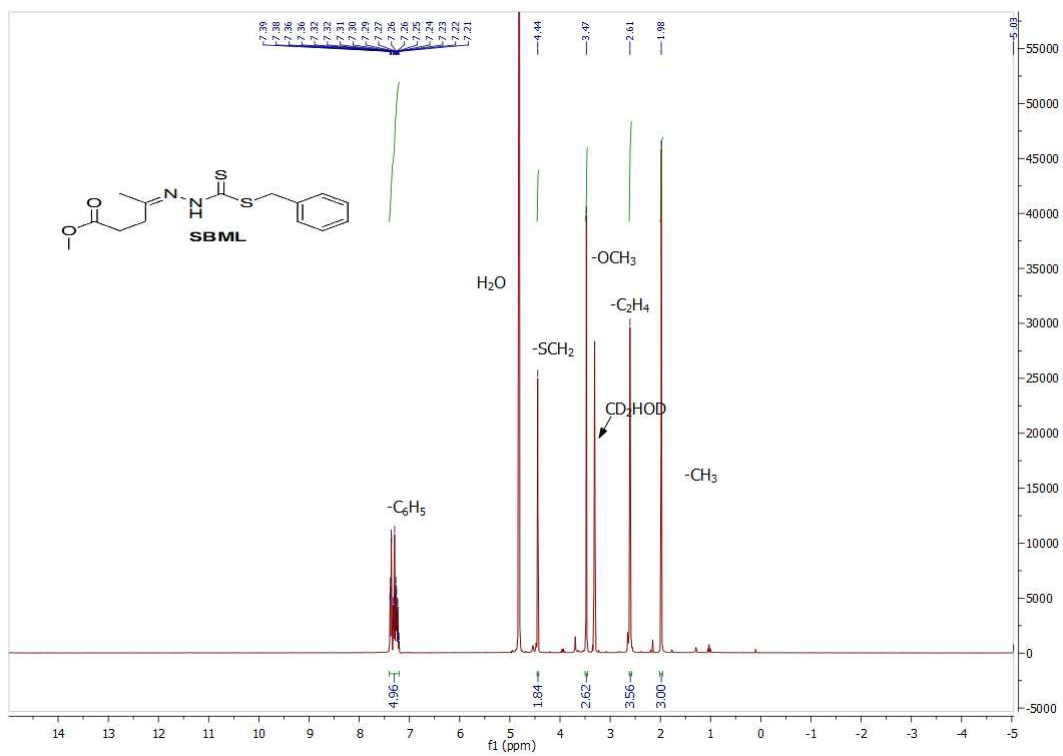


Figure A6. ¹³C NMR spectrum of SBPY





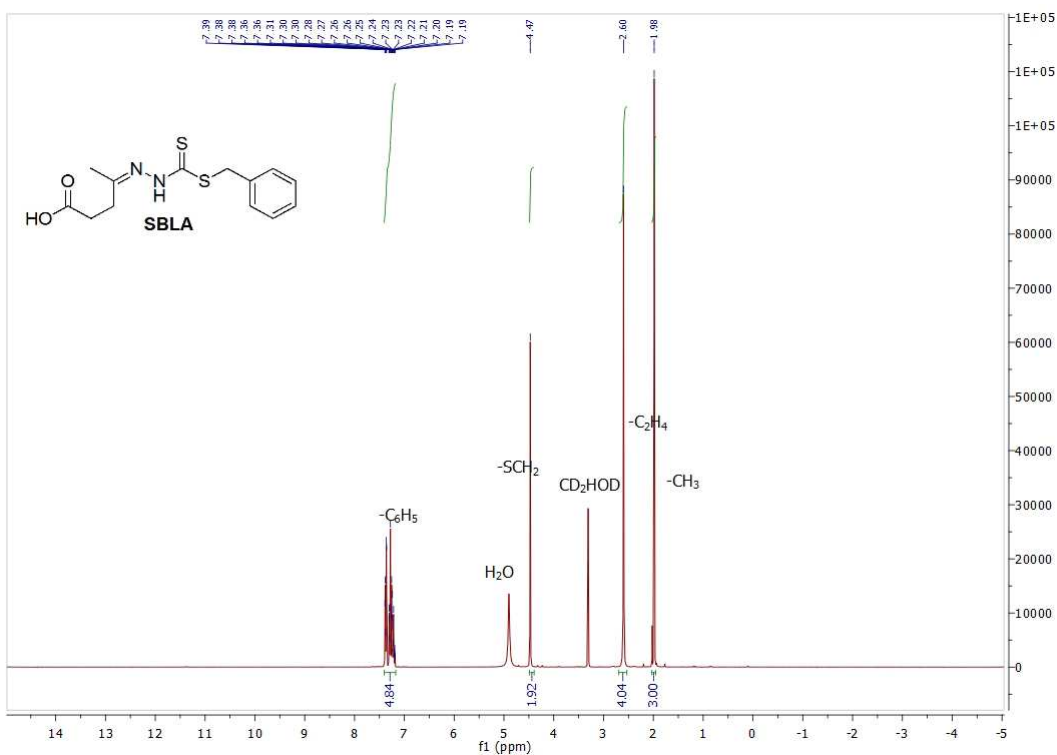


Figure A11. ¹H NMR spectrum of SBLA

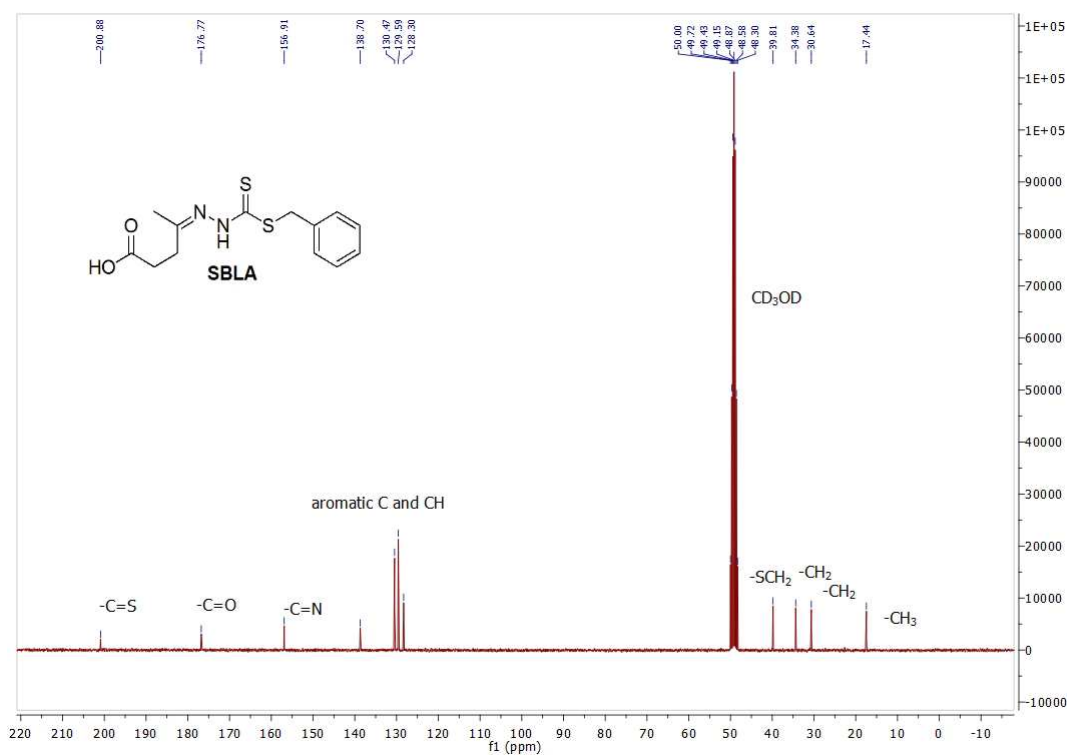


Figure A12. ¹³C NMR spectrum of SBLA

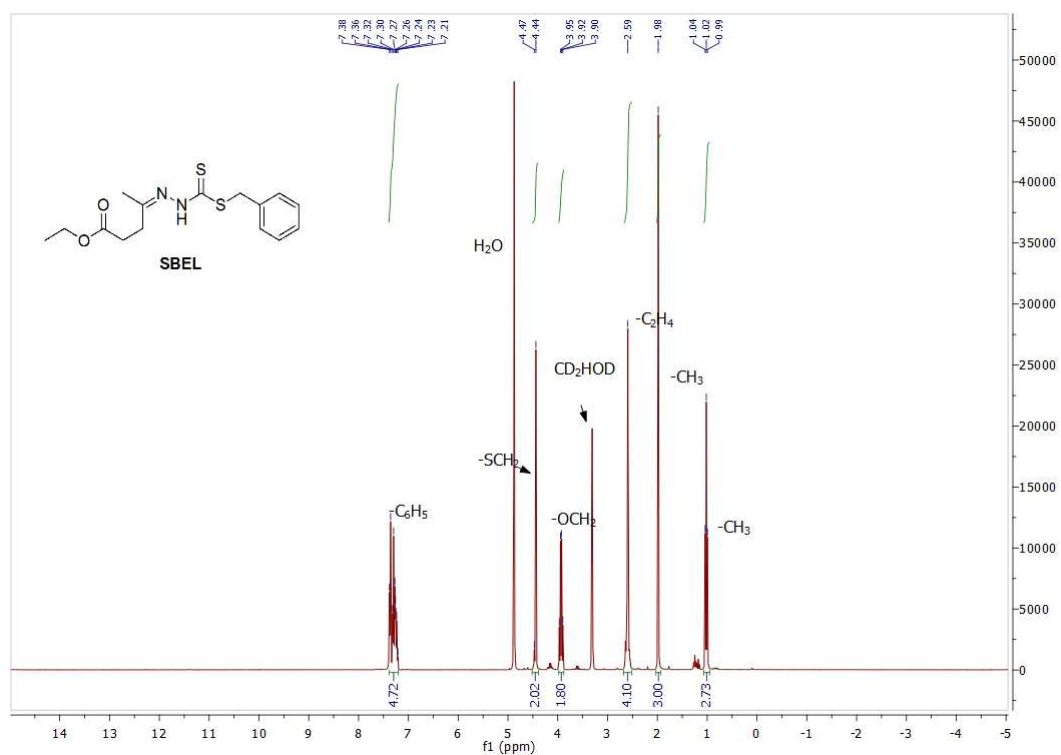


Figure A13. ^1H NMR spectrum of SBEL

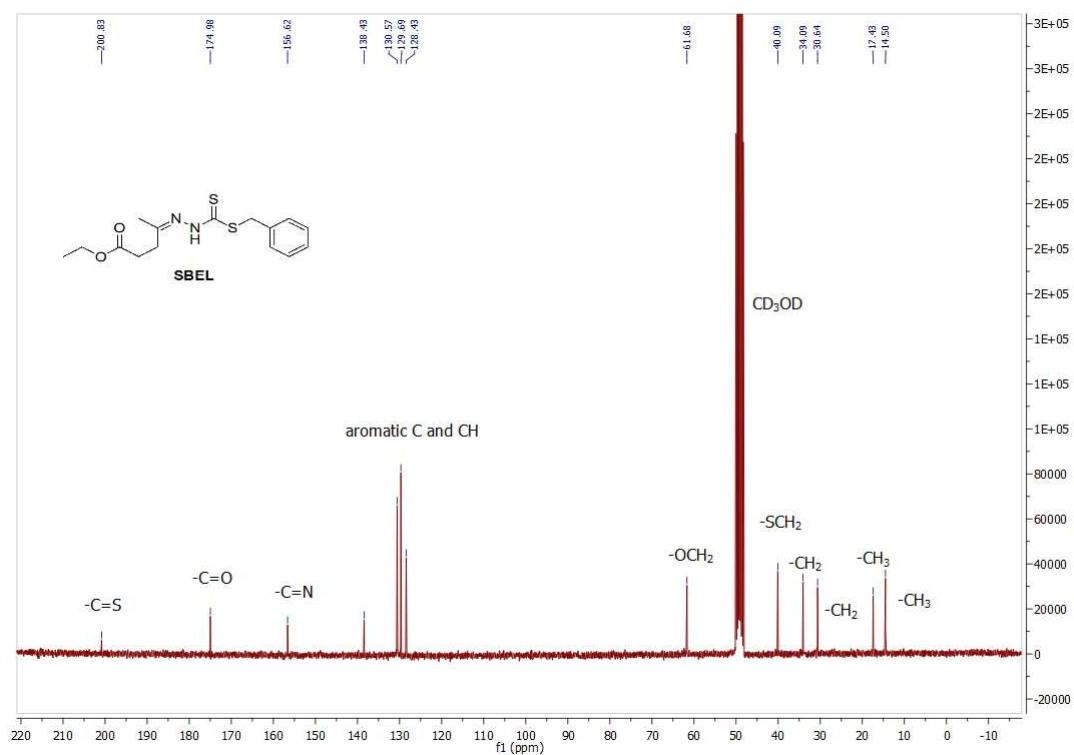


Figure A14. ^{13}C NMR spectrum of SBEL

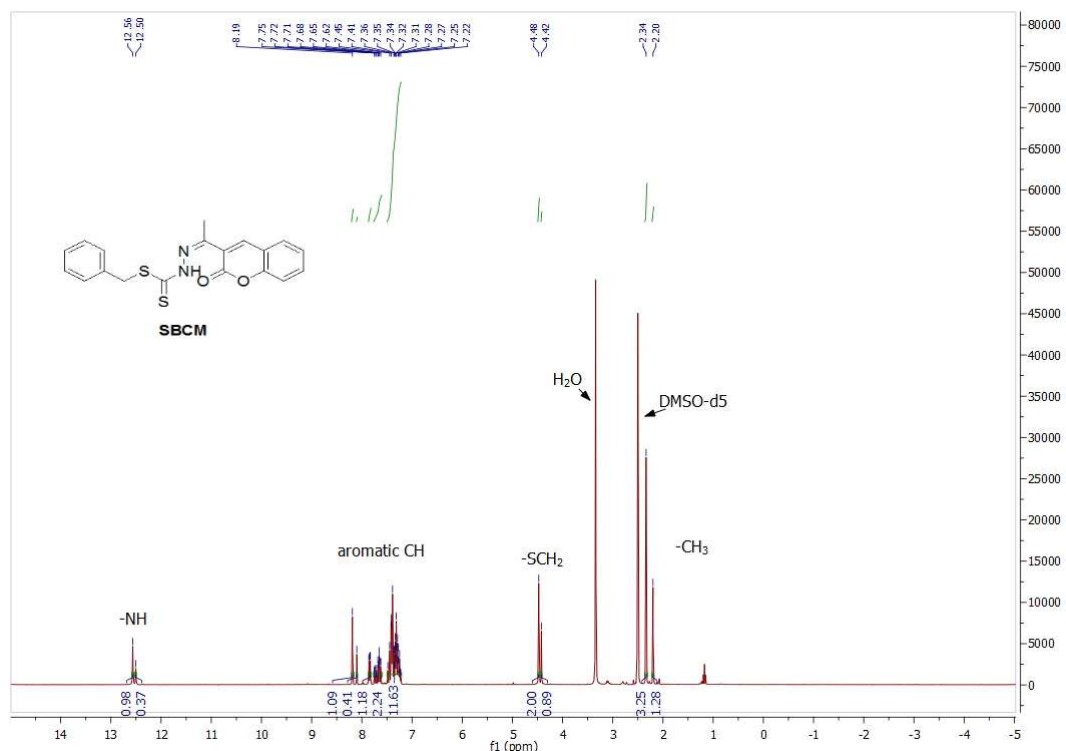


Figure A17. ^1H NMR spectrum of SBCM

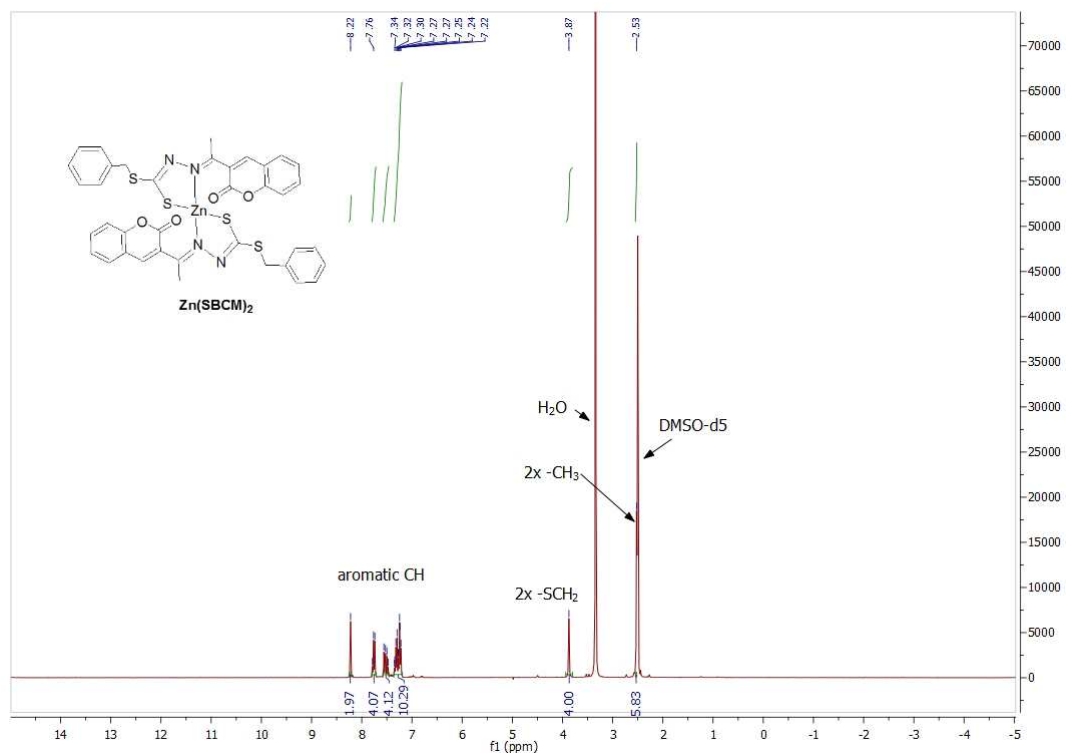


Figure A18. ^1H NMR spectrum of $\text{Zn}(\text{SBCM})_2$

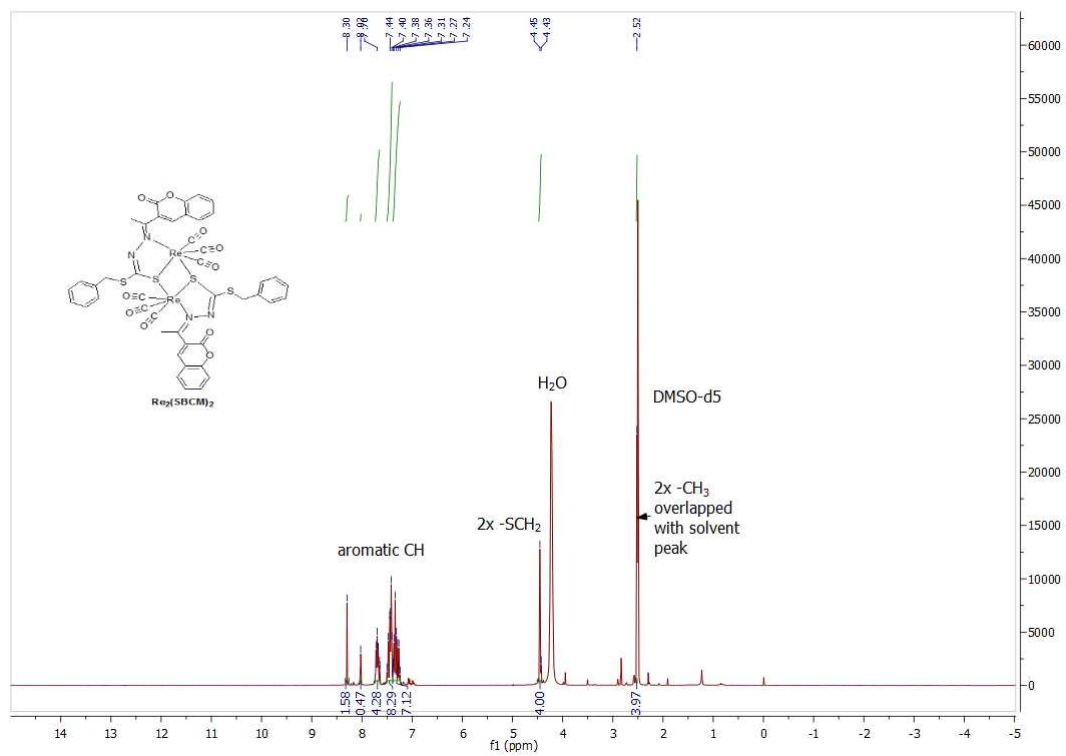


Figure A19. ^1H NMR spectrum of $\text{Re}_2(\text{SBCM})_2$

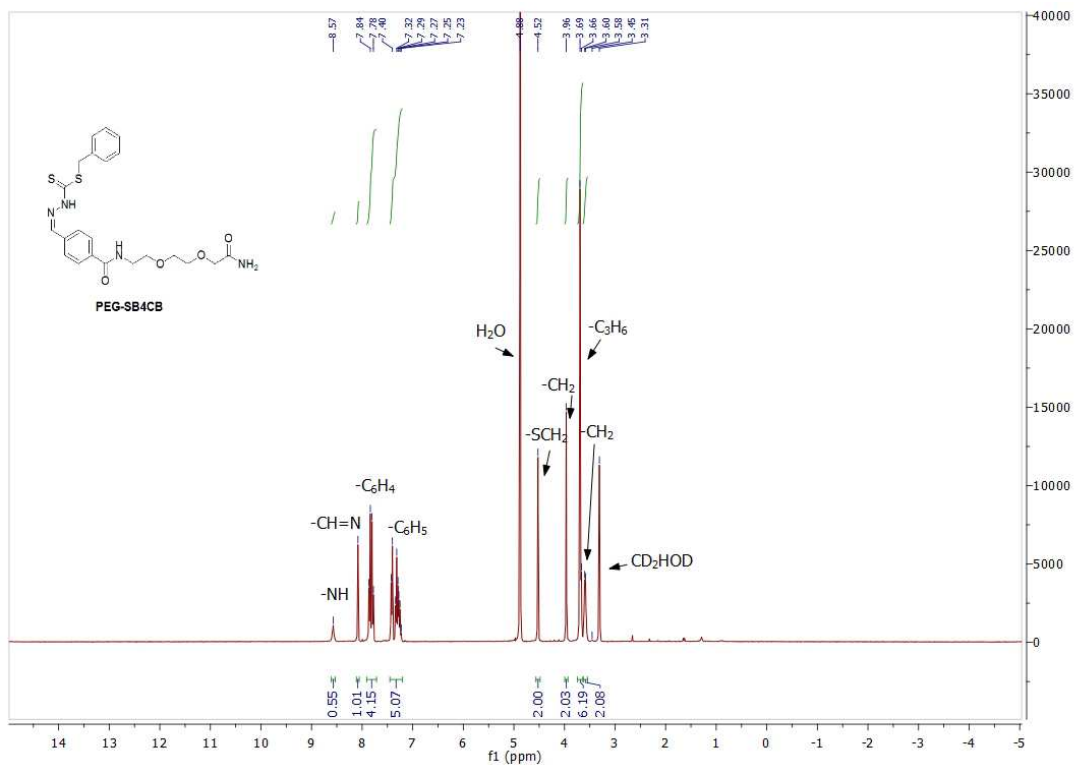


Figure A20. ¹H NMR spectrum of PEG-SB4CB

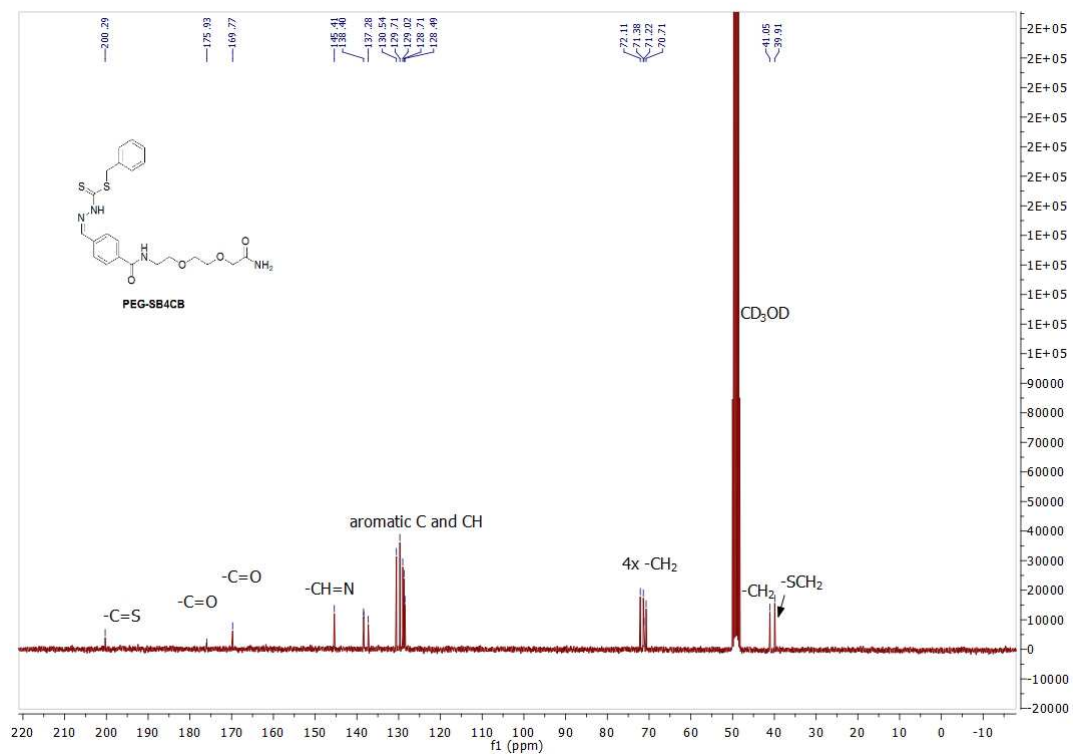
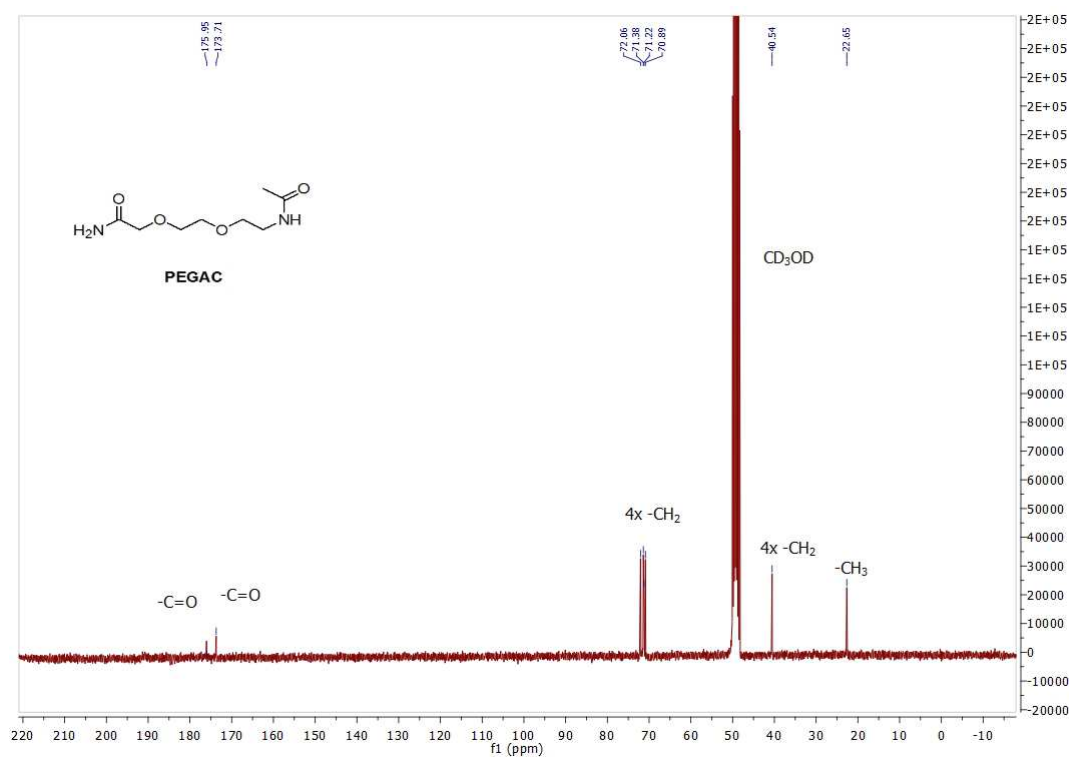
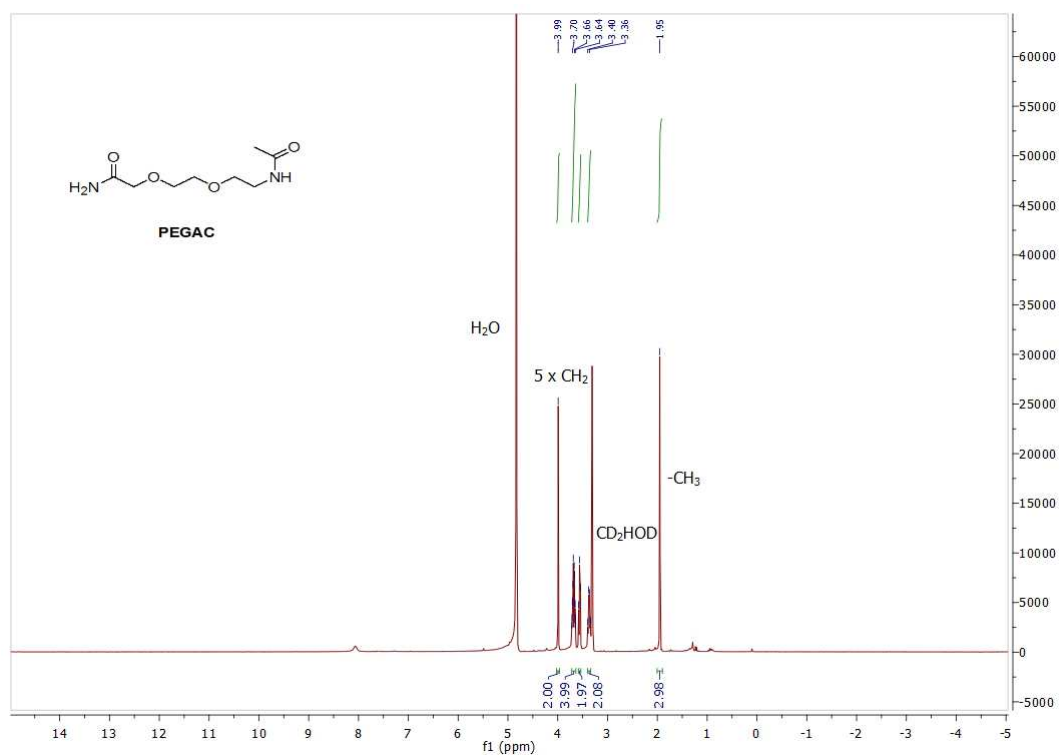


Figure A21. ¹³C NMR spectrum of PEG-SB4CB



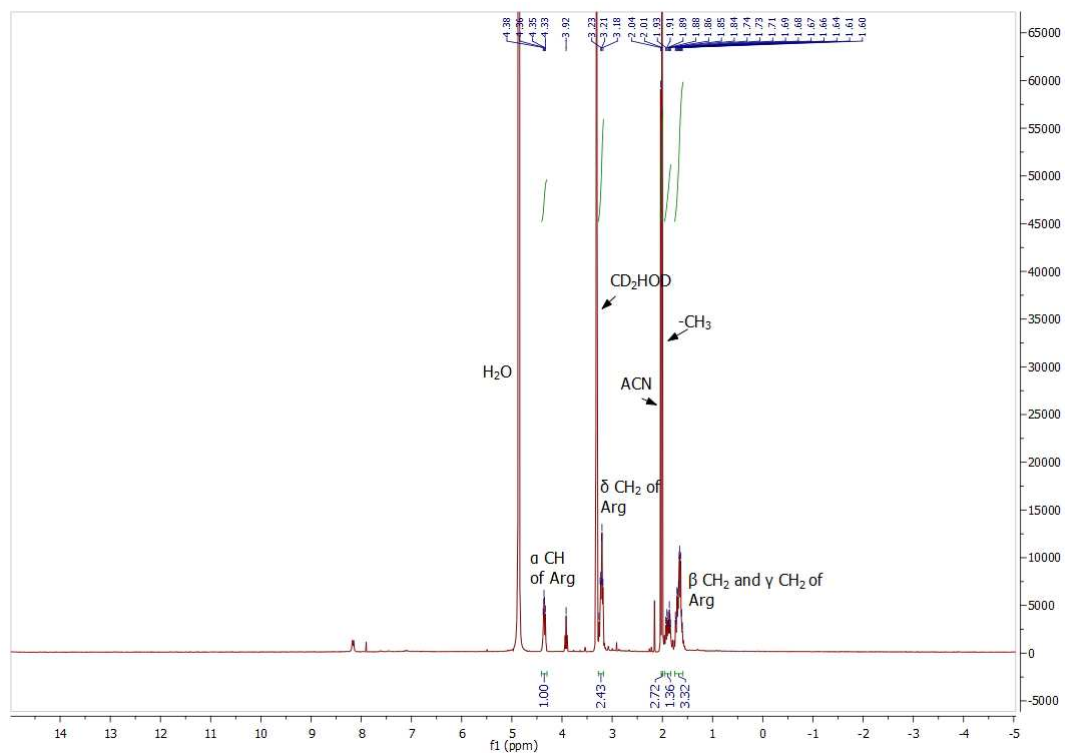


Figure A24. ¹H NMR spectrum of R1AC

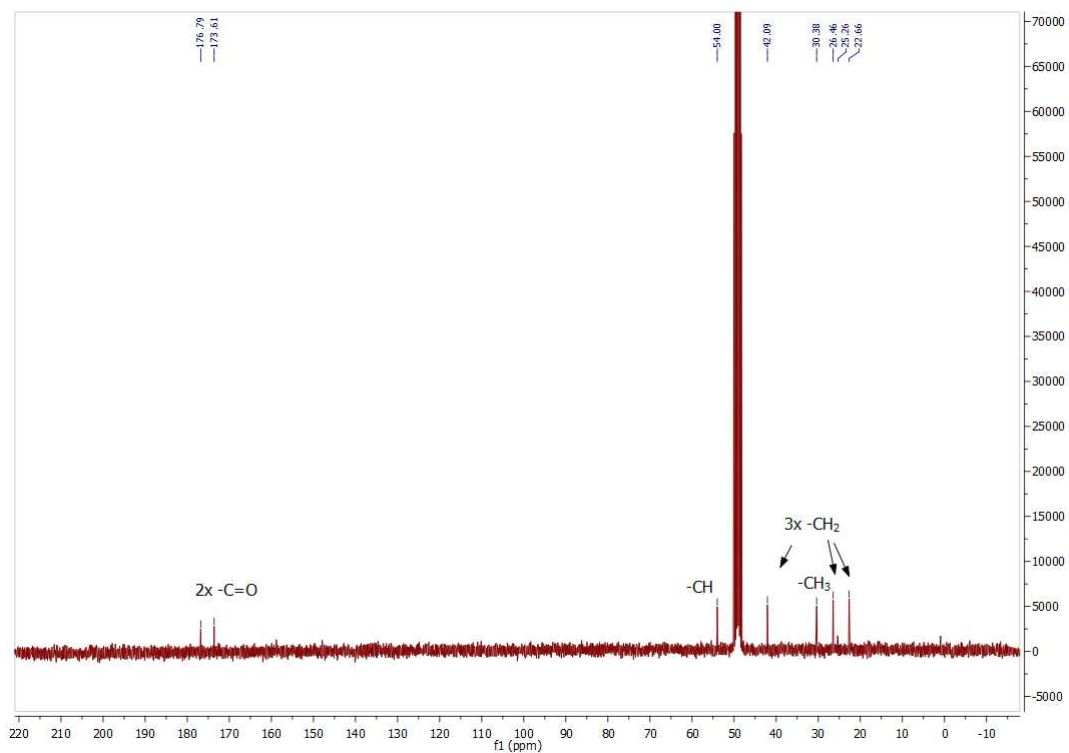


Figure A25. ¹³C NMR spectrum of R1AC

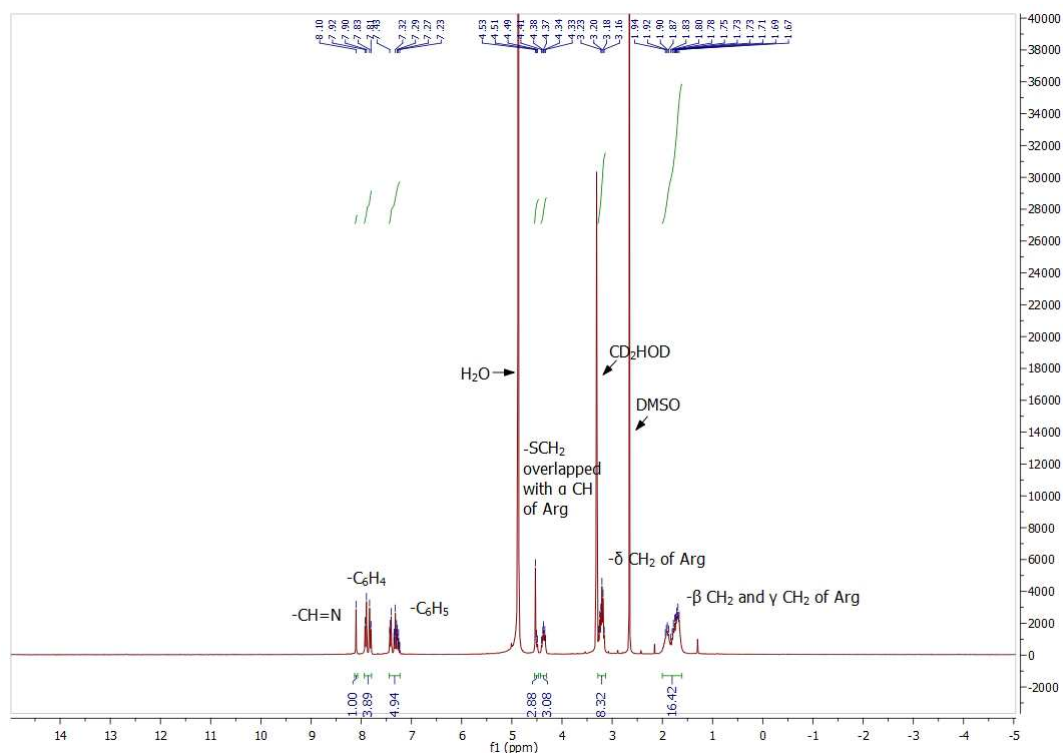


Figure A26. ^1H NMR spectrum of R4-SB4CB

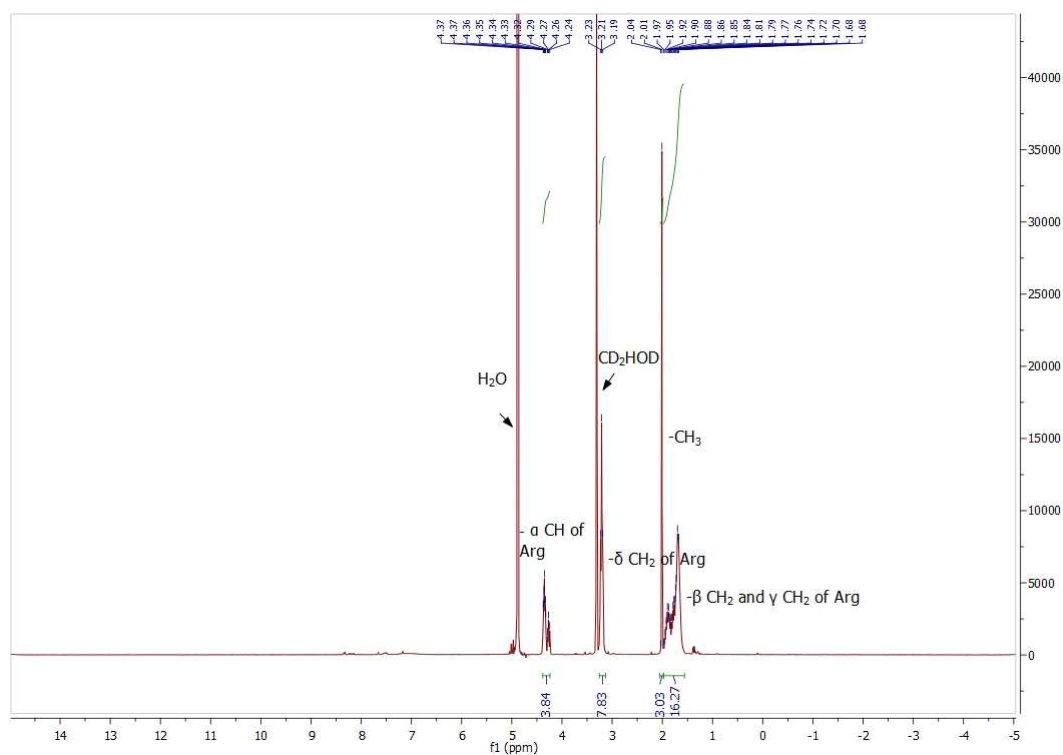


Figure A27. ^1H NMR spectrum of R4-AC

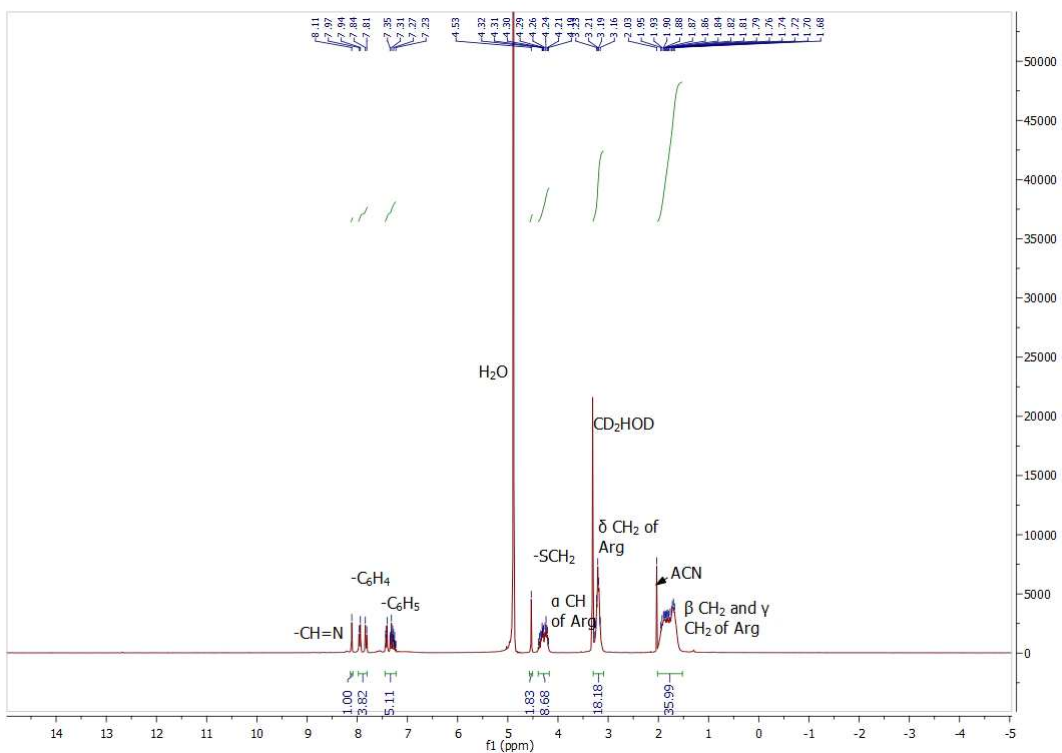


Figure A28. ^1H NMR spectrum of R9-SB4CB

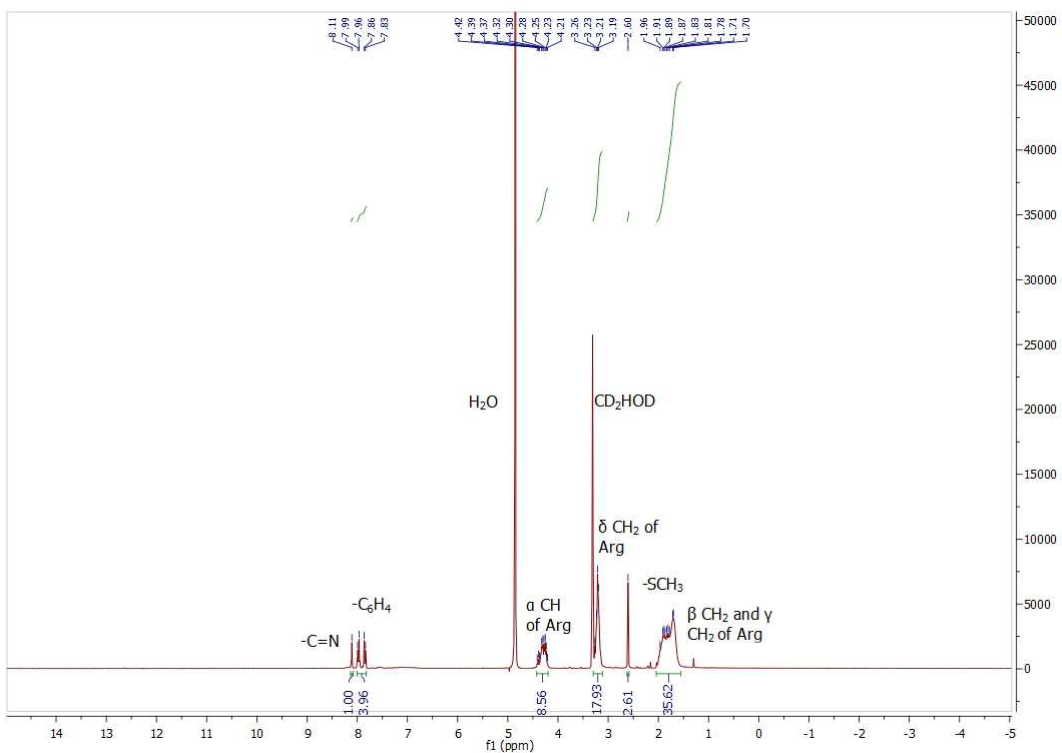


Figure A29. ^1H NMR spectrum of R9-SM4CB

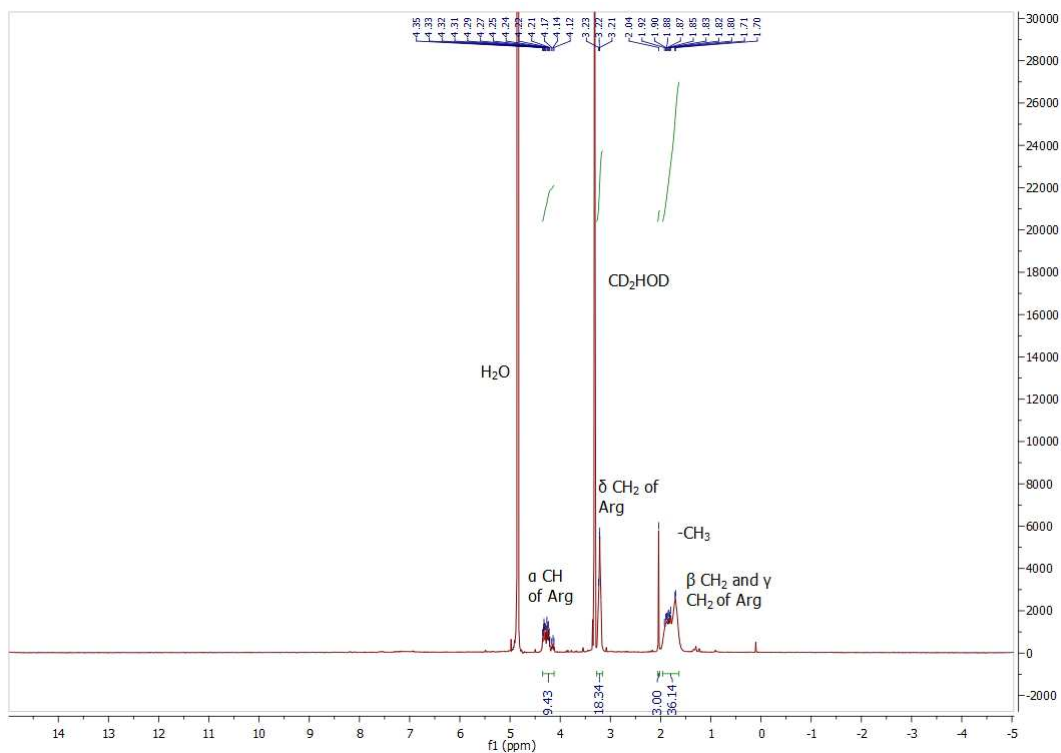


Figure A30. ^1H NMR spectrum of R9AC

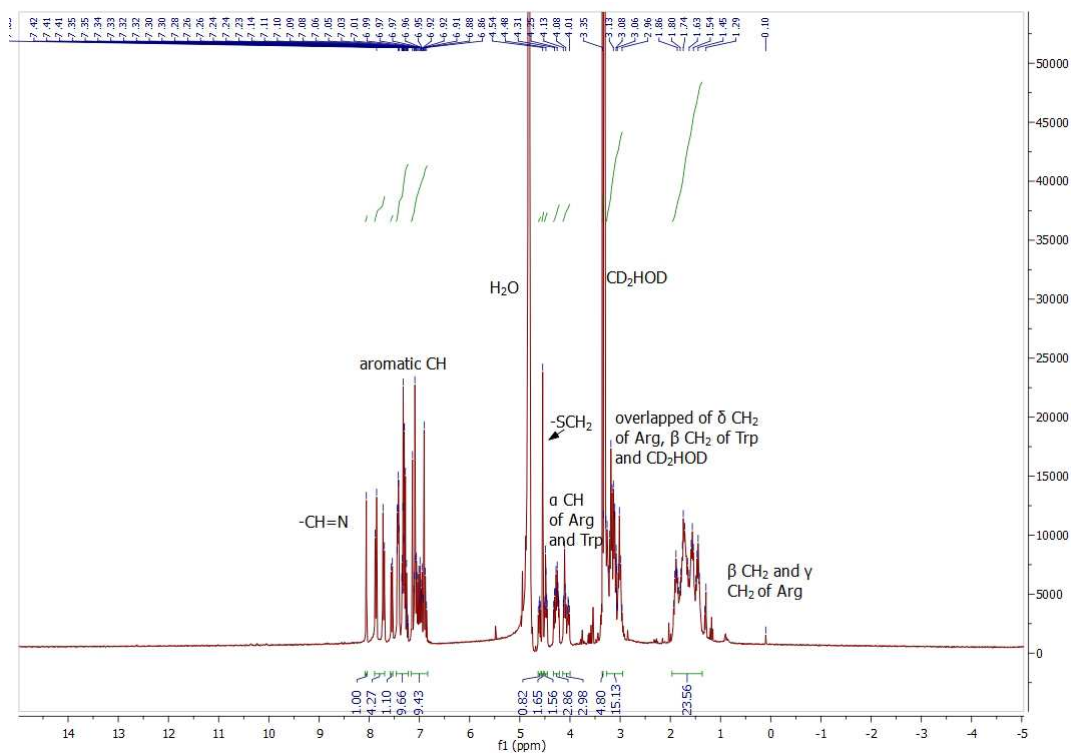


Figure A31. ^1H NMR spectrum of RW9-SB4CB

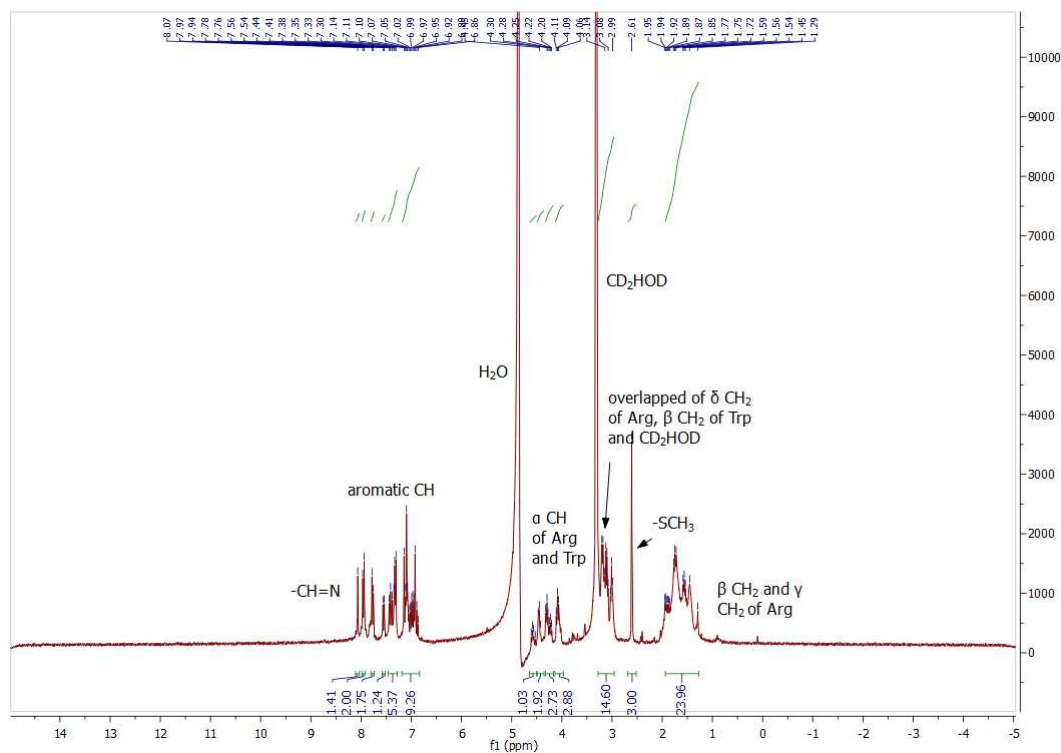


Figure A32. ^1H NMR spectrum of RW9-SM4CB

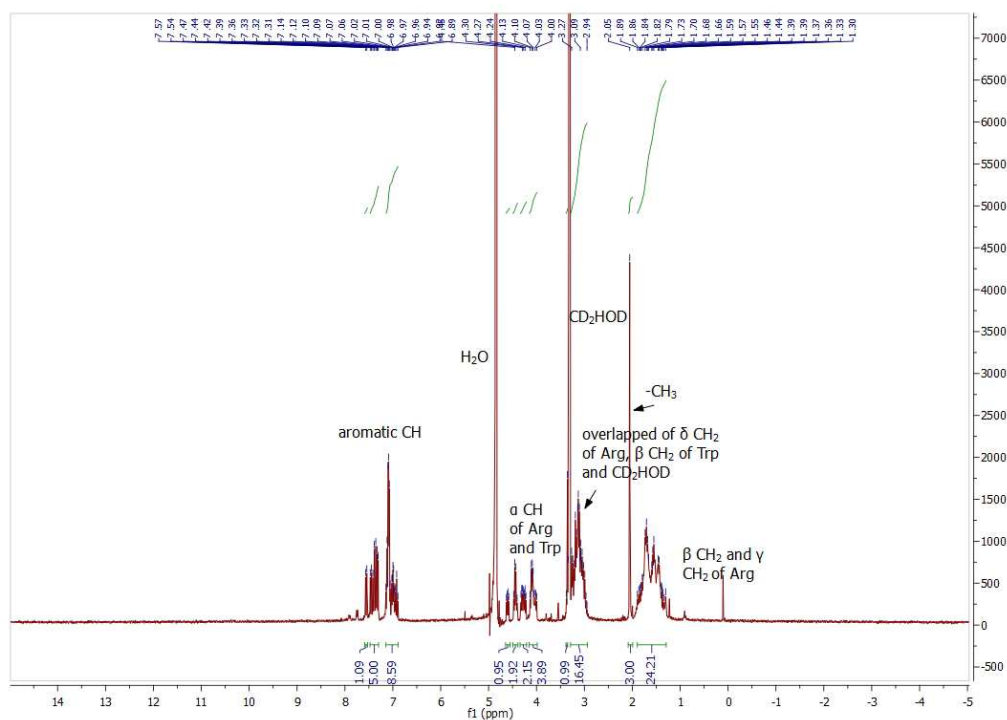


Figure A33. ^1H NMR spectrum of RW9AC

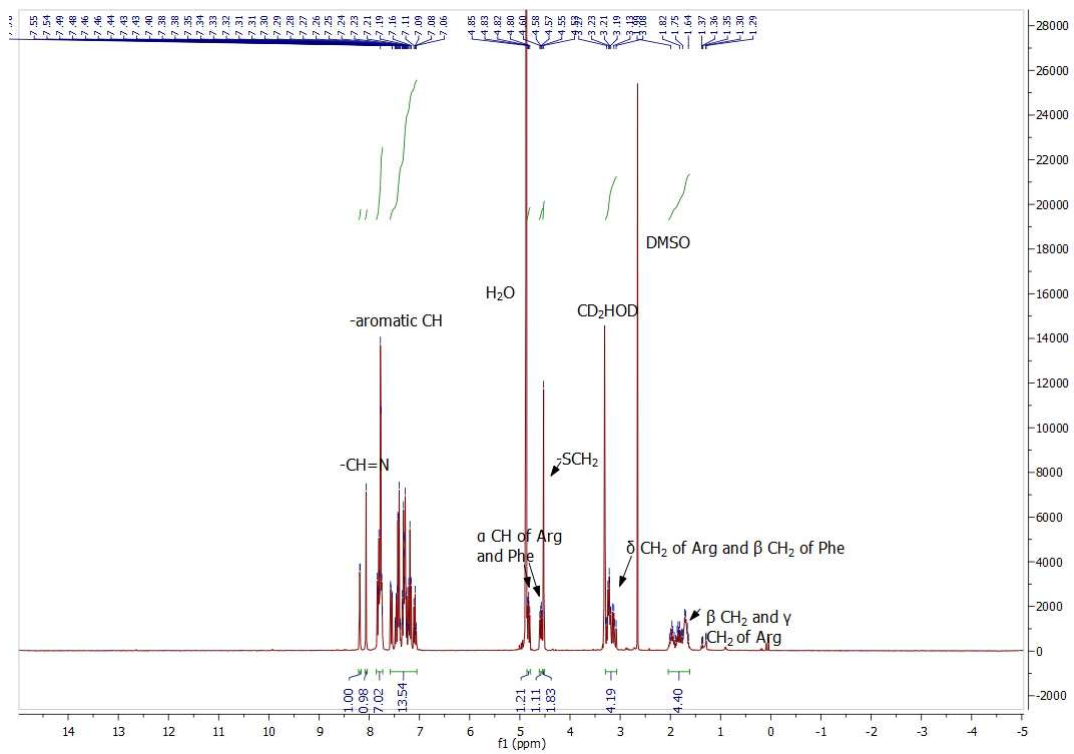


Figure A34. ^1H NMR spectrum of PA β N-SB4CB

B. Mass Spectra

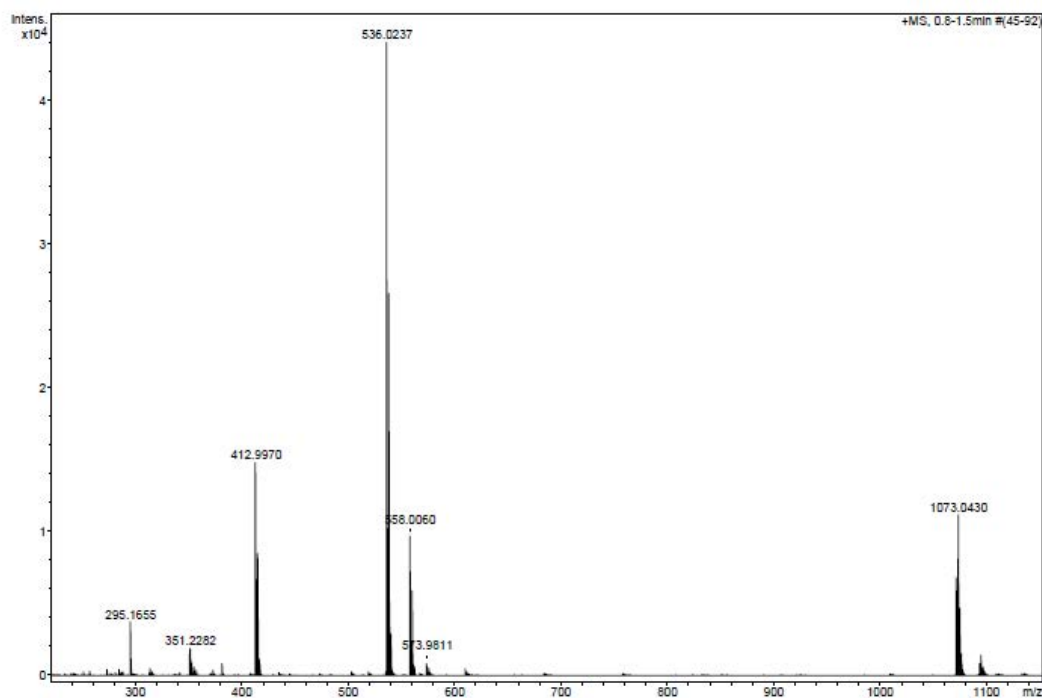


Figure B1. ESI-MS spectrum of CuSBHD

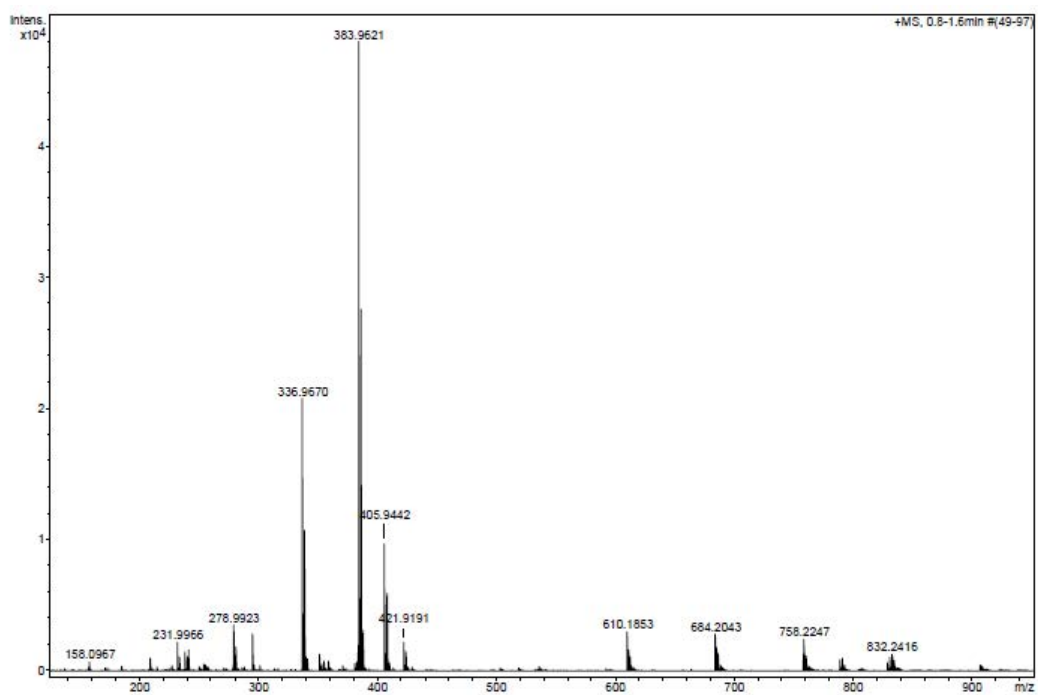


Figure B2. ESI-MS spectrum of CuSMHD

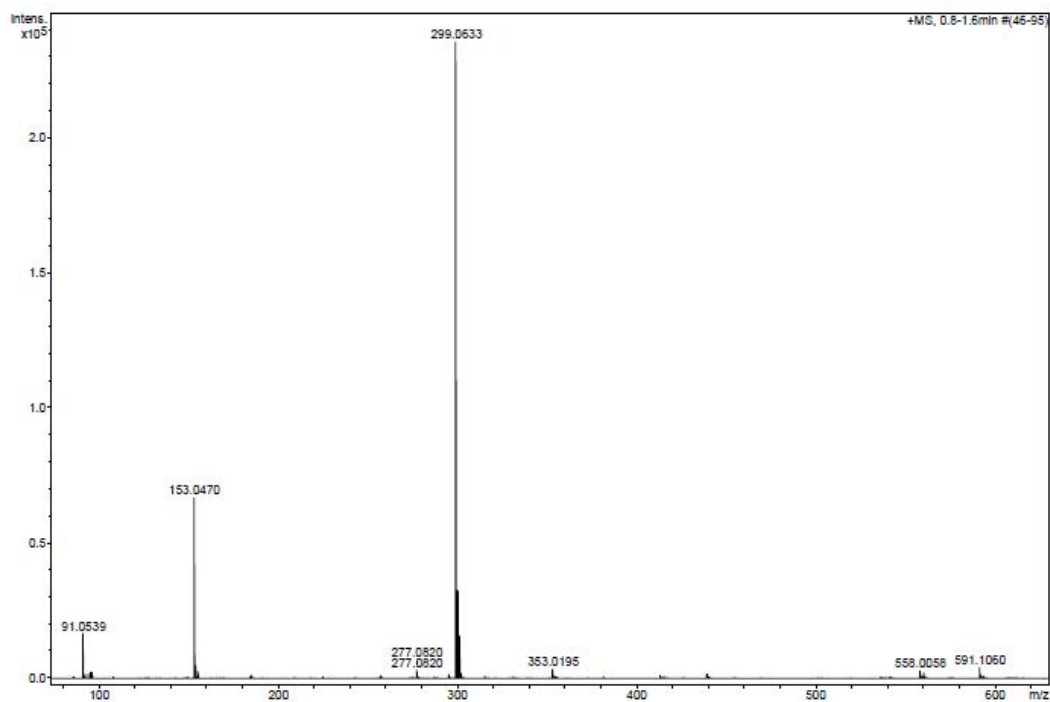
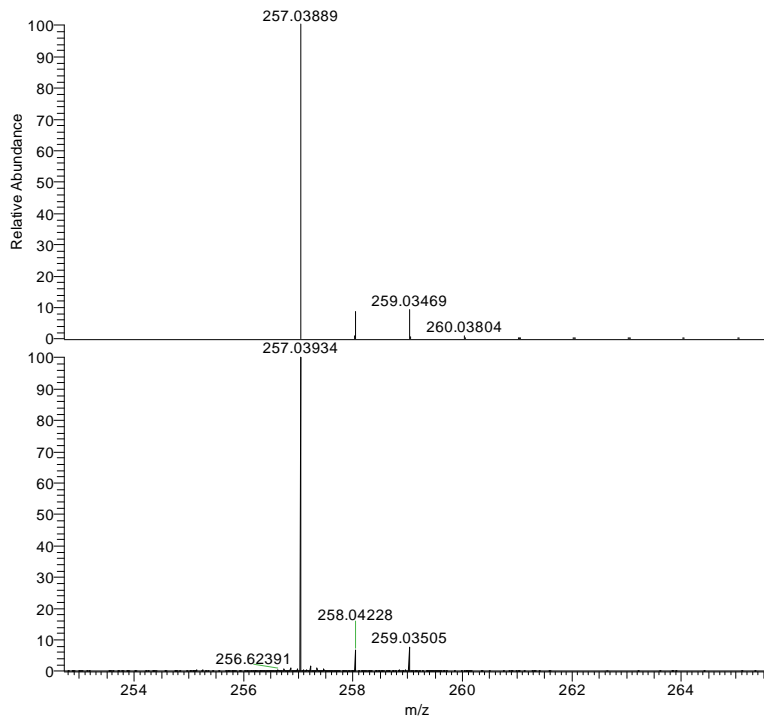


Figure B3. ESI-MS spectrum of SBPY

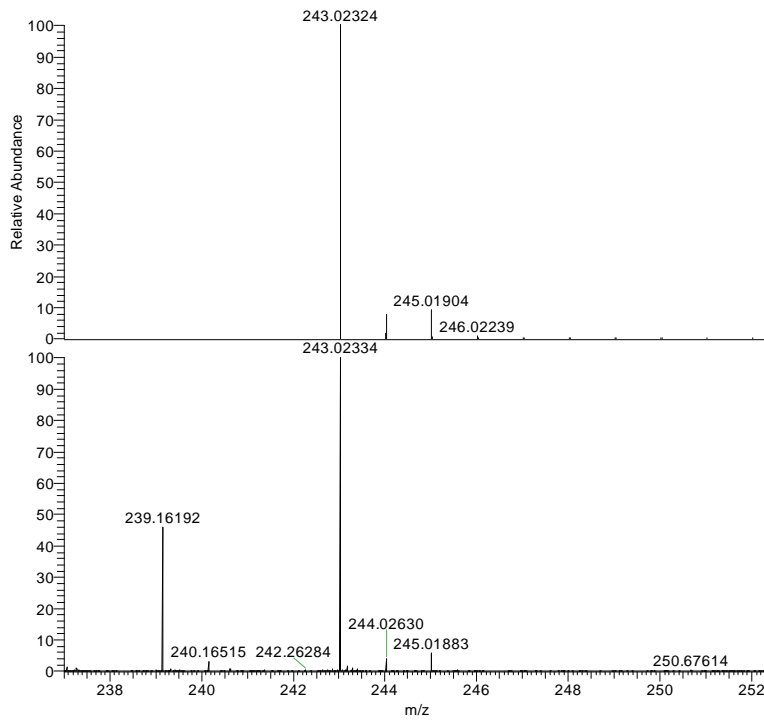


NL:
8.15E5
C₈H₁₄O₂N₂NaS₂:
C₈H₁₄O₂N₂Na₁S₂
pa Chrg 1

NL:
1.02E8
A12-0846#9-21 RT:
0.20-0.53 AV: 13 T:
FTMS + p ESI Full ms
[110.00-1200.00]

Error = 0.8 ppm

Figure B4. HR-MS spectrum of SMML

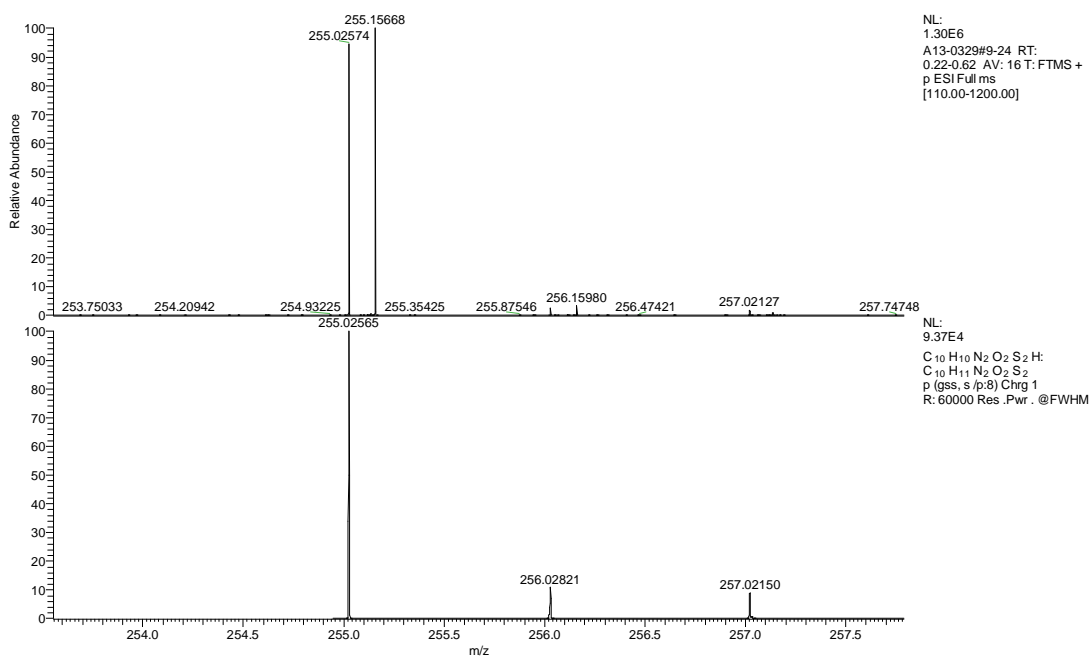


NL:
8.24E5
C₇H₁₂O₂N₂NaS₂:
C₇H₁₂O₂N₂Na₁S₂
pa Chrg 1

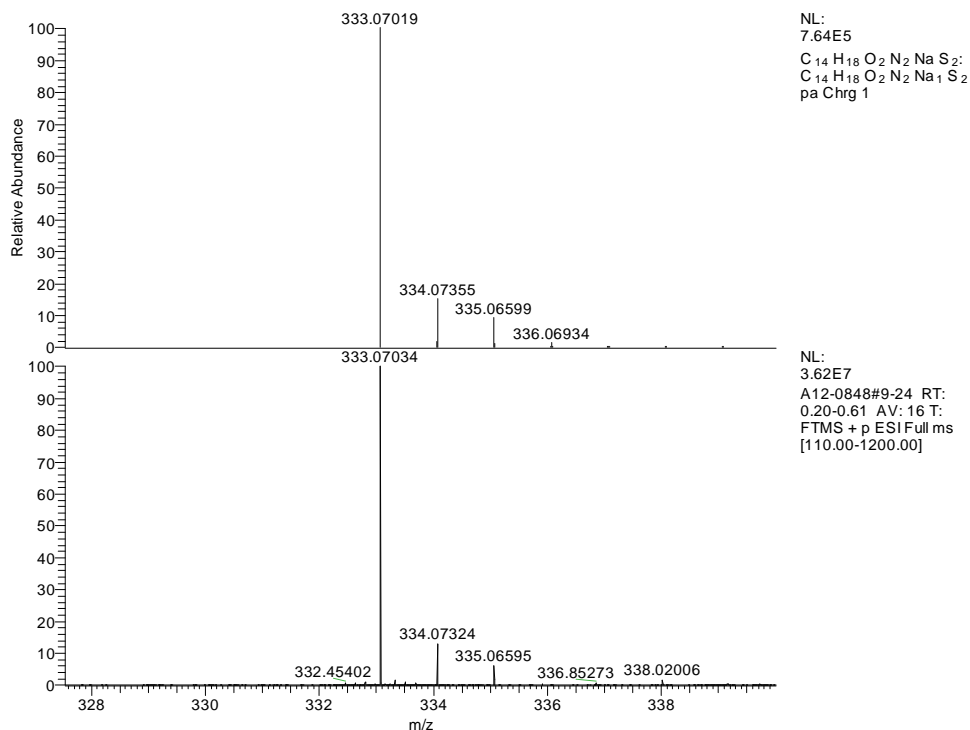
NL:
1.51E7
A12-0847#12-23 RT:
0.28-0.59 AV: 12 T:
FTMS + p ESI Full ms
[110.00-1200.00]

Error = 0.5 ppm

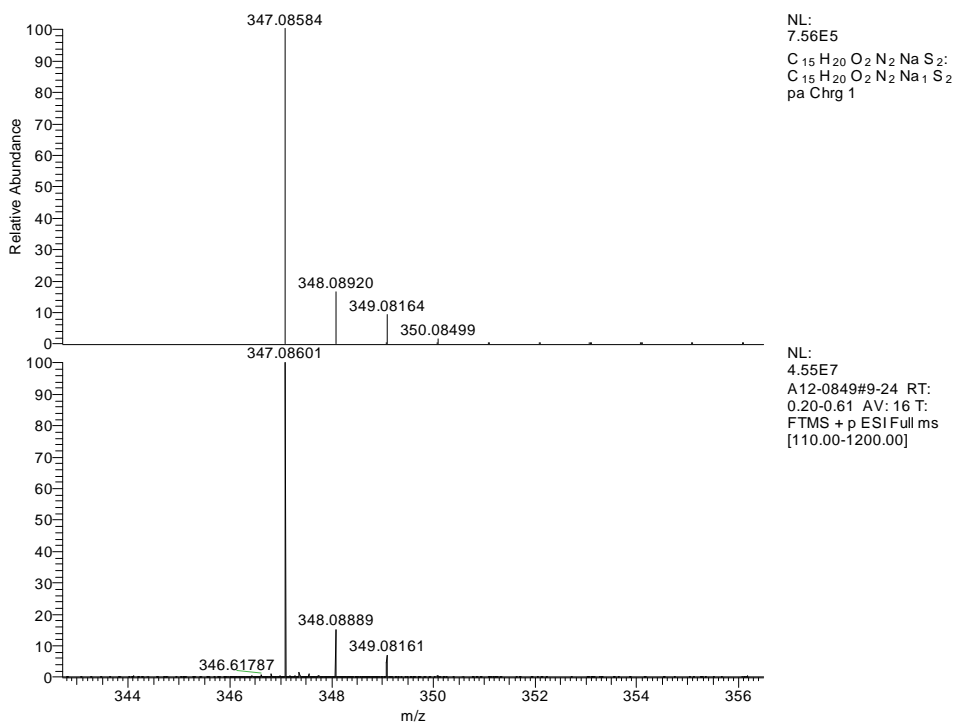
Figure B5. HR-MS spectrum of SMLA



Error = 0.4 ppm
Figure B6. HR-MS spectrum of SM4CB

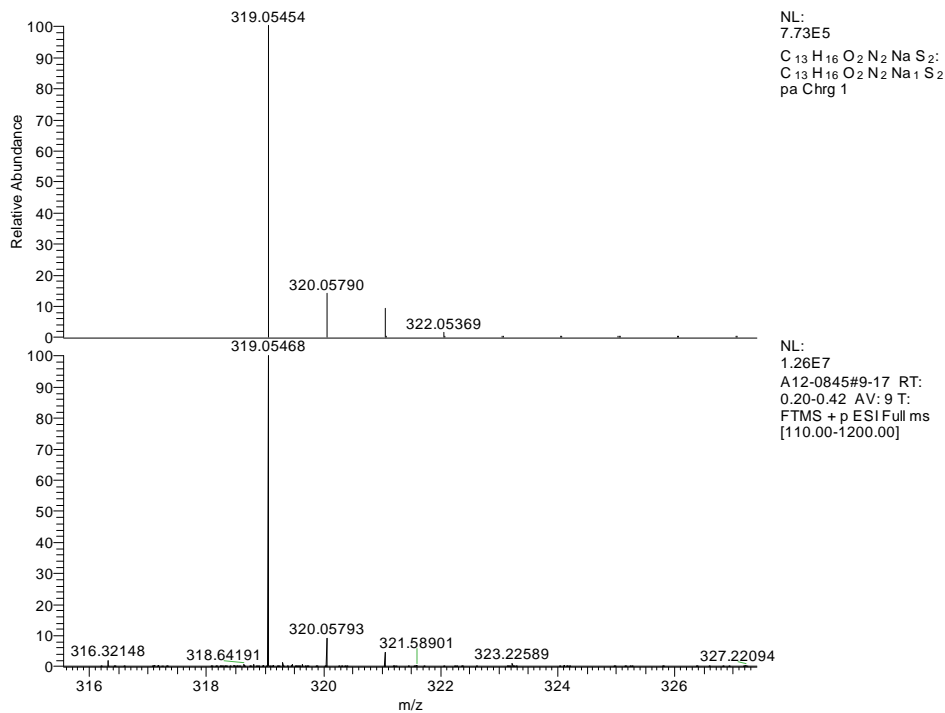


Error = 0.5 ppm
Figure B7. HR-MS spectrum of SBML



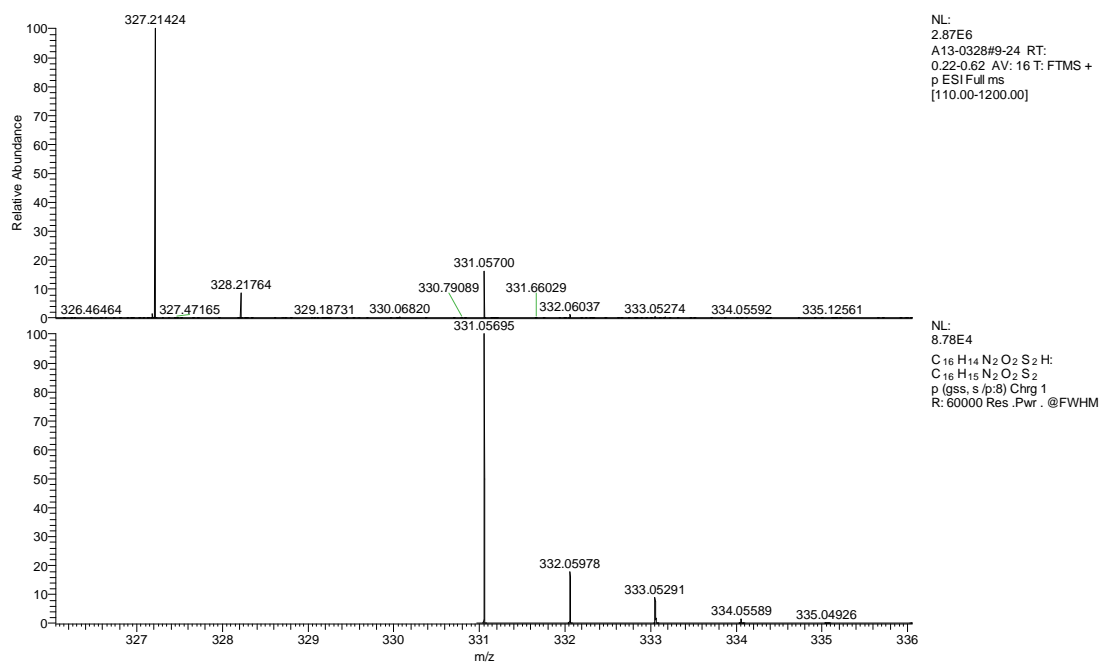
Error = 0.5 ppm

Figure B8. HR-MS spectrum of SBEL



Error = 0.5 ppm

Figure B9. HR-MS spectrum of SBLA



Error = 0.2 ppm

Figure B10. HR-MS spectrum of SB4CB

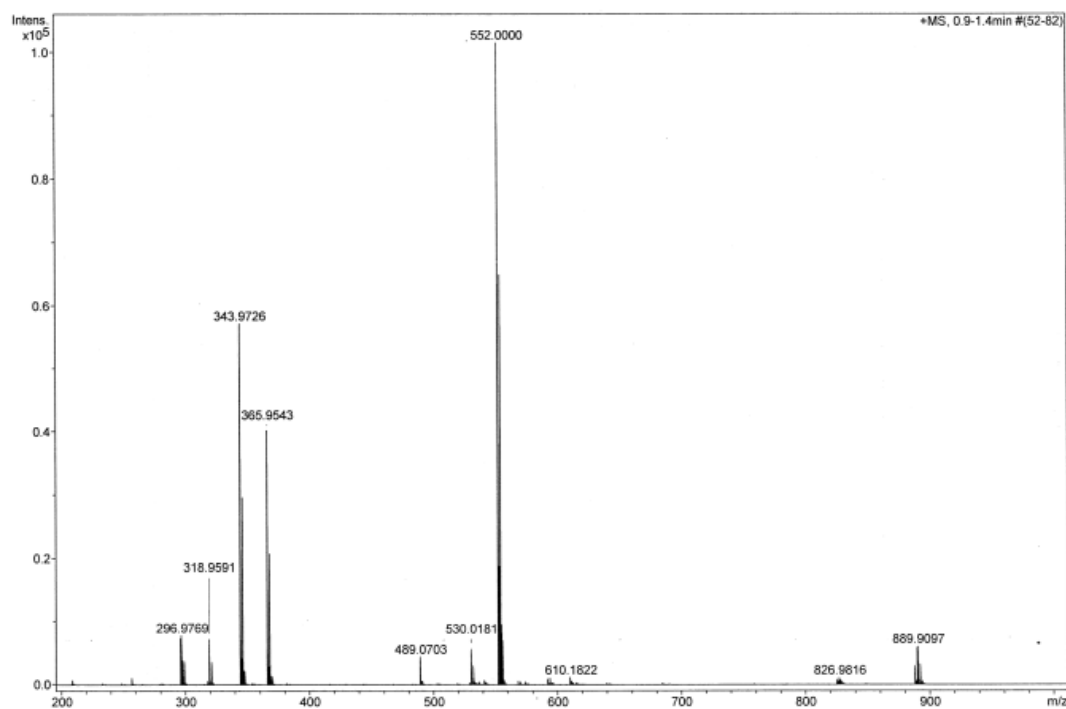


Figure B11. ESI-MS spectrum of Cu(SMML)₂

130530-8B #15-24 RT: 0.37-0.61 AV: 10 SB: 7 1.79-1.95 NL: 2.00E7
T: FTMS + p ESI Full ms [110.00-1200.00]

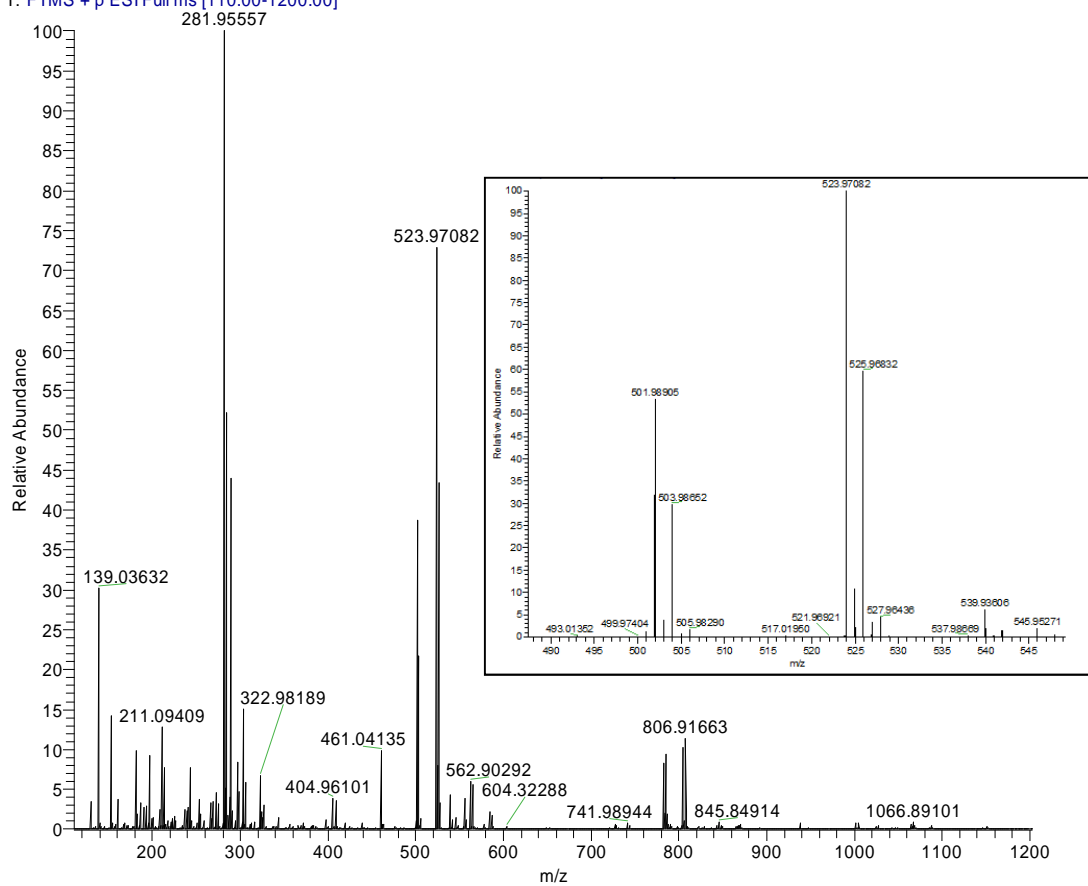


Figure B12. ESI-MS spectrum of Cu(SMLA)₂

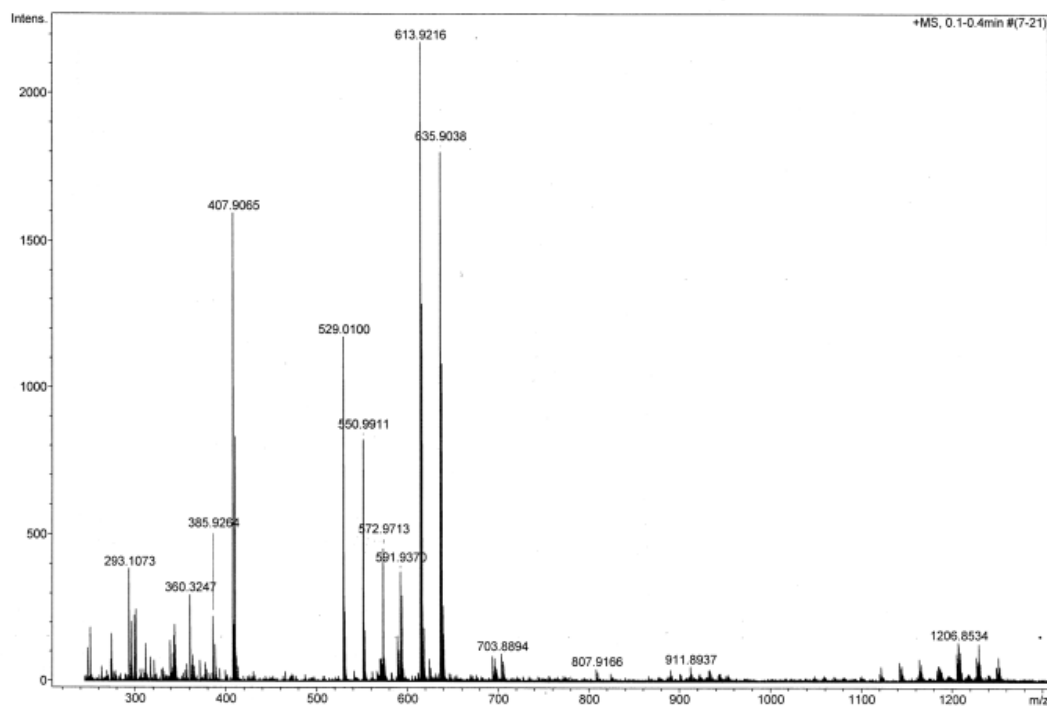


Figure B13. ESI-MS spectrum of Cu(SM4CB)₂

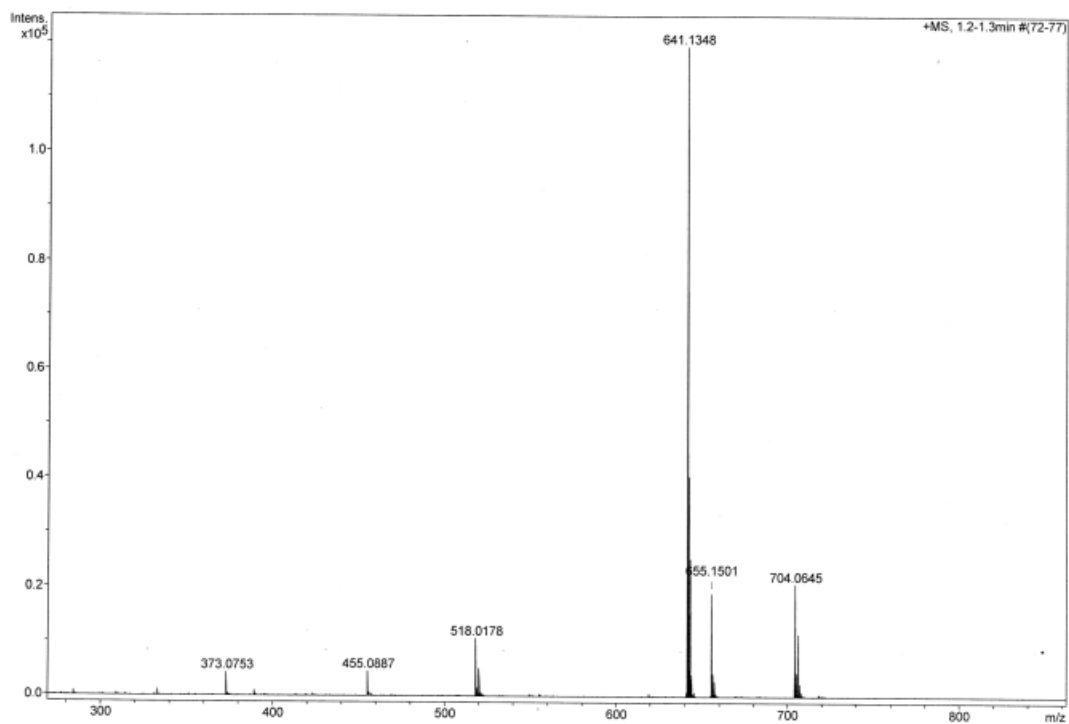


Figure B14. ESI-MS spectrum of Cu(SBML)₂

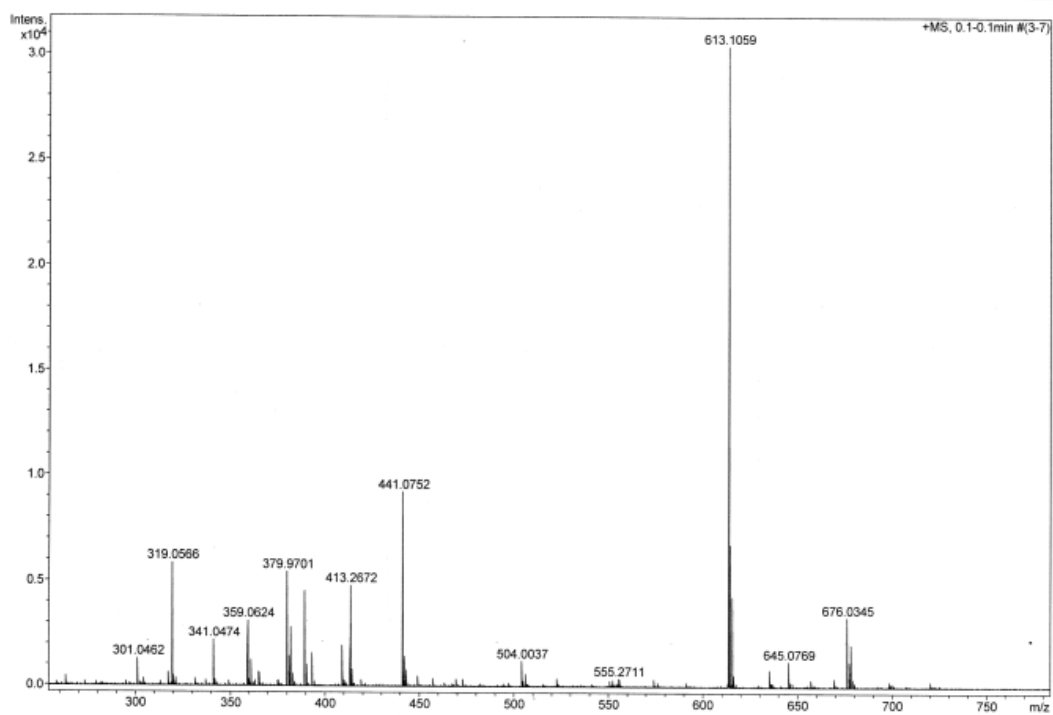


Figure B15. ESI-MS spectrum of Cu(SBLA)₂

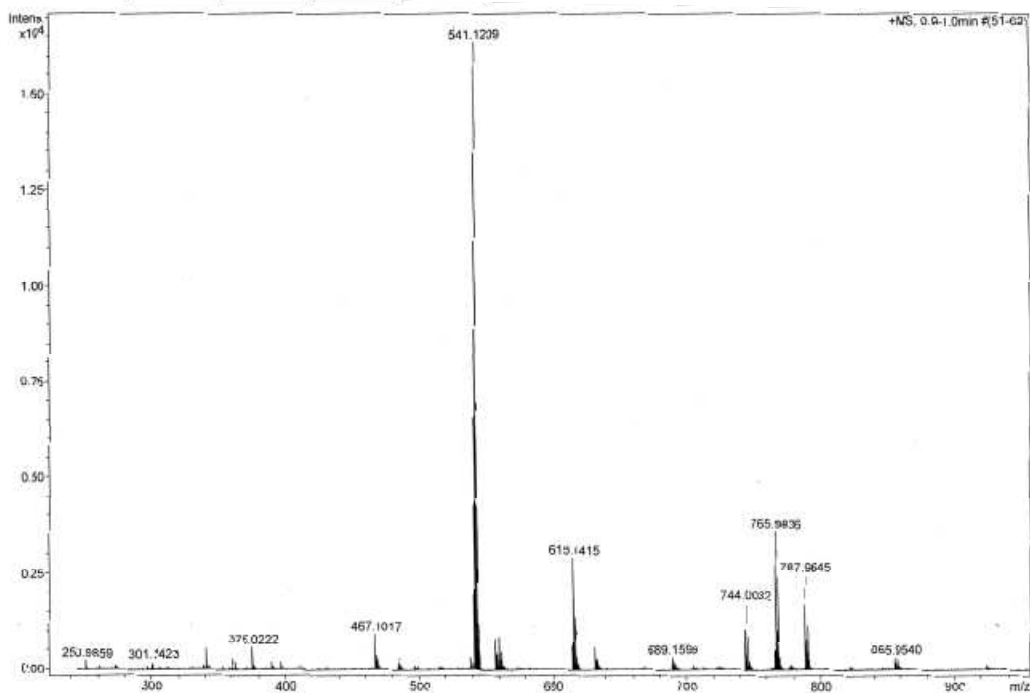
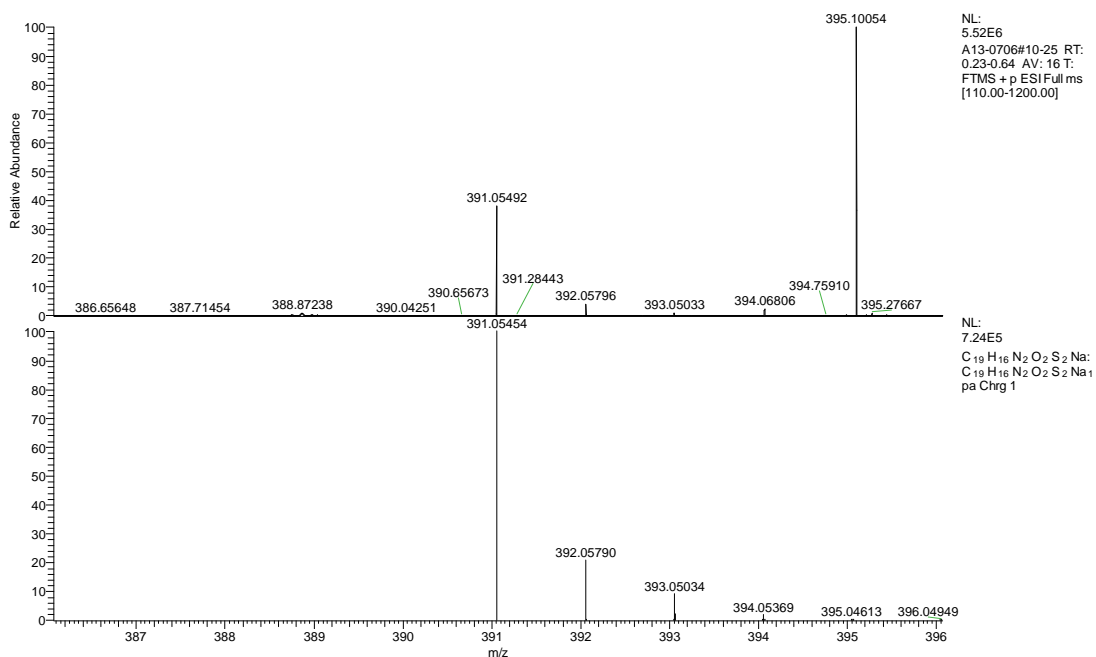


Figure B16. ESI-MS spectrum of $\text{Cu}(\text{SB4CB})_2$

C:\Analyses\TestAuto\A13-0706
13.06

27/06/2013 12:03:11

May Lee Low SBCM



Error = 1.0 ppm

Figure B17. HR-MS spectrum of SBCM

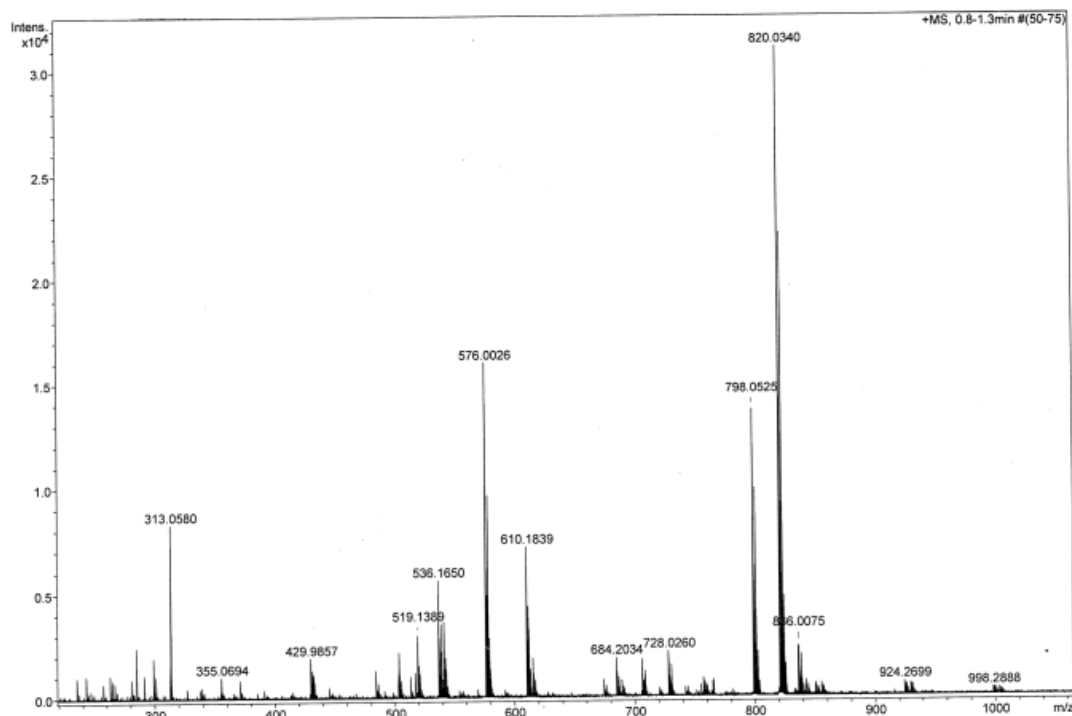


Figure B18. ESI-MS spectrum of Cu(SBCM)₂

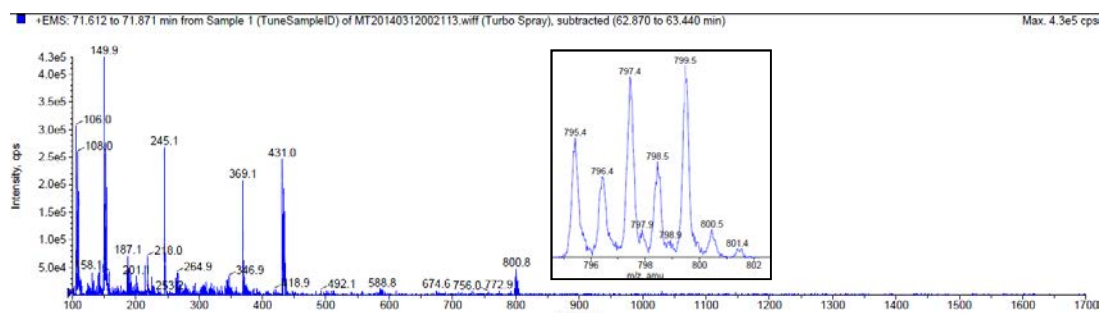


Figure B19. ESI-MS spectrum of Zn(SBCM)₂

130530-10 #13-22 RT: 0.31-0.56 AV: 10 SB: 8 1.80-1.99 NL: 4.06E6
T: FTMS + p ESI Full ms [110.00-2000.00]

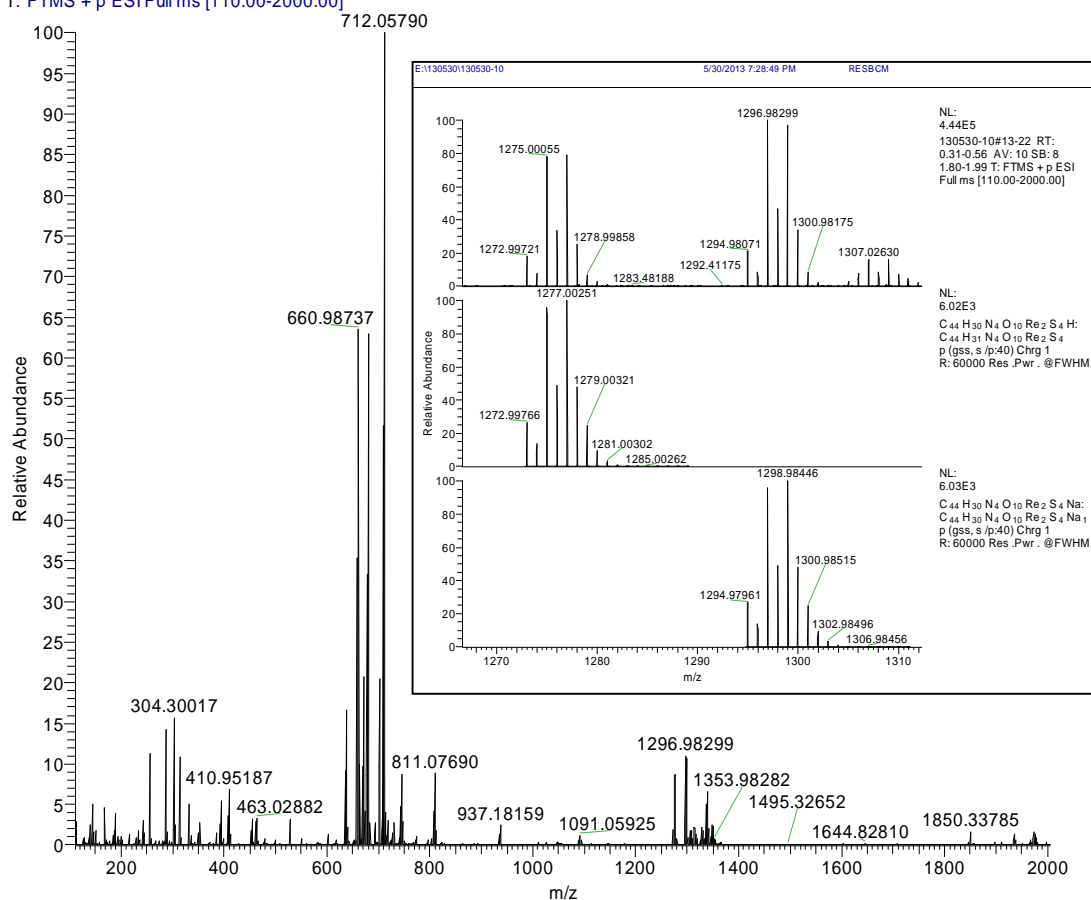
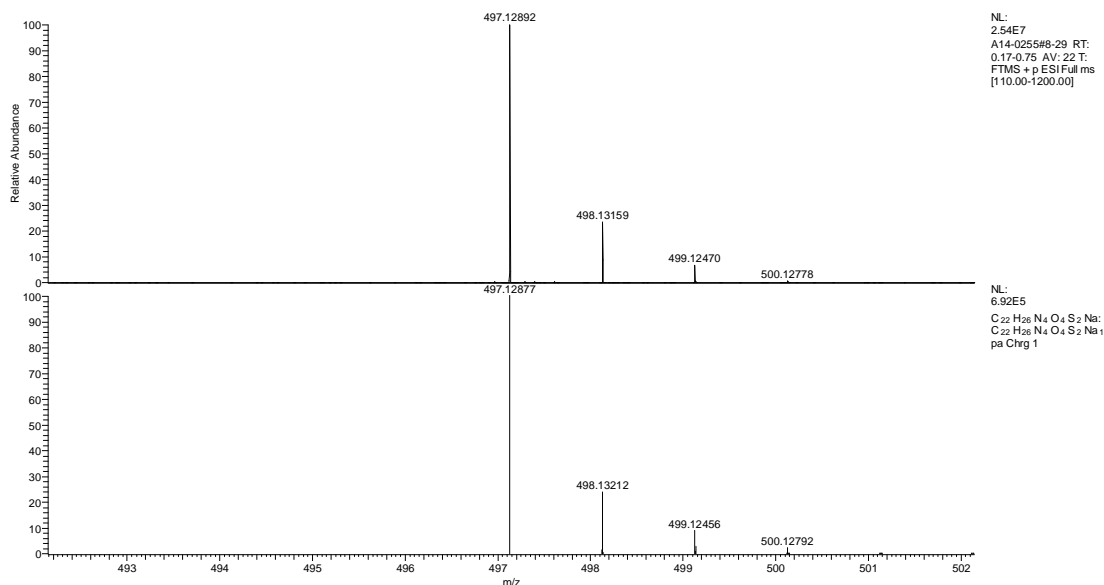
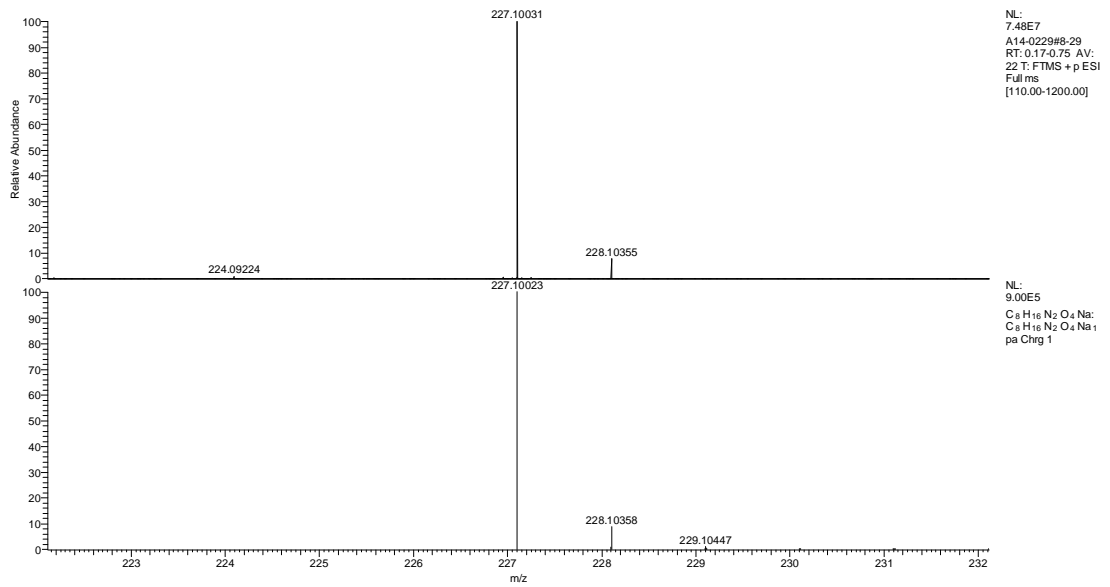


Figure B20. ESI-MS spectrum of $\text{Re}_2(\text{SBCM})_2$



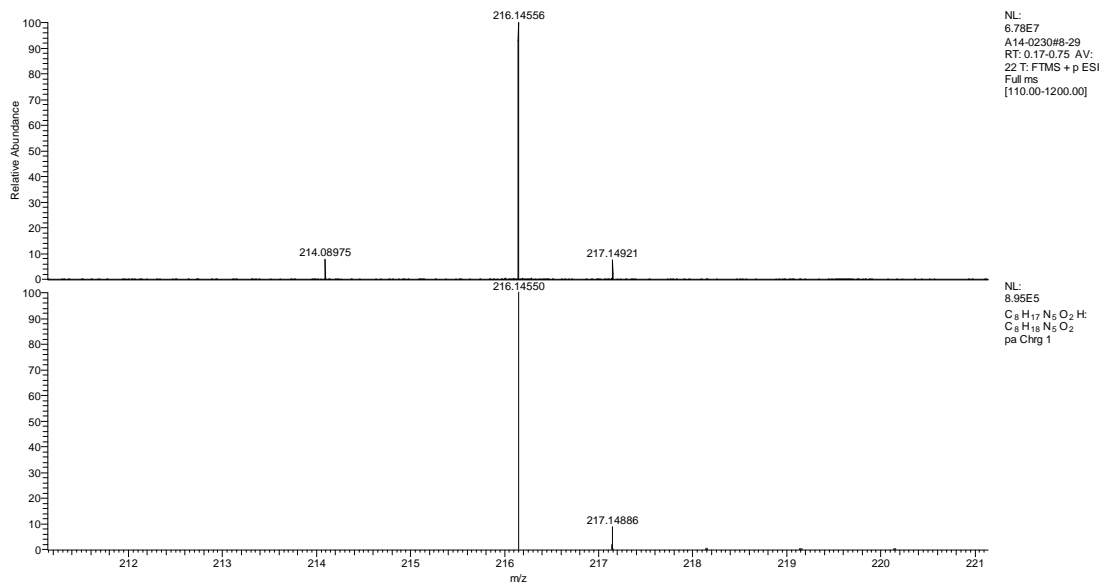
Error = 0.3 ppm

Figure B21. HR-MS spectrum of PEG-SB4CB



Error = 0.4 ppm

Figure B22. HR-MS spectrum of PEGAC



Error = 0.3 ppm

Figure B23. HR-MS spectrum of R1AC

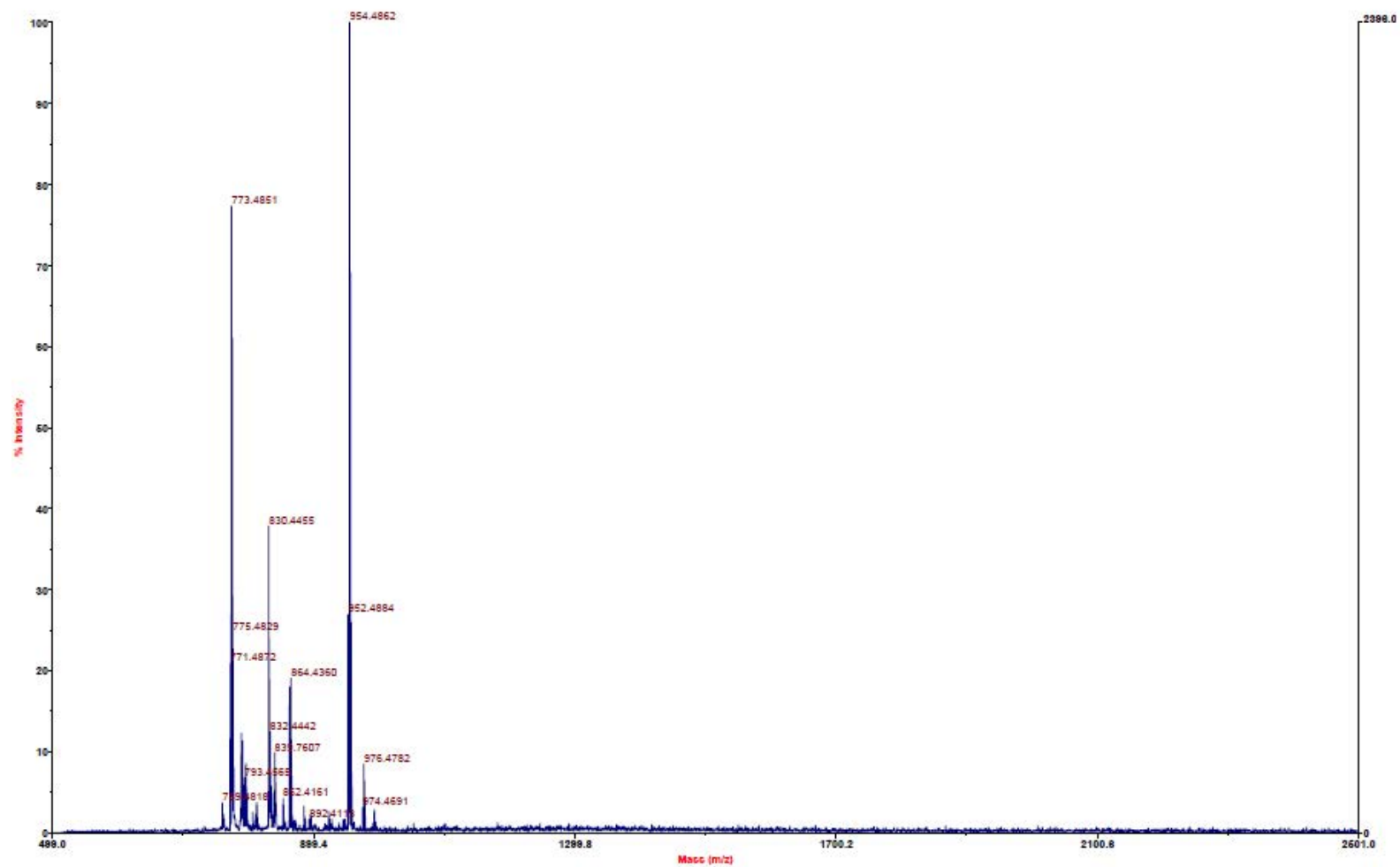


Figure B24. MALDI-TOF-MS full spectrum of R4-SB4CB

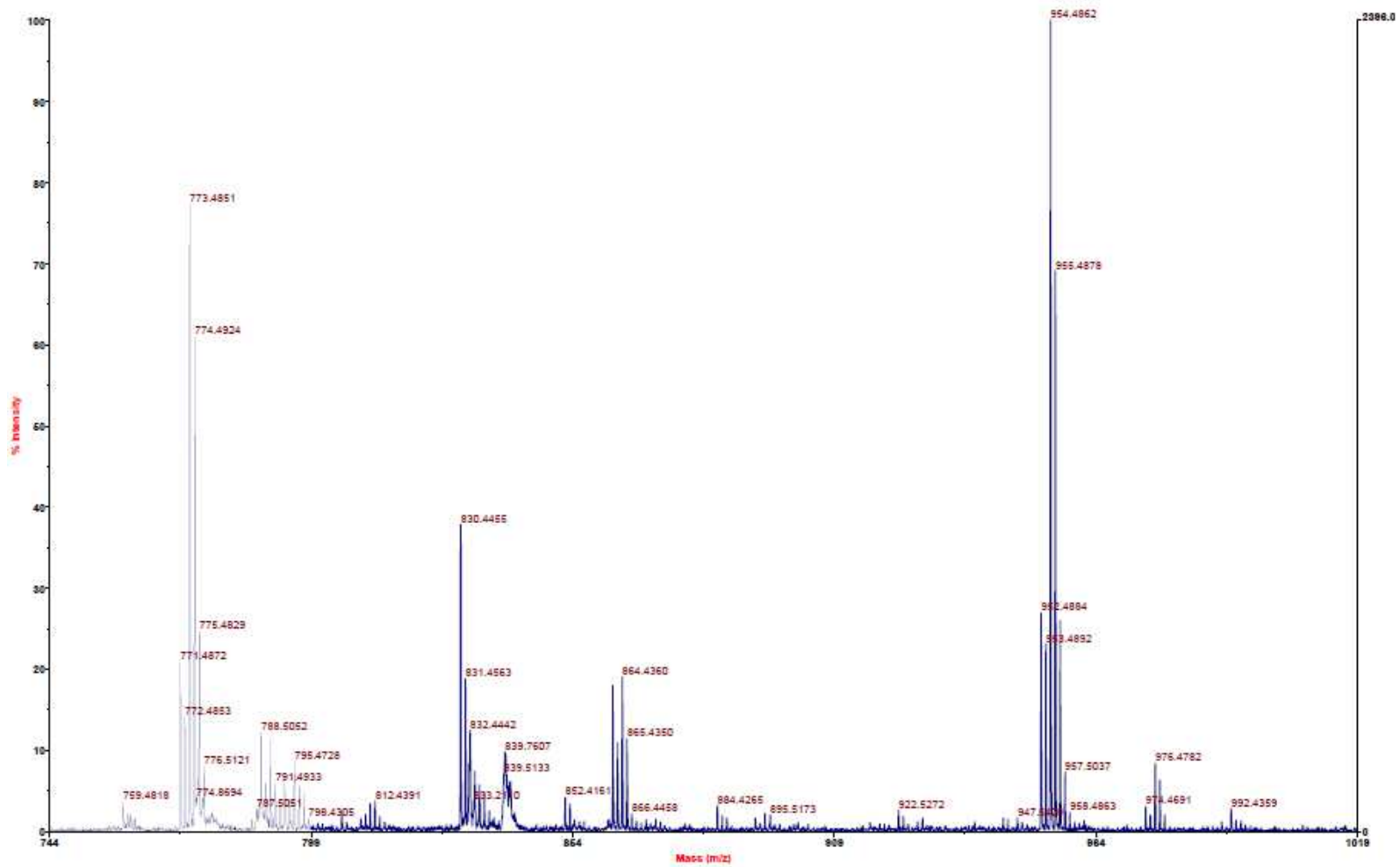


Figure B25. MALDI-TOF-MS enlarged spectrum of R4-SB4CB

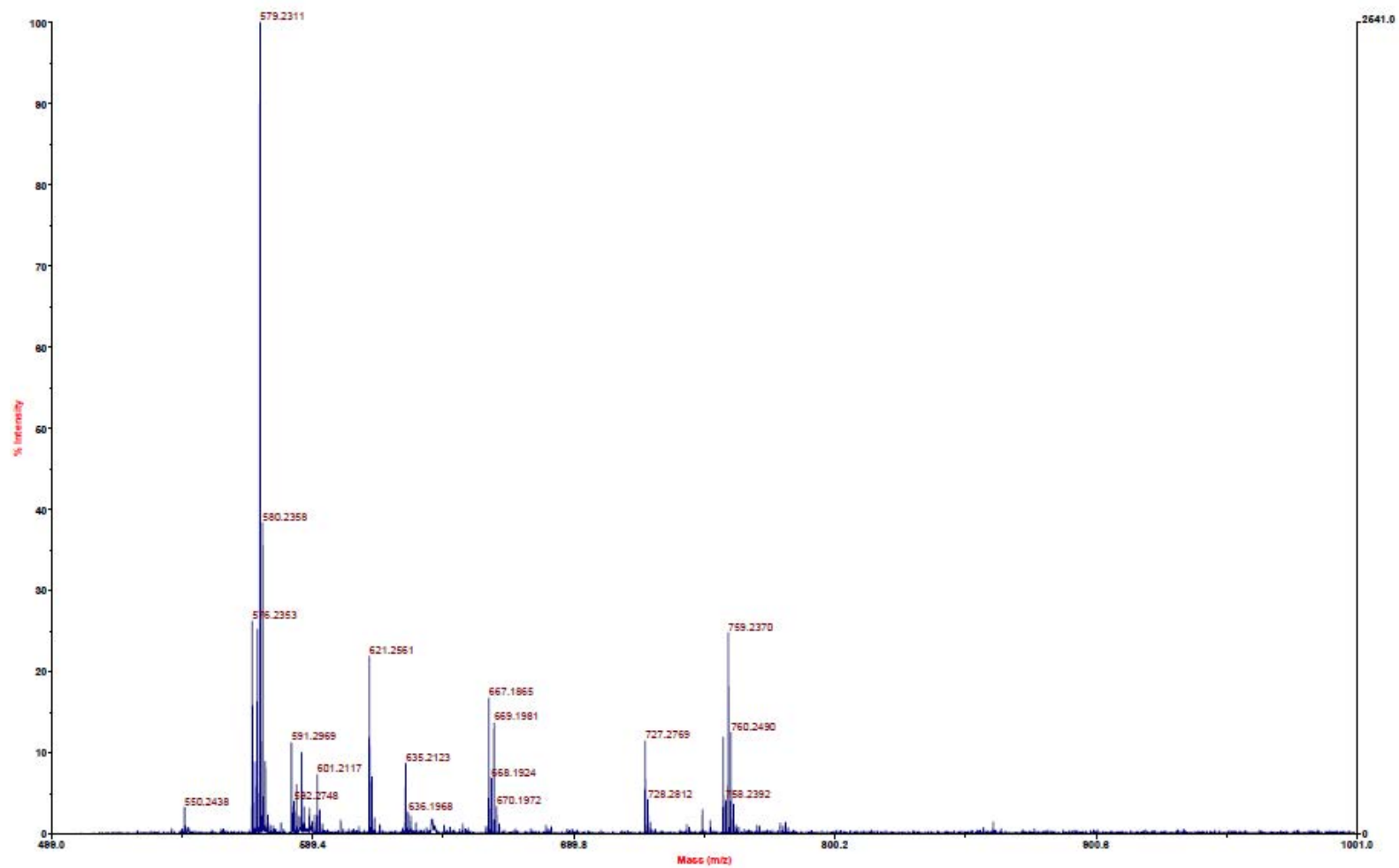


Figure B26. MALDI-TOF-MS full spectrum of PAβN-SB4CB

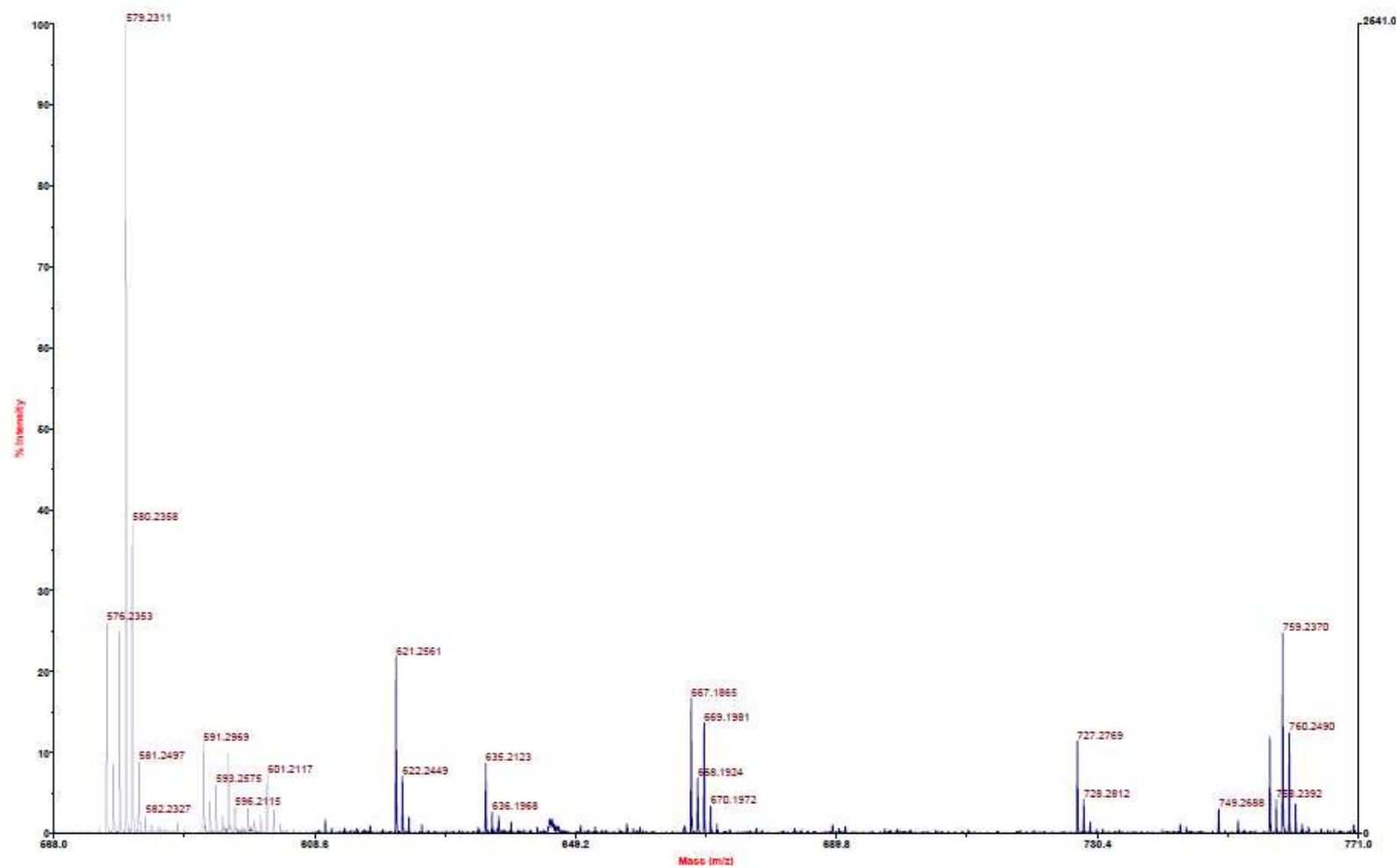


Figure B27. MALDI-TOF-MS enlarged spectrum of PA β N-SB4CB

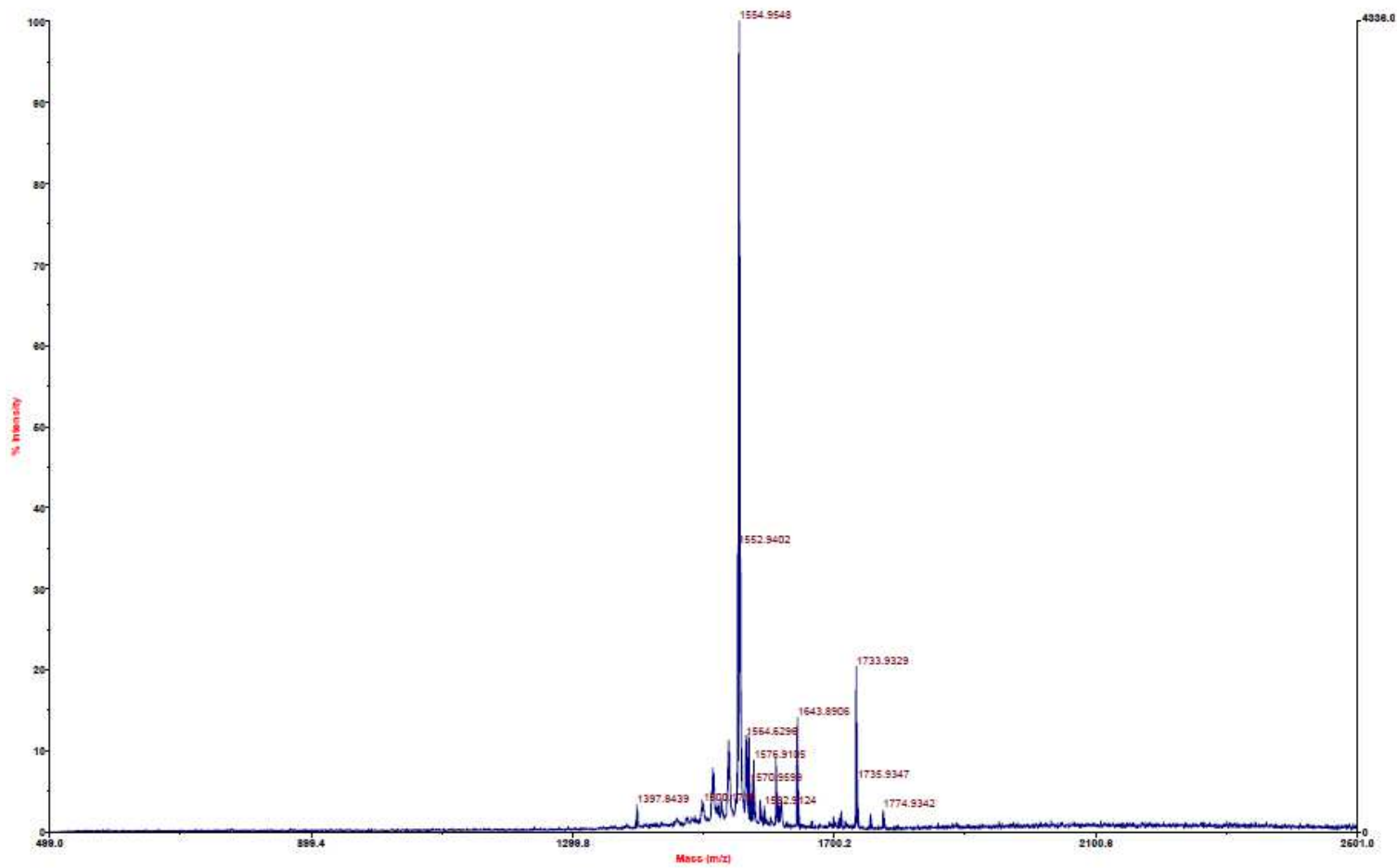


Figure B28. MALDI-TOF-MS full spectrum of R9-SB4CB

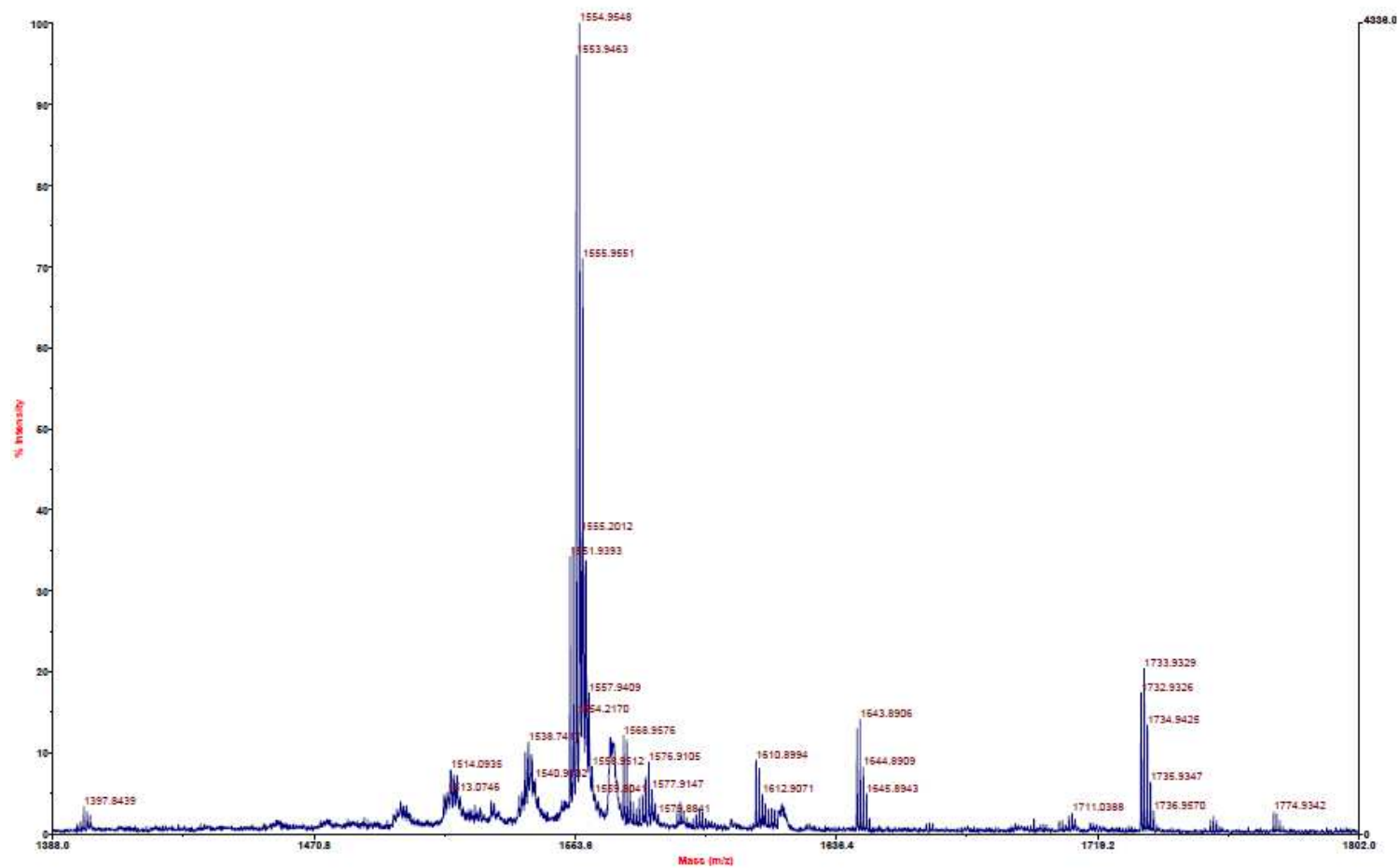


Figure B29. MALDI-TOF-MS enlarged spectrum of R9-SB4CB

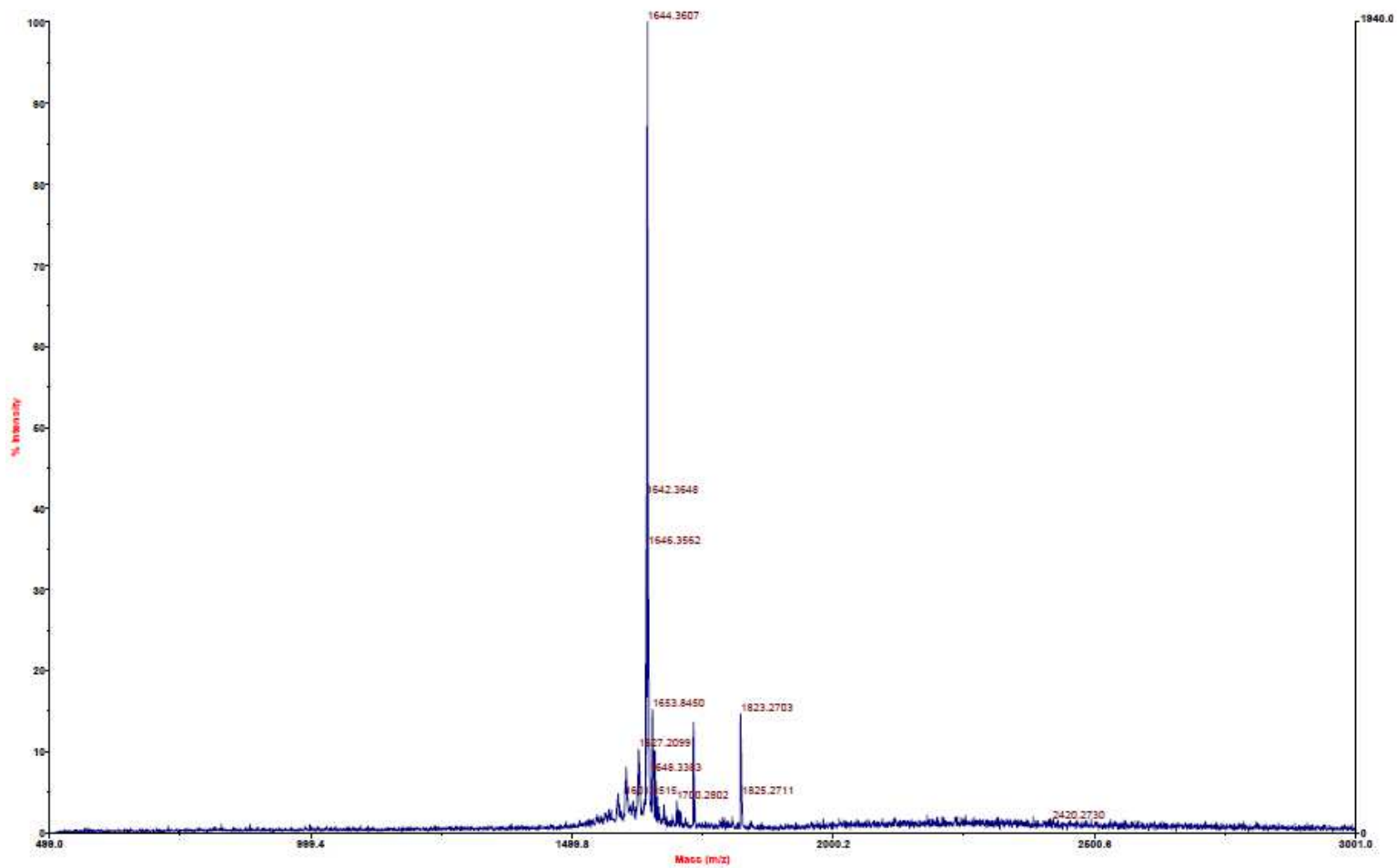


Figure B30. MALDI-TOF-MS full spectrum of RW9-SB4CB

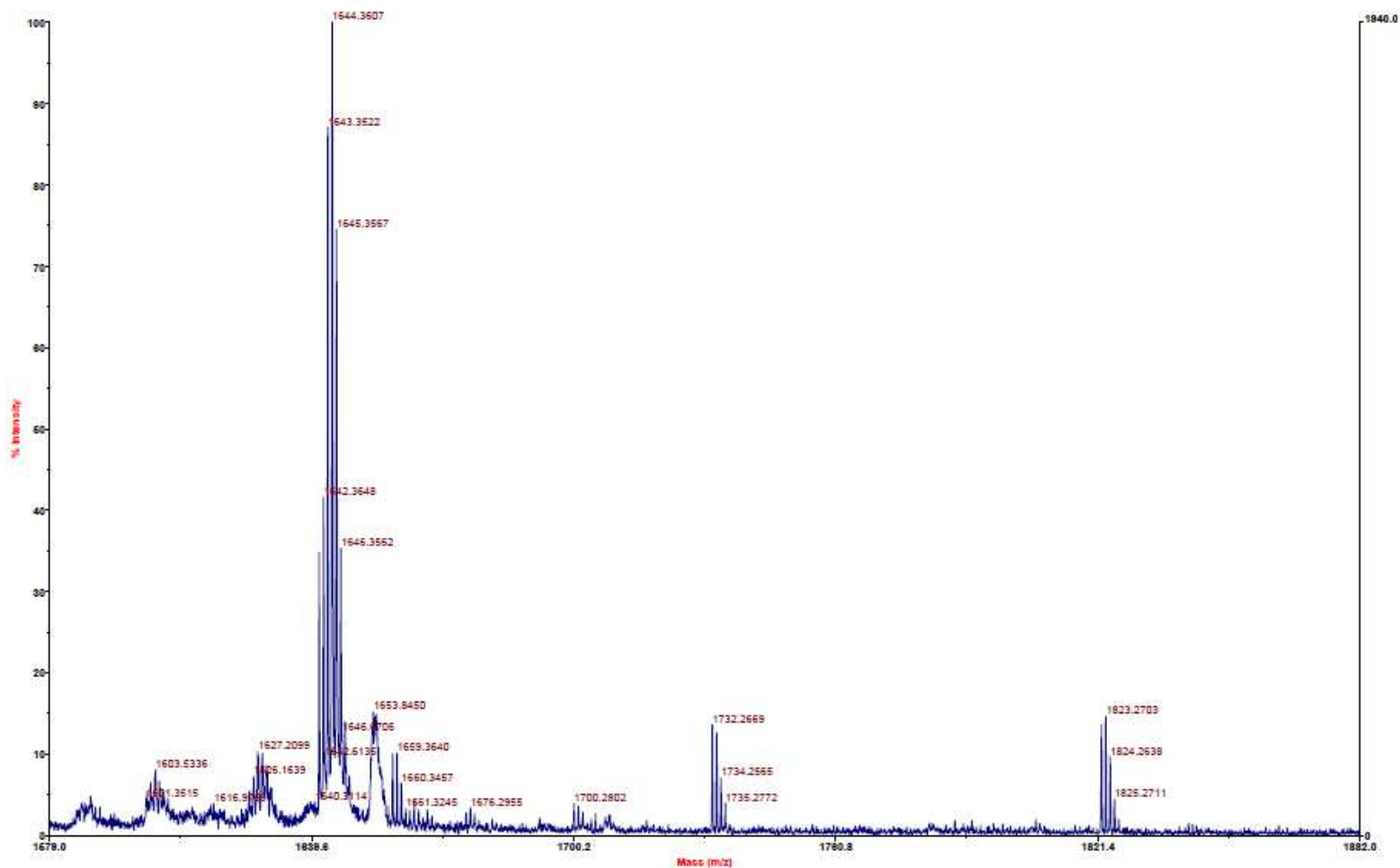


Figure B31. MALDI-TOF-MS enlarged spectrum of RW9-SB4CB

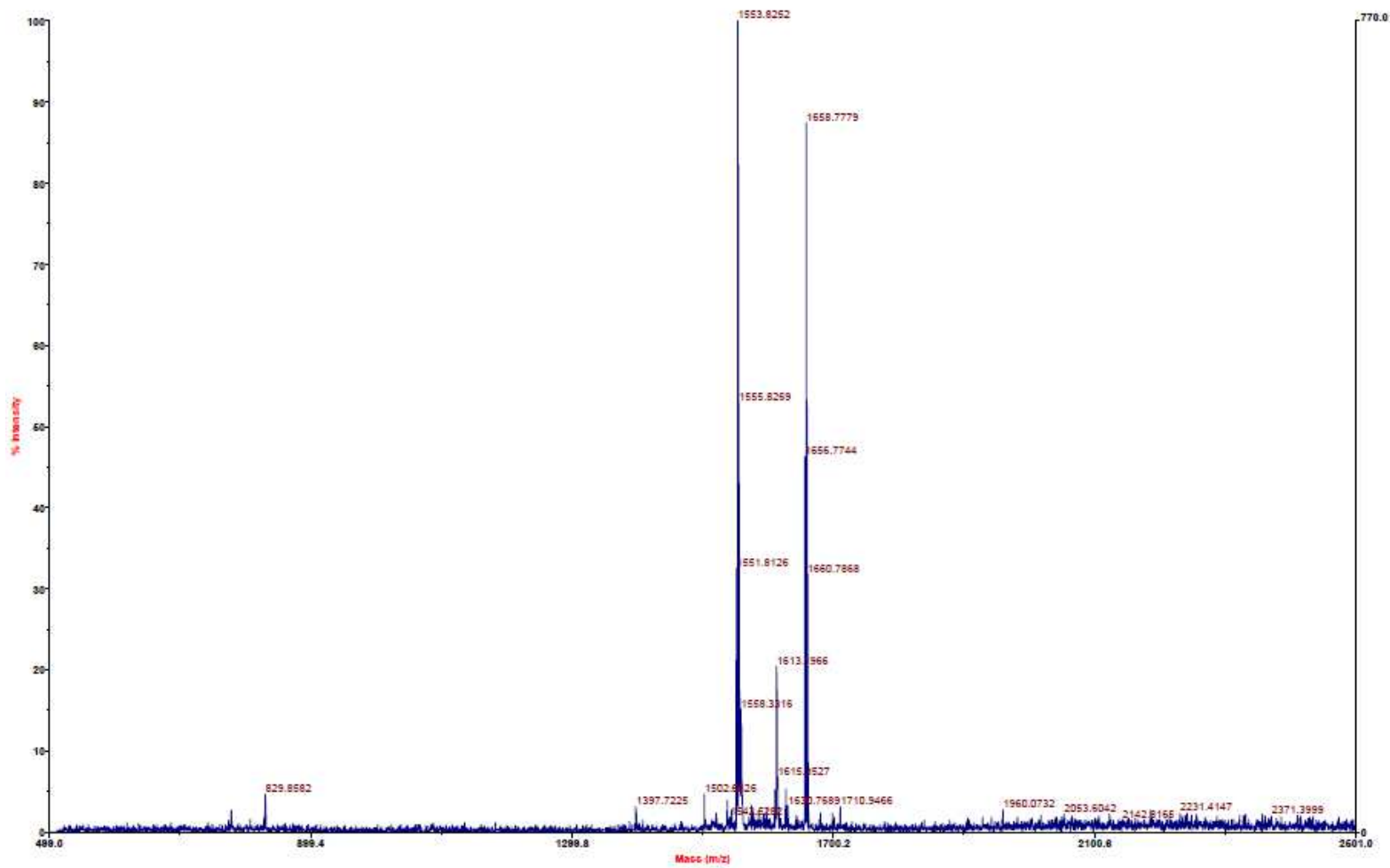


Figure B32. MALDI-TOF-MS full spectrum of R9-SM4CB

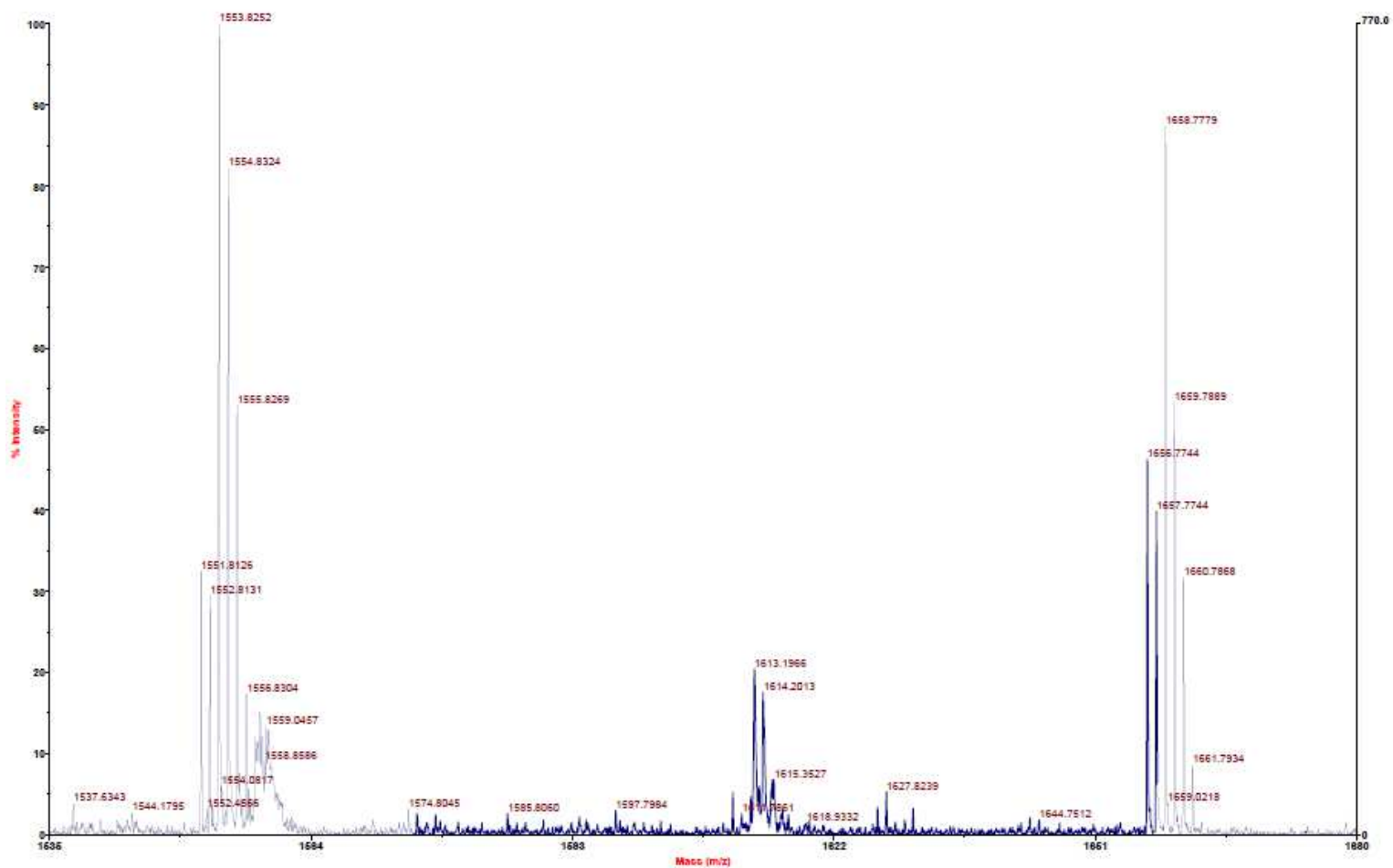


Figure B33. MALDI-TOF-MS enlarged spectrum of R9-SM4CB

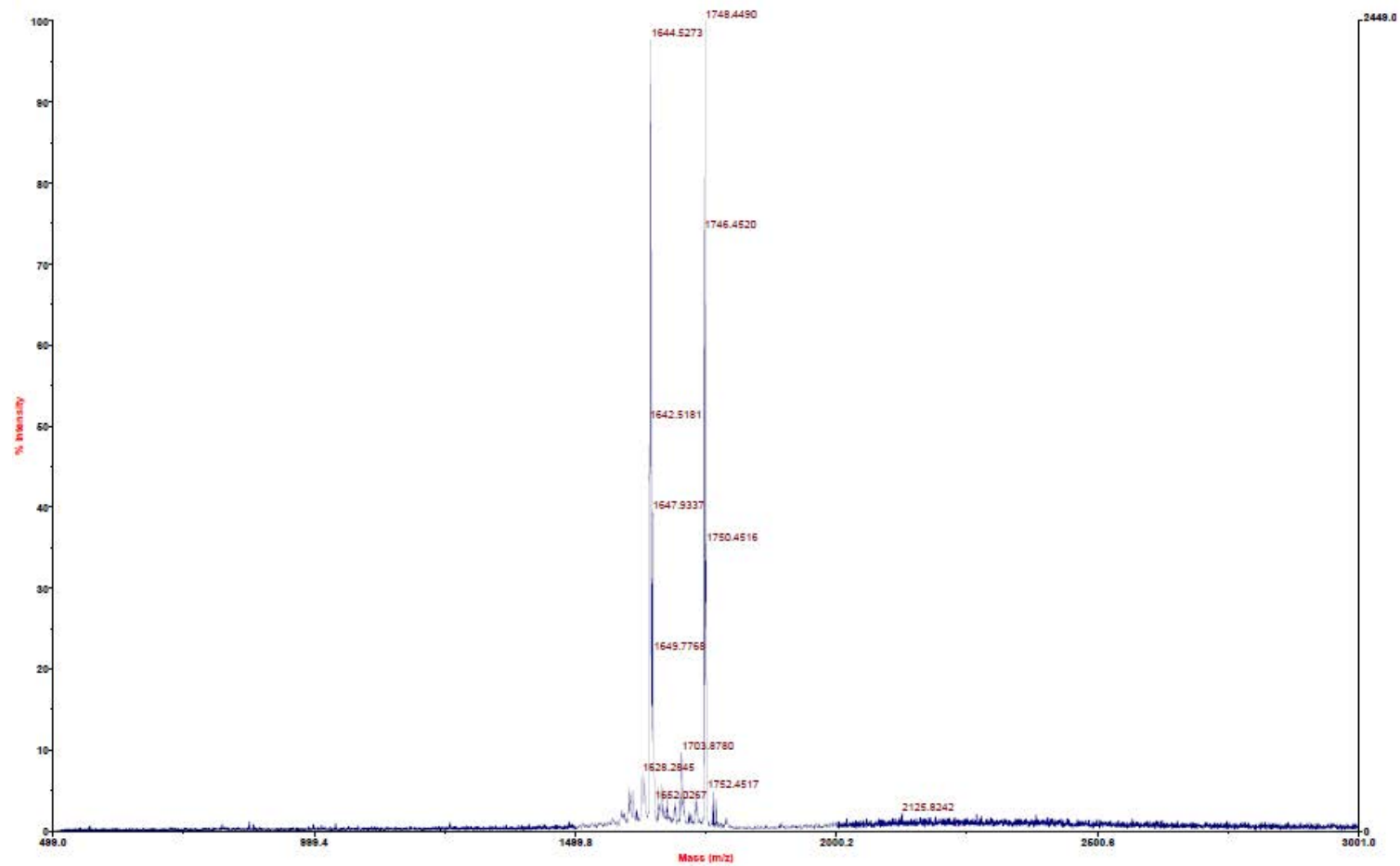


Figure B34. MALDI-TOF-MS full spectrum of RW9-SM4CB

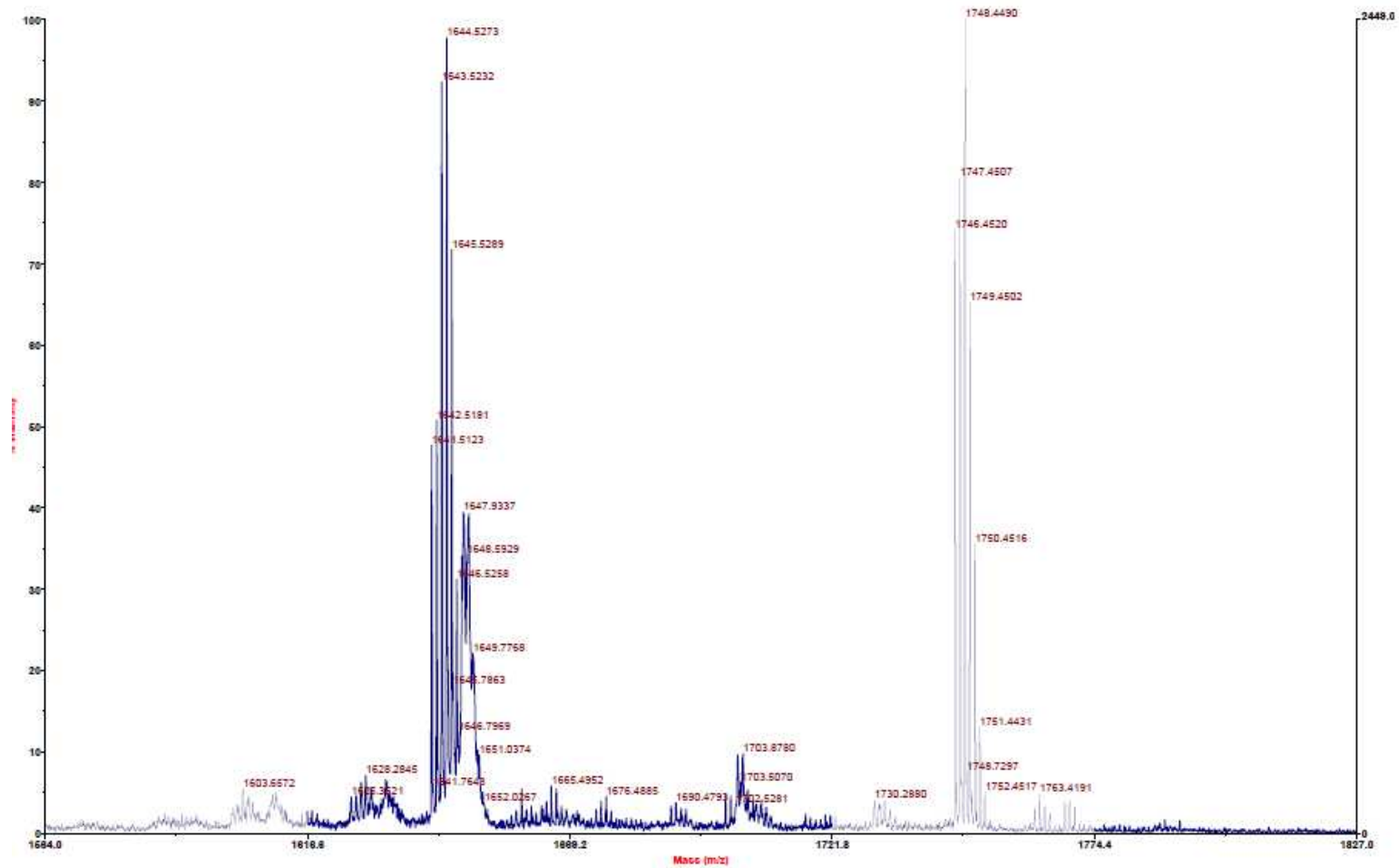


Figure B35. MALDI-TOF-MS enlarged spectrum of RW9-SM4CB

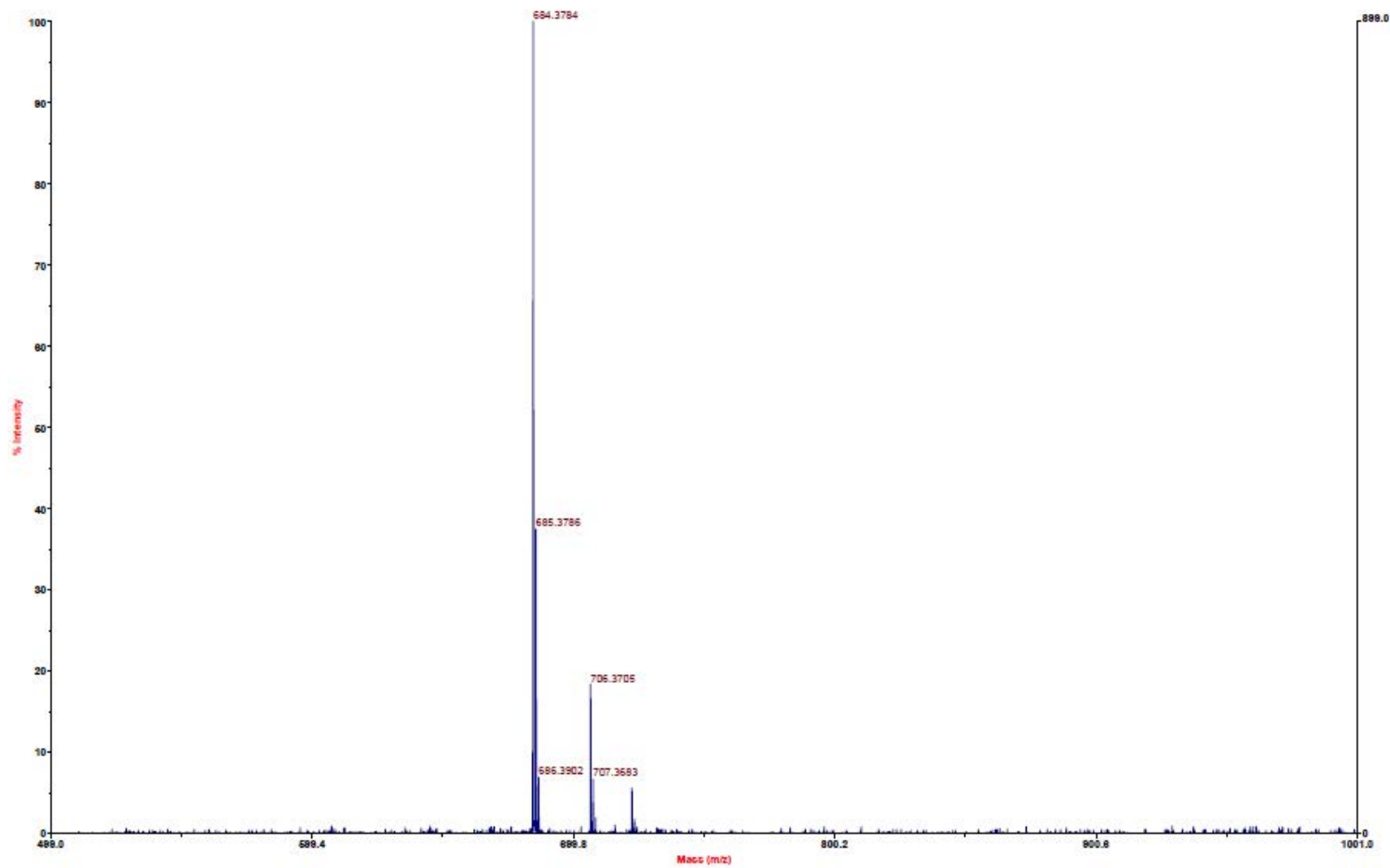


Figure B36. MALDI-TOF-MS full spectrum of R4AC

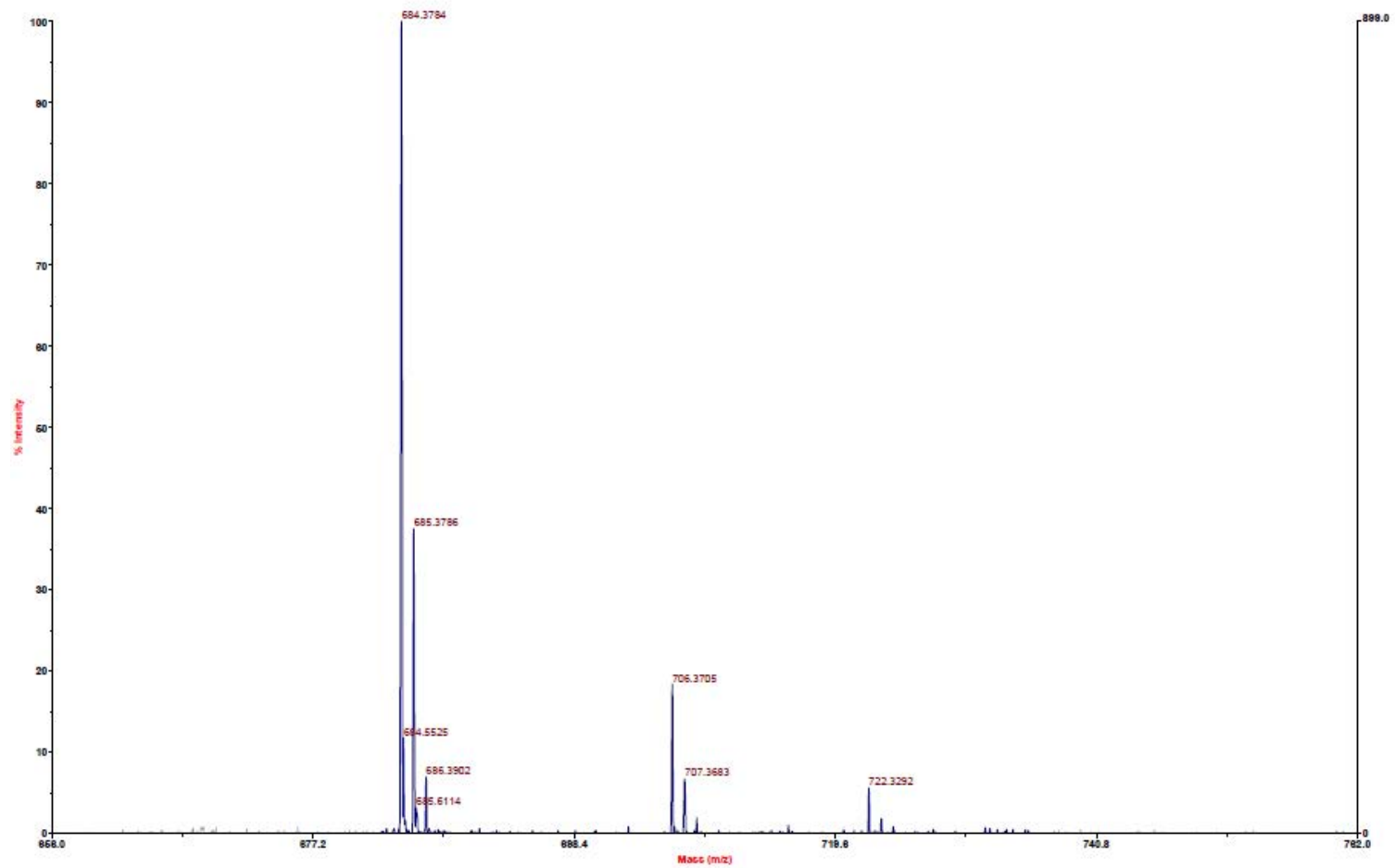


Figure B37. MALDI-TOF-MS enlarged spectrum of R4AC

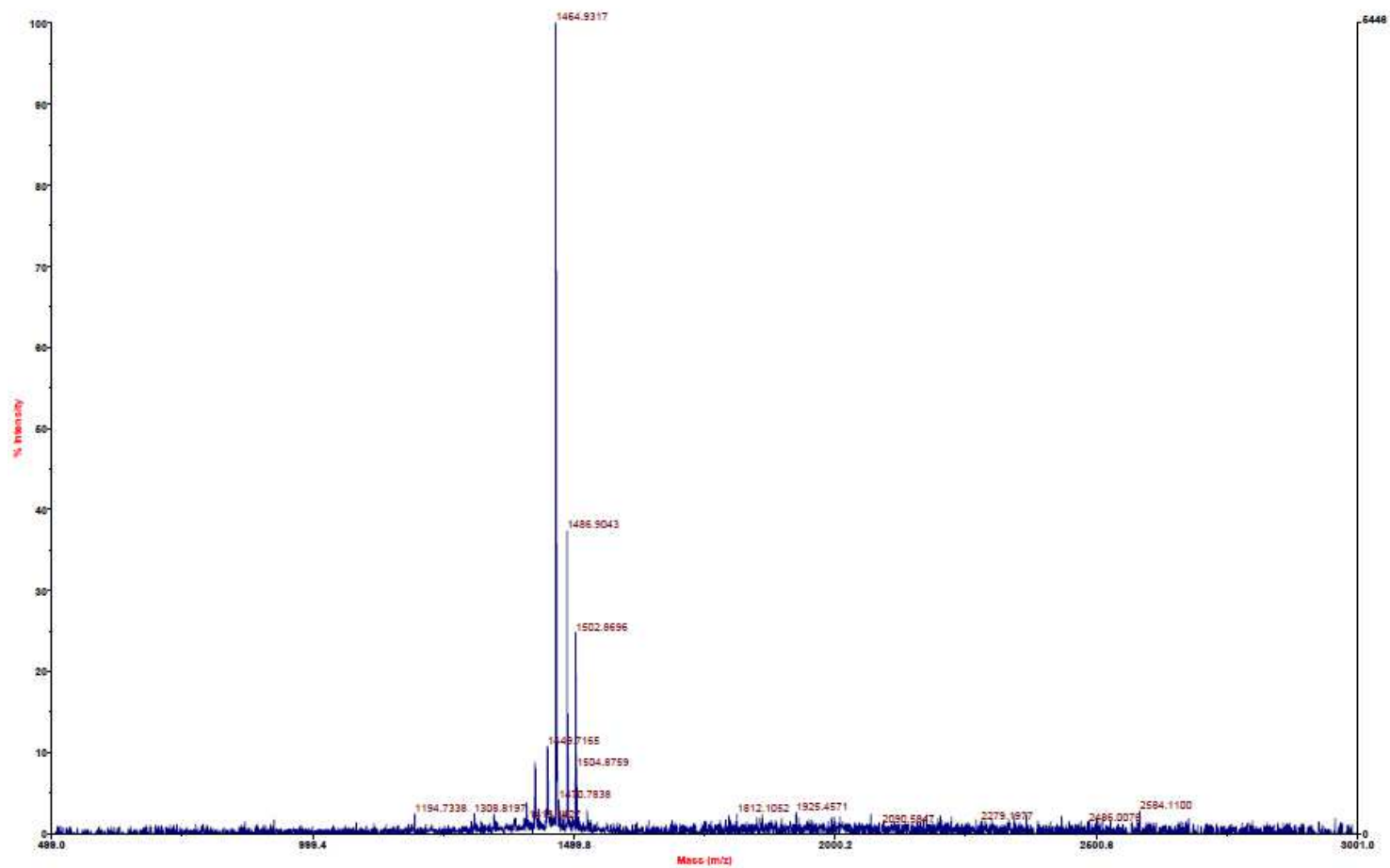


Figure B38. MALDI-TOF-MS full spectrum of R9AC

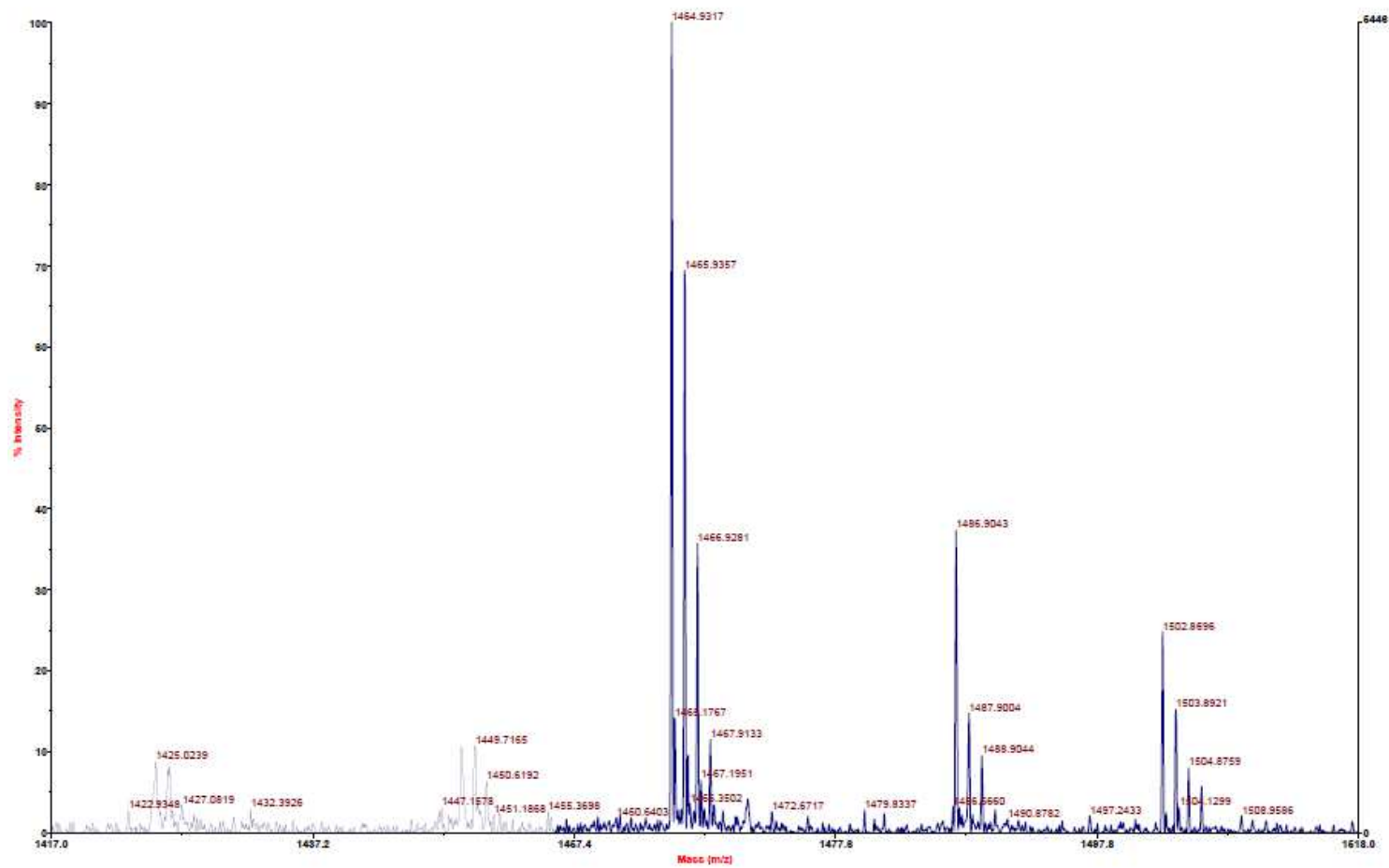


Figure B39. MALDI-TOF-MS enlarged spectrum of R9AC

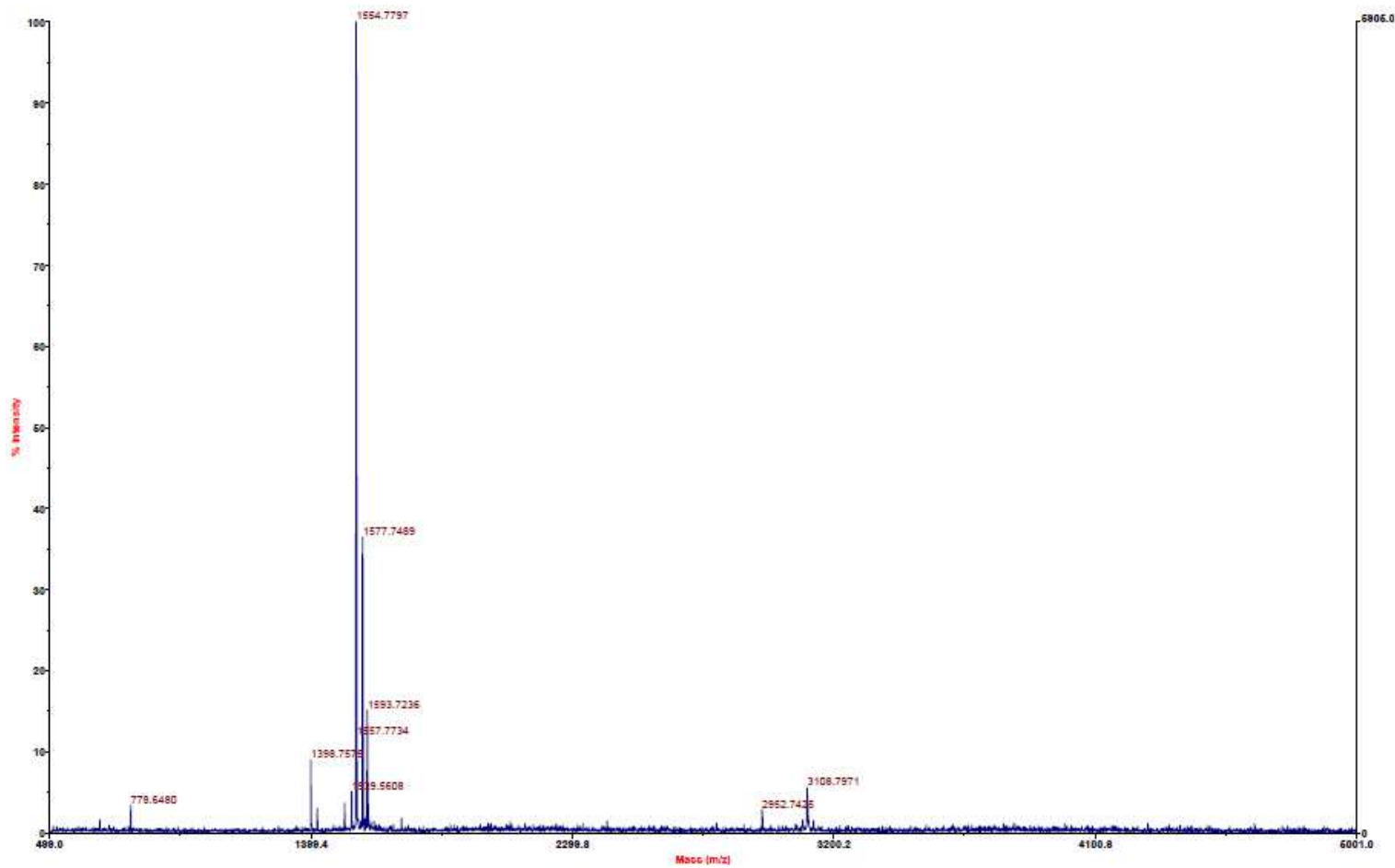


Figure B40. MALDI-TOF-MS full spectrum of RW9AC

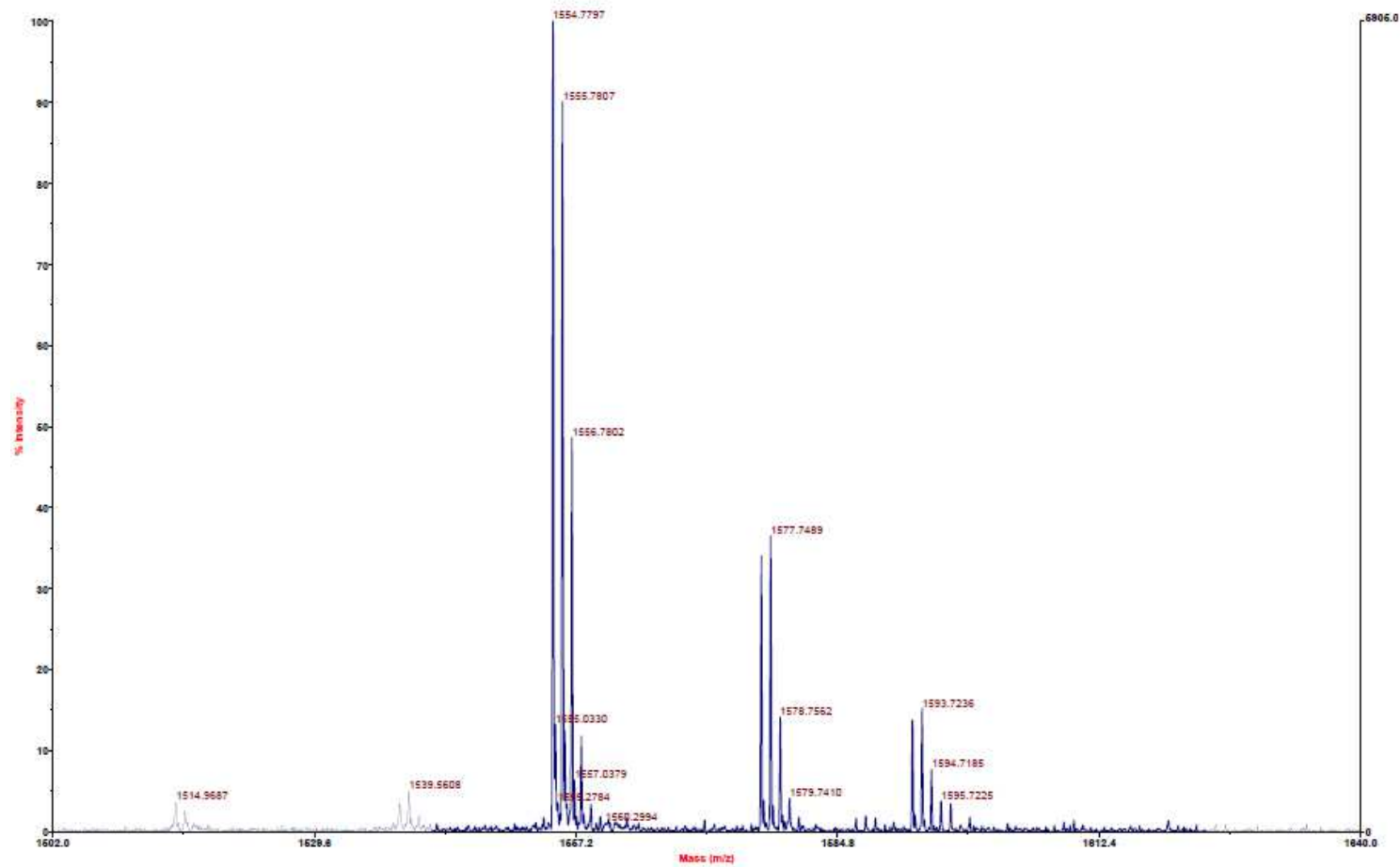


Figure B41. MALDI-TOF-MS enlarged spectrum of RW9AC

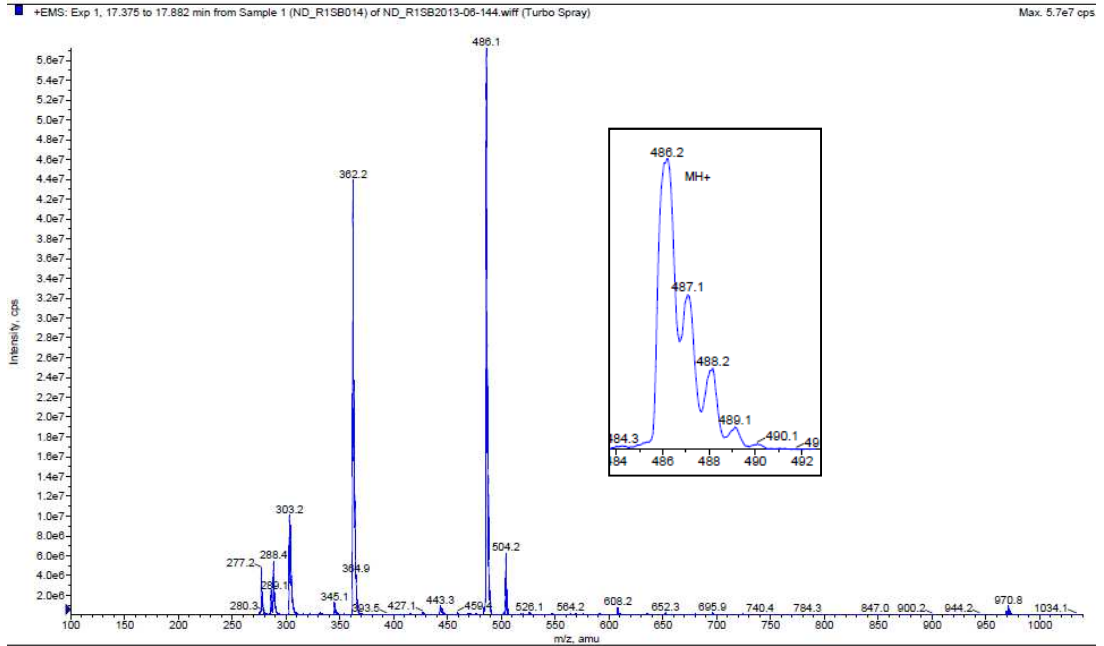


Figure B42. LC-MS (EMS) spectrum of R1-SB4CB at 17.6 min

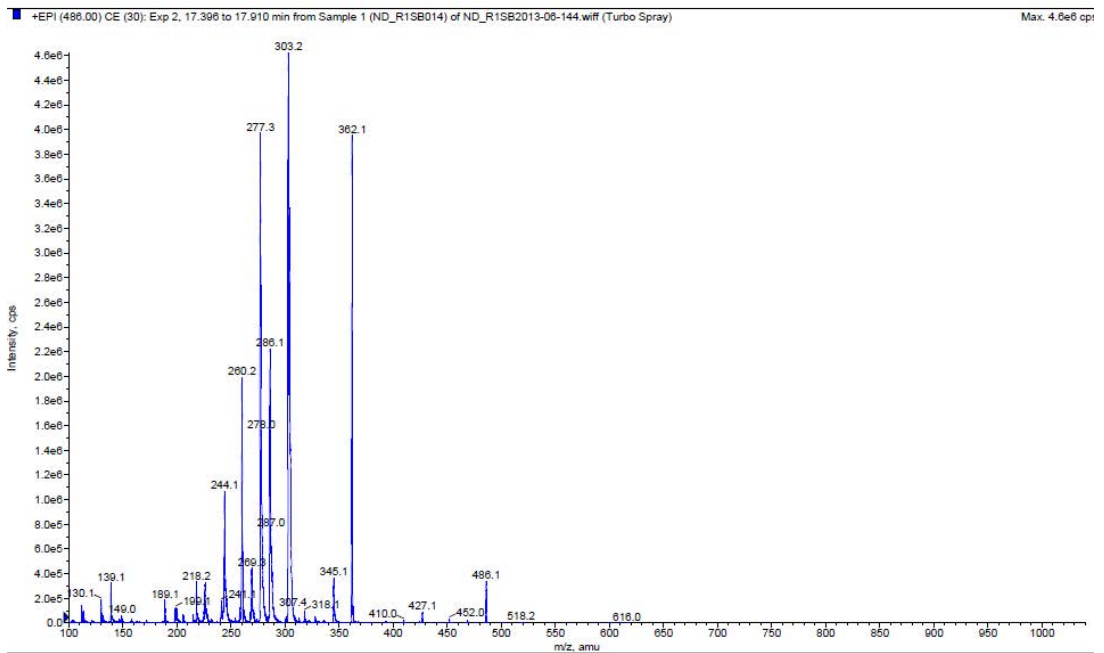


Figure B43. LC-MS (EPI) spectrum of R1-SB4CB at 17.6 min

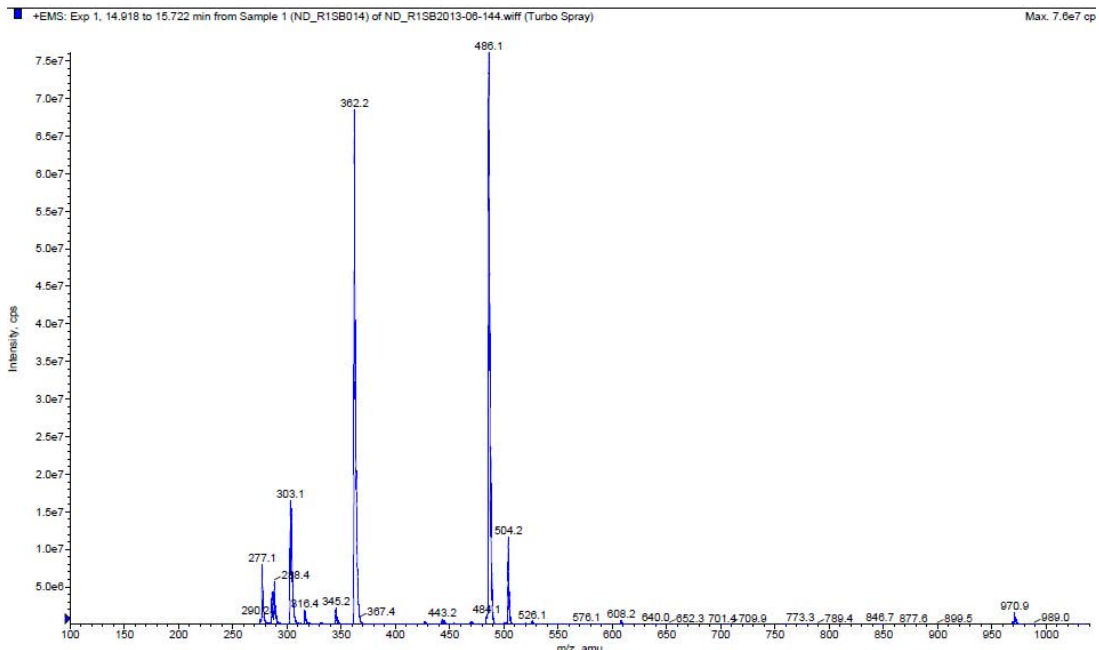


Figure B44. LC-MS (EMS) spectrum of R1-SB4CB at 15.3 min

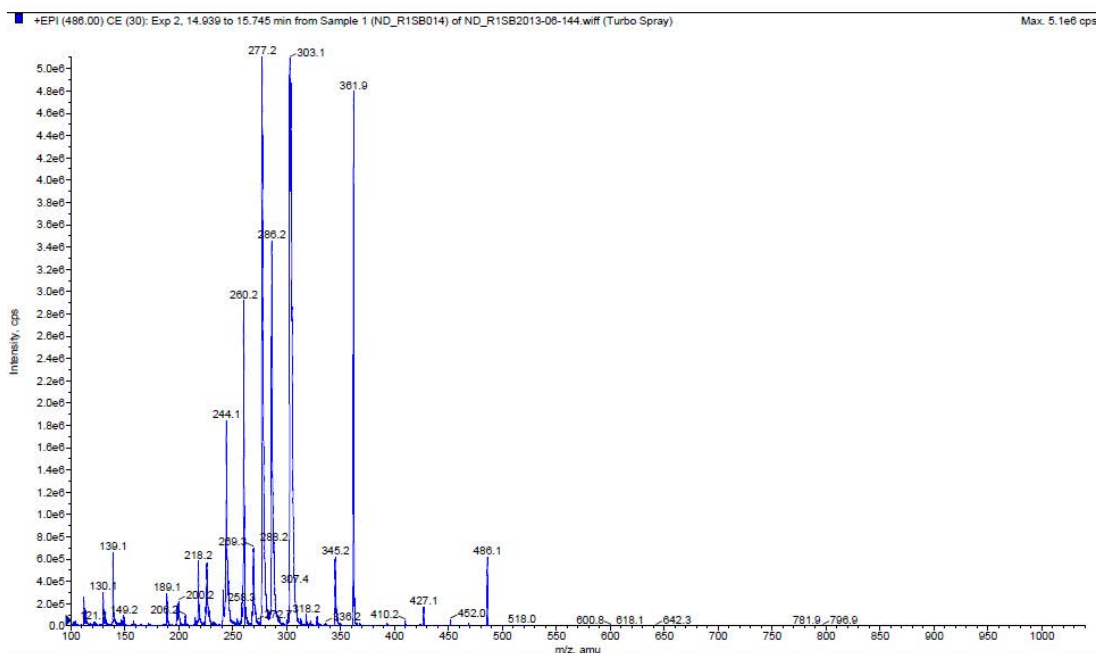


Figure B45. LC-MS (EPI) spectrum of R1-SB4CB at 15.3 min

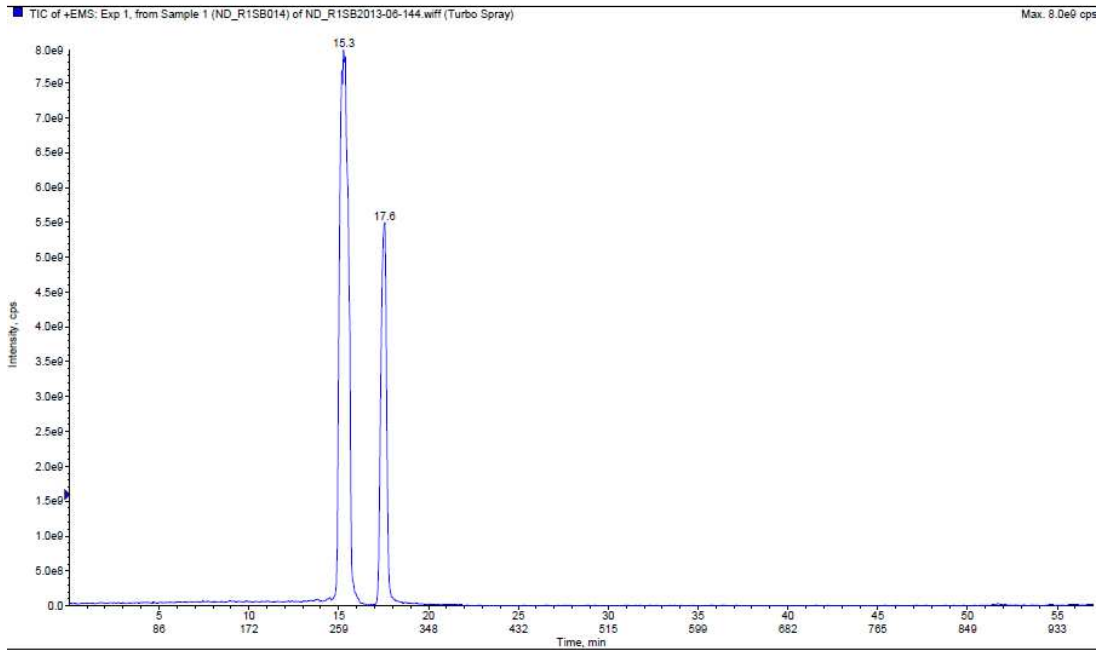


Figure B46. TIC (EMS) chromatogram of R1-SB4CB

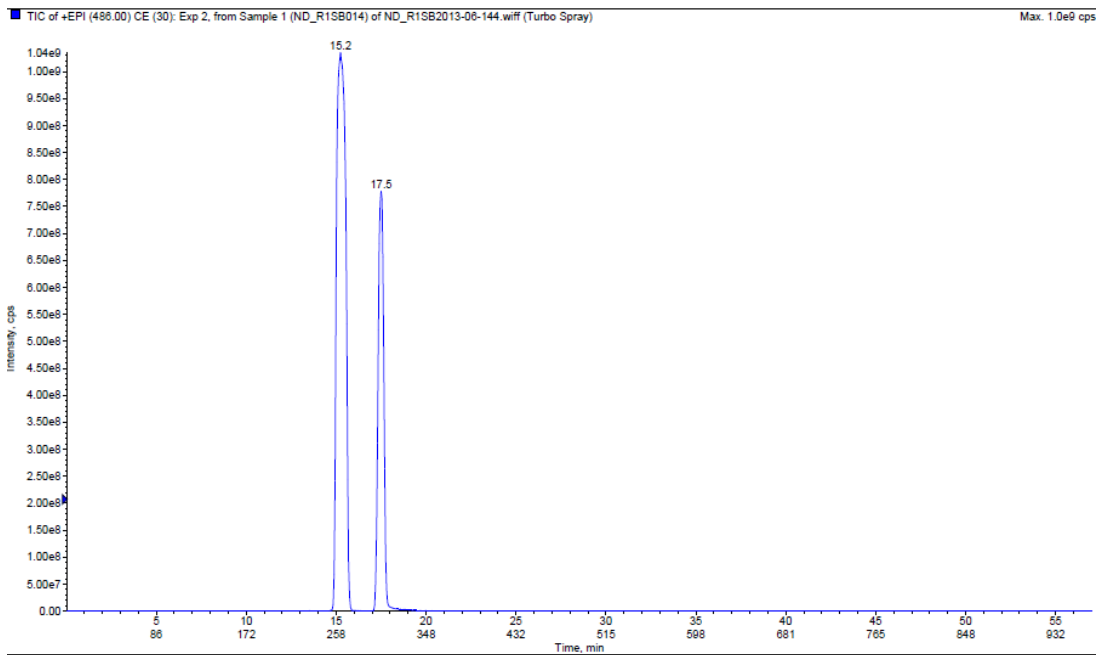


Figure B47. TIC (EPI) chromatogram of R1-SB4CB

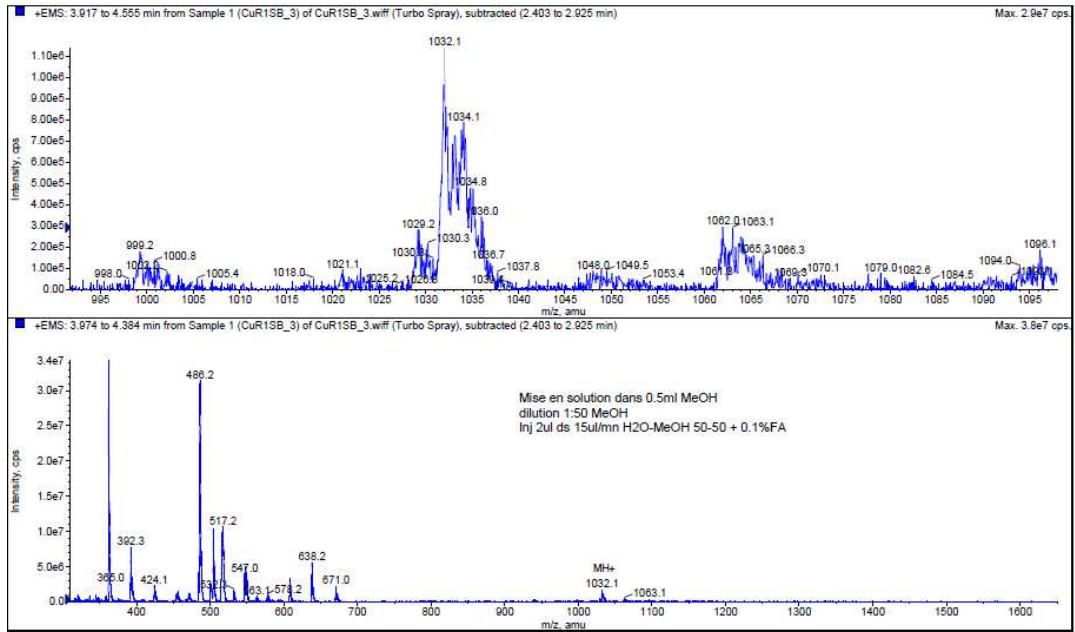


Figure B48. ESI-MS spectrum of $\text{Cu}(\text{R1-SB4CB})_2$

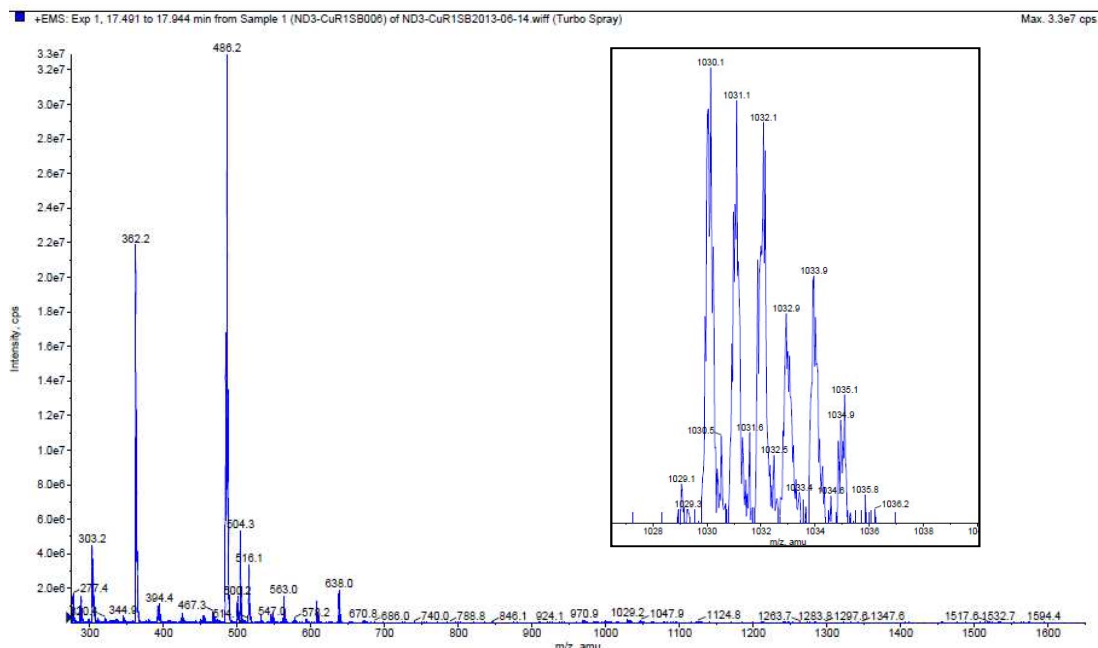


Figure B49. LC-MS [EMS and ER (inset)] spectra of $\text{Cu}(\text{R1-SB4CB})_2$ at 17.6 min

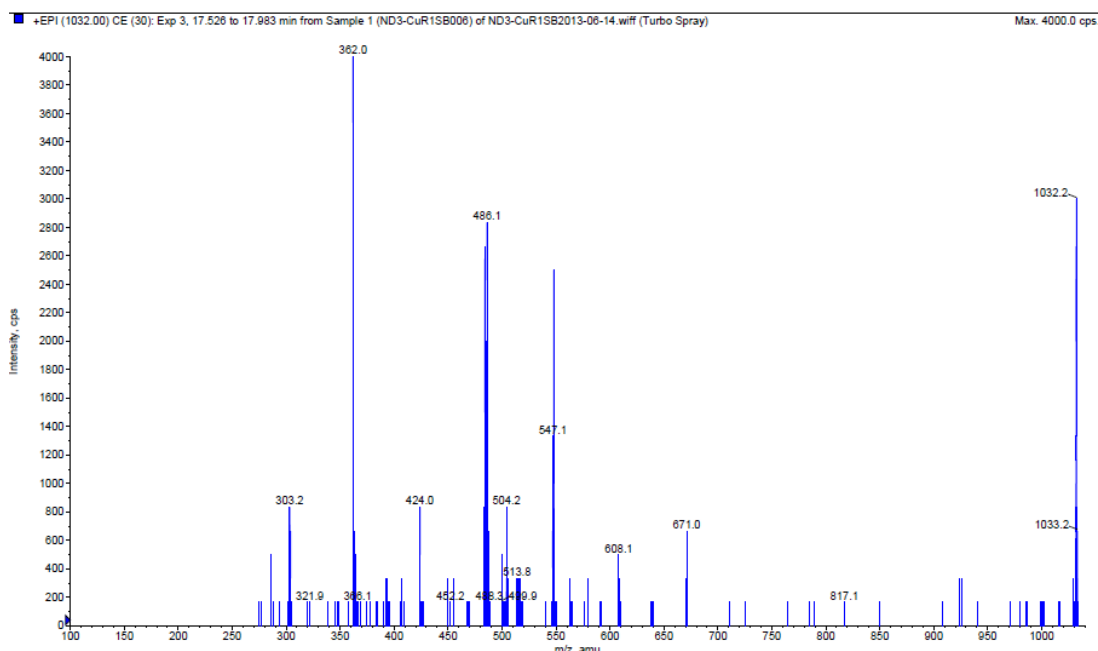


Figure B50. LC-MS (EPI) spectrum of $\text{Cu}(\text{R1-SB4CB})_2$ at 17.6 min

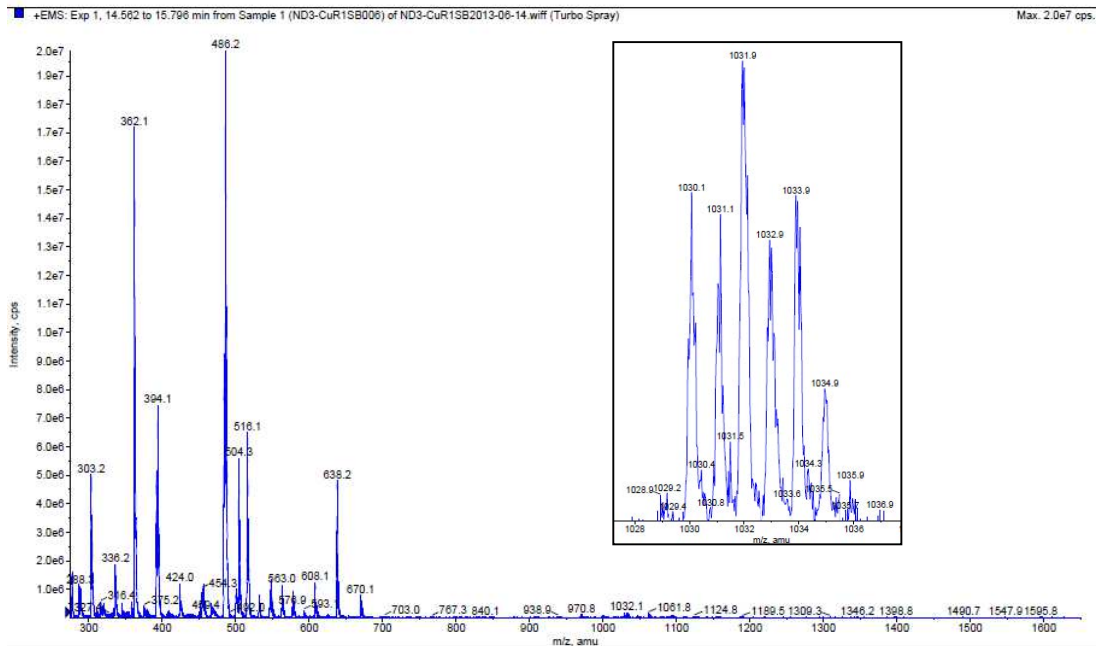


Figure B51. LC-MS [EMS and ER (inset)] spectra of $\text{Cu}(\text{R1-SB4CB})_2$ at 15.3 min

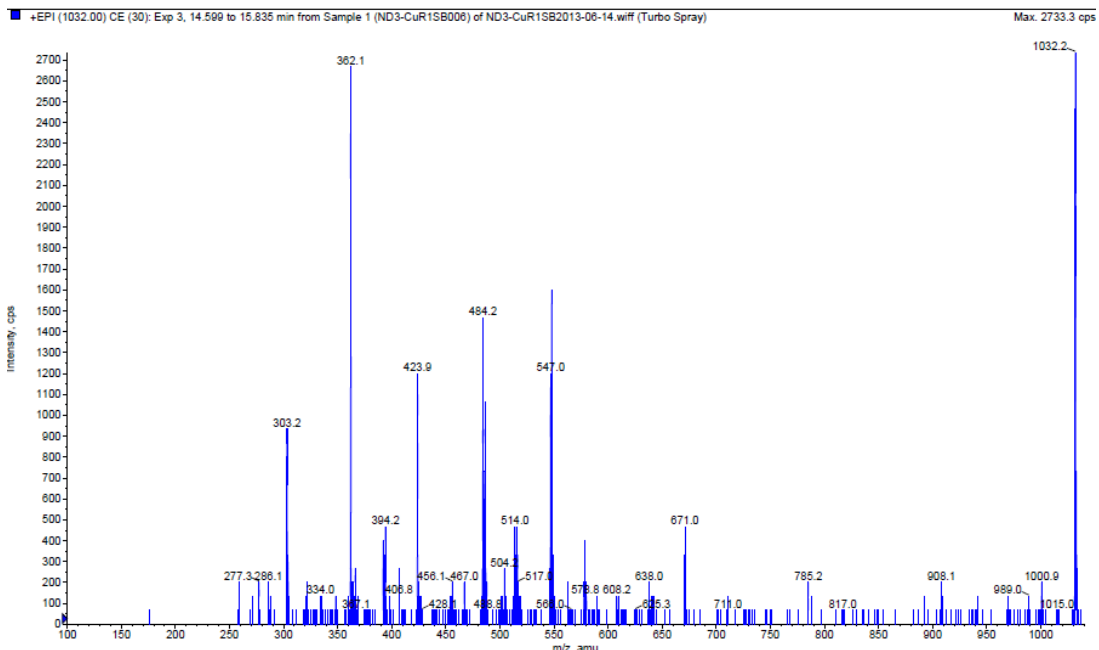


Figure B52. LC-MS (EPI) spectrum of $\text{Cu}(\text{R1-SB4CB})_2$ at 15.3 min

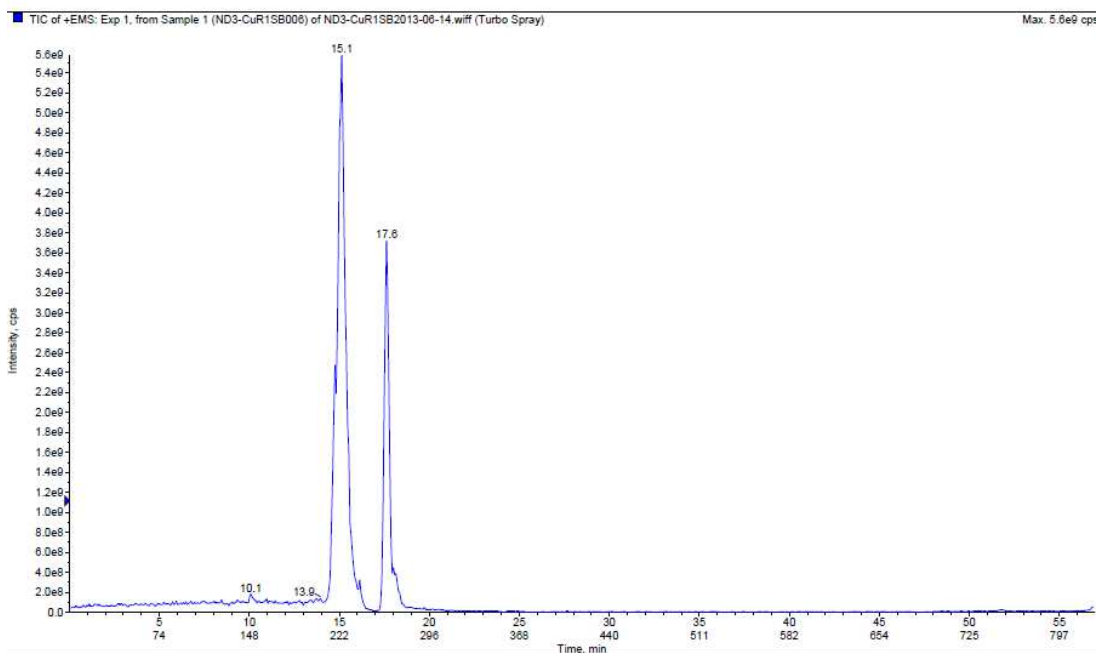


Figure B53. TIC (EMS) chromatogram of Cu(R1-SB4CB)₂

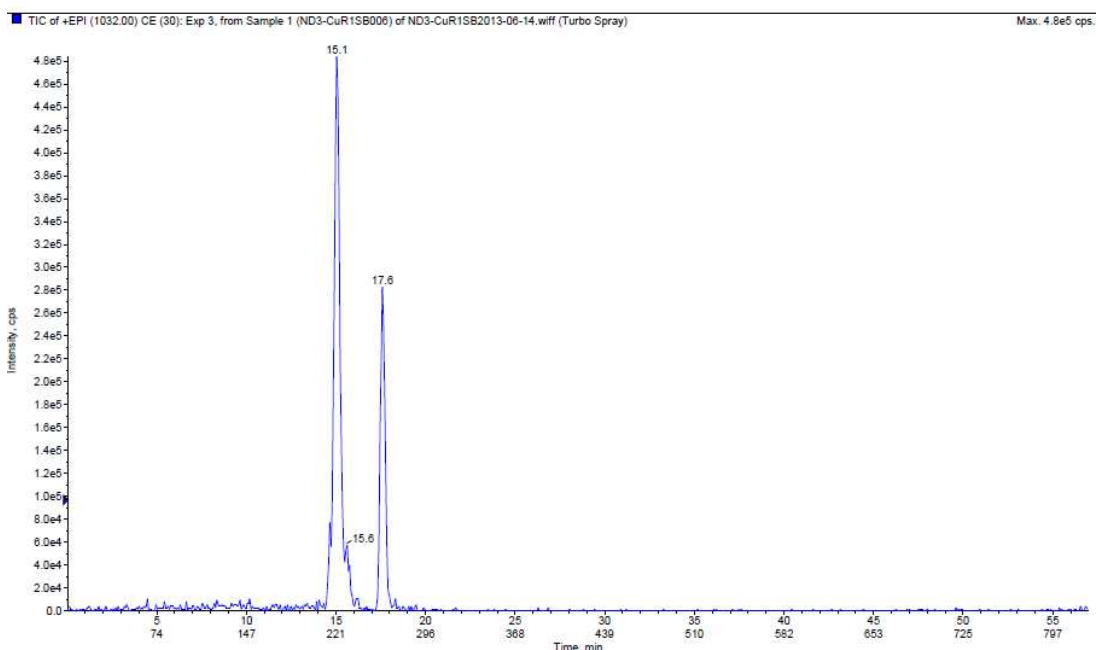


Figure B54. TIC (EPI) chromatogram of Cu(R1-SB4CB)₂

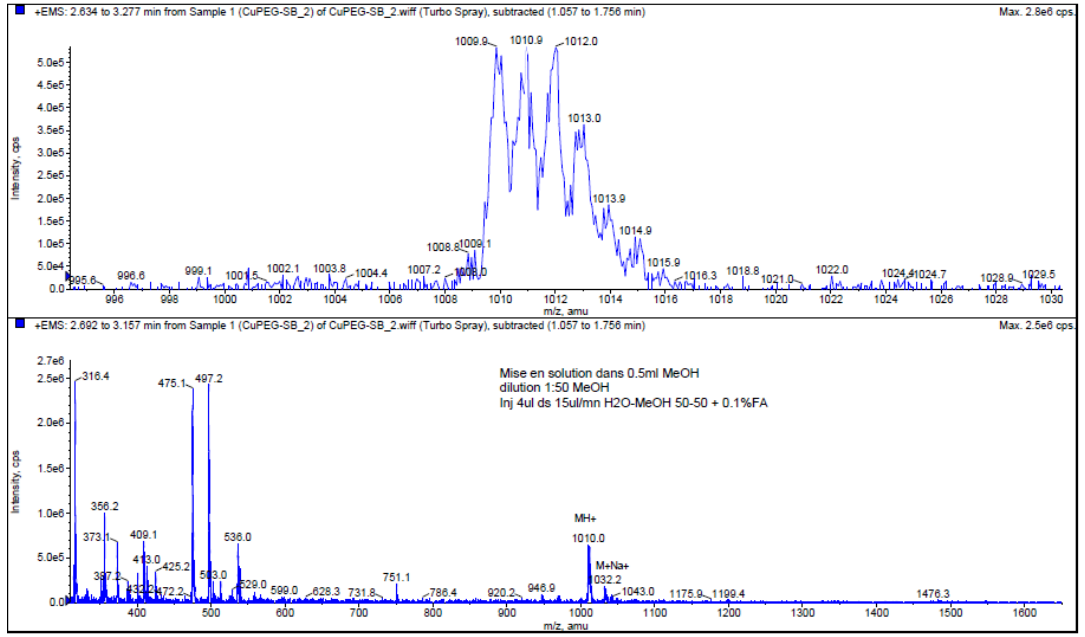


Figure B55. ESI-MS spectrum of Cu(PEG-SB4CB)₂

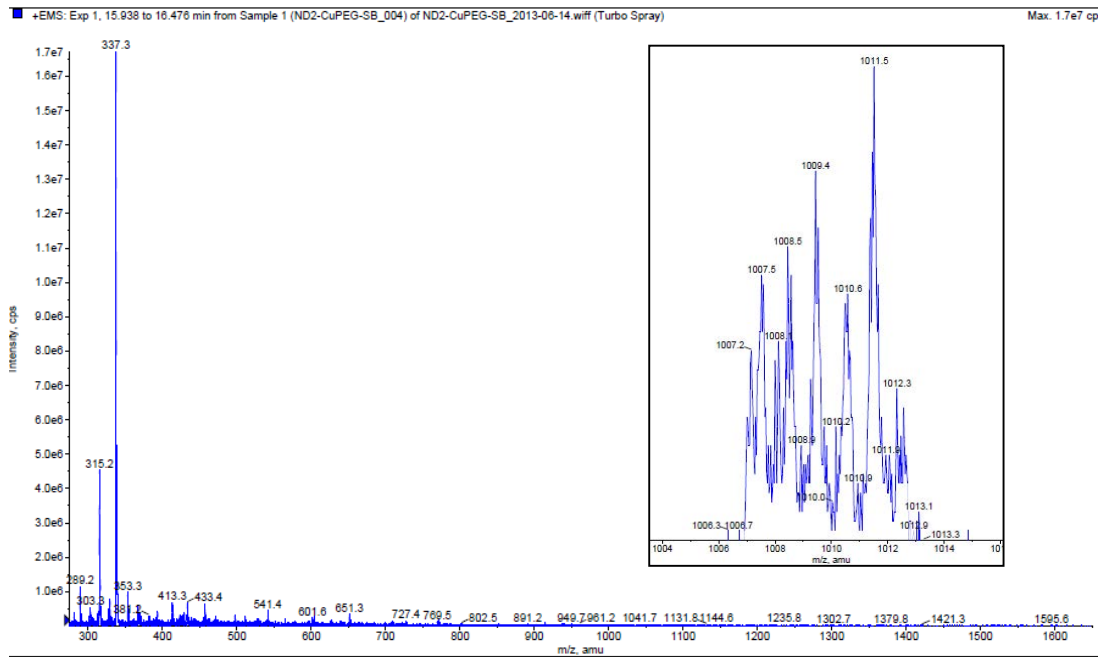


Figure B56. LC-MS [EMS and ER (inset)] spectra of $\text{Cu}(\text{PEG-SB4CB})_2$ at 16.1 min

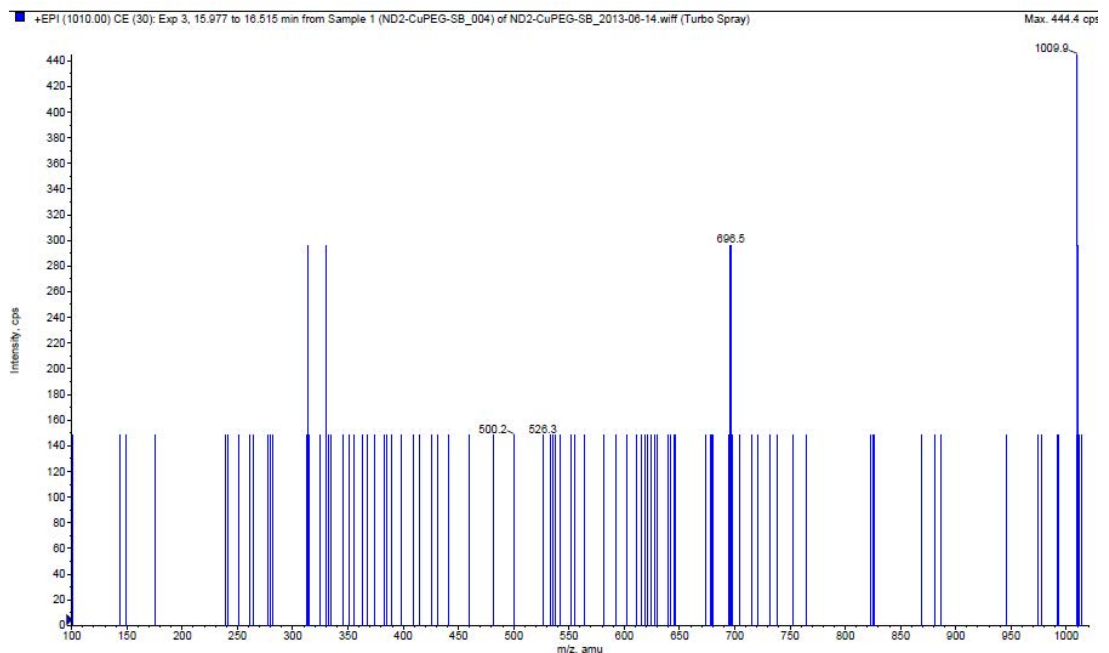


Figure B57. LC-MS (EPI) spectrum of $\text{Cu}(\text{PEG-SB4CB})_2$ at 16.1 min

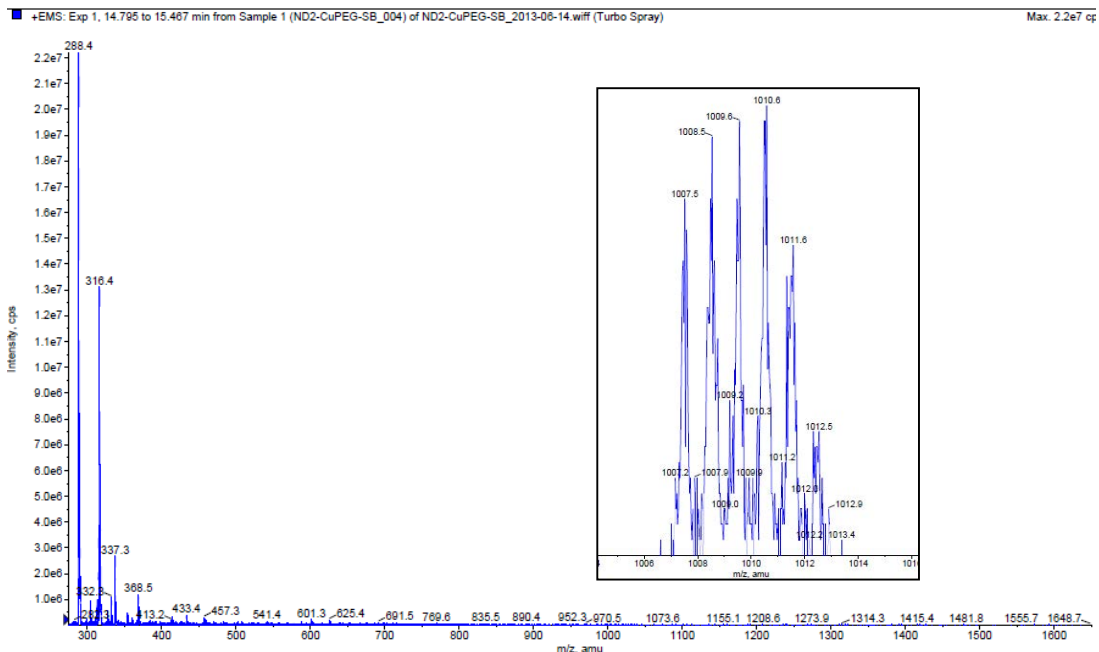


Figure B58. LC-MS [EMS and ER (inset)] spectra of $\text{Cu}(\text{PEG-SB4CB})_2$ at 15.2 min

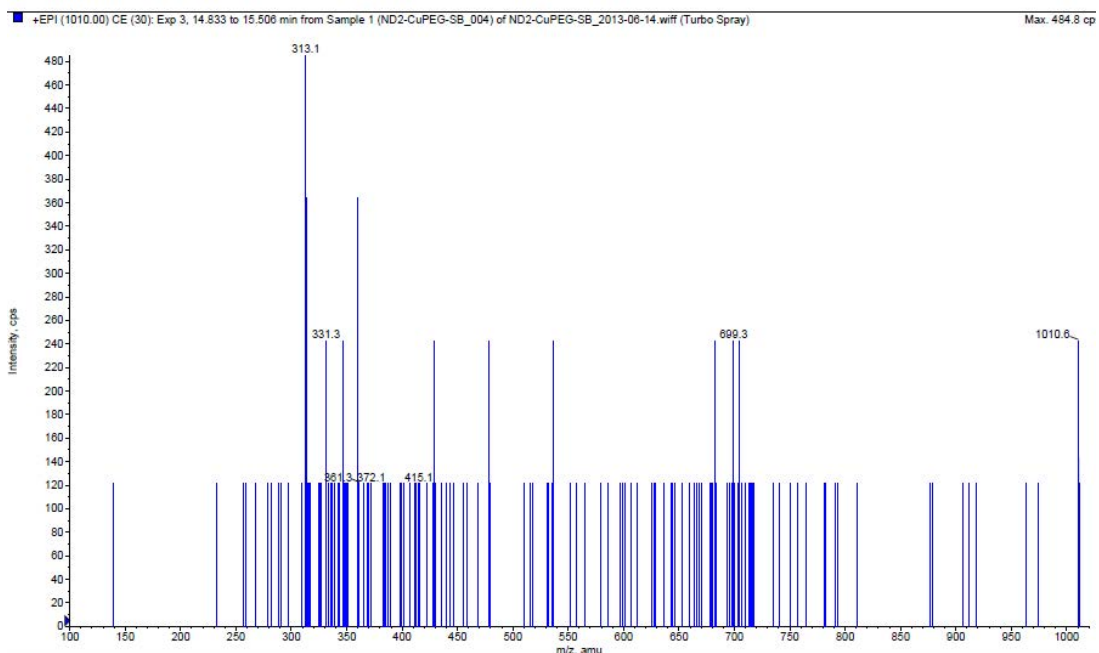


Figure B59. LC-MS (EPI) spectrum of $\text{Cu}(\text{PEG-SB4CB})_2$ at 15.2 min

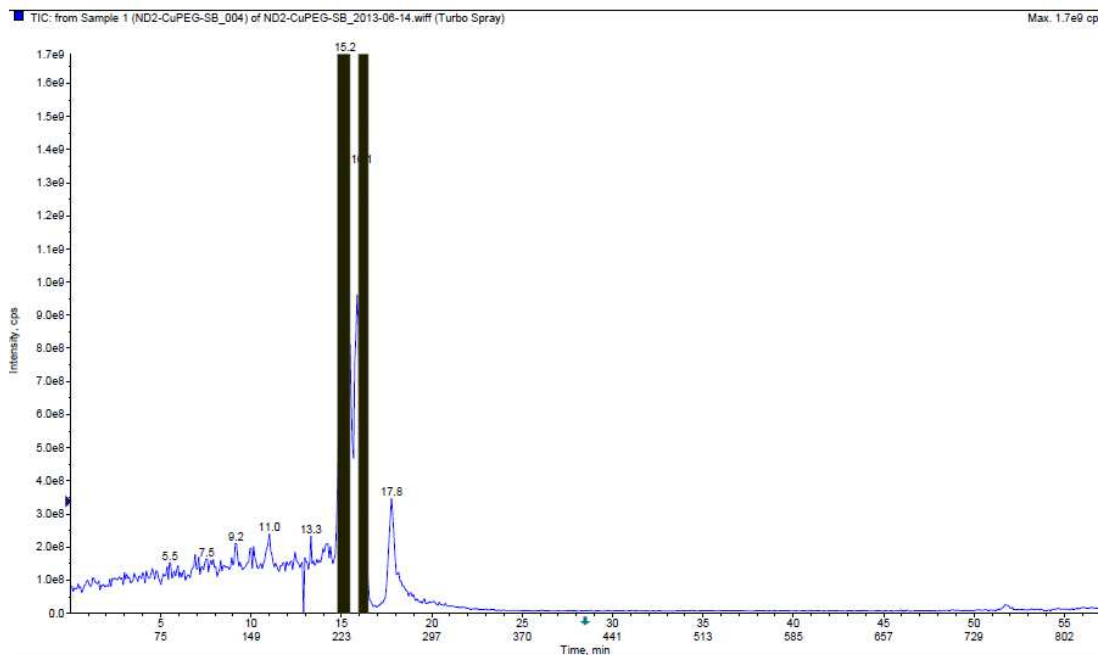


Figure B60. TIC chromatogram of $\text{Cu}(\text{PEG-SB4CB})_2$

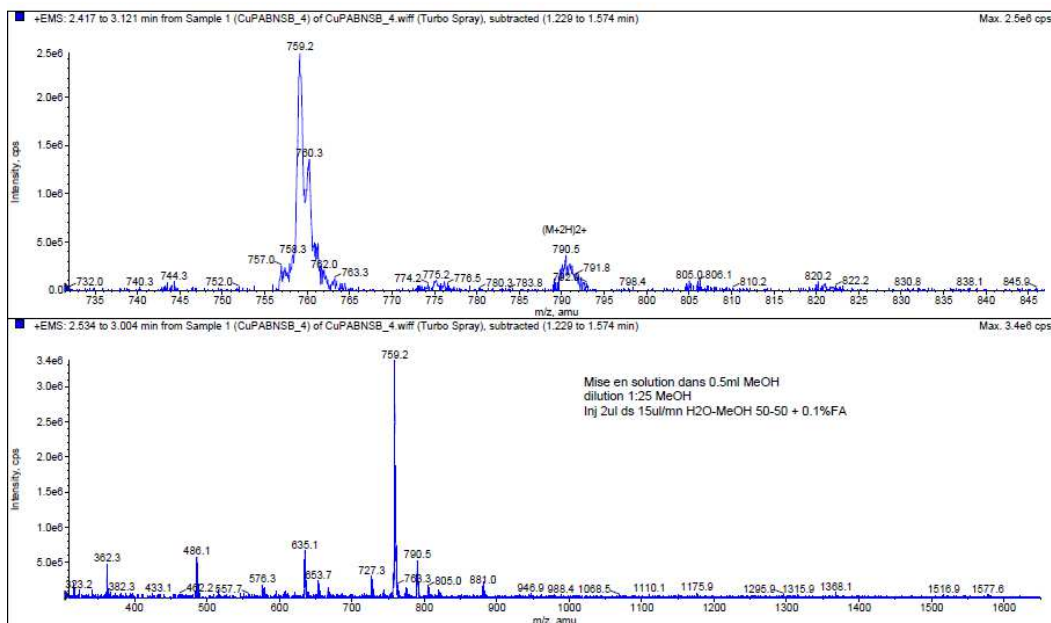


Figure B61. ESI-MS spectrum of $\text{Cu}(\text{P}\alpha\beta\text{N-SB4CB})_2$

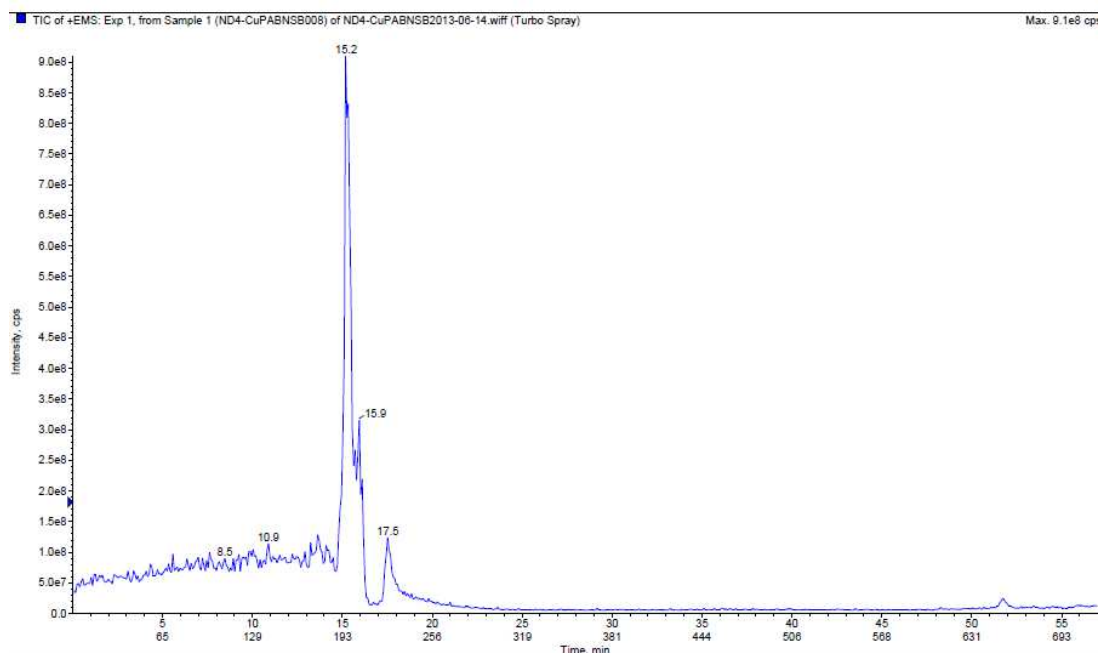


Figure B62. TIC (EMS) chromatogram of $\text{Cu}(\text{PA}\beta\text{N-SB4CB})_2$

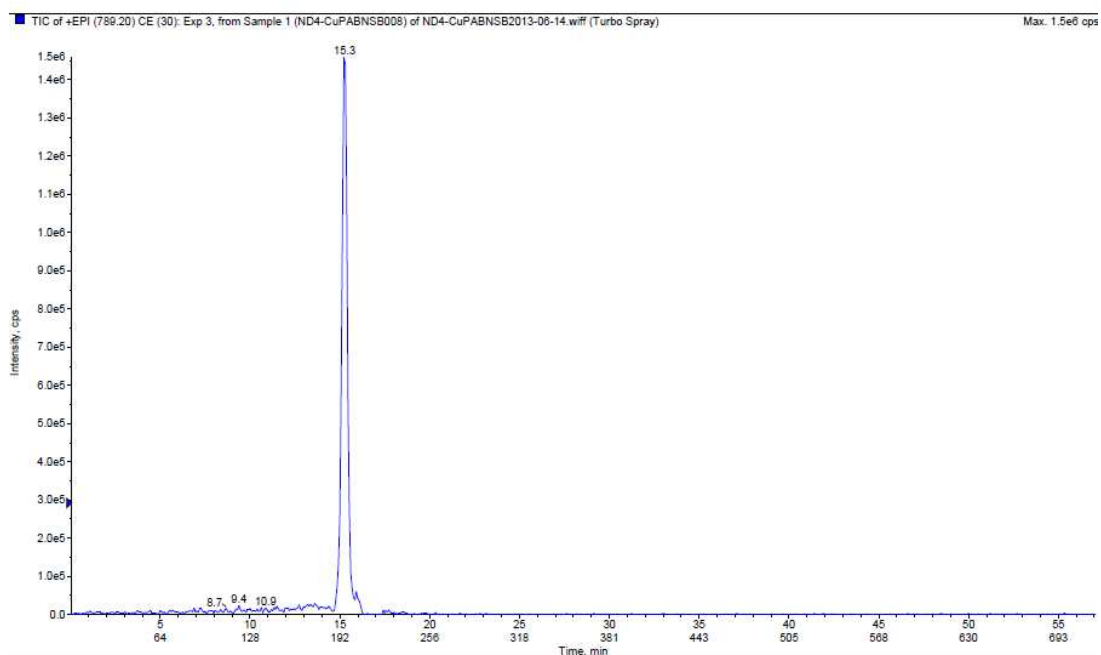


Figure B63. TIC (EPI) chromatogram of $\text{Cu}(\text{PA}\beta\text{N-SB4CB})_2$

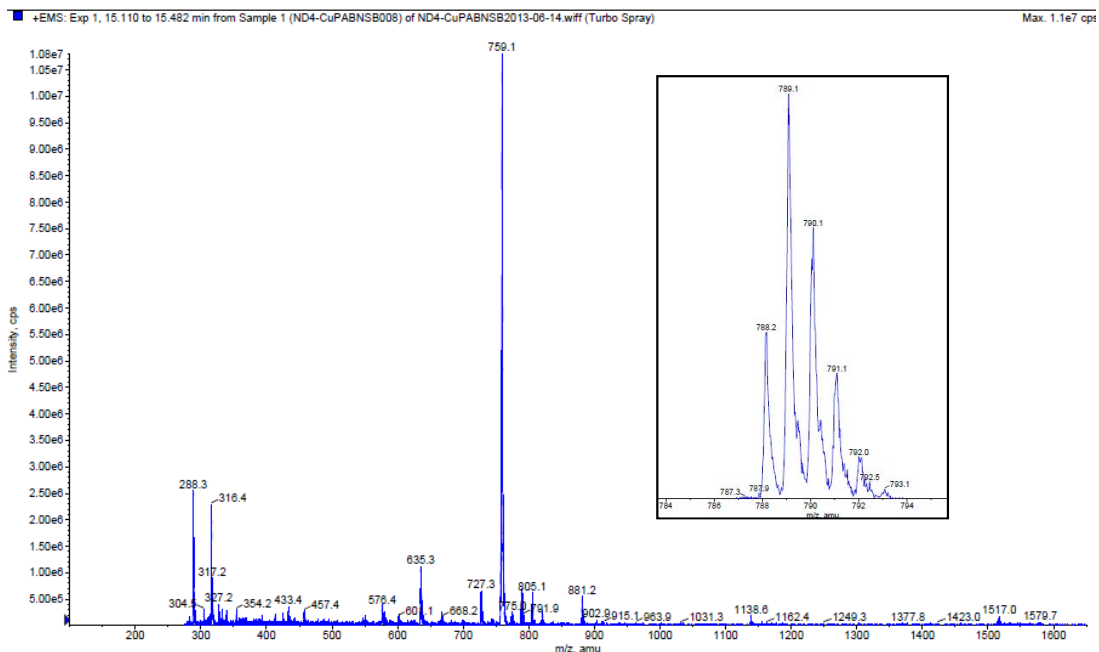


Figure B64. LC-MS [EMS and ER (inset)] spectra of $\text{Cu}(\text{PA}\beta\text{N-SB4CB})_2$

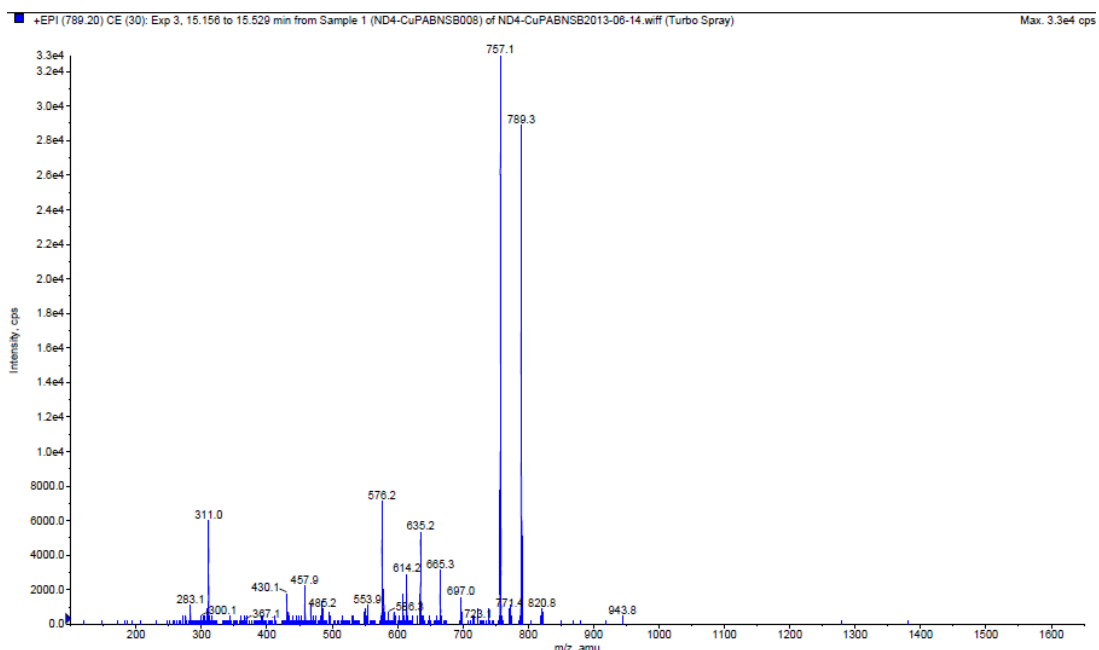


Figure B65. LC-MS (EPI) spectrum of $\text{Cu}(\text{PA}\beta\text{N-SB4CB})_2$

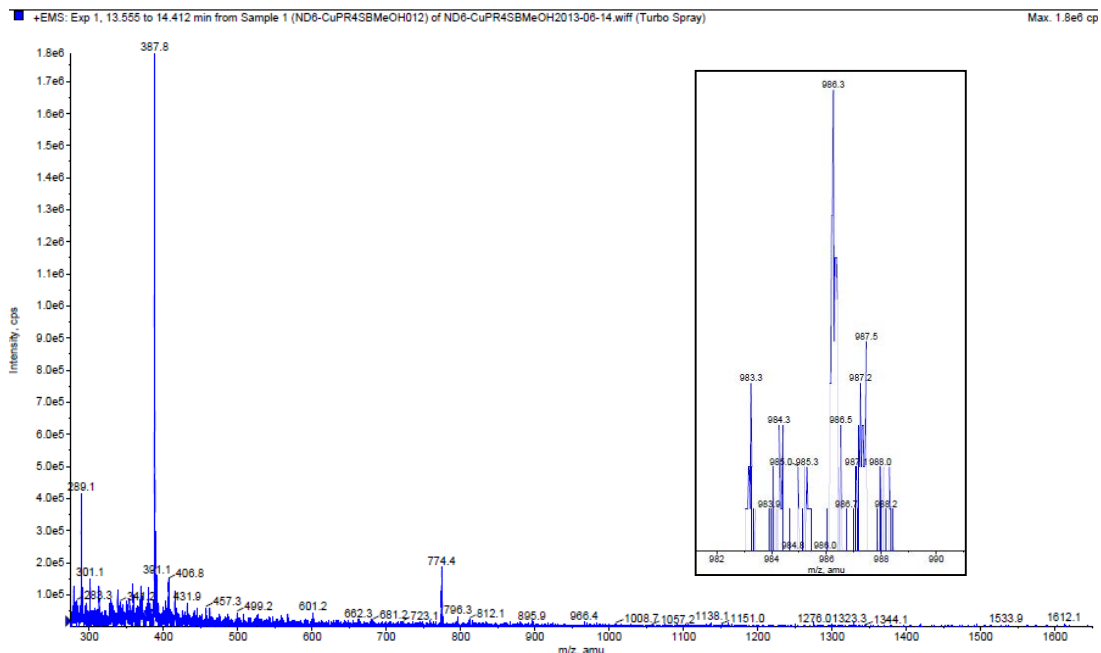


Figure B66. LC-MS [EMS and ER (inset)] spectra of $\text{Cu}(\text{R4-SB4CB})_2$ at 14.0 min

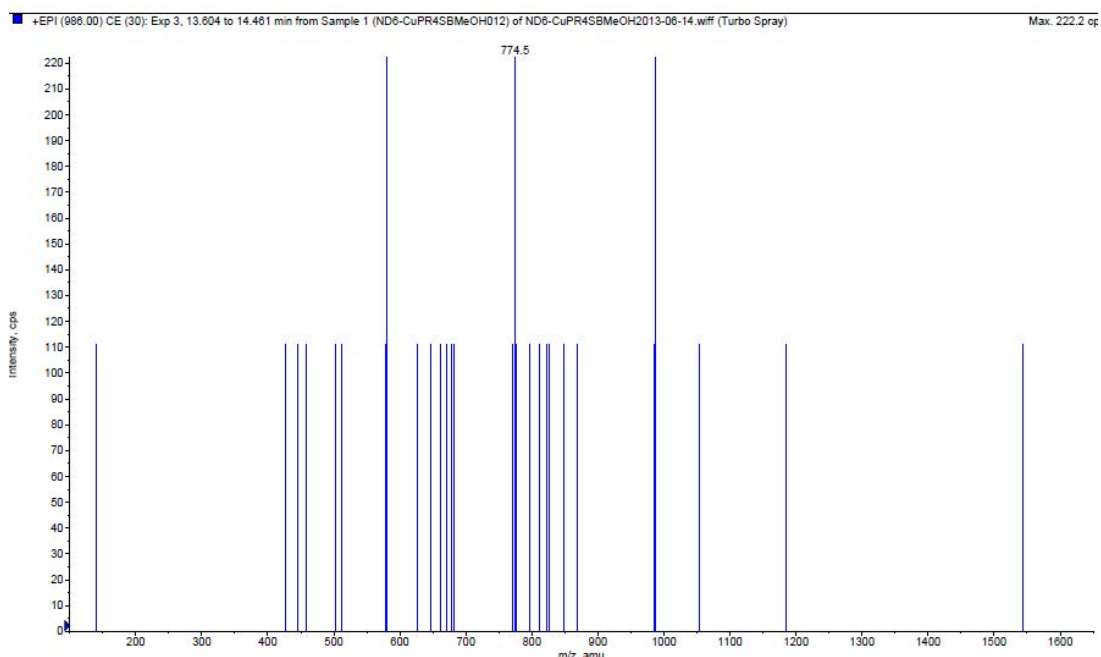


Figure B67. LC-MS (EPI) spectrum of $\text{Cu}(\text{R4-SB4CB})_2$ at 14.0 min

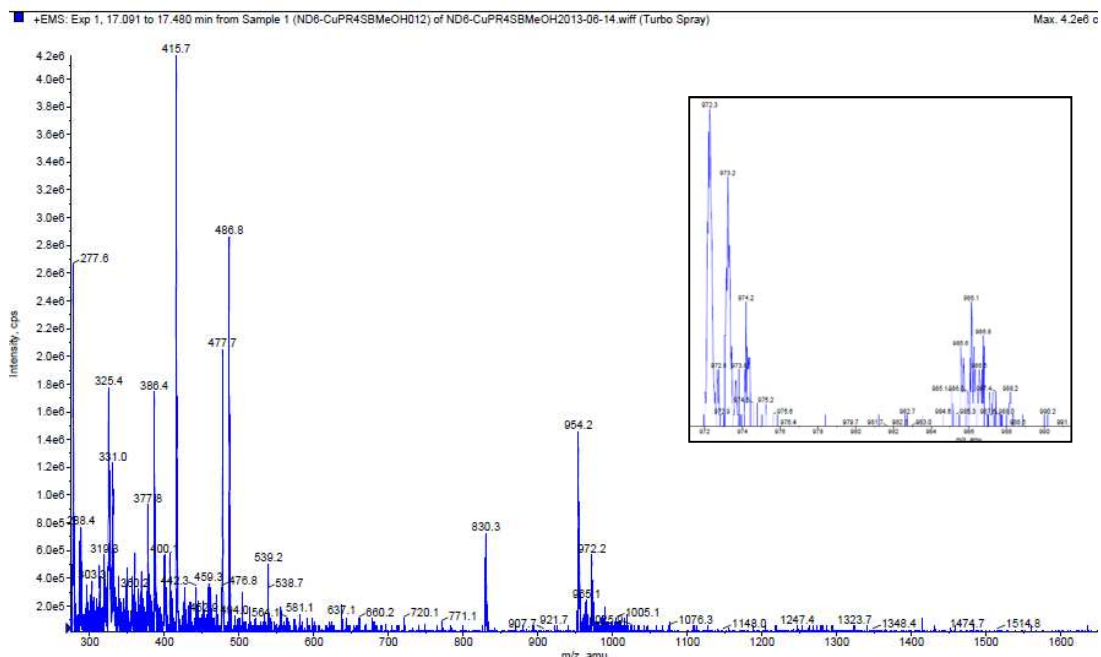


Figure B68. LC-MS [EMS and ER (inset)] spectra of $\text{Cu}(\text{R4-SB4CB})_2$ at 17.3 min

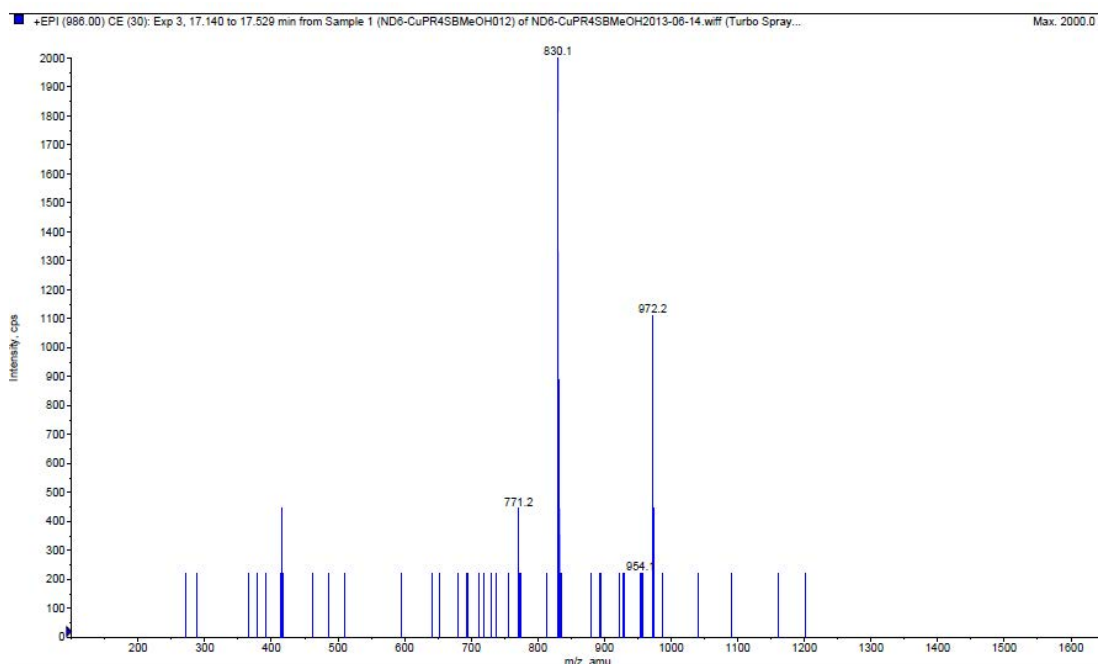


Figure B69. LC-MS (EPI) spectrum of $\text{Cu}(\text{R4-SB4CB})_2$ at 17.3 min

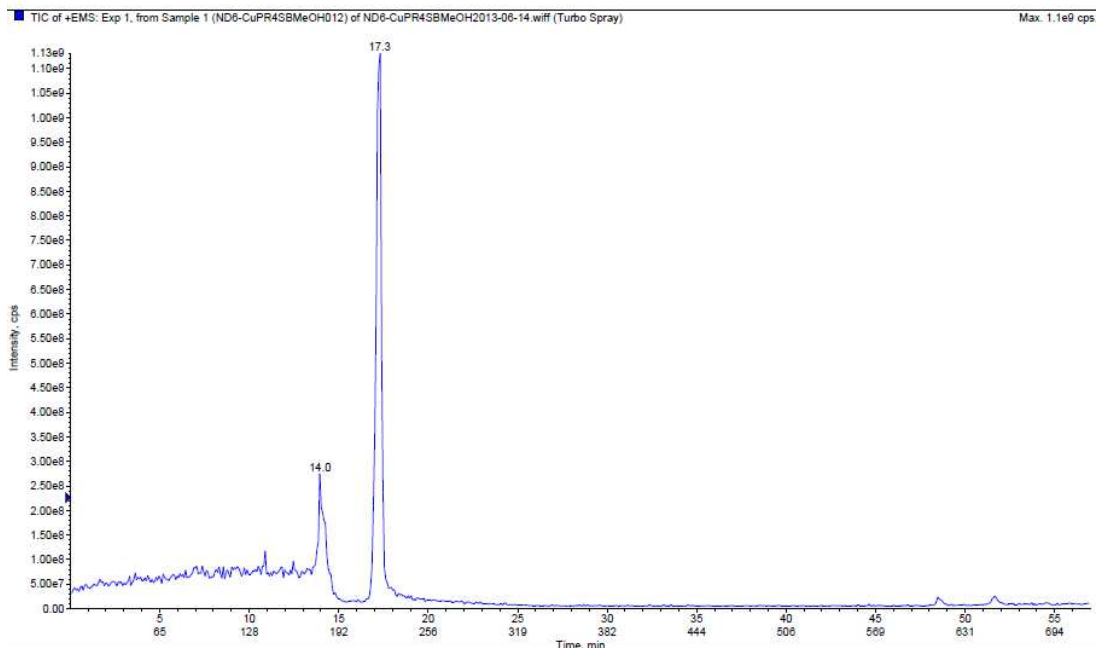


Figure B70. TIC (EMS) chromatogram of Cu(R4-SB4CB)₂

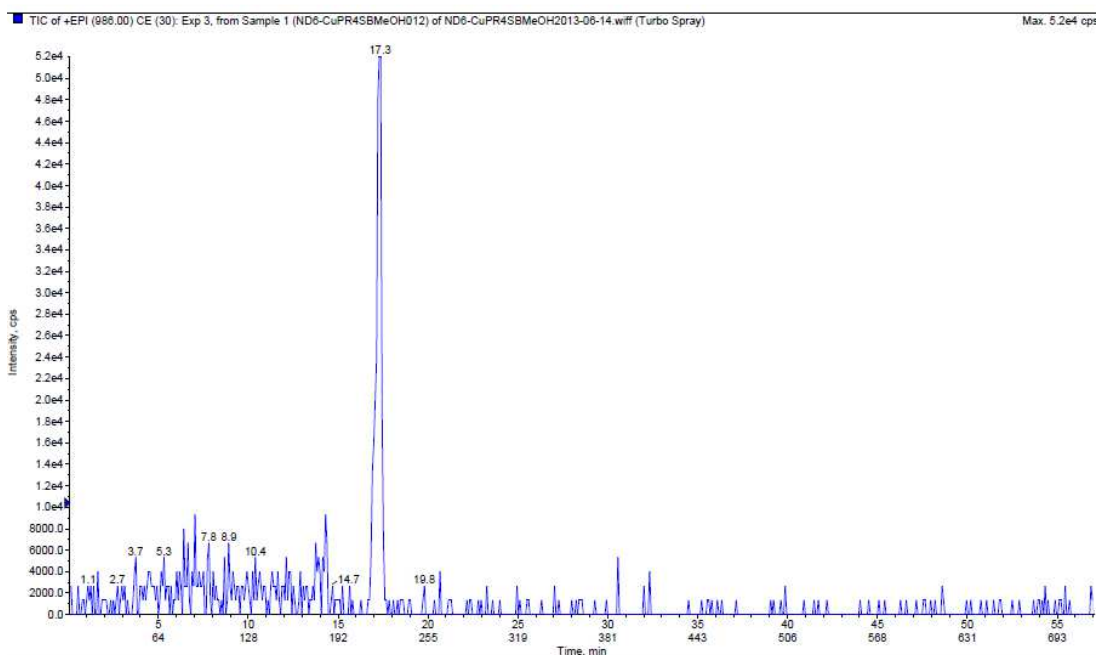


Figure B71. TIC (EPI) chromatogram of Cu(R4-SB4CB)₂

C. UV-Vis spectra

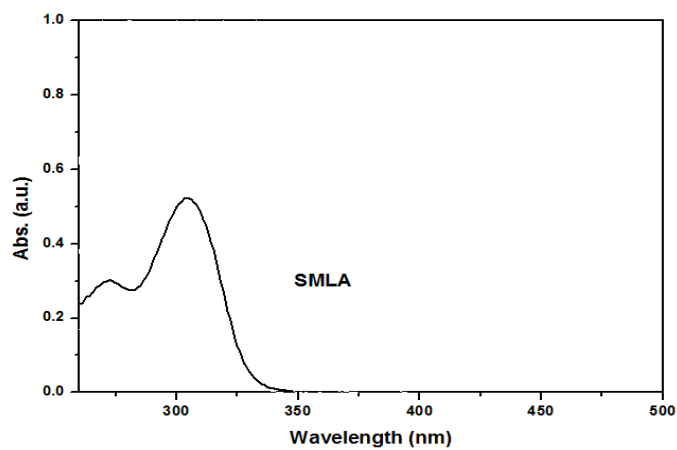


Figure C1. UV-Vis spectrum of SMLA at 25 μM

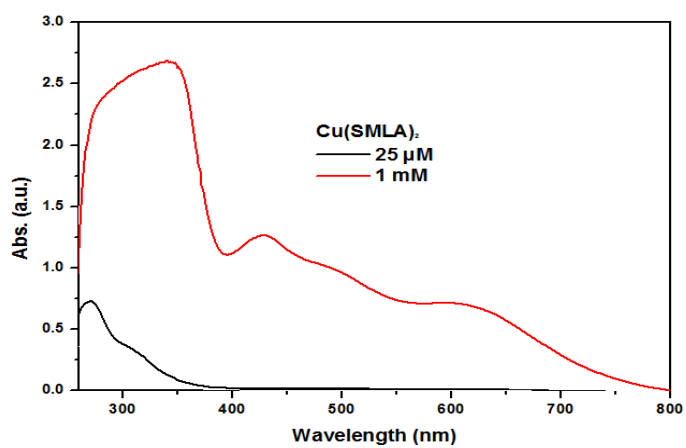


Figure C2. UV-Vis spectrum of Cu(SMLA)₂ at 25 μM and 1 mM

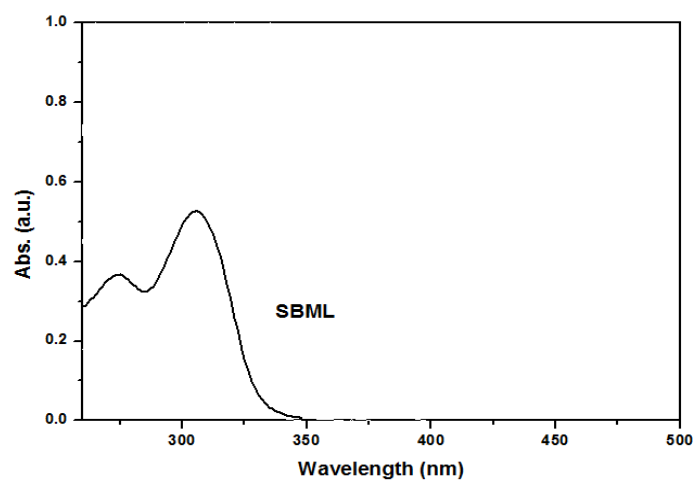


Figure C3. UV-Vis spectrum of SBML at 25 μM

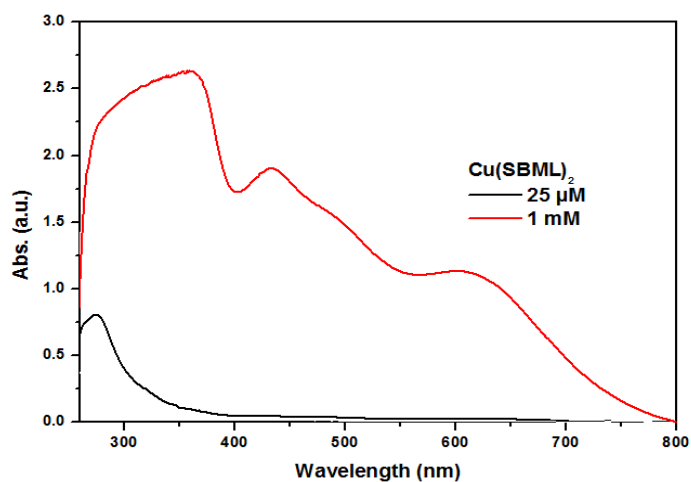


Figure C4. UV-Vis spectrum of Cu(SBML)₂ at 25 μM and 1 mM

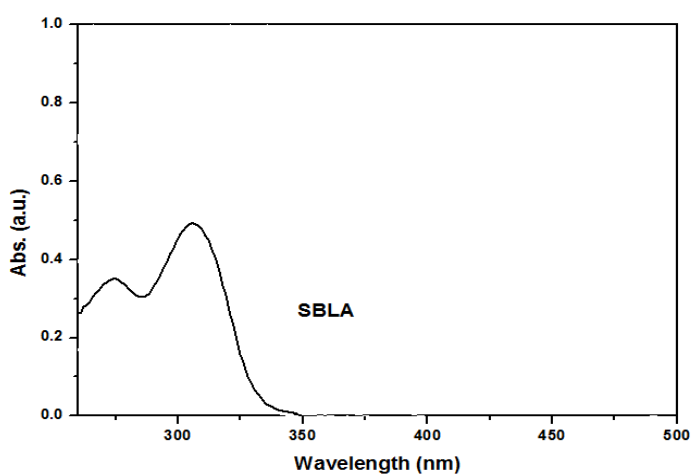


Figure C5. UV-Vis spectrum of SBLA at 25 μM

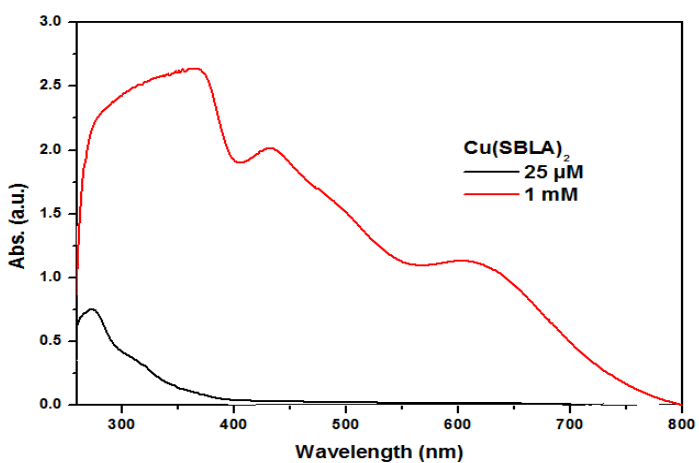


Figure C6. UV-Vis spectrum of Cu(SBLA)₂ at 25 μM and 1 mM

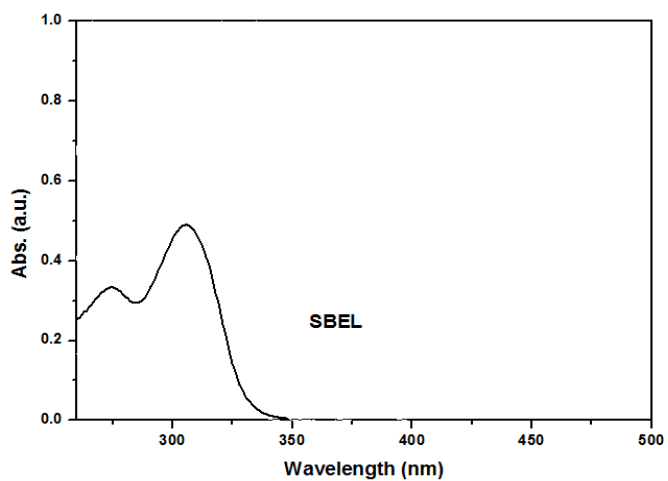


Figure C7. UV-Vis spectrum of SBEL at 25 μM

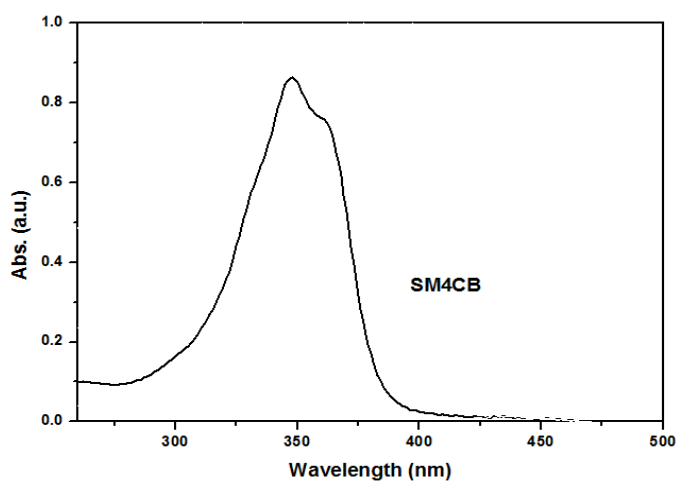


Figure C8. UV-Vis spectrum of SM4CB at 25 μM

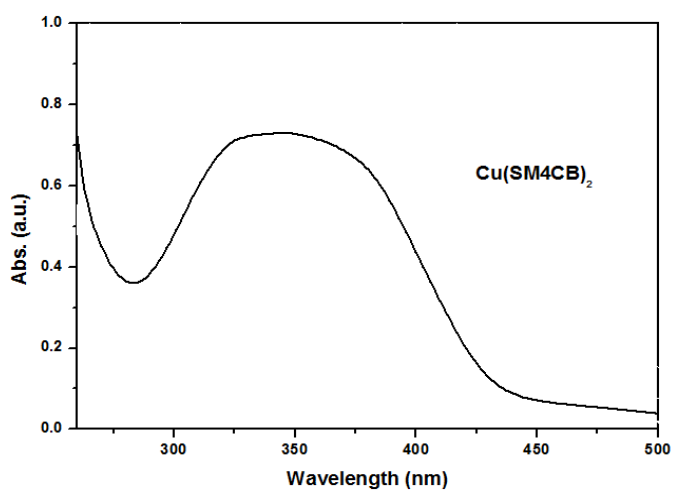


Figure C9. UV-Vis spectrum of $\text{Cu}(\text{SM4CB})_2$ at 25 μM

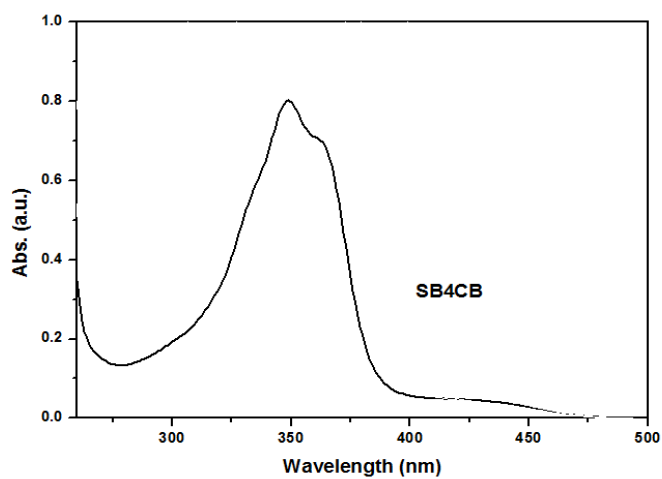


Figure C10. UV-Vis spectrum of SB4CB at 25 μ M

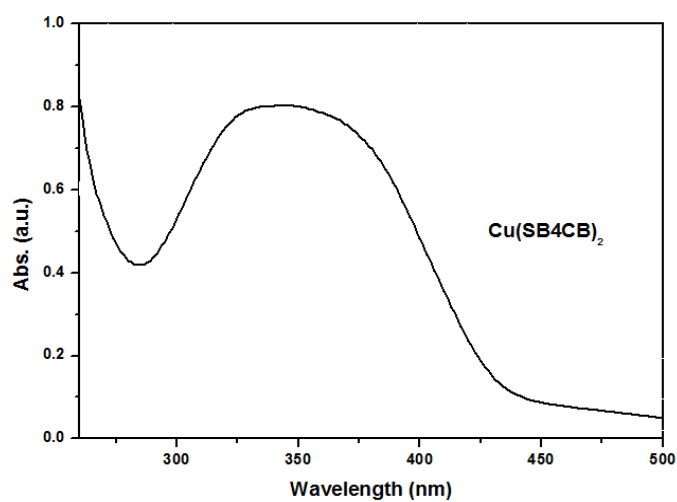


Figure C11. UV-Vis spectrum of Cu(SB4CB)₂ at 25 μ M

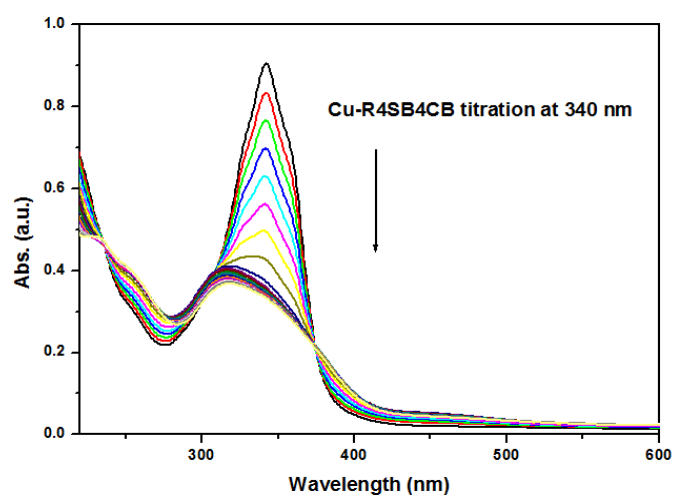


Figure C12. UV-Vis titration of Cu-R4SB4CB

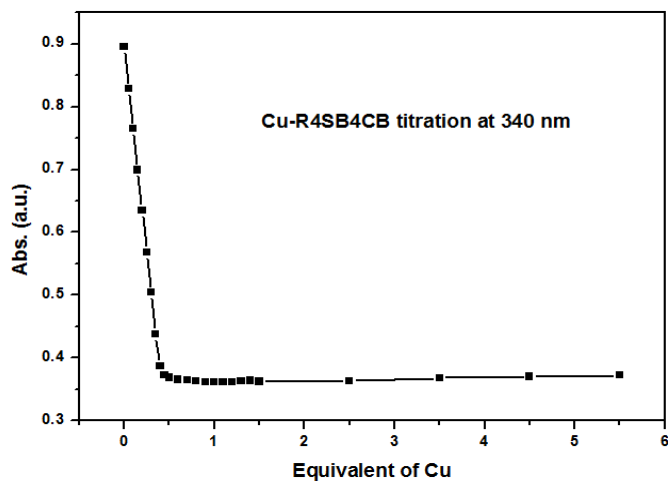


Figure C13. Plot of absorbance against equivalent of Cu for UV-Vis titration of Cu-R4SB4CB

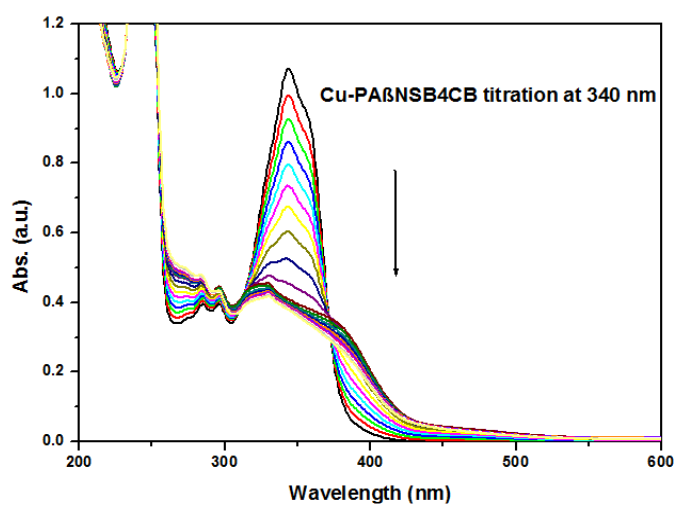


Figure C14. UV-Vis titration of Cu-PABNSB4CB

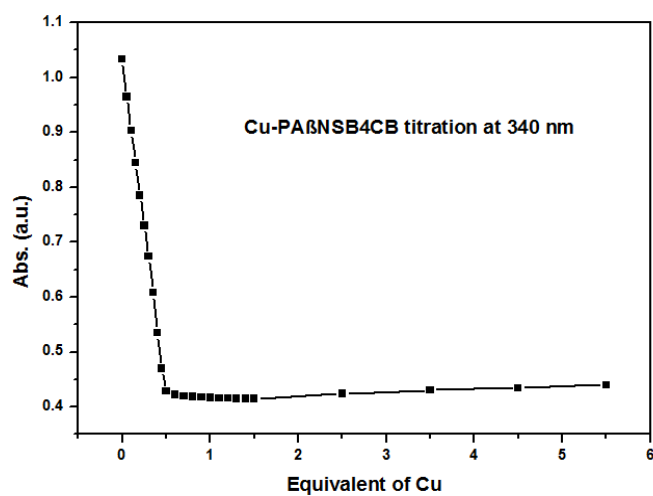


Figure C15. Plot of absorbance against equivalent of Cu for UV-Vis titration of Cu-PABNSB4CB

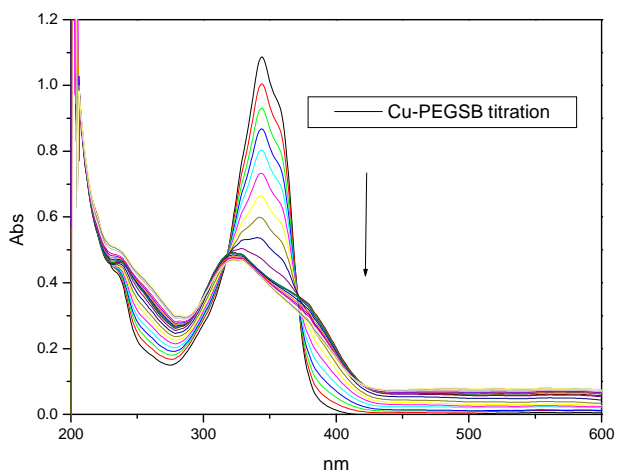


Figure C16. UV-Vis titration of Cu-PEGSB4CB

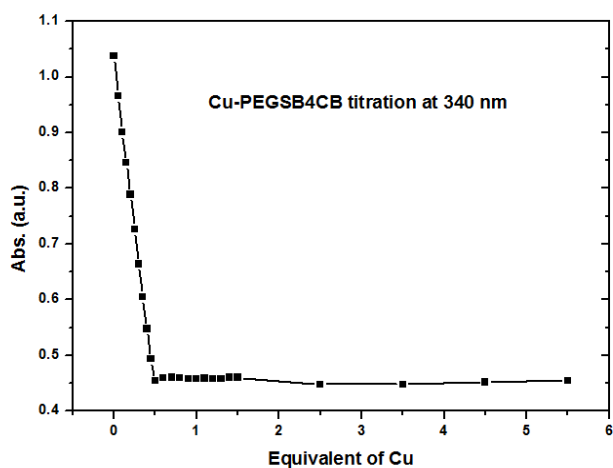


Figure C17. Plot of absorbance against equivalent of Cu for UV-Vis titration of Cu-PEGSB4CB

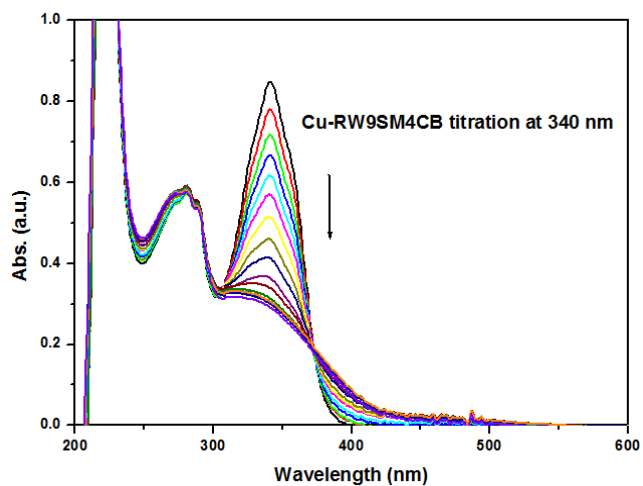


Figure C18. UV-Vis titration of Cu-RW9SM4CB

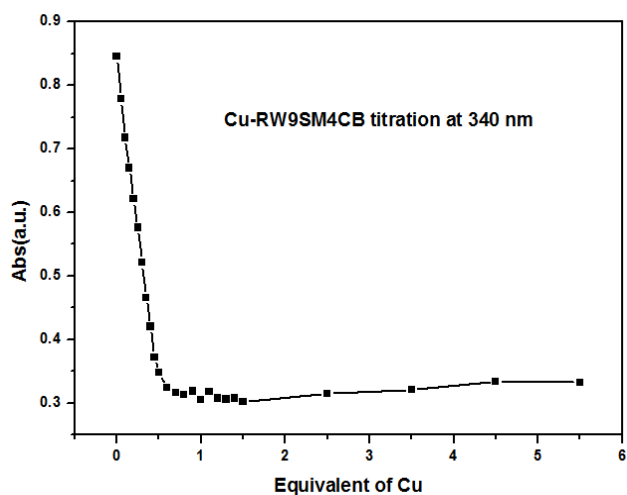


Figure C19. Plot of absorbance against equivalent of Cu for UV-Vis titration of Cu-RW9SM4CB

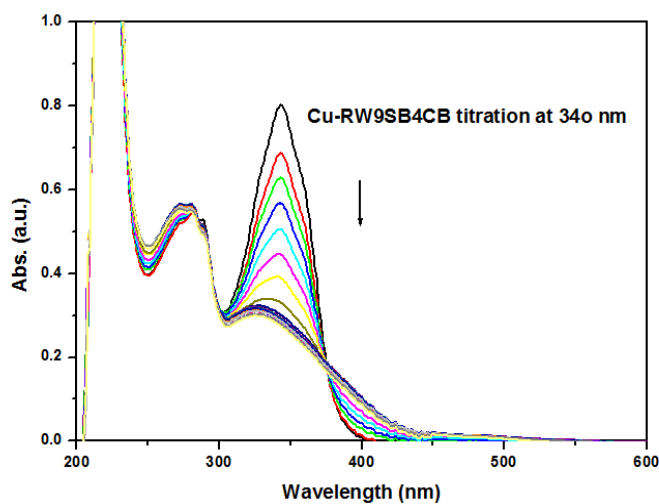


Figure C20. UV-Vis titration of Cu- RW9SB4CB

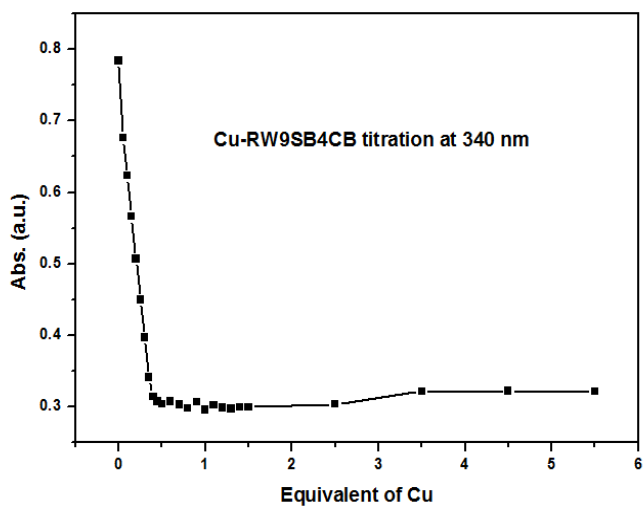


Figure C21. Plot of absorbance against equivalent of Cu for UV-Vis titration of Cu-RW9SB4CB

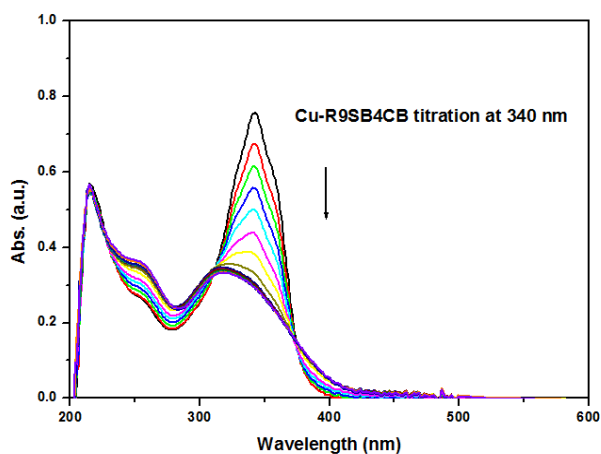


Figure C22. UV-Vis titration of Cu-R9SB4CB

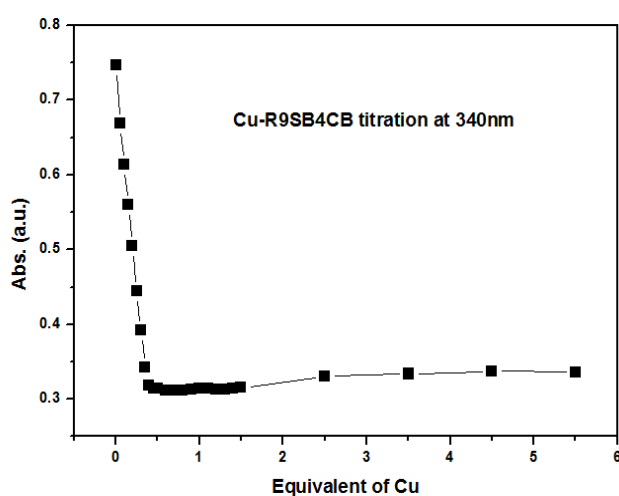


Figure C23. Plot of absorbance against equivalent of Cu for UV-Vis titration of Cu-R9SB4CB

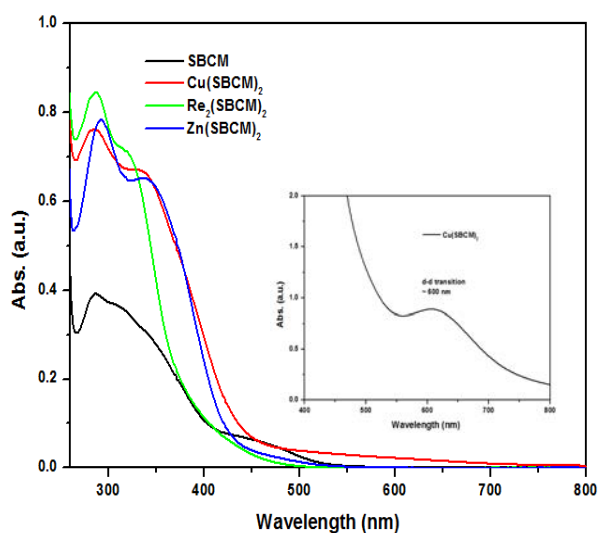


Figure C24. UV-vis spectra of SBCM, $\text{Cu}(\text{SBCM})_2$, $\text{Zn}(\text{SBCM})_2$ and $\text{Re}_2(\text{SBCM})_2$ recorded at $25 \mu\text{M}$ in DMSO using a cell length of 1 cm. The insert shows the d-d band of the complex $\text{Cu}(\text{SBCM})_2$ at concentration of 1 mM.

D. FT-IR spectra

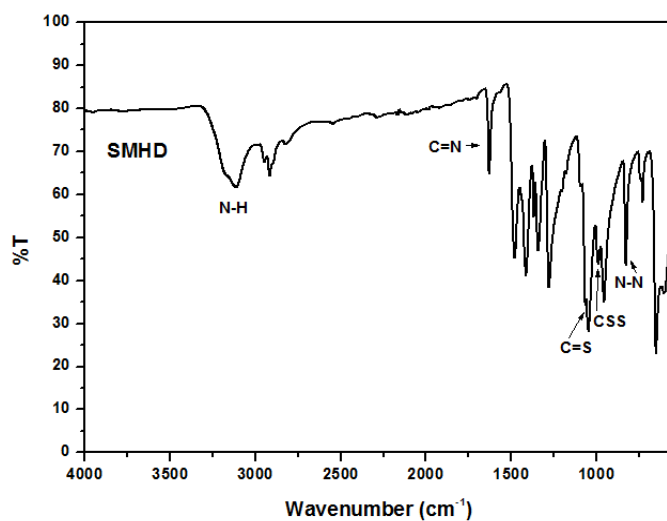


Figure D1. FT-IR spectrum of SMHD

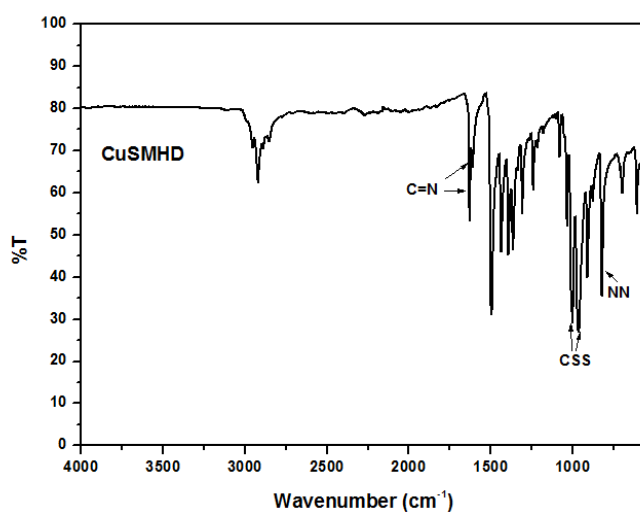


Figure D2. FT-IR spectrum of CuSMHD

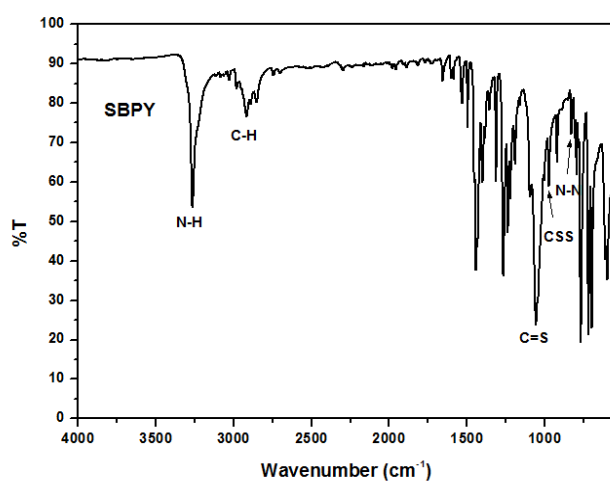


Figure D3. FT-IR spectrum of SBPY

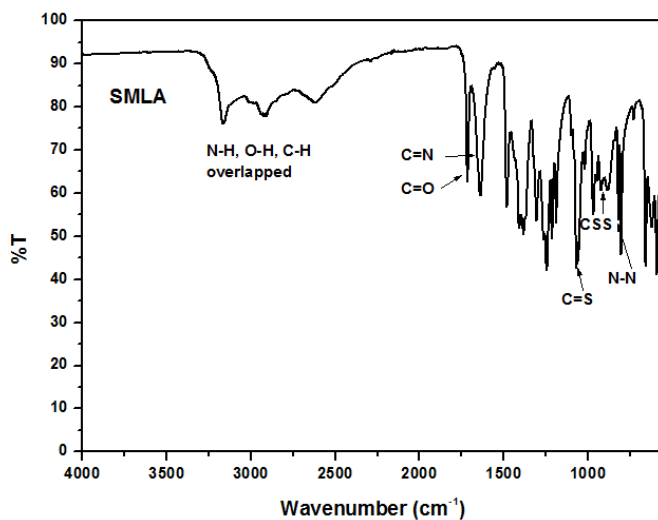


Figure D4. FT-IR spectrum of SMLA

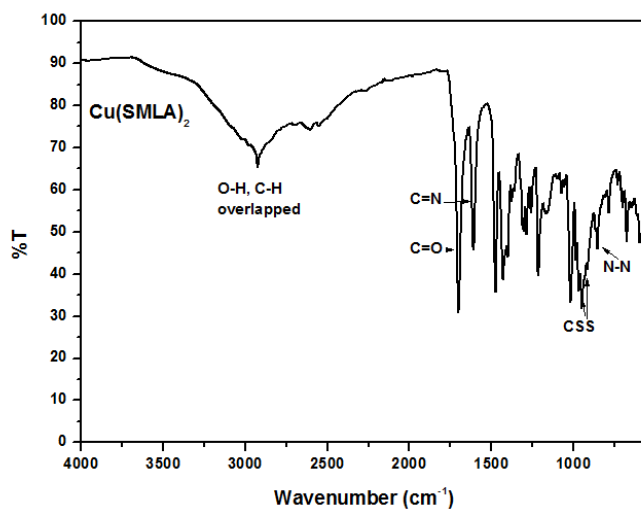


Figure D5. FT-IR spectrum of Cu(SMLA)₂

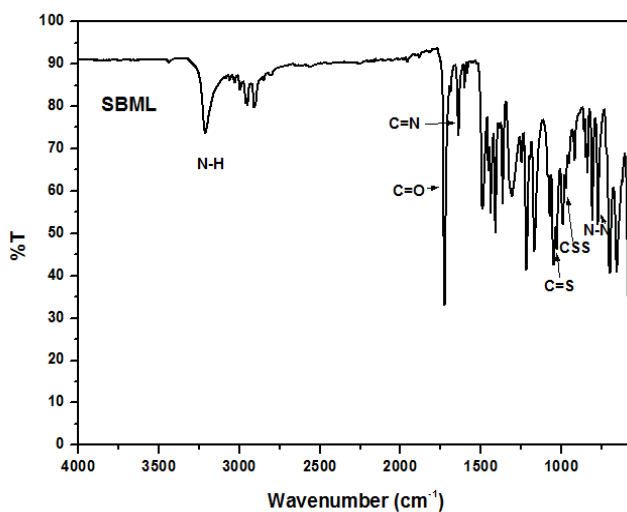


Figure D6. FT-IR spectrum of SBML

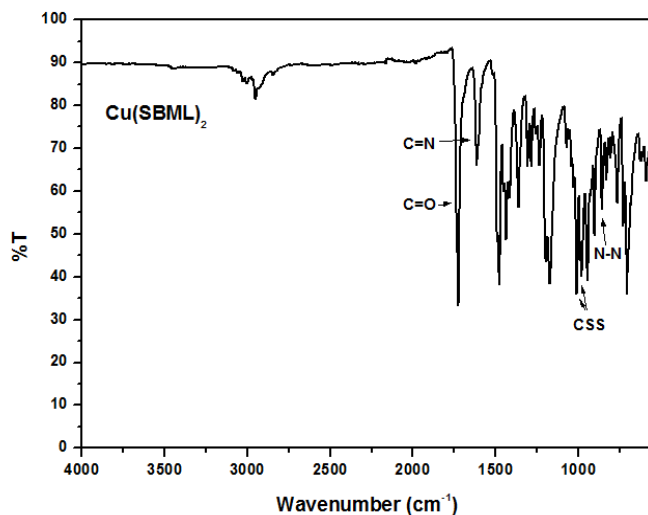


Figure D7. FT-IR spectrum of Cu(SBML)_2

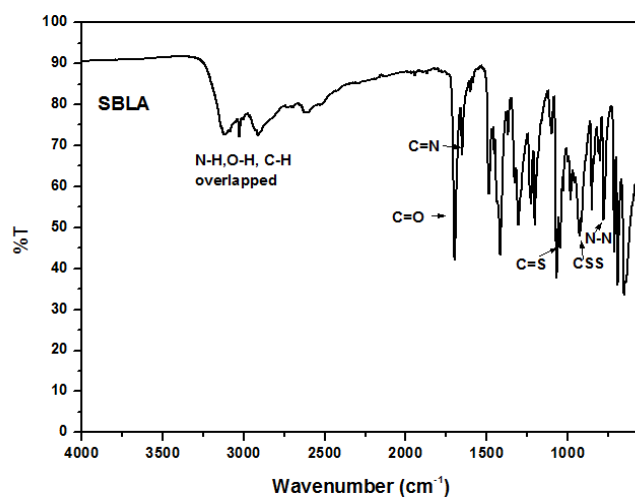


Figure D8. FT-IR spectrum of SBLA

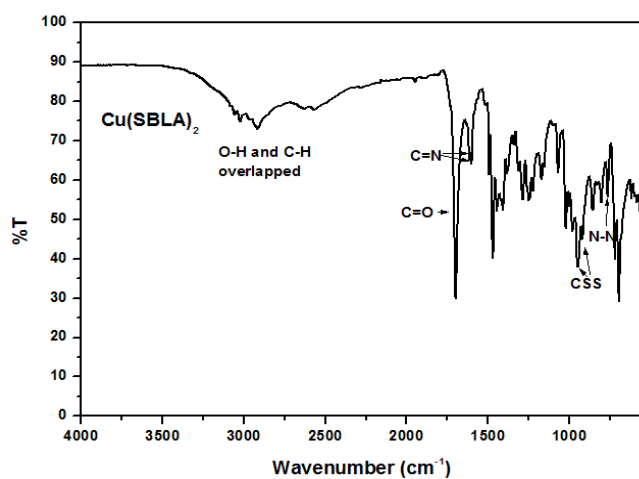


Figure D9. FT-IR spectrum of Cu(SBLA)_2

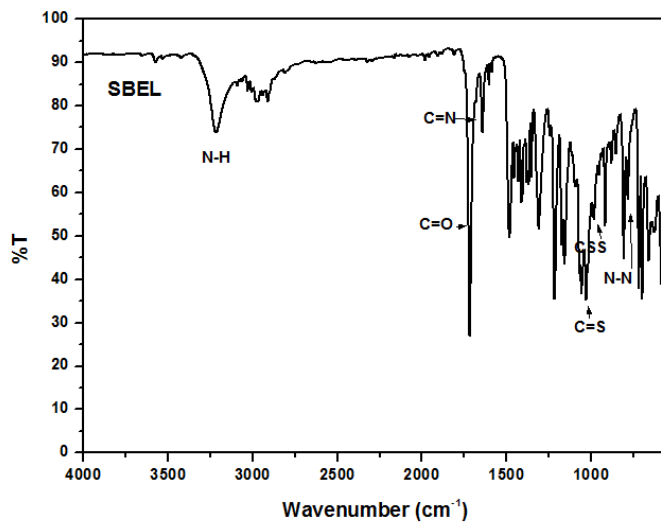


Figure D10. FT-IR spectrum of SBEL

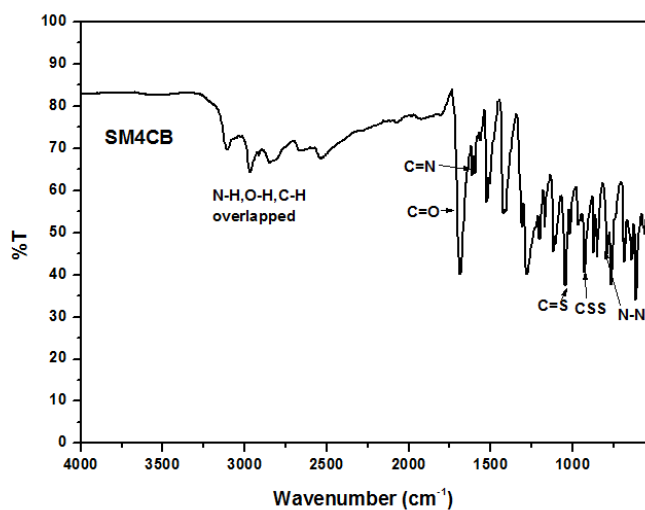


Figure D11. FT-IR spectrum of SM4CB

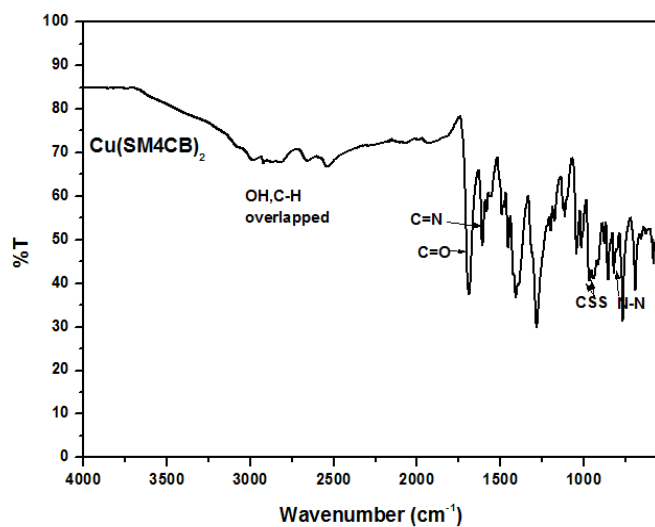


Figure D12. FT-IR spectrum of Cu(SM4CB)₂

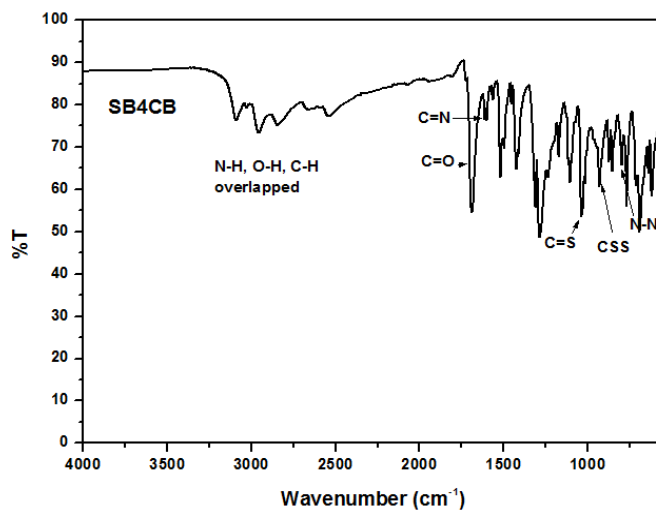


Figure D13. FT-IR spectrum of SB4CB

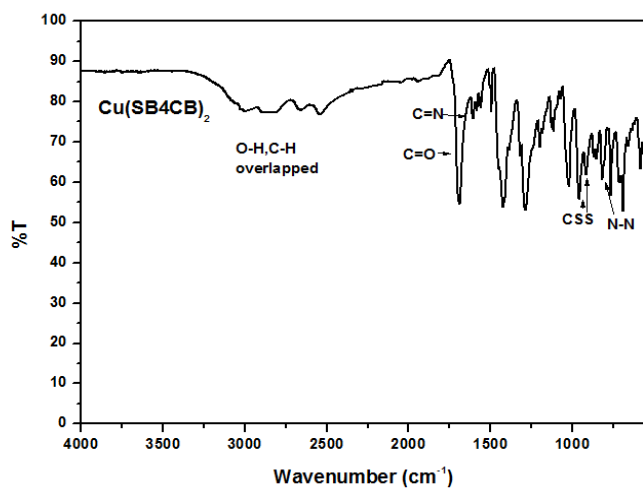


Figure D14. FT-IR spectrum of CuS(SB4CB)₂

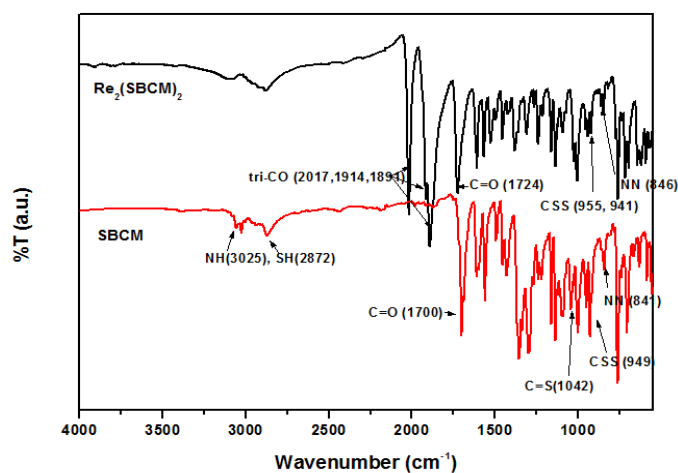


Figure D15. FT-IR spectrum of Re₂(SBCM)₂ and SBCM

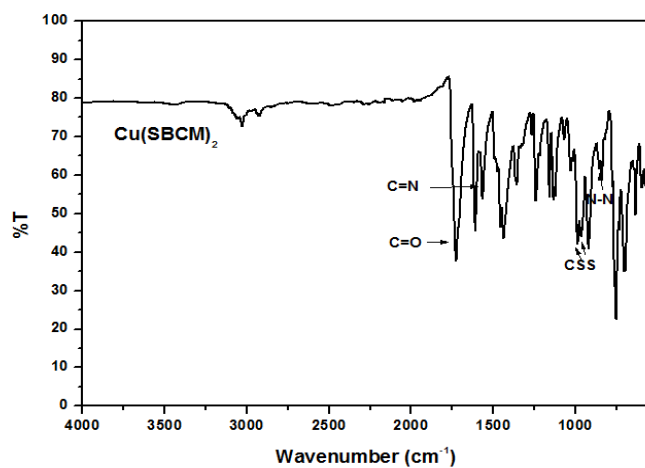


Figure D16. FT-IR spectrum of Cu(SBCM)₂

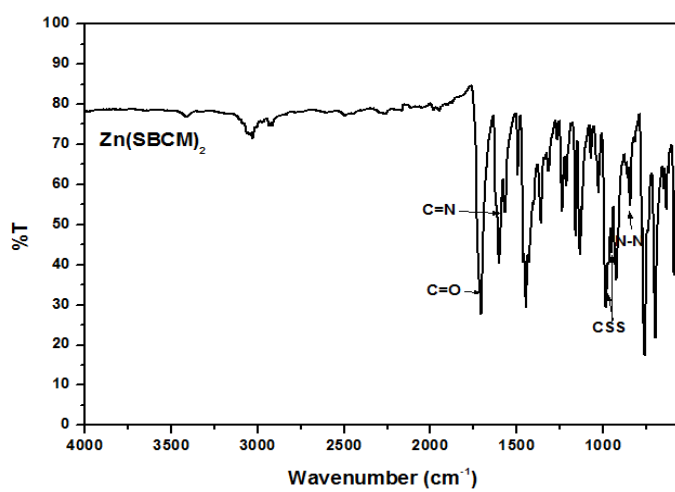


Figure D17. FT-IR spectrum of Zn(SBCM)₂

E. Crystal structures parameters

Table E1: Crystallographic data and structure refinement details for compounds SBPY, SMHD, CuSMHD and CuSBHD.

Compounds	SBPY	SMHD	CuSMHD	CuSBHD
CCDC	930513			
Formula	C ₁₄ H ₁₆ N ₂ S ₂	C ₁₀ H ₁₈ N ₄ S	C ₁₀ H ₁₆ CuN ₄ S ₄	C ₂₂ H ₂₄ CuN ₄ S ₄
M _r	276.41	322.54	384.07	536.27
Crystal size, mm ³	0.21 x 0.20 x 0.04	0.24 × 0.06 × 0.03	0.4×0.12×0.18	0.28 × 0.22 × 0.11
Crystal system	monoclinic	triclinic	monoclinic	monoclinic
Space group	<i>P</i> 2 ₁ / <i>c</i>	<i>P</i> 1	<i>C</i> 2/ <i>c</i>	<i>P</i> 2 ₁ / <i>c</i>
a, Å	9.2991(4)	5.1646 (5)	24.6441 (8)	10.79369 (13)
b, Å	15.9635(8)	7.2792 (8)	7.9100 (2)	18.8337 (2)
c, Å	9.4848(5)	10.7840 (12)	16.8972 (6)	11.84121 (15)
α, °	90	100.65 (1)	90	90
β, °	96.1550(10)	90.751 (9)	111.167(4)	103.4104(13)
γ, °	90	107.305 (10)	90	90
Cell volume, Å ³	1399.87(12)	379.39 (8)	3071.62 (19)	2341.51 (5)
Z	4	1	8	4
T, K	100	150	150	150
F ₀₀₀	584	170	1576	1108
μ, mm ⁻¹	0.364	5.662	1.956	1.308
θ range, °	2.51 – 32.16	4.18-71.56	2.55-28.96	2.22-28.98
Reflection collected	22 601	4869	19393	59768
Reflections unique	4 867	1455	3704	5779
R _{int}	0.0431	0.042	0.029	0.033
GOF	1.175	1.0039	0.9869	0.9773
Refl. obs. (I>2σ(I))	4 092	1209	3483	5129
Parameters	165	82	172	280

R, wR (all data)	0.0733,0.1273	0.0552, 0.1208	0.0217, 0.0498	0.0338,0.0736
Final R, wR ($I > 2\sigma(I)$)	0.0603,0.1217	0.0457, 0.1126	0.0198, 0.0488	0.0287, 0.0698
Largest diff. peak and hole ($e \cdot \text{\AA}^{-3}$)	-0.344; 0.536	-0.35; 0.52	-0.34; 0.36	-0.56; 0.72

Table E2: Crystallographic data and structure refinement details for compounds for compounds SMML, SBML and SBEL.

Compound	SMML	SBML	SBEL
CCDC	CCDC 999789	CCDC 999788	CCDC 999786
Empirical Formula	C ₈ H ₁₄ N ₂ O ₂ S ₂	C ₁₄ H ₁₈ N ₂ O ₂ S ₂	C ₁₅ H ₂₀ N ₂ O ₂ S ₂
<i>M_r</i>	234.33	310.42	324.45
Crystal size, mm ³	0.31 x 0.30 x 0.28	0.33 x 0.31 x 0.19	0.31 x 0.29 x 0.22
Crystal system	monoclinic	monoclinic	monoclinic
Space group	<i>P</i> 2 ₁ / <i>c</i>	<i>P</i> 2 ₁ / <i>n</i>	<i>P</i> 2 ₁ / <i>n</i>
<i>a</i> , Å	8.1149(2)	12.7266(4)	12.7529(5)
<i>b</i> , Å	13.0536(3)	7.2329(2)	7.4369(3)
<i>c</i> , Å	11.0433(3)	16.7849(5)	17.3690(7)
α , °	90	90	90
β , °	105.4960(10)	97.5740(10)	97.5530(10)
γ , °	90	90	90
Cell volume, Å ³	1127.28(5)	1531.57(8)	1633.02(11)
Z ; Z'	4 ; 1	4 ; 1	4 ; 1
T, K	100(1)	100(1)	100(1)
F ₀₀₀	496	656	688
μ , mm ⁻¹	0.450	0.350	0.331
θ range, °	2.47 – 36.41	1.89 – 33.74	1.87 – 36.30
Reflection collected	36 241	16 603	21 234
Reflections unique	5 508	4 539	6 657
R _{int}	0.0213	0.0429	0.0315
GOF	1.090	1.041	1.046
Refl. obs. (<i>I</i> > 2 σ (<i>I</i>))	5 091	4 102	5 868
Parameters	130	183	192
wR ₂ (all data)	0.0811	0.0978	0.0905
R value (<i>I</i> > 2 σ (<i>I</i>))	0.0674	0.0352	0.0319
Largest diff. peak and hole (e ⁻ ·Å ⁻³)	-0.386 ; 0.423	-0.406 ; 0.632	-0.380 ; 0.473

Table E3: Crystallographic data and structure refinement details for compounds for compounds SBLA, Cu(SMML)₂ and Cu(SMLA)₂.

Compound	SBLA	Cu(SMML) ₂	Cu(SMLA) ₂
CCDC	CCDC 999787	CCDC 999785	CCDC 999784
Empirical Formula	C ₁₃ H ₁₆ N ₂ O ₂ S ₂	C ₁₆ H ₂₆ Cu N ₄ O ₄ S ₄	C ₁₅ H ₂₆ Cu N ₄ O ₅ S ₄
<i>M_r</i>	296.40	530.19	534.18
Crystal size, mm ³	0.13 x 0.10 x 0.02	0.16 x 0.11 x 0.07	0.18 x 0.14 x 0.08
Crystal system	triclinic	monoclinic	monoclinic
Space group	<i>P</i> -1	<i>C</i> 2/ <i>c</i>	<i>P</i> 2 ₁ / <i>n</i>
a, Å	6.708(3)	12.9400(3)	11.8086(6)
b, Å	10.448(4)	12.4444(3)	9.1068(5)
c, Å	11.565(5)	13.8556(3)	21.0888(11)
α, °	76.170(9)	90	90
β, °	87.778(9)	91.4150(10)	97.626(2)
γ, °	71.867(10)	90	90
Cell volume, Å ³	747.4(5)	2230.49(9)	2247.8(2)
Z ; Z'	2 ; 1	4 ; ½	4 ; 1
T, K	100(1)	100(1)	100(1)
F ₀₀₀	312	1100	1108
μ, mm ⁻¹	0.355	1.384	1.377
θ range, °	1.81 – 30.05	2.27 – 36.33	1.88 – 30.63
Reflection collected	9 990	41 767	52 414
Reflections unique	3 748	5 390	6 889
R _{int}	0.0224	0.0401	0.0301
GOF	1.013	1.028	1.154
Refl. obs. (<i>I</i> > 2σ(<i>I</i>))	2 250	4 325	6 006
Parameters	174	135	270
wR ₂ (all data)	0.1732	0.0711	0.0855
R value (<i>I</i> > 2σ(<i>I</i>))	0.0617	0.0283	0.0342
Largest diff. peak and hole (e ⁻ ·Å ⁻³)	-0.642 ; 0.441	-0.380 ; 0.616	-0.428 ; 0.584

Table E4: Crystallographic data and structure refinement details for compounds for compounds $\text{Re}_2(\text{SBCM})_2$.

Compound	$\text{Re}_2(\text{SBCM})_2$
CCDC	1001600
Empirical Formula	$\text{C}_{44} \text{H}_{30} \text{N}_4 \text{O}_{10} \text{Re}_2 \text{S}_4$
M_r	1275.36
Crystal size, mm^3	0.19 x 0.14 x 0.03
Crystal system	monoclinic
Space group	$P 2_1/c$
a, Å	14.7072(4)
b, Å	12.6588(3)
c, Å	12.1386(3)
α , °	90
β , °	99.3740(10)
γ , °	90
Cell volume, Å ³	2229.73(10)
Z ; Z'	2 ; 1/2
T, K	100(1)
F_{000}	1232
μ , mm^{-1}	5.674
θ range, °	2.13 – 30.65
Reflection collected	54 115
Reflections unique	6 872
R_{int}	0.0446
GOF	1.028
Refl. obs. ($I > 2\sigma(I)$)	5 059
Parameters	290
w R_2 (all data)	0.0519
R value ($I > 2\sigma(I)$)	0.0225
Largest diff. peak and hole ($\text{e} \cdot \text{Å}^{-3}$)	-0.901 ; 1.625

F. RP-HPLC chromatograms

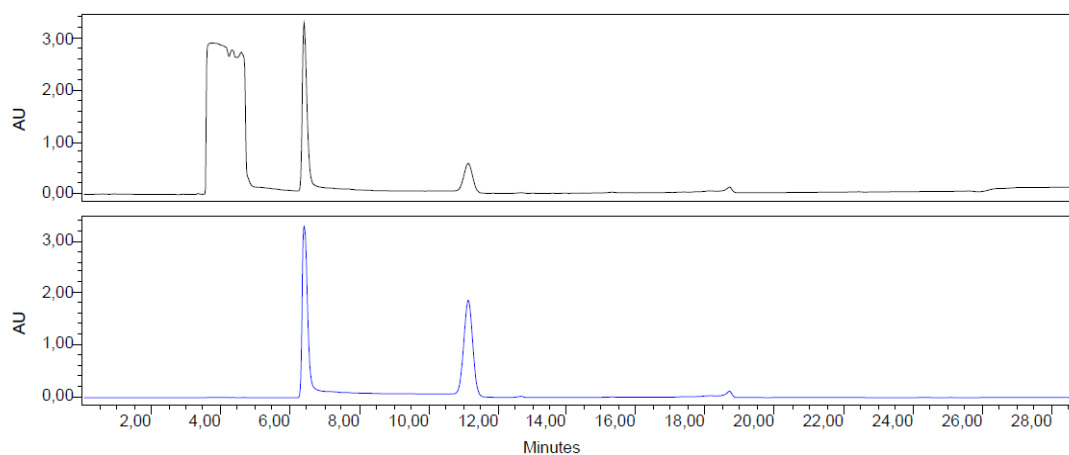


Figure F1. RP-HPLC chromatogram of SMHD

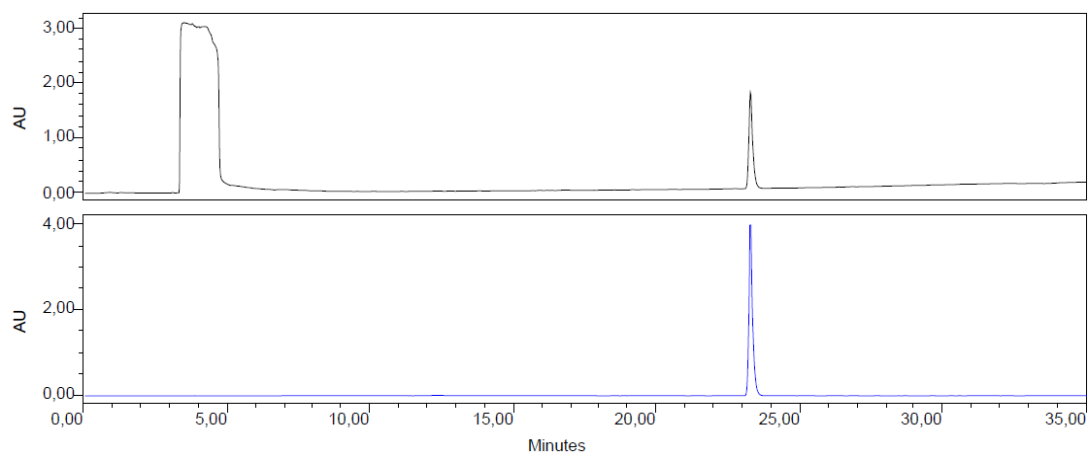


Figure F2. RP-HPLC chromatogram of CuSMHD

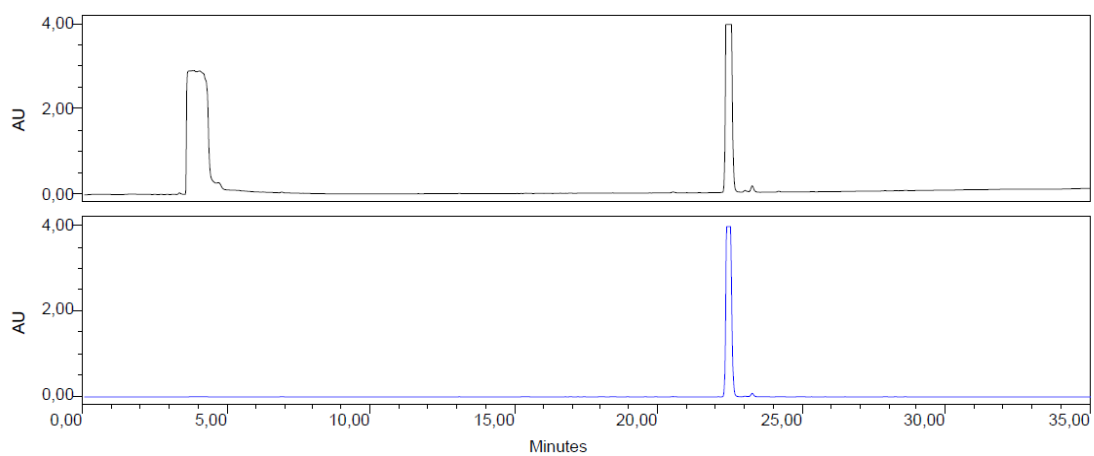


Figure F3. RP-HPLC chromatogram of SBPY

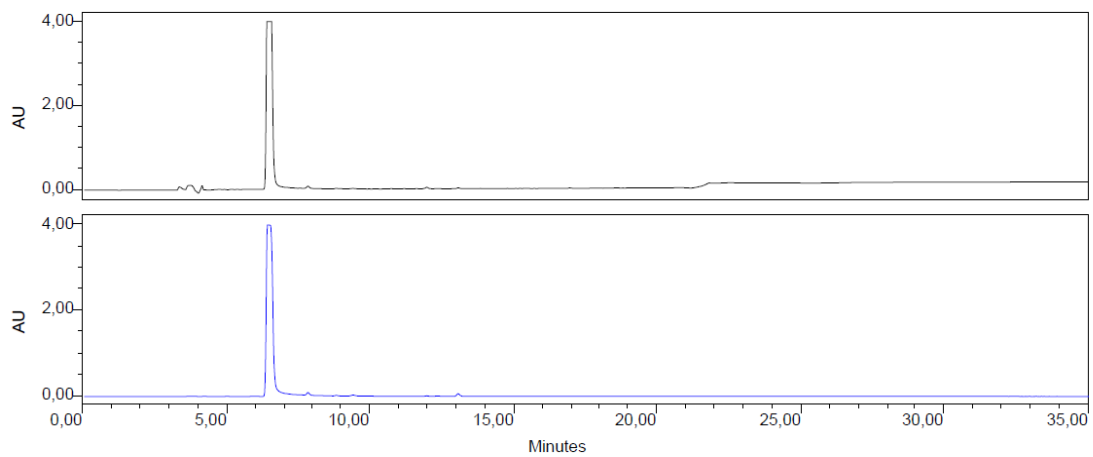


Figure F4. RP-HPLC chromatogram of SMDTC

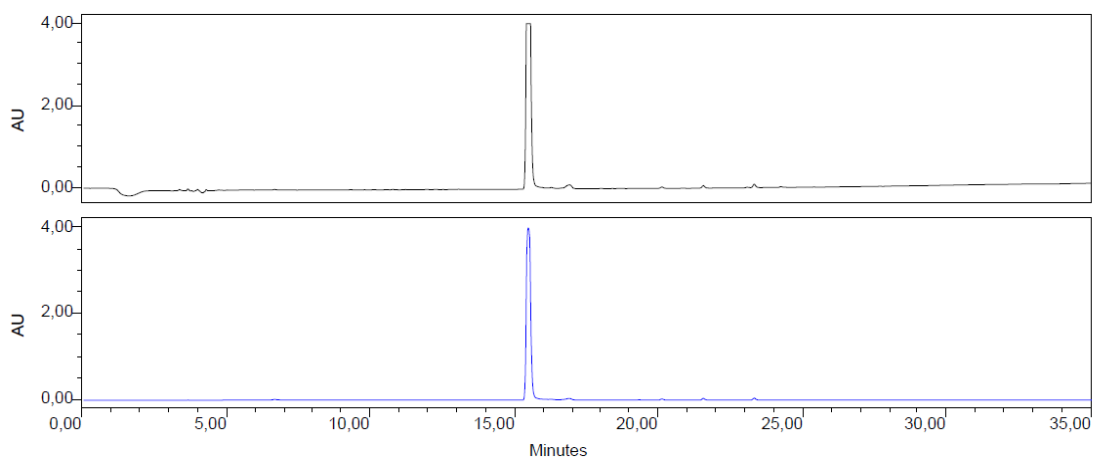


Figure F5. RP-HPLC chromatogram of SBDTC

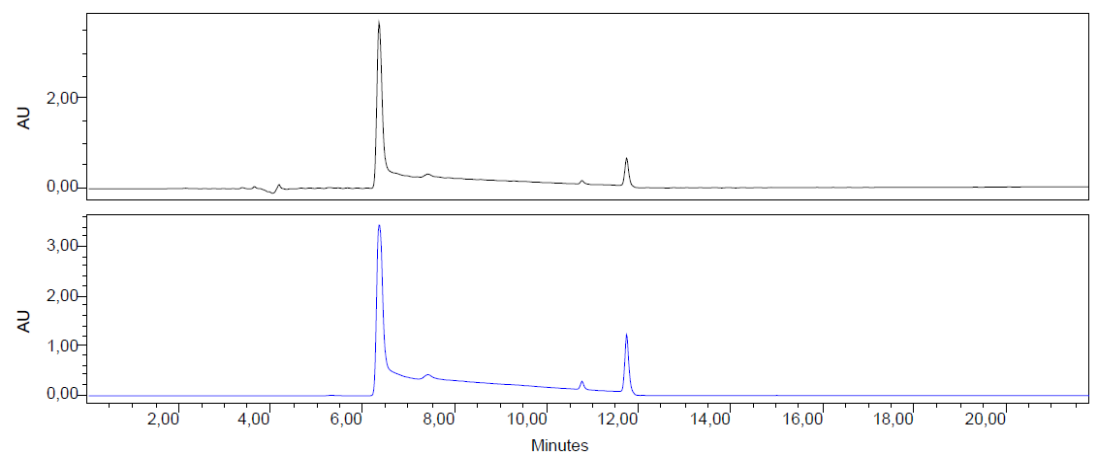


Figure F6. RP-HPLC chromatogram of SMLA

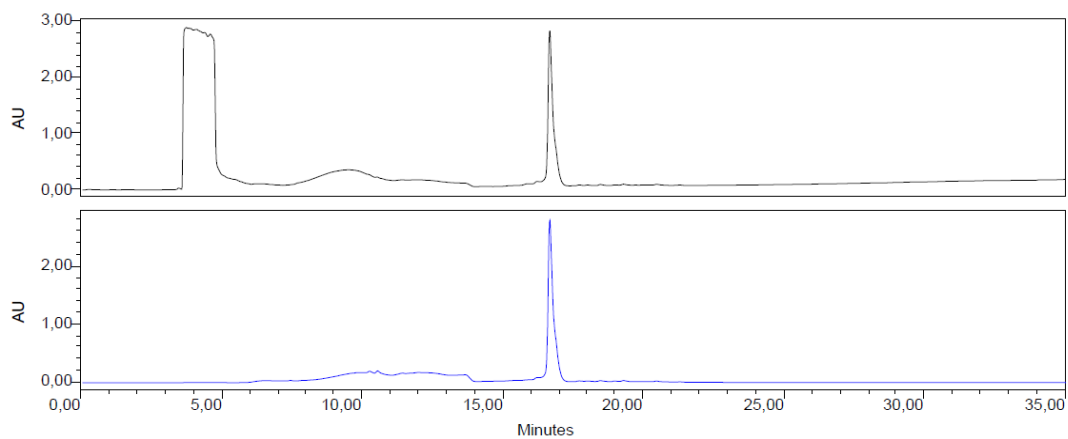


Figure F7. RP-HPLC chromatogram of Cu(SMLA)₂

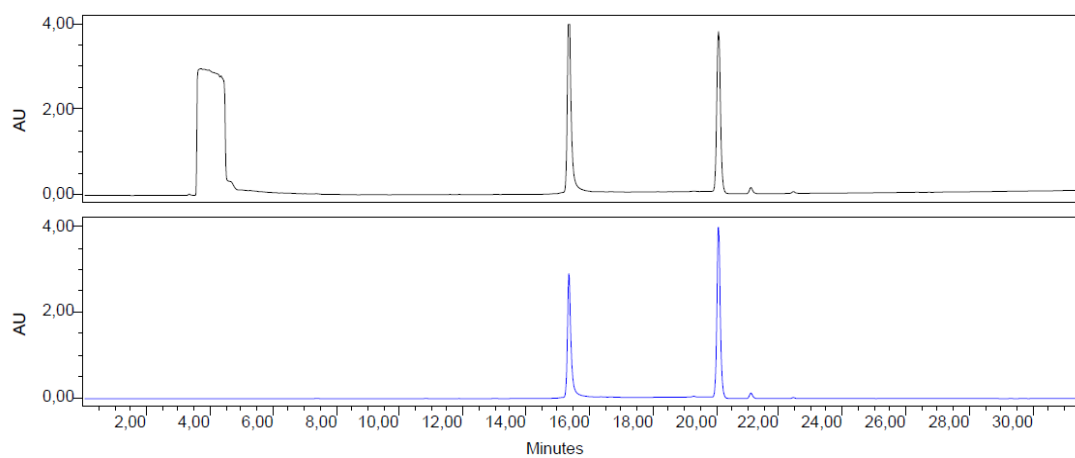


Figure F8. RP-HPLC chromatogram of SBML

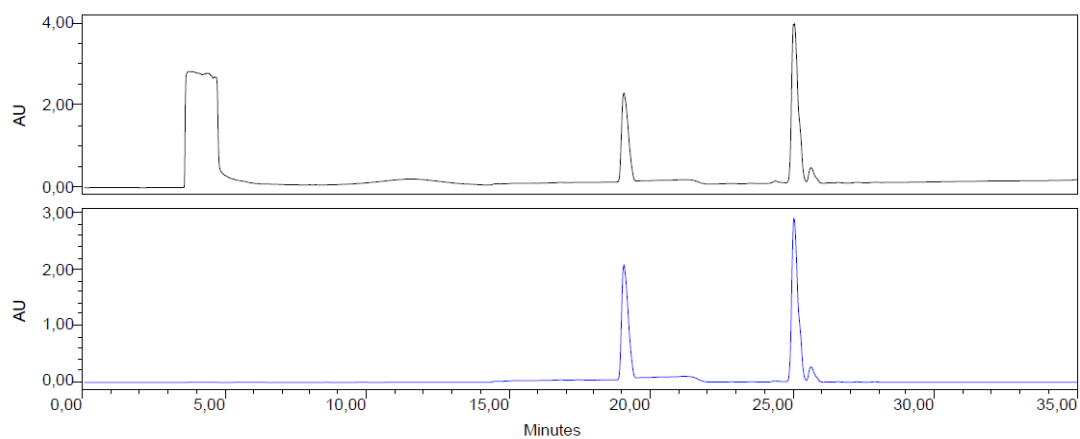


Figure F9. RP-HPLC chromatogram of Cu(SBML)₂

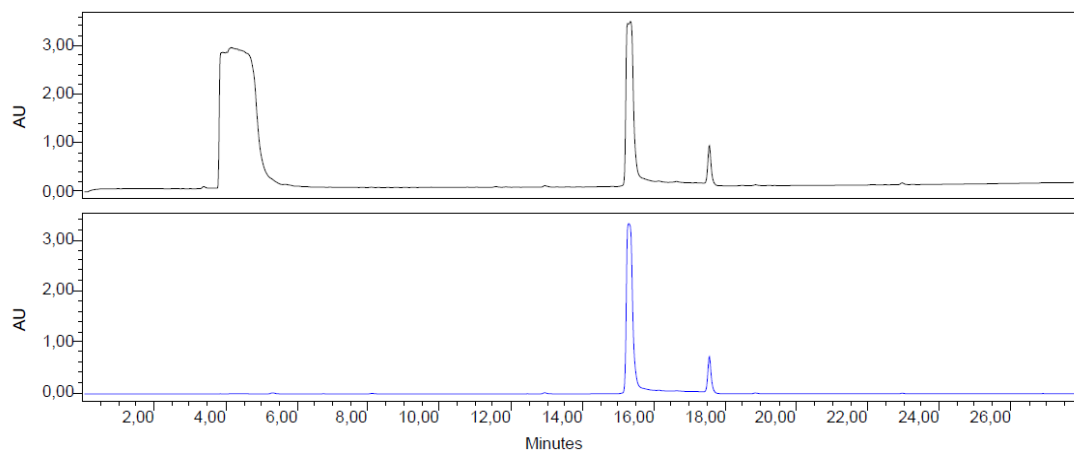


Figure F10. RP-HPLC chromatogram of SBLA

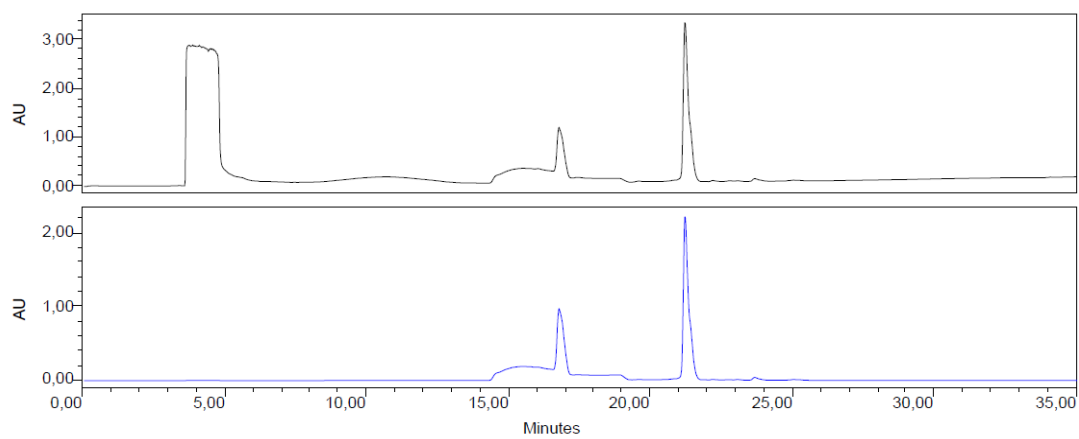


Figure F11. RP-HPLC chromatogram of Cu(SBLA)₂

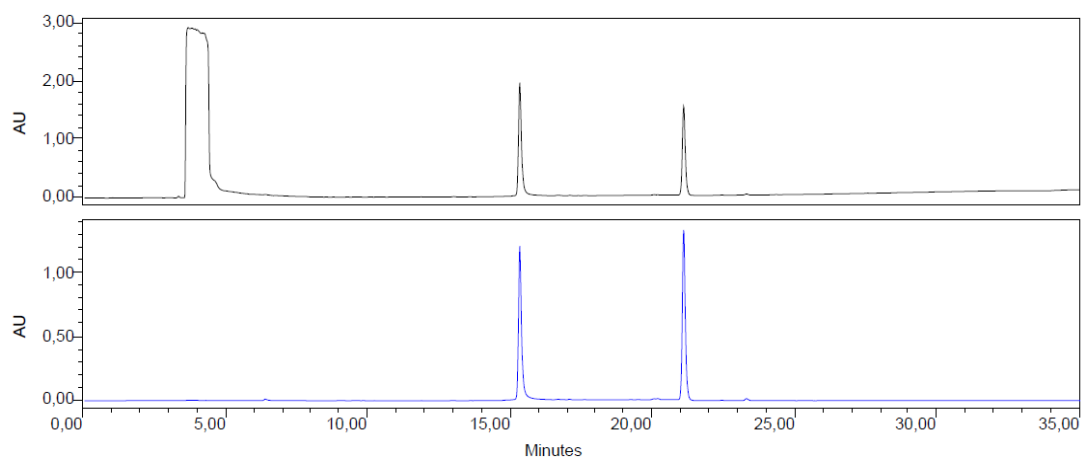


Figure F12. RP-HPLC chromatogram of SBEL

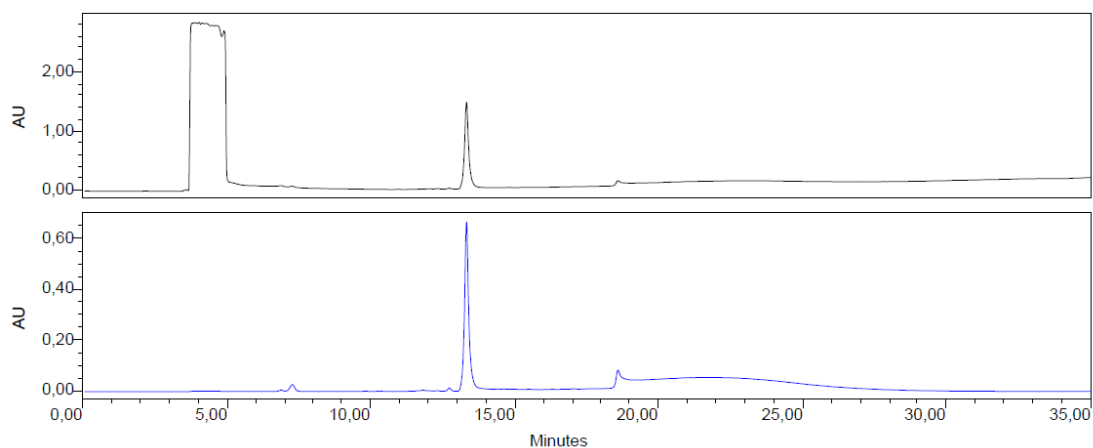


Figure F13. RP-HPLC chromatogram of CuSM4CB

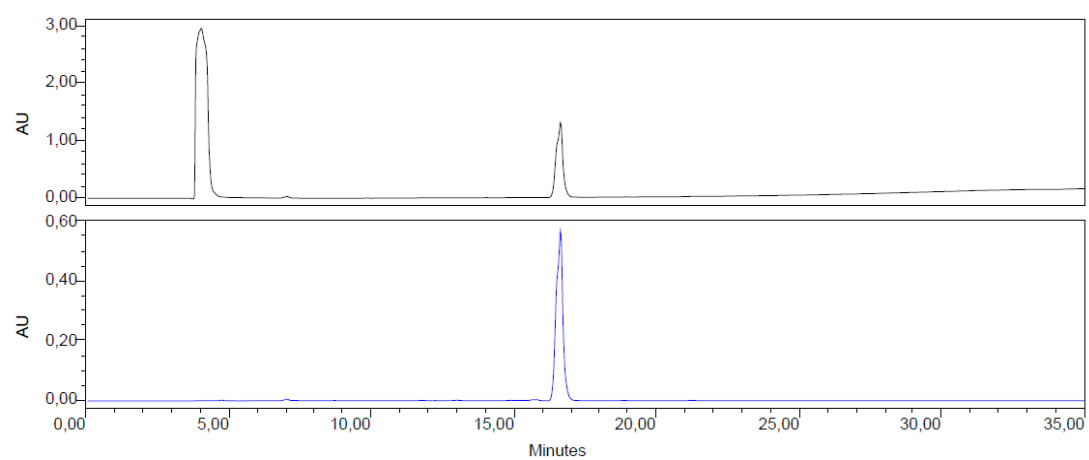


Figure F14. RP-HPLC chromatogram of SB4CB

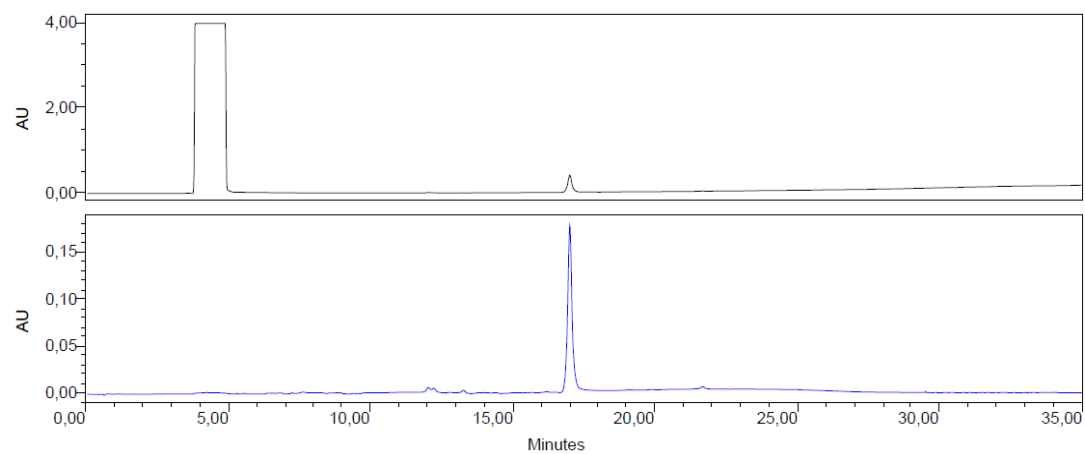


Figure F15. RP-HPLC chromatogram of CuSB4CB

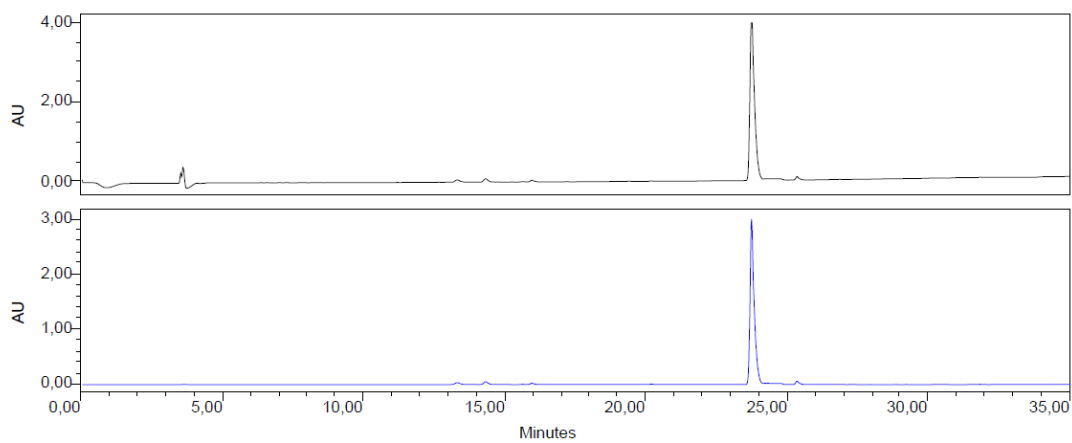


Figure F16. RP-HPLC chromatogram of SBCM

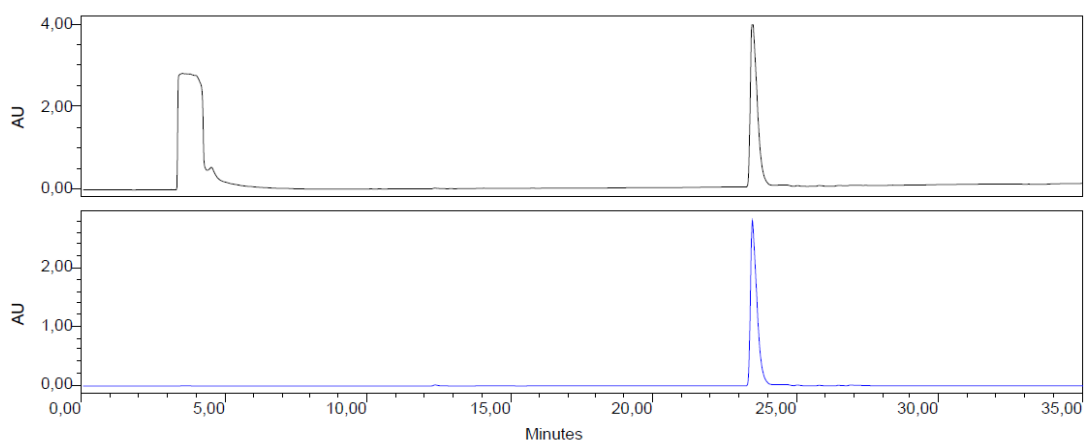


Figure F17. RP-HPLC chromatogram of Zn(SBCM)₂

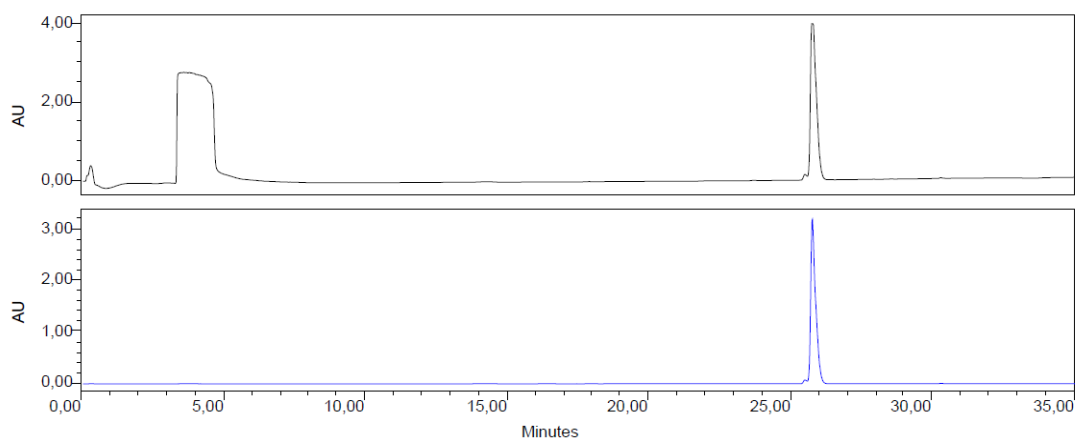


Figure F18. RP-HPLC chromatogram of Re₂(SBCM)₂

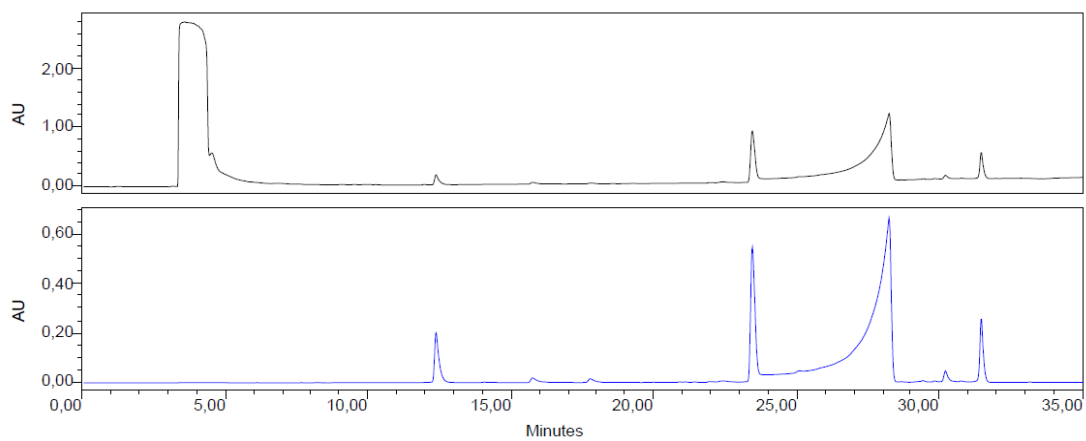


Figure F19. RP-HPLC chromatogram of Cu(SBCM)₂

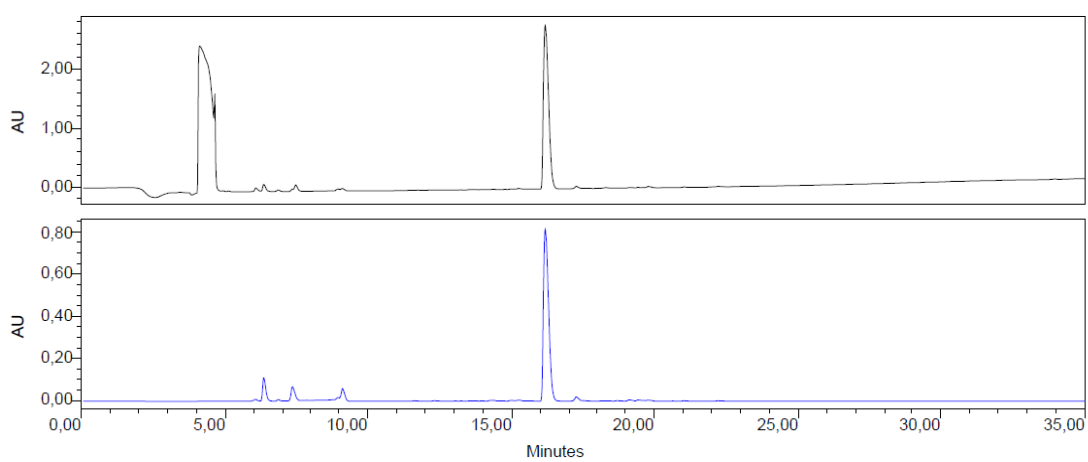


Figure F20. RP-HPLC chromatogram of R1-SB4CB (crude)

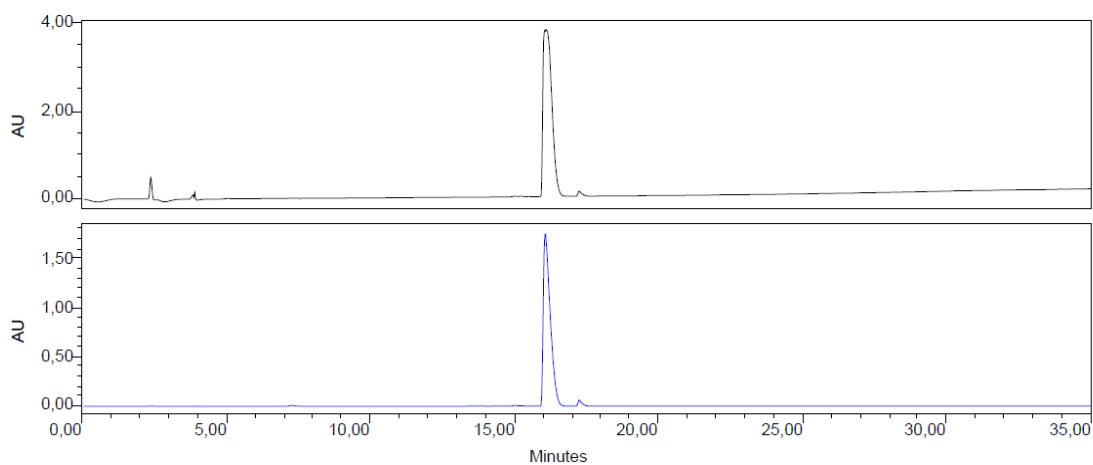


Figure F21. RP-HPLC chromatogram of R1-SB4CB (purified)

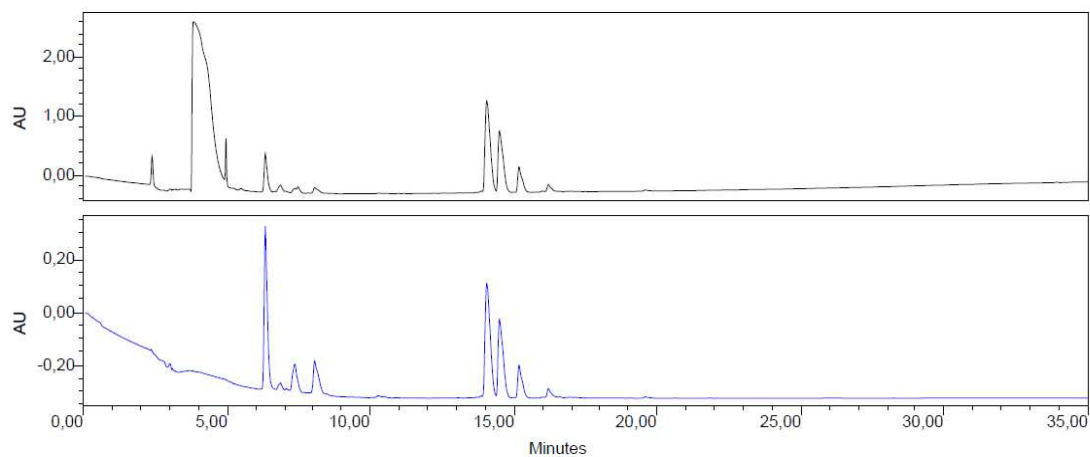


Figure F22. RP-HPLC chromatogram of R4-SB4CB (crude)

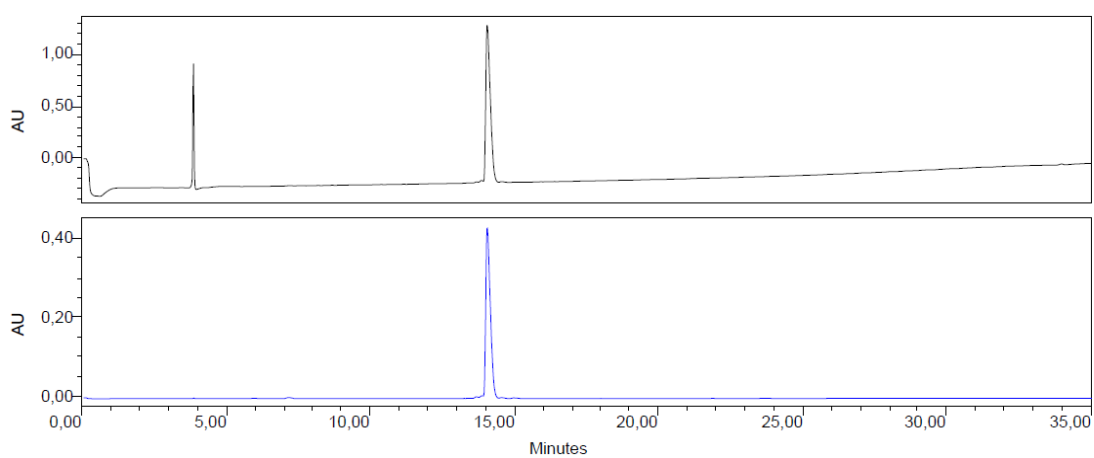


Figure F23. RP-HPLC chromatogram of R4-SB4CB (purified)

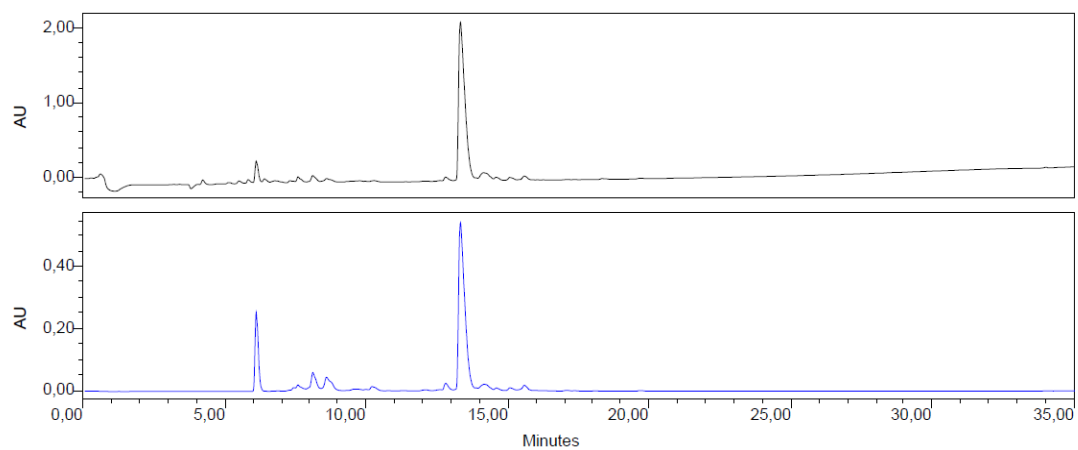


Figure F24. RP-HPLC chromatogram of R9-SB4CB (crude)

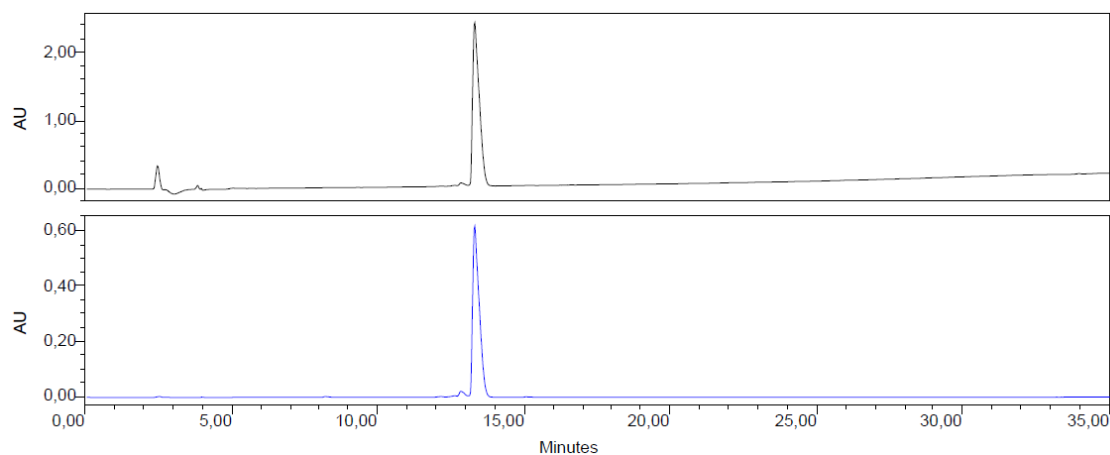


Figure F25. RP-HPLC chromatogram of R9-SB4CB (purified)

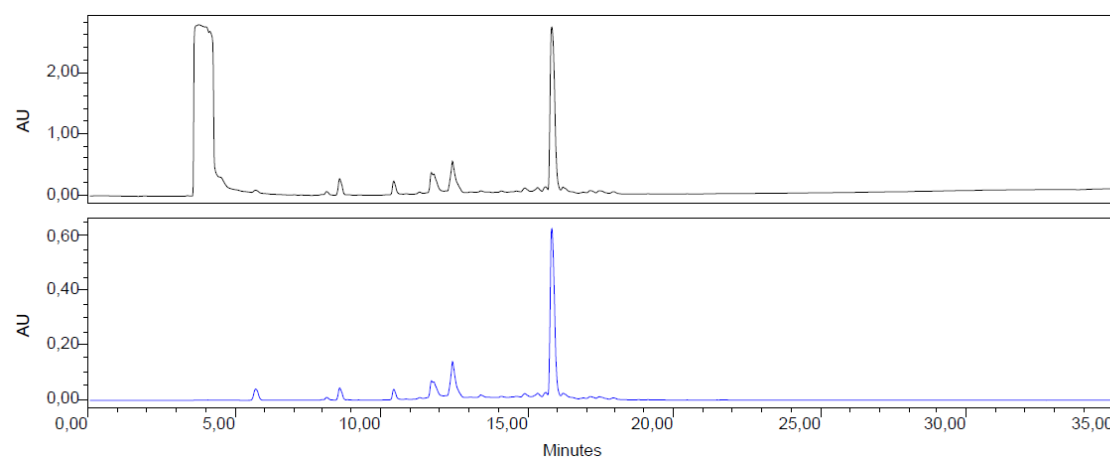


Figure F26. RP-HPLC chromatogram of RW9-SB4CB (crude)

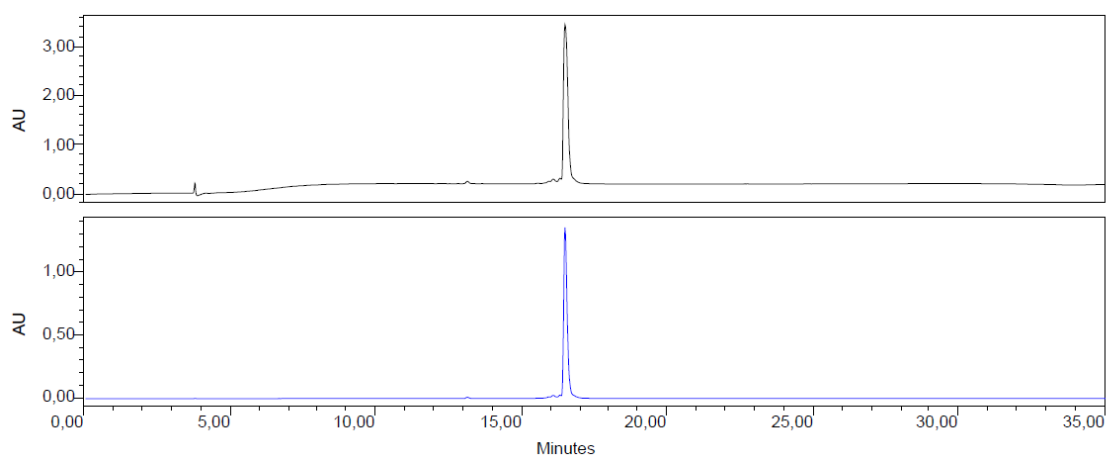


Figure F27. RP-HPLC chromatogram of RW9-SB4CB (purified)

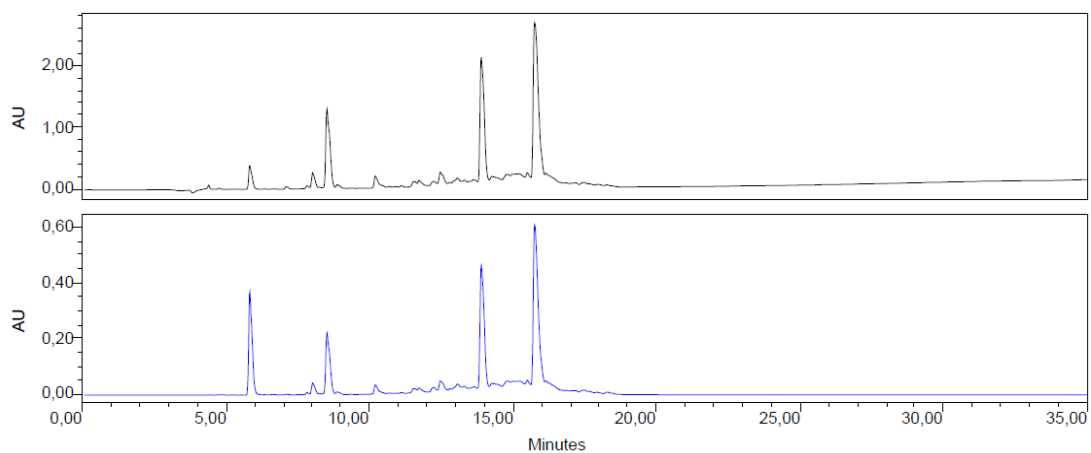


Figure F28. RP-HPLC chromatogram of RW9-SM4CB (crude)

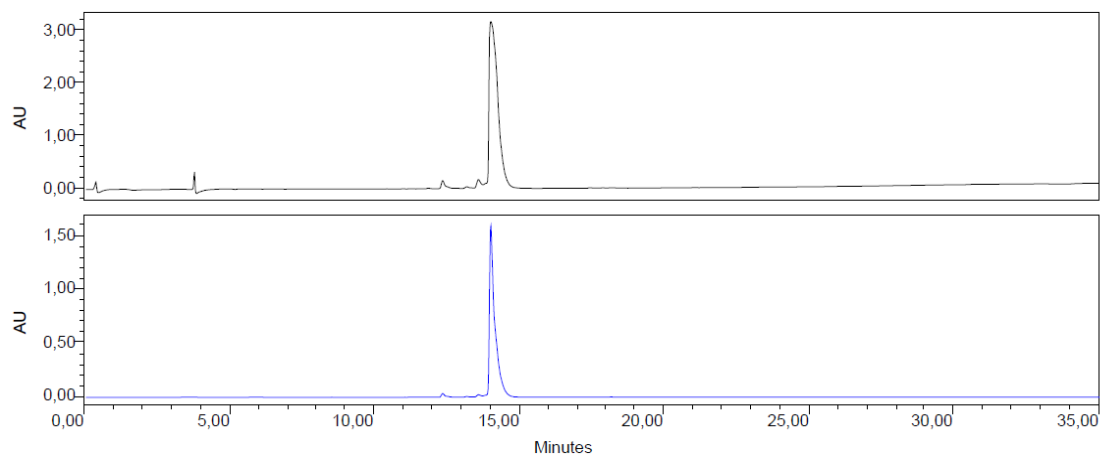


Figure F29. RP-HPLC chromatogram of RW9-SM4CB (purified)

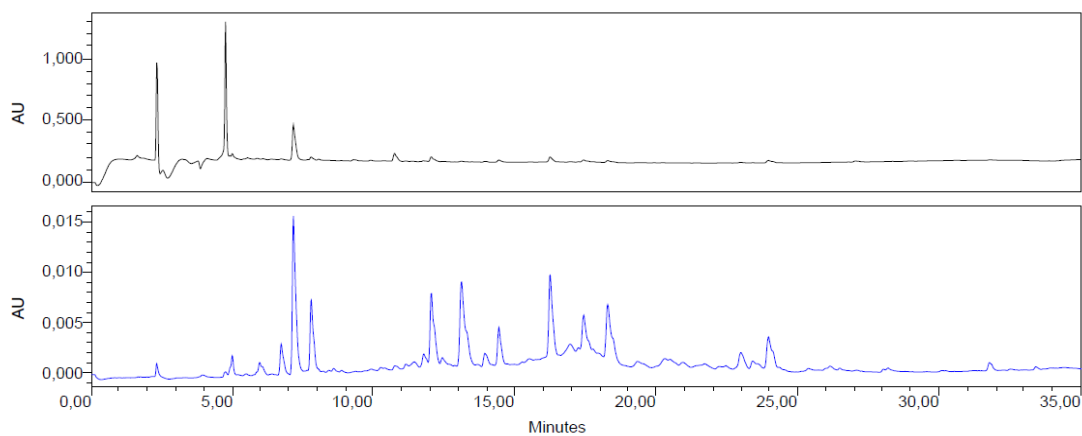


Figure F30. RP-HPLC chromatogram of R1-Ac (crude)

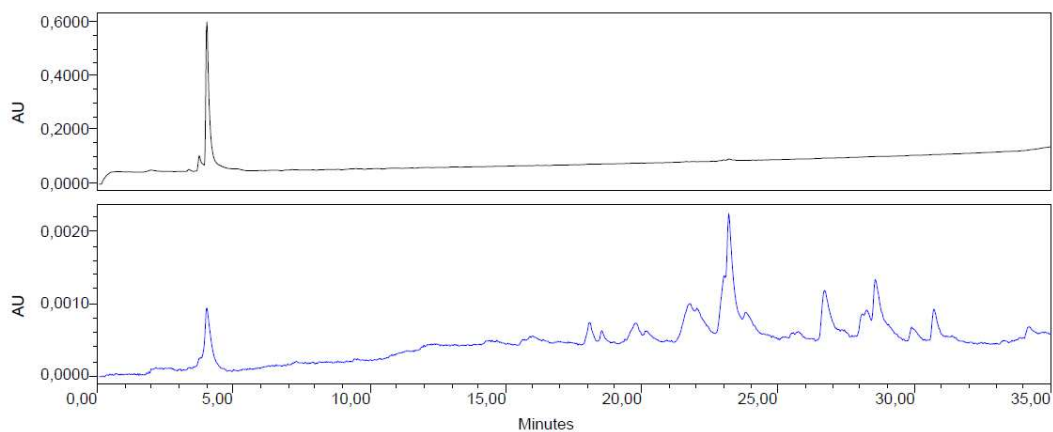


Figure F31. RP-HPLC chromatogram of R1-Ac (purified)

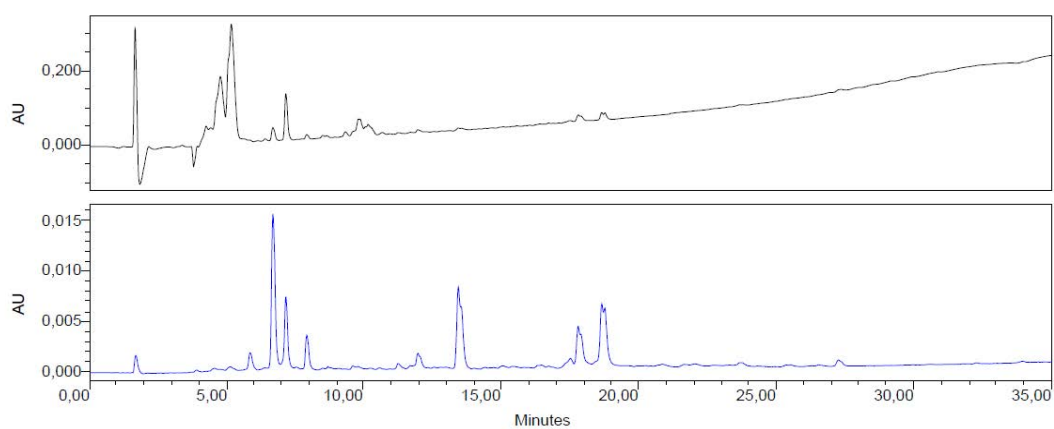


Figure F32. RP-HPLC chromatogram of R4-Ac (crude)

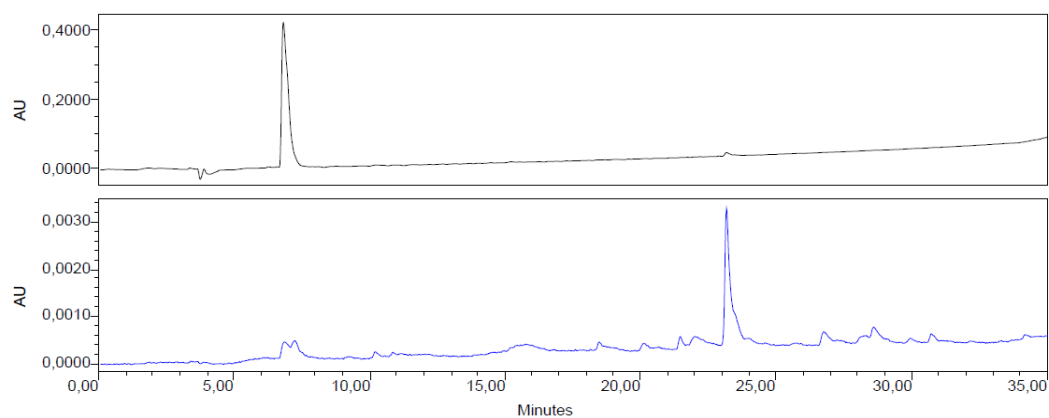


Figure F33. RP-HPLC chromatogram of R4-Ac (purified)

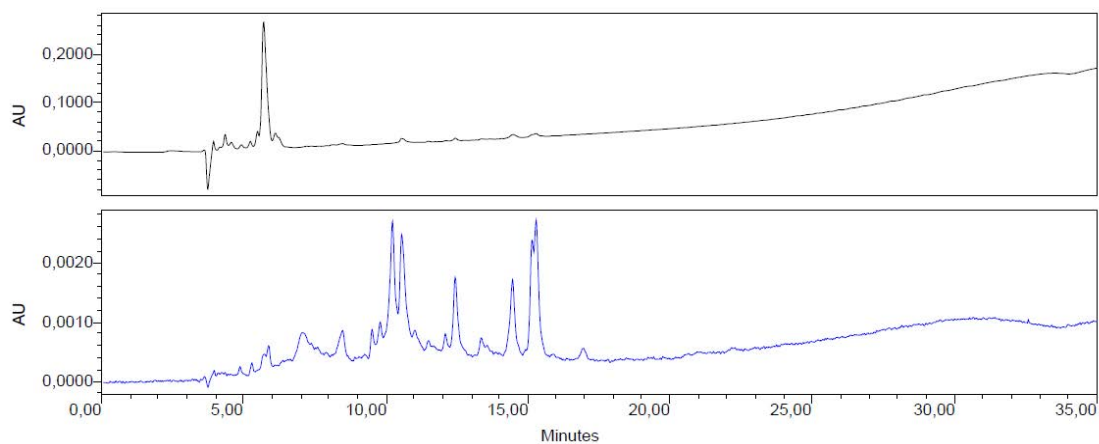


Figure F34. RP-HPLC chromatogram of R9-Ac (crude)

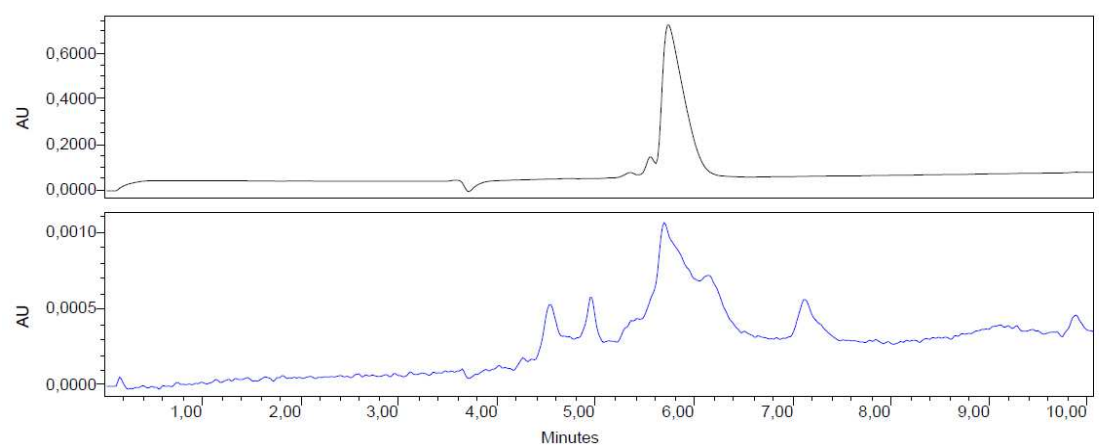


Figure F35. RP-HPLC chromatogram of R9-Ac (purified)

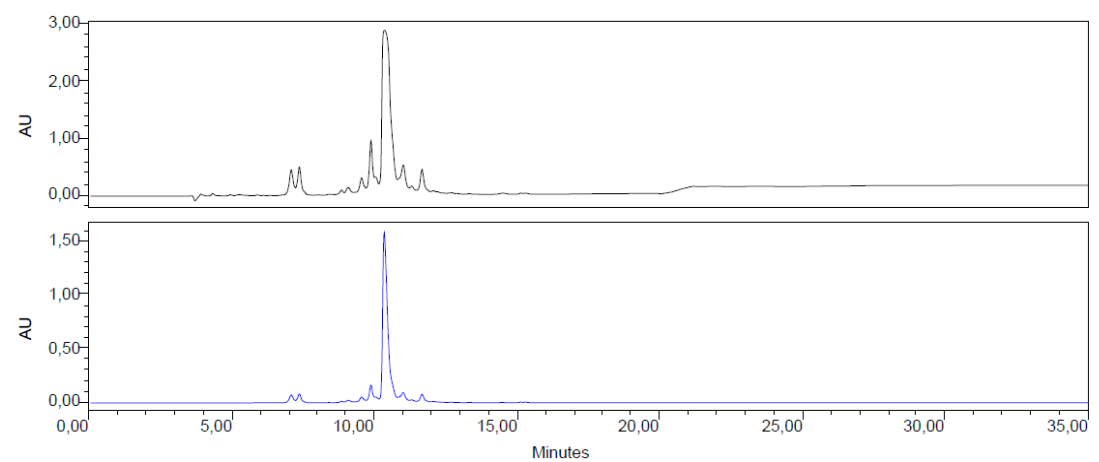


Figure F36. RP-HPLC chromatogram of RW9-Ac (crude)

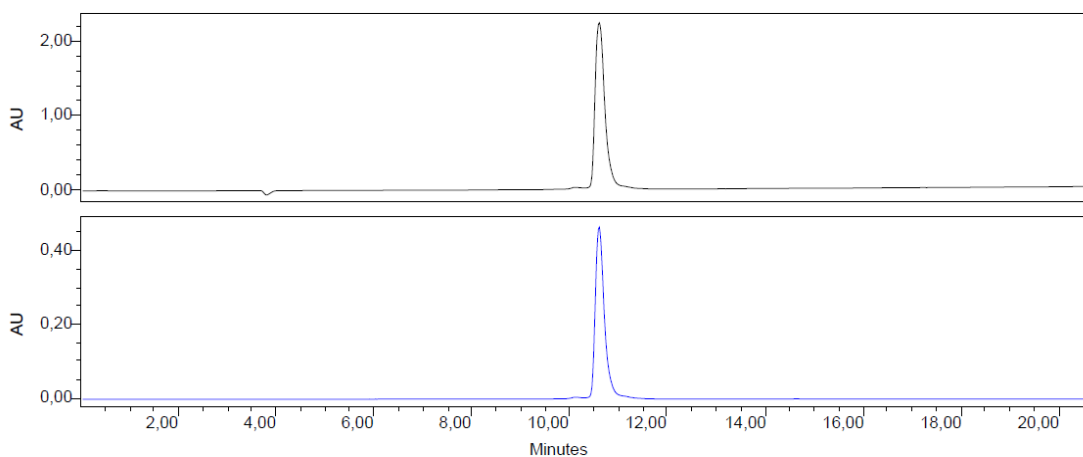


Figure F37. RP-HPLC chromatogram of RW9-Ac (purified)

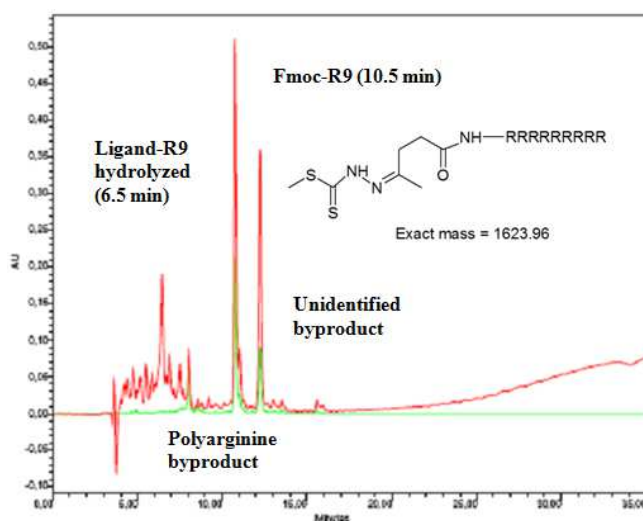


Figure F38. RP-HPLC chromatogram obtained from the SPPS Fmoc synthesis of the aliphatic ligand, SMLA-R9 conjugate. None of the major peaks correspond to the desired product as observed by MALDI-TOF-MS. The coupling and deprotection were difficult and the Schiff base was hydrolysed resulting in the product R9-ketone (m/z : 1521, R_T = 6.5 min) and R9-Fmoc (m/z : 1645, R_T = 10.5 min).

G. CV

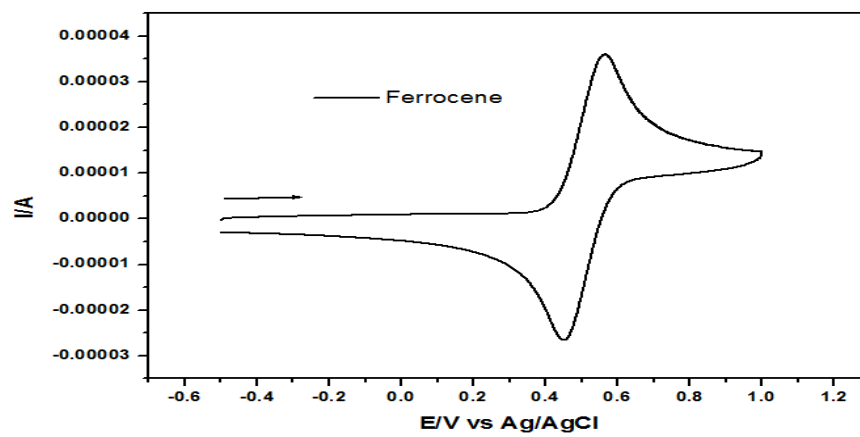


Figure G1. Cyclic voltammograms of ferrocene

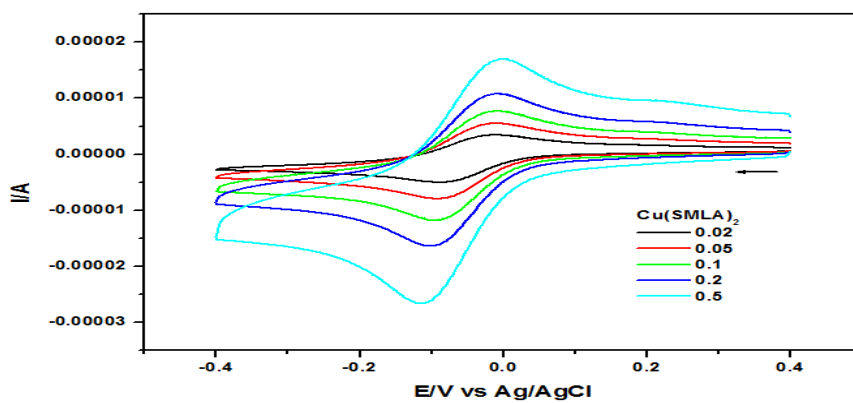
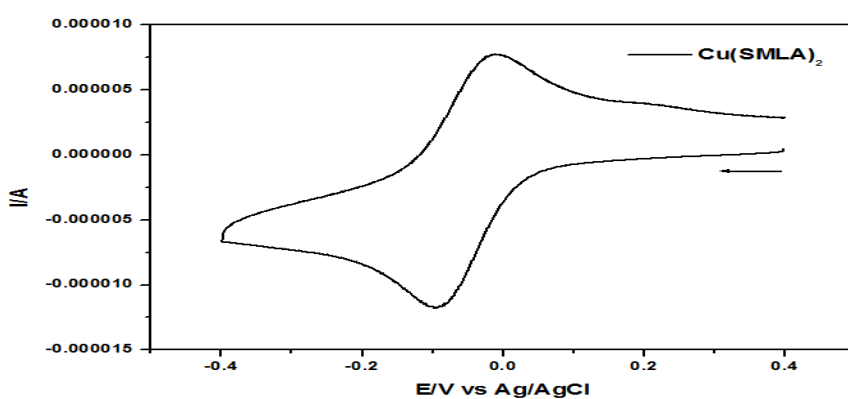
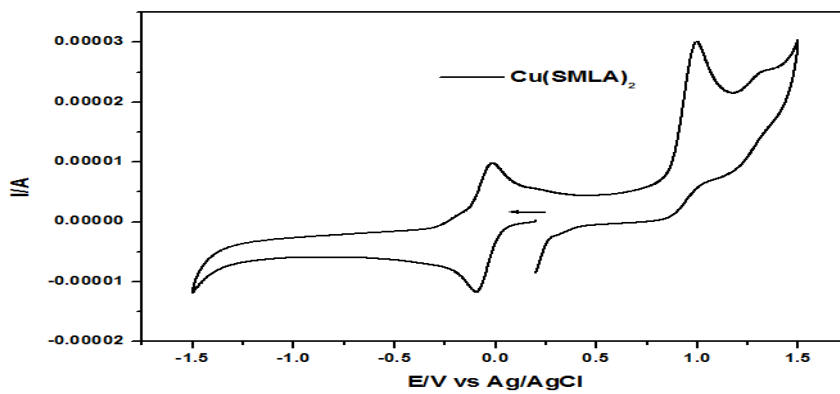


Figure G2. Cyclic voltammograms of the Cu(SMLA)_2

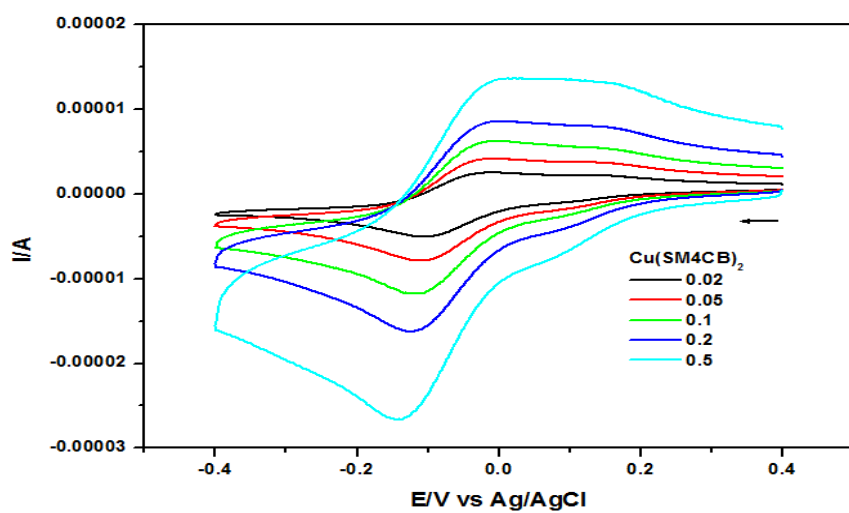
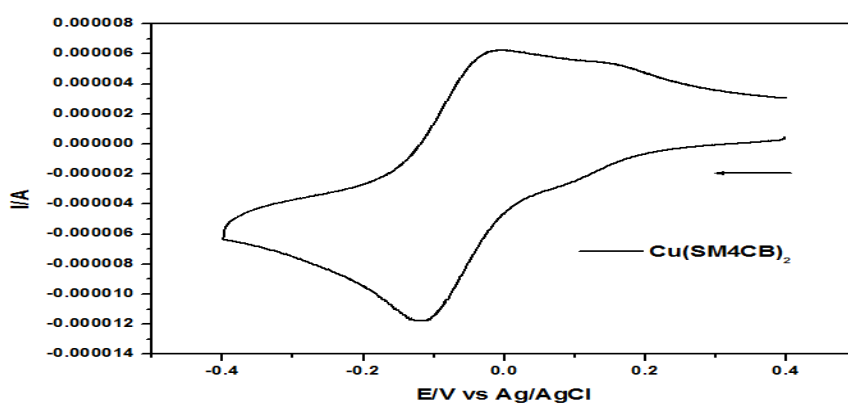
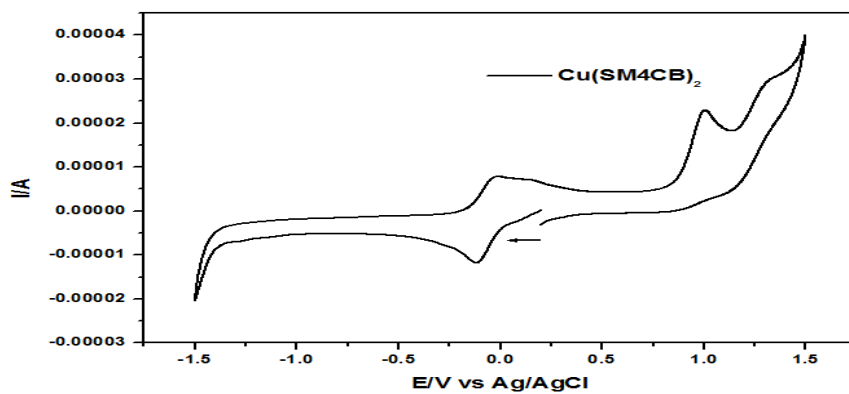


Figure G3. Cyclic voltammograms of the $\text{Cu}(\text{SM4CB})_2$

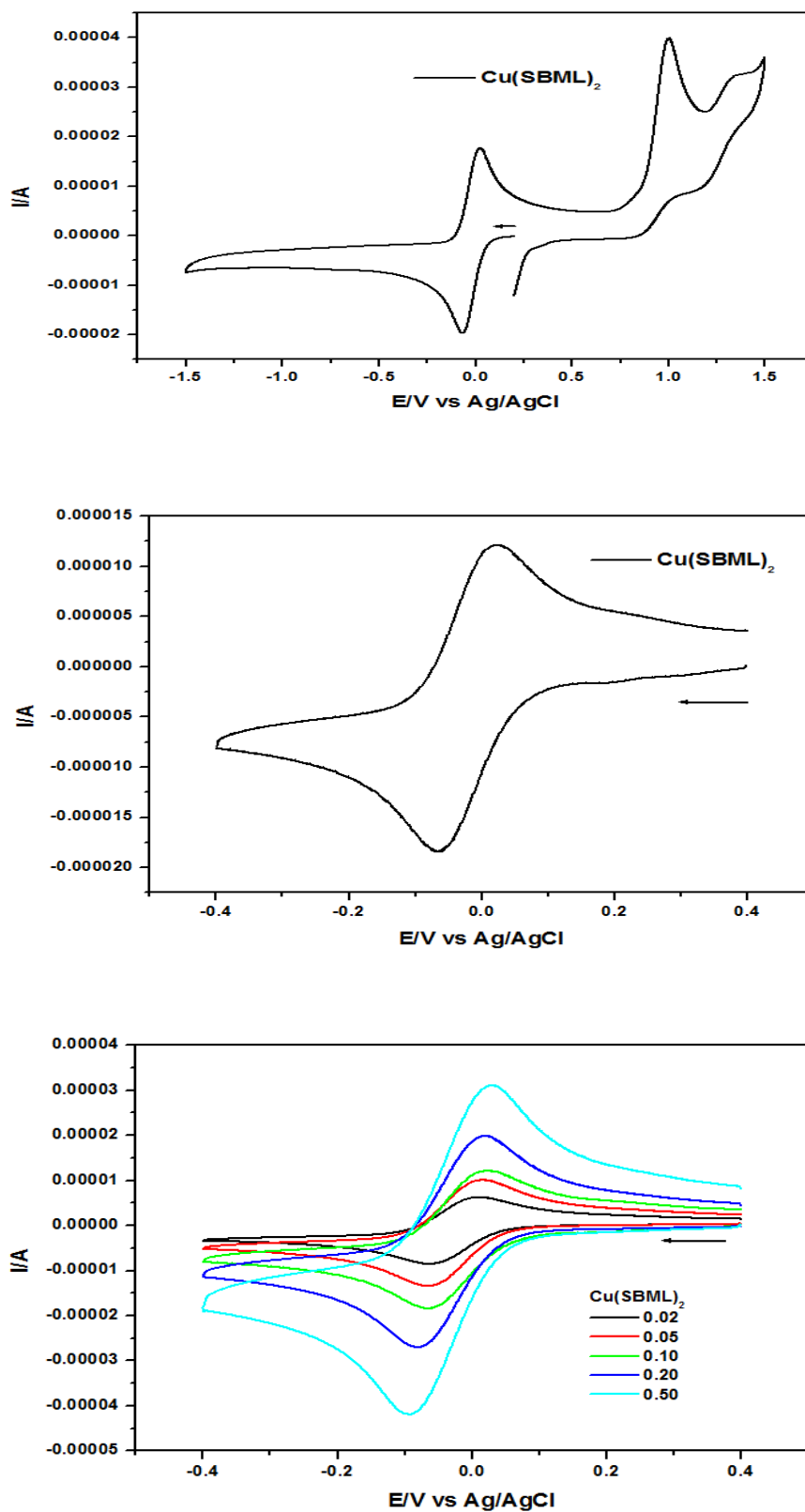


Figure G4. Cyclic voltammograms of the $\text{Cu}(\text{SBML})_2$

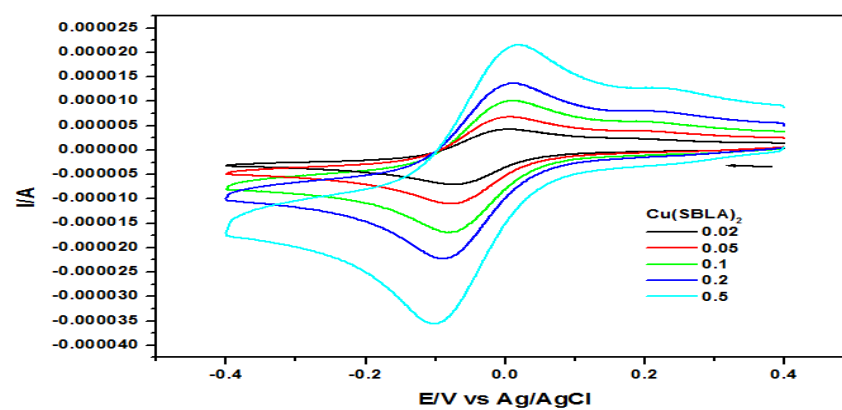
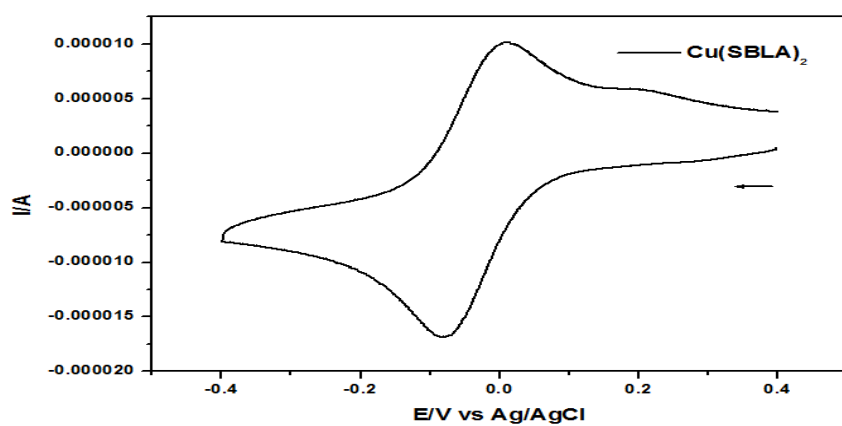
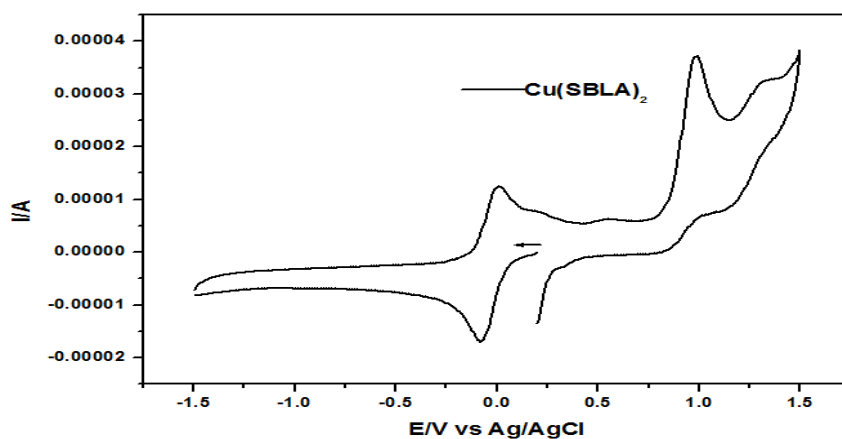


Figure G5. Cyclic voltammograms of the Cu(SBLA)_2

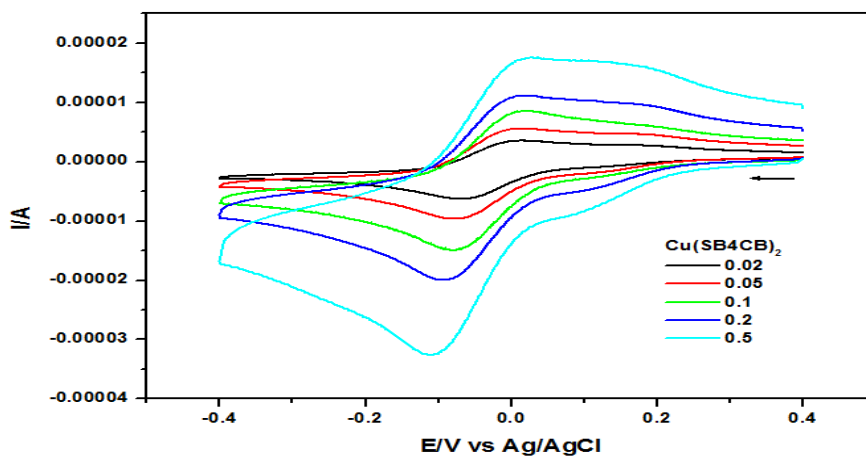
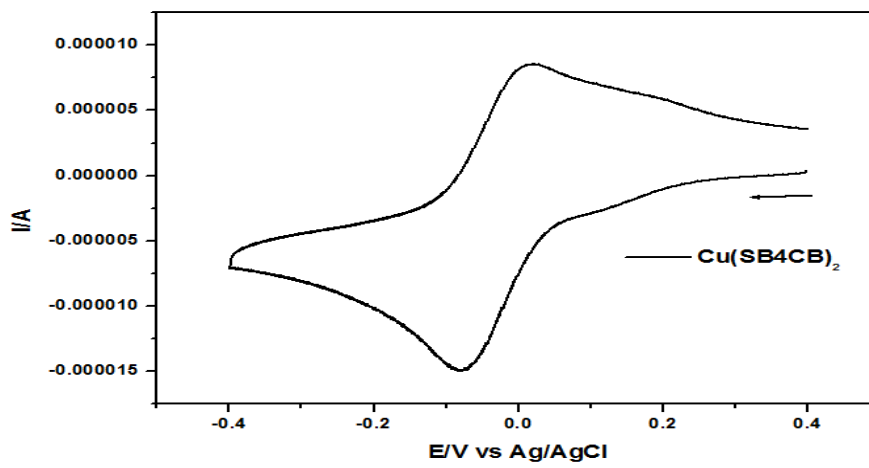
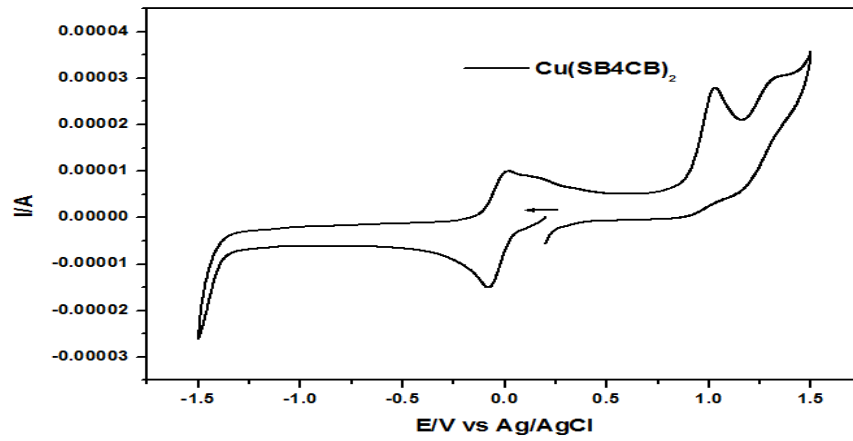


Figure G6. Cyclic voltammograms of the $\text{Cu}(\text{SB4CB})_2$

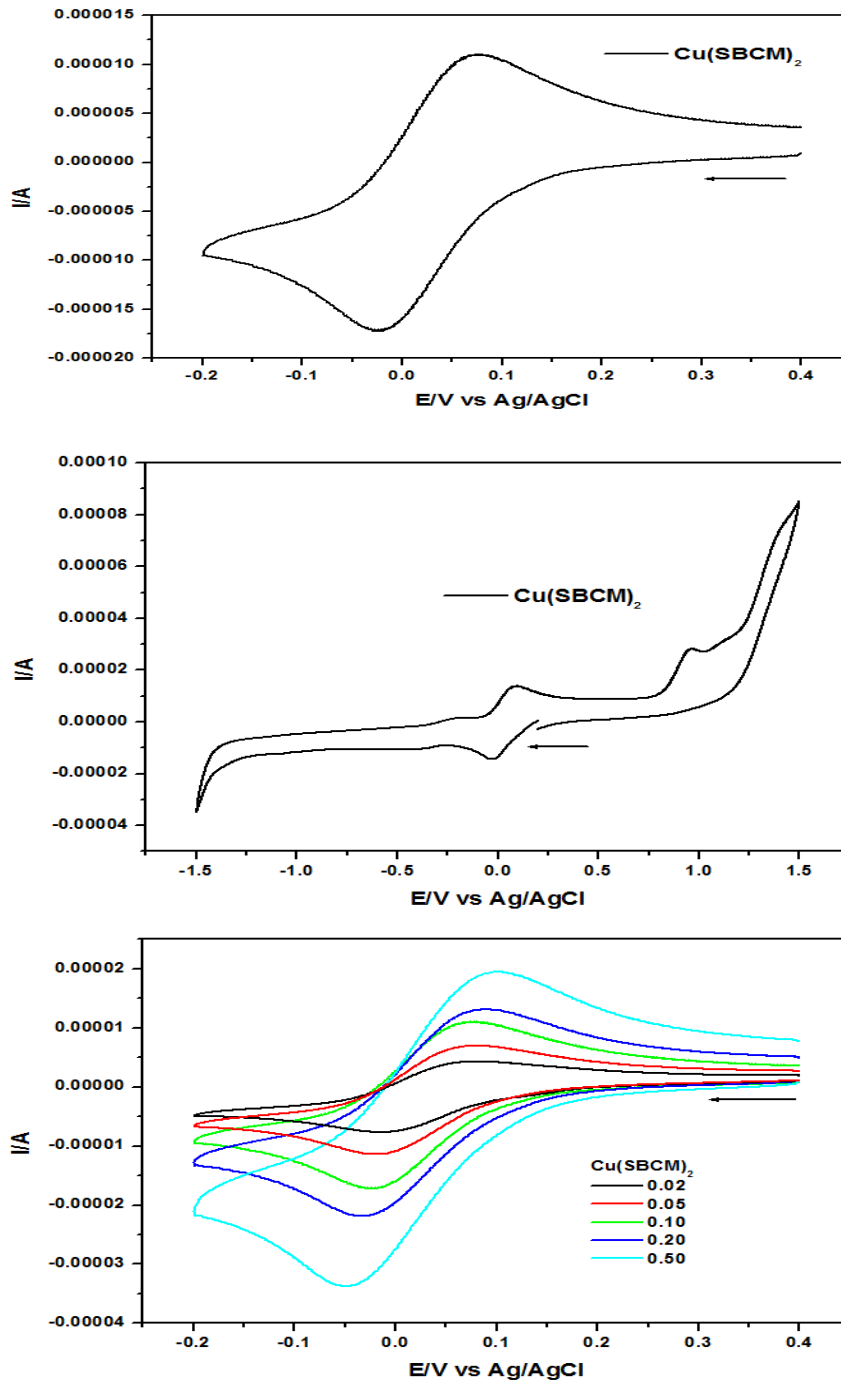


Figure G7. Cyclic voltammograms of the Cu(SBCM)_2

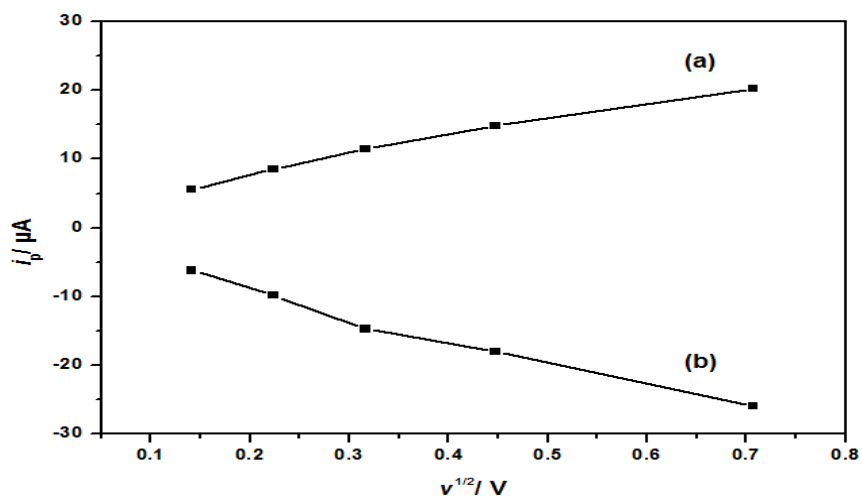


Figure G8. Plot of the anodic (I_{pa}) and cathodic (I_{pc}) current with the square root of scan rate for $Cu(SBCM)_2$ and (above) cyclic voltammograms of $Cu(SBCM)_2$ at 0.1 V/s in the range of -1.5 V to 1.5 V.

Table G1. Electrochemical data for the $Cu(SBCM)_2$ vs Ag/AgCl at various scan rate (V/s).

Cu(SMML) ₂	Cu(II)/Cu(I)				ia/ic	$i_{pc} / v^{1/2}$
	Epa[V]	Epc[V]	$\Delta E_p = E_{pa} - E_{pc}$ [mV]	$\Delta E_{1/2} = 0.5 (E_{pa} + E_{pc})$ [V]		
0.02	0.082	-0.015	97	0.034	0.91	-43.6
0.05	0.079	-0.019	98	0.060	0.87	-43.9
0.10	0.089	-0.027	116	0.031	0.78	-46.5
0.20	0.089	-0.033	122	0.056	0.83	-40.2
0.50	0.102	-0.049	151	0.053	0.78	-36.6

H. ITC

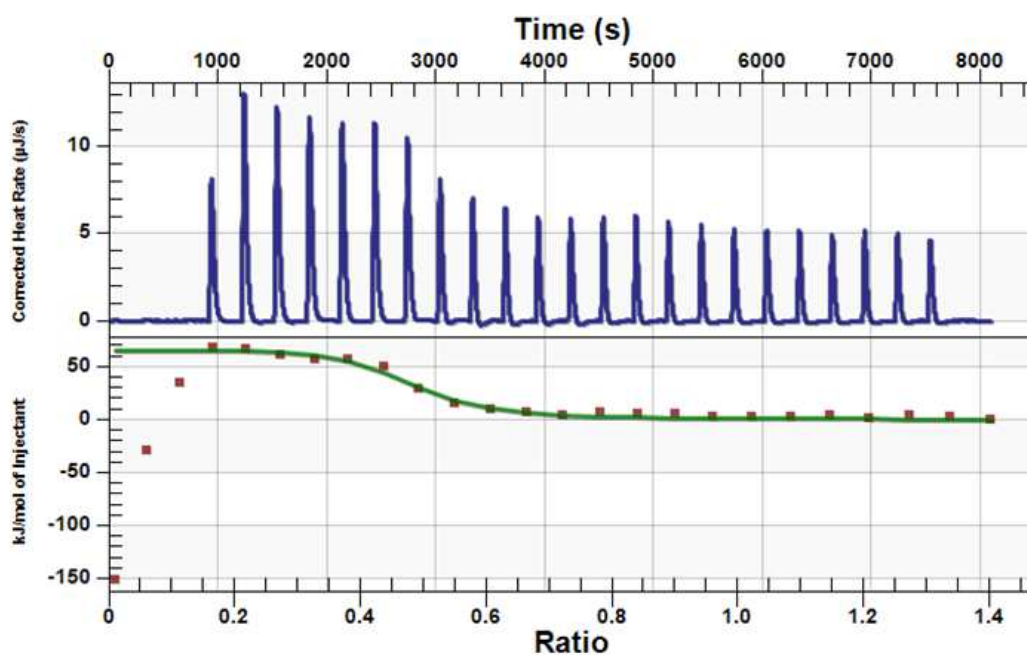


Figure H1. ITC titration of Cu(R1-SB4CB)₂

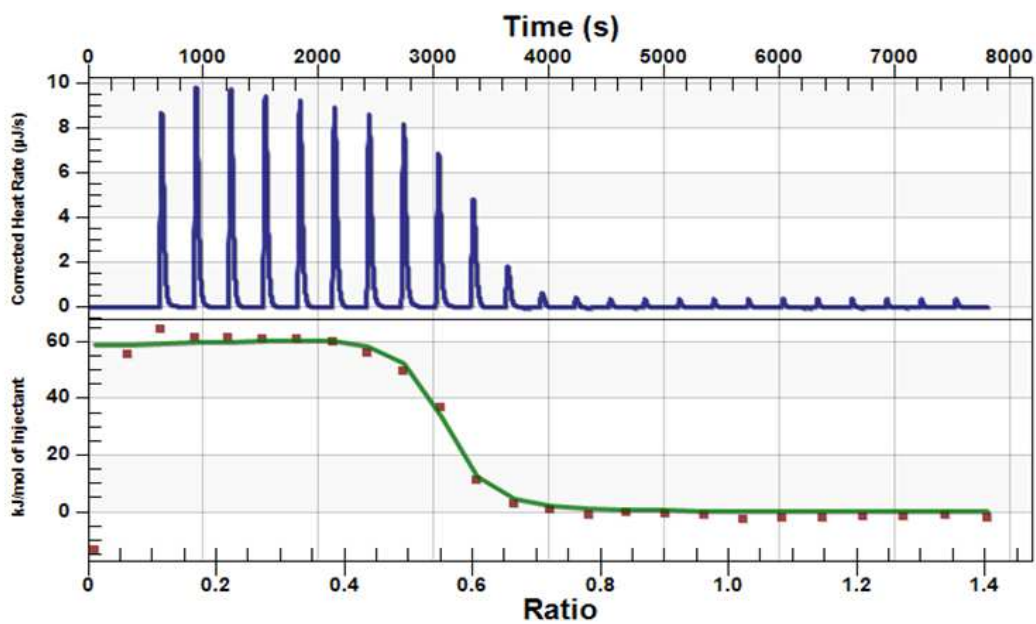


Figure H2. ITC titration of Cu(RW9-SB4CB)₂

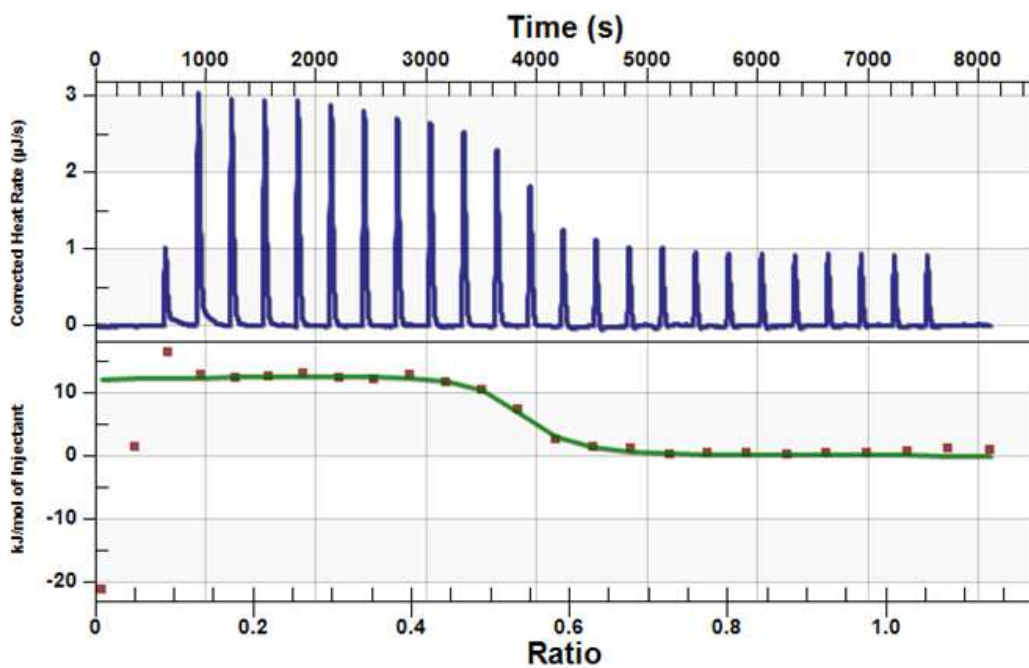


Figure H3. ITC titration of Cu(R9-SM4CB)₂

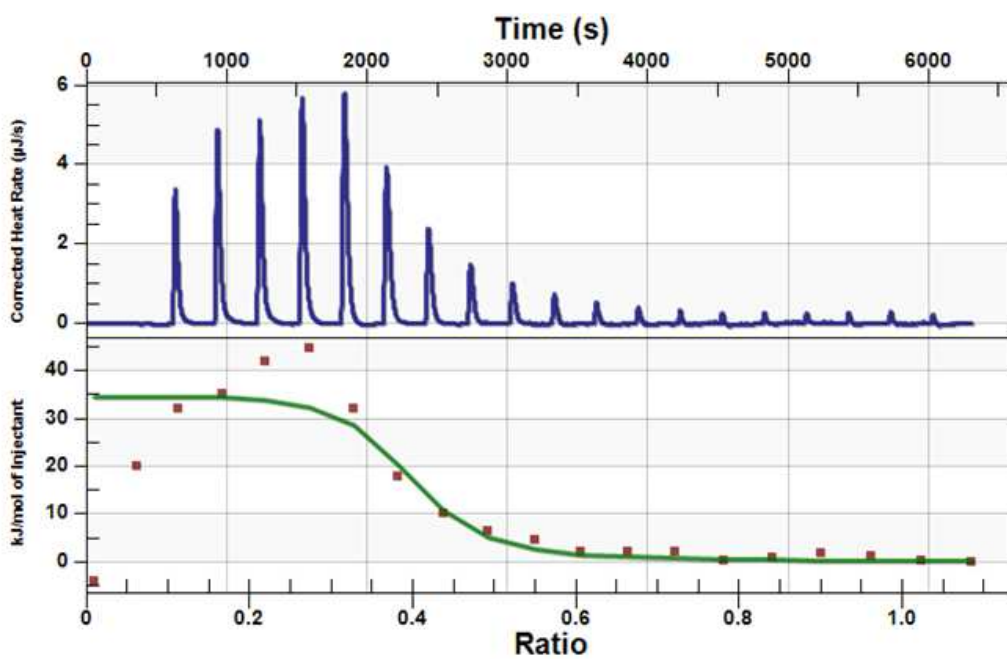


Figure H4. ITC titration of Cu(RW9-SM4CB)₂

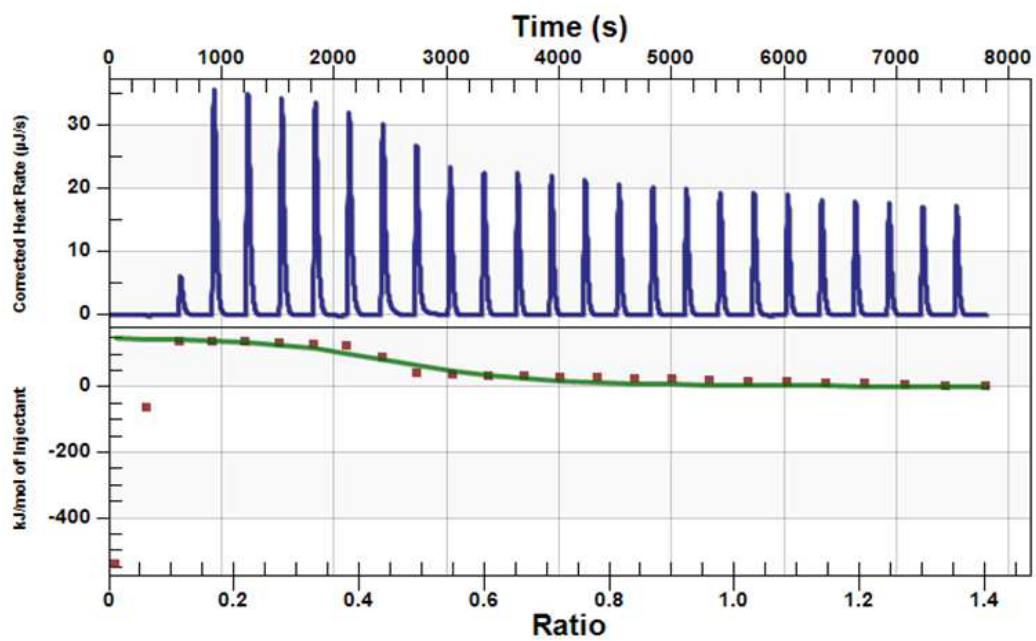


Figure H5. ITC titration of $\text{Cu}(\text{SB4CB})_2$

I. EPR

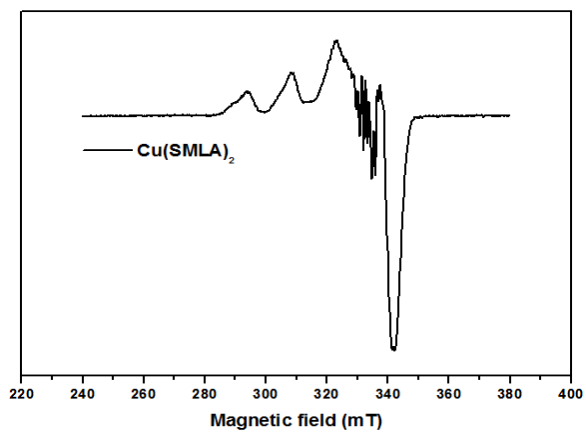


Figure I1. The EPR spectrum of Cu(SMLA)_2 at 1 mM

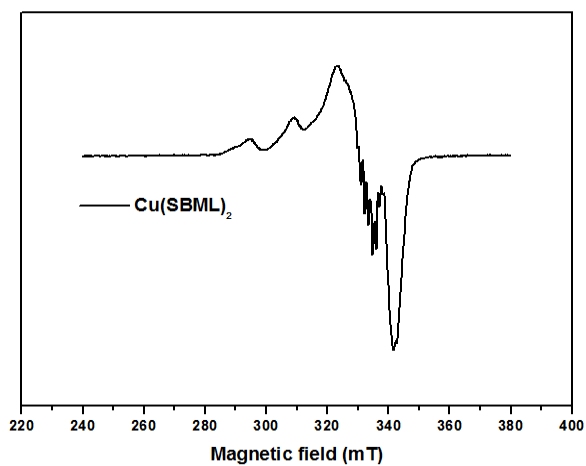


Figure I2. The EPR spectrum of Cu(SBML)_2 at 1 mM

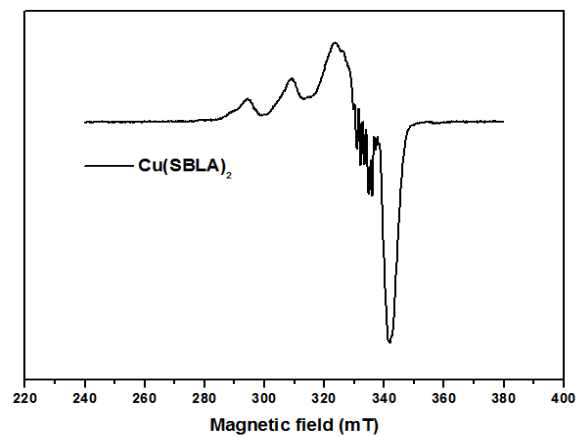


Figure I3. The EPR spectrum of Cu(SBLA)_2 at 1 mM

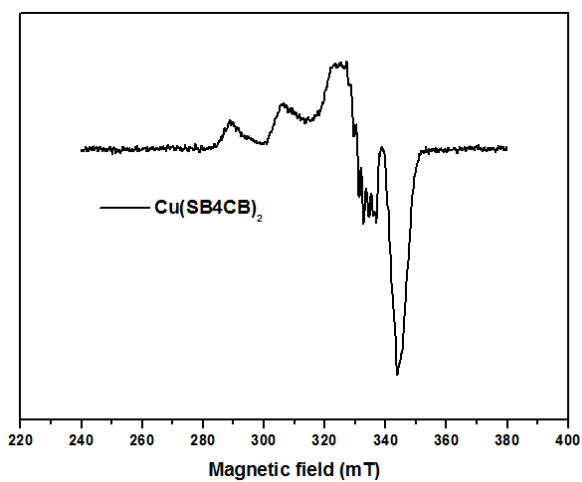


Figure I4. The EPR spectrum of $\text{Cu}(\text{SB4CB})_2$ at 1 mM

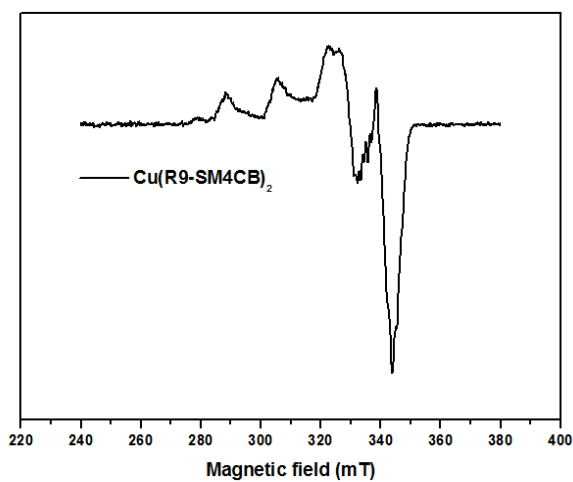


Figure I5. The EPR spectrum of $\text{Cu}(\text{R9-SM4CB})_2$ at 1 mM

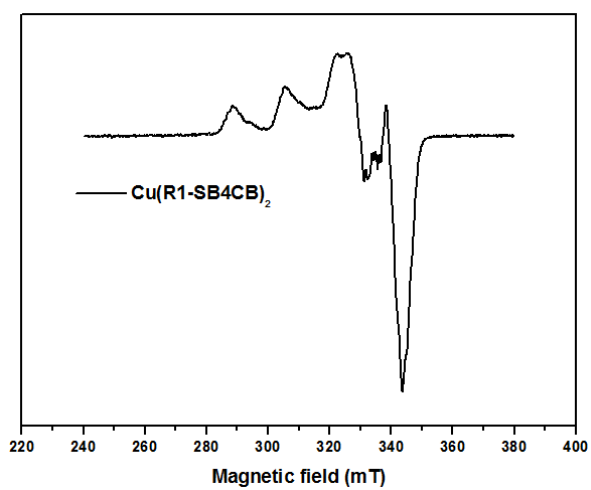


Figure I6. The EPR spectrum of $\text{Cu}(\text{R1-SB4CB})_2$ at 1 mM

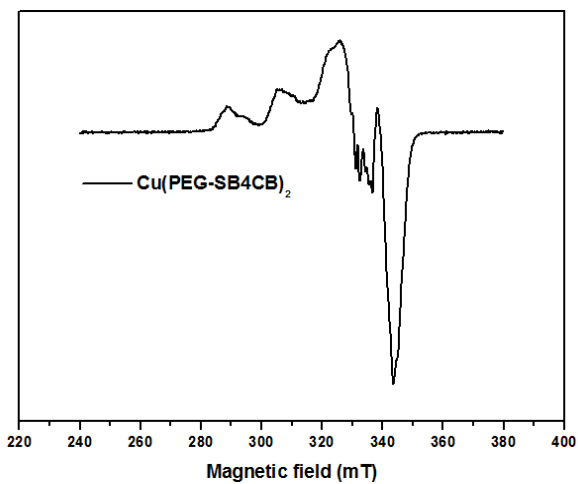


Figure I7. The EPR spectrum of $\text{Cu}(\text{PEG-SB4CB})_2$ at 1 mM

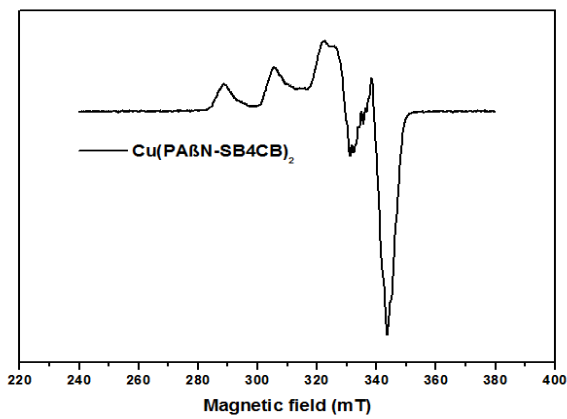


Figure I8. The EPR spectrum of $\text{Cu}(\text{PA}\beta\text{N-SB4CB})_2$ at 1 mM

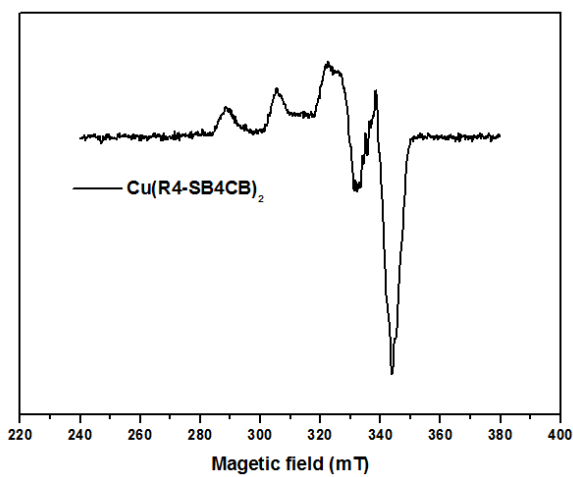


Figure I9. The EPR spectrum of $\text{Cu}(\text{R4-SB4CB})_2$ at 1 mM

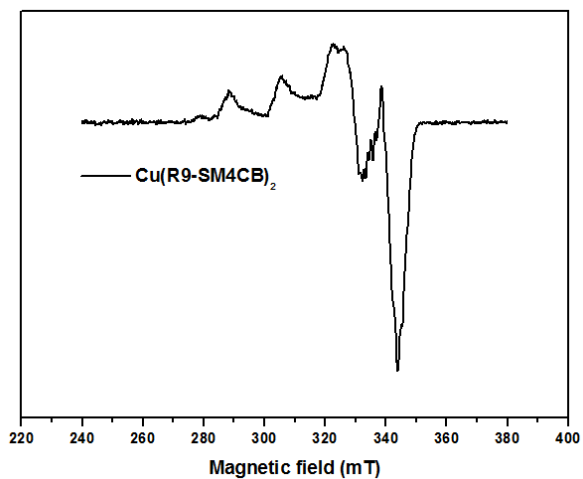


Figure I10. The EPR spectrum of Cu(R9-SM4CB)_2 at 1 mM

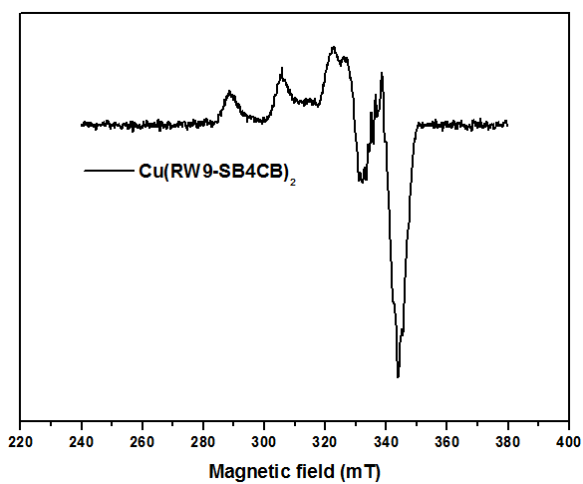


Figure I11. The EPR spectrum of Cu(RW9-SB4CB)_2 at 1 mM

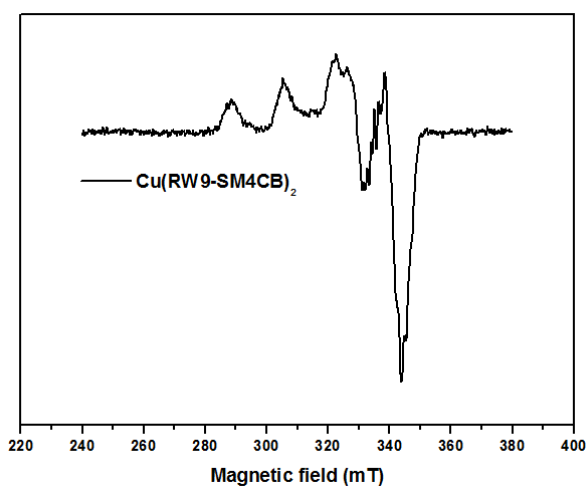


Figure I12. The EPR spectrum of Cu(RW9-SM4CB)_2 at 1 mM

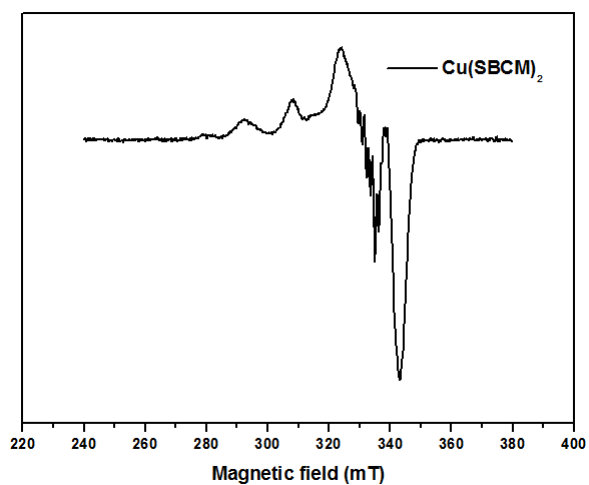


Figure I13. The EPR spectrum of Cu(SBCM)₂ at 1 mM

J. Elemental analysis

Table J1. CHNS data

CuSMHD

Elément	Mesure 1
% Carbone	31.35
% Hydrogène	4.24
% Azote	14.64
% Soufre	33.30

Cu(SM4CB)₂

Elément	Mesure 1
% Carbone	41.84
% Hydrogène	3.39
% Azote	9.65
% Soufre	22.35

Cu(SMLA)₂

Elément	Mesure 1
% Carbone	31.58
% Hydrogène	4.31
% Azote	10.48
% Soufre	23.65

Cu(SBLA)₂

Elément	Mesure 1
% Carbone	47.15
% Hydrogène	4.64
% Azote	8.51
% Soufre	19.35

Cu(SB4CB)2

Elément	Mesure 1
% Carbone	53.39
% Hydrogène	3.81
% Azote	7.65
% Soufre	17.74

Cu(SMML)₂

Elément	Mesure 1
% Carbone	36.41
% Hydrogène	5.03
% Azote	10.64
% Soufre	24.24

CuSBHD

Elément	Mesure 1
% Carbone	49.40
% Hydrogène	4.63
% Azote	10.46
% Soufre	23.98

Cu(SBML)₂

Elément	Mesure 1
% Carbone	50.07
% Hydrogène	5.09
% Azote	8.31
% Soufre	18.74

Cu(SBCM)₂

Elément	Mesure 1
% Carbone	56.53
% Hydrogène	3.80
% Azote	7.02
% Soufre	15.58

SBHD

18:28:41 April 04, 2011

Analysis Date: 4/4/2011 6:28:41 PM Name: Hexan Re Mass mg: 2.0800 Location: 27 Operator: Ismail

Carbon % 54.793

Hydrogen % 5.5918

Nitrogen % 11.750

Sulfur % 27.340

User name

SMHD

948 DB08 07 2.108 37.86 4.873 17.84 34.37

Re₂(SBCM)₂ (mass = 2.183 mg) and Zn(SBCM)₂ (mass = 1.997 mg)

Mass mg	Method	Carbon %	Hydrogen %	Nitrogen %	Sulfur %
2.152	UPM CHNS	51.84	5.102	19.61	12.28
2.182	UPM CHNS	51.87	5.114	19.57	11.77
1.922	UPM CHNS	55.35	3.749	7.216	15.78
1.997	UPM CHNS	56.49	3.838	7.103	16.72
1.893	UPM CHNS	56.43	3.864	7.274	16.58
1.36	UPM CHNS	37.51	2.491	4.405	6.839
2.183	UPM CHNS	40.04	2.409	4.428	8.886
2	UPM CHNS	-0.0037	-0.0395	0.1465	-0.318
2	UPM CHNS	-0.0055	0.0327	0.1797	-0.013

LIST OF PUBLICATIONS AND CONFERENCES ATTENDED

List of Publications

1. Low, M. L., Ravooof, T. B. S., Tahir, M. I. M., Crouse, K. A., & Tiekink, E. R. (2013). (Pyridin-4-yl) methyl N'-(3-phenylallylidene) hydrazinecarbodithioate. *Acta Crystallographica Section E: Structure Reports Online*, 69(2), o167-o168.
2. May Lee Low, Laure Maigre, Pierre Dorlet, Régis Guillot, Jean-Marie Pagès, Nicolas Delsuc, Clotilde Policar and Karen A. Crouse. A New Series of Copper(II) Dithiocarbazate Schiff Bases: Synthesis, Conjugation to Polyarginine and Effect On Antimicrobial Activity. *Manuscript in preparation*.
3. May Lee Low, Georgiana Paulus, Pierre Dorlet, Régis Guillot, Rozita Rosli, Nicolas Delsuc, Clotilde Policar and Karen A. Crouse. Synthesis, Characterization and Biological Activity of Cu(II), Zn(II) And Re(I) Complexes Derived from S-Benzyl Dithiocarbazate and 3-Acetylcoumarin. *Manuscript in preparation*.
4. May Lee Low, Laure Maigre, Mohamed Ibrahim M. Tahir, Pierre Dorlet, Régis Guillot, Thahira Begum Ravooof, Rozita Rosli, Jean-Marie Pagès, Nicolas Delsuc, Clotilde Policar and Karen A. Crouse. X-Ray and Solution Structure of Copper (II) Macroacyclic Bis(dithiocarbazate): Influence on Their Redox Properties and Bioactivities. *Manuscript in preparation*.

List of Conferences Attended

1. May Lee Low, Laure Maigre, Pierre Dorlet, Régis Guillot, Jean-Marie Pagès, Nicolas Delsuc, Clotilde Policar, Karen A. Crouse. A New Series of Copper(II) Dithiocarbazate Schiff Bases: Synthesis, Conjugation to Polyarginine and Effect on Antimicrobial Activity. *16th International Conference of Bioinorganic Chemistry (ICBIC), Grenoble, France (22nd - 26th July 2013)*. Poster presentation.
2. May Lee Low, Laure Maigre, Pierre Dorlet, Régis Guillot, Jean-Marie Pagès, Nicolas Delsuc, Clotilde Policar, Karen A. Crouse. A New Series of Copper(II) Dithiocarbazate Schiff Bases: Synthesis, Conjugation to Polyarginine and Effect on Antimicrobial Activity. *Group Français de Chimie Bio-Inorganique, Reunion Annuelle, Aussois, France (24-27th March 2013)*. Oral communication.
3. May Lee Low, Laure Maigre, Mohamed Ibrahim M. Tahir, Pierre Dorlet, Régis Guillot, Thahira Begum Ravooof, Rozita Rosli, Jean-Marie Pagès, Nicolas Delsuc, Clotilde Policar, Karen A. Crouse. Macroacyclic Bis(dithiocarbazate): Synthesis, Characterization and Bioactivities. *40th International Conference on Coordination Chemistry (ICCC), Valencia, Spain (9-13th September 2012)*. Poster presentation.

4. May Lee Low, Laure Maigre, Mohamed Ibrahim M. Tahir, Pierre Dorlet, Régis Guillot, Thahira Begum Ravoof, Rozita Rosli, Jean-Marie Pagés, Nicolas Delsuc, Clotilde Policar, Karen A. Crouse. Synthesis, Characterisation and Biological Activities of Cu(II) Complex Containing Macroacyclic Tetradentate (N₂S₂) Schiff Base Ligand Derived from Dithiocarbazate. *Club Metalloproteines et Modeles, Reunion Annuelle, Mittelwihr, France (25-28th March 2012)*. Poster presentation.
5. *The 3rd Fundamental Science Congress 2011, Universiti Putra Malaysia (5-6th July 2011)*, As Participant.
6. *13th BCA/CCG Intensive Teaching School in X-Ray Structure Analysis, Durham, UK (26th March-3rd April 2011)*, As Participant.

BIODATA OF THE AUTHOR

Low May Lee was born on the 27th of March 1988 in Melaka, Malaysia. She received her primary and secondary education in Air Panas Setapak Girls School, Kuala Lumpur. In 2010, she obtained her B.Sc. (Honours) in Chemistry with first class from Universiti Putra Malaysia and was awarded for the Highest Academic Achievement in the B.Sc. (Honours) in Chemistry program for the 2010 graduating class. During her undergraduate studies, she did her industrial training with the Material Characterization Unit (MCU) at Rubber Research Institute of Malaysia (RRIM). She also carried out her final year project in the field of solid state chemistry working on the synthesis and characterization of bismuth ferrite materials under the supervision of Dr. Tan Kar Ban. In the same year 2010, she started her Doctor of Philosophy in Synthesis program at Universiti Putra Malaysia under the supervision of Professor Karen A. Crouse and in November 2011, she was granted the Erasmus Mundus: MAHEVA Scholarship to continue her doctoral research in the group of Professor Clotilde Policar at the Laboratoire des BioMolécules (UMR 7203) in Paris, France for 22 months.